

OPEN ACCESS

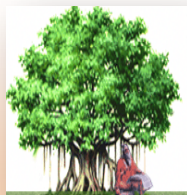
www.ijceronline.com

Volume 3, Issue 3, March, 2013

ISSN: 2250-3005



IjcerOnline



Editorial Board

Editor-In-Chief

Prof. Chetan Sharma

Specialization: Electronics Engineering, India
Qualification: Ph.d, Nanotechnology, IIT Delhi, India

Editorial Committees

DR.Qais Faryadi

Qualification: PhD Computer Science
Affiliation: USIM(Islamic Science University of Malaysia)

Dr. Lingyan Cao

Qualification: Ph.D. Applied Mathematics in Finance
Affiliation: University of Maryland College Park,MD, US

Dr. A.V.L.N.S.H. HARIHARAN

Qualification: Phd Chemistry
Affiliation: GITAM UNIVERSITY, VISAKHAPATNAM, India

DR. MD. MUSTAFIZUR RAHMAN

Qualification: Phd Mechanical and Materials Engineering
Affiliation: University Kebangsaan Malaysia (UKM)

Dr. S. Morteza Bayareh

Qualificatio: Phd Mechanical Engineering, IUT
Affiliation: Islamic Azad University, Lamerd Branch
Daneshjoo Square, Lamerd, Fars, Iran

Dr. Zahéra Mekkioui

Qualification: Phd Electronics
Affiliation: University of Tlemcen, Algeria

Dr. Yilun Shang

Qualification: Postdoctoral Fellow Computer Science
Affiliation: University of Texas at San Antonio, TX 78249

Lugen M.Zake Sheet

Qualification: Phd, Department of Mathematics
Affiliation: University of Mosul, Iraq

Mohamed Abdellatif

Qualification: PhD Intelligence Technology
Affiliation: Graduate School of Natural Science and Technology

Meisam Mahdavi

Qualification: Phd Electrical and Computer Engineering

Affiliation: University of Tehran, North Kargar st. (across the ninth lane), Tehran, Iran

Dr. Ahmed Nabih Zaki Rashed

Qualification: Ph. D Electronic Engineering

Affiliation: Menoufia University, Egypt

Dr. José M. Merigó Lindahl

Qualification: Phd Business Administration

Affiliation: Department of Business Administration, University of Barcelona, Spain

Dr. Mohamed Shokry Nayle

Qualification: Phd, Engineering

Affiliation: faculty of engineering Tanta University Egypt

CONTENTS :

S.No.	Title Name	Page No.
1.	Optimized Color Transforms for Image Demosaicing Evgeny Gershikov	01-7
2.	A Study of H-Function Transform And Its Inversion With Properties Dr. A.K. Ronghe, Mrs. Kulwant Kaur Ahluwalia	08-11
3.	Genealogy, Occurrences, Social and Psychological Consequences Of Violence In Nigeria Dr Falana Bernard Akinlabi, Fasina Bosede Oluwayemisi	12-16
4.	Cloud Documentation and Centralized Compiler for Java & Php Namrata Raut, Darshana Parab, Shephali Sontakke, Sukanya Hanagandi	17-20
5.	Real –Time Envirnorment Monitoring System and Data Logger Using Arm Processor B.Hari Babu, Y.Varthamanan M.E	21-25
6.	An Approach for Effective Use of Pattern Discovery for Detection of Fraudulent Patterns In Railway Reservation Dataset Rasika Ingle, Manali Kshirsagar	26-29
7.	Effective Service Security Schemes In Cloud Computing K.Sravani, K.L.A.Nivedita	30-35
8.	Development of Robotic Automated Storage and Retrieval System (AS/RS) Smita U.Chakole	36-40
9.	Theoretical Investigation/Research On Binding Energy Of A Donor In A Spherical Quantum Dot At Various Locations On It S.R.Chitra	41-45
10.	Modified Conjugate Cancellation Algorithm Forofdm Systems Mohamed Tayebi , Merahi Bouziani	46-48
11.	Estimation of the Population Total of Nigeria Using One Unit per Stratum (Based On 2006 Census Result) T.J. Akingbade , O.S. Balogun	49-53
12.	Evaluation Of Logistics Regression In Classification Of Drug Data In Kwara State O.S. Balogun, t.J. Akingbade , A.A Akinrefon	54-58
13.	A Study on Visualizing Semantically Similar Frequent Patterns in Dynamic Datasets Y.N.Jyothsna Mallampalli, S.Jayaprada, Dr S.Vasavi	59-64
14.	CFD Simulation in Township Planning – A Case Study Nilesh S. Varkute, R.S. Maurya	65-72
15.	Adhesive Wear Theory of Micromechanical Surface Contact Biswajit Bera	73-78
16.	Birads Score For Mammographic Images Parveen Jaseela Regina .O. M	79-86

17.	Concept Drawing For Oil Draining Machine For Vtu With Numerical Analysis Prajwal Shantalwar, Smitesh Bobde, Bhojraj Kale, Vivek Patil	87-91
18	Newly Developed Automatic Lay-Up Process for Manufacturing of FRP Sheets Prof. A. R. Chaple, Prof. S.S. Khedakar, Prof. S.R. Dharmadhikari, Mr. N.R. Chaple	92-97
19.	Methodology of Special Purpose Spot Facing Machine Prof. Hansini S. Rahate, Prof. R. B. Chadge, Prof. P. H. Dahake, Prof. S. Rewatkar	98-102
20.	Application of Image Processing For Development of Automated Inspection System Ms. Shubhada.K. Nagrale, Mr. S.T.Bagde	103-107
21.	Invention of The Plane Geometrical Formulae - Part I Mr. Satish M. Kaple	108-122
22.	Underground Water Prospecting In Rural Settings E. C. Mabunda, Beng, Msc	123-132
23.	Biosensors Based on Nano-Particles Sidharth Singh Sisodia, Shalinee Dumoliya, Deepak Koli	133-140
24.	Comparative Study of Transcritical CO ₂ Cycle with and Without Suction Line Heat Exchanger at High Ambienttemperature A..D. Kadam, A.S. Padalkar, V.U.Walekar	141-145
25.	Novel Encoding and Decoding Algorithm for Block Turbo Codes over Rayleigh Fading Channel M.Christhu Raju, Dr. Ch. D.V. Paradesi Rao	146-154
26.	Secured Reversible Data Transmission by Using Gzip Deflector Algorithm for Encoded AVC Video Gokiladeepa.G, Gayathri.S,Heeba.S.D, Pavithra.R	155-160
27.	“Isolation of Microorganism from Dairy Effluent for Activated Sludge Treatment” Vishakha S. Shivsharan , Minal P. Wani , Suhas W. Kulkarani	161-167
28.	Determining Pinpoint of Mobile Location in Global System for Mobile Communication Network (Gsm) Adnan Affandi, Mubashshir Husain	168-176
29.	Fabrication And Implementation Of Turbo Charger In Two-Wheeler Amalorpava Dass. J, Mr.Sankarlal.P	177-180
30.	Mining Association Rules From Time Series Data Using Hybrid Approaches Hima Suresh, Dr. Kumudha Raimond	181-188
31.	A Study of Influence of Electrochemical Process Parameters on the Material Removal Rate and Surface Roughness of SS AISI 304 S. S. Uttarwar, Dr. I. K. Chopde	189-197

32.	Implementation of Data Mining Techniques for Weather Report Guidance for Ships Using Global Positioning System P.Hemalatha	198-202
33.	Equalization of Doppler Effect Using Constellation Diagram of 8-PSK Modulation Vinay Negi, Sanjeev Kumar Shah, Sandeep Singh, Arun Shekhar, Tanuja Sundriyal	203-208
34.	Spectroscopic Constants & Potential Energy Function for Diatomic Molecules Ratikant Thakur ,Jagdhhar Mandal	209-215
35.	Lockme – Android Security Application Sumaiya Patel, Darshana Thakur ,Sujit Sherkar, Priyanka Dhamane	216-218
36.	Computer Aided Engineering (CAE) Techniques Applied To Hip Implant M. S. Abo_ Elkhair, M. E. Abo-Elnor, A. E. Radi	219-225
37.	New Methods for Horizon Line Detection in Infrared and Visible Sea Images Ilan Lifshitz , Evgeny Gershikov, Benjamin Milgrom	226-233
38.	A Study on Customer Preference of LG Lap-Top Dr. Srinivasa Rao Kasisomayajula	234-237
39.	Flowshop Scheduling Using Multiagents with Adaptive Auction Amar Jukuntla , Dr. E. Grace Mary Kanaga	238-242
40.	Five Dimensional String Cosmological Model In General Relativity Kalpana Pawar (Mody), Vidhya Chauhan , G. D. Rathod	243-245
41.	Role of Software Agents in E-Commerce Ramya S. Gowda	246-251
42.	Water Audit- A Tool for Assessment Of Water Losses R.A.Ganorkar, P.I.Rode, S.A Deshmukh, Dr.R.M.Dhoble	252-256
43.	An Efficient Semantic Web Through Semantic Mapping Jenice Aroma R, Mathew Kurian	257-261
44.	Lightweight Decentralized Algorithm for Localizing Reactive Jam-ers in Wireless Sensor Network Vinothkumar.G, Ramya.G, Rengarajan.A	262-266
45.	Secure Data Forwarding In Distributed Environment Using Cloud Storage System S.Amritha , S.Saravana Kumar	267-271
46.	Seismic Analysis of High-Rise Building by Response Spectrum Method Prof. S.S. Patil , Miss. S.A. Ghadge , Prof. C.G. Konapure, Prof. Mrs. C.A. Ghadge	272-279
47.	Sensing of Faults and Condition Monitoring in Gearbox of the Wind Turbine Mr.B.Babu , Mr.R.Vinod Kumar Reddy , Mr. R.Devananda Reddy	280-295

48.	Estimation of Wind Power Generation Based On Performance Curves Mr.B.Babu , Mr.J.Vikram Kumar Reddy, A.Keerthi	296-308
49.	Automatic Cash Deposite Machine With Currency Detection Using Fluorescent And UV Light Dhiraj Vasant Kapare , Sadashiv Lokhande , Sayaji Kale	309-311
50.	Simulink Design Of Pipelined CORDIC For Generation of Sine and Cosine Values Richa Upadhyay , Dr. Nisha Sarwade , Shrugal Varde	312-316
51.	Discrimination of Fault from Non-Fault Event in Transformer Using Concept of Symmetrical Component Mr. R.V.KATRE , Prof. Mr. D. S. Chavan, Prof.S.S.Sardey	317-322
52.	Image Segmentation and Classification of Mri Brain Tumors Based On Cellular Automata and Neural Network R.Fany Jesintha Darathi , K.S.Archana	323-327
53.	The Industrial Maintenance Management and Implementing Maintenance Policies for Improvement in Productivity Ajay S. Bonde, Ashwadeep C. Fulzele	328-331
54.	Azotobacter Chroococcum Mass Culture for Production of Bio-Fertilizer, Its Sustained Efficacy on Nitrogen Fixation and Crop Productivity in Mulberry Garden S.Rajaram , Klisdamon Nongrang , S.K.Mandal, M.K.Ghosh , B.B.Bindroo.	332-340
55.	Realization Of Gateway Relocation Using AC And LB Algorithms In Mobile Wimax Networks K.Sujatha , C.Nandagopal	341-346
56.	Convective Heat Transfer in Maxwell-Cattaneo Dielectric Fluids S. Maruthamanikandan , Smita S. Nagouda	347-355
57.	Enhancing Degraded Color Images Using Fuzzy Logic and Artificial Bee Colony Adlin Sharo T, Dr. Kumudha Raimond	356-361

Optimized Color Transforms for Image Demosaicing

Evgeny Gershikov

Department of Electrical Engineering, Ort Braude Academic College of Engineering,
Karmiel 21982, Israel
and Department of Electrical Engineering, Technion - IIT, Haifa 32000, Israel

Abstract:

Most demosaicing algorithms today are based on first reconstructing the green (G) color component followed by the reconstruction of the red (R) and the blue (B) components based on the green. This approach and the associated methods of using the differences $R-G$ and $B-G$ are arbitrary and in most cases not optimal. Instead, we propose optimal color transforms for demosaicing. This optimization is based on energy compactness and smoothness of the color components. We compare the performance of the proposed algorithms to presently available demosaicing methods and show that the new optimized approaches are superior both visually and quantitatively. Our conclusion is that the proposed color transforms improve the performance of demosaicing algorithms.

Keywords: Bayer pattern, Color transform, Demosaicing, Energy compactness, Image interpolation, Optimization, Smoothness

1. Introduction

Since many acquisition devices are based on a single sensor using a color filter array (CFA), only partially sampled versions of the primary colors R, G, B are recorded. This is done in most cases according to the Bayer pattern [1], as shown in Fig. 1. In this case, the green has twice as much samples as the red and the blue, making the green interpolation easier to accomplish due to reduced potential of aliasing [2,3]. Then the red and the blue components can be reconstructed based on inter-color correlations, which are usually high in natural images [4-8]. Straightforward algorithms for demosaicing, such as bilinear or bicubic interpolation methods, however, do not use these inter-color correlations and operate on each color component independently. Better performance is achieved by algorithms that are based on the above sequential scenario of reconstructing G first, followed by the reconstruction of R and B, e.g., [9-14]. In such algorithms the inter-color correlations are usually exploited by interpolating the differences $R-G$ and $B-G$. However, since no optimization is performed, it can be shown that using these differences is not the best method to perform the task efficiently. For the sake of completeness, we should add that non-sequential demosaicing methods have also been proposed, e.g. the iterative techniques of [15] or [16] as well as vector CFA demosaicing [17]. In this work we propose methods of choosing other color transforms for the interpolation of the red and the blue according to different optimization criteria.

We consider the following demosaicing algorithm.

1.1 The basic demosaicing algorithm

The stages of the algorithm are:

1. The green color component is interpolated using the method in [9]. It consists of filtering the CFA pattern horizontally and vertically, then choosing the direction of interpolation corresponding to the smaller estimated gradient (to avoid interpolation across edges): horizontal or vertical. In case of equal gradients the average of the horizontal and vertical interpolators is taken. This technique of interpolation was chosen because it provides good performance at low complexity.
2. The interpolated green component \hat{G} is used in the reconstruction of the red and the blue colors. The color differences $\Delta^{RG} \square R - \hat{G}$, $\Delta^{BG} \square B - \hat{G}$ are calculated at the known pixels of the red and the blue colors, respectively. Then the red-green difference is interpolated at the locations of the known blue samples and the blue-green difference at the locations of the red samples using the local polynomial approximation (LPA) filter [13]. Better performance can be achieved by this filter compared to simple bilinear interpolation.

- The missing pixels in the red and blue - those at the locations of the known green pixels are interpolated using simple averaging of their two vertical and two horizontal pixels (bilinear interpolation). The interpolation is performed once again on the Δ^{RG} and Δ^{BG} differences resulting in full images $\hat{\Delta}^{RG}$ and $\hat{\Delta}^{BG}$.

The final red and blue components are calculated according to $\hat{R} = \hat{G} + \hat{\Delta}^{RG}$ and

$$\hat{B} = \hat{G} + \hat{\Delta}^{BG}.$$

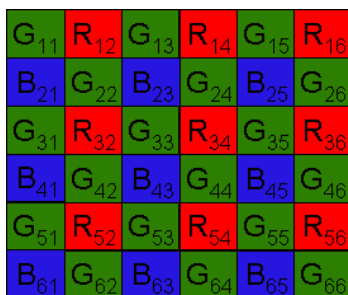


Figure 1. The Bayer CFA pattern.

The structure of this work is as follows. Color transforms for demosaicing based on optimization of different properties of the image are presented in Section 2. Demosaicing results for the proposed method and comparison to other available techniques are given in Section 3. Section 4 provides summary and conclusions.

2. Optimal Color Transforms

All printed material, including text, illustrations, and charts, must be kept within a print area of 6-1/2 inches (16.51 cm) wide by 8-7/8 inches (22.51 cm) high. Do not write or print anything outside the print area. All *text* must be in a single-column format. Columns are to be 3-1/16 inches (7.85 cm) wide, with The basic algorithm performs its interpolation in the $G, R - G, B - G$ color space. This choice is not necessarily optimal and thus other color transforms can be considered following an optimization process [18]. The change of the color space is not possible prior to the reconstruction of the green since at each pixel of the image only one of the primary colors is available. However, it becomes possible after the reconstruction of G in Subsection 1.1, Step 1. We thus propose a new general color space:

$$(1) C_1 = G, \quad C_2 = a_1R + a_2G, \quad C_3 = d_1B + d_2G$$

for some constants a_1, a_2, d_1, d_2 instead of the regular choice. To avoid the solution of $a_1 = a_2 = 0$ in the optimization problems presented below, a constraint has to be added forcing the L1 norm, for example, of the a coefficients to be 1 (similarly for the d coefficients). Thus

$$(2) |a_1| + |a_2| = 1 \quad \text{and} \quad |d_1| + |d_2| = 1.$$

2.1 Energy compactness and non-singularity

A Rate-Distortion model for color image coders was developed and optimized in [19]. As a result the optimal Color Transform (CT) was derived. Denoting the CT matrix by \mathbf{M} , the target function to be minimized for the optimal CT was found to be $\prod_{k=1}^3 \left((\mathbf{M}\mathbf{M}^T)^{-1} \right)_{kk} GM_k$, where GM_k is the geometric mean of the subband variances. Based on this result, the following target function can be proposed for our demosaicing algorithm:

$$(3) \prod_{k=2}^3 \left((\mathbf{M}\mathbf{M}^T)^{-1} \right)_{kk} var(C_k),$$

where C_k and the RGB components are connected by

$$(4) \quad \begin{bmatrix} C_1 \\ C_2 \\ C_3 \end{bmatrix} = \mathbf{M} \begin{bmatrix} R \\ G \\ B \end{bmatrix}, \quad \mathbf{M} = \begin{pmatrix} 0 & 1 & 0 \\ a_1 & a_2 & 0 \\ 0 & d_2 & d_1 \end{pmatrix}.$$

The expression in (3) is made of two terms: $\prod_{k=2}^3 \text{var}(C_k)$, which is a measure of the energy compactness in the new color space and $\prod_{k=2}^3 \left((\mathbf{M}\mathbf{M}^T)^{-1} \right)_{kk}$, which is a measure of the non-singularity of M. The optimal coefficients minimizing (3) under the norm constraint of (2) are

$$(5) \quad a_1 = \frac{\text{var}(G)}{\text{var}(G) + \text{cov}(R, G)}, \quad a_2 = -\frac{\text{cov}(R, G)}{\text{var}(G) + \text{cov}(R, G)}, \quad d_1 = \frac{\text{var}(G)}{\text{var}(G) + \text{cov}(B, G)}, \quad d_2 = -\frac{\text{cov}(B, G)}{\text{var}(G) + \text{cov}(B, G)}.$$

Since the target function of (3) combines the properties of energy compactness and non-singularity of the color transform, we refer to this algorithm as ECNS, which is the acronym of Energy Compactness and Non-Singularity.

2.2 Smoothness of the C2 and C3 components

The energy of the difference signals $\Delta^{RG} = R - G$ and $\Delta^{BG} = B - G$ is mostly concentrated in the low frequencies [11]. This is the reason for the good performance achieved by interpolating these differences using averaging [11-13]. This also means that Δ^{RG} and Δ^{BG} are smooth. To further impose this smoothness on C_2 and C_3 , the following methods are proposed.

2.2.1 Minimal high pass energy

The idea here is to minimize the energy of C_2 and C_3 , filtered by a two dimensional High Pass (HP) filter. We denote the filtered color components at pixel (i, j) by $(C_k^{HP})_{ij}$ and minimize $\sum_{i=1}^M \sum_{j=1}^N (C_k^{HP})_{ij}^2$, $k = 2, 3$ for an image of size $M \times N$. Alternatively, a pair of one dimensional HP filters HP_x and HP_y can be used to filter C_2 or C_3 horizontally and vertically, respectively. Usually, HP_y is chosen as $HP_y = HP_x^T$. Then the expression to be minimized becomes $\sum_i \sum_j (C_k^{HP_x})_{ij}^2 + \sum_i \sum_j (C_k^{HP_y})_{ij}^2$, $k = 2, 3$, where $C_k^{HP_x}$ is C_k filtered by HP_x and similarly for $C_k^{HP_y}$. The optimal a_1, a_2 coefficients for this problem are

$$(6) \quad a_1 = \frac{\alpha_{12} + \alpha_{22}}{\alpha_{11} + 2\alpha_{12} + \alpha_{22}}, \quad a_2 = -\frac{\alpha_{12} + \alpha_{11}}{\alpha_{11} + 2\alpha_{12} + \alpha_{22}},$$

where

$$(7) \quad \alpha_{11} \square \sum_i \sum_j \left[(R^{HP_x})_{ij}^2 + (R^{HP_y})_{ij}^2 \right], \quad \alpha_{22} \square \sum_i \sum_j \left[(G^{HP_x})_{ij}^2 + (G^{HP_y})_{ij}^2 \right], \\ \alpha_{12} \square \sum_i \sum_j \left[(R^{HP_x})_{ij} (G^{HP_x})_{ij} + (R^{HP_y})_{ij} (G^{HP_y})_{ij} \right].$$

The solution for the d_1 and d_2 coefficients is the same as the solution for a_1 and a_2 , respectively, in (6) with B replacing R everywhere in (7). For simple choices of HP_x , such as the backward/forward approximation of the horizontal derivative

($HP_x = [1 - 1]$), the calculations can be performed on the available small images obtained from the CFA (Fig. 2). Alternatively, R and B can be first reconstructed using a simple technique, such as bilinear filtering of the $R - G$ and $B - G$ differences, and then used for the estimation of the derivatives. In this work we use the Sobel

gradient operator given by $HP_x = \begin{pmatrix} 1 & 0 & -1 \\ 2 & 0 & -2 \\ 1 & 0 & -1 \end{pmatrix}$.

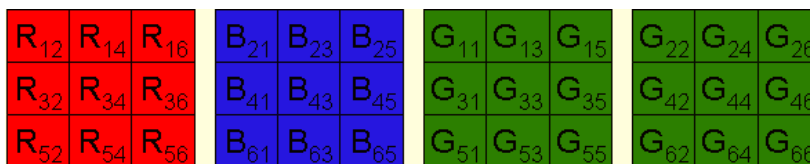


Figure 2. The Bayer pattern components: RR, BB, GR and GB (from left to right).

2.2.2 Minimal energy in the wavelet domain

Another approach is to consider the energy of the C_2 and C_3 color components in the high frequencies and to search for the coefficients a_k and d_k ($k = 2, 3$) that minimize this energy. One possible formulation for this problem is to minimize $\sum_{f \in \{LH, HL, HH\}} \sum_m \sum_n W_f^{C_k}(m, n)^2$, $k = 2, 3$, where $W_f^{C_k}(m, n)$ is the one level Discrete Wavelet Transform (DWT) of C_k at position (m, n) in subband f , which is one of the high frequency subbands (LH, HL or HH) above. The solution for this problem is as in (6), but now

$$(8) \quad \alpha_{11} \square \sum_{f \in \{LH, HL, HH\}} \sum_m \sum_n W_f^R(m, n)^2, \quad \alpha_{22} \square \sum_{f \in \{LH, HL, HH\}} \sum_m \sum_n W_f^G(m, n)^2, \\ \alpha_{12} \square \sum_{f \in \{LH, HL, HH\}} \sum_m \sum_n W_f^R(m, n)W_f^G(m, n).$$

The solution for d_1 and d_2 is similar.

2.2.3 Minimal relative energy in the Fourier domain

The energy in the high frequencies can be expressed in the frequency domain of the Discrete Fourier Transform (DFT) as well. In this case taking the relative energy of C_2 or C_3 provides better results. Therefore, we seek to minimize (for an image of size $M \times N$ assuming M and N are multiples of 4)

$$(9) \quad E \square \frac{\sum_{m=M/4}^{M/2-1} \sum_{n=N/4}^{N/2-1} |DFT^{C_k}(m, n)|^2}{\sum_{m=0}^{M/2-1} \sum_{n=0}^{N/2-1} |DFT^{C_k}(m, n)|^2}, \quad k = 2, 3.$$

$DFT^{C_k}(m, n)$ here denotes the DFT coefficient of C_k at position (m, n) in the frequency domain. The solution of this problem requires solving third order polynomial equations resulting in long expressions for the a and d coefficients. For simplicity we do not provide them here.

3. Demosaicing Results

The basic algorithm (Section 1.1) was implemented with and without the optimization techniques of Section 2. We also added the refinement method [20] as post-processing. This method provides further utilization of the inter-color and intra-color correlations and works well with our algorithms. The set of images given in Fig. 3 was used in our simulations, i.e., for each one the Bayer pattern was built, interpolated by the different algorithms and compared to the original image. The distortion measure used was the S-CIELAB metric [21]. The comparison of the proposed algorithms is given on the left side of Table 1. We can see that all the proposed algorithms achieve better results than the basic algorithm and the bilinear interpolation. The best performance with respect to the S-CIELAB metric is achieved by the minimal high pass energy (Min HP)

algorithm (Section 2.2.1). This shows the importance of the smoothness of the C_2 or C_3 color components for our interpolation process. The second best algorithm is ECNS, which means energy compactness and non-singularity of the color transform are important for demosaicing as well as image coding [18]. It is of interest to compare the proposed methods to other available algorithms. We have chosen some of the available state of the art techniques: Alternating Projections (AP [10]), Directional Linear Minimum Mean Square Error (DLMMSE [11]), Variance of Color Differences (VCD [12]), Local Polynomial Approximation (LPA [13]) and Successive Approximation (SAP [16]). The results for these algorithms can be seen on the right side of Table 1. From the table we can see that the Min HP algorithm is superior to the

other methods, while the performance of ECNS is similar to that of the VCD method that provides the best results among the algorithms chosen for comparison. Visual results for the new methods as well as existing algorithms for part of Image 8 are given in Fig. 4. As can be seen, the proposed methods provide better results than the other algorithms (including VCD that provides the most competitive performance). The values of the a and d coefficients for these algorithms are given in Table 2. Note that even if the values are close to $a_1 = -a_2 = 0.5$ and $d_1 = -d_2 = 0.5$, which would result in taking the common $R-G$ and $B-G$ differences (after scaling), the new methods outperform the basic algorithm.

4. Summary And Conclusions

An optimization approach to demosaicing has been introduced. Instead of using the common choice of the $R-G$ and $B-G$ differences for the reconstruction process, better performance can be achieved by choosing an optimized color space according to the desired properties of the image. Such properties can be energy compactness as in the ECNS algorithm or smoothness as in the Min HP algorithm. A basic demosaicing algorithm has been optimized to achieve these properties and compared to other available demosaicing methods. Our results show that the proposed optimization method significantly improves the interpolation performance and that the best performance is achieved by minimizing the high pass energy in the new color space. The second best is the algorithm that combines energy compactness and non-singularity of the color transform, providing better results also in the case of color image coding [18]. Our conclusion is that the proposed optimization approach is useful for demosaicing of color images.

Table 1. S-CIELAB results for the algorithms (from left to right): minimal High Pass energy, ECNS, minimal DWT energy, minimal relative DFT energy, the basic algorithm, bi-linear interpolation, AP, SAP, DLMMSE, LPA and VCD.

Image	Proposed Algorithms				Other Algorithms						
	Min HP	ECNS	Min DWT	Min Rel DFT	Basic	BL	AP	SAP	DL MMSE	LPA	VCD
1	0.733	0.729	0.752	0.730	0.769	1.505	0.851	0.897	0.723	0.758	0.850
2	0.779	0.786	0.794	0.830	0.796	1.201	1.032	1.215	0.749	0.766	0.778
3	0.747	0.732	0.791	0.812	0.808	1.501	1.165	1.177	0.832	0.832	0.795
4	0.645	0.654	0.650	0.659	0.656	0.833	0.787	0.877	0.644	0.611	0.687
5	0.579	0.595	0.571	0.593	0.578	0.928	0.838	0.828	0.561	0.530	0.593
6	0.576	0.611	0.594	0.577	0.606	1.149	0.654	0.760	0.524	0.581	0.526
7	1.408	1.475	1.456	1.467	1.488	3.272	1.862	1.810	1.431	1.321	1.312
8	1.490	1.508	1.569	1.569	1.608	2.742	1.867	2.168	1.689	2.154	1.563
Mean	0.870	0.886	0.897	0.905	0.914	1.641	1.132	1.216	0.894	0.944	0.888

Table 2. a and d coefficients for Image 8 for the proposed algorithms (same order of columns as in Table 1). Even if the values are close to $a_1 = -a_2 = 0.5$ and $d_1 = -d_2 = 0.5$ as in the basic method, the new methods outperform the basic algorithm.

	Min HP	ECNS	Min DWT	Min Rel DFT
a_1	0.539	0.578	0.506	0.460
a_2	-0.461	-0.422	-0.494	-0.540
d_1	0.551	0.597	0.509	0.559
d_2	-0.449	-0.403	-0.491	-0.441



Figure 3. The demosaicing test images.

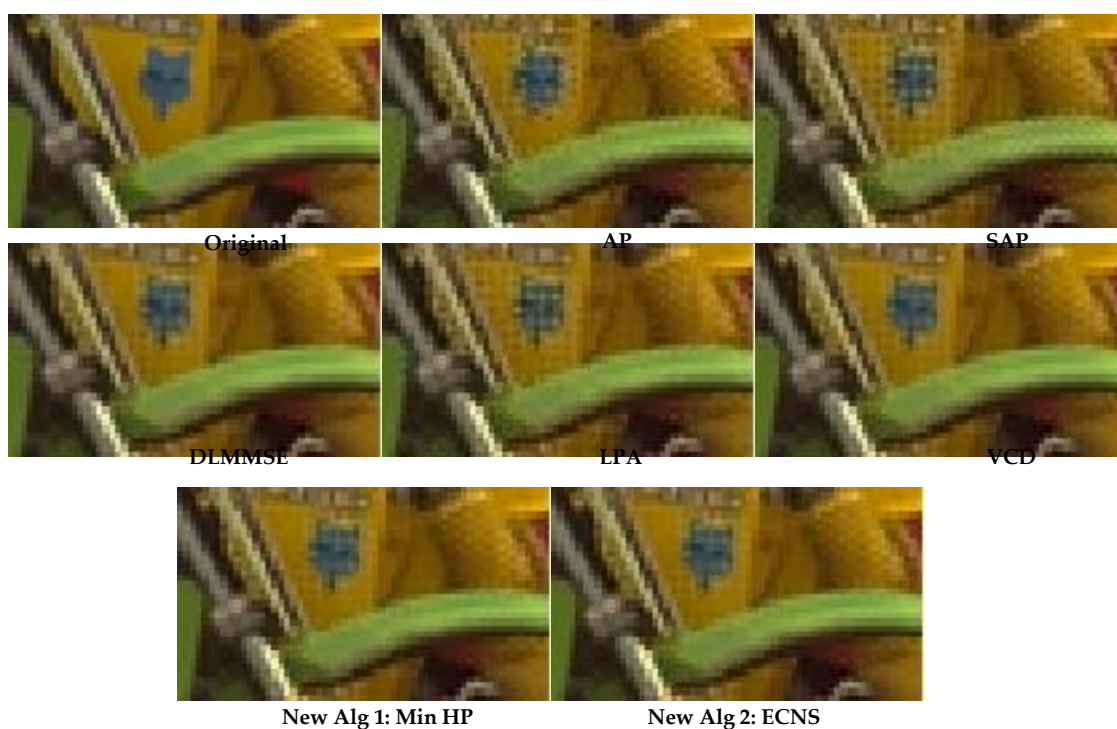




Figure 4. Demosaicing results for the different algorithms for part of Image 8. New Alg. 1-4 are the new algorithms.

References

- [1] B. E. Bayer. Color imaging array. U.S. Patent 3971065, July 1976.
- [2] B. Gunturk, X. Li and L. Zhang. Image demosaicing: A systematic survey. In Proc. of SPIE, 68221J-68221J-15, 2008.
- [3] H. Kirshner and M. Porat. On the Approximation of L2 Inner Products from Sampled Data. IEEE Trans. on Signal Processing 55:2136-2144, 2007.
- [4] H. Kotera and K. Kanamori. A Novel Coding Algorithm for Representing Full Color Images by a Single Color Image. J. Imaging Technology 16:142-152, Aug. 1990.
- [5] J. O. Limb and C.B. Rubinstein. Statistical Dependence Between Components of A Differentially Quantized Color Signal. IEEE Trans. on Communications 20:890-899, Oct. 1971.
- [6] H. Yamaguchi. Efficient Encoding of Colored Pictures in R, G, B Components. IEEE Trans. on Communications 32:1201-1209, Nov. 1984.
- [7] Y. Roterman and M. Porat. Color image coding using regional correlation of primary colors. Image and Vision Computing 25:637-651, 2007.
- [8] E. Gershikov and M. Porat. Optimal color image compression using localized color component transforms. In Proc. EUSIPCO 2008, Lausanne, Switzerland, Aug. 2008.
- [9] J. F. Hamilton and J. E. Adams. Adaptive Color Plane Interpolation in Single Sensor Color Electronic Camera. U.S. Patent 5629734, 1997.
- [10] B. K. Gunturk, Y. Altunbasak, and R. M. Mersereau. Color plane interpolation using alternating projections. IEEE Trans. Image Processing 11:997-1013, 2002.
- [11] L. Zhang and X. Wu. Color demosaicking via directional linear minimum mean square-error estimation. IEEE Trans. on Image Processing 14:2167-2178, 2005.
- [12] K.-H. Chung and Y.-H. Chan. Color demosaicing using variance of color differences. IEEE Trans. on Image Processing 15:2944-2955, 2006.
- [13] D. Paliy, V. Katkovnik, R. Bilcu, S. Alenius, and K. Egiazarian. Spatially adaptive color filter array interpolation for noiseless and noisy data. Int. Journal of Imag. Sys. and Technology 17:105-122, 2007.
- [14] R. Sher and M. Porat. CCD Image Demosaicing using Localized Correlations. In Proc. of EUSIPCO, Poznan, Poland, Sept. 2007.
- [15] R. Kimmel. Demosaicing: Image reconstruction from color ccd samples. IEEE Trans. on Image Processing 8:1221-1228, 1999.
- [16] X. Li. Demosaicing by successive approximation. IEEE Trans. Image Processing 14:370-379.
- [17] M. R. Gupta and T. Chen. Vector color filter array demosaicing. In Proc. of SPIE, Sensors and Camera Systems for Scientific, Industrial, and Digital Photography Applications II 4306:374-382, 2001.
- [18] E. Gershikov and M. Porat. A rate-distortion approach to optimal color image compression. In Proc. EUSIPCO, Florence, Italy, Sept. 2006.
- [19] E. Gershikov and M. Porat. On color transforms and bit allocation for optimal subband image compression. Signal Processing: Image Communication 22:1-18, 2007.
- [20] L. Chang and Y. P. Tam. Effective use of spatial and spectral correlations for color filter array demosaicing. IEEE Trans. Consumer Electronics, 50:355-365, Feb 2004.
- [21] X. Zhang and B. A. Wandell. A spatial extension of CIELAB for digital color image reproduction. SID Journal 5:61-63, 1997.

“A Study of \tilde{H} – Function Transform And Its Inversion With Properties”

¹Dr. A.K. Ronghe, ² Mrs. Kulwant Kaur Ahluwalia

¹,(S.S.L. Jain, P.G. College, Vidisha, MP (India) Pin-464001)

²,(Mata Gujri Mahila Mahavidyalaya, Jabalpur, MP (India) Pin-482002)

Abstract: In this research paper we have defined \tilde{H} – function transform and developed its inversion formula, and it is further detected that particular cases of \tilde{H} – function transform comes out as Fox’s H-function transform defined by Gupta and Mittal [6.7], G-function transform defined by Bhise [1] and other etc.

1. Introduction And Preliminaries:

The Mellin transform of the \tilde{H} – function is defined as follows:

$$\int_0^1 x^{\xi-1} H_{p,q}^{m,n} \left[ax \left| \begin{matrix} (a_j, A_j; \alpha_j)_{1,n} \\ (b_j, B_j)_{1,m} \end{matrix} \right. , (a_j, A_j)_{n+1,p} \right] dx \cdot d\xi = a^{-\xi} \theta(-\xi) \quad [1.1]$$

Where,

$$\theta(-\xi) = \frac{\prod_{j=1}^m \Gamma(b_j + B_j \xi) \prod_{j=1}^n \{\Gamma(1 - a_j - A_j \xi)\}^{\alpha_j}}{\prod_{j=m+1}^q \{\Gamma(1 - b_j - B_j \xi)\}^{\beta_j} \prod_{j=n+1}^p \Gamma(a_j + A_j \xi)} \quad [1.2]$$

$$\text{Provided } \min_{1 \leq j \leq m} \left[\text{Re} \left(\frac{b_j}{\beta_j} \right) \right] < \text{Re}(\xi) < \left\{ \min_{1 \leq j \leq n} \left[\text{Re} \left(\frac{1 - a_j}{a_j} \right) \right] \right\} \quad [1.3]$$

And other convergence conditions will be those of the \tilde{H} – function associated in the definition of \tilde{H} – function, see [(3), (8), (9)] etc. Integral involving product of Hyper geometric function and \tilde{H} – function given as follows,

$$\int_0^{\infty} x^{-\alpha} (x-1)^{\beta-1} {}_2F_1 \left[\begin{matrix} \gamma + \beta + \alpha, \lambda + \beta - \alpha \\ \beta \end{matrix} ; (1-x) \right] \times \tilde{H}_{p,q}^{m,n} \left[(ax) \left| \begin{matrix} (a_j, A_j; \alpha_j)_{1,n} \\ (b_j, B_j)_{1,m} \end{matrix} \right. , (a_j, A_j)_{n+1,p} \right] dx = \Gamma(\beta) \tilde{H}_{p+3,q+3}^{m+1,n+2} \left[a \left| \begin{matrix} (\alpha - \beta; 1, 1), (\gamma + \beta + \lambda - \alpha; 1, 1) \\ (\alpha - \beta; 1), (b_j, \beta_j)_{1,m} \end{matrix} \right. , (b_j, B_j, \beta_j)_{m+1,q} \right] \left. \begin{matrix} (a_j, A_j; \alpha_j)_{1,n} \\ (\gamma, 1, 1), (\lambda, 1, 1) \end{matrix} \right. , (a_j, A_j)_{n+1,p} , (\alpha, 1) \right] \quad [1.4]$$

and other convergence conditions stated in definition of \tilde{H} – function, see [(8) and (9)].

Proof: To establish (1.4), we first express \tilde{H} and ${}_2F_1$, occurring in the left hand side of (1.4) in term of Mellin Barnes contour integral with the help of definition of \tilde{H} – function, given by Inayat Hussain [8] and [9], series form of ${}_2F_1$ and using the property of Gamma-function, we arrive at the R.H.S. of (1.4) after a little simplification.

2. The \tilde{H} – Function Transform:

An integral transform of function $f(x)$ whose kernel is \tilde{H} – function defined by Inayat Hussain is called \tilde{H} – function transform, which is defined as follows:

$$\phi(\xi) = \int_0^{\infty} (\xi x)^{\rho} \tilde{H}_{p,q}^{m,n} \left[(\xi x) \left| \begin{matrix} (a_j, A_j; \alpha_j)_{1,n}, (a_j, A_j)_{n+1,p} \\ (b_j, B_j)_{1,m}, (b_j, B_j, \beta_j)_{m+1,q} \end{matrix} \right. \right] \times f(x) dx,$$

Provided $\text{Re}(\xi) > 0, \text{Re}(\rho + 1) > 0$,

We may represent \tilde{H} – function transform as follows:

$$\bar{f}(x) \text{ or } \{ \bar{f}(x); \xi \}$$

3. Special Cases:

(i) If $\rho = 0, \alpha_j = \beta_j = 1$, in (2.1) we get Fox's H-function transform defined by Gupta and Mittal (6) in 1970 is as follows:

$$\phi(\xi) = \int_0^{\infty} H_{p,q}^{m,n} \left[(\xi x) \left| \begin{matrix} (a_j, \alpha_j)_{1,p} \\ (b_j, \beta_j)_{1,q} \end{matrix} \right. \right] f(x) dx$$

(ii) If $\rho = 0, \alpha_j = \beta_j = 1, a_j = c_j + d_j, b_j = d_j, m = m + 1, n = 0, p = m, q = m + 1$ in (2.1) we get G-function transform defined by Bhise [1] in 1959 as follows:

$$\phi(\xi) = \int_0^{\infty} G_{m,m+1}^{m+1,0} \left[(\xi x) \left| \begin{matrix} (c_j + d_j)_{1,m} \\ (d_j)_{1,m}, 1 \end{matrix} \right. \right]$$

Note: A number of other transform involving various special functions which are the special cases of \tilde{H} – function given by Saxena [11] can also be obtained from \tilde{H} – function transform, but we do not record them here, due to lack of space for that see [10].

4. Inversion formula for \tilde{H} – function transform: Multiplying on both sides of equation (2.1) by ξ^{-k} and integrating with respect to “ ξ ” between the limits $[0, \infty]$, we have,

$$\int_0^{\infty} \xi^{-k} \phi(\xi) d\xi = \int_0^{\infty} \xi^{-k} \left\{ \int_0^{\infty} (\xi x)^{\rho} \times \tilde{H}_{p,q}^{m,n} \left[(\xi x) \left| \begin{matrix} (a_j, A_j; \alpha_j)_{1,n}, (a_j, A_j)_{n+1,p} \\ (b_j, B_j)_{1,m}, (b_j, B_j, \beta_j)_{m+1,q} \end{matrix} \right. \right] f(x) dx \right\} d\xi,$$

Now changing the order of integration and using the definition of Mellin transform of H-function given in (1.1) we get,

$$\int_0^{\infty} \xi^{-k} \phi(\xi) d\xi = \int_0^{\infty} \theta[(k - 1 - \rho)] x^{k-1} f(x) dx,$$

Where,

$$\theta[(k - 1 - \rho)] = \frac{\prod_{j=1}^m \Gamma(b_j + \beta_j (1 - k + \rho)) \prod_{j=1}^n \Gamma(1 - a_j + \alpha_j (1 - k + \rho))^{\alpha_j}}{\prod_{j=m+1}^q \left\{ \Gamma(1 - b_j - \beta_j (1 - k + \rho)) \right\}^{\beta_j} \prod_{j=n+1}^p \Gamma(a_j + \alpha_j (1 - k + \rho))}$$

$$\text{Let } \int_0^{\infty} \xi^{-k} \phi(\xi) d\xi = F(x),$$

$$\text{Then, } F(x) = \int_0^{\infty} \theta[(k - 1 - \rho)] x^{k-1} f(x) dx,$$

OR

$$\int_0^\infty x^{k-1} f(x) dx = \frac{F(x)}{\theta[k-1-\rho]}, \quad [4.6]$$

Now using the definition of inverse Mellin transform we get,

$$\frac{f(x-0) + f(x+0)}{2} = \frac{1}{2\pi\omega} \int_{c-i\infty}^{c+i\infty} \frac{x^{-k} F(x)}{\theta[(k-1-\rho)]} dx \quad [4.7]$$

Where, $F(x)$ is given by (4.5) and $\theta[(k-1-\rho)]$ is given by (4.2).

Provided $\min_{1 \leq j \leq m} [\rho + \operatorname{Re}(\frac{b_j}{\beta_j})] < (1-c) \left\{ \min_{1 \leq j \leq m} [\rho + \operatorname{Re}(\frac{1-a_j}{\alpha_j})] \right\}$ and other convergence conditions

are stated in the definition of \tilde{H} – function.

4. Special Cases:

(i) If $\rho = 0, \alpha_j = \beta_j = 1$ in (4.7) we get inversion formula for Fox's H-function transform, which developed by Gupta and Mittal [7] as follows:

$$\frac{f(x-0) + f(x+0)}{2} = \frac{1}{2\pi\omega} \int_{c-i\omega\theta}^{c+i\omega\theta} \frac{x^{-k} F(x)}{\theta_1[(k-1)]} dx, \quad [4.8]$$

Where,

$$\theta_1[(k-1)] = \frac{\prod_{j=1}^m \Gamma(b_j + \beta_j(1-k)) \prod_{j=1}^n \Gamma(1-a_j + \alpha_j(1-k))^1}{\prod_{j=m+1}^q \{\Gamma(1-b_j + \beta_j(1-k))\}^1 \prod_{j=n+1}^p \Gamma(a_j + \alpha_j(1-k))} \quad [4.9]$$

(ii) $\alpha_j = \beta_j = \text{unity}, a_j = c_j + d_j, b_j = d_j, m = m+1, n = 0, p = m, q = m+1$, in (4.7), we get an inversion formula for G-function transform which developed by Bhise [1] as follows:

$$\frac{f(x-0) + f(x+0)}{2} = \frac{1}{2\pi\omega} \int_{c-i\omega\theta}^{c+i\omega\theta} \frac{x^{-k} F(x)}{\theta_2[(k-1)]} dk,$$

Where,

$$\theta_2[(k-1)] = \frac{\prod_{j=1}^m \Gamma(d_j + (1-k)) \prod_{j=1}^n \Gamma(\sigma_j + (1-k))^1}{\prod_{j=1}^m \Gamma[(c_j + d_j) + (1-k)]^1}$$

5. Properties of \tilde{H} – function transform:

Ist property:

If, $\tilde{H}\{f(x) : \xi\} = \phi_1(\xi)$ and $\tilde{H}\{f_2(x) : \xi\} = \phi_2(\xi)$ then

$$\tilde{H}\{C_1 f_2(x) \pm C_2 f_2(x) : \xi\} = C_1 \phi_1(\xi) \pm C_2 \phi_2(\xi) \quad [5.1]$$

Where C_1 and C_2 are arbitrary constant.

IInd Property:

$$\text{If } \tilde{H}\{f(x) : \xi\} = \phi(\xi) \text{ and } \tilde{H}\{(\lambda x) : \xi\} = \phi_1(\xi) \text{ then } \phi_1(\xi) = \frac{1}{\lambda} \phi\left(\frac{s}{\lambda}\right) \quad [5.2]$$

6. Property:

If $\tilde{H}\{f(x) : \xi\} = \phi(\xi)$ and $\tilde{H}\{f(x^\sigma) : \xi\} = \phi_1(\xi)$, then $\phi_1(\xi) = \xi^{\sigma-1} \phi(\xi^\sigma)$, where

$$\operatorname{Re}(\sigma) > 0, \quad [5.3]$$

IVth Property:

$$\text{If } \tilde{H}\{f(x) : \xi\} = \phi(\xi) \text{ and } \tilde{H}\left\{f\left(\frac{1}{2}\right) : \xi\right\} = \phi_1(\xi) \quad [5.4]$$

Proof of all properties given in [10, P, 110]

7. Acknowledgement:

The author are thankful to prof. R.D Agrawal (SATI Vidisha) for useful discussions.

References

- [1] Bhise, V.M., (1959); Inversion Formula For Generalized Laplace, Transform, Vikram, Univ. 3, (P- 57-63)
- [2] Bhise. V.M. (1967); Certain Properties Of Meijer Laplace Transform, Comp. Math. 18, (P- 1.6). Bushman, R.G. And The H-Function Associated With A Certain Class Of
- [3] Shrivastava, H.M. (1990); Feynmann Integrals. J. Phys.; A Math, Gen (23), (P- 4707-4710).
- [4] Fox, C. (1961); The G Function And H-Function As Symmetrical Fourier Kernels, Trans. Amer. Math. Soc. 98. (P- 395-429).
- [5] Gupta, K.C. (1964); On The Inverse Meijer Transform Of G-Function. Collect Math 16. (P- 45-54).
- [6] Gupta K.C. And The H-Function Transform, J. Austral Math. Soc. Mittal P.K. (1970); 11 (P- 142-148).
- [7] Gupta K.C. And; The H-Function Transform II. J Austral. Math. Soc. Mittal P.K. (1971) 12. (P- 444-450).
- [8] Inayat Hussain A.A. (1987); New Properties Of Hypergeometric Series Derivable From Feynmann Integrals : I Transformation And Reduction Formulae J. Phys. A Math. Gen 20 (P- 4109-4117).
- [9] Inayat-Hussain A.A. (1987); New Properties Of Hypergeometric Series Derivable From Feynmann Integral II Generalization Of The \tilde{H} – Function J. Phys. A. Math. Gen (20), (P- 4119-4129). Ahluwalia K.K. (2013);
- [10] Comparative Study Of The I-Function, The \tilde{H} – Function, The Generalized Legendre's Associated Function And Their Applications, Ph.D. Thesis, Univ. Of B.U. Bhopal, India.
- [11] Saxena, R.K. J. Ram And Unified Fractional Integrals Formulae For The
- [12] And Kalla, S.L. (2002); Generalized \tilde{H} – Function Rev. Acad. Canor Cienc. 14 (P- 97-101)

Genealogy, Occurrences, Social and Psychological Consequences Of Violence In Nigeria

¹Dr Falana Bernard Akinlabi, ²Fasina Bosede Oluwayemisi (Mrs.)

¹Department Of Guidance And Counselling Faculty Of Education
Ekiti State University

²Department Of Guidance And Counselling Faculty Of Education

Abstract

The study investigated the genealogy, occurrence, social and psychological consequences of violence in Nigeria. The researcher surveyed the entire population of Nigeria while he used descriptive research design. The researcher observed that the occurrence of violence in Nigeria is genealogical and that the state of social and psychological insecurity in Nigeria corroborates the state of low or delay in all spheres of life of Nigerians. Based on the observation and revelations; There should be critical incident stress management techniques, there should be outreach to affected population in form of crises counselling, distribution of materials on stress reactions. There should be moral reawakening beyond rhetoric, responsible and responsive leadership. There should be reduction in the social-economic gap between the rich and the poor. The political situation should be reorganised, the situation should not be winner takes all. There should be provision of jobs to the youths as well as reorientation programmes, provision of adequate infrastructure, repositioning and strengthening of health sector and agencies responsible for emergencies.

Keywords:Genealogy, occurrence, violence, social consequences, psychological consequences.

1. Introduction

The United Nations (UN) Secretary General said in 2004 that violence or terrorism is any act intended to cause death or serious body harm to civilians or noncombatants with the purpose of intimidating a population or compelling a government or an international organization to do or abstain from doing any act. The purpose of violence or terrorism includes destruction, seeking provocation, economic collapse, back lash, hatred, division, elimination of tolerance and chaos. There are some insignificant traces of violence in Nigeria prior independence of 1960. The emergence of severe violence in Nigeria came into limelight during the lethal or civil war that took place in the year 1967. It was known as Nigerian-Biafra war which took place between 6th of July and 15th of January 1970. The Nigeria civil war was fought to integrate and reunify the country. The colonial masters decided to keep the non-homogenous Nigeria in order to control effectively vital resources for their economic interests. For administrative convenience the Northern and southern Nigeria were amalgamated in 1914. The only thing they've been having together was the name Nigeria. Amalgamation ought to have brought the various people together and provided a firm basis for the arduous task of establishing closer cultural social, religious and linguistic ties vital for true unity among the people. There have been disunity, division, hatred, unhealthy rivalry and disparity in development. Political parties emerged and based on ethnic, rather than national interests. The battle to consolidate the legacy of political and military dominance of a section of Nigeria over the rest of the federation began with increased intensity. It is this ugly occurrence and struggle that degenerated to incessant coup; counter coup and a bloody civil war. The federal government however used political diplomatic psychological and military strategies to prosecute the war. The relics of this war still raise its ugly heads up till today. This is because people still nurture grievances resulting into violence up till today. The technology used in provision of weapons and weaponry are still in vogue in Nigeria. This has in fact imbued in Nigerians the tenacity and intensity to use the weapons that escaped to Nigeria populace. Immediately after the civil war the rate of violence subsided. The resurgence of violence that heralded destruction was the bomb blast in Nigeria traceable to 1986 during the regime of General Ibrahim Babangida when Mr. Dele Giwa the Founding Editor of Newswatch magazine was massacred by a mail bomb in his home; but because it was home based and individual Nigerians does not rip it the bud. Since then various kinds of bombing incidents has erupted Nigeria. Majority have been reported in Nigeria under the despotic rule of General Sanni Abacha who was acclaimed and accused of masterminding and executing killings to intimidate opponents of his regime. There was an isolated case of accidental bombs explosion that took place at Ikeja cantonment in 2002 leading to the death of more than one thousands persons. There is no gainsaying the fact that Nigeria government should look backward in order to reduce the rate of violence in Nigeria . Violence began with military men in Nigeria

and to eliminate violence, the Nigeria government should be made to look for way of reducing violence in Nigeria. Year 2010 marked the resurgence of bomb blast as an act of terrorism in the civilian era when some bomb blast went off in Warri during Amnesty dialogue organized by vanguard newspapers in support of the amnesty programme of the then President Umaru Yaradua to arrest the cases of militancy in the Niger Delta region. There have been series of blasts in Nigeria. Nigeria capital city is supposed to be the most secured place; unfortunately it appears to be the most unsafe place to dwell. There was a bomb blast on October 1, 2010 during the Nigeria's 50th independence anniversary celebration in Abuja. It was suspected to be sponsored by the movement for the emancipation of the Niger Delta (MEND) a group of Niger Delta militants. On January 1, 2011 there was a blast at the Mammy market in Abuja, on April 26, 2011 in Maduguri the Borno state capital in Bauchi an army barracks was bombed on June 16, 2011, an Islamic sect popularly called Boko Haram claimed responsibilities for some of the blasts. A lot of lives have been lost in Nigeria in fact Nigerians are engulfed in fear and are prone to all the diseases related to fear. In December 2012 American citizens are warned to desist from travelling to Nigeria and certain zones and states were particularised as hot zones where life are unsafe as there may be bomblasts in the zones. Americans were intimated that if they should visit, Nigeria should contact the America embassy before embarking on any travelling. According to a united states security group Clayton consultants, Nigeria is among the worlds top eight kidnapping hotspots, along side war zones and failed states such as Afghanistan, Iraq and Somalia.

2. Personalities and Characteristics Of Violent Individuals

The National Association of Resident Doctors (NARD), Neuro-Psychiatric Hospital Yaba declared in a seminar the upsurge in violence, bombings and kidnapping the psychological impact on Nigerians and the coping strategies. The seminar was organized because many Nigerians are engulfed in fear as a result of bombing and occurrence of kidnapping. They observed that major psychological impact are shock and acute stress reactions, this has culminated in today's epidemic proportion. These acts are perpetrated by antisocial personalities or by psychopath terrorists. Psychopath can be intelligent and have contact with reality. They are law breakers, deceitful, aggressive and reckless in disregarding safety. Psychopaths can not feel empathy or affection for others. Those who are present or nearly exposed to trauma of violence or in a bid to help victims, societies, communities or corporate bodies are engulfed in psychological reactions. Nwokedi (2000) reported that kidnapping and terrorism is a fall out of youth unemployment and display of stupendous inexplicable ill-gotten wealth by leaders. Kidnapping, according to criminal law is the taking away or transportation of a person or persons against his or her will, usually to hold the person in false imprisonment or confinement without legal authority. This may be done for a ransom or in furtherance of another crime. While terrorism means to frighten "The terror cum bricus was a panic and state of emergency in Rome in response to the approach of warriors of the cumbri tribe in 105BC. Factors of Violent Behaviours Different or various factors accounts for Involvement in violence and terrorism. There are biological, psychological, and social factors that enhances violence:

Age: Males between the ages of 15 and 30 years tend to be the most violent subgroup irrespective of culture (Blumenrath 1993; Faretta 1981; Kroll & Mackenzie 1983; Shah Fineberg & James 1991). The elderly are disproportionately represented in the population that may become violent (Astroen, Bucht, Eisemann, Nombery & Saveman (2002) Hindley of Gordon 2000; Petrie 1984). In a study of 200 cases of assault at the Cincinnati Veterans Administration of Medical centre, Jones (1985) discovered that 58.5% of the assaults took place in the geriatric facility. The statistics is noteworthy because the institution also had a larger psychotic and substance abusing population.

Substance Abuse: There is probably no psychotropic or psychoactive drug either legal or illegal that does not correlate with violence when it is abused. Whether the abuse is going on a meth high, coming off vacuum or experiencing the withdrawal or heroine, violence and drug use to have a strong relationship. (Blumenrath 1993b; Piercy 1984, Rada 1981; Simonds & Kashani 1980). Alcohol has been associated with more than half of reported cases in psychiatric institutions (Bachy Rita, Lion & Climent 1971). The potential for violence is further increased when individuals who have a history of psychosis engage in alcohol or drug use (Klassen' Connor 1988; Yesavage & Zarcone 1983)

Predisposing History of Violence: A history of serious violence, homicide, sexual attacks, assault or threat of assault with a deadly weapon is one of the best predictors of future violence (California Occupational Safety and Health Administration 1998, Faretta 1981, Monahan 1981).

3. Psychological Disturbance

A variety of mental disorders may be predisposing to violence the anti social personality type who has a history of violent behaviours, emotional callousness, impulsivity and manipulative behaviour. The borderline personality who lacks adequate ego to continue intense emotional drives and repeatedly exhibits emotional outbursts. The paranoid is on guard against and constantly anticipating external threat, the manic who has elevated moods, hyperactively and excessive involvement in activities that may have painful consequences, the explosive personality who has sudden escalating periods of anger, the schizophreme who is actively hallucinating and has a bizarre or grandiose delusions, the attack victim, who is fearful dissociative and has extreme flight or fight reactions and acting out suicidal plans (Blumenriach 1993; Greenfield, McNal& Binder, 1959; Heilbrum, 1990; Heilbrum&Halmbrum, 1989; Klassan O.Connor, 1988; Murdach 1993).

Social Stressors

Blumenreich(1993) & Munoz: Joaquin, NovalMoringo, Garcia & Concha (2002) reported that loss of job, job stress, break up in a relationship, a past history of physical or sexual abuse and financial reversals are a few of the social stressors that cause acute frustration and rage in an out of control social environment that leads to violence.

Family History

A history of violence within the family is often carried into other environment. An early childhood characterized by an unstable and violent home is an excellent model for future violence (Wood &Khuri 1984). A history of social isolation or lack of family & environmental support also may heighten the potential for violence (Halbrun&Halbrun, 1989, Munoz 2000).

Bases Of Violence

There are biological, psychological and social bases for violence. Biologically low intelligence, hormonal imbalance, organic brain disorders, neurological and systemic changes of a psychiatric nature diseases, chemicals, intense chrome pain or traumatic head injury may lead to more violence-prone behavior (Fish bain Cutler, Rosomoff, & Steele-Rosomoff (2000); Hamsfra 1986; Helbrun 1990; Heibrum&Heibrum 1989). Psychologically specific situational problems, certain functional psychoses and character disorder are predisposing to violence (Greenfield, McNal&Buder1989), Klassen&D' Connor 1988). Socially, modeling the violent behavioural norms of family, peers & the environment within which one lives can trigger violent tendencies (Nisbelt 1993, Tardif 1984, Wood &Khuri 1984). Specific on site physical environmental stressors such as heat, crowding, noise, conflict and poor communication can trigger violence (Anderson 2001, Jensen &Absher 1984). When all these ingredient are mixed together, the result start to resemble the kinds of people and environments with which the crises worker is likely to come in contact (Tardiff 1984).

4. Symptoms In People Exhibiting Violence Behaviours

Most people react to the stress of violence with an emotional or somatic response which are normal reaction and do not constitute mental disorders in themselves. Some people seek help from their Doctors or Counsellor, some people faces sleeping problems, eating problems, head aches, increased level of arousal, cognitive confusion, poor concentration, memory difficulties, distressing dreams or nightmares, intrusive thoughts or images, behavioural withdrawal or isolation, increased compulsiveness, increased use of drugs and alcohol, hyper vigilance, reluctance to leave home, emotional fear, sadness, anger and irritability are other challenges. Adebayo(2004) reported that acute stress reaction is another psychological impact which is said to be transient response which sometimes occurs immediately following exposure to or during an exceptionally severe event but subsides within a short period of time usually hours or days. He also observed that Post Traumatic Stress Disorder (PTSD) is an intense prolonged and sometimes delayed reaction to an intensely stressful event. The core symptoms are hyper arousal, poor concentration, irritability and persistent anxiety.

Research Rationale

There are reports on the national daily bases and sophisticated media about the occurrences, tenacity and waves of violence. There appears to be increment in the rate of ailments and diseases associated with fear. Economically, investors desert Nigeria because of the fear of mishap and dangers that may erupt their business as a result of violence occurring in daily basis in Nigeria. The reports of disasters in print and visual media about violence throws Nigerians into social and psychological problems. The researcher therefore traces the genealogy, occurrences and reported that it appears to be one of the tendencious problems ravaging Nigeria. One continue to languish that Nigerians image is dented nationally and internationally, Nigeria is rated as one of the 8 hot zones or war zones in the world where violence of bombing and kidnapping is very high.

5. Conclusion

Based on the aforementioned it can be concluded that majority of Nigerians are susceptible to social and psychological stress resulting to violence. The bases of Nigerians violent behaviors are historical looking at the antecedents. The violent behavior in Nigeria has historical background. Majority of Nigerians experience somatic and psychosomatic ailments that are not alien to violence.

6. Significance Of The Study

The study could be of benefit to the students, teachers, counsellors, curriculum planners, religious organizations, health care Practitioners, law enforcement agents, parents and guardians. Student could learn about the occurrence effects and remedies for involvement in violence. Teachers would be able to teach courses that would stem the tides of violence. Curriculum planners would be able to incorporate into the national curriculum areas to be taught and reduce the wave of violence, counsellors would counsel the students and Nigerians about the causes, symptoms and consequences of violence. Religious leaders; Pastors and Imams could preach to the congregation the evil effects of violence. The health care practitioners could diagnose and do prognoses to the clients manifesting violence related ailments, the law enforcement agents could be able to mount surveillance and handle cases involving violence with reduced problems. Parents and guardians could be able to understand children showing violent behaviours and handle their wards manifesting behaviour problems resulting to violence.

7. Recommendations

There should be critical stress management techniques such as debriefing. It should be incorporated into the national curriculum education imbued in stress management. There should be outreach to affected population, provision should be made in form of crisis counselling, bereavement counselling and distribution of materials on stress reactions. There should be moral reawakening beyond persuasive insincere language or rhetoric. Nigeria leaders should be responsible and responsive, there should be reduction in the gap between the rich and the poor. Election of political leaders should go beyond winners takes all. There should be reconsideration and reconciliation after election. The rigging and fraud that permeates all the political system of Nigeria should be eschewed. Above all Nigerians should be trained and taught to be job creators and not seekers. Reorientation programmes should be timely provided for Nigeria youths. Also adequate infrastructure and facilities should be provided. There should be repositioning and strengthening of the health sector and agencies responsible and responsive for emergences should be in place.

References

- [1]. Anderson C.A. (2001) Heat and Violence Current Directions in psychological science 10 (1), 33-38
- [2]. Astrolm S, Bucht G, Fisengmn M, Norberg A. & Saveman B (2002). Incidence of violence towards staff caring for the elderly. Scan-dinavian Journal of caring services 16 (1) 66-72.
- [3]. Bach y Rita G, Lion J.R & Climent C.E (1971) Episodic dyscontrol: A Study of 630 violent patients, *American journal of Psychiatry* 128, 1473-1478.
- [4]. Blumenrach P.E (1993) Assessment: In P.E. Blumereich & S Lewis (Eds), managing the violent patient. *A clinician's guide* (pp. 35-40) New York: Brunner/Mazel.
- [5]. California Occupational Safety and Health Administration (1998) Guidance of Security and Safety of health Care and community service workers. Sacramento, CA: Author
- [6]. Faretta G (1981) A profile of aggression from adolescence to adulthood: An 18 year follow up of psychiatrically disturbed and violent adolescents, *American Journal of Orthopsychiatry* 51, 439-453.
- [7]. Fishbain D.A, Cutler, R.B Rosomoff H.L & Steele – Rosomoff R. (2000) Risk for violent behavior in patients with chronic pain: Evaluation and management in the pain facility setting. *Pain Medicine* 1 (2), 140-155.
- [8]. Grassi L, Peron L, MaFangoni C, Zanchi P & Vanni A (2001) Characteristics of violent behavior in acute psychiatric in patients: A 5 year Italian Study, *Acta Psychiatrica Scandinavica* 104(4), 273-279
- [9]. Greenfield T.K, McNeil D.E & Binder R.L (1989) Violent behavior and Length of psychiatry hospitalization Hospital and community psychiatry 40, 809-814.
- [10]. Hamstra B (1986) Neurobiological substrates of violence: An overview for forensic clinicians. *Journal of psychiatry and Law* 14, 349-374.
- [11]. Heibrun A.B & Heilbrun M.R (1989) Dangerousness and legal insanity. *Journal of psychiatry and Law* 17, 39-53.
- [12]. Hindley N & Gordon H (2000). The elderly, dementia aggression and risk management. *International journal of Geriatrics* 15 (3) 254-259.
- [13]. Jensen, D & Absher, J. (1994) Associative behavior, the crisis is over: Preventing another crisis Paper presented at the Eighteenth Annual Convening of crisis intervention personnel, Chicago.
- [14]. Jones M.K (1985) Patient Violence: Report of 200 incidents, *Journal of Psychosocial Nursing and Mental Health* 23, 12-17.

- [15]. Klassen, D & O' Connor W.A. (1988) A prospective study of predictors of violence in adult male mental health admissions. *Law and Human Behaviour* 12, 143-158.
- [16]. Kroll J & Mackenzie T.B (1983) when psychiatrists are liable: Risk management and violent patiente *Hospital and Community Psychiatry*, 34, 29-37.
- [17]. Monahan J (1981) The clinical prediction of violent behaviors Rockville, MD! National Institute of Mental Health.
- [18]. Munoz, M Joaquin C, Noval D Moringo A & Garcia de la Concha J.A (2000) Factorespredictores de agresividad en esquizofrenicoshospitalizados. *ActasEspanolas de Psiquiatria*, 28 (3) 151-155.
- [19]. Nisbett R.E. (1993) Violence and U.S regional culture *American Psychologist* 48, 441-449.
- [20]. Petrie W.M (1984) Violence.The geriatric patient.In J.T Turner (Ed) Violence in the medical care setting. *A survival guide* (PP.107-122). Rock Ville M.D Aspen systems.
- [21]. Piercy D. (1984) Violence the drug and alcohol patient.In J.T. Turner (Ed) Violence in the medical care setting. *A survival guide* (pp. 107-122) Rock Ville M.D. Aspen Systems.
- [22]. Rada R.T. (1981) the violent patient: Rapid assessment and management. *Psychosomatics* 22, 101-109
- [23]. Shah A.K., Fineberg N.A. & James D.V. (1991) Violence among psychiatric in patients, *Actapsychiatrica, Scandinavica*, 84, 305-309
- [24]. Simonds J.F &Kashani J (1980) Specific drug use and Violence in delinquent boys. *American Journal of Drug and Alcohol Abuse* 7, 305-309
- [25]. Tardiff K. (1980) Violence: The Psychiatric patient in J.T. Turner Ed Violence in the medical care setting: *A Survival Guide* (pp. 33-55). Rockville MD. Aspen Systems.
- [26]. Wood K.A. F Khuri R. (1984) Violence: The emergency room patient in J.T. Turner (Ed) Violence in the medical care setting: *A Survival Guide* (pp.57-84) Rockville, M.D: Aspen systems.
- [27]. Yesavage J.A &Zarcone, V (1983) History of drug abuse and dangerous behavior in inpatient Schizophrenics, *Journal of Clinical Psychiatry*, 44, 259-261

Cloud Documentation and Centralized Compiler for Java & Php

¹Namrata Raut, ²Darshana Parab ³Shephali Sontakke, ⁴Sukanya Hanagandi

^{1,2,3,4}Student, Department of Computer Engineering, JSPM's BSIOTR(W)

Abstract

Cloud computing is an Internet based computing which aims at providing hardware and software resources. It enables the users to access and share information from devices like laptops, desktops, smart phones, etc. which have ability to connect to the Internet. Cloud computing caters to dynamism, abstraction and resource sharing. The project mainly deals with the creation of Integrated Development Environment for the java language to code, compile, run, test and debug the code using the browser based IDE through the Internet and a web browser. The project is aimed at creating a browser based IDE to code in Java language in the cloud which will allow real time collaboration with the peers.

Keywords: Centralized Compiler, Cloud Computing, Collaborative Learning Tools, Peer Reviewing, Browser Based IDEs, Compiler, Document Sharing.

1. Introduction

Cloud Computing describes a new supplement, consumption and delivery model for IT services based on Internet protocols and it typically involves provisioning of dynamically scalable and often virtualized resources. It is a byproduct and consequence of the ease-of-access to remote computing sites provided by the Internet according to their own needs. This may take the form of web-based tools or applications that users can access and use through a web browser as if the programs were installed locally on their own computers. There are five known ways of providing cloud computing currently viz. public, private, community, combined and hybrid cloud computing. The users need not care how to buy servers, software. This project mainly deals with the creation of Integrated Development Environment for the java language to code, compile, run, test and debug the code using the browser based IDE through the Internet and a web browser. The IDE will permit easy development, testing and debugging of applications. Cloud computing is a model for providing computation, software, data access and storage services that do not require end-user knowledge of the physical location and configuration of the system that delivers the services.

1.1 Collaborative Writing

The cloud will allow the real time collaboration with peers. Collaborative writing allows the users to work concurrently on single document. Computer-supported collaborative writing has received attention since computers have been used for word processing. Research that analyzes collaborative writing in terms of group work processes, focusing on issues such as process loss, productivity, and quality of the outcomes [5], [6]; and research that studies collaborative writing in terms of group learning processes, focusing on topics such as establishing common ground, knowledge building, and learning outcomes [4]. Collaborative writing is an iterative and social process that involves a team focused on a common objective that negotiates, coordinates, and communicates during the creation of a common document is a cognitively and organizationally demanding process.

1.2 Centralized Compiler

The paper aims to describe centralized compiler which helps to reduce the problems of time, cost and storage space by making use of the concept of cloud computing. Also, the trouble of installing the compiler on each computer is avoided. The main reason for creating the project is to provide a centralized compiling scheme [2], [3]. Also, it will act as a centralized repository for all the codes written. The other major advantage that this system will have over the others is that it will make the users system lightweight i.e. there will be no need to maintain separate compilers at the client side [2],[3]. Also, the process of maintenance and distribution of dynamic usernames and passwords will be greatly simplified. Also, authentication and personalized task distribution will be made possible. A compiler, which is the heart of any computing system, transforms source code from a higher level language to a lower, machine level language. This is mainly done in order to create executable files which can then be run in order to execute the program and its instructions [2].

2. Related Work

(1) Cloud computing implies a service oriented architecture, reduced information technology overhead for the end-user, great flexibility, reduced total cost of ownership and on demand services among other advantages. The National Institute of Standards and Technology (NIST) defines Cloud Computing⁴ as a model for enabling easy, on demand network access to a shared pool of configurable computing resources (e.g., networks, servers, storage, applications, and services) that can be rapidly provisioned and released with minimal management effort or service provider interaction. Some of them are lower costs, better computing, location independence, better security (although this advantage in clouded with doubts of loss of some sensitive data) [8].

(2) Cloud computing can be viewed from two different aspects. One is about the cloud infrastructure which is the building block for the up layer cloud application. The other is of course the cloud application. By means of three technical methods, cloud computing has achieved two important goals for the distributed computing: high scalability and high availability. Scalability means that the cloud infrastructure can be expanded to very large scale even to thousands of nodes. Availability means that the services are available even when quite a number of nodes fault. SaaS provides Internet application to the customer also provides the software the off-line operation and the local data storage, lets software and service which the user all may use it anytime and anywhere to order.

(3) The concept of computing comes from grid, public computing and SaaS. It is a new method that shares basic framework. The basic principles of cloud computing is to make the computing be assigned in a great number of distributed computers, rather than local computer or remoter server. This article also introduces the application field the merit of cloud computing, such as, it do not need user's high level equipment, so it reduces the user's cost [9]. It provides secure and dependable data storage center, so user needn't do the awful things such storing data and killing virus, this kind of task can be done by professionals. Users can enjoy the service even he knows nothing about the technology of cloud computing and the professional knowledge in this field and the power to control it.

3. System Architecture

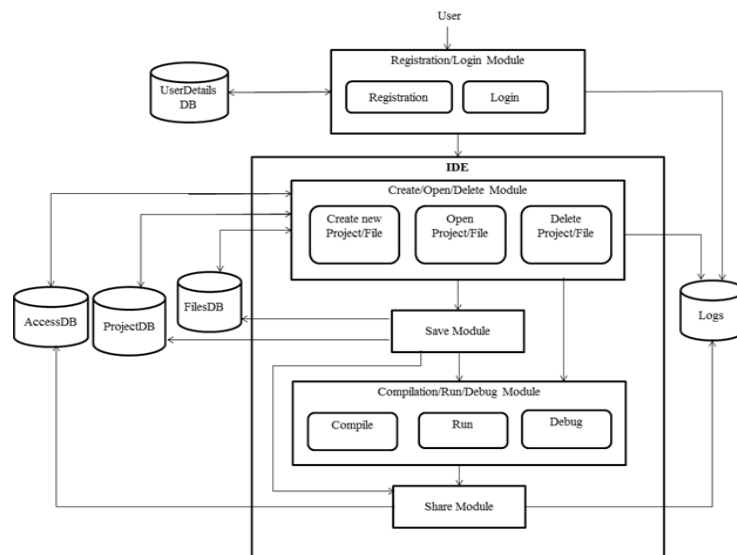


Fig1.System Architecture

The various modules involved in Browser Based IDE to Code in the Cloud are as follows:

- 1. Registration:-**This module accepts the details of a new user and stores it in the UserDetailsDB database. This action is logged in the Logs database. This module ensures that the user is registered before the first login.
- 2. Login:-**A registered user should login with his username and password to use the IDE. This module facilitates login and user authentication using UserDetailsDB database. This action is logged in the Logs database.
- 3. Create new Project/ File:-**This module permits valid users to create new projects with the name of their choice. They can also create new files within these projects. The details of the projects are stored in the

ProjectDB database and those of the files are stored in FilesDB database. These actions are logged in the Logs database.

4. **Open Project/ File:-**This module permits valid users to open existing projects and files. The user's access rights to the projects and files are checked from the AccessDB database. The action of opening project is logged in the Logs database.
5. **Delete Project/ File:-** This module permits the valid users to either delete certain files of a project or delete the entire project itself. The time at which the delete action is performed along with the User ID of the user who performs it is logged in the Logs database.
6. **Save:-** This module allows the valid users to save their projects and files. These projects are stored in ProjectDB database and the files are stored in FilesDB database.
7. **Compile:-** This module allows the users to compile their Java code by invoking a compiler. The result of compilation is displayed to the user.
8. **Run:-** This module allows users to run the compiled Java code. The result of this action is displayed to the user.
9. **Debug:-** This module permits the users to insert breakpoints in the code for the purpose of debugging.
10. **Share:-** This module permits valid users to share the projects with other users. The User ID of the peer with whom the project is shared and the access rights granted are store in the AccessDB database. This action is logged in the Logs database.

4. Features

1. **Ability to create new projects and files:-** The IDE will allow the users to create new projects and to name the projects according to their choice. It will permit the creation of new files within the project to write Java code.
2. **Easy modification of existing code:-** The IDE will have the ability to edit and modify the already written code in various files.
3. **Saving the files and project for future access:-** The files and projects will be saved on the cloud itself and will be easily available to the users from anywhere and at anytime.
4. **Easy development, testing and debugging of applications:-**
The IDE will have tools for easy development of the applications. It will have an integrated Java compiler to review the build errors. It will also allow users to employ breakpoints in their code in order to debug the code.
5. **Sharing projects with peers:** - The IDE will allow users to share the projects with peers.
6. **Real time collaboration:-** The IDE will allow the users to share code and to modify the same files by real time collaboration feature.

5. Future Scope

The software can be extended in the future to include Java EE technologies like JSP, Servlets and also other advanced functionalities like code completion, syntax highlighting, sharing code with hyperlinks and support for other languages.

6. Conclusion

The project aims at creating & compiling Java & Php code in the cloud and also aims to provide the special feature of real time collaboration for the users. As compared to the current scenario where each machine need to install compilers separately. This would eliminate the need to install compilers separately. So we can check our code at the centralized server. Advantage of this project is that whenever the compiler package is to be upgraded it can be done easily without again installing it on each and every machine.

References

- [1] M.L. Kreth, "A Survey of the Co-Op Writing Experiences of Recent Engineering Graduates," IEEE Trans. Professional Comm., vol. 43, no. 2, pp. 137-152, June 2000.
- [2] Aamir Nizam Ansari, Siddharth Patil, Arundhati Navada, Aditya Peshave, Venkatesh Borole, "Online C/C++ Compiler using Cloud Computing", Multimedia Technology (ICMT), July 2011
- [3] Shuai Zhang Shufen Zhang Xuebin Chen Xiuzhen Huo, "Cloud Computing Research and Development Trends", Future Networks, 2010. ICFN '10. Second International Conference.
- [4] M. Scardamalia and C. Bereiter, "Higher Levels of Agency for Children in Knowledge Building: A Challenge for the Design of New Knowledge Media," The J. Learning Sciences, vol. 1, pp. 37-68, 1991.
- [5] P.B. Lowry, A. Curtis, and M.R. Lowry, "Building a Taxonomy and Nomenclature of Collaborative Writing to Improve Interdisciplinary Research and Practice," J. Business Comm., vol. 41, pp. 66-99, 2004.
- [6] G. Erkens, J. Jaspers, M. Prangma, and G. Kanselaar, "Coordination Processes in Computer Supported Collaborative Writing," Computers in Human Behavior, vol. 21, pp. 463-486, 2005
- [7] Chunye Gong Jie Liu Qiang Zhang Haitao Chen Zhenghu Gong, "The Characteristics of Cloud Computing", Parallel Processing Workshops (ICPPW), 2010 39th International Conference.
- [8] A.RABIYATHUL BASARIYA and K.TAMIL SELVI, Computer Science and Engineering, Sudharsan Engineering College-centralized C# compiler using cloud computing, 2nd march 2012
- [9] Rafael A. Calvo, Senior Member, IEEE, Stephen T. O'Rourke, Janet Jones, Kalina Yacef, and Peter Reimann- Collaborative writing support tools on the cloud, Jan-March 2011

Real –Time Envirnorment Monitoring System and Data Logger Using Arm Processor

¹**B.Hari Babu**, ²**Y.Varthamanan M.E**

^{1,2} (Department of Electronics and Communication Engineering, Sathyabama University, India)

Abstract: This paper describes is to monitoring the real time environment and data logger using ARM processor. The various parameters of the surrounding system such as temperature, humidity, gas, fire and battery are acquired and processed through the Arm microcontroller and stored in a data logger and also we can analysis in Graphical Lcd.Additional features of this project is to locate the exact position of the sensed data from the sensors through Gps.The paper will describe decision regarding what resources were included in the device as well as how to provide flexibility in order to meet a diverse range of application.

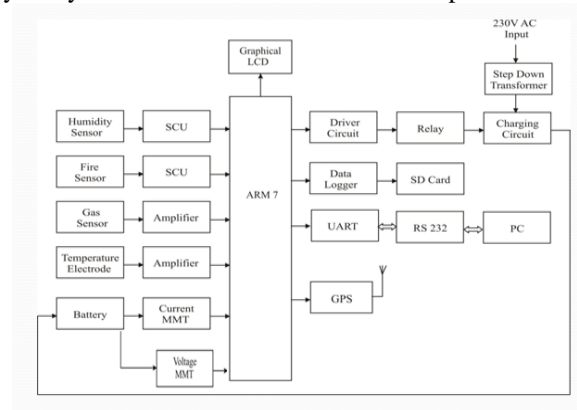
Keywords-:Bms, Data Logger, hyper terminal,LPG, POT, Sd card,Tdmi

1. Introduction

We had multiple upcoming projects that appeared to require the low power of a 32-bit CPU, so we set out to design a board that would work for these projects as well as future projects. A board was designed around the Microchip ARM7TDMI LPC2148.This paper describes the project hardware and software requirements and other considerations in the board design as well as component selection and flexibility issues.

2. Block Diagram

In the below, Block diagram there are three main applications involved they are: Industrial, Battery management system and Data logger. In Industrial application we measure (temperature, humidity, gas and pressure) through sensors. This sensed data are conditioned (by amplification) and given to the Microcontroller. In Battery Management System (BMS) for every periodic of time it monitor the (current) through sensors and send the data to the Microcontroller. This obtained data from the Microcontroller are sent to data logger for storing in sd card without any delay in a real time and viewed in a Graphical Lcd



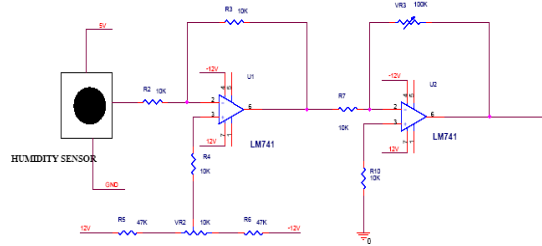
Sensors are interfaced with ARM Processor

3. Sensors

A sensor (also called detector)is a converter that measures a physical quantity and converts into a signal which can be ready by an observer or by an (today mostly electronic)instrument.

3.1: HUMIDITY:

Humidity is the amount of water vapor in an air sample.

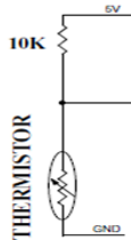


Circuit diagram of humidity sensor

Circuit description:

This circuit is designed to measure the humidity level in the atmosphere air. The humidity sensor is used for the measurement device. The humidity sensor consists of an astable multivibrator in which the capacitance is varied depending on the humidity level. So the multivibrator produces a varying pulse signal which is converted into a corresponding voltage signal. The voltage signal is given to the inverting input terminal of the comparator. The reference voltage is given to the non-inverting input terminal. The comparator is designed by the LM 741 operational amplifier. The comparator is compared with the reference humidity level and delivers the corresponding error voltage at its output, which is given to the next stage of a gain amplifier in which a variable resistor is connected in the feedback path. By adjusting the resistor, we can get the desired gain. Then the final voltage is given to a microcontroller or other circuit in order to find the humidity level in the atmosphere.

3.2: Temperature:

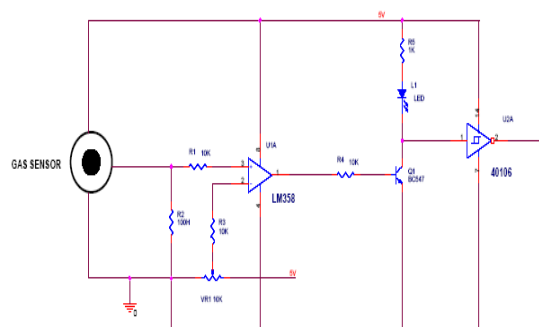


Temperature measurement using thermistor

In this circuit, the thermistor is used to measure the temperature. A thermistor is nothing but a temperature-sensitive resistor. There are two types of thermistors available, such as positive temperature coefficient and negative temperature coefficient. Here we are using a negative temperature coefficient in which the resistance value is decreased when the temperature is increased.

3.3: Gas:

An ideal sensor for use to detect the presence of a dangerous LPG leak in your car or in a service station, storage tank environment. This unit can be easily incorporated into an alarm unit, to sound an alarm or give a visual indication of the LPG concentration. The sensor has excellent sensitivity combined with a quick response time. The sensor can also sense iso-butane, propane. The unit will work with a simple drive circuit and offers excellent stability with a long life.



Circuit diagram of gas sensor

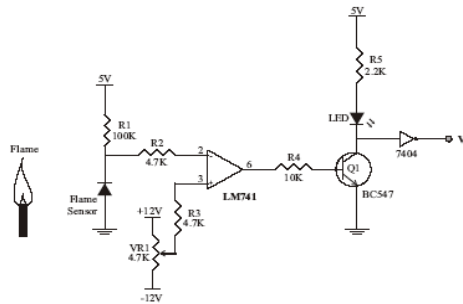
Circuit description:

This circuit is mainly designed to sense the present LPG GAS in the atmosphere. The LPG GAS (Propane) is sensed by the gas sensor. The gas sensor is the one type of transducer which produces the voltage signal depends on the gas level. Then the voltage signal is given to inverting input terminal of the comparator. The comparator is constructed by the operational amplifier LM 741. The reference voltage is given to non inverting input terminal. The comparator compares with normal reference signal and produces the corresponding output error signal. Then the output voltage is given to microcontroller in order to determine the presence of a dangerous LPG leak.

3.4: Fire:

3.4 .a: Flame sensor:

The flame sensor is used to detect the flame occurrence. When the sensor detects the fire then it became short-circuit. When there is no fire the sensor become open circuit

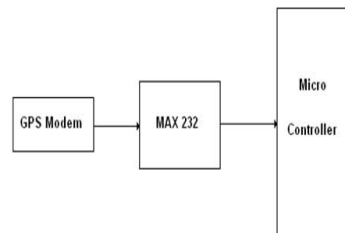


Circuit diagram of fire sensor

Circuit description:

The flame sensor is connected with resistor. This connection formed the voltage divider network which is connected with inverting input terminal of the comparator. The reference voltage is given to non inverting input terminal. The comparator is constructed with LM 741 operational amplifier. When there is no fire, the flame sensor became open circuit. So the inverting input terminal voltage is greater than non inverting input terminal (reference voltage). Now the comparator output is -12V which is given to the base of the switching transistor BC547. So the transistor is cutoff region. The 5v is given to 7404 IC. The 7404 is the hex inverter with buffer. Hence zero voltage is given to microcontroller. When there is fire occurred, the flame sensor became short circuit. So the inverting input terminal voltage is less than non inverting input terminal (reference voltage). Now the comparator output is +12V which is given to the base of the switching transistor BC547. So the transistor is turned ON. The zero voltage is given to 7404 IC. Hence +5v voltage is given to microcontroller. In the microcontroller we can detect the fire with the help of software.

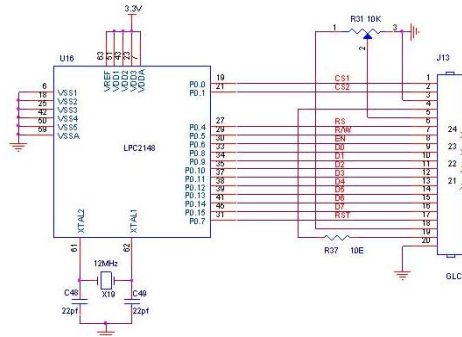
4. Interfacing With Gps



This is a third generation POT (Patch Antenna On Top) GPS module. This POT GPS receiver providing a solution that high position and speed accuracy performances as well as high sensitivity and tracking capabilities in urban conditions & provides standard NMEA0183 strings in “raw” mode for any microcontroller. The module provides current time, date, latitude, longitude, speed, altitude and travel direction / heading among other data, and can be used in a host of applications, including navigation, tracking systems, fleet management, mapping and robotics. This is a standalone GPS Module and requires no external components except power supply decoupling capacitors. It is built with internal RTC Back up battery. It can be directly connected to Microcontroller's USART. The module is having option for connecting external active antenna if necessary. The

GPS chipsets inside the module are designed by MediaTek Inc., which is the world's leading digital media solution provider and largest fab-less IC company in Taiwan. The module can support up to 51 channels. The GPS solution enables small form factor devices. They deliver major advancements in GPS performances, accuracy, integration, computing power and flexibility. They are designed to simplify the embedded system integration process.

5. Interfacing with Graphical LCD



This project is designed to interface graphical: CD to ARM based microcontroller. Data entry is through PC's hyper terminal and the received data is displayed on graphical LCD. MAX 232 is used to communicate with the hyper terminal. The LPC2148 are based on a 16/32 bit ARM7TDMI-S™ CPU with real-time emulation and embedded trace support, together with 128/512 kilobytes (kB) of embedded high speed flash memory. A 128-bit wide memory interface and a unique accelerator architecture enable 32-bit code execution at maximum clock rate. For critical code size applications, the alternative 16-bit Thumb Mode reduces code by more than 30% with minimal performance penalty. With their compact 64 pin package, low power consumption, various 32-bit timers, 4- channel 10-bit ADC, USB PORT,PWM channels and 46 GPIO lines with up to 9 external interrupt pins these microcontrollers are particularly suitable for industrial control, medical systems, access control and point-of-sale. With a wide range of serial communications interfaces, they are also very well suited for communication gateways, protocol converters and embedded soft modems as well as many other general-purpose applications.

6. Flow Chart And Result



Flow chart of the project





7. Conclusion

The ARM7TDMI LPC2148 board has proven to be efficacious and robust in the above projects. Its flexibility to adapt to a wide range of Application. Future plans for this board include the all automated Management System described above as well as remote access and replacement of an embedded PC system controlling an industrial machine.

8. REFERENCES

- [1] Subramanian, R., Venhovens, P.J., Keane, B.P., "Accelerated Design and Optimization of Battery Management Systems using HIL Simulation and Rapid Control Prototyping", 2012 IEEE International Electric Vehicle Conference, March 4-8, 2012, Greenville, sc.
- [2] DU Chun-lei. ARM Architecture and Programming [M]. Beijing_Tsinghua university press, 2003. (in Chinese)
- [3] Zhang Da-bo. principles, Design and application of embedded system [M]. Beijing Machinery industry press_2004. (in Chinese)
- [4] Kyberd, Peter and Poulton, Adrian (2012). The use of multiple sensors in the control of prosthetic arms. In: Trent International Prosthetic Symposium TIPS 2012, 21-23 May 2012, Loughborough, UK.

An Approach for Effective Use of Pattern Discovery for Detection of Fraudulent Patterns In Railway Reservation Dataset

Rasika Ingle¹, Manali Kshirsagar²

¹Dept. of Computer Technology, Yeshwantrao Chavan College of Engineering,
Nagpur, Maharashtra, India

²Dept. of Computer Technology, Yeshwantrao Chavan College of Engineering, Nagpur, Maharashtra, India

Abstract:

Data mining concepts and techniques can help in solving many problems. Useful knowledge may be hidden in the data stored. This knowledge, if extracted, may provide good support for planners, decision makers, and legal institutions or organizations. Hence Pattern discovery, as one of the powerful intelligent decision support platforms, is being increasingly applied to large scale complicated systems and domains. It has been shown that it has the capacity to extract useful knowledge from a large data space and present to the decision makers. This will contribute to the detection of illegal activities, the governance of systems, and improvements in systems. This paper proposes a work to develop a mechanism that allows the system to work interactively with a user in detecting, characterizing and learning unusual and previously unknown patterns over groups of records depending on the characteristics of the decisions. The data mining in real time could even help to alert Railways when something untoward happens. Hence this innovative mechanism focuses on detecting anomalous and potentially fraudulent behavioral patterns within set of railway reservation transactional data. The pattern based analysis will include the possible detection of fake ids, fake booking, an unusual pattern like reservation of a person for trains in two different directions on a given date from the same starting city etc.

Keywords: Anomalous transactions, data mining, fraudulent transactions, hash map, pattern, pattern discovery, rule based discovery.

1. Introduction

All Data Mining is the process of discovering new correlations, patterns, and trends by digging into (mining) large amounts of data stored in warehouses, using artificial intelligence, statistical and mathematical techniques. Data mining is the principle of sorting through large amounts of data and picking out relevant information. It has been described as "finding hidden information in a database. Alternatively, it has been called exploratory data analysis, data driven discovery, and deductive learning" [13] and "the science of extracting useful information from large data sets or databases". The interesting patterns are presented to the user and may be stored as new knowledge in the knowledge base. According to this view, data mining is only one step in the entire process, albeit an essential one because it uncovers hidden patterns for evaluation [14]. It is usually used by business intelligence organizations, and financial analysts, but it is increasingly used in the sciences to extract information from the enormous data sets generated by modern experimental and observational methods. One of main area where data mining can be used in the industry is in monitoring systems. The specific tasks in automated transaction monitoring systems are the identification of suspicious and unusual electronic transactions. An unusual pattern is an observation or a point that is considerably dissimilar to or inconsistent with the remainder of the data. Detection of such outliers or patterns is important for many applications and has recently attracted much attention in the data mining research community.

Pattern-based analysis looks for anomalies indicative of fraud or error in normal patterns of data. It is growing gradually and becomes more important with the quick development of computer technologies with increasing capacity to collect massive amounts of valuable data for pattern analysis. In real life, fraudulent transactions are interspersed with genuine transactions and simple pattern matching is not often sufficient to detect them accurately. Often times, discrepancies in transaction data are missed when analysis doesn't go beyond known problems. Discrepancies may result from unanticipated behavior that pattern-based analysis is more apt to uncover. The basic question asked by all detection systems is whether anything strange has occurred in recent events. This question requires defining what it means to be recent and what it means to be strange. "What's strange about recent events". WSARE operates on discrete data sets with the aim of finding rules that characterize significant patterns of anomalies [9]. In general, anomalies can be defined as any observations that are different from the normal behaviour of the data. Many traditional anomaly detection techniques look at the data records individually, and try to determine whether each record is anomalous with respect to the historical distribution of data. A Bayesian Network likelihood model and a conditional anomaly

detection method are considered by [10],[11]. In terms of data mining, fraud detection can be understood as the classification of the data. Research on fraud detection has been focused on the pattern matching in which abnormal patterns are identified from the normality [12]. Input data is analysed with the appropriate model and determined whether it implies any fraudulent activities or not. One could use the classical data mining tools to get supporting data to confirm or refute existing personal perception, but one also cannot be assured that there are no better-fitting explanations for the discovered patterns, or even that no important information has been missed in the entire data mining process. For a relatively complex real problem with a large data space, all traditional knowledge acquisition and data mining tools would become obviously inefficient, even helpless in some ways. For a larger mixed-mode database with more unanticipated variations than normal ones, even the domain experts would find it difficult to reach useful results. Hence this limitation motivates to develop a technique that searches for suspicious patterns in the form of more complex combinations of transactions and other evidence using background knowledge. There are many indicators of possible suspicious (abnormal) transactions in traditional illegal business. Here we concentrate on fraudulent patterns; This paper proposes a work that aims to identify certain forms of knowledge that can be inferred from the information infrastructure that supports railway reservation booking systems. It will also assess the integration of data mining with these systems as a means to facilitate the extraction of useful knowledge. The purpose of this short paper is to present an idea of finding fraudulent patterns from a railway reservation dataset and proposing a mechanism to achieve the same. The structure of the rest of the paper consists of an introduction to data mining and pattern discovery concepts, followed by a brief description of the key aspects of proposed work. This section sets the scene for the main methodology for a fraudulent pattern discovery. The paper then concludes with a scope and limitation.

2. Methodology

2.1. Problem Definition

Pattern discovery from large datasets has been an active field of research for the past two decades. These studies are driven by a desire for automated systems which can search, analyse, and extract knowledge from the massive amount of data collected in many fields. The main goal is to replace the conventional manual examination methods which are expensive, inaccurate, error prone and limited in scope. Reservation records should also be searched for unusual patterns and undiscovered knowledge. This proposed work demonstrates that different kinds of illegal manipulation or ways used in railway reservation transactions can be discovered by identifying particular patterns and track them in the datasets. Fraud indicators in the railway reservation transactions are the focus of this work. The problem is formulated by,

Recognising those indicators, the patterns associated with them, and the human behaviour underlying these patterns;

A data mining approach to automate the discovery of the illegal activities that generate the patterns.

2.2. Significance

This study will contribute to current efforts in establishing better systems to support the railway reservation governance. To achieve this, two main problems are addressed.

Assessing the patterns hidden in reservation transaction records which can be used to point out useful knowledge.

Automating the discovery of some of these patterns from reservation records by applying data mining techniques.

A major problem is the lack of published work that addresses the automatic extraction of knowledge from railway reservation systems. Therefore, in some aspects, this is a pioneering study.

2.3. Research Objectives

The primary objective of this work is,

To explore the use of data mining in railway reservation systems and to develop knowledge of where and how data mining can be applied and integrated into these systems, to contribute to the discovery and alleviation of fraud in railway reservation transactions.

As stated, the primary objective of this work is set to provide a solution to fraud bookings by agents and to railway reservation governance by detecting fraud. To serve this primary objective, four main activities or sub-objectives are set. They are,

2.3.1 Identify different fraudulent activities in reservation record datasets, in a variety of contexts where these activities may take place.

2.3.2 Identify suitable data mining techniques that may help in detecting some of the fraud activities found in (2.3.1).

2.3.3 Design and develop a data simulator to generate reservation record datasets.

2.3.4 Identify existing tools or techniques to apply the methods found in (2.3.2) above and develop a mechanism which serves the main objective.

2.4. Suggested Approach

This section of the paper describes the activities that would be carried out by the authors in order to address the problem of the research.

2.4.1 Acquisition of Domain Knowledge

In addition to the literature review; a qualitative survey was conducted using unstructured interviews because literature is sparse. This survey asked experts in the field of railway reservation systems (Railway employees, travel agents and consultants), about their knowledge in indicating the types of frauds or unusual patterns that may occur in reservation records.

2.4.2 Data collection

For the proposed work the relevant data set is the records of railway reservation transactional data. Hence the required data set is collected and studied successfully. It has been studied that this transactional database mainly consist of master files as

- Train Index
- Station Index
- Category Index
- Fare Index
- PNR Index
- Current Index
- Reservation Index

These master files contain the overall details of specific nature. Based on the observations made from the collected railway reservation transactional data set, the required relevant database is created following the same structures.

2.4.3 Creation of fraud schemes based on the findings from the first two activities above

In this activity the author studied and analysed the behaviours found in the first two activities to come up with a set of racketeering methods and schemes that are used in the real world. For each scheme, the author tried to find the effect of conducting it on the datasets and how the corresponding records differ from the records of any other usual reservation activity. The findings are summarized in lists of fraud patterns and indicators. Based on the patterns and indicators studied for the schemes, some of the schemes would be selected for the testing of data mining. This selection process is mostly based on the available data.

2.4.4 Data mining methods used in pattern discovery

This phase encompasses two activities. First performs the study of data mining concepts and techniques [5]. This will help in understanding the problems data mining techniques might be useful in solving. The second activity is to understand the existing fraud detection techniques and examine some case studies of fraud detection in different fields [12]. This is an important activity since the focus of this study is more toward detecting fraudulent activities in railway reservation transactions. This review helps to understand how to formulate schemes found in order to apply detection methods.

2.4.5 Data simulation

In this step, a reservation records simulation system was developed to provide the required data for the experiments in this research. The need for a simulator stems from not only the lack of uniform data sources but also the lack of access to railway reservation bookings data.

2.4.6 Formulation of domain specific algorithms

For each fraud method selected in activity mentioned above (2.4.3) the rule of detecting fraudulent activities in that scheme is formulated. A search is conducted for available tools such as data mining toolboxes provided in MATLAB or the machine learning/data mining software (WEKA) .These tools can provide detection methods that can be applied to extract the targeted pattern from the records. If no appropriate available tools were found, then database queries will be implemented by the author. By analyzing the filtered

transactions, a domain specific rule based algorithm will be designed for finding abnormal transactions at this step.

2.4.7 Testing

Perform the tests for the developed mechanism on the appropriate datasets and analyse the results. This step includes performance evaluation for the used methods.

3. Scope And Limitation

Data mining concepts and techniques can help in solving many problems. This paper suggests that data mining should be studied and applied in railway management; however, it only investigates the application of a set of techniques that are used for fraud detection. Furthermore, it is not the purpose to compare and evaluate performance and efficiency of different algorithms; the main goal is to evaluate the usability and the efficiency of data mining algorithm in the context of the pattern discovery. The reason of this scoping of the current work is because it is pioneering work and more focused on addressing the problem and the solutions while efficiency can be developed later. One of the major limitations of this study is the lack of real datasets. As data is a major factor in the success of achieving the objectives, the existence of real datasets would have helped substantially in the progress of the research. A property transactions data simulator was developed to overcome the lack of data availability. While this simulator has advantages, it has some limitations and creates a finer scope for the type of data to be worked with.

References

- [1] Junjie Wu, Shiwei Zhu, Hui Xiong, Jian Chen, and Jianming Zhu, "Adapting the Right Measures for Pattern Discovery: A Unified View", IEEE Trans. On Systems, Man and Cybernetics-Part B, Vol.42, No.4, Aug 2012.
- [2] Ning Zhong, Yuefeng Li, and Sheng-Tang Wu, "Effective Pattern Discovery for Text Mining", IEEE Trans. Knowledge Data Eng., Vol. 24, No. 1, Jan 2012.
- [3] Mehmet Koyuturk, Ananth Grama, and Naren Ramakrishnan, "Compression, Clustering, and Pattern Discovery in Very High-Dimensional Discrete-Attribute Data Sets", IEEE Trans. Knowledge Data Eng., VOL. 17, NO. 4, APRIL 2005.
- [4] Dongsong Zhang and Lina Zhou, "Discovering Golden Nuggets: Data Mining in Financial Application" IEEE Trans. On Systems, Man and Cybernetics-Part C: Application and Reviews, vol. 34, no. 4, Nov 2004.
- [5] Kovalerchuk, B., Vityaev, E., "Detecting patterns of fraudulent behavior in forensic accounting", In Proc. of the Seventh International Conference "Knowledge-based Intelligent Information and Engineering on Systems", Oxford, UK, part 1, pp. 502-509, Sept, 2003.
- [6] Andrew K. C. Wong, Senior Member, IEEE, and Yang Wang, Member, IEEE, "Pattern Discovery: A data driven approach to decision support", IEEE Trans. On Systems, Man and Cybernetics-Part C: Application and Reviews, vol. 33, no. 1, Feb 2003.
- [7] T. Chau and A. K. C. Wong, "Pattern discovery by residual analysis and recursive partitioning," IEEE Trans. Knowledge Data Eng., vol. 11, pp.833-852, Nov./Dec. 1999.
- [8] Nitin Jindal, Bing Liu, Ee-Peng Lim, "Finding Unusual Review Patterns Using Unexpected Rules".
- [9] Weng-Keen Wong, Andrew Moore, Gregory Cooper, and Michael Wagner, "Rule-Based Anomaly Pattern Detection for Detecting Disease Outbreaks".
- [10] Kaustav Das, Jeff Schneider, Daniel B. Neill, "Anomaly Pattern Detection in Categorical Datasets".
- [11] Kaustav Das, Jeff Schneider, "Detecting Anomalous Records in Categorical Datasets".
- [12] Jia Wu and Jongwoo Park, "Intelligent Agents and Fraud Detection".
- [13] Margaret H. Dunham, Data mining: Introductory and advanced topics, Dorling Kindersley (India) Pvt. Ltd., Pearson, 2006.
- [14] Jiawei Han, Micheline Kamber, Data mining: Concepts and Techniques, M Morgan Kaufmann, 2005.

Effective Service Security Schemes In Cloud Computing

¹K.Sravani, ²K.L.A.Nivedita

^{1,2}Assistant Professor Department of CSE Swarna Bharathi College of Engineering
Khammam, Andhra Pradesh

Abstract

The cloud computing is the fastest growing concept in IT industry. The IT companies have realized that the cloud computing is going to be the hottest topic in the field of IT. Cloud Computing reduces cost by sharing computing and storage resources, merged with an on demand provisioning mechanism relying on a pay-per use business model. Due to varied degree of security features and management schemes within the cloud entities security in the cloud is challenging. Security issues ranging from system misconfiguration, lack of proper updates, or unwise user behaviour from remote data storage that can expose user's private data and information to unwanted access can plague a Cloud Computing. The intent of this paper is to investigate the security related issues and challenges in Cloud computing environment. We also proposed a security scheme for protecting services keeping in view the issues and challenges faced by cloud computing.

Keywords— Cloud Computing, Data Protection, Security, Application Program Interface, Average Revenue Per user.

1. Introduction

The basic principle of cloud computing is to make the computing be assigned in a large number of computers, rather than local computer or remote server. The cloud computing is extension of grid computing, distributed computing and parallel computing [3]. In cloud computing the recourses are shared via internet. Cloud computing provides the fast, quick and convenient data storage and other computing services via internet. The cloud computing system is like your virtual computer that is a virtual location of your resources. The user can access their resources those are placed on a cloud as on their real system resources. The user can install applications, store data etc. and can access through internet anywhere. The user do not need to buy or install any hardware to upgrade his machine. They can do it via internet. In future we may need only notebook PC or a mobile phone to access our powerful computer and our resources anywhere. Security aspects of cloud computing are gaining interests of researchers as there are still numerous unresolved issues which needed to be addressed before large scale exploitation take place. Cloud computing is not something that suddenly appeared overnight; in some form it may trace back to a time when computer systems remotely time -shared computing resources and applications. More currently though, cloud computing refers to the many different types of services and applications being delivered in the internet cloud, and the fact that, in many cases, the devices used to access these services and applications do not require any special applications [2].



Figure1: The Cloud

The basic idea of cloud computing is that it describes a new supplement, consumption, and delivery model for IT services based on Internet protocols, and it typically involves provisioning of dynamically scalable and often virtualized resources. The attractive feature of Cloud computing is that it has made access to computing resources a lot easier, but with that convenience has come a whole new universe of threats and vulnerabilities. In this paper, we explore the security issues and challenges for next generation CC and discuss the crucial parameters that require extensive investigations. Basically the major challenge for employing any efficient security scheme in CC is created by taking some of the important characteristics into considerations such as Shared Infrastructure, Dynamic Provisioning, Network Access and Managed Metering.

2. Cloud Computing Security Issues

Security issues are the most concerned challenges in cloud computing [3]. Cloud is expected to offer the capabilities like encryption strategies to ensure safe data storage environment, strict access control, secure and stable backup of user data. However, cloud allows users to achieve the power of computing which beats their own physical domain. It leads to many security problems. We will discuss the major security concerns in the following:

2.1. Identification and Authentication:

The multi tenancy in cloud computing allows a single instance of the software to be accessed by more than one users [3]. This will cause identification and authentication problem because different users use different tokens and protocols, that may cause interpretability problems.

2.2. Access control:

Confidential data can be illegally accessed due to lenient access control. If adequate security mechanisms are not applied then unauthorized access may exist. As data exists for a long time in a cloud, the higher the risk of illegal access [3].

2.3. Data Seizure:

The company providing service may violate the law. There is a risk of data seizure by the some foreign government.

2.4. Encryption/ Decryption:

There is an issue of the Encryption/ Decryption key that are provided. The keys should be provided by the customer itself.

2.5. Policy Integration: Different cloud servers can use different tools to ensure the security of client data. So integration policy is one of the major concerns of security.

2.6. Audit: In cloud computing the Cloud Service Provider (CSP) controls the data being processed. CSP may use data while being processed [3]. So the process must be audited. The all user activities must be traceable. The amount of data in Cloud Computing may be very large. So it is not possible to audit everything.

2.7. Availability: Availability is the major concern in the cloud computing. When the client data is virtualized, clients have no control on the physical data [3]. If in the cloud, the data or service is not available, it is rigid to fetch the data.

2.8 Network Consideration

Cloud computing is a technique of resource sharing where servers and storage in multiple locations are connected by networks to create a pool of resources. When applications are run, resources are allocated from this pool and connected to the user as needed. The missions of connecting the resources (servers and storage) into a resource pool and then connecting users to the correct resources create the network's mission in cloud computing. For many cloud computing applications, network performance will be the key to cloud computing performance.

2.9. Virtualization Paradigm

In order to process a user request in CC environment, a service provider can draw the necessary resources on demand, perform a specific job and then relinquish the unneeded resources and often dispose them after the job is done. Contrary to traditional computing paradigms, in a cloud computing environment, data and the application is controlled by the service provider. This leads to a natural concern about data safety and also its protection from internal as well as external threats. Usually, in a cloud computing paradigm, data storage and computation are performed in a single data enter that may led to the development of various security related failure.

2.10. Mapping machines

Cloud computing offers a means to decouple the application activities from the physical resources required. This has enabled consolidation of multiple applications onto a lesser number of physical servers resulting in an increase in server utilization. Such decoupling of resources is facilitated by the concept of a virtual machine which encapsulates an application with a specific set of functionalities. Physical resources are made available to the virtual machine by a guest operating system running on each physical machine. The virtual machine runs over this guest operating system which also provides facilities for creation, destruction and migration of virtual machines. The different security parameters are required to facilitate these functions in cloud computing.

2.11 Secure Data Management

As data is an important tool of CC the some aspects of the secure cloud, namely aspects of the cloud storage and data layers. In particular the security issues ranging from ways of efficiently store the data in foreign machines to querying encrypted data, as much of the data on the cloud may be encrypted is a critical challenge for implementing security schemes in Cloud Computing [8].

2.12 Resource Allocation

With the cloud model, we lose control over physical security. In a public cloud, we are sharing computing resources with other companies. In a shared pool outside the enterprise, we don't have any knowledge or control of where the resources run. Exposing our data in an environment shared with other companies could give the government "reasonable cause" to seize your assets because another company has violated the law. Simply because we share the environment in the cloud, may put your data at risk of seizure. Storage services provided by one cloud vendor may be incompatible with another vendor's services should decide to move from one to the other. Thus to secure the resources in a cloud demand highly encrypted schemes.

3. Challenges Of Security Schemes

Cloud Computing represents one of the most significant shifts in information technology many of us are likely to see in our lifetimes. Basically the major challenge for employing any efficient security scheme in CC is created by the tasks expected from the clouds. Security schemes look like a defense tool which every organization needs. However there are some challenges the organizations face while deploying a security system in Cloud computing. Some of them are:

3.1 Abuse and Nefarious Use of Cloud Computing

Providers offer their customers the illusion of unlimited computer, network, and storage capacity often coupled with a friction less registration process where anyone with a valid credit card can register and immediately begin using cloud services. Some providers even offer free limited trial periods. By abusing the relative anonymity behind these registration and usage models, spammers, malicious code authors, and other criminals have been able to conduct their activities with relative impunity.

3.2 Insecure Interfaces and APIs

Cloud computing providers expose a set of software interfaces or APIs that customers use to manage and interact with cloud services. Provisioning, management, orchestration, and monitoring are all performed using these interfaces. The security and availability of general cloud services is dependent upon the security of these basic APIs. From authentication and access control to encryption and activity monitoring, these interfaces must be designed to protect against both accidental and malicious attempts to circumvent policy. Furthermore, organizations and third parties often build upon these interfaces to offer value-added services to their customers. This introduces the complexity of the new layered API; it also increases risk, as organizations may be required to relinquish their credentials to third parties in order to enable their agency.

3.3 Malicious Insiders

Another important challenge regarding implementing security schemes is the threat of a malicious insider. This threat is amplified for consumers of cloud services by the convergence of IT services and customers under a single management domain, combined with a general lack of transparency into provider process and procedure. For example, a provider may not reveal how it grants employees access to physical and virtual assets, how it monitors these employees, or how it analyzes and reports on policy compliance (e.g. [7], [1]). To complicate matters, there is often little or no visibility into the hiring standards and practices for cloud employees. This kind of situation clearly creates an attractive opportunity for an adversary — ranging from the hobbyist hacker, to organized crime, to corporate espionage, or even nation-state sponsored intrusion. The level of access granted could enable such an adversary to harvest confidential data or gain complete control over the cloud services with little or no risk of detection.

3.4 Shared Technology Issues

Vendors deliver their services in a scalable way by sharing infrastructure. Often, the underlying components that make up this infrastructure (e.g., CPU caches, GPUs, etc.) were not designed to offer strong isolation properties for a multi-tenant architecture. To address this gap, a virtualization hypervisor mediates access between guest operating systems and the physical compute resources. Still, even hypervisors have exhibited flaws that have enabled guest operating systems to gain inappropriate levels of control or influence on the underlying platform. A defence in depth strategy is recommended, and should include compute, storage, and network security enforcement and monitoring. Strong compartmentalization should be employed to ensure that individual customers do not impact the operations of other tenants running on the same cloud provider. Customers should not have access to any other tenant's actual or residual data, network traffic etc.

3.5 Data Loss or Leakage

There are many ways to compromise data. Deletion or alteration of records without a backup of the original content is an obvious example [6]. Unlinking a record from a larger context may render it unrecoverable, as can storage on unreliable media. Loss of an encoding key may result in effective destruction. Finally, unauthorized parties must be prevented from gaining access to sensitive data. The threat of data compromise increases in the cloud, due to the number of and interactions between risks and challenges which are either unique to cloud, or more dangerous because of the architectural or operational characteristics of the cloud environment.

4. PROPOSED SECURITY FRAMEWORK

In the recent years, CC security has been able to attract the attentions of a no. of researchers around the world [4]. In this section we proposed a security scheme taking regarding issues and challenges keeping in mind. Our aim is to design and develop a security proposal that would be accurate, secure data in shared pool, secure for unexpected intrusions, adaptive and be of real time. The proposed secure model provides the security of cloud services by the following ways:

4.1 Secure Cloud service

The cloud service providers with the highest margins, highest ARPU, lowest operating costs, and lowest churn will have a significant competitive advantage in the long run. To achieve this advantage, they will need a comprehensive cloud service delivery platform and the cost of developing such a platform with security parameter is a factor they will need to take into account. Not all cloud service providers are the same. While some are giants with multiple data centers worldwide, some, in particular niche service providers. That is not all bad computing still is their business, which means they invest all their operating and capital budgets in IT operations. And even the largest providers are not immune to security problems as the hacking of the Sony network and the major crash of Amazon's infrastructures- a-service installation demonstrated. The security of service provider managed by:

- Check out its security staff.
- Ask where its data centres are, how many it has, and what its security parameters and proposals are.
- Separating the company data from company operations has many security advantages.
- Stricter initial registration and validation processes for customers.
- To enhanced credit card fraud monitoring and coordination.
- Comprehensive introspection of customer network traffic.
- Monitoring public blacklists for one's own network blocks.

4.2 Secure Web Platform

Cloud platform services deliver a computing platform and solution stack as a service often consuming cloud applications [5]. It facilitates deployment of applications without the cost and complexity of buying and managing the underlying hardware and software layers. The security of the web platform is to securing all content and data traffic - including email, web and identity traffic - moving between an organization and the Cloud. Some schemes that protect the data and its travels within or outside the organization to the Cloud are:

- i. Analyze the security model of cloud provider interfaces.
- ii. Ensure strong authentication and access controls in concert with encrypted transmission.
- iii. Understand the dependency chain associated with the API.

4.3 Secure Cloud Infrastructure

Cloud infrastructure is a platform which holds the development environments and within it one would find managed hosting environment where various applications are built. To secure this Using a secure password management service that protects user ID and password data and can flag users that repeat passwords across various systems. For secure cloud Infrastructure we have used:

- LDAP controls and administering credentials that keep access information from being scattered around.
- Running scripts to remove access when employees leave the organization are also proposed for identity management security.
- Determine security breach notification processes.
- Monitor environment for unauthorized changes/activity.
- Promote strong authentication and access control for administrative access and operations [3].
- Conduct vulnerability scanning and configuration audits.

4.4 Secure Cloud Data Pool

- When enterprises adopt cloud computing and deploy databases in virtual environments, they run the risk of exposing highly-sensitive data to a broad base of internal and external attacks [3]. Here, we enlist strategies to help enterprises protect their data when implementing a database security strategy in cloud or virtualized environments.
- Multi-tenancy: To be used for single backup system to protect multiple business units or customers and to allocate resources to them dynamically on-demand. Therefore, every storage pool needs to be kept secure and fully independent from the others.
- Chargeback systems: For data protection resources allocated by end-user needs, storage providers need to track this usage by a wide range of criteria for both chargeback and billing purposes and for infrastructure optimization purposes.
- Robust Reporting: CC environment need an accurate way to forecast their capacity and processing needs for budgeting purposes. It also needs to analyze usage to optimize available system resources for better efficiencies. Thus detailed reporting and analytics not only helps in managing the current environment but also enables trending and modelling for planning future investments.
- Quality of Service delivery: Storage pooling enables CC environment to set replication priorities for each pool so that the most mission critical data is replicated before less important data. This QoS orientation can be set to specific backup policies with different retention periods for a particular storage pool.
- Storage Tiering: Storage tiering is the mechanism to allocate disk drives to a storage pool according to the capacity or performance requirements for a specific set of data under protection.
- Global Deduplication: De duplication is a critical part of an effective data protection environment. It is not only necessary for cost-effective optimization of the overall storage capacity but also provides a cost effective WAN implementation for replication and movement of data to a remote location for disaster recovery.

5. Conclusion

The proposed secure model has to ensure security of each service by applying the various security schemes on each cloud architectural component. While most of the risk against security in Cloud computing are caused by the involvement of computing in different plate forms. For defending the threats, developing the secure system that will be efficient is a great research challenge. Again, ensuring each component secure is a major research issue. Many of today's security schemes based on specific component mode but there is a lack of combined effort to take a common model to ensure security of each architectural component, in future though the security mechanism become well - established for each individual component, combining all the mechanism together for making them work in collaboration with each other will incur a hard research challenge.

References

- [1] P.F. da Silva and C.B. Westphall, "Improvements in the Model for Interoperability of Intrusion Detection Responses Compatible with the IDWG Model" *Int'l J. Network Management*, vol. 17, no. 4, 2011, pp. 287–294.
- [2] Chunye Gong, Jie Liu, Qiang Zhang, Haitao Chen and Zhenghu Gong, "Characteristics of cloud computing", 39th International Conference on Parallel Processing Workshops, 2012
- [3] Ziyuan Wang, "Security and privacy issues within the Cloud Computing", International Conference on Computational and Information Sciences, 2011
- [4] Shuai Zhang, Shufen Zhang, Xuebin Chen and Xiuzhen Huo, "The Comparison Between Cloud Computing and Grid Computing", International Conference on Computer Application and System Modeling (ICCASM 2010), 2010
- [5] Siani Pearson and Azzedine Benameur, "Privacy, Security and Trust Issues Arising from Cloud Computing", 2nd IEEE International Conference on Cloud Computing Technology and Science
- [6] Zhidong Shen and Qiang Tong, "The Security of Cloud Computing System enabled by Trusted Computing Technology", 2nd International Conference on Signal Processing Systems (ICSPS), 2010
- [7] Shuai Zhang, Shufen Zhang, Xuebin Chen and Xiuzhen Huo, "Cloud Computing Research and Development Trend", Second International Conference on Future Networks, 2010
- [8] D. Nurmi, R. Wolski, C. Grzegorzczak, G. Obertelli, S. Soman, L. Youseff, and D. Zagorodnov, "The Eucalyptus open source cloud-computing system" in *Proceedings of the 9th IEEE/ACM International Symposium on Cluster Computing and the Grid (CCGRID 09)*, May 2011, pp. 124–131.
- [9] Q. Wang, K. Ren, W. Lou, and Y. Zhang, "Dependable and Secure Sensor Data Storage with Dynamic Integrity Assurance" *Proc. of IEEE INFOCOM*, 2010.
- [10] T. Ristenpart, E. Tromer, H. Shacham, and S. Savage, "Hey, you, get off of my cloud: exploring information leakage in third-party compute clouds," in *CCS 09: Proceedings of the 16th ACM conference on Computer and communications security*. New York, NY, USA: ACM, 2011, pp. 199–212.
- [11] K. Hamlin, M. Kantarcioglu, L. Khan and B. Thuraisingham "Security Issues for Cloud Computing" *Journal of Information Security and Privacy*, vol. 4, no. 2, pp. 39–51, April-June 2010.

Development of Robotic Automated Storage and Retrieval System (AS/RS)

¹**Smita U.Chakole**

¹Mtech student, Mechanical Department Yeshwantrao Chavan College of Engineering, Hingna Road, Wanadongri, Nagpur-441110(India)

Abstract

The automated storage and retrieval systems (AS/RS) are major material handling support systems that are commonly used in the automated factories, distribution centers, warehousing, and non manufacturing environments. Their applications vary widely from a simple storage and retrieval system for small parts to central systems where production, assembly, and manufacturing operations are concentrically located around them. This paper summarizes the literature study of a Robotic automated storage and retrieval system and development of a dedicated automated storage and retrieval system for YCCE Flexible manufacturing system laboratory. The prototype model of automated storage and retrieval system developed consist of the control hardware and software communicating over a field bus network. This also includes study of literature for types of automated storage and retrieval system, study of literature for suitable environment for automated storage and retrieval system, order processing for automated storage and retrieval system. This study of automated storage and retrieval system and the physical model of automated storage and retrieval system will ensure better understanding of automated storage and retrieval system for student. The development of physical prototype is highly beneficial to acquisition of tactic knowledge and greatly benefits the development of students by understanding the automated storage and retrieval system. This model will contribute to the ongoing development of dedicated FMS. And this prototype model for AS/RS will be the foot step ahead to achieve the goal.

Keywords :AS/RS, Dwell point analysis, FEM, Network system, Robotic

1. Introduction

An automated storage/retrieval system (AS/RS) can be defined as a storage system under which a defined degree of automation is to be implemented to ensure precision accuracy and speed in performing storage and retrieval operations. This dedicated robotic automated storage and retrieval system will be foot step ahead to contribute to flexible manufacturing system. Development of integrated manufacturing environment has been going on in YCCE mechanical engineering department from last few batches of PG projects. The continuous efforts are going on towards the flexible manufacturing system for mechanical department FMS laboratory he term flexible manufacturing cell is commonly used to refer to machine grouping that consists of either manually operated or automated material handling, and it may or may not be computer controlled. The term flexible manufacturing system generally means a fully automated system consisting of automated workstations, automated material handling and computer control. Storage is an essential function in an automation system. The material storage system allows materials to be stocked for a specified period of time, before they are re-introduced, or are introduced for the first time, into the automation system. The sorts of stored material are related to the product (e.g. raw materials, purchased parts, work-in-process, finished products, and scrap and rework), the process (e.g. process refuse, such as process waste products; and tooling), and the overall support functions in the factory (e.g. maintenance spare parts, office supplies, and plant records). Each of these material types is typically stored under different conditions and controls. Robotic AS/RS is designed to pick and palletize goods onto a mixed pallet which allow retrieving orders in a ready to ship sequence. Robots have frequently been used to palletize these specialized loads. The first Robotic ASRS system has been developed by Bastian in the world which helps to create store ready pallet.

2. Literature Review

Jeroen P Vanden Berg explains Analytical expression for the optimal dwell point in an AS/RS” he was concentrates on deciding the dwell point in an AS/RS, to minimize the expected travel time to the position of next operation. Report that on the basis of a simulation study the nearest-neighbor rule gives the best results for selecting an open location within the storage area for randomized storage or within a class-region for class-based storage. When an incoming load cannot be stored within its dedicated region it is better to assign it to a location further away from the input and output station, than to a location that is nearer than its dedicated region. The latter is likely to fill up the storage space for fast moving products, which may result in increased mean travel times. They also considered three criteria when evaluating good due date performance; mean response

time, maximum response time or the number of late requests and report that these criteria were satisfied better when using a FCFS sequence for the retrievals than by applying specific urgency rules (giving priority to retrievals with long waiting times). Hausman et al (1976) deal with optimal storage assignment. Results are obtained which compare the operating performance of three storage assignment rules: random assignment, which is similar to the closest-open-location rule used by many currently operating systems; full turnover-based assignment; and class-based turnover assignment. It is shown that significant reductions in crane travel time (and distance) are obtainable from class-based turnover-based rules rather than closest-open-location (essentially random) policies. These improvements can, under certain circumstances, be directly translated into increased throughput capacity for existing systems and may be used to alter the design (e.g. size and number of racks, speed of cranes, etc.) of proposed systems in order to achieve a more desirable system balance between throughput and storage capacity. According to Moon & Kim (2001) were explain shuffling or relocations are helpful to maintain stable throughputs with all the three types of ASRS operation policies (random, 2 class-based and 3-class-based). They are also helpful to avoid losses caused by crane travel distance increase and lack of storage with a system under unstable production plans. Relocation does not cause any crane operation problems since the time to re-locate items in an ASRS is too minor to affect the crane utilization. With class-based storage policies, better throughputs and lower rack and crane utilizations are achieved. An applicable operation policy can be selected based on the production plan variation, or a necessary variation point for relocation to the current policy can be determined using the simulation results. Bozer & White (1990) have developed travel-time models for ASRS machines. The S/R machine is taken to travel simultaneously horizontally and vertically as it moves along a storage aisle. For randomized storage conditions expected travel times are determined for both single and dual command cycles. Alternative input/output locations are considered and various dwell-point strategies for the storage/retrieval machine are examined.

3. Concepts

The objective of this project is to develop a dedicated prototype model of Robotic automated storage and retrieval system to facilitate study of automated storage and retrieval system for students in flexible manufacturing system laboratory. And will be the test bed for the ongoing project for the extension for FMS laboratory with ongoing projects in PG CAD/CAM course. And will allow for analysis of control strategies for knowledge acquisition, knowledge development, knowledge extension, knowledge spiraling. As the lab model are also available in the market, but they are available in standard sizes. Standard controllers they are using which are very costly. They mostly use pneumatic controllers. As they are using pneumatic controllers the maintenance is high due to leakages. These will be avoided as we are generating fully mechanical controls. And it is drafted and designed according to FMS lab layout and the sizes of the work parts that will be processed on the CNC machine tools available with YCCE FMS lab.

3.1 FLEXIBLE MANUFACTURING SYSTEM

The term flexible manufacturing cell is commonly used to refer to machine grouping that consists of either manually operated or automated material handling, and it may or may not be computer controlled. The term flexible manufacturing system generally means a fully automated system consisting of automated workstations, automated material handling and computer control. In contrast to this defines a FMS as an automated computer controlled cell and a FMC with the addition of automated storage and the retrieval as FMS. The four basic elements of any FMS are

Robot

Workstations,

Material transport and storage system,

Computer controlled system.

3.2 AUTOMATED STORAGE AND RETRIEVAL SYSTEM

Storage is an essential function in an automation system. The material storage system allows materials to be stocked for a specified period of time, before they are re-introduced, or are introduced for the first time, into the automation system. The sorts of stored material are related to the product (e.g. raw materials, purchased parts, work-in-process, finished products, and scrap and rework), the process (e.g. process refuse, such as process waste products; and tooling), and the overall support functions in the factory (e.g. maintenance spare parts, office supplies, and plant records). Each of these material types is typically stored under different conditions and controls.

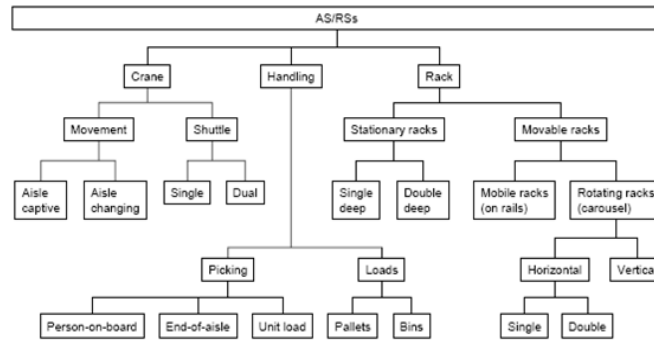


Figure 1:- different types for automated storage and retrieval system

3.3 Layout Development for robotic AS/RS system

The objective of this project is to develop a dedicated prototype model of robotic automated storage and retrieval system to facilitate study of automated storage and retrieval system in flexible manufacturing system laboratory.

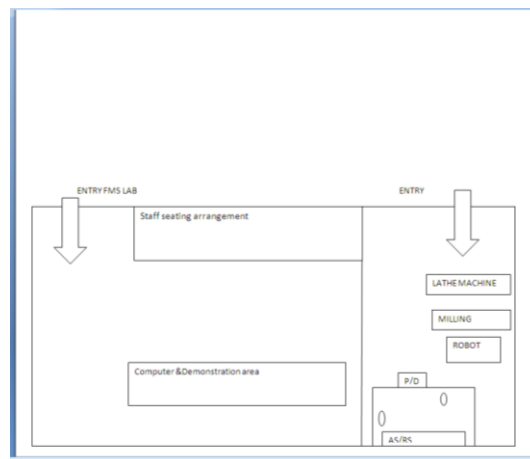


Fig:-2 block dig. For FMS lab layout

This work done concentrates on development of robotic automated storage and retrieval system. The components for robotic automated storage and retrieval system are storage structure, automated storage and retrieval machine i.e. robot and pick and deposit station. The system is grid following system means robot is follow the grid system and decided its path by which it can travel the minimum distance. This system consists of IR sensor system and use the interfacing for remote control. System receives the unit load part from Lathe and milling machine which are present in the FMS lab. Then sensor provided all this information to the robots then robot check the two conditions i.e. load/unload means robot is already with work part or ready to accept the work part from pick and drop station. Second condition is that it check the nearest one condition means those Robot is near from pick and drop station or rack that robot performs storage and retrieval according to the requirements.

Controller should be checking the two conditions and then decided which perform the given task.

- 1) Load/unload condition
- 2) Nearest one condition

Dimension of layout 3' * 4'

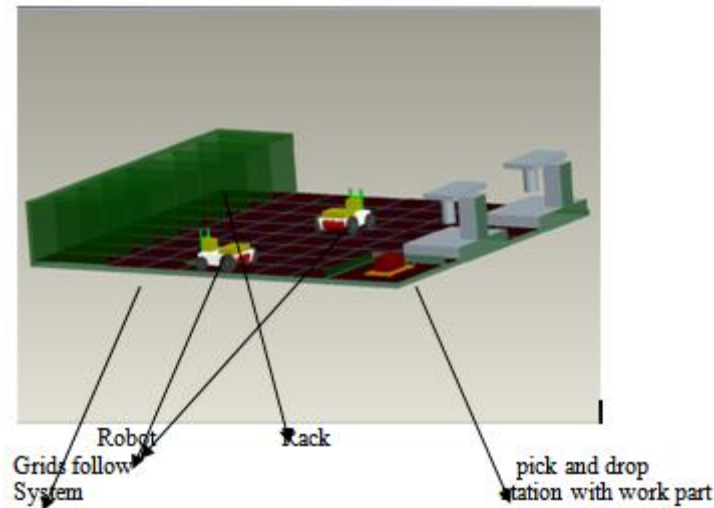


Fig 3:- layout of the robotic AS/RS system

3.4 Robotic AS/RS Rack structure

The total storage capacity of one storage aisle depends on how many storage compartments are arranged horizontally and vertically in the aisle. There are one row and six columns are present with the single rack. total length of rack is 3'

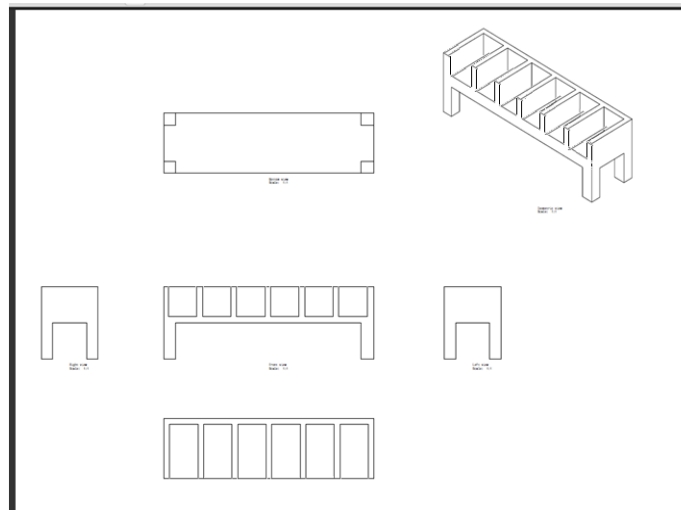


Fig 4:-Rack structure

3.5 Robot with Fork Lift Mechanism

In this system two robots will be used with fork lift mechanism. Most of us probably have a general idea of what a forklift is, but there are a number of different classifications, power sources, sizes, uses and new technologies that make up these useful machines. Some are used on rugged construction sites and lift heavy materials and equipment while other forklifts drive themselves inside modernized warehouses. Whether indoors or out, forklifts are a necessary tool in most warehouses and an integral part of our industries. Forklifts might seem more industrial than inventive, but consider that they're typically the size of a small car yet they can lift loads that are thousands of pounds, often several stories into the air, all without tipping over. These machines work long hours each day lifting and moving heavy loads to keep our manufacturing, automotive, aerospace and other industries humming along. Forklifts have been around for nearly 100 years and they continue to make our jobs more efficient just as much as they did when they were invented. Whether they're forklifts that use batteries, liquid propane, hydrogen fuel cells or another power source, without these machines we wouldn't be able to build ship or move manufactured goods efficiently.

3.6 Function

A forklift has two forks that are located on the front of the machine. These two forks only move up and down, but they can also tilt upward and downward. The operator controls these movements, and uses a Battery system to move the forks. The battery system applies pressure to a bar with rolling chains that is located in the forklift. Forklifts can get their power from many different sources, including electricity, gasoline, diesel or propane. In this system it shall get power from battery. Height of fork lift =15 cm.

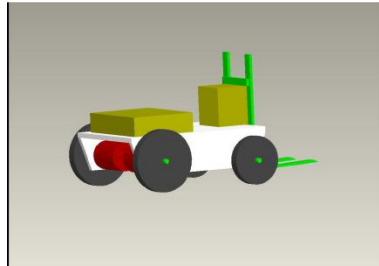


Fig 5: - Robot with fork lift mechanism

Dimensions for unit load

Dimension of unit load 100*100*10 mm and weight one kg

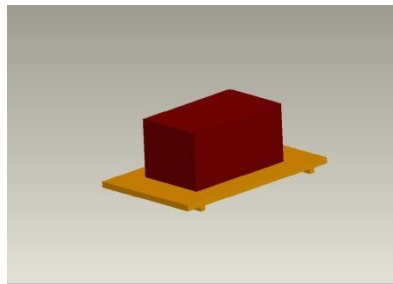


Fig 6:-unit load

4. Conclusion:-

Automated storage and retrieval system (AS/RS) is complex in design and fabrication which needs exclusive study of transmitting devices, motors to control movements of the various axes, positioning techniques and feedback control system, power circuitry, behavior of electronics devices it support first user microcontroller system. Automated storage and retrieval system development is divide in layers i.e. fabrication of the mechanical components and their assembly, the electrical circuitry, the electronic circuitry, microcontroller programming and interfacing.

References

- [1] JEROEN P. VAN DEN BERG and A. J. R. M. (NOUD) GADEMANN "Simulation study of an automated storage/retrieval system" int. j. prod. res., 2000, vol. 38, no.6, 1339± 1356
- [2] Min S. KO G.N. Wang and Hye S. Shin Sang C. Park Dept. of Industrial Engineering Paldalgwan-822, Ajou University Paldalgwan-822, Suwon, 443-749, SOUTH KOREA" Machine control level simulation of an AS/RS in the automotive industry" Proceedings of the 2010 Winter Simulation Conference B. Johansson, S. Jain, J. Montoya-Torres, J. Hagan, and E. Yücesan, eds
- [3] Chuanyu CHEN Shell-Ying HUANG Wen-Jing HSU and Ah Cheong TOH CheeKit LOH "Platform-based AS/RS for Container Storage" Center for Advanced Information Systems, *Robotics & Automation* Taipei, Taiwan, September 14-19, 2003
- [4] JEROEN P VANDEN BERG "Analytical expression for the optimal dwell point in an AS/RS" International journal production economics 76(2002) 13-25
- [5] http://www.bastiansolutions.com/automation/automated-storage-and-retrieval-system/robotic_asrs.asp#ixzz239DeIYfs
- [6] Tamio Arai, Enrico Pagello, Lynne E. Parker, "Editorial: Advances in Multi-Robot Systems" IEEE Transaction on Robotics and automation, VOL. 18, NO. 5, OCTOBER 2002: 655-661
- [7] B. Park, "optimal dwell point policies for automated storage/retrieval system with dedicated storage ", IIE Trans, vol. 31, 1999, pp 1011-1013.

Theoretical Investigation/Research On Binding Energy Of A Donor In A Spherical Quantum Dot At Various Locations On It

S.R.Chitra.,

M.Sc., M.Phil., PGDCA.,[Ph.D].,

[working as Lecturer in Physics, @ N.P.R College in Natham, Dindigul Dt and doing Ph.D., at Anna University , Thiruchirappalli ,Tamil Nadu in India]

Abstract

The binding energy of a donor in spherical quantum dots (QDs) is calculated, using a variational approach within the effective mass approximation. The binding energy is computed for GaAs QD as a function of the dot size for different impurity positions, and also as a function of the impurity position for different dot sizes. The results of mine show that when the impurity binding energy increases with the reduction in the dot dimension. The binding energy is also found to depend on the location of the impurity, and the same is the maximum for the on-center impurity. Also I found that the value of the polarizability obtained is several orders higher than the hydrogen atom value.

Keywords: Spherical quantum dot, Donor binding energy, Impurity state, Parabolic confinement Quantum dots , quantum wells [gallium arsenide](#), [III-V semiconductors](#), [impurity states](#), [effective mass](#), donor Binding , [Semiconductor compounds](#)

PACS 73.20.Dx , 73.20.Hb , [73.21.La](#) , [73.21.-b](#) , [73.61.Ey](#) , [73.20.Hb](#) , [71.18.+y](#), 71.38.+I , 71.20.Nr

1. Introduction.

The work on the binding energy of a donor atom within an infinite potential well initiated several studies on the impurity states in quantum wells. Similar studies have also been extended for structures with lower dimensionality, such as quantum-well wires (QWWs) and quantum dots (QDs). The study of low – dimensional systems has received much attention in recent years , especially due to the discovery of such effects as the quantum Hall Effect in two – dimensional (2D) systems. The physics or even lower – dimensional systems present intriguing challenges both theoretically and experimentally. With the development of modern technology, it is now possible to produce (Quasi-) 0D systems that confine electrons in all three spatial dimensions. In this communication, we shall study the effect of polarizability and the binding energy of donor in a spherical QD of a wide gap material; the derived results will be computed for GaAs QD. The binding energy will be computed as a function of the dot dimension for different impurity positions, and also as a function of the impurity position for different dot sizes.

2. Theory

In the effective mass approximation, the Hamiltonian of a single hydrogenic impurity in a spherical QD with parabolic confinement can be written as

$$H = [P^2/2m^*] + 1/2 [m^* \omega^2 r^2] - e^2 / \epsilon |r-r_i|$$

Where e and m^* are, respectively, the electronic charge and effective mass, P is a momentum, ω is a characteristic frequency, ϵ is the dielectric constant of the dot material, and r_i gives the location of the impurity with respect to the center of the dot. In order to calculate the ground state of the impurity binding energy, the variational technique is used, and for this the trial wave function is taken as

$$\psi(r) = N(\lambda) \exp(-\beta r^2/2) \exp(-\lambda |r-r_i|) ,$$

Where $\beta = m^* \omega / \hbar / 2\pi$.

Here \hbar being the Planck's constant. λ is the variational parameter and $N(\lambda)$ is the normalization constant. The ground state energy of the hydrogenic impurity is worked out from the above equations by using the below relation.

$$E(\lambda, \beta, r_i) = \langle \psi^* / H / \psi \rangle / \langle \psi^* / \psi \rangle$$

Here ψ^* means the conjugate of the eigen function ψ .

Our work consists of two cases.

That is, we derived the binding energy for two cases:

- (i) $r_i = 0$., ie., the location of the impurity is zero.
- (ii) $r_i = a$.r., ie., impurity at the inner surface of the dot.

Cases:

Case 1:

At $r_i = 0$, the location of the impurity is zero.

Therefore the Hamiltonian of a single hydrogenic impurity in a spherical QD with parabolic confinement can be written as

$$H = [P^2/2m] + 1/2 [m^*\omega^2 r^2] - e^2 / \epsilon|(r-r_i)|$$

The trial wave function is taken as

$$\psi(r) = N(\lambda) \exp(-\beta r^2 / 2) \exp(-\lambda|(r-r_i)|),$$

Where $\beta = m^*\omega / \hbar / 2\pi$.

Here \hbar being the Planck's constant. λ is the variational parameter and $N(\lambda)$ is the normalization constant.

Normalization condition:

$$\langle \psi^* / \psi \rangle = 1$$

By equating everything, we get

$$\int |\psi(r)|^2 [1/2 m^*\omega^2 r^2] \psi(r) d\tau = 2\pi N^2 e^2 e^{\lambda\beta} / m^* [\lambda(\sqrt{\pi}) / \beta^{3/2} - 1/2\beta]$$

This is the final solution for case (i). Then the binding energy will be,

$$\langle E \rangle = 2\pi N^2 \hbar^2 e^{\lambda\beta} / m^* \{-5(\sqrt{\pi}) / 2\beta^{1/2}\} - \dots\dots$$

By using this the binding energy was computed for GaAs QD as a function of the dot size. The results are tabulated in Table 1:

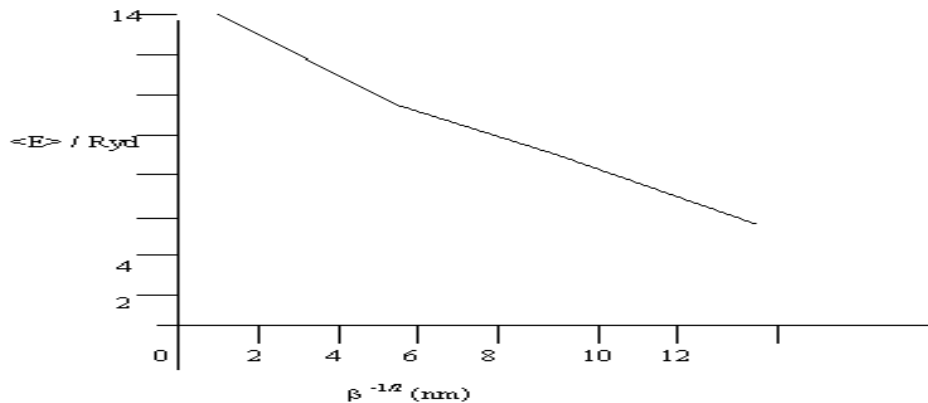
Table 1:

$\beta^{-1/2}$ (nm)	λ (cm ⁻¹)	$\langle E \rangle$ in Ryd* (Present)	$\langle E \rangle$ in Ryd* (Reference)
2	0.47*10 ⁵	13.18	13.1
4	0.46*10 ⁵	12.10	12.0
6	0.44*10 ⁵	7.93	7.4
8	0.42*10 ⁵	4.99	4.5
10	0.41*10 ⁵	3.18	3.0

*1 Ryd = 5.3 meV for GaAs

In this the present works are compared with the values of the references . Finally a graph is drawn between the impurity binding energy versus the dot size.

Graph:



For the case $r_i = 0$. From this figure it follows that the donor binding energy decreases as the dot size increases. As the size $\rightarrow \infty$, the energy should 1 Ryd.

The impurity binding energy in spherical GaAs QDs with parabolic confinement versus the dot size.

Case 2:

At $r_i = a$, the location of the impurity is at the inner surface of the dot.

Therefore the Hamiltonian of a single hydrogenic impurity in a spherical QD with parabolic confinement can be written as

$$H = [P^2/2m^*] + 1/2 [m^*\omega^2 r^2] - e^2 / \epsilon|(r-a)|$$

The trial wave function is taken as

$$\psi(r) = N(\lambda) \exp(-\beta r^2 / 2) \exp(-\lambda|(r-a)|),$$

Where $\beta = m^*\omega / \hbar / 2\pi$. Here \hbar being the Planck's constant. λ is the variational parameter and $N(\lambda)$ is the normalization constant.

Normalization condition:

$$\langle \psi^* / \psi \rangle = 1$$

By equating everything, we get

$$\int |\psi(r)|^2 [1/2 m^*\omega^2 r^2] \psi(r) d\tau = 2\pi N^2 e^2 e^{\lambda\beta} / m^* [\lambda(\sqrt{\pi}) / \beta^{3/2} - (2\lambda / \beta) + (1/2\beta) - \dots]$$

This is the final solution for case (i). Then the binding energy will be,

$$\langle E \rangle = 2\pi N^2 \hbar^2 e^{\lambda\beta} / m^* \{ 25 (\sqrt{\pi}) / 8\beta^{1/2} \} - \dots$$

By using this the binding energy was computed for GaAs QD as a function of the dot size. The results are tabulated in Table 2:

Table 2:

$\beta^{-1/2}$ (nm)	λ (cm ⁻¹)	$\langle E \rangle$ in Ryd* (Present)	$\langle E \rangle$ in Ryd* (Reference)
2	0.46*10 ⁵	12.28	12.0
4	0.45*10 ⁵	11.48	10.9
6	0.42*10 ⁵	7.10	6.9
8	0.40*10 ⁵	4.21	4.0
10	0.39*10 ⁵	3.16	3.08

*1 Ryd = 5.3 meV for Ga As

In this the present works are compared with the values of the references .

Finally a graph is drawn between the impurity binding energy versus the dot size. For the case $r_i = a$.

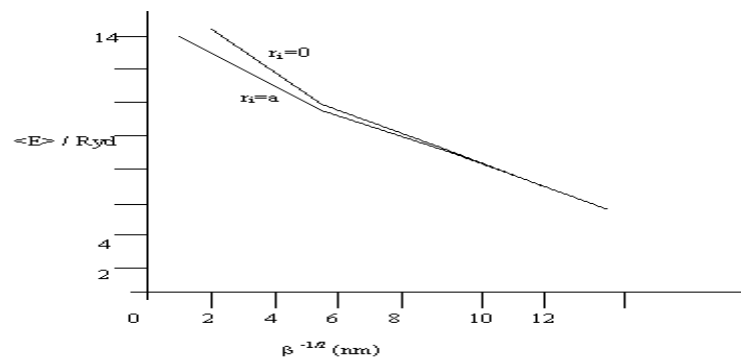
From this figure it follows that the donor binding energy decreases as the dot size increases. As the size $\rightarrow \infty$, the energy should 1 Ryd.

The impurity binding energy in spherical GaAs QDs with parabolic confinement versus the dot size.

From Table II, it follows that as in the previous case, the binding energy decreases when the dot size increases.

Comparisons of Table I & II reveals that the binding energy is larger in the case where the impurity is at the centre of the dot. The graph is drawn between the beta values and the energy values.

Graph:



The impurity binding energy in spherical GaAs QDs with parabolic confinement versus the dot size.

3. Program For Calculating Binding Energy.

```
#include <stdio.h>
#include <conio.h>
#include <math.h>
void main()
{ double int n,h,m,e,x,y,y0,y1,y2,beta,A,B,C,D,E,F,G,H,I,J,K,L,E1;
float PI;
clrscr();
PI = 3.14;
n = 1;
h = 6.626 *pow10(-27);
m = 6.097 *pow10(-29);
e = 4.8 *pow10(-10);
x = 12.5;
printf ("Enter the value of y:");
printf ("Enter the value of beta:");
scanf ("%lf",&y);
scanf ("%lf",&beta);
y0 = y*y;
y1 = y0*y;
y2 = y1*y;
A=(2*PI*n*n*exp(y0/beta)*[(h/2II)*(h/2II)] /m;
B=-5*sqrt(PI)/2*pow(beta,(1/2));
C=-(e*e*m)/(2*x*beta*(h/2II)*(h/2II));
D=7/(2*beta);
E=(e*e*m*sqrt(PI))/(x*pow(beta,(3/2))*(h/2II)*(h/2II));
F=14*sqrt(PI)/4*pow(beta,(3/2));
G=6/pow(beta,2);
H=sqrt(PI)/2*pow(beta,(5/2));
I=B+C;
J=(D-E)*y;
K=F*y0;
L=G*y1;
M=H*y2;
E1=A*(I-J+K+L-M);
printf ("%0.3f",E1);
getch();}
```

4. Polarizability With An Effect Of An Electric Field.

The donor atom in our system in an external electric field is given by,

$$H = [P^2/2m] + 1/2 [m*\omega^2 r^2] - e^2 / \epsilon |(r-r_i)| + \epsilon z$$

We use the trial wave function,

$$\psi (r) = N(\lambda) \exp(-\beta r^2 / 2) \exp(-\lambda |r-a|) (1+\alpha z)$$

where $z = r \cos \theta$. And α is treated as a variational parameter.

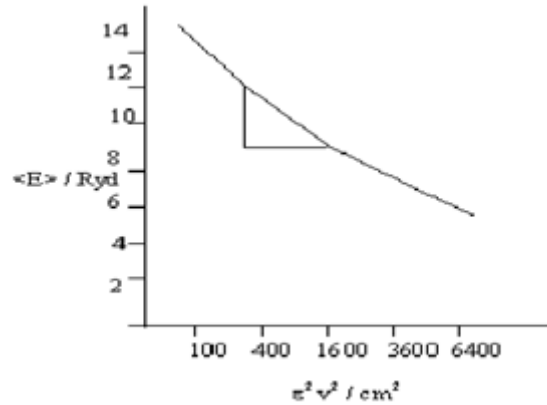
In the case of 'On- Centre' impurity ($r_i = 0$), the normalization condition yields,

$$N^2 = 1 / 4\pi e^{\lambda/\beta} \left[\left[\sqrt{\pi} / \beta^{3/2} (\dots) - \lambda / \beta [1 + (\epsilon^2 \alpha^2) / 3] + (\lambda^2 / \beta^{5/2}) (\dots) - \dots \right] \right]$$

If we put $\alpha = 0$, then we get the N^2 value for case 1. (i.e., $r_i = 0$)

I simplified this for second case also and I found out the expectation value of the Hamiltonian and also the binding energies were computed for different values of the electric fields. The results are presented in the Table 3.

Graph:



Using these datas, a graph was drawn for binding energy Vs ϵ^2 , (see in figure). The curve is linear. However for small values of ϵ , it is linear and gives the value of α_p as $0.7 * 10^2 * (10^{-24} \text{ cm}^3)$ for polarizability which is defined as

Table 3:

$\beta^{-1/2}$ (nm)	$\langle E \rangle$ in Ryd*				
	$\epsilon = 0$	$\epsilon = 10$	$\epsilon = 20$	$\epsilon = 40$	$\epsilon = 60$
2	13.18	13.48	13.47	13.46	13.44
4	12.10	12.42	12.39	12.35	12.27
6	7.93	8.16	8.12	8.10	8.02
8	4.99	5.42	5.39	5.37	5.26
10	3.18	3.57	3.49	3.46	3.38

*1 Ryd = 5.3 meV for Ga As

$$\alpha_p = [\partial \langle E \rangle / \partial \epsilon^2] |_{\epsilon \rightarrow 0} = 0.7 * 10^2 * (10^{-24} \text{ cm}^3)$$

5. Conclusion.

We have presented a calculation for the binding energy of the ground state for a shallow hydrogenic donor in spherical GaAs QDs with parabolic confinement, following variational procedure within the effective mass approximations. The computed result shows that the binding energy increases as the dot size decreases. In spherical quantum dots, with an isotropic parabolic potential, the impurity binding energy is found to decrease as the impurity moves away from the center, the effect being more pronounced for dots of smaller sizes.

Reference Books:

- [1] Bastard G 1981 Phys.Rev.B24 4714
- [2] Chayanika Bose , 1998 J,Appl. Phys. 83 3089
- [3] Sakaki H 1981 J.Vac.Sci. Technol. 19 148
- [4] Vojak B.A., Laidig W.D, Holonyak N.Camras M D, Coleman J J and Dapkus
- [5] Schiff. L. I. (1968) Quantum Mechanics, III rd Edition, Phys.265
- [6] Lorke, J.P.Kotthaus, and K.Ploog, phys.Rev. Lett. 64 , 2559(1990)

Modified Conjugate Cancellation Algorithm For ofdm Systems

Mohamed Tayebi¹, Merahi Bouziani²

¹Telecommunications And Signal Processing Lab, Djillaliliabès University, Sidibelabbès, Algeria

Abstract:

The Inter-Carrier Interference Created By The Carrier Frequency Offset Significantly Degrades The Performances Of The Orthogonal Frequency Division Multiplexing Signal. If These Offsets Are Random, Then The Performances Fluctuate With This Shift. In This Letter, We Give Various Reasons For The CFO And Propose A New Technique To Inhibit The Effect Of ICI And Achieve Performance Almost Independent Of Carrier Frequency Offset. This New Technique Is A Variant Of The Method Of Combined Data Using The Conjugate Cancellation Algorithm. When Compared To Other Techniques, It Offers Better Performance In Terms Of Stability And Consistency.

Keywords:Carrier Frequency Offset (CFO), Carrier To Interferences Ratio (CIR), Doppler-Effect, Inter Carriers Interferences (ICI), Orthogonal Frequency Division Multiplexing (OFDM).

1. Introduction

The Orthogonal Frequency Division Multiplexing (OFDM), For Its Simplicity Of Implementation Using The Pair FFT/IFFT And Its Innumerable Benefits Such Its High Spectral Efficiency And Robustness Against The Effects Of Multipath Enabled Modern Telecommunications Systems Go A Significant Step Forward And Have Access To New Perspectives [1]. It Has Found Its Place In A Variety Of Broadcast Standards Such As Digital Audio Broadcasting (DAB), Digital Video Broadcasting (DVB) And In Optical Applications [2]. However, Its Main Drawback Is Its Sensitivity To Carrier Frequency Offset (CFO). This Is Mainly Due To Imperfections Of Local Oscillators And The Doppler-Effect Present In Radio Mobile Channels [3]. The CFO Gives Rise To Inter-Carrier Interference (ICI) That Degrades System Performances [4]-[8]. For A Given Link, The Offset Due To Imperfections Of Local Oscillators Is Constant Where The Doppler-Effect Generates Variable And Random Shifts, Which Not Only Degrade Performances, But Also Let Them, Fluctuate To The Rhythm Of The Doppler-Effect. A Number Of Methods Have Been Proposed To Reduce The Interference, But None Was Interested In The Stability Of Performance. Among The Methods That Do Not Require A Channel Estimation, We Cite The Technique Of ICI Self-Cancellation [9]-[10], The Symmetric Symbol Repetition Scheme (SSR) [7] And The Conjugate Cancellation (CC) [11]. In This Letter, We Propose A New Method Inspired By The Conjugate Cancellation Algorithm [11]. The Results Show Stable Performances Furthermore Being Practically Independent Of The CFO. This Is A Major Advantage In Highly Variable Channel As The Radio Mobile-Channel.

2. Ofdm With Carrier Frequency Offset (Cfo)

In Transmission Using OFDM, Frequency Offset Effects Are Mainly Due To The Imperfections Of Local Oscillators And The Doppler-Effect. The Normalized Values Are Respectively Denoted By ε_o , And ε_d Where:

$$\varepsilon_o = T \Delta f \quad (1)$$

And

$$\varepsilon_d = T f_p \frac{v}{c} \cos \alpha \quad (2)$$

Where Δf represents The Frequency difference between The Transmitter And The Receiver, T Is The Symbol Duration, v The Relative Velocity Between The Transmitter And Receiver, f_p The Carrier Frequency, c The Speed Of Light And α The Angle Formed By The Direction Of The Wave And The Velocity Vector. The Influence Of The Doppler-Effect Depends On Several Factors, All May To Vary. What Makes It A Real Problem With Uniformity And Consistency Of Performance When It Varies In Large Proportion. In OFDM Transmission Characterized By A Carrier Frequency Offset, We Denote By $X(k)$ The Transmitted Symbols And Which Is Denoted By $x(n)$, The IFFT Of $X(k)$, It Will Be Expressed By :

$$x(n) = \sum_{k=0}^{N-1} X(k) \text{Exp} \left(j 2\pi \frac{nk}{N} \right) \quad (3)$$

The Channel Is Affected By A Carrier Frequency Offset; The Received Signal Is Then Equal To:

$$y(n) = \text{Exp} \left(j2\pi \frac{n\varepsilon}{N} \right) \sum_{k=0}^{N-1} X(k) \text{Exp} \left(j2\pi \frac{nk}{N} \right) \quad (4)$$

To Recover The Signal, We Apply An FFT To The Signal. The Resulting Signal Is Equal To:

$$Y(k) = \frac{1}{N} \sum_{n=0}^{N-1} y(n) \text{Exp} \left(-j2\pi \frac{nk}{N} \right) \quad (5)$$

After Some Manipulations, The Signal Can Be Written [10]:

$$Y(k) = X(k)S(0) + \sum_{\substack{l=0 \\ l \neq k}}^{N-1} X(l)S(l-k) \quad (6)$$

Where:

$$S(l-k) = \frac{\sin \pi (l-k+\varepsilon)}{N \sin \frac{\pi}{N} (l-k+\varepsilon)} \exp j\pi \left(1 - \frac{1}{N} \right) (l-k+\varepsilon) \quad (7)$$

If The Transmitted Signal Is The Instead Of Emitting $x(n)$, We Transmit Its Conjugate:

$$x^*(n) = \left(\sum_{k=0}^{N-1} X(k) \text{Exp} \left(j2\pi \frac{nk}{N} \right) \right)^* = \sum_{k=0}^{N-1} X^*(k) \text{Exp} \left(-j2\pi \frac{nk}{N} \right) \quad (8)$$

Then, The Received Signal Is Written:

$$y(n) = \text{Exp} \left(j2\pi \frac{n\varepsilon}{N} \right) \sum_{k=0}^{N-1} X^*(k) \text{Exp} \left(-j2\pi \frac{nk}{N} \right) \quad (9)$$

Its Conjugate Is Then Equal To:

$$y^*(n) = \text{Exp} \left(-j2\pi \frac{n\varepsilon}{N} \right) \sum_{k=0}^{N-1} X(k) \text{Exp} \left(j2\pi \frac{nk}{N} \right) \quad (10)$$

To Recover The Signal, We Apply To A Signal An FFT, The Resulting Signal Is Then Equal To [11]:

$$Y(k) = X(k)S'(0) + \sum_{\substack{l=0 \\ l \neq k}}^{N-1} X(l)S'(l-k) \quad (11)$$

Where:

$$S'(l-k) = \frac{\sin \pi (l-k-\varepsilon)}{N \sin \frac{\pi}{N} (l-k-\varepsilon)} \exp j\pi \left(1 - \frac{1}{N} \right) (l-k-\varepsilon) \quad (12)$$

3. Modified Conjugate Cancellation algorithm

In Our Proposed Algorithm, We Reconsider The Idea Of Conjugate Cancellation [11], But With A Different Combination, The CIR Obtained Will Be:

$$CIR = \frac{|S(0) - S'(0)|^2}{\sum_{l=1}^{N-1} |S(l) - S'(l)|^2} \quad (13)$$

Figure 1 Plots The Variations Of The CIR For The Proposed Method And Standard OFDM. Note That The Modified Conjugate Cancellation Algorithm Provides An Improvement Over The Standard OFDM Beyond $\varepsilon = 0.15$. Comparing The Proposed Algorithm To The Existing Ones, We Can Clearly Notice That For The Range $0.01 \leq \varepsilon \leq 0.5$, The CIR Degradation Is About 35 Db For The Standard OFDM, Which In Terms Of Performance Shows That It Is Very Sensitive To The Carrier Frequency Offset, While For The Proposed Method, For The Same Range Of CFO, The Degradation Is Only 2 Db. Furthermore, It Maintains An Average

Value Of The CIR Equal To 10 Db. In An Environment, Where The CFO Is Strongly Variable, The Proposed Algorithm Is Clearly More Appropriate.

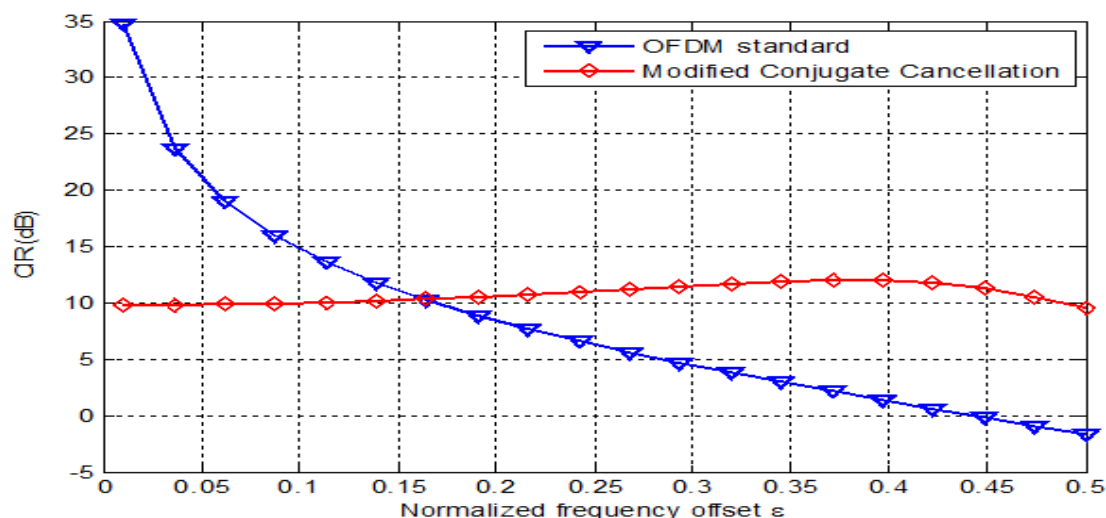


Figure 1: Comparison Of OFDM CIR And CIR With Modified Conjugate Cancellation

4. Conclusion

In This Paper, We Studied The OFDM In A Radio Mobile Channel. We Cited Several Methods To Reduce Inter-Carrier Interference (ICI) Created By The Carrier Frequency Offset (CFO). Compared To Existing Methods, The Proposed Method Has The Advantage Of Being Very Weakly Dependent On The Carrier Frequency Offset, Which Makes It Is Feasible And Attractive Solution For Links To Great Variation In CFO Due To Doppler-Effect.

References

- [1] S. Weinstein And P. Ebert, "Data Transmission By Frequency-Division Multiplexing Using The Discrete Fourier Transform," IEEE Trans. Commun., Vol. 19, Pp. 628-634, Oct. 1971.
- [2] J. Armstrong, "OFDM For Optical Communications", Journal Of Lightwavetechnology, Vol. 27, N°. 3, February 1, 2009.
- [3] M. Russell And G. L. S. Stüber, "Interchannel Interference Analysis Of OFDM In A Mobile Environment," In Proc. VTC'95, Chicago, IL, July 1995, Pp. 820-824.
- [4] J. Armstrong, "Analysis Of New And Existing Methods Of Intercarrier Interference Due To Carrier Frequency Offset In OFDM", IEEE Trans. Commun., Vol 47, No.3, Pp. 365-369, Mar. 1999.
- [5] K. Sathananthan And C. Tellambura, "Performance Analysis Of An OFDM System With Carrier Frequency Offset And Phase Noise," IEEE Vehicular Technology Conference, VTC 2001 Fall, Atlantic City, NJ, USA, Vol. 4, Pp. 2329-2332, Oct. 7-11, 2001.
- [6] K. Sathananthan And C. Tellambura, "Probability Of Error Calculation Of OFDM Systems With Frequency Offset," IEEE Trans. Commun., Vol. 49, No. 11, Pp. 1884-1888, Nov. 2001.
- [7] K. Sathananthan, R. M. A. P. Rajatheva, And S. B. Slimane, "Analysis Of OFDM In The Presence Of Frequency Offset And A Method To Reduce Performance Degradation," In Proc. IEEE Globecom, Vol. 1, San Francisco, CA, Nov. 2000, Pp. 72-76.
- [8] J. Lee, H. Lou, D. Toumpakaris, And J. Cioffi, "SNR Analysis Of OFDM Systems In The Presence Of Carrier Frequency Offset For Fading Channels" IEEE Transactions On Wireless Communications, Vol. 5, N°. 12, December 2006
- [9] Y. Zhao And S.-G. Häggman, "Sensitivity To Doppler Shift And Carrier Frequency Errors In OFDM Systems—The Consequences And Solutions," In Proc. IEEE 46th Vehicular Technology Conf., Atlanta, GA, Apr. 28–May 1, 1996, Pp. 1564–1568.
- [10] Y. Zhao And S.-G. Häggman, "Intercarrier Interference Self-Cancellation Scheme For OFDM Mobile Communication Systems," IEEE Trans. Commun., Vol. 49, Pp. 1185–1191, 2001.
- [11] H. Yeh, Y. Chang, And B. Hassibi "A Scheme For Cancelling Intercarrier Interference Using Conjugate Transmission In Multicarrier Communication Systems" IEEE Transactions On Wireless Communications, Vol. 6, N°. 1, January 2007

Estimation of the Population Total of Nigeria Using One Unit per Stratum (Based On 2006 Census Result)

¹T.J. Akingbade, ²O.S. Balogun,

¹Department of Mathematical Sciences, Kogi State University, Anyigba, Kogi State, Nigeria

²Department of Statistics and Operations Research, Modibbo Adama University of Technology, P.M.B 2076, Yola, Adamawa State, Nigeria

Abstract

This research has been done to show the point estimate of the population total of Nigeria based on 2006 census result to examine the effect of the use of auxiliary information in estimating variance in collapsing of strata with one unit per stratum. Two stage sampling method was used for the sample selection, which involves two phases of selection. In the first stage, 12 states were selected out of 36 states using random number table. The Local Government Areas (774) were taken to be the second stage and purposive sampling method was used. Based on the research work, considering one unit per stratum, that is selecting one Local Government Area was selected from each of the selected state. Based on the result obtained, using stratified random sampling with addition of auxiliary variable, the least standard error of \hat{Y}_{str} was **3,501,901.105** under the collapsing of 12 strata in six into two groups with an estimated population total of **139,295,482** which was very close to the actual population total of Nigeria based on 2006 census result (**140,003,542**). Estimation using stratified sampling with addition of an auxiliary variable gave a better result than estimation with variable of interest only

Keywords: Population, Collapse strata, Stratified sampling, Stratum

1. Introduction

The general knowledge of our day to day activities is all based to a very large extent on sample. Hence, sample survey has been very useful in almost every area of lives. Sample survey theory deals with the method and processes of sampling, data collection and estimation of the population parameters.

2. Collapsing Of Strata

A feature of many surveys Sample design is the selection of a single primary sampling unit (PSU) per stratum. The selection of a single PSU per stratum gives efficiency in design since stratification is carried out to fullest possible extent, but it does not generally permit an unbiased variance estimator to be obtained. A widely used method of variance estimation for this situation is known as collapsed strata technique (Rust and Kalton, 1987). With this techniques, strata and their corresponding sample PSU's are collapsed together in groups and then the variability among the unit within these groups is used to derive a variance estimator. If the strata can be ordered approximately in ascending order of the stratum means, the method of successive difference (Kish, 1965) is attractive. This method is an extension of collapsing of strata in pairs. Frequently, these methods have similar biases but the method of successive differences has some-what greater precision. Isaki (1983) used auxiliary information to reduce the bias of the collapse strata variance estimator. The results suggest that when auxiliary variable is highly correlated with the survey variables, there is a substantial improvement in the accuracy of variance estimation. The collapsed strata estimator (Cochran, 1977, section 5A.12) is a well-known estimator of variance estimation in one-per-stratum problem. The procedure collapses strata with one unit per stratum into groups and treats the strata in a group as independent samples from the combined stratum. In this research, collapsing can be accomplished separately among the strata containing small and medium sized districts with one district in the sample. First arrange the strata in a non-increasing sequence based on total enrolment size. Then collapse strata into pairs or groups sequentially. The variance estimator of a group is given by (5A.56) in Cochran's (1977).

2.1 Estimation of Variance with One Unit per Stratum ($n_h=1$)

Let the sample observation in a typical pair be y_{j1}, y_{j2} , where j goes from 1 to $L/2$. Let $\hat{y}_{j1} = N_{g1}y_{g1}$, $\hat{y}_{j2} = N_{g2}y_{g2}$ be the estimated stratum totals.

$$V_{CS}(\hat{Y}_{str}) = \sum_{g=1}^{L/2} \frac{L_g}{L_{g-1}} \sum_{k=1}^{L_g} \left(\hat{Y}_{gh} - \frac{\hat{Y}_g}{L_g} \right)^2 \quad (\text{Cochran, 1977})$$

Where \hat{Y}_g is the estimated total for group g for $L_g = 2$ when $\hat{Y}_g = \hat{Y}_{g1} + \hat{Y}_{g2}$. This method of estimation is called “*collapsed strata*”.

When an auxiliary variate X_h is known for each stratum that predicts the total Y_h , (Hansen, Hurwitz, and Madow, 1953) suggested the alternative variance estimator.

$$V_{CSx}(\hat{Y}_{str}) = \sum_{g=1}^{L/2} \frac{L_g}{L_g - 1} \sum_{k=1}^{L_g} \left(\hat{Y}_{gh} - \frac{x_{gh} \hat{Y}_g}{x_g} \right)^2 \quad (\text{Hansen, Hurwitz \& Madow, 1953})$$

Strata pairs are formed so that the strata in each pair are as similar as possible in respect to the characteristics of interest. In addition, strata that do not vary much in size as measured by an auxiliary variate are often collapsed. Pairs are not formed on the basis of selected sample units.

When to Collapse Strata

- (a) When the sample contains only one unit per stratum in such a way that variance estimation within stratum (S_{yh}) is not possible to estimate.
- (b) When the first stage of sampling consist of primary sampling unit such as cities or counties and the ultimate sampling unit are households.

3. Methodology and Data Presentation

The data were collected based on female population, male population and total population for each of the 36 states and 774 local government areas (LGA) in Nigeria based on 2006 census result. The number of states was taken to be the first stage and there were 36 states in Nigeria. The second selection is known as second stage unit. The number of the Local Government Areas in the selected states was taken as the second stage. The method of selection used here was a non probability sampling schemes using purposive sampling. Based on this research work, considering one unit per stratum, the 36 states are called 36 strata and each of the state is called a stratum and each state constitute a number of LGA’s Therefore, one LG was selected from each of the selected states. The LGA that has a close value to the average value of the state was chosen as a representative for the selected state.

4. Collapsed strata method used

Deterministic mixing method was employed.

Procedure: The probability $P_g = x_g/X$ were determined and were rearrange in ascending order with respect to P_1 for each of the tables. That is:

Estimation based on sample size 12, were rearrange in ascending order and were also collapsed in pair, three, four and six w.r.t. P_i in order to form homogeneous collapsed strata.

For example, if $L=12$, $L/2=6$ groups, taking the first two strata as a group and the next two strata as another group until the sixth group is obtained.

Table 1: Random digits of the selected 12 states with the Population Total, Female Population of the selected LGA and the number of LGA in the selected states

Random No Digits	selected States-L.G.A.	Pop Total of LGA	Female Pop of LGA	No of LGA
03	Akwa-Ibom-Itu	127033	59467	31
29	Osun -Obokun	116511	60965	30
13	Ekiti -Aiyekire	148193	70980	16
02	Adamawa-Mubi North	151072	72850	21
16	Imo-Ikeredu	149316	73084	27
25	Nasarawa-Obi	148874	74462	13
21	Kebbi-KokoBesse	154605	76201	21
26	Niger-Paikoro	158086	77280	25
33	Sokoto-Wurno	162307	78964	23
12	Edo-Orhionmwon	182717	90051	18
11	Ebonyi-Ohaukwu	196337	103489	13
18	Kaduna-Je,a'a	278735	133068	23

Data analysis and Result

In this section, the analysis of this research was carried out. Estimation of population total (\hat{Y}), Bias percentage(\hat{Y}) and variance of the population total ($V(\hat{Y})$) with one unit per stratum were estimated with $n= 12$ using stratified random sampling

Estimation of population total \hat{Y}_{str} with variable of interest only

$$\bar{Y}_{str} = \sum_{h=1}^n W_h \bar{y}_h \quad \hat{Y}_{str} = \frac{N}{n} M \sum_{h=1}^n W_h \bar{y}_h$$

$$n=12, \quad N=36, \quad M=774, \quad \sum W_h \bar{y}_h = 54428.8825$$

$$\hat{Y}_{str} = \frac{36}{12} \times 774 \times 54428.8825 = 126,383,865$$

$$\text{Bias Percentage} = \frac{\text{Actual Pop. Total} - \text{Estimated Pop. Total}}{\text{Actual Pop. Total}} * 100$$

Actual Pop. Total

$$(140003542 - 126383865) / 140003542 \times 100 = 9.728\%$$

Estimation of population total \hat{Y}_{str} with addition of auxiliary variable using combine Ratio Stratified Random Sampling

$$X=68,293,683$$

No of groups	Pop. Total (y_{gh})	Female Pop (x_{gh})	$P_{gh} = \frac{x_{gh}}{X}$	N_{gh}	$N_{gh} y_{gh} = \hat{Y}_{gh}$	$\left(\frac{\hat{Y}_{gh} - \hat{Y}_g}{2} \right)^2$	$\left(\hat{Y}_{gh} - \frac{x_{gh}}{x_g} \hat{Y}_g \right)^2$	
1	Akwa-Ibom	127033	59467	0.000871	31	3938023	48994273062	71597227953
	Osun	116511	60965	0.000893	30	3495330	48994273062	71597227953
	Subtotal	243544	120432			7433353	97988546125	1.43194E+11
2	Ekiti	148193	70980	0.00104	16	2371088	1.6057E+11	1.32988E+11
	Adamawa	151072	72850	0.00107	21	3172512	1.6057E+11	1.32988E+11
	Subtotal	299265	143830			5543600	3.2114E+11	2.65975E+11
3	Imo	149316	73084	0.00107	27	4031532	1.09848E+12	1.15767E+12
	Nassarawa	148874	74462	0.00109	13	1935362	1.09848E+12	1.15767E+12
	Subtotal	298190	147546			5966894	2.19696E+12	2.31533E+12
4	Kebbi	154605	76201	0.00112	21	3246705	1.24413E+11	1.07202E+11
	Niger	158086	77280	0.00113	25	3952150	1.24413E+11	1.07202E+11
	Subtotal	312691	153481			7198855	2.48826E+11	2.14405E+11
5	Sokoto	162307	78964	0.00116	23	3733061	49318416006	2.04657E+11
	Edo	182717	90051	0.00132	18	3288906	49318416006	2.04657E+11
	Subtotal	345024	169015			7021967	98636832013	4.09313E+11

6	Ebonyi	196337	103489	0.00152	13	2552381	3.72205E+12	1.87383E+12
	Kaduna	278735	133068	0.00194	23	6410905	3.72205E+12	1.87383E+12
	Subtotal	475072	236557			8963286	7.4441E+12	3.74766E+12
	Overall Total						1.04077E+13	7.09588E+12

$$\hat{Y}_{rcstr} = \frac{\bar{y}_{str}}{\bar{x}_{str}} X$$

$$\hat{Y}_{rcstr} = \frac{\sum_{h=1}^{12} W_h \bar{y}_h}{\sum_{h=1}^{12} W_h \bar{x}_h} X = \frac{54428.88}{26685.35} * 68293683 = 139,295,482$$

Bias Percentage=

$$\frac{(140003542 - 139295482)}{140003542} \times 100 = 0.506\%$$

TABLE 2: Estimation of variance in collapsing of 12 strata pair into 6 groups

Estimation of $V(\hat{Y}_{str})$ in collapsing of strata in pair into six groups

- a) Estimation of $V(\hat{Y}_{str})$ with variable of interest only

$$V_{cs}(\hat{Y}_{str}) = \sum_{g=1}^G \frac{L_g}{L_g - 1} \sum_{h=1}^{L_g} \left(\hat{Y}_{gh} - \frac{\hat{Y}_g}{L_g} \right)^2$$

$$L_g = 2, g = 1, \dots, 6$$

$$\sum_{g=1}^6 \sum_{h=1}^2 \left(\hat{Y}_{gh} - \frac{\hat{Y}_g}{L_g} \right)^2 = 1.040765998 \times 10^{13}$$

$$V_{CS(2)}(\hat{Y}_{str}) = 2 \times (1.040765998 \times 10^{13}) = 2.081531996 \times 10^{13}$$

Standard error of \hat{Y}_{str}

$$SE_{cs(2)}(\hat{Y}_{str}) = \sqrt{V_{cs(2)}(\hat{Y}_{str})} = 4562380.953$$

- b) Estimation of $V(\hat{Y}_{str})$ with addition of Auxiliary Variable

$$V_{csx}(\hat{Y}_{str}) = \sum_{g=1}^G \frac{L_g}{L_g - 1} \sum_{h=1}^{L_g} \left(\hat{Y}_{gh} - \frac{x_{gh}}{x_g} \hat{Y}_g \right)^2$$

$$\sum_{g=1}^6 \sum_{h=1}^2 \left(\hat{Y}_{gh} - \frac{x_{gh}}{x_g} \hat{Y}_g \right)^2 = 7.095878997 \times 10^{12}$$

$$V_{csx(2)}(\hat{Y}_{str}) = 2 \times (7.095878997 \times 10^{12}) = 1.419175799 \times 10^{13}$$

Standard error of \hat{Y}_{str}

$$SE_{csx(2)}(\hat{Y}_{str}) = \sqrt{V_{csx(2)}(\hat{Y}_{str})} = 3767194.977$$

Summary of the findings

Summary for the Estimated \hat{Y} and $S.E(\hat{Y})$ Based on Sample Size 12

Table 3: Summary Table for the Estimated \hat{Y} and $S.E(\hat{Y})$ Using Stratified Random Sampling with Sample Size 12

Methods	$\hat{Y}_{str} = 126,383,865$ $Bias(\hat{Y}_{str}) = 9.728\%$ $S.E_{cs}(\hat{Y}_{str})$	$\hat{Y}_{str} = 139,295,482$ $Bias(\hat{Y}_{str}) = 0.506\%$ $S.E_{csx}(Y_{str})$
Collapsing in pair	4,562,380.953	3,767,194.927
Collapsing in three	4,274,185.051	3,652,067.891
Collapsing in four	4,102,367.353	3,580,511.818
Collapsing in six	3,879,691.526	3,501,901.105

Conclusions

Stratified random sampling with addition of auxiliary variable seems to be more precise estimator, because it gives the least standard error of \hat{Y}_{str} to be **3,501,901.105** under the collapsing of 12 strata in six into two groups and least bias of **0.506** percentage and the estimated population total was **139,295,482** which was very close to the actual population total of Nigeria based on 2006 census result (**140,003,542**)

References

- [1] Cochran, William G., description of method of “collapsed strata” in Sampling Techniques, 1977, pp 139-140.
- [2] Hansen, M.H., Hurwitz, W.N., and Madow, W.G.(1953): Sample Survey Methods and Theory. Vol.II. Methods and Applications.
- [3] Kish, L. (1965): Survey sampling. John Wiley and Sons, New York.
- [4] Parsons, V.L. and Eltinge, J.L. (1999). Stratum partition, collapse and mixing in construction of balanced repeated replication variance estimators. Paper presented at the 1999 Joint Statistical Meetings, Baltimore, Maryland.
- [5] Rust, K. and Kalton, G. (1987). Strategies for collapsing strata for variance estimation. Journal of Official Statistics **3**, pp69-81

Evaluation Of Logistic Regression In Classification Of Drug Data In Kwara State

¹O.S. Balogun, ²T.J. Akingbade ¹, A.A. Akinrefon

¹Department of Statistics and Operations Research, Modibbo Adama University of Technology, P.M.B. 2076, Yola, Adamawa State, Nigeria

²Department of Mathematical Sciences, Kogi State University, Anyigba, Kogi State, Nigeria

Abstract

The classification of individuals who engage in illicit drugs into drug peddlers and non-peddlers on the basis of oral evidence, type and the quantity of exhibit found with them usually pose problem for the purpose of prosecution. This paper uses logistic regression to classify offenders into the two dichotomous dependent variable (peddlers or non-peddlers) in order to ease the work of the agency, National Drug Law Enforcement Agency (NDLEA), responsible for illicit drugs. The data used in this study include age of offenders, type and weight of exhibit collected from the agency. The discriminant analysis was first used by Abdulkadir and Emmanuel (2010) to classify the illicit drug offenders into peddlers and non-peddlers based on the data and then used by Balogun et al (2012) including some other variable to it. In literature the author discovered that the discriminant analysis cannot handle mixed data (discrete and continuous data) effectively instead logistic regression better fit the data. The model correctly classified 95.4% original grouped cases with positive and negative predictive values 92.44% and 97.90% respectively, which are higher than values obtained under the discriminant analysis. It was discovered that large quantity of exhibit has more effect than other variables, yet their inclusion significantly improves the outcome of the findings.

Keyword: Logistic regression, classification, odds ratio, discriminant Analysis.

1. Introduction

Logistic regression is a mathematical modeling approach that can be used to describe the relationship between independent or predictor variables to dichotomous dependent variable (Kleinbaum et al.1998). The model has traditional been appealing due to its performance in classification, the potential to use its output as probabilistic estimates since they are in the range[0, 1], and interpretation of the coefficients in terms of the log-odds ratio. It is especially in biostatistical application where binary classification tasks occur frequently (Hastie et al.2001).Agresti (1996) asserted that relationships between the probability of success $\pi(x)$ and X are usually nonlinear rather than linear. Therefore a fixed change in X may have less impact when $\pi(x)$ is near 0 or 1 than $\pi(x)$ is in the middle of its range.Logistic regression is often chosen if the predictor variables are a mixture of continuous and categorical variables and/or if they are not nicely distributed, that is, logistic regression makes no assumptions about the distribution of predictor variables. The logit analysis is usually employed if all the predictors are categorized while discriminant function analysis is used if all the predictors are continuous and nicely distributed (see <http://www.math.toronto.edu/mathnet>). This paragraph motivated the author to re-analyze the data obtained on illicit drug using logistic regression analysis (Abdulkadri, 2012). The data was first used in a paper by Balogun et al, 2012 using discriminant analysis while the data includes both qualitative and categorized predictor variables. In the paper the authors believed that the agency, The National Drug Law Enforcement Agency charged with the responsibility of dealing with drug and drug related offences, in some occasion, may not be able to distinguish between drug peddlers and non- peddlers on the basis of oral evidence on possession and dealing with illicit drugs. Therefore, there is need for a scientific method to employ in order to classify future offenders into peddler or non-peddler if some variables such as age of offenders, length of dealing in illicit drugs, type of exhibit, weight of exhibit and so on are known.

The involvement in illicit drug has so many social implications some of which include prostitution, theft, sexual assaults on female folks. According to Odejide (1992), those involved in peddling are ignorant of the problem emanating from it. It is true that a small number of people, mainly those organizing the illicit drug trade, make large profits from illicit crop cultivation, but the vast majority of people, including most of those benefiting from such trade, are adversely affected by the illicit activity. In the long term, the illicit industry causes major problem that eventually affect the economic development of the country concern. (<http://www.incb.org/>). On this premise the author believe offenders, especially peddlers/traffickers deserve stiff penalty than the users, because without seller buyer will not exist and invariably reduces or eliminate the activity in the system. Therefore, the laws concerning the illicit drug need to be reformed to reflect the new idea of treating peddlers with stiffer penalty than non-peddlers. This will be the responsibility of the legislators to appropriate the enabling laws.

In USA the amount of quantity of illicit drug determines the length of sentence pass on the offenders. However, the large quantity or numbers of item seized usually make the calculation of total quantity cumbersome, hence the use of statistical sampling such as multistage, composite and simple random samplings have been adopted.

A rule of thumb developed by Izenman (2001) for determination of sample size is square root of N, \sqrt{N} , where N is the number of items in a container is popular. A 95% confidence interval is developed to reduce the error for using the rule. Since the aim of the study is to determine whether or not an offender can be classified as a peddler/trafficker on the bases of age of offender, type, and weight of substance, therefore large quantity as never been reported in literature to have influenced the logistic regression model. However, some large quantity which could have been considered as outliers in the data collected was included/removed to determine the effect on the result of the study.

The logistic regression is employed for classification of objects into binary variable as

$$Y = \begin{cases} 1 & \text{Drug - peddler} \\ 0 & \text{Non - peddler} \end{cases}$$

According to Ganesalingam (1989), classification of objects to groups is usually thought of as partition of objects into subsets in which the members are more similar. Classifying individuals into groups such that there is relative homogeneity within the groups and heterogeneity between the groups is a problem which has been considered for many years. For this paper the author intends to re-classify objects into groups in which they were known to belong using logistic regression analysis.

2. Logistic Model

Let X_1, X_2, \dots, X_p be predictor variables which consist of qualitative and quantitative variables and Y as a dichotomous dependent variable, where Y is coded as 1 or 0 for its two categories as indicated above.

$$E(X) = \frac{1}{1 + \exp[-(B_0 + \sum_{j=1}^k B_j x_j)]} \dots\dots\dots (1)$$

This equation can be written in a form that describes the probability of occurrence of one of the two possible outcomes of Y , as follow

$$P(Y=1) = \frac{1}{1 + \exp[-(B_0 + \sum_{j=1}^k B_j x_j)]} \dots\dots\dots (2)$$

In general,

$$f(Z) = \frac{1}{1 + e^{-z}} \text{ where } z = B_0 + \sum_{j=1}^k B_j X_j$$

The function $f(z)$ is called logistic function. This function is well suited to modeling a probability, since the values of $f(z)$ varies from $-\infty$ to $+\infty$. The logistic model, therefore, is set up to ensure that, whatever estimate of risk we get, it always falls between 0 and 1. This is not true for other models, which is why the logistic model is often used when a probability must be estimated.

3. Estimating The Odds Ratio Using Logistic Regression

The regression coefficients B_j in the logistic model given in (1) play an important role in providing information about the relationships of the predictors in the model to the exposure variable. The qualification of this relationship involves a parameter called the odd ratio (Kleinbaum *et.al*, 1998) The odd ratio is a measure of effect because it is a measure that compares two or more groups in predicting the outcome variable.

The odd of an event $D = \{Y=1\}$

$$\text{Odds (D)} = \frac{\text{Pr}(D)}{1 - \text{Pr}(D)}$$

Any odds ratio is defined as a ratio of two odds.

The logistic regression is written as

$$\text{Logit } [\text{Pr}(Y=1)] = \log_e [\text{odds}(Y=1)]$$

$$= \log_e \left[\frac{\Pr(Y = 1)}{1 - \Pr(Y = 1)} \right].$$

Thus, equation (1) becomes

$$\text{Logit} [\Pr(Y=1)] = B_0 + \sum_{j=1}^k B_j X_j$$

The odds ratio, say, for groups A and B can be defined as

$$e^{\sum_{j=1}^k (X_{Aj} - X_{Bj}) B_j}$$

In general the odds ratio for groups A and B in given by

$$\frac{\text{Odds for } X_A}{\text{Odds for } X_B} = \frac{e^{(B_0 + \sum_{j=1}^k B_j X_{Aj})}}{e^{(B_0 + \sum_{j=1}^k B_j X_{Bj})}} = e^{\sum_{j=1}^k (X_{Aj} - X_{Bj}) B_j} \dots (3)$$

The constant term B_0 in the logistic model (1) drops out of the odds ratio expression in (3). The expression (3) describes a population odds ratio parameter because the B_j terms in the expression are themselves unknown population parameter. An estimate of this population odds ratio is obtained by fitting the logistic model using maximum likelihood estimation and substitute in the ML estimates B_j , together with the values of X_{Aj} and X_{Bj} , into the formula (3) to obtain a numerical value for the odds ratio.

4. Results And Discussion

A total number of 262 cases of illicit drugs which comprises of 119 drug peddlers and 143 non-peddlers was extracted from the record of NDLEA in Kwara and considered for this study. The average age of the peddlers is 27.76 years with a standard deviation of 8.611 while the average age of non-peddlers is 28.07 years with standard deviation of 9.763. The exhibit type for the peddlers and non-peddlers are 1.04 and 1.06 respectively. The average weights of exhibit caught with peddlers and non-peddlers are 5211.52 grams and 2430.21 grams respectively. The table below depicts the Nagelkerke R square of 88% of the total variation in the outcome variable (drug status- peddlers and non-peddlers) explained by the logistic regression model fitted into the data.

Table 1: Model summary

Step	-2 Log likelihood	Cox & Snell R Square	Nagelkerke R Square
1	79.640	0.658	0.880

The estimates of the logistic regression model parameters are presented in Table 2 below. The Wald statistics for age, exhibit weights and gender are 2.345, 43.462 and 8.880 respectively. These show that the three are important risk factors to determine the status of illicit drug offenders. The exhibit weight and gender are more important than the age going by the value of the Wald statistic, besides the Wald value for age is not significant while that of exhibit weight and gender is highly significant (P-value of 0.000 and 0.003) respectively. The odds ratio for age is 1.065 meaning that an increase in age by one year will increase the rate of peddling by 0.065 (95% C.I. 0.983 to 1.154).

Table 2: Estimates of the Logistic Regression Model

							95% C.I. for Exp(B)	
	B	S.E.	Wald	df	Sig	Exp(B)	Lower	Upper
Exhibit type	-0.726	1.680	0.187	1	0.666	0.484	0.018	13.037
Age	0.063	0.041	2.345	1	0.126	1.065	0.983	1.154
Exhibit Weight	-0.010	0.001	43.462	1	0.000	0.990	0.987	0.993
Gender	2.651	0.890	8.880	1	0.003	14.173	2.478	81.061
Constant	1.108	2.026	0.299	1	0.585	3.027		

The overall accuracy of this model (logistic regression) to predict becoming a drug peddler, with a (predicted probability of 0.5 or greater) is 95.4% as shown in Table 3. The predictive model is $z = 2.026 + 0.063age + 2.651gender - 0.726Exhibit\ Type - 0.010Exhibit\ Weight$. The interest is to use this model (logistic regression) to predict the outcome for a new case. To determine how good the model is we computed the followings: The sensitivity from Table 3 is 96.35%

Table 3: Classification Result (for logistic model)

Observed	Predicted		% Correct
	1	0	
1	110	9	92.4
0	3	140	97.9
Overall %			95.4

95.4% of the original grouped cases correctly classified.

and specificity is 93.96%. The positive predictive value (PPV) is 92.44% and the negative predictive value (NPV) is 97.90%. These results show that whenever we have a new subject, we can use logistic model to predict his probability of becoming a drug peddler. For instance, if given the gender, age of a new subject, the weight and the type of exhibit caught with him and if the predictive model gives a low probability, it means that the subject is very unlikely to become a drug peddler because the NPV reveals that we should be 97.90% confident and on the other hand if the model gives high probability it means that the subject is very likely to become a drug peddler because the PPV gives 92.44% confidence. The summary results obtained under the discriminant analysis are presented in Table 4 and 5 to justify the need to use logistic regression when variables contain both discrete and continuous data.

Table 4: Test for Equality of Group Means (through Discriminant Analysis ANOVA tests)

	Wilks' Lambda	F	Df1	Df2	Sig
Y ₁	0.993	1.878	1	260	0.172
Y ₂	1.000	0.075	1	260	0.785
Y ₃	0.930	19.499	1	260	0.000
Y ₄	1.000	0.006	1	260	0.937

The above Table 4 contains the results obtained when discriminant analysis was employed to classify the drug traffickers. In the table the Y₁ represents type of exhibit, Y₂ the age of offender, Y₃ the weight of exhibit and Y₄ the gender of the offender. All the four variables used in the model except one, Y₃, is significant. This implies that only weight of exhibit can be used to predict whether a drug offender is a peddler of illicit drug or not.

Table 5: Classification Results (for Discriminant Analysis)

Observed	Predicted		% Correct
	1	0	
1	67	52	56.30
0	22	121	43.70
Overall %			71.80

71.8% of original grouped cases correctly classified.

Comparing Tables 3 and 5 of classification above the overall percent grouped cases correctly classified is higher when logistic regression model was employ to classify the illicit drug offenders. The positive predictive value is 56.30% while the negative predictive value is 84.62%

Conclusion

The logistic regression model and discriminant analysis were used to classify data collected on illicit drug offenders. The results obtained when logistic regression was employed shows that 95.6% of the original grouped cases correctly classified while discriminant analysis correctly classified 46.45% of the same group. Moreover, the discriminant analysis results indicate that only weight of exhibit is significant in classification of offenders, but the logistic regression includes, in addition, the type of exhibit and age of offenders as important variables in the classification. Although the large quantity of exhibit has more effect than other variables, yet their inclusion significantly improves the outcome of the findings.

References

- [1] Abdulkadir, S.S. and Emmanuel, T. (2010), Discriminant Analysis and Classification of Drug Peddlers and Non-Peddlers. Journal of Research in National Development. Vol8(1)
- [2] Abdulkadir, S.S., Assessment of Logistics Regression for Classification of Drug Data. International Journal of Science and Technology Volume 1 No. 10, October, 2012
- [3] Agresti, A. (1996), An Introduction to Categorical Data Analysis. John Wiley and Sons. New York
- [4] Balogun, O.S.; Oyejola, B.A.; Akingbade, T.J. (2012), Use of Discriminant Analysis in Classification of Drug Peddlers and Non-Drug Peddlers in Kwara. International Journal of Engineering Research and Application. Vol.2, Issue 5, Pp. 936-938.
- [5] Ganesalingam, S. (1989), "Classification and Mixture Approaches to Clustering via Maximum likelihood." Applied Statistics, 38, no 3, Pp. 455 – 466.
- [6] Hastie, T.; Tibshirani, R.; and Friedman, J.H. (2001), The Elements of Statistical Learning. Springer.
- [7] Izenman, A. J. (2001), Legal and Statistical aspect of the forensic study of illicit drugs, Statistical Science, 16.
- [8] Kleinbaum, D.G; Kupper, L.L; Muller, K.E., and Nizam, A. (1998) Applied Analysis and Multivariate Methods. Third Edition. Duxbury Press.
- [9] Odejide, A.O. (1992), Drugs in the Third World. In Drugs and Society to Year 2000, Ed by Vamos and Corriveau Pp 116 – 119.
- [10] <http://www.math.toronto.edu/mathnet>
- [11] <http://www.incb.org/>

A Study on Visualizing Semantically Similar Frequent Patterns in Dynamic Datasets

¹Y.N.Jyothsna Mallampalli, ² S.Jayaprada, ³Dr S.Vasavi

¹M-Tech II Year, ²Senior Assistant Professor, ³Professor

^{1,2,3} Department of Computer Science & Engineering, V.R.Siddhartha Engineering College(Autonomous), Affiliated to JNTU Kakinada, KANURU, Vijayawada, Krishna (DT), Andhra Pradesh, India.

Abstract

Discovering frequent and interesting patterns is an important area of data mining. Transactional databases cannot serve the requirement of analyzing current trends in shopping; it is required to focus on analyzing dynamic data sets. Existing data mining algorithms when applied on dynamic data sets takes lot of time as they generate very huge number of frequent patterns making the analyst with the task to go through all the rules and discover interesting ones. Works that are reported until now in reducing number of rules are either time consuming or does not consider the interestingness of the user and does not focus on analysis of rules. This paper extends SSFPOA algorithm which produces clusters of semantically similar frequent patterns and presents these clusters using data visualization.

Keywords: Clusters, Dynamic Datasets, Ontology, Semantically similar frequent patterns, Data Visualization.

1. Introduction

One important area in data mining is concerned with the discovery of frequent patterns and interesting association rules. While considering the transactional databases, the patterns are extracted over a certain period of time like and at the end of the day. But, as the trends are continuously changing, the patterns extracted by previous day transactions may not suit to the present trends. Hence there is a need in extracting frequent patterns in dynamic datasets. The standard approach to update dynamic dataset is, applying the data mining algorithms continuously for every update in the dataset. The most general algorithm used for this purpose is “Apriori Algorithm”. Apriori algorithm extracts all association rules satisfying minimum thresholds of support and confidence. If the threshold is high, some rules may be omitted and if the threshold is low then a large set of all rules will be extracted. Solutions such as frequent closed patterns, using filters, using redundancy rules, ontologies with semantics were proposed to solve this problem. Also compression on appropriate set of frequent patterns, frequent patterns asserting the interestingness of association rules which is evaluated by using relatedness based on relationship between item pair are investigated but there are still many challenges. First, the problem of mining such patterns is difficult as algorithms are very time and memory-consuming. Second, as usual in data mining problems, the number of patterns extracted by current solutions is too large to be easily handled by end-users. Fig.1 presents the traditional approach to association rule mining where support and confidence are used to produce best rules.

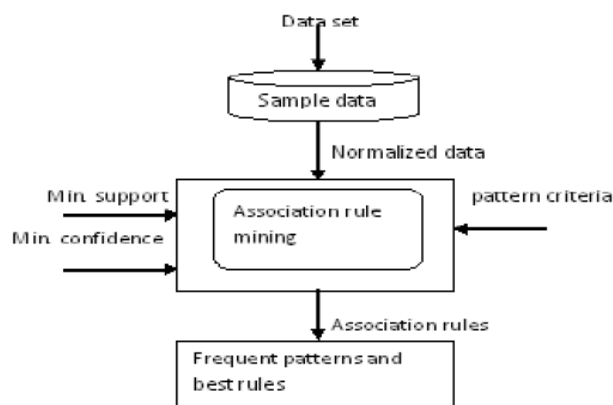


Figure 1: Traditional approach for association rule mining.

Hence, we are considering the methods for finding similarity within frequent patterns and from those patterns we can extract association rules. Then, we will apply clustering techniques on them. i.e. each cluster contains semantically similar patterns. The paper is organised as follows: section 2 discusses about related work, section 3 about Proposed Work, section 4 about Conclusions and Future Work.

2. Related Work

The interesting association rules and frequent patterns can be discovered by using 3 types of measures such as i) Objective Measures (ii) Subjective Measures and (iii) Semantic Measures. Objective measure [1] as given in Table 1 is a data-driven approach for evaluating the quality of association patterns. Since, these measures calculate the frequent patterns based on the statistical parameters, different measures produce different results. So, these are insufficient for determining the interestingness of a discovered rule. Subjective measures [2] generally operate by comparing the beliefs of a user against the patterns discovered by the data mining algorithm. But these measures are also not sufficient as the rules generated by these measures are user biased. Semantic measures uses natural language processing techniques such as domain ontologies, web ontologies to identify relationships amongst the patterns. Resnik's approach [3] finds semantic similarity based on the distance from one node to another. i.e.

the path between the 2 nodes is shorter; they are treated as more similar. This approach is mainly based on the domain independent ontology such as Wordnet[4] But problem with Wordnet is, words which are not identified by it is treated as noise. Also, shortest path is not only sufficient to conform on semantic similarity. KEOPS methodology [5] works by comparing the extracted rules with expert's knowledge and it uses IMAK partway interestingness measure that considers relative confidence values and knowledge certainty for determining the rule quality. KEOPS only focused on "Rules based Patterns" and is mainly based on IMAK measure. But, IMAK is computed by quality indices like Support, confidence and lift, which are easily interpretable. Since, the patterns generated by this methodology are heterogeneous, it is very difficult to access as well as analyzing them. The work SSFPOA [6] extracts and clusters semantically similar frequent patterns. It uses both domain dependent and domain independent ontologies, and considers the entire path to conform the semantic similarity between elements along with their structural information such as the number of the children for each node of schema, the number of subclasses for each class within the ontology. We extend SSFPOA by adding visualization techniques for easy analysis of the extracted patterns. This paper proposes visualization techniques for the clusters of rules extracted by SSFPOA.

[7,8] uses Scatter plots to display data as a collection of points. These are used when a variable exists that is under the control of the experimenter. Mosaic plots [8,9] are often used to visualize relationship between two or more categorical values. Parallel co-ordinate plots [8] visualise the distribution of the values of a variable over the different values of another variable (For example, calculation of annual expenditure etc).

In, Matrix-visualization [10], the Antecedent is represented on the X-axis and Consequent on the Y-axis. Intersection of Antecedent and Consequent represents the Selected interest measure. All these techniques can visualize only small amounts of data. In [11] the results of association rule mining algorithms are represented as directed graphs. Items, item-sets and association rules are represented as nodes, where as the links between items and item-sets or association rules are represented as edges. But, this approach can visualize only frequent item-sets and binary association rules derived from transactional data. Line graphs are most useful in displaying data or information that changes continuously over time. Histograms are the special type of bar charts, for visualizing showing a visual impression of the distribution of data. It can display large amounts of data that are difficult to understand in a tabular, or spreadsheet form. So, line graphs and histograms will be more suitable for visualizing semantically similar frequent patterns in dynamic datasets.

3. Proposed Work

Many mining methods use measures such as support and confidence for mining association rules efficiently and also for measuring the quality of the mined rules. While considering the transactional databases, the patterns are extracted over a certain period of time like, at the end of the day. But, as the shopping trends are continuously changing, the patterns extracted by previous day transactions may not be useful to the present trends. So that, we have to consider the problem of extracting frequent patterns in dynamic datasets, in which the dataset is updated in small intervals of time. The measure SSFPOA uses domain dependent as well as domain independent ontologies to construct semantic similarity matrix between all pairs of frequent items and then clusters all the frequent patterns which have high similarity. These clusters are further used to generate association rules with high level abstraction[12]. But, analyzing these association rules is a more difficult task, we are extending this method with visualizing these clusters graphically. Figure 2 shows our extended approach.

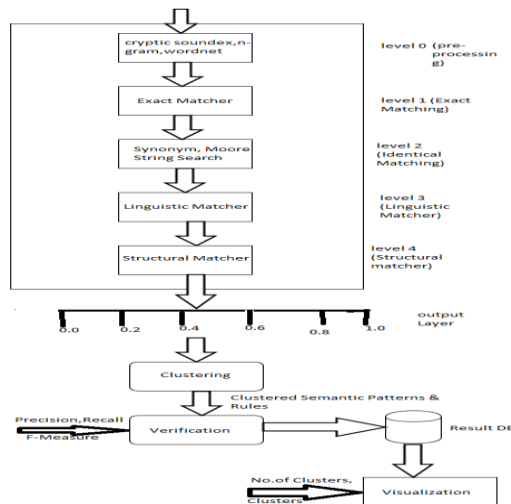


Figure 2: Extended Approach of Visualizing Semantically Similar Frequent Patterns

In this approach Level 1 to level 4 are the hidden layers. Here, each layer evaluates and output of this layer is given as input to the next layer. Layer 1 is an exact string matcher which gives either 0 or 1 depending on equality. If it generates 1 then level 2, 3 are not performed and is directed to level 4 for context matching. Layer 2 uses 2 matchers (neuron units) and layer 3 uses 6 matchers. Structural matcher considers the depth of the node within the tree along with the other structural features such as :

- (i) Number of children for each node
- (ii) Number of subclasses for each class of ontology

Also semantic similarity is measured in the range of 0-1. The algorithm SSFPOA has focused on interpreting the frequent patterns that are mined, especially extracting semantically similar items and clustering them, instead of generating large number of distinct rules for semantically similar items with separate support values, related rules can be reduced. Our algorithm VSSFPOA extends, SSFPOA by visualizing the clusters of semantically similar frequent item sets using Line graphs and Histograms. Table 2 presents semantically similar frequent patterns produced by SSFPOA for product domain available at [13]. Similar patterns are clustered to generate rules which are in higher level of abstraction. For example, the semantically similar items of Table 2 can be clustered as 3 clusters, (i). Beauty/Health (ii) Foods and (iii) Other items. These can be formed by clustering the similar patterns which are in the lower level of ontology. i.e. Beauty/Health cluster can be formed by clustering Toothpaste, Creams, Hair products, Health and Soaps. Biscuit/Rusk contains Biscuits, Papad, Dal/pulses, Roti, Snacks and Pickles. The 3rd cluster Other items contains, Vegetables, Miscellaneous and Phone cards. In Line graph Visualization, we represent the cluster numbers on X-axis and the semantic similarity value on Y-axis. By plotting respective clusters with their corresponding similar value, one can easily visualize the clusters for easy analysis as shown in Fig.3.

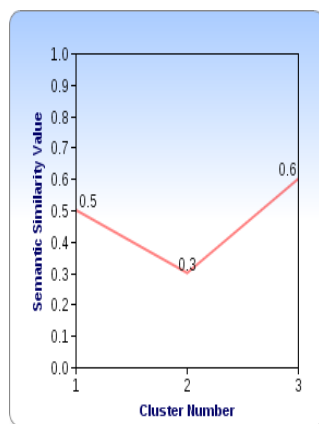


Figure 3: Line graph visualization of semantically similar frequent patterns for Table 2. In Fig.4 visualization, we first calculate the centroid of each cluster. The cluster numbers are represented on X-axis and the centres on the Y-axis. By plotting respective clusters with their centroid, one can easily visualize the clusters for easy analysis as shown in Fig.4.

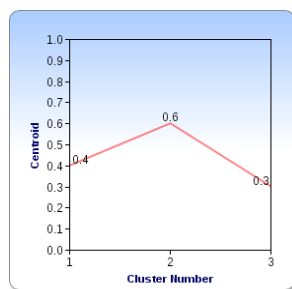


Figure 4: Line graph visualization of semantically similar frequent patterns for Table 2.

In Histogram visualization, we consider the number of rules or items each cluster have. By representing the clusters on X-axis and number of rules on Y-axis, the visualization is more effective for the analysis as shown in Fig.5.

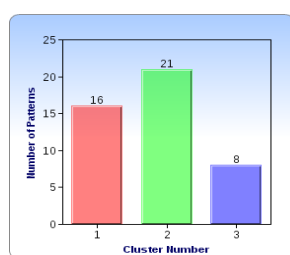


Figure 5: Histogram visualization of semantically similar frequent patterns for Table 2.

4. Conclusion And Future Work

According to the rapidly changing present shopping trends, it is essential to consider dynamic Datasets for extracting frequent patterns. Existing data mining algorithms are very time consuming and they generate very huge number of frequent patterns, hence we extend SSFPOA algorithm which results the semantically similar frequent patterns at higher levels of abstraction and further clusters them. This paper extends SSFPOA as VSSFPOA by adding visualization techniques like line graphs and histograms to clusters for easy analysis of patterns. Our future work concentrates on providing visualizations in 3-D and the comparison of performance of various visualization techniques.

References

- [1]. Guillaume, Sylvie, Dhouha Grissa, and Engelbert Mephu Nguifo, Categorization of interestingness measures for knowledge extraction, arXiv preprint arXiv:1206.6741 (2012).
- [2]. Bing Liu , Wynne Hsu , Shu Chen , Yiming Ma, Analyzing the Subjective Interestingness of Association Rules, IEEE Intelligent Systems(journal) - Volume 15 Issue 5, September 2000, Pages 47 - 55.
- [3]. Resnik P, Using information content to evaluate semantic similarity in a taxonomy(1995).
- [4]. <http://www.wordnet.princeton.edu>
- [5]. Laurent Brisson and Martine Collard, How to Semantically Enhance a Data Mining Process?, ICEIS 2008: 103-116.
- [6]. S. Vasavi, S. Jayaprada, V. Srinivasa Rao, Extracting Semantically Similar Frequent Patterns Using Ontologies, SEMCCO'11 Proceedings of the Second international conference on Swarm, Evolutionary, and Memetic Computing - Volume Part II, Pages 157-165.
- [7]. http://en.wikipedia.org/wiki/Scatter_plot
- [8]. Hashler M. and Chelluboina S., Visualizing Association Rules: Introduction to the R-extension Package arulesViz(2011)
- [9]. Hofmann H., Siebes A., and Wilhelm A.F.X.,(2000), Visualizing Association Rules with Interactive Mosaic Plots, in KDD, pp. 227-235.
- [10]. Michael Hahsler and Sudheer Chelluboina, Visualizing association rules in hierarchical groups, In Computing Science and Statistics, Vol. 42, 42nd Symposium on the Interface: Statistical, Machine Learning, and Visualization Algorithms” (Interface 2011).
- [11]. Ertek G. and Demiriz A, (2006), A Framework for Visualizing Association Mining Results, in ISCIS, pp. 593-602
- [12]. S.Vasavi, S.Jayaprada, Clustering Semantically Similar Frequent Patterns using SSFPOA, International Journal of Data Ware housing & Mining, Vol 2 Issue 1 pg 45-51,2012 ISSN:2249-7161.
- [13]. <http://www.indianmart.com.au/shopping/index.php>

Table 1: Definition of Objective Measures

N ^o	Measure	Formula
1	Correlation coefficient	$\frac{p(XY) - p(X)p(Y)}{\sqrt{p(X)p(Y)p(X)p(Y)}}$
2	Cohen or Kappa	$2 \frac{p(XY) - p(X)p(Y)}{p(X) + p(Y) - 2p(X)p(Y)}$
3	Confidence or precision	$\frac{p(XY)}{p(X)}$
4	Causal Confidence	$1 - \frac{1}{2} \left(\frac{1}{p(X)} + \frac{1}{p(Y)} \right) p(XY)$
5	Centered Confidence or Favillon	$\frac{p(XY)}{p(Y)} - p(Y)$
6	Descriptive Confirm Confidence or Giasscia	$1 - 2 \frac{p(XY)}{p(X)}$
7	Causal Confirm Confidence	$1 - \frac{1}{2} \left(\frac{1}{p(X)} + \frac{1}{p(Y)} \right) p(XY)$
8	Causal Confirm	$p(X) + p(Y) - 4p(XY)$
9	Descriptive Confirm	$p(XY) - p(XY)$
10	Conviction	$\frac{p(XY)p(Y)}{p(X)p(Y)}$
11	Cosinus or Ohiai	$\frac{p(XY)}{\sqrt{p(X)p(Y)}}$
12	Coverage	$p(X)$
13	Czekanowski-Dice or F-measure	$2 \frac{p(XY)}{p(XY) + 1 - p(XY)}$
14	Dependency	$\ p(Y) - \frac{p(XY)}{p(X)}\ $
15	Putative Causal Dependency	$\frac{3}{2} + 2p(X) - \frac{3}{2}p(Y) - \left(\frac{3}{2p(X)} + \frac{3}{2p(Y)} \right) p(XY)$
16	Gray and Orlowska's Interestingness Weighting Dependency	$\left(\left(\frac{p(XY)}{p(X)p(Y)} \right)^k - 1 \right) \times p(XY)^m$
17	Esyes factor or Odd multiplier	$\frac{p(XY)p(Y)}{p(X)p(Y)}$
18	Certainty factor or Loevinger or Satisfaction	$\frac{p(XY) - p(X)p(Y)}{p(X)p(Y)}$
19	Negative reliability	$\frac{p(XY)}{p(Y)}$
20	Collective Strength	$\frac{p(XY) + \frac{p(XY)}{p(X)}}{p(X)p(Y) + p(X)p(Y)} \times \frac{1 - p(X)p(Y) - p(X)p(Y)}{1 - p(XY) - \frac{p(XY)}{p(X)}}$
21	Fukuda	$n \left(p(XY) - \sigma_0 p(X) \right)$
22	Informational gain	$\log_2 \left(\frac{p(XY)}{p(X)p(Y)} \right)$
23	Gini	$p(X) \left(\frac{p^2(XY)}{p^2(X)} + \frac{p^2(XY)}{p^2(X)} \right) + p(X) \left(\frac{p^2(XY)}{p^2(X)} + \frac{p^2(XY)}{p^2(X)} \right) - p^2(Y) - p^2(Y)$

Table 1: Definition of Objective Measures(Continued)

24	Goodman-Kruskal	$\frac{\sum_{j,k} \max_k P(X_j, Y_k) + \sum_{j,k} \max_j P(X_j, Y_k) - \max_j P(X_j) - \max_k P(Y_k)}{2 - \max_j P(X_j) - \max_k P(Y_k)}$
25	Implication index	$\sqrt{n} \frac{p(XY) - p(X)p(Y)}{\sqrt{p(X)p(Y)}}$
26	Probabilistic intensity of deviation from equilibrium (IPEE)	$P \left[N(0, 1) \geq \frac{nXY - nXY}{\sqrt{max}}$
27	Entropic probabilistic intensity of deviation from equilibrium (IPSE)	$\sqrt{\left[\frac{1}{2} \left((1 - h_1(P(XY)))^2 \times (1 - h_2(P(XY)))^2 \right)^{\frac{1}{2}} + 1 \right]} \times \sqrt{IPEE}$ with $h_1(t) = -\left(1 - \frac{t}{p(X)}\right) \log_2 \left(1 - \frac{t}{p(X)}\right) - \frac{t}{p(X)} \log_2 \left(\frac{t}{p(X)}\right)$ for $t \in [0, \frac{p(X)}{2}]$, else $h_1(t) = 1$ $h_2(t) = -\left(1 - \frac{t}{p(Y)}\right) \log_2 \left(1 - \frac{t}{p(Y)}\right) - \frac{t}{p(Y)} \log_2 \left(\frac{t}{p(Y)}\right)$ for $t \in [0, \frac{p(Y)}{2}]$, else $h_2(t) = 1$
28	Probabilistic discriminant index (FDI)	$P \left[N(0, 1) \geq IICR/B \right]$ where $IICR/B$ indicate that II is reduced-centred according to the values taken by II on the extracted rules set.
29	Mutual Information	$-P(X) \log_2 P(X) - P(X) \log_2 P(X)$
30	Intensity of Implication (II)	$P \left[Poisson(nP(X)P(Y)) \geq P(XY) \right]$
31	Entropic intensity of implication (IIE)	$\sqrt{\left[\left(1 - h_1(P(XY))\right)^2 \times \left(1 - h_2(P(XY))\right)^2 \right]^{\frac{1}{2}}} \times II$
32	Entropic intensity of revised implication (IIEr)	$\sqrt{\left[\left(1 - h_1(P(XY))\right)^2 \times \left(1 - h_2(P(XY))\right)^2 \right]^{\frac{1}{2}}} \times \sqrt{max(2 \times II - 1, 0)}$
33	Likelihood discriminant index	$P \left[Poisson(nP(X)P(Y)) < P(XY) \right]$
34	Interest or Lift	$\frac{p(XY)}{p(X)p(Y)}$
35	Jaccard	$\frac{p(XY)}{p(XY) + p(Y)}$
36	J-Measure	$p(XY) \log \left(\frac{p(XY)}{p(X)p(Y)} \right) + p(XY) \log \left(\frac{p(XY)}{p(X)p(Y)} \right)$
37	Klcegen	$\sqrt{p(XY) \left(\frac{p(XY)}{p(X)} - p(Y) \right)}$
38	Kulczynski or Agreement and disagreement index	$\frac{p(XY)}{p(XY) + p(XY)}$
39	Laplace	$\frac{2p(XY) + 1}{2p(X) + 2}$
40	Leverage	$\frac{p(XY)}{p(X)} - p(X)p(Y)$
41	Mgk	$\frac{p(XY)}{p(Y)}$ If $P(Y/X) \geq P(Y)$ then $Mgk(X \rightarrow Y) = \frac{p(XY)}{p(Y)}$ Else $Mgk(X \rightarrow Y) = \frac{p(XY)}{p(X)}$
42	Least contradiction or Surprise	$\frac{p(XY) - p(XY)}{p(Y)}$

Table 1: Definition of Objective Measures(Continued)

43	Novelty	$p(XY) - p(X)p(Y)$
44	Pearl	$p(X) \left \frac{p(XY)}{p(X)} - p(Y) \right $
45	Piatetsky-Shapiro	$n \times \left(p(XY) - p(X)p(Y) \right)$
46	Accuracy	$p(XY) + p(X\bar{Y})$
47	Prevalence	$p(Y)$
48	Yule's Q	$\frac{p(XY)p(X\bar{Y}) - p(X\bar{Y})p(XY)}{p(XY)p(X\bar{Y}) + p(X\bar{Y})p(XY)}$
49	Recall	$\frac{p(XY)}{p(Y)}$
50	Odds Ratio	$\frac{p(XY)p(X\bar{Y})}{p(X\bar{Y})p(XY)}$
51	Relative Risk	$\frac{p(Y/X)}{p(Y/\bar{X})}$
52	Sebag-Schoenauer	$\frac{p(XY)}{p(X\bar{Y})}$
53	Specificity	$\frac{p(X\bar{Y})}{p(\bar{X})}$
54	Support or Rusesel and Rao index	$p(XY)$
55	Yao and Liu's One Way Support	$\frac{p(XY)}{p(X)} \log_2 \frac{p(XY)}{p(X)p(Y)}$
56	Yao and Liu's Two Way Support	$p(XY) \log_2 \frac{p(XY)}{p(X)p(Y)}$
57	Examples and counter-examples rate	$\frac{p(XY) - p(X\bar{Y})}{p(XY)}$
58	Test value VT100	$\phi^{-1}(P[\text{Hypergeometric}(100P(X)P(Y)) \leq P(XY)])$
59	Yao and Liu's Two Way Support Variation	$p(XY) \log_2 \frac{p(XY)}{p(X)p(Y)} + p(X\bar{Y}) \log_2 \frac{p(X\bar{Y})}{p(X)p(\bar{Y})} + p(\bar{X}Y) \log_2 \frac{p(\bar{X}Y)}{p(\bar{X})p(Y)}$
60	Yule's Y	$\frac{\sqrt{p(XY)p(X\bar{Y})} - \sqrt{p(X\bar{Y})p(XY)}}{\sqrt{p(XY)p(X\bar{Y})} + \sqrt{p(X\bar{Y})p(XY)}}$
61	Zhang	$\max \left\{ p(XY)p(\bar{Y}), p(Y)p(X\bar{Y}) \right\}$

Table 2: Semantically similar frequent patterns for product domain

SNO	Semantically similar items	Parent node
1	Vicco vajardanti 100gm 3.75\$ Vicco vajardanti 100gm 6.50\$	Tooth paste
2	Gori Gori blue fairness bleach 50gm \$4.95 Gori Gori fairness bleach 50gm \$4.95	Creams
3	Godrej renew hair color cream black 120ml \$6.95 Godrej renew hair color cream brown 120ml \$6.95	Hair products
4	Supreme Dark brown henna 150gm \$2.95 Supreme Maroon henna 150gm \$2.95	Hair products
5	Eno lemon 100gm \$2.95 Eno regular 100gm \$2.95	Health
6	Hajmola imli 120 tbs \$3.95 Hajmola regular 120 tbs	Health
7	Godrej No.1 natural \$2.75 Godrej No.1 rose \$2.75	Soaps
8	Neem active toothpaste 125gm \$3.25 Neem toothpaste 125gm \$3.25	Tooth paste
9	Pattu Jeera khari biscuit - 200gm \$2.95 Pattu Masala khari biscuit - 200gm \$2.95 Pattu plain khari biscuit - 200gm \$2.95 Pattu Tomato khari biscuit - 200gm \$2.95	Biscuit
10	Indian Mart Black Urid 1kg \$3.75 Indian Mart Black Urid split 1kg \$3.75	Dal/pulses
11	Indian Mart Kabuli Channa (10mm) 1kg \$3.75 Indian Mart Kabuli Channa (9mm) 1kg \$3.75	Dal/pulses
12	Indian Mart Toor Daal 1kg \$3.75 Indian Mart Toor Daal premium 1kg \$3.75	Dal/pulses
13	Katoomba Roti Parantha (20 roti) \$7.25 Katoomba Roti Parantha lite (20 roti) \$7.25	Roti
14	Mezban Gajar Halwa 280gms \$6.25 Mezban Loli Halwa 280gms \$6.25	Snacks
15	Taj Valor Lilva (indian beans) 400gm \$2.00 Taj Valor Papdi (indian beans) 400gm \$2.00	Vegetables
16	Food Color - Orange \$2.00 Food Color - Red \$2.00 Food Color - Yellow \$2.00	Miscellaneous
17	Aithra sago papad 200gm \$2.25 Aithra sago papad color 200gm \$2.25	Papad
18	Lijjat papad - garlic 200gm \$2.00 Lijjat papad -red chilli 200gm \$2.00 Lijjat papad - Urad 200gm \$2.00	Papad
19	South Asia Phone Card \$8.00 South Asia Phone Card \$16.00 South Asia Phone Card \$40.00	Phone cards
20	Priya garlic pickle \$2.50 Priya garlic pickle \$6.50	Pickles

CFD Simulation in Township Planning – A Case Study

¹Nilesh S. Varkute²R.S. Maurya

¹ Sardar Patel College Of Engineering, Mumbai, Maharashtra, India.

² Sardar Patel College Of Engineering, Mumbai, Maharashtra, India.

Abstract

There are increasing concerns regarding the quality of urban public spaces. Wind is one important environmental factor that influences pedestrians' comfort and safety. In modern cities there are increasing numbers of high constructions and complex forms which can involve problems of significant wind discomfort around these buildings. Architects and town planners need guidelines and simple design tools to take account of wind in their projects. In recent years the numerical investigation has emerged as powerful and sufficient tool for building optimization and a better township planning. Present work proposes the methodology to carry out exterior numerical on a cluster of existing structures and concludes with significant outcomes which are mostly neglected by the planners. Present work uses a three dimensional scale down model of buildings where steady incompressible flow analysis has been done. It has been implemented through ANSYS Fluent 12.0 using SIMPLE algorithm as solver. The effect of turbulence has been captured using k- ϵ model. Simulated work validates well with the available experimental result. The work progresses with single building simulation to a cluster of building with common external amenities. Some of the significant conclusion are changing ventilation pattern of air among buildings with wind direction, flow separation, wind shadow effect, location of amenities such as garden, playground etc.

Keywords: Building, CFD, Environment, High Rise Building, k- ϵ model, Optimization, Simulation, Township.

1. Introduction

With the development in technology taller and taller structures are being designed and constructed to care of the local need and desire. Such structures have a significant effect on the surrounding wind patterns due to the change in the local wind flows. This causes many environmental problems in nearby areas such as accelerated wind flow at the ground level impacting the comfort, and sometimes safety, of the users of the building and the pedestrians in the surrounding street canyons. Sometimes it creates permanent pollutant dispersion problem in the locality. Other significant effects of changed wind flow pattern are wind-sun shadow effect and locating amenities like playground, garden, swimming pool etc. For the city planners and building designers, prior knowledge of the air flow around builds play a significant role in finalizing their design. At the building scale, the theoretical challenges are inherent in the complex interplay of thousands of components, each with their own complex physical behavior and a multiplicity of interactions among them. Such kind of complexity can be easily handled numerically. Therefore numerical investigation for building has gained a well-respected role in the prediction, assessment, and verification of building behavior. Two conventional approaches i.e. Building energy balance model (BES) and Zonal airflow network (AFN) models are slowly losing their significance and now the focus is more towards CFD based simulation which is based on mass, momentum and energy conservation in the flow domain. But CFD simulation of building design is a challenging task due to large length scale with complex geometry, the uncertainty in assigning boundary condition and wide range of physical processes occurring in the surrounding.

The most important physical phenomena in the externally built environment are the atmospheric boundary layers, the unsteady flow, the separating bluff body flow and dispersion. In spite of such computational difficulties, CFD has become an influential tool in the building industry, especially with its capability to visualize air flow in and around the building. It is used to justify the selection of design option. Not only as a justification or confirmation tool, it has emerged as a shaping and molding tool also on the drawing board where the design is refined. Most of the work on building simulation is dedicated to optimizing internal environment of the rooms or interiors where location and orientation of the building were prime focus. Feustel and diamond [1] carried out an experimental and a numerical study to investigate air flow pattern and ventilation systems in the high-rise buildings. Using a building energy simulation program and a computational fluid dynamics program, Zhai [2] investigated the influence of building scales on building cooling energy consumption with and without natural ventilation. Investigations on natural ventilation design by Carriho-dagrac et al. [3], prediction of smoke and fire in buildings by Lo et al. [4] and Yeoh et al. [5], particulate dispersion in indoor environment by Quinn et al. [6], building element design by Manz [7], and space indoor

environment analysis by Eckhardt and Zori [8] are some significant work on internal simulation on buildings. Often, the outdoor environment has a significant impact on the indoor environment. Therefore to solve the problems related to natural ventilation requires the study of both the indoor and outdoor environment together. Few such research work are simulations of outdoor airflow and pollutant dispersion by Sahm et al. [9] and Swaddiwudhipong and Khan [10], and combined indoor and airflow studies by Jiang and Chen [11]. Due to large spatial scale external building simulation could not progress at same pace as internal building simulation. But several efforts have been made by researchers in this direction also. Baskaran and Stathopoulos [12] presented the computer simulation of wind pressures on buildings. Cheng et al. [13] reported a systematic computational study of wind-induced natural ventilation and pollutant transport of re-entrant. Thepmongkorn et al. [14] investigated interference effects of neighboring tall buildings on wind-induced coupled translational and torsional motion. Investigation was carried out through a series of wind tunnel aero elastic model experiments. Baskaran and Kashef [15] used numerical techniques to predict wind flow conditions around a single building, between two parallel buildings and around a multiple building configuration. Bosch et al. [16] presented an experimental investigation on the flow past a square cylinder placed near a wall at $Re = 22,000$. Lakehal and Rodi [17] presented a 3D steady simulation of flow around a cube placed in developed-channel flow with various versions of the $k-\epsilon$ model. Rodi [18] compared LES and RANS calculation of flow around bluff bodies. Castelli et al.[19] investigated flow pattern around dome shaped structure by using proper boundary conditions like velocity inlet, pressure outlet, and symmetry in lateral and top direction, wall for ground and building wall surfaces. The review of literature indicates insufficient work in the area of external wind simulation around building structures which are useful for architects, city planner and building designers. The objective of the present work is to illustrate the capability and potential of modern CFD tool through a detailed case study of a cluster of high rise building located in Mumbai city.

Investigation would be helpful for the planners to take many critical decisions such as influence of high rise buildings and building clustering on surrounding settlements, locating garden area, play area, community centers, internal roads etc. to make their project better and effective from environmental view point. It contributes in structural analysis of the buildings also with the knowledge of wind drag data. A systematic investigation is proposed where following important parameters like effect of wind flow direction, building orientation, in between building spacing, building layouts are discussed. Based on available metrological data of Mumbai city, all simulation has been executed using wind speed of 10 m/s. Any kind of thermal effect arising due to the building is not a part of the investigation.

2. Problem Definition

Present problem is to carry out numerical investigation of air flow pattern around a cluster of existing high rise structures located in west coast mega city i.e. Mumbai of India. The bird eye view of this small township is shown in Fig.1. It consists of fourteen structures of different height and orientations. The objective is to know the effect of changing wind direction and predict the optimum location of garden, play area, community centers, and internal roads along with its influence on surrounding settlements. The investigation starts with the numerical study of single building, two buildings and multi building's inline and staggering layouts. The orientation of single building with L, B and H are length, breadth and height respectively is depicted in Fig.2. To investigate the channeling effect created by wind in between the buildings, two buildings of same size is proposed as shown in Fig.3.



It is not a part of CFD analysis

Figure 1. Bird view of township

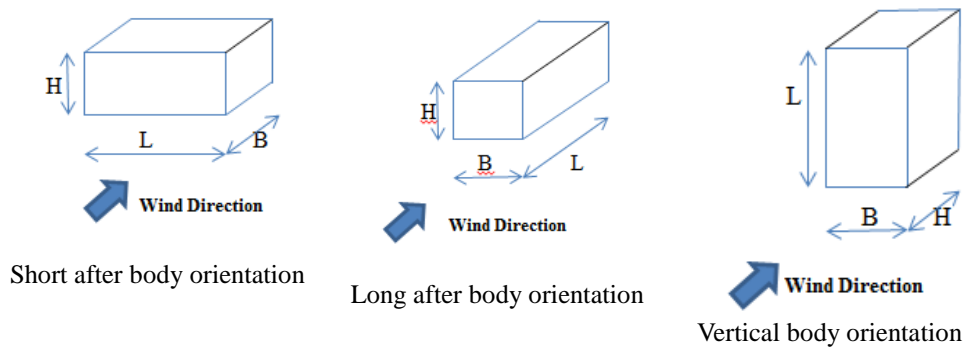


Figure 2. Orientation of building

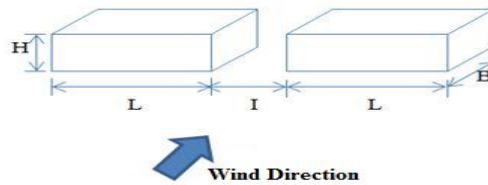


Figure 3. Two Building Model

3. Modeling of Problem

3.1. Mathematical Model

The average wind speed of Mumbai region is about 10 meters per second based on the available metrological data. The movement of air around the building can be modeled as Newtonian fluid with turbulent, viscous, incompressible and steady flow in nature. The flow behavior is governed by mass and momentum conservation with appropriate turbulence model where the body force can be neglected.

3.1.1. Governing Equations

The governing equation for Newtonian, incompressible and steady flow without turbulence is presented here, To turbulence is captured by using standard K-ε Model which leads to two additions transport equation i.e. kinetic energy(k) and turbulence diffusivity (ε).

Mass Balance,

$$\frac{\partial u}{\partial x} + \frac{\partial v}{\partial y} + \frac{\partial w}{\partial z} = 0 \quad \dots (1)$$

X- Momentum Equation,

$$\rho \left(u \frac{\partial u}{\partial x} + v \frac{\partial u}{\partial y} + w \frac{\partial u}{\partial z} \right) = -\frac{\partial p}{\partial x} + \mu \left(\frac{\partial^2 u}{\partial x^2} + \frac{\partial^2 u}{\partial y^2} + \frac{\partial^2 u}{\partial z^2} \right) \quad \dots (2)$$

Y- Momentum Equation,

$$\rho \left(u \frac{\partial v}{\partial x} + v \frac{\partial v}{\partial y} + w \frac{\partial v}{\partial z} \right) = -\frac{\partial p}{\partial y} + \mu \left(\frac{\partial^2 v}{\partial x^2} + \frac{\partial^2 v}{\partial y^2} + \frac{\partial^2 v}{\partial z^2} \right) \quad \dots (3)$$

Z- Momentum Equation,

$$\rho \left(u \frac{\partial w}{\partial x} + v \frac{\partial w}{\partial y} + w \frac{\partial w}{\partial z} \right) = -\frac{\partial p}{\partial z} + \mu \left(\frac{\partial^2 w}{\partial x^2} + \frac{\partial^2 w}{\partial y^2} + \frac{\partial^2 w}{\partial z^2} \right) \quad \dots (4)$$

Turbulence Equation: K-ε Model

Air flow simulation around the building needs scale down of the actual building size for the sake of computational efficiency. Being external flow investigation, a judicious selection of appropriate computational domain considering the geometrical scale of the problem is must along with suitable boundary condition.

- a. The inlet boundary condition is based on finite velocity which is obtained from the average wind speed of the location collected from metrological department of India based on past 10 years data.

- b. Model of air behaving like a viscous fluid, no-slip wall boundary condition is used for ground part of the computational domain.
- c. Remaining parts of the computational domain is assumed to be at ambient condition i.e. zero gauge pressure.

3.2. Numerical Implementation

Numerical simulation of the cases presented in the previous section is done through the ANSYS Fluent 12.0. It starts with the selection and modeling of the computational domain and its meshing. Physics of the problem demands sufficiently lengthy downstream length to care of vortex formation behind the structure. To capture presence of velocity gradient near the structures sufficient fine meshing is required. The selection of proper solver settings is essential for successful simulation. For pressure velocity decoupling SIMPLE algorithm is used and turbulence is captured by standard k-ε model. The convective terms present in momentum, kinetic energy and turbulent dissipation is treated by using first order upwind scheme, to interpolate pressure cell based pressure data is averaged at the faces and the pressure gradient is estimated using least square cell based technique.

4. Results and Discussion

This section deals with the result and discussion associated with air flow distribution around single body, two body, multi-body and actual existing cluster of building respectively. The work has been validated with experimental result. For the sake of completeness of the investigation the parameter like air flow distribution, direction of wind, recirculation zone and drag forces have been considered for the analysis and conclusion.

4.1 Single Building Simulation

The investigation is performed on a building of dimension L=40 m, B=20 m, H=20 m with short, long and vertical body orientation which is depicted in Fig.2. Figure 4 shows a movement of air around building under different orientations through velocity vectors. The flow can be observed to be getting stagnated as it approaches the building. A separation of flow from the front edges of the building and development of a weak velocity recirculation zone behind the building can be observed in all three orientations. With the length of recirculation zone, and total drag force data for each building orientation is presented in Table 1. The total force component along the specified force vector \vec{a} on a wall zone is computed by summing the dot product of the pressure and viscous forces on each face with the specified force vector. The terms in this summation represent the pressure and viscous force components in the direction of the vector \vec{a} .

$$F_a(\text{Total Force}) = \vec{a} \cdot \vec{F}_p (\text{Pressure Force Component}) + \vec{a} \cdot \vec{F}_v (\text{Viscous Force Component})$$

Where \vec{F}_p and \vec{F}_v are specified, pressure and viscous force vector respectively.

Table 1. Comparison between orientations of building

Parameter/Orientation	Short after body orientation	Long after body orientation	Vertical body orientation
Recirculation Zone length (m)	37	24	31.5
Total Drag Force (N)	49912.35	25015.21	52273.75

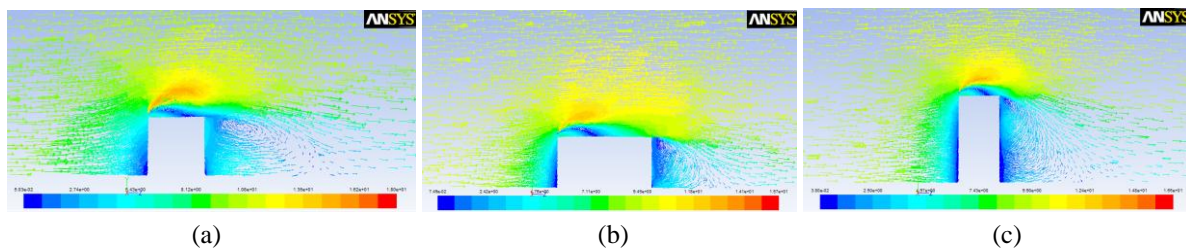


Figure 4. Velocity vectors (a) short after body, (b) long after body and (c) vertical body orientation

A low value of recirculation zone length and drag force acting on the structure can be observed for long body orientation of the structure. This can be attributed to the nature of flow separation occurring in all three orientations. Reattachment of flow in early length part and second separation at extreme downstream leads to lesser pressure and viscous drag. So long body orientation is best from good in design point of view.

4.2. Two Buildings Simulation

The simulation investigates the optimum nearness between two buildings for human comfort and good city planning. The model considered for investigation is depicted in Fig.5 which has been experimentally investigated by Baskaran and Kashef [10]. The simulated results for velocity at mid-section in between the building spacing along z- direction of flow is validated with experimental data and presented in Fig.6 for in-between building gap of 6 meter. Here U and V are local and average incoming wind speed. It is found that the magnitude of flow velocity between two buildings is increases first and then it decreases. Numerical result matches well with the experimental work with maximum error of 5%.

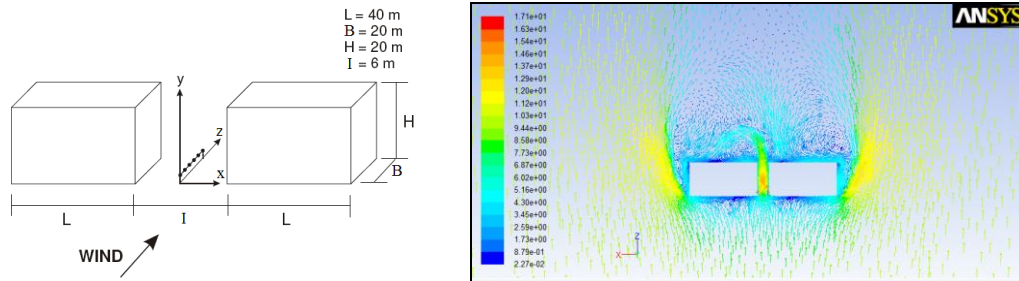


Figure 5. Model and velocity vector

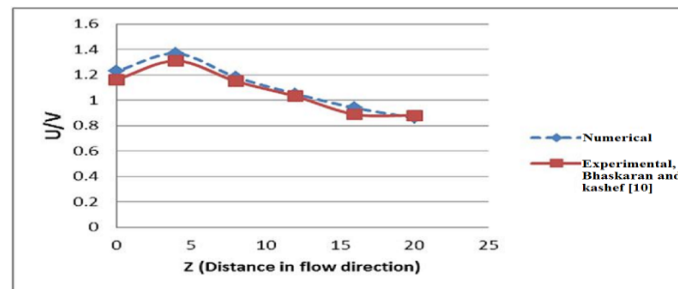


Figure 6. Validation graph for two building model

A numerical investigation of in-between building gap (I) on velocity along the downstream at height of 2 meter from the ground is presented in Fig.7. The building gap (I) is varied from 6 meters to 20 meters. This variation can be attributed to the venturi effect created in between the building spacing. The maximum and average both wind velocity can be observed to be rising and then decreasing. The magnitude of several parameters is presented in Table 2.

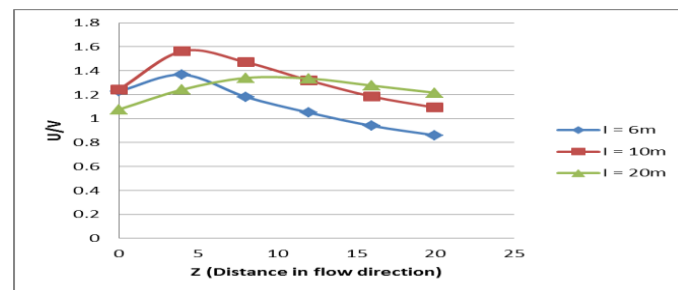


Figure 7. Comparison of channeling effect between two buildings for various spacing

Table 2. Parametric comparison of channeling effect between two buildings

Parameter	I = 6 m	I = 10 m	I = 20 m
Maximum Velocity rise along the flow (m/s)	13.67	15.64	13.40
Flow pattern behind buildings	Non-uniform	Uniform	Uniform
Total Drag Forces (N)	139791.68	113159.12	132608.37

4.3. Existing Cluster of High Rise Structures

The bird eye view of existing structures as depicted in Fig.1, consisting of many tall structures with few small and many amenities such as playground, garden and swimming pool etc. In numerical simulation some of small structures have been removed to find air flow distribution only due to tall structures (50 meter high). Simulation presents the investigation for natural ventilation around, location of external amenities and drag data due to changing wind direction. The computational domain as shown in Fig.8 is chosen for the simulation is with: Upstream distance = 400 m, Downstream distance = 1180 m, Side distances = 400 m and top distance = 250 m. The domain meshed with 3.3 lakhs tetrahedral mesh as computational cells with maintaining fine meshes near the structures and ground. The simulation has been carried out under north, west, SW and south wind directions.

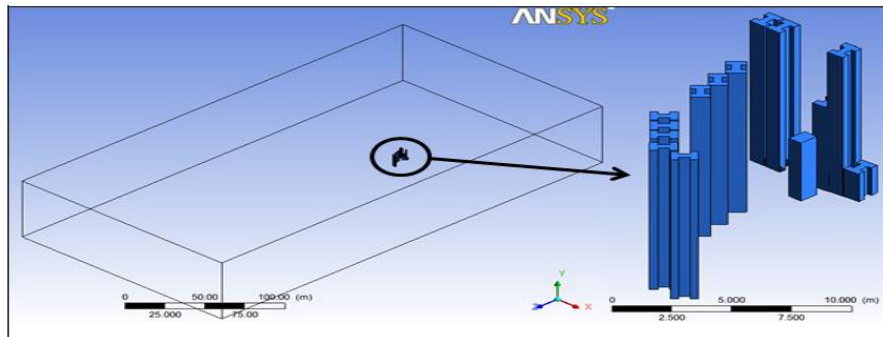
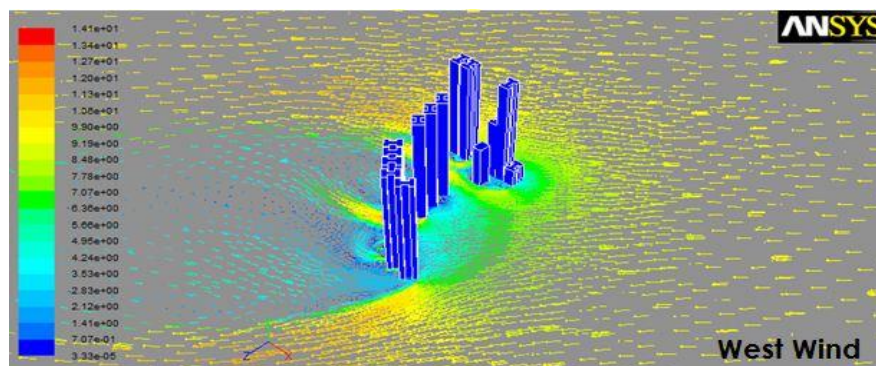


Figure 8. Computational domain for cluster of structures

Figure 9 shows the effect of wind direction on velocity distribution around the structures. The formation of vortex and wind shadow zone can be observed under each wind direction simulation. A wake region and stagnant zone develops behind the building. This is not good for pleasant ambience. The town planners need to be careful in minimizing such wind effects. In the west coastal region where Mumbai is located, have wind direction throughout the year is either north or west direction. Therefore all external amenities must be located on the upstream side for better ventilation and pleasant ambience. For the case under investigation the playground, swimming pool and landscape garden is properly located. There is no wind shadow effect of one structure over others. In case of southward or south west wind has sever wind shadow effect and the layout of the building is not good for these two wind directions. Figure 10 shows the zoomed view of air flow in-between the structure. It illustrates the qualitative results which is good enough for building planners to take critical decision such as exterior layout of building, building spacing, stagnant pockets created by wind flow. In present vector plot it can be seen that except few places where the structures are extremely nearby there is a development of stagnant zone which is not good from building planning point of view.



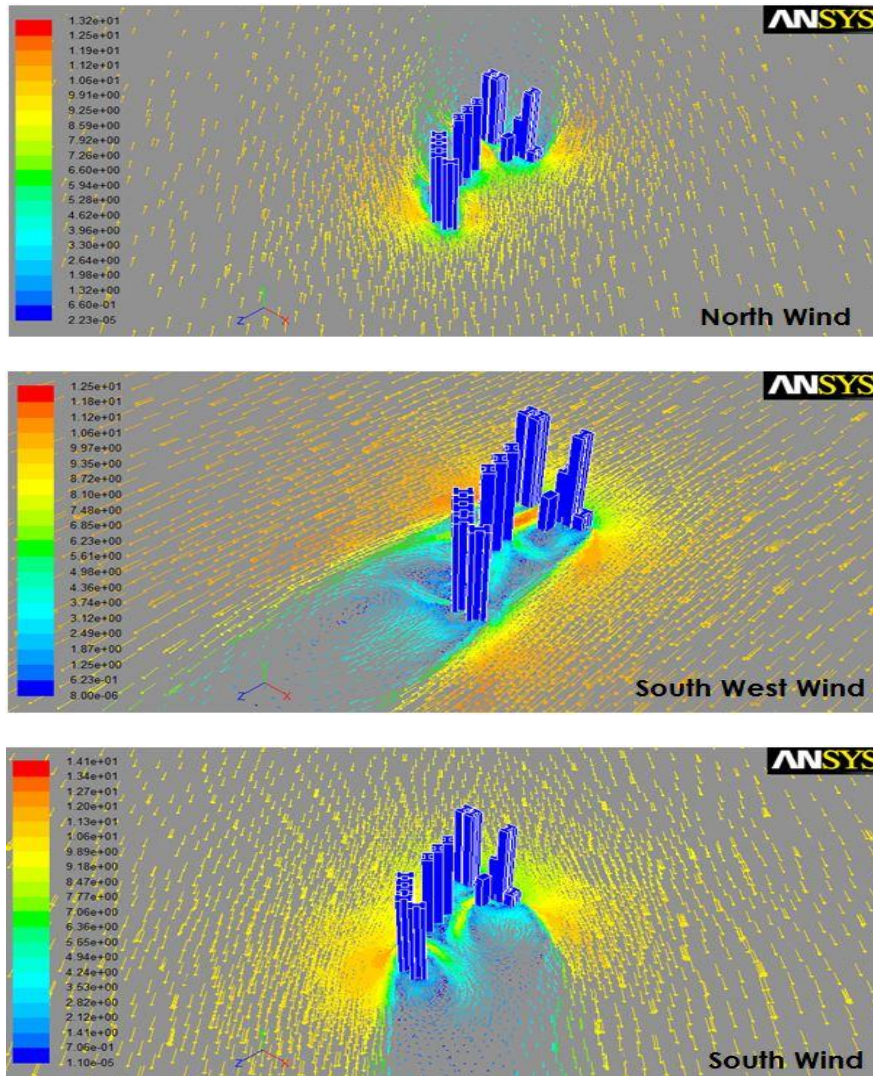


Figure 9. Velocity vector in different wind direction

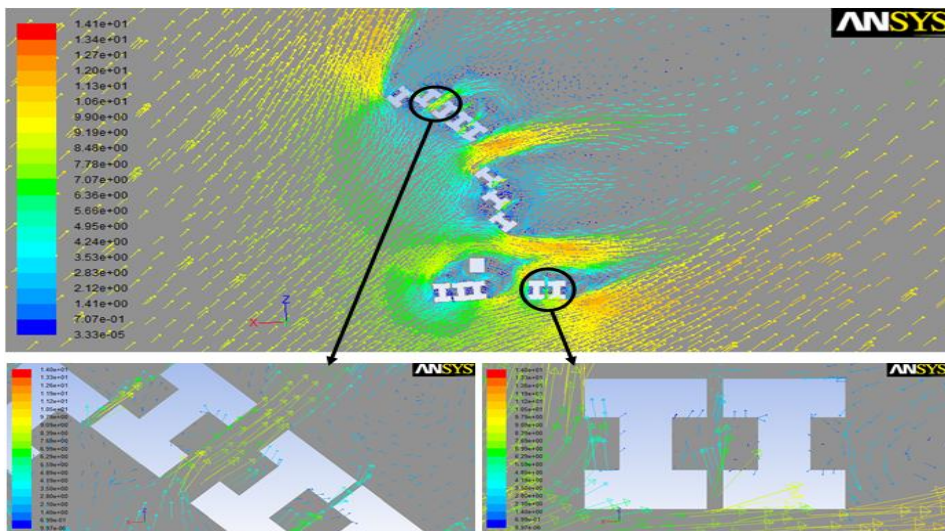


Figure 10. Wind velocity in-between two buildings

5. Conclusion

A three-dimensional numerical model is developed to analyze the flow pattern around buildings. From the preceding discussions, the following conclusions can be made:

- a. Computation fluid dynamics is a powerful tool for the investigation of building air flow applications. It provides detailed predictions of air velocities around buildings.
- b. Gap between two buildings is significant and needs to be investigated before planning.
- c. Due to the detailed study of flow pattern around the buildings we are able to capture correct location of air conditioning systems, heating installations etc.
- d. A good natural ventilated location around an existing can be easily located with the help of CFD analysis.

References

- [1] H.E. Feustel and R.C.Diamond. Air flow distribution in a high-rise residential Building. Lawrence Berkeley National Laboratory, Berkeley, 1996.
- [2] Z. Zhai. Numerical study of optimal building scales with low cooling load in both hot and mild climate regions. In Proceedings of the 17th Annual North American Waste-to-Energy Conference, May 18-20, Chantilly, Virginia, 2009.
- [3] G. Carrilho da Graca, Q. Chen, L.R. Glicksman, and L.K. Norford. Simulation of wind-driven ventilate cooling systems for an apartment building in Beijing and Shanghai. *Energy and Buildings*, 34(1):1–11, 2002.
- [4] S.M. Lo, K.K.Yuen, W.Z. Lu, and D.H. Chen. A CFD study of buoyancy effects on smoke spread in a refuge floor of a high-rise building. *Journal of Fire Sciences*, 20(6):439–463, 2002.
- [5] G.H.Yeoh, R.K.K.Yuen, S.M. Lo, and D.H. Chen. On numerical comparison of enclosure fire in a multi-compartment building. *Fire Safety Journal*, 38(1):85–94, 2003.
- [6] A.D. Quinn, M. Wilson, A.M. Reynolds, S.B. Couling, and R.P. Hoxey. Modelling the dispersion of aerial pollutants from agricultural buildings—an evaluation of computational fluid dynamics (CFD). *Computers and Electronics in Agriculture*, 30(1): 219–235. 2001.
- [7] H. Manz. Numerical simulation of heat transfer by natural convection in cavities of facade elements. *Energy and Buildings*, 35(3):305–311, 2003.
- [8] B. Eckhardt and L. Zori. Computer simulation helps keep down costs for NASA’s ‘lifeboat’ for the international space station. *Aircraft Engineering and Aerospace Technology: An International Journal*, 74(5):442–446. 2002.
- [9] P. Sahm, P. Louka, M. Ketzler, E. Guilloteau, and J.F. Sini. Inter-comparison of numerical urban dispersion models—part I: Street canyon and single building configurations. *Water, Air and Soil Pollution: Focus*, 2(5–6):587–601, 2002.
- [10] S. Swanddiwudhipong and M.S. Khan. Dynamic response of wind-excited building using CFD. *Journal of Sound and Vibration*, 253(4):735–754, 2002.
- [11] Y. Jiang and Q. Chen. Effect of fluctuating wind direction on cross natural ventilation in building from large eddy simulation. *Building and Environment*, 37(4):379–386, 2002.
- [12] Baskaran and T. Stathopoulos. Prediction of wind effects on buildings using computational methods review of the state of the art. *Canadian Journal of Civil Engineering*, 21:805-822, 1994.
- [13] C.K.C. Cheng, K.M. Lam, Y.T.A. Leung, K. Yang, H.W Danny and C.P. Cheung Sherman. Wind-induced natural ventilation of re-entrant bays in a high-rise building. *Journal of Wind Engineering and Industrial Aerodynamics*, 99:79–90, 2011.
- [14] S. Thepmongkorn, G.S. Wood, K.C.S. Kwok. Interference effects on wind-induced coupled motion of a tall building. *Journal of Wind Engineering and Industrial Aerodynamics*, 90:1807–1815, 2002.
- [15] A.Baskaran, and A. Kashef. Investigation of air flow around buildings using computational fluid dynamics techniques *Engineering Structures*, 18(11):861-875,1996.
- [16] G. Bosch, M. Kappler, W. Rodi. Experiments on the flow past a square cylinder placed near a wall. *Experimental Thermal and Fluid Science*, 13:292-305, 1996.
- [17] D. Lakehal, W. Rodi. Calculation of the flow past a surface-mounted cube with two-layer turbulence models. *Journal of Wind Engineering and Industrial Aerodynamics* 67-68:65-78, 1997.
- [18] W. Rodi. Comparison of LES and RANS calculations of the flow around bluff bodies. *Journal of Wind Engineering and Industrial Aerodynamics*, 69-71:55-75, 1997.
- [19] M.R.Castelli, S.Toniato and E. Benini. Numerical analysis of wind loads on a hemi cylindrical roof building. *World Academy of Science, Engineering and Technology*,56, 2011.

Adhesive Wear Theory of Micromechanical Surface Contact

Biswajit Bera

Department of Mechanical Engineering National Institute of Technology Durgapur, India

Abstract: Microscopically, when two surfaces come in contact, strong adhesive bond is formed at the tip of the asperities and consequently, adhesive wear particle is formed by shearing the interface caused by sliding. On the basis of JKR adhesion theory, dimensionless real area of contact and wear volume are computed numerically for multiasperity contact and It is found, their ratio is almost constant for different pair of MEMS surfaces. From which adhesive wear law is derived and accordingly, adhesive wear volume is the multiplication of real area of contact and rms roughness (sigma).

Keyword: JKR adhesion theory, Real area of contact, Adhesive wear volume, Coefficient of adhesive wear

1. Introduction

Wear is a complex process of material removal from the interface of mating surfaces under sliding motion. According to adhesive wear theory, when two smooth and clean rough surfaces come in contact, cold welded junctions are formed at the pick of the asperities through plastic deformation and the subsequent shearing of the junctions from softer material causes adhesive wear particle. Existing almost all laws of adhesive wear are based on experimental findings and empirical in nature. Holm [1] assumed that adhesive wear was an atomic transfer process occurring at the real area of contact formed by plastic deformation of the contacting asperities. Holm proposed an equation for adhesive wear, as $v = \frac{P}{H}Z$ where P, H and Z are load, hardness and

number of atoms removed per atomic encounter respectively. Similarly, Archard [2] quantified adhesive wear for rough surface contact based on single asperity contact as adhesive wear, $v = K \frac{P}{H}L$ where L is sliding distance

and K is wear coefficient which should be evaluated experimentally. Still, now, Archard's adhesive wear law is well accepted but it does not quantify the adhesive wear volume theoretically. In this study, effort has paid to quantify adhesive wear volume theoretically. It is considered that asperities would deform elastically and they cold weld due to intermolecular adhesion at the contact zone of asperity. Strong adhesive bond is formed according to JKR adhesion theory [3] i.e. adhesive force would act within Hertzian contact zone of deformed asperities. This idea is implemented to find adhesive wear volume and real area of contact for multiasperity contact of rough surfaces such as adhesive MEMS surface contact. Thereafter, from the interrelation of both the parameters, new adhesive wear law has developed and finally, the new adhesive law is compared and interrelated with existing Archard's adhesive wear law.

2. Theoretical Formulation

2.1 Single asperity contact

2.1.1 Single asperity real area of contact

JKR theory has modified Hertz theory of spherical contact. It predicts a contact radius at light loads greater than the calculated Hertz radius. As asperity tip is considered spherical, the adhesion model of single asperity contact could be extended to multiasperity of rough surface contact. So, real contact area of single asperity is

$$A_a = \pi \left[\frac{R}{K} \left(F_0 + 3\pi\gamma R + \sqrt{6\pi\gamma R F_0 + (3\pi\gamma R)^2} \right) \right]^{\frac{2}{3}}$$

Substituting $F_0 = \frac{K(R\delta)^{1.5}}{R}$, we get

$$A_a = \pi \left[R^{1.5} \delta^{1.5} + \frac{3\pi\gamma R^2}{K} + \sqrt{\frac{6\pi\gamma R^{3.5} \delta^{1.5}}{K} + \frac{9\pi^2 \gamma^2 R^4}{K^2}} \right]^{\frac{2}{3}} \quad \text{--(1)}$$

2.1.2 Single asperity adhesive wear volume

If wear particle is in the shape of hemispherical and is cut off from tip of the asperity through shearing of cold welded junction, wear volume,

$$V_a = \frac{2}{3}\pi a^3$$

$$= \frac{2}{3}\pi \left[\frac{R}{K} \left(F_0 + 3\pi\gamma R + \sqrt{6\pi\gamma R F_0 + (3\pi\gamma R)^2} \right) \right]$$

Substituting $F_0 = \frac{K(R\delta)^{1.5}}{R}$, we get

$$V_a = \frac{2}{3}\pi \left[R^{1.5}\delta^{1.5} + \frac{3\pi\gamma R^2}{K} + \sqrt{\frac{6\pi\gamma R^{3.5}\delta^{1.5}}{K} + \frac{9\pi^2\gamma^2 R^4}{K^2}} \right] \quad \text{--(2)}$$

2.2 Multiasperity contact

First of all, Greenwood and Williamson [4] developed statistical multiasperity contact model of rough surface under very low loading condition and it was assumed that asperities are deformed elastically according Hertz theory. Same model is modified here in adhesive rough surface contact and it is based on following assumptions:

- a. The rough surface is isotropic.
- b. Asperities are spherical near their summits.
- c. All asperity summits have the same radius R but their heights vary randomly followed by Gaussian distribution.
- d. Asperities are far apart and there is no interaction between them.
- e. Asperities are deformed elastically and adhesive bonded according to JKR adhesion theory
- f. There is no bulk deformation. Only, the asperities deform during contact.

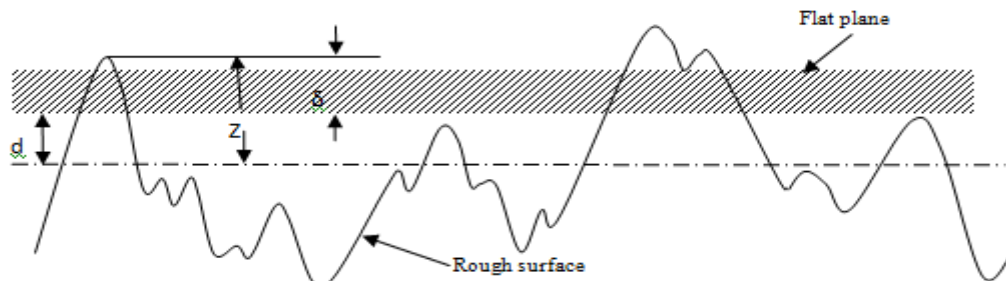


Fig. 1 Rough surfaces contact

Multiasperity contact of adhesive rough surface has shown in Fig.1 According to, GW model, two rough surface contact could be considered equivalently, contact between rough surface and smooth rigid surface. Let z and d represents the asperity height and separation of the surfaces respectively, measured from the reference plane defined by the mean of the asperity height. δ denotes deformation of asperity by flat surface. Number of asperity contact is

$$N_c = N \int_d^\infty \phi(z) dz \quad \text{--(3)}$$

where N is total number of asperity and $\phi(z)$ is the Gaussian asperity height distribution function.

2.2.1 Multiasperity real area of contact

So, from eqⁿ (1) and (3), total real area of contact for multiasperity contact is

$$A = N \int_d^\infty A_a \phi(z) dz$$

$$= N \int_d^{\infty} \pi \left[R^{1.5} \delta^{1.5} + \frac{3\pi\gamma R^2}{K} + \sqrt{\frac{6\pi\gamma R^{3.5} \delta^{1.5}}{K} + \frac{9\pi^2 \gamma^2 R^4}{K^2}} \right]^{\frac{2}{3}} \phi(z) dz$$

Dividing both side by apparent area of contact A_n

$$A^* = \int_0^{\infty} \left[\pi^{1.5} (\eta R \sigma)^{1.5} \Delta^{1.5} + 3\pi^{2.5} (\eta R \sigma)^{1.5} \left(\frac{\gamma}{K\sigma} \right) \left(\frac{R}{\sigma} \right)^{0.5} + \sqrt{6\pi^4 (\eta R \sigma)^3 \left(\frac{\gamma}{K\sigma} \right) \left(\frac{R}{\sigma} \right)^{0.5} \Delta^{1.5} + 9\pi^5 (\eta R \sigma)^3 \left(\frac{\gamma}{K\sigma} \right)^2 \left(\frac{R}{\sigma} \right)^2} \right] \phi(\Delta) d\Delta$$

$$= \int_0^{\infty} \left[\pi^{1.5} A_0^{1.5} \Delta^{1.5} + 3\pi^{2.5} A_0^{1.5} B_0 R_0^{0.5} + \sqrt{6\pi^4 A_0^3 B_0 R_0^{0.5} \Delta^{1.5} + 9\pi^5 A_0^3 B_0^2 R_0^2} \right] \frac{1}{\sqrt{2\pi}} \exp \left[-\frac{(h+\Delta)^2}{2} \right] d\Delta$$

2.2.2 Multiasperity adhesive wear volume

So, , from eqⁿ (2) and (3) adhesive wear volume for multiasperity contact is

$$V = N_c V_a$$

$$= N \int_d^{\infty} V_a \phi(z) dz$$

$$= N \int_d^{\infty} \frac{2}{3} \pi \left[R^{1.5} \delta^{1.5} + \frac{3\pi\gamma R^2}{K} + \sqrt{\frac{6\pi\gamma R^{3.5} \delta^{1.5}}{K} + \frac{9\pi^2 \gamma^2 R^4}{K^2}} \right] \phi(z) dz$$

Dividing both side by $A_n \sigma$

$$V^* = \frac{2}{3} \pi \int_0^{\infty} \left[(\eta R \sigma) \left(\frac{R}{\sigma} \right)^{0.5} \Delta^{1.5} + 3\pi (\eta R \sigma) \left(\frac{\gamma}{K\sigma} \right) \left(\frac{R}{\sigma} \right) + \sqrt{6\pi (\eta R \sigma)^2 \left(\frac{\gamma}{K\sigma} \right) \left(\frac{R}{\sigma} \right)^{1.5} \Delta^{1.5} + 9\pi^2 (\eta R \sigma)^2 \left(\frac{\gamma}{K\sigma} \right)^2 \left(\frac{R}{\sigma} \right)^2} \right] \phi(\Delta) d\Delta$$

$$= \frac{2}{3} \pi \int_0^{\infty} \left[A_0 R_0^{0.5} \Delta^{1.5} + 3\pi A_0 B_0 R_0 + \sqrt{6\pi A_0^2 B_0 R_0^{1.5} \Delta^{1.5} + 9\pi^2 A_0^2 B_0^2 R_0^2} \right] \frac{1}{\sqrt{2\pi}} \exp \left[-\frac{(h+\Delta)^2}{2} \right] d\Delta$$

3. Results and Discussion

Tayebi and Polycarpou [5] have done extensive study on polysilicon MEMS surfaces and four different MEMS surface pairs. Here, surface roughness, surface energy, and material parameters of the clean and smooth MEMS surfaces are being considered for present study as input data as given in Table.1. The material properties of MEMS surface samples are modulus of elasticity, $K = \frac{4}{3}E = 112$ GPa, modulus of rigidity, $G = 18.42$ GPa hardness, $H = 12.5$ GPa, and poisions ratio, $\nu_1 = \nu_2 = 0.22$

Johnson et.al. first mentioned that deformation of spherical contact would be greater than the deformation predicted by Hertzian spherical contact. It is mentioned that only attractive adhesive force acts within Hertzian contact area and it increases deformation of sphere resulting higher contact area. From Fig.2, dimensionless real area of contact increases with decrement of dimensionless mean separation exponentially. It is found that maximum real areas of contact for the all cases of MEMS surfaces increase as smoothness of MEMS surfaces increase. Dimensionless real area of contact for super smooth MEMS surface is very high almost near to the apparent area of contact due to presence of strong attractive adhesive force. On the other hand, real area of contact is very small for the rough MEMS surface contact.

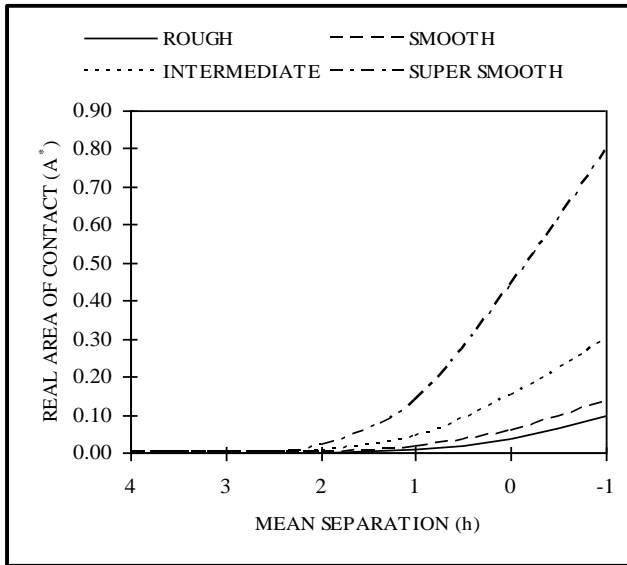


Fig.2 Real area of contact

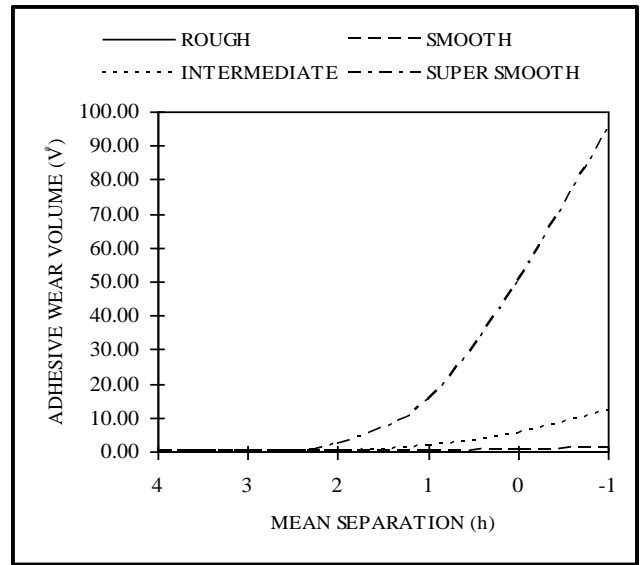


Fig.3 Adhesive wear volume

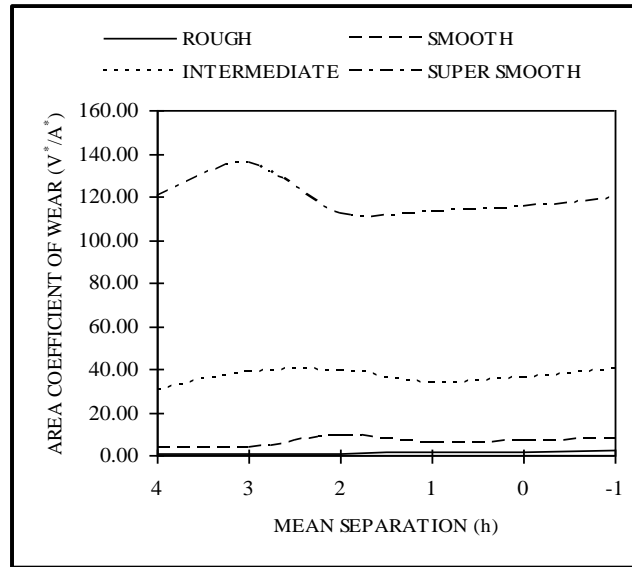


Fig.4 Area coefficient of wear

Fig.3 depicts variation of adhesive wear volume with mean separation. It is found that maximum adhesive wear volume for the all cases of MEMS surfaces increase as smoothness of MEMS surfaces increase. So, super smooth MEMS surface produces maximum adhesive wear volume whereas rough MEMS surface produces very low adhesive wear volume. Fig.4 shows area coefficient of wear verses dimensionless mean separation. This coefficient is considered to understand the relationship in between real area of contact and wear volume. From the nature of curves, it is found that dimensionless adhesive wear volume is almost linearly proportional with dimensionless real area of contact. So, area coefficient of wear is almost constant.

$$\text{So, Area coefficient of wear} = \frac{V^*}{A^*} = \frac{V}{A\sigma} = K_{adh}$$

$$\text{or, } V = K_{ad}A\sigma$$

Considering yielding of asperity of asperity tip due to loading force, real area of surface contact, $A = \frac{P}{H}$

$$\text{So, } V = K_{adh} \frac{P}{H} \sigma$$

where V = Wear volume, K_{adh} = adhesive wear coefficient (i.e. area coefficient of wear), P = loading force (i.e. Contact force), H = soft material hardness, σ = rms roughness of surface

According to new adhesive wear law, adhesive wear coefficient increases with increment of MEMS surface contact. And $K_{adh} = 0.25$ for rough surface, $K_{adh} = 5$ for smooth surface, $K_{adh} = 30$ for intermediate surface, and $K_{adh} = 120$ for super smooth surface.

Now, wear rate, $\dot{V} = V \times \text{no. of pass per revolution} \times \text{RPS} = v \times n_p \times \text{RPS}$

Generally, Pin on Disk tester are commonly used to measure wear rate. If circular cross sectional pin of diameter, d is placed on disk at diameter, D ,

$$\text{no. of pass per revolution, } n_p = \frac{\text{Total area crossed}}{\text{Cross sectional area of pin}} = \frac{\pi D d}{\pi d^2 / 4} = 4 \frac{D}{d}$$

In comparison of new adhesive wear law with Archard's law of adhesive wear, the new law is much more appropriate from the point view of volume concept. In case of well accepted Archard's law of adhesive wear, sliding distance is on the plane of real area of contact and so, how does multiplication of both the two parameter produce volume whereas in case of new law of adhesive wear, r.m.s. roughness perpendicular to the plane of real area of contact which produces volume removal in the form of adhesive wear.

Now, let us see the interrelation in between new adhesive wear law and existing Archard's adhesive wear law. Archard's adhesive wear law was developed from single asperity contact directly as follows;

$$\text{Elementary wear volume of hemispherical shape of wear particle, } V_a = \frac{2}{3} \pi a^3 = \frac{1}{3} (\pi a^3). (2a)$$

= 1/3 Area of contact of asperity \times sliding distance of asperity

Now, for multiasperity contact of rough surface, we have wear volume; $V = K_{adh} \cdot \text{Real area of contact} \times \text{Apparent sliding distance} = K_{adh} A \cdot L = K_{adh} \frac{P}{H} L$

First, Archard have developed interrelation of wear volume with real area of contact and apparent sliding distance but wear volume could not be calculated theoretically because coefficient of adhesive wear have to be quantified experimentally. Experimentally, it is found that coefficient of adhesive wear is of the order of 10^{-6} to 10^{-9} . Actually, for unit meter sliding distance, $K_{adh} \cdot L$ is real sliding distance of truncated asperities only which is of the order of 10^{-6} to 10^{-9} m. In comparison with new adhesive wear law, real sliding distance is the parameter of rms surface roughness (σ) which is also of the order of 10^{-6} to 10^{-9} m. So, new adhesive wear law is an alternative law of adhesive wear by which wear volume could be calculated theoretically.

4. Conclusion

Finally, alternative adhesive wear theory could be developed according to Mindlin's concept of stick-slip mechanism as follows.

- Microscopically, when two rough surfaces come in contact, spherical tip of asperity would deform elastically and it will stick and cold weld at the contact zone due to interatomic adhesive force under loading condition.
- Subsequent impending sliding produces maximum frictional traction at the junction of asperity contact. After maximum limit, it would slip radially inward at the circular contact zone of asperity and correspondingly, real area of contact of asperity decreases producing ultimate gross slip / sliding.
- During slipping, if shearing strength at asperity junction is much more than bulk shear strength of one of the surface, fragment of material would be removed from the softer surface. As a result one adhesive wear particle would be formed.

- At the end of one pass of sliding, volume of adhesive wear would be proportional to Real area of contact \times rms roughness. It would be of the order of nm^3 to μm^3 .
- So, Adhesive wear rate is linearly proportional to real area of contact (= Load / Hardness), rms roughness and no. of pass per unit time.

References

[1] Holm, Electric contact, H Gerbers, Stockholm, Sweden,
 [2] J F Archard, Contact and rubbing of flat surfaces. Journal of Applied Physics, 24, 1953, 981-988
 [3] K L Jhonson, K Kendall, and A D Roberts, Surface energy and the contact of elastic solids, Proc. R. Soc. Lond., A 324, 1971, 301-313
 [4] J A Greenwood, and J B P Williamson, Contact of nominally flat surfaces. Proc. R. Soc. Lond., A 295, 1966, 300-319
 [5] N Tayebi and A A Polycarpou, Adhesion and contact modeling and experiments in microelectromechanical systems including roughness effects, Microsyst. Technol., 12, 2006, 854-869

Table.1 Input data

Combined MEMS Surfaces	Rough	Smooth	Intermediate	Super Smooth
Asperity density η (m^{-2})	$14.7 \cdot 10^{12}$	$11.1 \cdot 10^{12}$	$17 \cdot 10^{12}$	$26 \cdot 10^{12}$
Asperity radius R (m)	$0.116 \cdot 10^{-6}$	$0.45 \cdot 10^{-6}$	$1.7 \cdot 10^{-6}$	$26 \cdot 10^{-6}$
Standard deviation of asperity height σ (m)	$15.8 \cdot 10^{-9}$	$6.8 \cdot 10^{-9}$	$1.4 \cdot 10^{-9}$	$0.42 \cdot 10^{-9}$
Surface energy γ (N/m)	0.5	0.5	0.5	0.5
Modulus of elasticity K (N/m^2)	$112 \cdot 10^9$	$112 \cdot 10^9$	$112 \cdot 10^9$	$112 \cdot 10^9$
Modulus of rigidity G (N/m^2)	$18.42 \cdot 10^9$	$18.42 \cdot 10^9$	$18.42 \cdot 10^9$	$18.42 \cdot 10^9$
Roughness parameter A_0	$27 \cdot 10^{-3}$	$34 \cdot 10^{-3}$	$41 \cdot 10^{-3}$	$53 \cdot 10^{-3}$
Surface energy parameter B_0	$2.825 \cdot 10^{-4}$	$6.565 \cdot 10^{-4}$	$31.887 \cdot 10^{-4}$	$74.405 \cdot 10^{-4}$
Asperity radius parameter R_0	7.342	66.176	1214.285	5600.000

Birads Score For Mammographic Images

Parveen Jaseela Regina .O. M

Regional Centre Of Anna University, Tirunelveli

Abstract

Breast imaging and screening has evolved for accurate diagnosis of breast cancer at earlier stages of development. 20% of malignant cases which has been proved as cancerous have been misinterpreted as non-detected cancers owing to technical problems in imaging procedure. These cancers is generally referred to as missed cancers (MC). Various image segmentation algorithms like K-Means Clustering , Expectation Maximization has proved for segmenting cancerous part from tumour part and statistically proved approaches for extracting features such as Area, Entropy, Clustering image, Uniformity, Mean evolved for classifying features of abnormal tissue. Evidences prove that about 65-80% of breast biopsies result in benign diagnosis and many false negative errors in retrospect considered as false positive biopsies. Hence clearer vision of classifying image based on textures provide wider view for radiologists in assessing the categories.

Keyword-malignant, missedcancers, K-Means Clustering,biopsies

1. INTRODUCTION

Breast Cancer is a malignant tumour which is a collection of cancer cells arising from the cells of the breast. BC is the one of the most leading cancer which exhibits an exceptionally heterogenous phenotype in histopathology[7]. The availability of a computerized image analysis for automated quantification will enable development of an inexpensive image-based system for predicting disease survival and outcome. Definitive diagnosis of BC is performed by a pathologists via examination of tissue histopathology typically obtained via a needle biopsy. Hence, a clinician's ability to predict survival and disease outcome may be affected by inter and intra observer variability. introduction of a novel method that enables professionals to efficiently produce medical reports that are less error-prone and can be used in decision support systems without extensive post-processing methodology[3]. Filtering algorithm begins by storing the data points in a kd-tree Recall that, in each stage of Lloyd's algorithm, the nearest center to each data point is computed and each center is moved to the centroid of the associated neighbors[10]. Accordingly, K-Means Clustering algorithm results in a partitioning of the data space into Voronoi cells where each observation is a d-dimensional real vector. Staging is the process of determining the extent of the cancer and its spread in the body. Together with the type of cancer, staging is used to determine the appropriate therapy and to predict chances for survival. Staging system is used by the health care team to summarize in a standard way the extent and spread of the cancer. This staging can then be used to determine the treatment most appropriate type of cancer. Staging is the process of determining the extent of the cancer and its spread in the body. Together with the type of cancer, staging is used to determine the appropriate therapy and to predict chances for survival. Staging system is used by the health care team to summarize in a standard way the extent and spread of the cancer. This staging can then be used to determine the treatment most appropriate type of cancer.

The most widely used system in the U.S. is the American Joint Committee on Cancer TNM system. Besides the information gained from the imaging tests, this system also uses the results from surgical procedures. After surgery, a pathologist looks at the breast cancer and associated lymph nodes under the microscope. This information gained is incorporated into the staging as it tends to be more accurate than the physical exam and X-ray findings alone. . The system, called BI-RADS, includes seven standardized categories, or levels. Each BI-RADS category has a follow-up plan associated with it to help radiologists and other physicians appropriately manage a patient's care. BI-RADS is a quality assurance tool designed to standardize mammography reporting, reduce confusion in breast imaging interpretations, and facilitate outcome monitoring. It is a lexicon of standardized terminology, a reporting organization and assessment structure, a coding system and a data collection structure Results are communicated to the referring physician in a clear fashion with a final assessment that indicates a specific course of action. Results are compiled in a standardized manner that permits the maintenance and collection analysis of mammographic and outcome data. It is important for CAD to assess not only the computer performance, but also the performance by physicians. It is thus necessary to evaluate quantitatively and accurately by use of receiver operating characteristic (ROC) analysis whether the performance by physicians can be improved by use of the computer results. In fact, even if the ROC curve for computer results in detecting clustered micro calcifications on mammograms is substantially lower than that by radiologists, the ROC curve obtained by radiologists using the computer results can be improved[4]. The extent

of this improvement due to CAD was confirmed to be statistically significant. The higher the performance of the computer, the better the overall effect on the final diagnosis. The rest of the paper is organized as follows. Section II describes about lesion segmentation from normal tissue. Section III describes the experimental results and discussions. Section IV describes the conclusion and the further work.

2. PROPOSED METHOD

The Fig.1 describes the distinctions between detection and computer applications. The work presented here may be considered as the groundwork for an overall automated classification system for use in digital mammography (DM).

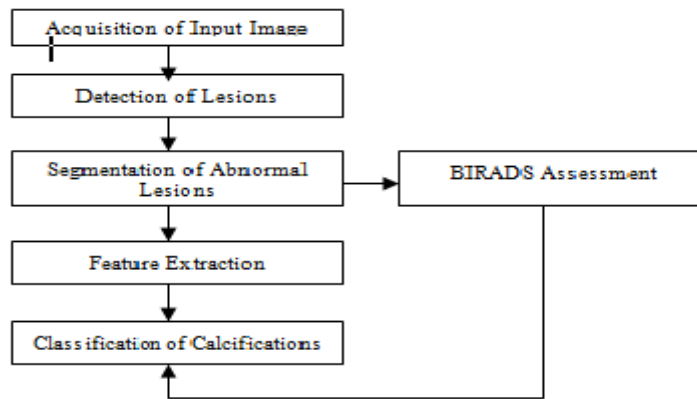


Fig.1. Block Diagram for Automated Mass classification System

Once the system is cued to the abnormality location, the classification consists of three main processing steps:

- Separate the abnormality from normal tissue
- Feature analysis.
- Classify the degree of malignancy.

3. Acquisition Of Input Image

The most common sign of breast cancer is a new lump or mass in the breast. The doctor will also look for lumps and calcifications. A lump or mass where the size, shape and edges of a lump sometimes can give doctors information about whether or not it may be cancer. On a mammogram a growth that is benign often looks smooth and round with a clear, defined edge. A digital mammogram also uses x-rays to produce an image of the breast, but instead of storing the image directly on film, the image is stored directly on a computer. This allows the recorded image to be magnified for the doctor to take a closer look. Even though mammography can detect tumors that cannot be felt, finding a small tumor does not always mean that a woman's life will be saved. Mammography may not help a woman with a fast growing cancer that has already spread to other parts of her body before being found. False negatives can happen. This means everything may look normal, but cancer is actually present. False negatives don't happen often. Younger women are more likely to have a false negative mammogram than are older women. The dense breasts of younger women make breast cancers harder to find in mammograms. False positives can happen. This is when the mammogram results look like cancer is present, even though it is not. The indifference exists between the selection of the processes and the acquisition of the image helps to classify the calcifications and provide ease for the radiologists in assessing the category of BIRADS formulated by ACR. The acquisition is followed by the detection of lesions that leads to confusion.

3.1 Detection of Lesions

Lesions may be comprised of calcifications of type micro and macro which means tiny specks of calcium and large deposits often caused by aging. If calcifications are grouped together, in a certain way, it may be a sign of cancer. Depending on how many calcium specks present, how big they are, and what they look like, doctors may suggest for further tests. Calcium in the diet does not create calcium deposits, or calcifications, in the breast. For detection the margins have to be sharply demarcated with an abrupt transition between the lesion and the surrounding tissue. Without additional modifiers there is nothing to suggest infiltration.

3.2 Segmentation of Abnormal Lesions

The most widely used segmentation algorithm preferred so far include Expectation Maximization algorithm. The EM algorithm is a general method of finding the maximum-likelihood estimate of the parameters of an underlying distribution from a given data set when the data is incomplete or has missing values. There are two main applications of the EM algorithm. The first occurs when the data indeed has missing values, due to problems with or limitations of the observation process. The second occurs when optimizing the likelihood function is analytically intractable but when the likelihood function can be simplified by assuming the existence of and values for additional but missing (or hidden) parameters. The latter application is more common in the computational pattern recognition community .

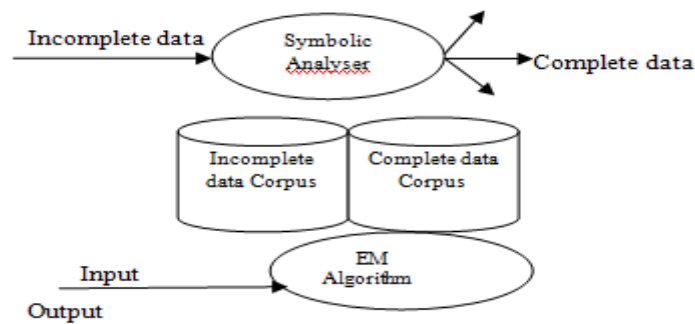


Fig. 2. Input and Output of EM Algorithm

The EM algorithm is more probabilistic in nature and more widely characterized for segmentation processes. The more appropriate algorithm that best suits for the spot detections is K-Means Clustering Algorithm since it can be refined by filtering processes. Given a set of observations (x_1, x_2, \dots, x_n) , where each observation is a d -dimensional real vector, k -means clustering aims to partition the n observations into k sets ($k \leq n$) $S = \{S_1, S_2, \dots, S_k\}$ so as to minimize the within-cluster sum of squares (WCSS).

$$(1)$$

where μ_i is the mean of points in S_i .

k -initial "means" (in this case $k=3$) are randomly generated within the data domain . k clusters are created by associating every observation with the nearest mean. The partitions here represent the Voronoi diagram generated by the means. The centroid of each of the k clusters becomes the new mean. The result of k -means can also be seen as the Voronoi cells of the cluster means. Since data is split halfway between cluster means, this can lead to suboptimal splits as can be seen in the "mouse. The Gaussian models used by the Expectation-maximization algorithm (which can be seen as a generalization of k -means) are more flexible here by having both variances and covariances. Attach label to each observation or data points in a set. You can say this "unsupervised classification" Clustering is alternatively called as "grouping".

Intuitively, if you would want to assign same label to a data points that are "close" to each other Thus, clustering algorithms rely on a distance metric between data points Sometimes, it is said that the for clustering, the distance metric is more important than the clustering algorithm. The EM result is thus able to accommodate clusters of variable size much better than k -means as well as correlated clusters .The parameters of the Gaussian mixture model were calculated for each texture in the image using EM algorithm. A likelihood function is calculated which gives the probability of a pixel as belonging to a particular class which forms the basis of labeling of the pixel. The segmentation step is the crucial stage addressed here; if it fails, the entire classification analysis fails. The goal of this work is to develop a robust method of segmenting breast masses from the normal background breast tissue. The success of automated classification requires knowledge of the mass, ambient normal-tissue, background border region, and the tumor area. The refining algorithms prevent the initial selection seed cluster points and the filtering processes makes ease of selecting the centroid that becomes a seed point to be a new cluster. The EM algorithm is applied to estimate the mean and variance of features for every texture in the image. At last a Bayesian classification rule is applied to attribute a label for each pixel by defining a likelihood function, which computes the probability for a given pixel as belonging to a given class. The Clustering algorithm will there provide simpler context in estimating the threshold value from which mean and variance need not be a probabilistic value. Algorithmically, very simple to implement . K -means converges, but it finds a local minimum of the cost function. Works only for numerical observations . K is a user input;

alternatively BIC (Bayesian information criterion) or MDL (minimum description length) can be used to estimate K. Outliers can considerable trouble to K-means.

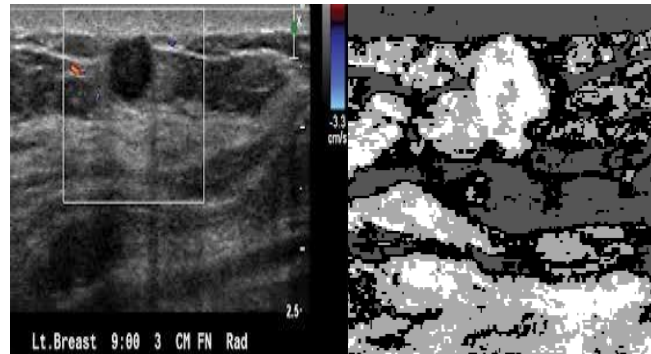


Fig. 3. Output of the Segmentation process

Where the cluster count $K=3$ and more the cluster count more the perfect segmentation and careful observation has to be performed for reducing the computational time.

4. D. Feature Extraction

To reduce the computational time required for extracting features for 256 pixel values the input image is quantized before applying the feature extraction process. Quantization can be done either to the pixel values or to the spatial coordinates. Operation on pixel values is referred to as gray-level reduction and operating on the spatial coordinates is called spatial reduction. Texture measures are derived using the gray-level co occurrence matrices. The EM algorithm is applied to estimate the mean and variance of features for every texture in the image. The feature extraction algorithms analyze the spatial distribution of pixels in grey scale images. The different methods capture how coarse or fine a texture is. The textural character of an image depends on the spatial size of texture primitives. Large primitives give rise to coarse texture and small primitives fine texture. To model these characteristics, spatial methods are found to be superior to spectral methods. Texture segmentation has long been an important topic in image processing. Basically, it aims at segmenting a textured image into several regions with the same texture features. An effective and efficient texture segmentation method will be very useful in applications like the analysis of aerial images, biomedical images and seismic images as well as the automation of industrial applications. Like the other segmentation problems ,the segmentation of textures requires the identification of proper texture-specific features with good discriminative power. Generally speaking, texture feature extraction methods can be classified into three major categories, namely, statistical, structural and spectral. In statistical approaches, texture statistics such as the moments of the gray-level histogram, or statistics based on gray-level co-occurrence matrix are computed to discriminate different textures. For structural approaches, “texture primitive”, the basic element of texture, is used to form more complex texture pattern by grammar rules which specify the generation of texture pattern. Finally, in spectral approaches, the textured image is transformed into frequency domain To circumvent the above-mentioned issue, in this study, based on the fact that each interior point in a texture region must posses similar properties with its neighbors, a new statistical method is proposed. The key idea is that if the pixels of the input image can be classified into interior pixels and boundary ones, the interior pixels stand for the interior parts of texture regions, then the segmentation can be achieved by applying region growing on the interior pixels.

4.1 Statistical approaches

A frequently used approach for texture analysis is based on statistical properties of intensity histogram. One such measure is based on statistical moments. Various features are as follows,

$$(2)$$

which gives a measure of average intensity.

$$\text{Variance}, \quad (z) \quad (3)$$

which gives a measure of average contrast.

$$(4)$$

which gives a measures the uniformity of intensity in the histogram.

$$Ent \quad (5)$$

which gives a measure of randomness.

Once the features are extracted from the input image set the threshold value thereby Area ,Entropy ,Clusterized image, Mean ,Variance are found using matlab code and the work will be made ease for the radiologists to assess the abnormalities. Statistical approaches like uniformity also specify the texture of the lesion and the probability of occurrence will be visually observed through the above mentioned features. The unit of specification is not mentioned as if predictions are based on the count of pixels and the image boundary.

5. RESULTS AND DISCUSSIONS

After number of simulations performed on the images varies statistical textures were obtained .

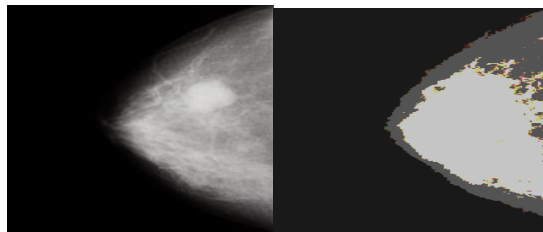


Fig .4 (a) Input Image

Fig .4 (b) Clusterized Image



Fig .4 (c) Binary Image

Fig .4 (d) Gray Image

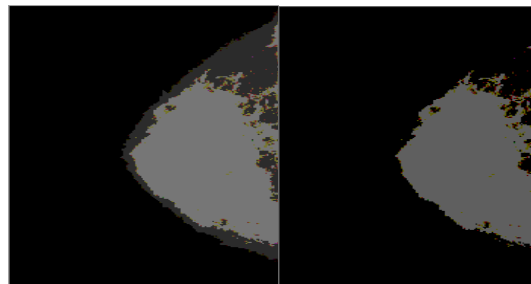


Fig .4(e) Area

Fig .4(f) Mean

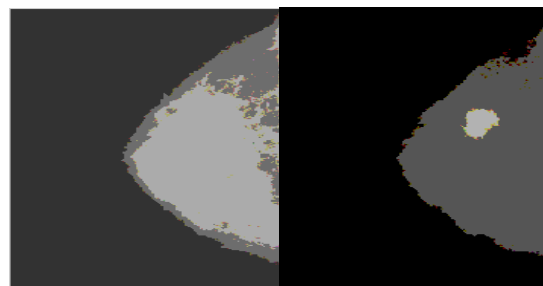


Fig .4(g) Variance

Fig .4(h) Resultant Image

Figure. 4(a) represents the calcification of size of the input $<400*267*3\text{uint}8>$. (b) represents the cluster count that has been taken here as $K=3$. (c) represents the Binary image which provides the differentiation of the object and background.(d) represents the gray image that provides the threshold range of 0.3137.(e) gives the spread

of metastasis state where the area of the image is clearly shown as 3449 and (f) represents the mean of about 4 that provides the average smooth of the spread and makes it easier for assessing the image. The assessment will be assisted by the use of CAD tool with automated tool for maintaining the patient archiving ,Medical data with CAD assess that leads to better diagnosis. (g) represents the average contrast that is a measure of uniformity and it varies depends upon the cluster count and (h) provides the final resultant image of the clusterized image from which the analysis of the category of the image begins. The further processing has been made for large number of samples for classifying the abnormalities such as Compressed tissue, fatty and Non-fatty that leads to complexion and the categories for biopsies are verified using these samples. In this paper three samples have been taken and the output is verified using the resultant image, Variance analyzing the contrast.

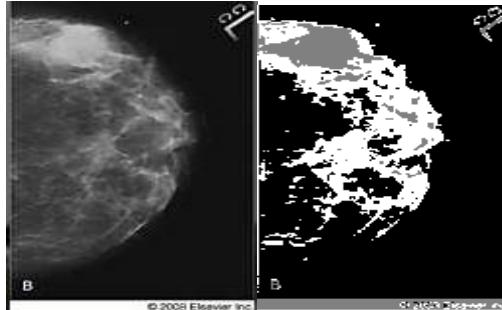


Fig. 5 (a) Input Image Fig. 5 (b) Clusterized Image

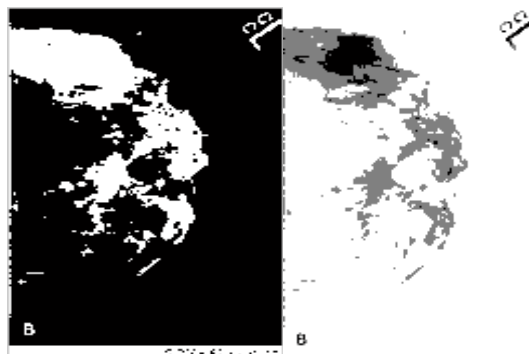


Fig. 5(c) Binary Image Fig. 5(d) Gray Image

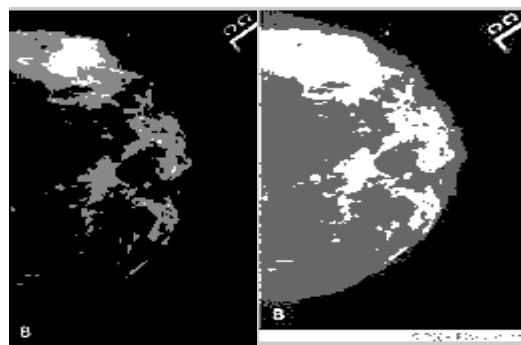


Fig. 5 (e) Area Fig. 5 (f) Mean

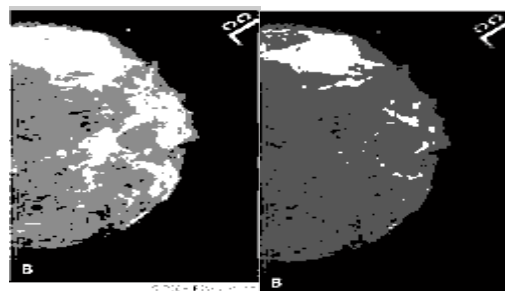


Fig. 5(g) Variance Fig. 5(h) Resultant Image

Figure. 5(a) represents the calcification of size of the input $<200*126*3uint8>$. (b) represents the cluster count that has been taken here as $K=3$. (c) represents the Binary image which provides the differentiation of the object and background.(d) represents the gray image that provides the threshold range of 0.3608(e) gives the spread of metastasis state where the area of the image is clearly shown as 2001 and (f) represents the mean the provides the average smooth of the spread and makes it easier for assessing the image. The assessment will be assisted by the use of CAD tool with automated tool for maintaining the patient archiving ,Medical data with CAD assess that leads to better diagnosis. (g) represents the average contrast that is a measure of uniformity and it varies depends upon the cluster count and (h) provides the final resultant image of the clusterized image from which the analysis of the category of the image begins.

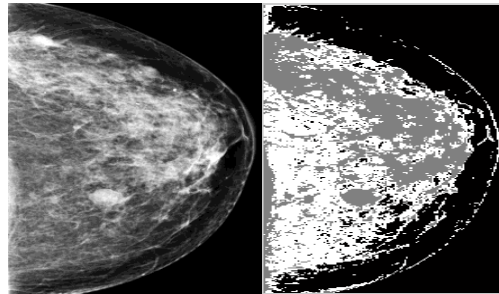


Fig. 6(a) Input Image Fig. 6 (b) Clusterized Image

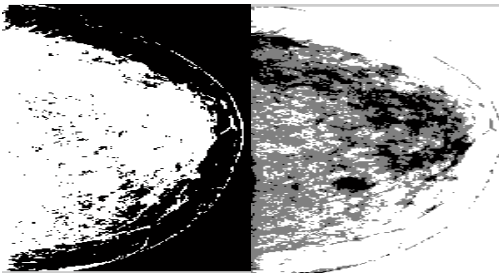


Fig. 6 (c) Binary Image Fig. 6 (d) Gray Image

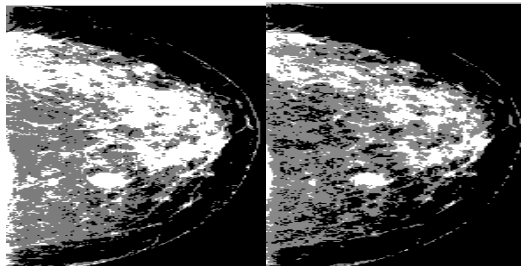


Fig. 6 (e) Area Fig. 6 (f) Mean

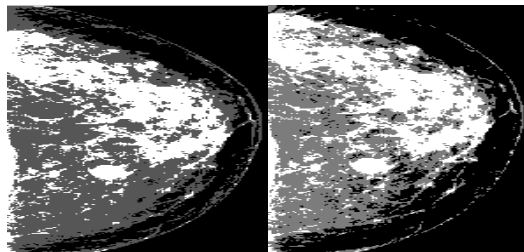


Fig. 6 (g) Variance Fig. 6 (h) Resultant Image

Figure. 6(a) represents the calcification of size of the input $<440*227*3uint8>$. (b) represents the cluster count that has been taken here as $K=3$. (c) represents the Binary image which provides the differentiation of the object and background.(d) represents the gray image that provides the threshold range of 0.3176.(e) gives the spread of metastasis state where the area of the image is clearly shown as 49813 and (f) represents the mean the provides the average smooth of the spread and makes it easier for assessing the image. The assessment will be assisted by the use of CAD tool with automated tool for maintaining the patient archiving ,Medical data with

CAD assess that leads to better diagnosis. (g) represents the average contrast that is a measure of uniformity and it varies depends upon the cluster count and (h) provides the final resultant image of the clusterized image from which the analysis of the category of the image begins.

Images	Cluster	Area	Threshold	Mean	Variance
			d	n	e
Image a	[185,161,17]	3449	0.3137	4	170
Image b	[25,83,197]	2001	0.3608	50	63
Image c	[50,171,109]	49813	0.3176	63	228

Table 1. Performance Analysis of Image Types

The above experimental results were performed for inputs that comes under the category of uncompressed fatty tissue since the benign and malignant stages were absolute for cluster count K=3. For more beneficiary outputs the computation time of CAD processing becomes more tedious and further analysis have to be made for detecting compressed and fatty tissues.

6. Conclusion

Cluster value chosen as K=3 and more the cluster count more the efficient image segmentation. My future work includes the Classification of images by a better algorithm that aids CAD system to help Radiologists even more better. For better performance analysis cluster count can raised and segmentation along with computer aids can be used for better radiological assessment. Raising the cluster count may take more time consuming and using refining filtering algorithm procedures differentiation from tumour, the cancerous part can be detected. The Radiologists will be able to provide report for biopsy proven cancer tissue and be able to categorize benign and malignant tissue.

7. Future Scope

The future scope includes the Classification of images by a comparison made with breast tomosynthesis and evaluated using thermographic analysis that aids CAD system to help Radiologists even more better for differentiating between masses and density. The Breast tomosynthesis method employ reconstruction method for improved detectability of microcalcifications (MCs).

References

- [1] Marwa A. Shaaban, Abo El-Ata K. Aly, "Real-time ultrasound elastography: Does it improve B mode ultrasound characterization of solid lesions." The Egyptian Journal of Radiology and Nuclear Medicine (2012) 43, 301-309.
- [2] BasakOztan, Hui Kong, Metin N. G'urcab, and B'ulentYener, "Follicular Lymphoma. Grading using Cell-Graphs and Multi-Scale Feature Analysis." Medical Imaging 2012: Computer-Aided Diagnosis, Proc. Of SPIE Vol .8315,831516.
- [3] Kuru, S. Girgin, K. Arda, U. Bozlar, "A novel report generation approach for medical applications: The SISDS methodology and its applications." International Journal of Medical Informatics (2012).
- [4] Arnau Oliver, Jordi Freixenet, Joan Marti, Elsa Perez, Josep Pont, Erika R.E., "A review of automatic mass detection and segmentation in mammographic images." Medical Image Analysis 14 (2010) 87 -110.
- [5] Georgia Giannakopoulou, George M.Spyrou, ArgyroAntaraki, IoannisAndreadi, "Downgrading BIRADS 3 to BIRADS 2 category using a computer -aided microcalcification analysis and risk assessment system for early breast cancer", Computers in Biology and Medicine 40 (2010) 853-859.
- [6] Ajay NageshBasavanhallyand James Peter Monaco, "Computerized Image-Based Detection and Grading of Lymphocytic Infiltration in HER2+Breast Cancer Histopathology". IEEE Transactions on Biomedical Engineering Vol 57, No 3 March (2010).
- [7] Hussian Fatakdawala, Jun Xu, Ajay Basavanhally, Gyan Bhanot, Shridhar Ganesan, "Expectation-Maximization-Driven Geodesic Active Contour with Overlap Resolution (EMaGACOR): Application to Lymphocyte Segmentation on Breast Cancer Histopathology." IEEE Transactions on Biomedical Engineering, Vol 57 No 7 July 2010.
- [8] H.S. Sheshadri and A. Kandaswamy, "Experimental investigation on breast tissue classification based on statistical feature extraction of mammograms". Computerized Medical Imaging and Graphics 31 (2007) 46-48."
- [9] Dr.K Revathy, Roshni V. S, "Applying EM Algorithm for Segmentation of Textured Images." Proceedings of the World Congress on Engineering 2007 Vol I.
- [10] Catarious, D.M., Baydush, A.H., Floyd, C.E., (2006). "Characterization of Difference of Gaussian filters in the detection of mammographic regions." Med.Phys.33(11)4104-4114.

CONCEPT DRAWING FOR OIL DRAINING MACHINE FOR VTU WITH NUMERICAL ANALYSIS

Prajwal Shantalwar¹, Smitesh Bobde², Bhojraj Kale³, Vivek Patil⁴

¹Prajwal Shantalwar, DBACER, ²Smitesh Bobde, DBACER ³Bhojraj Kale, DBACER
⁴Vivek Patil, DBACER

Abstract:

The aim of this Project is to Manufacture and design Oil Draining unit for Vary Touch Unit (VTU) to overcome the current problem of the industry and to make the efficient unit to increase the productivity and reduce the human fatigue. The proposed machine will be automated and will work with the help of PLC program. The machine will be compact as compared to the existing unit and it will be easy for the maintenance work whether it is mechanical or electrical or instrumental side as all the components on the machine will be easily approachable.

Keywords: The machine will be completely automated and will work on the PLC program.

1. Introduction:

Introduction Of Current System

The VARY TOUCH UNIT (VTU) is a part of TRACTOR which is use to hold the Plough. The VTU contains hydraulic oil due to which it can hold the weight of around 800kg firmly After Load testing of Vary Touch Unit in the process the parts which pass all the criteria are ready for the dispatch for final use before introduction of these parts in to the market the oil which it contains it must be drained out completely The current unit which is use for draining purpose has some limitations due to which the productivity of the plant is decreased and the plant is under maintenance for more time due to MECHANICAL and ELECTRICAL break downs. The problem which the industries are currently facing with current unit are listed below

- 1) Frequent breakage of hinges used in structure.
- 2) It is not PLC based.
- 3) OIL draining Problem.
- 4) Collection of drain Oil is also difficult
- 5) Cycle time req. for draining oil is more
- 6) The conveyor on which the VTU draining is done is not properly aligned with the before and after conveyor
- 7) After lifting and tilting the VTU for Oil draining it touches the VTU which lies behind it.
- 8) The clamping mechanism which is available for holding the VTU while lifting and tilting is manual.
- 9) The position of lifting cylinder is in the pit and the drain oil is deposited in the pit so that the floor is become slippery which may cause accident.

2. Proposed System:-

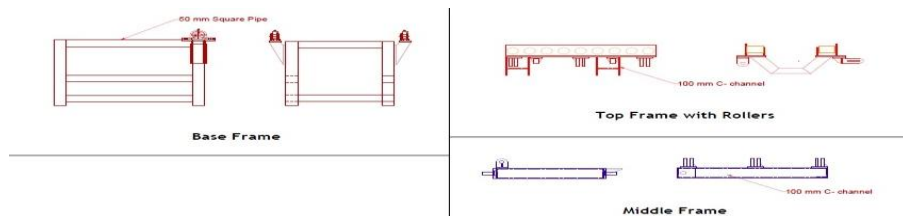
The proposed system will overcome the entire problem which is associated with the current system in terms of productivity and function ability; the proposed system will comprise the following characteristics

1. The hinges which will be used are machined hinges.
2. The entire unit will be PLC based.
3. Try to reduced maximum use of Hinges and instead of Hinges at few points will use Plummer Block for proper and smooth motion
4. For draining purpose there will be a drain tank on unit itself and it will contain the drain tap at the base so that the collected oil will be transferred easily to oil tank.
5. The unit will at the height of the before and after conveyor so that it will be align properly with the existing conveyor.
6. After lifting and tilting of VTU for Oil draining it will not touch the VTU which lies behind it.
7. The clamping will be automated in our unit and it will be hydraulically operated so that the it will hold the VTU firmly
8. The position of lifting cylinder will be on the structure itself and it will avoid the saturation of oil on the floor

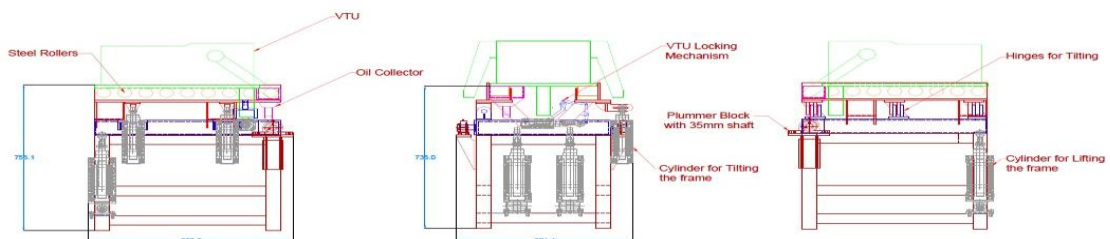
With this unit we will try to make the best draining unit and it will increase the productivity and the number of VTU dispatch per day will increase as the chances of breakdown of the unit will reduced. The unit which we are introducing will try to couple with the vacuum pump also so that the strain mark of the oil or the oil which will present in the oil chamber of VTU will be sucked completely. As soon as the draining cycle will complete the Vacuum pump will get actuated and it will be connected with the PLC itself.

3. CONCEPT DRAWING

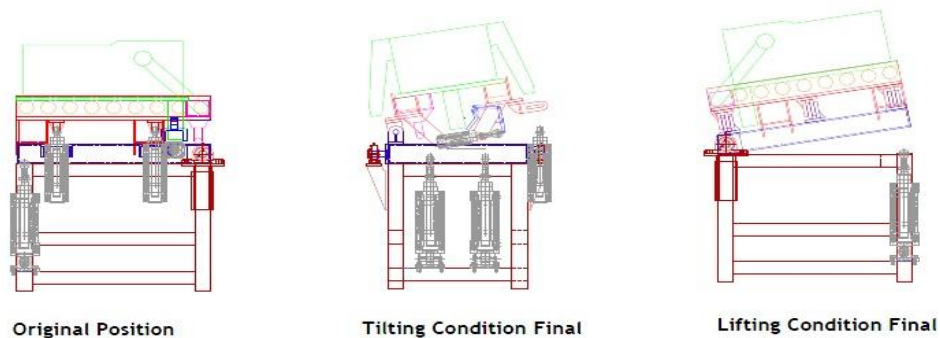
a) Part Drawing



b) Assembly Drawing



4. Proposed Working Condition



5. Proposed Sequence of Operation

1. Operator will press the start cycle button.
2. System will sense the presence of VTU on the drain unit and will start only if there is VTU present.
3. Lock cylinder between incoming VTU and drain unit will be actuated.
4. Next locking clamp cylinder for VTU locking on drain unit will be activated.
5. After 1 sec delay the first platform cylinder will be actuated and simultaneously a connection to vacuum pump will actuate to start the vacuum pump.
6. After delay of 3-5 sec, second platform's tilting cylinder will be actuated.
7. System will remain in tilted position for 30 Seconds (Can be set as required).
8. After cycle completion both tilting and lifting cylinders will be deactivated and system will come to its home position.
9. Next VTU will be unlocked by deactivating respective clamp cylinder
10. Lock cylinder will be deactivated after a delay of 5 second so that operator will get time to unload the VTU.

5.5 Numerical Calculation:-

Load of the object = 130Kg

Weight of Top Frame = 60Kg

Weight of Middle Frame = 60Kg

Total Weight = 250Kg

For Design Consideration

Assume Total Weight = 300Kg

a) Initial Condition

When the part is loaded on the machine and the machine is in **ideal** condition

$$\sigma = F/A$$

$$= (300 \times 9.81) / 100$$

$$= 29.43 \text{ N/mm}^2$$

$$\sigma \text{ (for Single leg)} = 7.35 \text{ N/mm}^2$$

Bending Moment:-

$$R_A + R_B = 300 \times 9.81$$

$$R_A + R_B = 2943 \text{ N}$$

$$\sum M_A = 0$$

$$R_B \times 0.56 = 2943 \times 0.28$$

$$R_B = 1471.5 \text{ N-m}$$

&

$$R_A = 1471.5 \text{ N-m}$$

Bending Moment at C

$$\sum M_c = 0$$

$$1471.5 \times 0.25 = R_c$$

$$R_c = 412.02 \text{ N-m}$$

Bending Stress

$$M / I = F / Y = E / R$$

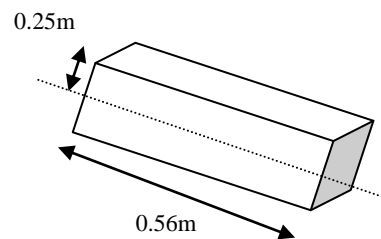
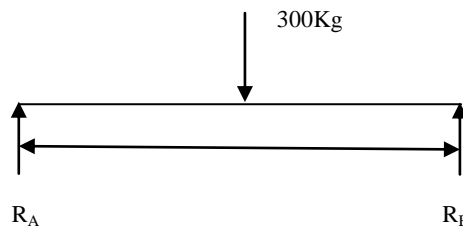
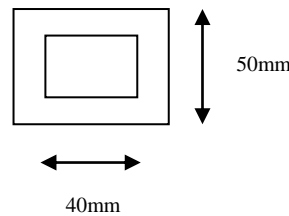
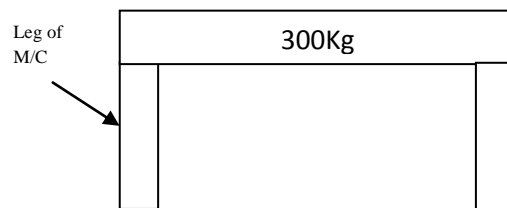
M = Max. Bending Moment

I = Moment of Inertia

F = Bending Stress

Y = Distance of Neutral Axis

$$Y = 0.25 \text{ m}$$



$$M = 412.02 * 10^3 \text{ N-mm}$$

$$I = (BD^3 / 12 - bd^3 / 12)$$

$$= (50^4 / 12 - 40^4 / 12)$$

$$= 307500 \text{ mm}^4$$

$$412.02 * 10^3 / 307500 = F/25$$

$$F = 33.49 \text{ N/mm}^2$$

b) Lifting Condition:-

$$300\text{Kg}/0.56\text{m} = X/1\text{m}$$

$$X = 535.71\text{Kg}$$

$$W = \frac{1}{2} * (535.71 * 9.81) * 0.56$$

$$= 1471.4\text{N}$$

$$R_A + R_B = 1471.4\text{N}$$

$$\Sigma M_A = 0$$

$$0.56 * R_B = 1471.4 * 0.186$$

$$R_B = 1471.4 * 0.186 / 0.56$$

$$R_B = 488.5\text{N}$$

$$R_A = 982.4\text{N}$$

$$A = \pi * D * W$$

$$= \pi * 25 * 5.4$$

$$A = 424.11\text{mm}^2$$

$$B = F/A$$

$$= 5255 / 424.11$$

$$B = 12.39\text{N/mm}^2$$

B

c) Tilting Condition:-

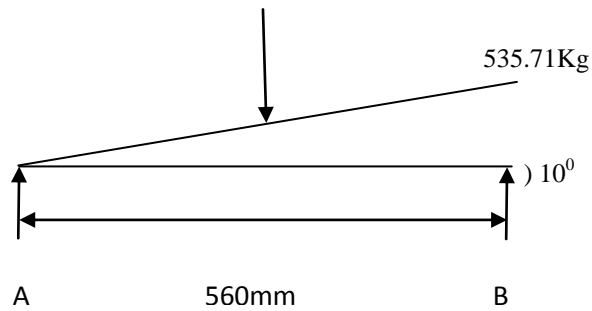
Weight of frame: - 240Kg

$$134.4 * 9.81 = 1318 \text{ N}$$

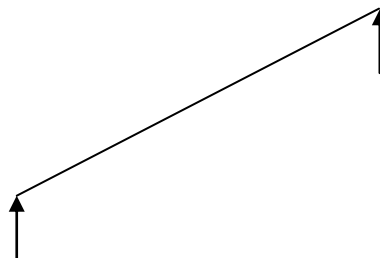
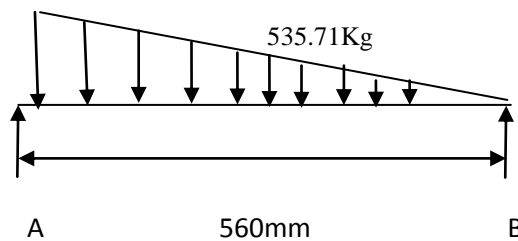
$$F = 1318 \text{ N}$$

$$R_A + R_B = 1318 \text{ N}$$

$$\Sigma M_A = 0$$



c



A

$$.56 R_B = 1318 \cdot 28$$

$$R_B = 659 \text{ N}$$

$$R_A = 659 \text{ N}$$

$$240 \cdot .56 = 134.4 \text{ Kg}$$

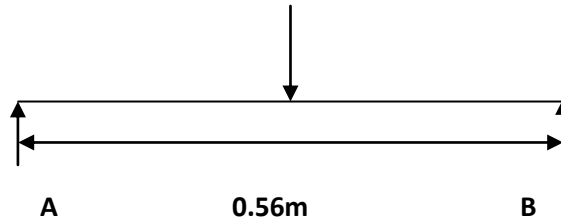
B.M. at A = 0

$$B=0$$

$$C = 659 \cdot 28$$

$$C = 184.52 \text{ N}$$

Bending Stress



$$M / I = F / Y = E / R$$

M = Max. Bending Moment

I = Moment of Inertia

F = Bending Stress

Y = Distance of Neutral Axis

$$M = WL/4$$

$$= 134.4 \cdot .56/4$$

$$= 18.8 \text{ N-M}$$

$$M = 18.8 \cdot 10^3 \text{ N-MM}$$

$$I_{XX1} = 122 \cdot 5^3 / 12 + (122 \cdot 5 \cdot 50^2)$$

$$I_{XX1} = 1.56 \cdot 10^6$$

$$I_{XX2} = 5 \cdot 90^3 / 12$$

$$= 3.03 \cdot 10^5$$

$$I_{XX2} = 3.03 \cdot 10^5$$

$$I_{XX3} = 122 \cdot 5^3 / 12 + (122 \cdot 5 \cdot 47.5^2)$$

$$= 1.3 \cdot 10^6$$

$$I_{XX3} = 1.3 \cdot 10^6$$

$$I_{XX} = I_{XX1} + I_{XX2} + I_{XX3}$$

$$= 1.56 \cdot 10^6 + 3.03 \cdot 10^5 + 1.3 \cdot 10^6$$

$$= 3.16 \cdot 10^6$$

$$F = M \cdot L / I_{xx}$$

$$= 18.8 \cdot 10^3 \cdot 50 / 3.16 \cdot 10^6$$

$$= .290 \text{ N / M}^2$$

$$F = 2.90 \text{ N / MM}^2$$

Bending Stress = 2.90 N / MM²

References

- [1] Design data book by B.D.Shivalkar
- [2] Auto CAD Software
- [3] Machine Design by R. K. Bansal
- [4] Machine Design by Khurmi Gupta

Newly Developed Automatic Lay-Up Process for Manufacturing of FRP Sheets

Prof. A. R. Chaple¹, Prof. S.S. Khedakar², Prof. S.R. Dharmadhikari³, Mr. N.R. Chaple⁴.

¹ Asst.Prof., Dept Of Mechanical Engg., DBACER, Nagpur (M.S.), India.

² Asst.Prof., Dept Of Mechanical Engg., YCCE, Nagpur (M.S.), India.

³ Asst.Prof., Dept Of Mechanical Engg., SDMP, Nagpur (M.S.), India.

⁴ M.E. (CAD/CAM), Dept Of Mechanical Engg., Prof.RMITR Badnera , Amravati (M.S.), India.

Abstract:

Hand lay-up process is fabrication process to manufacture of FRP products. FRP or fiberglass corrugated roof sheet also manufactured by hand lay-up process, but some problems has been arise with this method such that, mainly low production rate of sheets; uniform thickness not maintaining; lay-up does not uniformly perform, resin is harmful for human. These problems can be eliminated by hand lay-up process converted into Automatic lay-up process with providing safety environments for works. In this paper also discussed about different composite materials of methods for manufacturing of roof sheet and other products.

Keywords: Corrugated roof sheet, Composite materials, FRP, Fiberglass, Hand lay-up, Gantry structure, Automatic machine.

1. Introduction

Now days, the Fiber Reinforced Plastic (FRP) products are generally manufactured by the Hand Lay-up or spray-up process. Hand Lay-up process is a simple method and economically cheap process w.r.t. other methods of FRP product manufacturing. The paper describe about automatic lay-up method of manufacturing of corrugated fiberglass roofing sheets, now days, manufacturing by Hand Lay-up process, this process done by manually with the help of equipments, it consists of open mold, brush, squeeze roller. Fiberglass is the composite material of resin and chopped fiber strand or fiber mats. This process is simple and economical for production of FRP product, but some problems are arise from these process such that,

- Production rate of corrugated fiberglass sheet is low i.e. approximately 50-60 sheets per day (i.e. 12 hr. shift.),
- Thickness of sheet is not uniform.
- Lay-up process does not perform uniformly i.e. when perform lay-up of resin on mold; the amount of resin is not taken with specific amount for lay-up on mold surface.
- Resins are harmful to human.
- Fiberglass strand does not uniformly sprayed on mold, therefore, strength of sheet does not uniform on sheet.

These above problems are eliminated; Hand lay-up process is converted into Automatic Lay-up process.

1.1. What Is The Hand Lay-Up Process?

Hand Lay-up is fabrication process of FRP products (Fiber Reinforced Plastic). The FRP is composite material of Resin and Fiberglass strand or Fiberglass mat. It involved building up layers of chopped glass or woven glass mat impregnated with catalyzed resin around a suitable mould. The reinforcement is then rolled for better wet-out and removing trapped air.

1.2. Steps of Hand lay-up process

Hand lay-up process is an open mold process. It is a simple process to manufacturing of FRP products
Preparing Mold:-

We take mold and removing any dust and dirt from mold. The mold material may be plaster, wood or new fiberglass, apply soft wax, P.V.A. and buff with soft towel.

- **Applying Resin:-**

Resin is applied on mold by the brush. The brush is move like to painting of wall.

- **Lay-up of Fiberglass:-**

Brush is applied of resin on mold then chopped fiber glass strands spread over the resin layer.

- **Applying Resin:-**

Again apply the resin layer over the glass strand layer by using brush.

- **Squeeze Action:-**

Second layer of resin is applied then roller is move over the layers of resin-fiberglass-resin, for removing the air between in layers. This action called squeeze action. This squeeze action also used for compact the product.

- **Remold :-**

Lastly the sheet is removing from mold for hardening of sheet, the left in air at room temperature. And remold product is final of a corrugated fiber roofing sheet. We ask that authors follow some simple guidelines. In essence, we ask you to make your paper look exactly like this document. The easiest way to do this is simply to download the template, and replace the content with your own material.

2. Literature Review:

The main purpose of that paper, to improve the manufacturing method of corrugated fiberglass roofing sheet. Today's used manufacturing method of corrugated fiberglass roofing sheet of Hand Lay-up process is converted into Automatic Lay-up process. Today's in the market available of various types of corrugated roofing sheets with different materials such as Steel (G.I. steel), Plastic, Composite materials etc. composite materials of Cement fibrous, Fiber Reinforce Plastic. These different materials of sheets are manufactured by using different manufacturing methods. Like that, for Steel corrugated roofing sheets manufactured process by using roll forming method; for Plastic corrugated roofing sheets manufacturing process by using Extrusion method; for Cement fibrous corrugated roofing sheets manufacturing process by using Hatschek method; for FRP corrugated roofing sheets manufacturing by using Hand Lay-up or Spray Lay-up method.

Cement fibrous corrugated roofing sheets like to be fiberglass roofing sheets, the different between both sheets are made from different materials. Cement fibrous sheet is in the used cement materials for bounding the fibers. And FRP sheet is in used the resin for bounding the fiberglass. These both sheets materials group is belong to composite materials. The fiber is used in sheet for increase the wind strength of sheet. Different materials of sheets, so different manufacturing methods of these. Hashem Akbari, Ronnen Levinson, and Paul Berdahl [6], they are discussed about the methods for the manufacturing of Residential Roofing materials. Such that, shingles; Clay tiles; Concrete tiles; Metal roofing. In this paper discussed about climate of California, the demand for cooling energy, increasing roof solar reflectance reduces energy consumption in mechanical cooled building, and improves occupant comfort in non-conditioned buildings, with manufacturing methods and innovative methods for increasing the solar reflectance of these roofing materials. In cement fibrous sheets, the major components involved cement, water, silica, lime stone flour and fibers. The cement fibrous corrugated roofing sheets manufacture by different methods, AL Moselemi [1], to provide an overview of the different technologies that are currently in use to manufactured of cement fibrous sheets, the most popular technology used in fiber cement manufacturing is the Hatschek process and other processes are used such as Extrusion machine, Fourdrinier forming machine, Pour-on Technology, Wounder Board Process, Cement-Bonded particle board, Wood wool Boards, Block and Siabs. These technologies are currently used for manufacturing of cement sheets in factories. Hatschek process is very old method was developed in 1890's for production of asbestos cement product. Tony Cook [4], describes the details working mechanism about Hatschek machine process for manufacturing of fiber cement sheets. This method is helpful for film formation cement fibrous sheets in uniform thickness and flatness of sheet.

S. Delvasto, E.F. Toro, F. Perdomo [2], this are discussed about another technology for manufacturing of corrugated fiber reinforced cementitious sheets using Vacuum forming technology. The machinery used in cylinder forming process is simple; this technology appropriate for small scales of production and it is an environmental friendly low cost appropriate technology that does not need skilled labour. Ciarlini Sergio [3], the discussed about existing manufacturing methods and to improve the existing method for manufacturing of corrugated cement fiber sheet. In an existing method of corrugated sheets in find it microscopic discontinuities, formation of cracks, delaminations, breakages, these all drawback eliminated by improving and small changes in method for producing corrugated cement sheets. Bijkerk, Bakker and Deblauwe [5], in this paper invention about the finished product of fiber cements are protected from scuffing damage during storage, transport, handling and fixing or mounting. Therefore, to applied spacer of hot melt adhesive to the back side of finished product and described the manufacturing method for applying the spacer, to extend the Hatschek process which was originally applied to the asbestos cement technology. Above manufacturing methods and technology of to produce corrugated fiber cement sheets, these manufacturing technologies will be helping for to introduce the Automatic technology for manufacturing corrugated fiberglass roofing sheets.

3. Solution On Existing Systems Problems

In hand lay-up method arises above problems these problems are overcome by conversion of manually operated hand lay-up process into automatic lay-up process i.e. all operation steps are performed by the automatically using dedicated system.

Describe automatic systems are related to the existing system in following.

- [1] Preparing Mold:-
- [2] In existing system, removing of dust by soft cloth and apply wax and PVA by manually using soft towel.
- [3] In Automatic system, already die used dust free and PVA agent apply by spraying system on mold.
- [4] Applying Resin :-
- [5] In existing system, resin apply on mold with help of brush, the brush is move like to paint.
- [6] In Automatic system, resins apply by spray system or dumping of resin in mold.
- [7] Lay-up of fiberglass :-
- [8] In existing system, chopped fiber spread by hand on layer of resin.
- [9] In Automatic system, chopped fiber spread with help of fiber spread unit.
- [10] Again applying Resin:-
- [11] In existing system, second layer of resin applied on fiber with the help of brush. It is same like to first layer of resin.
- [12] In Automatic system, second layer of resin applied by spray system or dumping of resin in mold.
- [13] Squeeze Action:-
- [14] In existing system, squeezing action performs by roller applying hand force and move more layer of resin – fiber – resin.
- [15] In Automatic system, squeezing actions perform by automatic roller by self weight of roller for compacting and air releasing between layer of resin and fiber.
- [16] Remold:-
- [17] In existing system, after hardening of sheet, the remold by manually.
- [18] In Automatic system, the remold operation by using automatic ejection system to remove sheet from mold.

3.1. Required components for Automatic Lay-up System:-

- a. PVA Spray Unit.
- b. Resin Spray Unit.
- c. Fiber Spread Unit.
- d. Roller Unit for squeezing action.
- e. Ejection System.

4. Structure Of Automatic Machine

Structure is basic part of every machine for holding of all unit of any system. In Automatic lay-up system used gantry type of structure used for holding and performing of operations by separates units.

4.1 Construction of Structure:-

It consists of base table, columns, and guide ways rod. The base table is place on floor and four columns are mounted on table, at near about end corner of table. The column used for support to the guide ways rod shown in fig.1. These guide way rod used for the travelling the units on mold for performing operations.

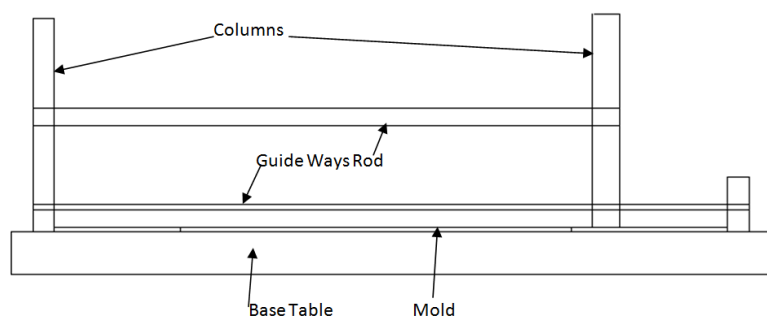


Figure 1 Basic Structure of Automatic Lay-up Process

5. Proposed System For Automatic Lay-Up Process

Three systems are proposed for Automatic lay-up process in following.

5.1. Proposed System “A”

Construction & Working of Machine: -

This system used in gantry type of structure it is shown in fig.2, it consists of base table, column, resin spray unit, PVA spray unit, flap system, fiber glass spread unit, roller unit, and mold. These arrangements show in fig.2, Base table mount on angle type of structure. Four columns are mounted on base table for supporting to guide ways rod. On this guide ways rod mounted spray units, flap system, fiber spread unit, roller unit for to travelling on mold for performing of operation simultaneously, with the help of motion mechanisms applying individual external sources. In this system three guide ways are used for holding units. On one guide way for fiber glass spread unit. Second guide way for flap and squeeze unit and third guide way for spraying unit.

Working of Machine:-

In this system, firstly applying the PVA agent on mold by using spray unit, these spray unit having two nozzle one for PVA and other for Resin. The spray unit move on y-direction of guide way for dumping of PVA in mold like to paste, now, flap system is activated for PVA apply on mold uniformly. This flap taken initial position after completion of laying process of PVA. Whenever flap activated before that nozzle tip is rotate to 90^0 at shown in fig.2, for avoiding of accident, then flap move for performs of work. Now nozzle position is taken original after flap comes to initial position. The nozzle is ready for dumping the resin in mold when the spray unit moves to initial position i.e. backward moment. Again nozzle tip is rotate at 90^0 . Flap is ready for perform the lay-up operation on mold. After completion of lay-up of resin operation the flap comes to initial position. Now, fiber glass spread by spread unit this units are place to other end of table i.e. left end it is shown in fig.2, after completion of fiber spread operation these comes to origin position. Next step is again activated resin nozzle for dumping of resin in mold same to move of spray unit in y-direction but now the completion of spraying of resin the unit comes to origin position, and taken rotate at 90^0 . Flap is move for performing of lay-up operation on fiber glass layer. Now, flap stop at the other end. The next step is squeezing operation by using roller units. The roller units move on layer of resin-fiber-resin for releasing of air and compacting of product. This roller unit two times of performing squeezing action, one forward direction and second is backward direction. Lastly roller unit comes to origin position as well as flap also comes to origin position, after hardening of sheet remove from mold. This cycle is repeated for manufacturing of sheets.

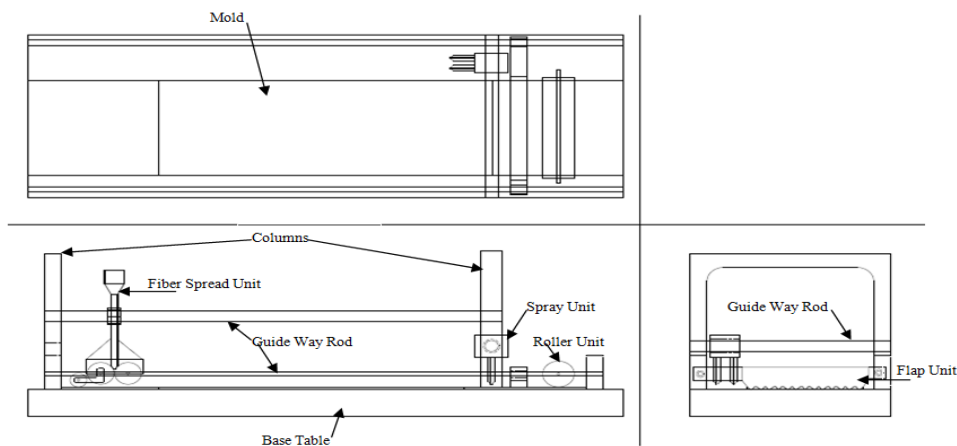


Figure 2. First Proposed System for Automatic Lay-up Process

5.2. Proposed System “B”

Construction & Working of Machine: -

In Second proposed system construction is same near about to first proposed system. The little change is spray unit motion and number of nozzles for dumping of resin in mold. In this spray unit move in vertical direction like up and down for dumping of resin in mold. It is shown in fig. the PVA nozzles and Resin nozzles are arrange to opposite side its shown in fig.3, first pair of PVA nozzle dump PVA in mold. Before that spray unit rotate 90^0 for avoiding accident and move the flap used for performing uniform lay-up operation. After that completion of lay-up for PVA. Now, spray unit rotate next at 90^0 and ready for dumping of resin in mold. After dumping of resin operation the spray unit again rotates at 90^0 , and flap activated for lay-up operation. After that the spray unit moves upward direction in vertically, place origin position of spray unit. Now, fiber glass spread

unit activated for spreading the fiber on first layer of resin, completion of fiber spreading operation, again dumping the resin in mold and lay-up by flap system. After that roller unit is activated for performing squeezing action. This cycle is repeated for manufacturing of sheets. In this system, two guide ways are used for holding and travelling of units for performing lay-up operation for manufacturing of sheets. One guide way rod is used for fiber spread unit and second guide way rod for flap system and roller system shown in fig.3.

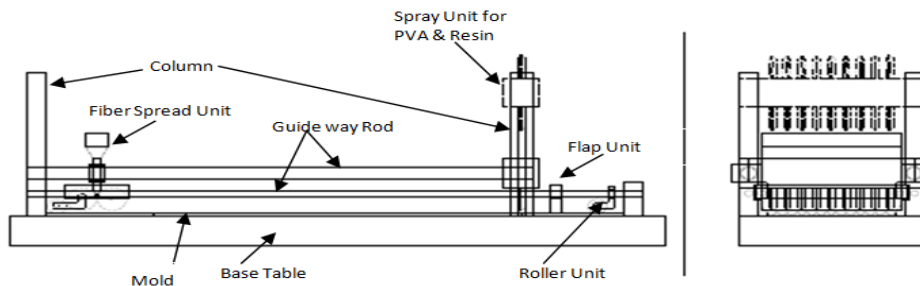


Figure 3. Second Proposed System for Automatic Lay-up Process

5.3. Proposed System “C”

Construction & Working of Machine: -

In third proposed system construction same like to above two systems. But in this system used only one guide way rod for holding and travelling of units for performing operation steps for manufacturing of sheets. On these guide way rod two spray units, one fiber spread unit, one rolling units are mounted. The two spray unit and fiber spread unit are place at right end of table and roller unit is placed at left end of table shown in fig.4. Working of these systems, firstly spray PVA on mold by spray unit, the moment of unit right to left direction and stop the unit at left end of table, after that resin spray move for spraying on mold in same direction of previous unit and stop there. Now, fiber glass spread unit ready for spreading of fiber on layer of resin, these unit move from right to left direction, and return to original position. Again spray the resin on layer of fiber glass by resin unit whenever these unit move to backward direction and takes the origin position. Now, PVA spray unit return to origin position but these time no any operation perform i.e. ideally move. After roller unit activated for performing of squeezing action for releasing of air in between layer of resin-fiber-resin, also compacting of product uniformly. These roller units perform squeezing action twice, and reset the origin position. This cycle repeated for manufacturing of sheets.

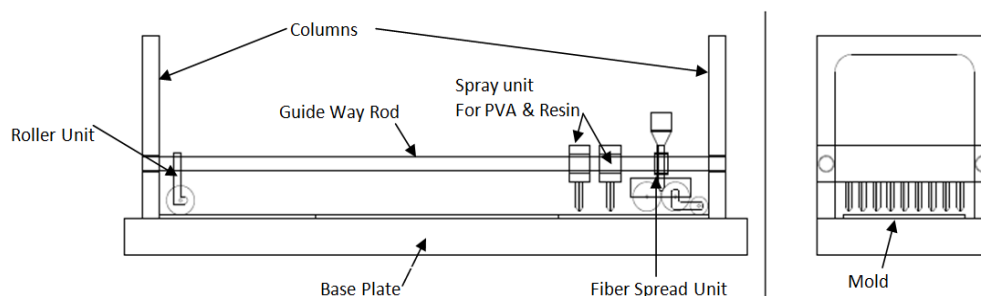


Figure 4. Third Proposed System for Automatic Lay-up Process

6. Conclusion

It is possible to existing lay-up process converted into Automatic Lay-up Process. Therefore, those problems are arise in existing lay-up process can be avoided with increasing the production rate of sheets. There, three systems are proposed for automatic lay-up system, so, can be possible to adopt these one from above system and also available more options for converting Automatic Lay-up system. If adopt the automatic lay-up process for manufacturing of FRP sheets, therefore achieving the uniform thickness of sheet as well as to providing safety environments to human. Also increasing the production rate with economical.

References

- [1] Moslemi, A. L., 2008. Technology & Market Consideration for Fiber Cement Composites. Int. Inorganic-Bonded Fiber Composite Conference. Spain.
- [2] Delvasto, S., Toro, E.F., and Perdommo, F. 2010. An appropriate Vacuumed technology for manufacturing of corrugated fibre fiber reinforced Cementitious sheets. Construction and Building Material, ELSEVIER Journal, 187-192.
- [3] Ciarlini Sergio. 1998. Method for manufacturing corrugated sheets made of Fibrous cements. European Patent Office.
- [4] Tony Cooke. Formation of Films on Hatschek machine. Building Materials and Technology pvt. Ltd. Australia.
- [5] Bijkerk, Bakker, and Deblauwe. 2009. Finished Product of fiber cement and method of manufacturing thereof. European Patent Office.
- [6] Hashem Akbari, Ronnen Levinson, and Paul Berdahl. 2003. A Review of Methods for the Manufacture of Residential Roofing Surfaces. Lawrence Berkeley National Laboratory Berkeley.

Methodology of Special Purpose Spot Facing Machine

Prof. Hansini S. Rahate¹, Prof. R. B. Chadge², Prof. P. H. Dahake³, Prof. S. Rewatkar⁴

¹ Asst. Professor Of Mechanical Department, Dbacer, Nagpur (M.S.) - India.,

² Asst. Professor Of Mechanical Department, Ycce, Nagpur (M.S.) - India.

³ asst. Professor Of Mechanical Department, Dbacer, Nagpur (M.S.) - India.

⁴ asst. Professor Of Mechanical Department, Dbacer, Nagpur (M.S.) - India.

Abstract:

Special purpose machine are widely used for special kind of operations, which are not economical on conventional machines. It is design for getting higher accuracy at desired condition. Spot facing in industrial valve is followed by a mechanical drilling or milling process. After the initial hole is drilled recess is develop on the valve with the help of required tool material. This aim of this paper is to presents the concept of spot facing in industrial valve, identified problems in flanges during spot facing and propose concept for avoiding the same.

Keywords: Back spot facing operation, Special purpose machine, Spot facing, Industrial valve.

1. Introduction

Special Purpose Machines (SPM) is not available off the Shelf. It is also not covered in standard manufacturing programs. They are designed and Tailor Made as Per the customer's specific requirements. They are also Called as Bespoke Machines. The use of SPM minimizes the human errors, human fatigue in repetitive operation etc. and increases the productivity at desired level. It also assures the quality and interchange ability of parts.

It is either cam operated machine or they use Hydraulics and Pneumatics as Actuating Elements or combination of all the three of them Many times a dedicated Programmable Logic Controller is used in Conjunction with Positional Sensors and Transducers, to give Commands to the Actuating Elements. Sometimes different special motors like Stepper Motor and Servo Motors are used as Actuating Element. Special mechanisms, drives, gears etc may also be used. The productivity achieved after all these efforts is very high. However to Fetch the Fruits of these highly specialized machines the pre condition is that the input to the automatic machine must have strict quality control.

1.1 Necessity Of The Back Spot Facing In The Valves:-

The back spot facing is needed in all flanges of the valves. It is provide the fittings for tightening the stud nuts or fasteners Back spot facing is so equally important like any other operation otherwise the stud nut can be fail during tightening or application of torque during the tightening of the stud nut. Here introduce the paper, and put a nomenclature if necessary, in a box with the same font size as the rest of the paper. The paragraphs continue from here and are only separated by headings, subheadings, images and formulae. The section headings are arranged by numbers, bold and 10 pt. Here follows further instructions for authors.

1.2 Current Available Facility For Back Spot Facing

The shape and geometry of the valve body is very different than any other component. The shape of the side and top flanges are intricate and difficult to machining.. Presently back spot facing operation is the last process after all the other process is completed.

The radial drilling machine is the only option on which the back spot facing operation can perform. There are so many aspects involved in the actual operation, but currently there is no other option other than radial drilling machine. This is an unnatural type of operation on the Radial drilling machine, since the spindle moving towards upward direction means opposite to gravity. This results the vibration on spindle and increasing the chances of run out of spindle. Sometimes at the time of drilling operation the accuracy of the machine is totally out of control. Clamping of component encountered a problem in radial drilling machine because it required more time and if clamping is not done properly the chances of accident may occurred.

1.3 Advantages And Disadvantages Of Current Facilities

Following are the advantages & disadvantages of the existing operation i.e. the back spot facing on the Radial drilling machine.

Advantages:-

- 1) No need of body indexing during spot facing of each drilled hole

- 2) Auto feed mechanism is available.
- 3) Any size can be spot face up to the capacity of the machine.

1.4 Disadvantages:-

- a) Rigid clamping required for the work piece.
- b) Special type of tooling attachment is required like socket as per the machines Morse taper.
- c) Tool clamping is difficult, since it is operating in opposite direction of the spindle.
- d) Tool changing time is much higher.
- e) No judgment of dimensions to be maintained, since it is very difficult to see the actual operation going on by operator.
- f) Special types of clamping devices are required to clamp the work piece.
- g) Skilled operator requires performing the desired operation.
- h) Cost per piece is very high.
- i) Other operation can delay due to this operation.
- j) Machine accuracy is affected very much due to this unconventional operation on this machine.
- k) Breakdown time is more.
- l) Tool breakage is very high since operator cannot see the condition of tool visually every time during operation.

2. Literature review:-

Many works have been done to carry out the various machining operations, for that special machine, tools, fixtures are invented. Some inventor had tried to carry out the spot facing operation by inventing special tool but very little inventor had tried to make special purpose machine for it. Burr et al. have worked on the back spot facing tool, A backspot facing tool includes a shaft and a cutting element. The shaft has a first and second end and a recess located near the first end. The shaft also includes an outer circumference and is centered on a first axis. The cutting element has an inner portion and an outer portion and is pivotally coupled to the shaft about a second axis.

The cutting element is movable between a closed position and an open position. Louis Belanger², This invention relates to rotary cutting tools for use in a drill press milling machine or other spindle type machine tools. An object of the invention is to provide a tool for performing an internal, substantially blind machining operation accurately and with a minimum of time and effort. Further object of the invention is to provide a tool especially useful to readily perform a spotting or facing operation upon an inaccessible inner face of a wall or other element adjacent to an aperture through the wall. Stuart A. Cogsdill³, This invention relates to cutting tools and particularly to a cutting tool that will spotface or counterbore the back side of a workpiece around a bore extending there through Kenneth P. Chamberlain⁴, His invention relates to rubber lined pipe and to the preparation of joints therefore, and has for its object the provision of an improved cutting tool and a machine for counterboring the rubber lining at the end of the pipe, for example to receive a joint sealing member, his machine effects a rapid, clean cut of various kinds of rubber, especially the soft resilient rubber, and is notable for its effective counter boring of soft rubber which could not be counterbored heretofore.

Henry F. Swenson⁴, His invention pertains to a back spot facing tool whose cutting blade is pivotally mounted on a spindle body and is axially actuated by a plunger rod so as to be moved to either a cutting or a concealed condition in response to either a manual manipulation or to a hydraulic actuation of this rod. Arlan W. way, Terrence M. McCarver⁶, A spot facing mechanism employs a self centering chuck, a stationary mandrel and housing. Axial feed controls are also stationary when the apparatus is operational. Incremental radial feeding of the tool head is provided, with the degree of feed being adjustable between zero feed and maximum feed. radial feed rate adjustment controls remain stationary while the apparatus is operating, enabling adjustment of feed rate without having to stop the machine. Walter C. Bergstorm⁷ His invention relates to new and useful improvements in countersinking and counterboring tools, An important object of the invention is the provision of construction for such tools which prevent chattering of the tool in use, provide precision smooth surfaces of the work, provide for more rapid ejection of the chips or shaving, and deburr the work.

3. Checklist of Information Useful in Investigation of Solution for Back Spot Facing

1. The spot facing on RD machine is a non conventional job, since the operation is reverse of the machine behaviour, so we need to develop the solution which is having parallel or same cutting action in the feed direction of the machine.

2. The mechanism which is suitable for the type of operation of spot facing.
3. Focus on some current available facility which is helpful to make some new economical and useful solution.
4. Selection of suitable drives for the mechanism like Belt drive, Chain drive and Gear drive. Also find the advantages and disadvantages of this drives.
5. Dimensional requirement, finishing requirement of spot facing and economy of the operation.
6. User friendly and low maintenance solution.
7. Properties of the materials which we have to cut or machine and cutting tools available for cutting these materials.

4. Proposed Mechanism of the Spot Facing Machine

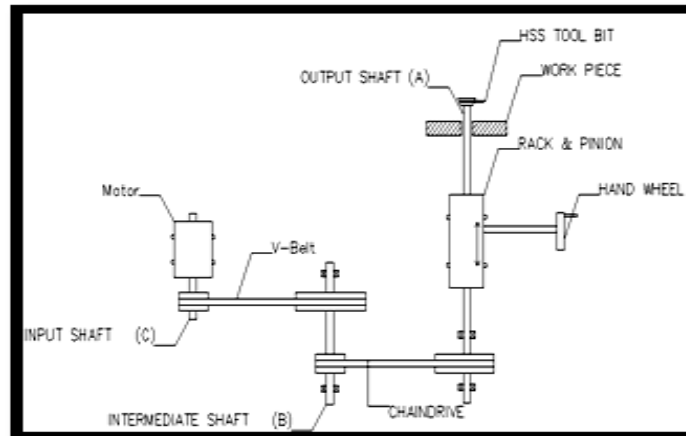


Fig. 1 Belt & Chain drive mechanism

- a) Belt drive mechanism
- b) Chain drive mechanism
- c) Gear drive mechanism

4.1 Construction And Working Of Mechanism (1):-

Belt Drive:-

This system is used for back spot facing operation. It consists of smaller pulley, V belt, larger pulley, Worm and worm wheel gear box, Guide way for worm gear box, Rack and pinion arrangement, Hand wheel. A Belt is a looped strip of flexible material, used to mechanically link two or more rotating shafts they may be used as a source of motion, to efficiently transmit POWER, or to track relative movement. Belts are looped over pulleys. Power transmission is achieved by specially designed belts and pulleys. Belts run smoothly and with little noise, and cushion motor and bearings against load changes, but have less strength than gears or chains.

Advantages

- Cheap
- Allows misalignment (parallel shafts)
- Protects from overload
- Absorbs noise and vibrations
- Cushion load fluctuations
- Needs little maintenance
- High efficiency (90-98%, usually 95%).

Disadvantages

- Speed ratio is not constant (slip & stretch)
- Heat accumulation
- Speed limited – 2000 m/min,
- Power limited - 700 kW
- Endless belts needs special attention to install

Chain Drive-

Like any method of power transmission, chain drives have advantages and disadvantages. Advantages of chain will be discussed initially, and the note will conclude with a discussion of chain disadvantages.

Advantages

- Virtually any length chain can be obtained (splicing).
- Positive drive provides synchronization of two shafts (Synchronous belts such as Poly Chain® also possess this characteristic).
- Bearing loads are generally lower than for belts (no slack side tension).
- Chain drives are 95-99% efficient (Poly Chain is 98-99% efficient).
- Due to chain's symmetric design characteristics, serpentine drives are possible (serpentine drives are also possible using twin tooth synchronous belts).
- Chain drives seem to give the appearance that they will do the job - i.e., steel is tough.
- Chain offers higher HP capacities on smaller diameters.

Disadvantages

- Lubrication is critical - unlubricated drives can wear 300 times faster than lubricated drives (difficult to properly re-lube chain).
- The lubrication attracts dirt which leads to wear problems.
- Life is usually low since an estimated 90-95% of chain drives are improperly lubricated.
- Frequent maintenance is required due to wear and stretch.
- Chain drives are noisy (proportional to speed) due to metal-to-metal contact.
- Linear speed is limited to 3000 ft. /min. for roller chain.
- Vertical drives may present problems since less slack can be permitted than in a horizontal drive in order to insure proper chain/sprocket engagement.
- Equipment damage can result upon chain failure due to steel construction.
- Available only in full box length increments except in rare cases.

Gear Drive Mechanism

A gear is a rotating machine part having cut teeth, or cogs, which mesh with another toothed part in order to transmit torque. Two or more gears working in tandem are called a transmission and can produce a mechanical advantage through a gear ratio and thus may be considered a simple machine. Geared devices can change the speed, torque, and direction of a power source. The most common situation is for a gear to mesh with another gear; however a gear can also mesh a non-rotating toothed part, called a rack, thereby producing translation instead of rotation. In transmissions which offer multiple gear ratios, such as bicycles and cars, the term gear, as in first gear, refers to a gear ratio rather than an actual physical gear. The term is used to describe similar devices even when gear ratio is continuous rather than discrete, or when the device does not actually contain any gears, as in a continuously variable transmission.

Advantages

- Provide Positive Drive without slip.
- Suitable for high speed, high torque & high power transmission.
- Properly designed & properly maintained gear system can run over decades.
- Very high transmission ratio is practicable.
- Compact machine train in limited space.
- Due to rigid construction gives rigidity to mechanism.
- Drastic speed variation is possible without any major problem.
- Low maintenance cost.

Disadvantages

- Needs Proper Lubrication System.
- Which involve high cost.
- Require skilled technician to maintain.

4.2 Construction And Working Of Mechanism (2)-

This system is also used for back spot facing. it consist of sun and planet gear mechanism, gear drive, variable frequency drive, lead screw, indexing table. By using this system we can spot face four hole of side flange of the valve by using four cutting tool at a time. Gear drive is used for power transmission.

Working: We can externally supply the power and speed from the motor to the gear drive mechanism. In gear drive mechanism there is sun and planet gear mechanism which is used for power transmission sun gear distributes power and speed to the planet gears which is used as a output power and output speed in this way we can done back spot facing operation on one side of flange of valve. After completion of back spot facing operation on one side we are apply same process for another side by providing rotary table indexing mechanism we can rotate table by 180 degree and done operation on another side of flange of valve.

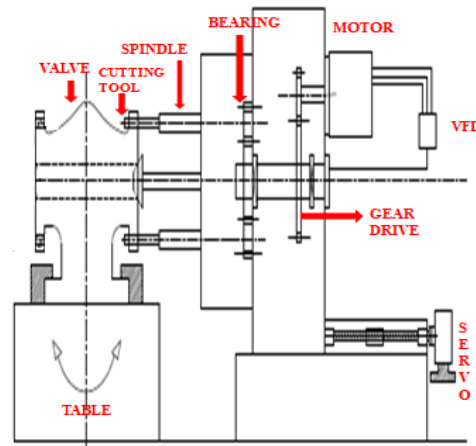


Fig.2. Sun and Planet Gear Mechanism

5. Conclusion:-

In this paper discussed about the spot facing operation and methodology. In this suggesting two special purpose machines for back spot facing operation perform on the industrial valves. In existing process required more time for completion of operation of back spot facing as well as difficult to achieving to each back spot facing . This problems eliminating by providing dedicated back spot facing machine i.e providing special purpose machine.

Above suggesting mechanisms in facilitated to loading the valve in short time as well as unloading, easily performing operation on back side of flange of valve. This system also increase rate of production with accurated dimensions.

References:

- [1]. United States Patents, Burr et al, Back Spot Facing Tool, Jul,1,2004
- [2]. United States Patent, Louis Belanger, Salem, Mass, Spot facing tool, July16,1946.
- [3]. United States Patent, Stuart A. Cogsdill, Back spotface tool , July31,1962
- [4]. United States Patent, Kenneth P. Chamberlain, Counterboring Tool, March27, 1948.
- [5]. United States Patent, Henry F. Swenson, Axially Actuated Back Spot Facing Tool, Aug 6, 1974.
- [6]. United States Patent, Arlan W. way, Terrence M. McCarver,Spot Facing Machine, Sep21,1999.
- [7]. United States Patent, Walter C. Bergstorm, Countersinking And Counterboring Tool, Dec7,1953.

Application of Image Processing For Development of Automated Inspection System

¹Ms. Shubhada.K. Nagrale, ²Mr. S.T.Bagde

¹P.G.Student(M-Tech, CAD/CAM), Dept. Of Mechanical Engg.,
Yeshwantrao College Of Engg, Wanadongri, Nagpur,India.

²Assistant Professor, Dept. Of Mechanical Engg.,Yeshwantrao College Of Engg, Wanadongri,
Nagpur,India

Abstract

In manufacturing industry, machine vision is very important nowadays. Computer vision has been developed widely in manufacturing for accurate automated inspection. A model of automated inspection system is presented in this conceptual paper. Image processing is used for inspection of part. It is assumed that the part after going through many previous operations comes to inspection system where the weight of the part as well as geometry made on that part is detected and later decided whether it is to be accepted or rejected with the help of image processing technique. Using MATLAB software a program is developed and pattern or geometry is detected.

Keywords: Automated Inspection System, Digital Camera, Image Processing, Machine Vision, MATLAB, Pattern Recognition, PRO-E Software .

1. Introduction

Automated inspection systems are continuously conveyed in the manufacturing process. The systems are capable of measuring predetermined parameters of various parts, comparing the measured parameters with predetermined values, evaluating from the measured parameters the integrity of the parts and determining whether such parts are acceptable or, alternatively, whether they should be rejected. Humans are able to find such defects with prior knowledge. Human judgment is influenced by expectations and prior knowledge. However, it is tedious, laborious, costly and inherently unreliable due to its subjective nature. Therefore, traditional visual quality inspection performed by human inspectors has the potential to be replaced by computer vision systems. The increased demands for objectivity, consistency and efficiency have necessitated the introduction of accurate automated inspection systems. These systems employ image processing techniques and can quantitatively characterize complex sizes, shapes, and the color and textural properties of products. Accurate automated inspection and classification can reduce human workloads and labor costs while increasing the throughput. Machine vision has been used to detect the part and take the image of the part which compares it with the standard dimensions given to it through programming language.

Machine vision (MV) is the process of applying a range of technologies and methods to provide imaging-based automatic inspection, process control and robot guidance in industrial applications. the first step in the MV sequence of operation is acquisition of an image, typically using cameras, lenses, and lighting that has been designed to provide the differentiation required by subsequent processing. MV software packages then employ various digital image processing techniques to extract the required information, and often make decisions (such as pass/fail) based on the extracted information. Though the vast majority of machine vision applications are still solved using 2 dimensional imaging, machine vision applications utilizing 3D imaging are growing niche within the industry.

Machine vision image processing methods include:

- Pixel counting: Counts the number of light or dark pixels
- Thresholding: Converts an image with gray tones to simply black and white or using separation based on a grayscale value.
- Segmentation: Partitioning a digital image into multiple segments to simplify and/or change the representation of an image into something that is more meaningful and easier to analyze.
- Blob discovery & manipulation: Inspecting an image for discrete blobs of connected pixels (e.g. a black hole in a grey object) as image landmarks. These blobs frequently represent optical targets for machining, robotic capture, or manufacturing failure.
- Pattern recognition including template matching: Finding, matching, and/or counting specific patterns. This may include location of an object that may be rotated, partially hidden by another object, or varying in size.
- Barcode, data matrix and 2D code reading.

- Optical character recognition: Automated reading of text such as serial number.
- Gauging: Measurement of object dimensions (e.g. in pixels, inches or millimeters).
- Edge detection: Finding object edge.
- Neural net processing: Weighted and self-training multi-variable decision making.
- Filtering (e.g. morphological filtering).

We assume that the part after going through many previous operation comes to the automated inspection system where it is decided whether to accept or reject the part. Based on the weight of the part as well as through image processing, pattern of the part is matched through the standard program and image fed beforehand. Aluminum block is the part which is to be weighed and geometric pattern is recognized and matched using image processing.

2. Review Of Papers

The manual activity of inspection could be subjective and highly dependent on the experience of human inspectors. So image analysis techniques are being increasingly used to automate industrial inspection. The machine vision system for automatic inspection of defects in textured surfaces has been developed. It aimed to solve the problem of detecting small surface defects which appear as local anomalies embedded in a homogeneous texture of textile fabrics and machined surfaces [1]. Computer vision has been for detection of defective packaging of tins of cigarettes[2]. A large amount of research has been carried out on automated inspection of tile surfaces[3],[4], biscuit bake color[5], the color of potato chips, textile fabrics, food products and wood[6]. However, relatively little work has been done in automated defect classification, mainly because of the difficult nature of the problem. Computer vision has been used to objectively measure the color of different food since it provides some additional and obvious advantages over conventional techniques such as using a colorimeter, namely, the possibility of analyzing each pixel of the entire surface of the food, and quantifying the surface characteristics and defects. Defective images are detected in textile fabrics by individually applying simple classification to discriminate knots from slubs according to the ratio of length to width [7], and pyramid linking scheme is employed to locate defects in wood and a hierarchical defect classification scheme to classify different types of wood defect [6]. An Automated Visual Inspection (AVI) system for weaving defect detection is developed based on image processing and recognition algorithms. The techniques from neural network for classifying the weaving defect are also used. The irregularities of the weaving fabrics are detected as defects [8].

3. Conceptual Designs

3.1. Rotary Disc Type Mechanism

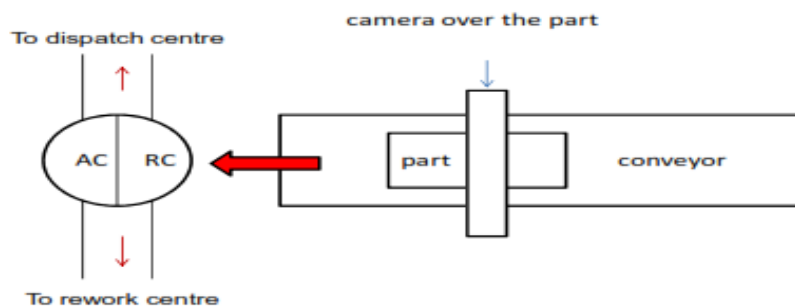


Figure 1. Rotary disc type mechanism

In this mechanism, the part is kept over conveyor with an overhead gantry. Camera is fitted on the gantry exactly over the part. Conveyor is used to transfer the part from one end to another end. As soon as the part is kept over the conveyor, the camera takes image of the part and matches with parameters of the program fed beforehand. After this the part goes to rotary disc where weighing machine is kept. If the weight and other parameters match exactly then the part goes to the acceptance centre. The disc is rotated 90° clockwise if part is to be accepted otherwise it directly drops the part in rejection centre (RC). After the part is accepted, it is sent to the dispatch centre for final packaging otherwise the part is sent to the rework centre where the rejected part is again operated for obtaining exact dimensions.

3.2. Pusher type mechanism

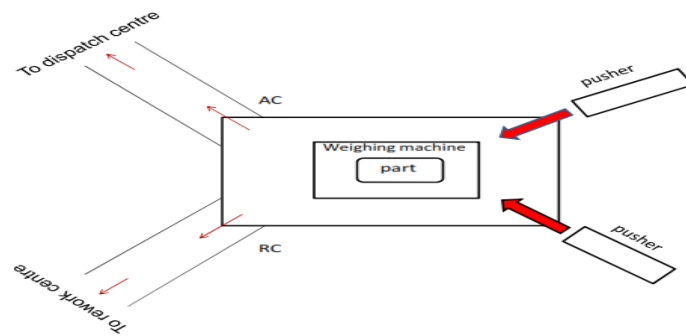


Figure 2. Pusher type mechanism

In pusher type mechanism, pusher is used to send the part to the acceptance centre or rejection centre. There is a rectangular block on which weighing machine is kept at the centre. The part is kept on the weighing machine. Camera is fitted on the weighing machine in such a way that camera comes exactly over the part. Weight is measured and other dimensions along with the weight are matched with the fed program. If the dimensions of the part are exactly matched, the lower pusher pushes the part towards acceptance centre from where the part is sent to dispatch centre for further processing otherwise the upper pusher pushes the part towards rejection centre from where the part goes to rework centre for further machining so that exact dimensions of the part are obtained.

3.3. Gantry type Mechanism

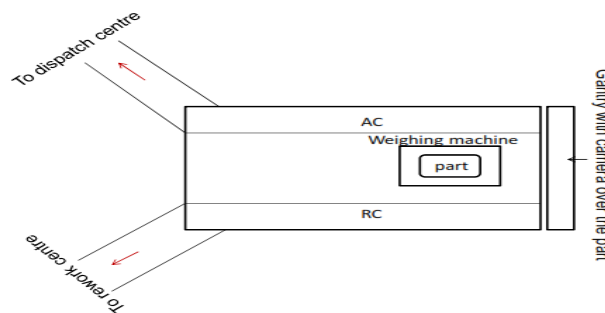


Figure 3. Gantry type mechanism

In this layout, the acceptance centre and rejection centre is kept besides weighing machine. Overhead Gantry is fitted at the extreme right of the layout so that camera fitted on the gantry comes exactly above the part. Other process is same as explained above. Now after the part is matched exactly, the part is transferred to acceptance centre through the arm (attached to the overhead gantry) otherwise it is transferred to rejection centre which in turn is sent to either dispatch centre or rework centre respectively.

3.4. Flip Drop mechanism

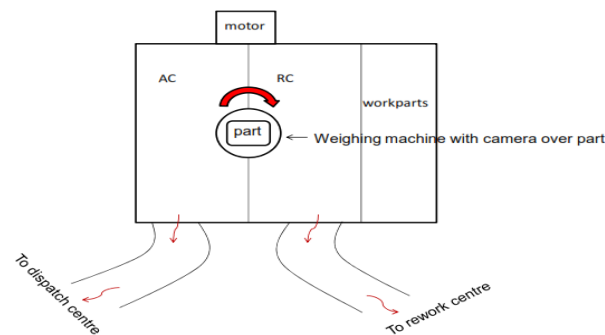


Figure 4. Flip drop mechanism

In this mechanism, the part is flipped with the help of motor. The part is either dropped in the acceptance centre or rejection centre by rotating the block through 90° (either clockwise or anticlockwise respectively). The part is kept over weighing machine where camera is fitted such that the camera is exactly over the part. Other procedure is same as mentioned above.

3.5 Oscillatory mechanism

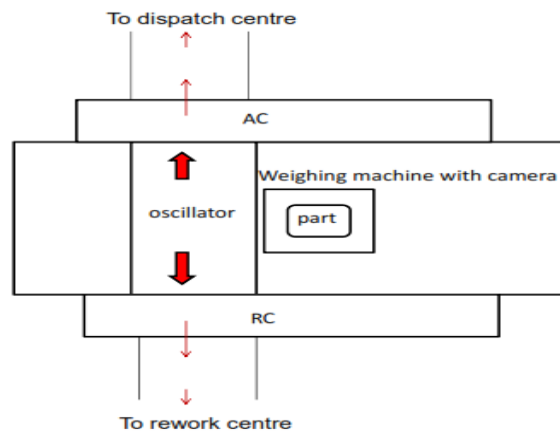


Figure 5. Oscillatory mechanism

In this, the oscillator is used to transfer the part either to acceptance centre or rejection centre by to and fro motion. If the part is exactly matched, the oscillator drops the part to the acceptance centre which in turn is sent to dispatch centre. The oscillator moves forward if the part is to be sent towards acceptance centre otherwise it moves backward to drop the part to rejection centre. Other processing is done as mentioned before.

4. Proposed Design

Flip drop Mechanism is the best suited design for the project as it requires

- less space
- less moving parts
- no gantry arm for placing the part in the respective centre.

The disadvantages of other models are: All other conceptual designs used gantry arm to place the part in the respective centre, conveyors were used which complicated the design. More floor space. Use of gantry arm will increase the computational time during processing. For weighing the Aluminium block, load cell is used.

3-D model of the system is represented below:

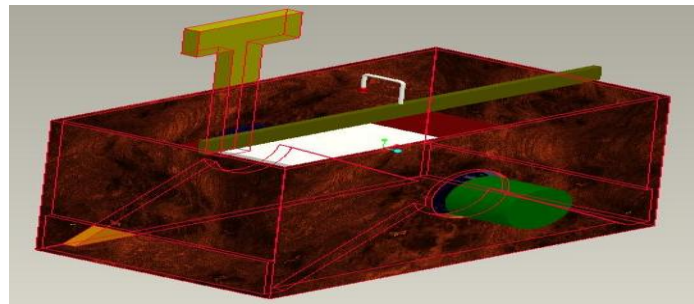


Figure 6. 3-D model of the system

This is the proposed concept of the system. Specification of the main components of system is given below:
Aluminium block

- DimensionsofAluminium block= $100\text{mm}\times 100\text{mm}\times 10\text{mm}$;
- Density of Aluminium= $2700\text{kg}/\text{m}^3$;
- Density=mass/volume;
- Volume= $100\times 100\times 10\times 10^{-9}\text{ m}^3$
- Mass= $2700\times 100\times 100\times 10\times 10^{-9}$
= 0.27 kg

Servo Motor

- Dimension: $23\text{mm}\times 12\text{mm}\times 25\text{mm}$
- Torque: $1.5\text{kg}/\text{cm}$ at 4.8V
- Motor weight: 30gms
- Operating speed: $0.15\text{sec}/60\text{ degree}$

- Operating voltage: 4.8V/6V
Camera
- Camera:3MP
- Model: HD Webcam C270

Load cell

- Type: VLC131 Single point load cell
- Capacity:5lb
-

5. Image Processing

Fundamental steps in image processing:

1. Image acquisition: This is the first step of image processing. In this a digital image is acquired
2. Image preprocessing: In the second step image is improved in a way that increase the chances for success of the other processes.
3. Image segmentation: It partitions an input image into its constituent parts or objects.
4. Image representation: It converts the input data to a form suitable for computer processing.
5. Image description: In this step features are extracted that result in some quantitative information of interest or features that are basic for differentiating one class of objects from another.
6. Image recognition: It assigns a label to an object based on the information provided by its descriptors.
7. Image interpretation: A meaning is assigned to an ensemble of recognized objects in this step.

General code for comparing two images in MATLAB is given below:

```
a = imread('image1.jpg');  
b = imread('image2.jpg');  
c = corr2(a,b);  
if c==1  
    disp('The images are same')  
else  
    disp('the images are not same')  
end;
```

6. Conclusion

In this paper, the proposed design is being developed. This design is advantageous than other papers as this is a portable type of machine which has acceptance and rejection centre placed in a single machine. Different types of geometries can be used for image processing. This design is more advantageous for small scale industries. Different types of models or objects can be used as a workpiece for testing.

7. References

- [1] D. M. Tsai and S. K. Wu, Machine Vision Lab, Department of Industrial Engineering and Management, Yuan-Ze University, Chung-Li, Taiwan, R.O.C "Automated surface inspection using Gabor filters".
- [2] Mira Park1, Jesse S. Jin1, Sherlock L. Au2, Suhuai Luo1, and Yue Cui1,1 The School of Design, Communication & IT, The University of Newcastle, Australia, 2Multi Base Ltd, Hong Kong, "Automated Defect Inspection Systems by Pattern Recognition", International Journal of Signal Processing, Image Processing and Pattern Recognition_Vol. 2, No. 2, June 2009.
- [3]. Costa, C. E. and Petrou, M., Automatic registration of ceramic tiles for the purpose of fault detection, Machine Vision and Applications, 11:225-230, 2000.
- [4]. Elbehiery, H., Hefnawy, A. and Elewa, M., Surface defects detection for ceramic tiles using image processing and morphological techniques, Proceedings of World Academy of Science, Engineering and Technology, 5:1307-6884, 2005.
- [5]. Yeh, J. C. H., Hamey, L. G. C., Westcott, T. and Sung, S. K. Y., Colour bake inspection system using hybrid artificial neural networks, IEEE International Conference of Neural Networks:37-42, 1995.
- [6]. Braxakovic, D., Beck, H. and Sufi, N., An approach to defect detection in materials characterized by complex textures, Pattern Recognition, 23(1/2):99-107, 1990.
- [7]. Zhang, Y. F. and Bresee, R. R., Fabric defect detection and classification using image analysis, Textile Research Journal, 65(1):1-9, 1995.
- [8]. Chi-ho Chan, Hugh Liu, Thomas Kwan, Grantham Pang, Dept. of Electrical and Electronic Engineering, The University of Hong Kong, Pokfulam Road, Hong Kong, "AUTOMATION TECHNOLOGY FOR FABRIC INSPECTION SYSTEM".
- [9]. M. Dar, W. Mahmood, G. Vachtsevanos, "Automated pilling detection and fuzzy classification of textile fabrics". Machine in industrial inspection V. SPIE Vol. 3029. pp. 26-36. 1997.
- [10]. H. C. Abril, M. S. Millan, R. Navarro, " Pilling evaluation in fabrics by digital image processing". Vision system: applications. SPIE Vol. 2786. pp. 19-28. 1996.

Invention of The Plane Geometrical Formulae - Part I

Mr. Satish M. Kaple

Asst. Teacher Mahatma Phule High School, Kherda Jalgaon (Jamod) - 443402 Dist- Buldana,
Maharashtra (India)

Abstract

In this paper, I have invented the formulae of the height of the triangle. My findings are based on pythagoras theorem.

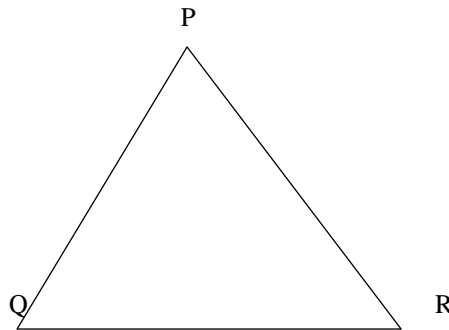
1. Introduction

A mathematician called Heron invented the formula for finding the area of a triangle, when all the three sides are known. From the three sides of a triangle, I have also invented the two new formulae of the height of the triangle by using pythagoras Theorem . Similarly, I have developed these new formulae for finding the area of a triangle. When all the three sides are known, only we can find out the area of a triangle by using Heron's formula. By my invention, it became not only possible to find the height of a triangle but also possible for finding the area of a triangle. I used pythagoras theorem with geometrical figures and algebric equations for the invention of the two new formulae of the height of the triangle. I Proved it by using geometrical formulae & figures, 50 and more examples, 50 verifications (proofs).

Here myself is giving you the summary of the research of the plane geometrical formulae- Part I

Method

First taking a scalene triangle PQR



Now taking a, b & c for the lengths of three sides of $\triangle PQR$.

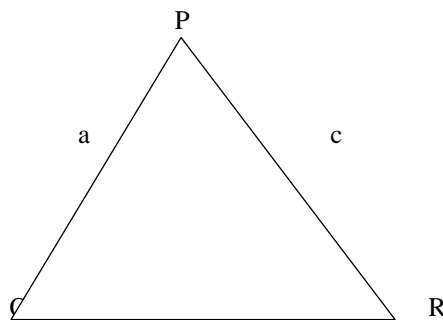
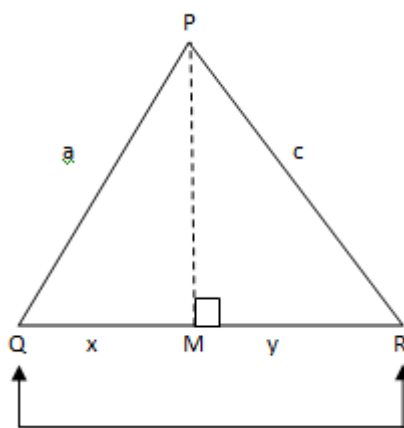


Fig. No. - 2



Draw perpendicular PM on QR.

b Fig. No. - 3

In $\triangle PQR$ given above,

$\triangle PQR$ is a scalene triangle and is also an acute angled triangle. PM is perpendicular to QR. Two other right angled triangles are formed by taking the height PM, on the side QR from the vertex P. These two right angled triangles are $\triangle PMQ$ and $\triangle PMR$. Due to the perpendicular drawn on the side QR, Side QR is divided into two other segment, namely, Seg MQ and Seg MR. QR is the base and PM is the height. Here, a, b and c are the lengths of three sides of $\triangle PQR$. Similarly, x and y are the lengths of Seg MQ and Seg MR.

Taking from the above figure,

$$PQ = a, QR = b, PR = c$$

$$\text{and height, } PM = h$$

But QR is the base, $QR = b$

$$MQ = x \text{ and } MR = y$$

$$QR = MQ + MR$$

Putting the value in above eqn.

$$\text{Hence, } QR = x + y$$

$$b = x + y$$

$$x + y = b \text{ ----- (1)}$$

Step (1) Taking first right angled $\triangle PMQ$,

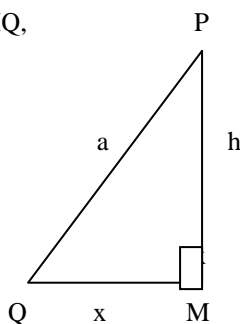


Fig. No.- 4

In $\triangle PMQ$,

Seg PM and Seg MQ are sides forming the right angle. Seg PQ is the hypotenuse and

$$\angle PMQ = 90^\circ$$

Let,

$$PQ = a, MQ = x \text{ and}$$

$$\text{height, } PM = h$$

According to Pythagoras theorem,

$$(\text{Hypotenuse})^2 = (\text{One side forming the right angle})^2 +$$

$$(\text{Second side forming the right angle})^2$$

In short,

$$(\text{Hypotenuse})^2 = (\text{One side})^2 + (\text{Second side})^2$$

$$PQ^2 = PM^2 + MQ^2$$

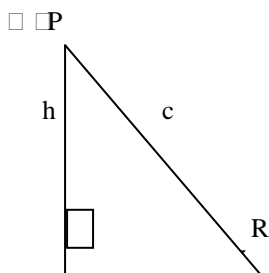
$$a^2 = h^2 + x^2$$

$$h^2 + x^2 = a^2$$

$$h^2 = a^2 - x^2 \text{ ----- (2)}$$

Step (2) Similarly,

Let us now a right angled triangle $\square PMR$



In $\square PMR$,

Seg PM and Seg MR are sides forming the right angle. Seg PR is the hypotenuse.

Let, $PR = c$, $MR = y$ and

height, $PM = h$ and $m \angle PMR = 90^\circ$

According to Pythagoras theorem,

$$(\text{Hypotenuse})^2 = (\text{One side})^2 + (\text{Second side})^2$$

$$PR^2 = PM^2 + MR^2$$

$$c^2 = h^2 + y^2$$

$$h^2 + y^2 = c^2$$

$$h^2 = c^2 - y^2 \text{ ----- (3)}$$

From the equations (2) and (3)

$$a^2 - x^2 = c^2 - y^2$$

$$a^2 - c^2 = x^2 - y^2$$

$$x^2 - y^2 = a^2 - c^2$$

By using the formula for factorization, $a^2 - b^2 = (a + b)(a - b)$

$$(x + y)(x - y) = a^2 - c^2$$

But, $x + y = b$ from eqn. (1)

$$b \times (x - y) = a^2 - c^2$$

Dividing both sides by b,

$$\frac{b \times (x - y)}{b} = \frac{a^2 - c^2}{b}$$

$$(x - y) = \frac{a^2 - c^2}{b} \text{(4)}$$

Now, adding the equations (1) and (4)

$$x + y = b$$

$$+ \quad x - y = \frac{a^2 - c^2}{b}$$

$$2x + 0 = b + \frac{a^2 - c^2}{b}$$

$$2x = b + \frac{a^2 - c^2}{b}$$

Solving R.H.S. by using cross multiplication

$$2x = \frac{b}{1} + \frac{a^2 - c^2}{b}$$

$$2x = \frac{b \times b + (a^2 - c^2) \times 1}{1 \times b}$$

$$2x = \frac{b^2 + a^2 - c^2}{b}$$

$$x = \frac{a^2 + b^2 - c^2}{b} \times \frac{1}{2}$$

$$x = \frac{a^2 + b^2 - c^2}{2b}$$

Substituting the value of x in equation (1)

$$x + y = b$$

$$\left(\frac{a^2 + b^2 - c^2}{2b} \right) + y = b$$

$$y = b - \left(\frac{a^2 + b^2 - c^2}{2b} \right)$$

$$y = \frac{b}{1} - \left(\frac{a^2 + b^2 - c^2}{2b} \right)$$

Solving R.H.S. by using cross multiplication.

$$y = \frac{b \times 2b - (a^2 + b^2 - c^2) \times 1}{1 \times 2b}$$

$$y = \frac{2b^2 - (a^2 + b^2 - c^2)}{2b}$$

$$y = \frac{2b^2 - a^2 - b^2 + c^2}{2b}$$

$$y = \frac{-a^2 + b^2 + c^2}{2b}$$

The obtained values of x and y are as follow.

$$x = \frac{a^2 + b^2 - c^2}{2b} \quad \text{and}$$

$$y = \frac{-a^2 + b^2 + c^2}{2b}$$

Substituting the value of x in equation (2).

$$h^2 = a^2 - x^2$$

$$h^2 = a^2 - \left(\frac{a^2 + b^2 - c^2}{2b} \right)^2$$

Taking the square root on both sides,

$$\sqrt{h^2} = \sqrt{a^2 - \left(\frac{a^2 + b^2 - c^2}{2b} \right)^2}$$

$$\text{Height, } h = \sqrt{a^2 - \left(\frac{a^2 + b^2 - c^2}{2b} \right)^2} \dots\dots\dots(5)$$

Similarly,

Substituting the value of y in equation (3)

$$h^2 = c^2 - y^2$$

$$h^2 = c^2 - \left(\frac{-a^2 + b^2 + c^2}{2b} \right)^2$$

Taking the square root on both sides.

$$\sqrt{h^2} = \sqrt{c^2 - \left(\frac{-a^2 + b^2 + c^2}{2b} \right)^2}$$

$$\sqrt{h^2} = \sqrt{c^2 - \left(\frac{-a^2 + b^2 + c^2}{2b} \right)^2}$$

$$\text{Height, } h = \sqrt{c^2 - \left(\frac{-a^2 + b^2 + c^2}{2b} \right)^2} \dots\dots\dots(6)$$

These above two new formulae of the height of a triangle are obtained.

By using the above two new formulae of the height of the triangle, new formulae of the area of a triangle are developed. These formulae of the area of a triangle are as follows :-

$$\begin{aligned} \therefore \text{Area of } \triangle PQR &= A (\triangle PQR) \quad \text{----- (A stands for area)} \\ &= \frac{1}{2} \times \text{Base} \times \text{Height} \\ &= \frac{1}{2} \times QR \times PM \\ &= \frac{1}{2} \times b \times h \quad \text{----- (b for base and h for height)} \end{aligned}$$

From equation (5), we get

$$\therefore \text{Area of } \triangle PQR = \frac{1}{2} \times b \times \left[a^2 - \left(\frac{a^2 + b^2 - c^2}{2b} \right)^2 \right]$$

OR

$$\begin{aligned} \therefore \text{Area of } \triangle PQR &= A (\triangle PQR) \\ &= \frac{1}{2} \times \text{Base} \times \text{Height} \\ &= \frac{1}{2} \times QR \times PM \\ &= \frac{1}{2} \times b \times h \end{aligned}$$

From equation (6), we get

$$\therefore \text{Area of } \triangle PQR = A (\triangle PQR) = \frac{1}{2} \times b \times \sqrt{c^2 - \left(\frac{-a^2 + b^2 + c^2}{2b} \right)^2}$$

From above formulae, we can find out the area of any type of triangle. Out of two formulae, anyone formula can use to find the area of triangle.

For example:-

Now consider the following examples :-

Ex. (1) If the sides of a triangle are 17 m, 25 m and 26 m, find its area.

Here,

□ DEF is a scalene triangle

l (DE) = a = 17 m

l (EF) = Base , b = 25 m

l (DF) = c = 26 m

By using The New Formula No (1)

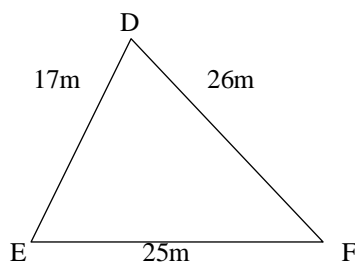


Fig.No.6

$$\text{Height, } h = \sqrt{a^2 - \left(\frac{a^2 + b^2 - c^2}{2b} \right)^2}$$

Area of □ DEF = A (□ DEF)

$$= \frac{1}{2} \times \text{Base} \times \text{Height}$$

$$= \frac{1}{2} \times b \times h$$

$$= \frac{1}{2} \times b \times \sqrt{a^2 - \left(\frac{a^2 + b^2 - c^2}{2b} \right)^2}$$

$$= \frac{1}{2} \times 25 \times \sqrt{17^2 - \left(\frac{17^2 + 25^2 - (26)^2}{2 \times 25} \right)^2}$$

$$= \frac{25}{2} \times \sqrt{17^2 - \left(\frac{289 + 625 - 676}{50} \right)^2}$$

$$= \frac{25}{2} \times \sqrt{17^2 - \left(\frac{238}{50} \right)^2}$$

The simplest form of $\frac{238}{50}$ is $\frac{119}{25}$

By using the formula for factorization,

$$a^2 - b^2 = (a - b)(a + b)$$

$$= \frac{25}{2} \times \sqrt{\left(17 - \frac{119}{25} \right) \left(17 + \frac{119}{25} \right)}$$

$$= \frac{25}{2} \times \sqrt{\left(\frac{425 - 119}{25}\right) \left(\frac{425 + 119}{25}\right)}$$

$$= \frac{25}{2} \times \sqrt{\left(\frac{306}{25}\right) \times \left(\frac{544}{25}\right)}$$

$$= \frac{25}{2} \times \sqrt{\frac{306 \times 544}{25 \times 25}}$$

$$= \frac{25}{2} \times \sqrt{\frac{166464}{625}}$$

The square root of $\frac{166464}{625}$ is $\frac{408}{25}$

$$= \frac{25}{2} \times \frac{408}{25}$$

$$= \frac{408}{2}$$

The simplest form of $\frac{408}{2}$ is 204

$$= 204 \text{ sq. m}$$

∴ Area of □ DEF = 204 sq.m.

By using the new formula No (2)

$$\text{Height, } h = \sqrt{c^2 - \left(\frac{-a^2 + b^2 + c^2}{2b}\right)^2}$$

Area of □ DEF = A (□ DEF)

$$= \frac{1}{2} \times \text{Base} \times \text{Height} = \frac{1}{2} \times b \times h$$

2

2

$$\begin{aligned}
 &= \frac{1}{2} \times b \times \sqrt{c^2 - \left(\frac{-a^2 + b^2 + c^2}{2b} \right)^2} \\
 &= \frac{1}{2} \times 25 \times \sqrt{(26)^2 - \left(\frac{-(17)^2 + 25^2 + 26^2}{2 \times 25} \right)^2} \\
 &= \frac{25}{2} \times \sqrt{(26)^2 - \left(\frac{-289 + 625 + 676}{50} \right)^2} \\
 &= \frac{25}{2} \times \sqrt{(26)^2 - \left(\frac{1012}{50} \right)^2}
 \end{aligned}$$

The simplest form of $\frac{1012}{25}$ is $\frac{506}{25}$

$$= \frac{25}{2} \times \sqrt{(26)^2 - \left(\frac{506}{25} \right)^2}$$

By using the formula for factorization,

$$a^2 - b^2 = (a - b)(a + b)$$

$$= \frac{25}{2} \times \sqrt{\left(\frac{26 - 506}{25} \right) \left(\frac{26 + 506}{25} \right)}$$

$$= \frac{25}{2} \times \sqrt{\left(\frac{650 - 506}{25} \right) \left(\frac{650 + 506}{25} \right)}$$

$$= \frac{25}{2} \times \sqrt{\left(\frac{144}{25} \right) \times \left(\frac{1156}{25} \right)}$$

$$= \frac{25}{2} \times \sqrt{\frac{144 \times 1156}{25 \times 25}}$$

$$= \frac{25}{2} \times \sqrt{\frac{166464}{625}}$$

The square root of $\frac{166464}{625}$ is $\frac{408}{25}$

$$= \frac{25}{2} \times \frac{408}{25}$$

$$= \frac{408}{2}$$

The simplest form of $\frac{408}{2}$ is 204

$$= 204 \text{ sq. m}$$

∴ Area of □ DEF = 204 sq. m.

Verification:-

Here, l (DE) = a = 17 m

l (EF) = b = 25 m

l (DF) = c = 26 m

By using the formula of Heron's

$$\begin{aligned} \text{Perimeter of } \square \text{ DEF} &= a + b + c \\ &= 17 + 25 + 26 \\ &= 68 \text{ m} \end{aligned}$$

Semiperimeter of □ DEF,

$$S = \frac{a + b + c}{2}$$

$$S = \frac{68}{2} = 34 \text{ m.}$$

Area of □ DEF = A (□ DEF)

$$= \sqrt{s(s-a)(s-b)(s-c)}$$

$$= \sqrt{34 \times (34 - 17) \times (34 - 25) \times (34 - 26)}$$

$$= \sqrt{34 \times 17 \times 9 \times 8}$$

$$= \sqrt{2 \times 17 \times 17 \times 9 \times 8}$$

$$= \sqrt{(17 \times 17) \times 9 \times (2 \times 8)}$$

$$= \sqrt{289 \times 9 \times 16}$$

$$= \sqrt{289} \times \sqrt{9} \times \sqrt{16}$$

The square root of 289 is 17,

The square root of 9 is 3 and

The square root of 16 is 4 respectively

$$= 17 \times 3 \times 4$$

$$= 204.$$

∴ Area of □ DEF = 204 sq .m.

Ex. (2) In □ ABC , l (AB) = 11 cm,

l (BC) = 4 cm and l (AC) = 7 cm

Find the area of □ ABC.

☞ □ ABC is a scalene triangle

Here,

$$l (AB) = a = 11 \text{ cm}$$

$$l (BC) = \text{Base} , b = 6 \text{ cm}$$

$$l (AC) = c = 7 \text{ cm}$$

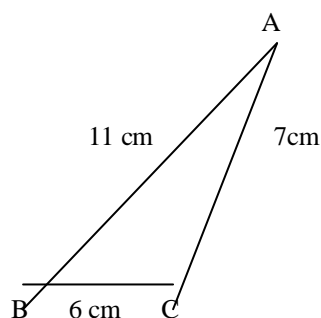


Fig.No.7

By using The New Formula No. (1)

Area of □ ABC = A (□ ABC)

$$= \frac{1}{2} \times \text{Base} \times \text{Height}$$

$$= \frac{1}{2} \times b \times h$$

$$= \frac{1}{2} \times b \times \sqrt{a^2 - \left(\frac{a^2 + b^2 - c^2}{2b} \right)^2}$$

$$= \frac{1}{2} \times 6 \times \sqrt{11^2 - \frac{11^2 + 6^2 - (7)^2}{2 \times 6}}$$

$$= \frac{6}{2} \times \sqrt{121 - \left(\frac{121 + 36 - 49}{12} \right)^2}$$

$$= 3 \times \sqrt{121 - \left(\frac{108}{12} \right)^2}$$

The simplest form of $\frac{108}{12}$ is 9

$$= 3 \times \sqrt{121 - (9)^2}$$

$$= 3 \times \sqrt{121 - 81}$$

$$= 3 \times \sqrt{40}$$

$$= 3 \times \sqrt{4 \times 10}$$

$$= 3 \times \sqrt{4} \times \sqrt{10}$$

The square root of 4 is 2

$$= 3 \times 2 \times \sqrt{10}$$

$$= 6 \sqrt{10} \text{ sq.cm}$$

$$\therefore \text{Area of } \square \text{ ABC} = 6 \sqrt{10} \text{ sq.cm}$$

By using The New Formula No. (2)

Area of $\square \text{ ABC} = A(\square \text{ ABC})$

$$= \frac{1}{2} \times \text{Base} \times \text{Height}$$

$$= \frac{1}{2} \times b \times h$$

$$= \frac{1}{2} \times b \times \sqrt{c^2 - \left(\frac{-a^2 + b^2 + c^2}{2b} \right)^2}$$

$$= \frac{1}{2} \times 6 \times \sqrt{7^2 - \left(\frac{-(11)^2 + 6^2 + 7^2}{2 \times 6} \right)^2}$$

$$= \frac{6}{2} \times \sqrt{49 - \left(\frac{-121 + 36 + 49}{12} \right)^2}$$

$$= 3 \times \sqrt{49 - \left(\frac{-36}{12} \right)^2}$$

The simplest form of $\frac{-36}{12}$ is (-3)

$$= 3 \times \sqrt{49 - (-3)^2}$$

The square of (-3) is 9

$$= 3 \times \sqrt{49 - 9}$$

$$= 3 \times \sqrt{40}$$

$$= 3 \times \sqrt{4 \times 10} = 3 \times \left(\sqrt{4} \times \sqrt{10} \right)$$

The square root of 4 is 2.

$$= 3 \times 2 \times \sqrt{10}$$

$$= 6 \sqrt{10} \text{ sq.cm}$$

Area of $\square ABC = 6\sqrt{10}$ sq. cm

Verification :-

EX (2) In $\square ABC$, l (AB) = 11 cm,
l (BC) = 6 cm and l (AC) = 7 cm

Find the area of $\square ABC$.

☞ Here, l (AB) = a = 11 cm

l (BC) = b = 6 cm

l (AC) = c = 7 cm

By using the formula of Heron's

Perimeter of $\square ABC = a + b + c$

Semiperimeter of $\square ABC$,

$$S = \frac{a + b + c}{2}$$

$$S = \frac{11 + 6 + 7}{2}$$

$$S = \frac{24}{2} = 12 \text{ cm.}$$

Area of $\square ABC = A(\square ABC)$

$$= \sqrt{s(s-a)(s-b)(s-c)}$$

$$= \sqrt{12 \times (12 - 11) \times (12 - 6) \times (12 - 7)}$$

$$= \sqrt{12 \times 1 \times 6 \times 5}$$

$$= \sqrt{6 \times 2 \times 6 \times 5}$$

$$= \sqrt{(6 \times 6) \times (2 \times 5)}$$

$$= \sqrt{36 \times 10}$$

$$= \sqrt{36} \times \sqrt{10} \quad (\text{The square root of 36 is 6.})$$

$$= 6 \times \sqrt{10}$$

$$\therefore \text{Area of } \square ABC = 6\sqrt{10} \text{ sq.cm}$$

2. Explanation

We observe the above solved examples and their verifications, it is seen that the values of solved examples and the values of their verifications are equal.

Hence, The New Formulae No. (1) and (2) are proved.

3. Conclusions

$$\text{Height, } h = a^2 - \sqrt{\left(\frac{a^2 + b^2 - c^2}{2b}\right)^2}$$

$$\therefore \text{Area of triangle} = \frac{1}{2} \times \text{Base} \times \text{Height}$$

$$= \frac{1}{2} \times b \times h$$

$$\text{Area of triangle} = \frac{1}{2} \times b \times \sqrt{a^2 - \left(\frac{a^2 + b^2 - c^2}{2b}\right)^2}$$

OR

$$\text{Height, } h = \sqrt{c^2 - \left(\frac{-a^2 + b^2 + c^2}{2b}\right)^2}$$

$$\therefore \text{Area of triangle} = \frac{1}{2} \times \text{Base} \times \text{Height}$$

$$= \frac{1}{2} \times b \times h$$

$$\text{Area of triangle} = \frac{1}{2} \times b \times \sqrt{c^2 - \left(\frac{-a^2 + b^2 + c^2}{2b}\right)^2}$$

From above two new formulae, we can find out the height & area of any types of triangles. These new formulae are useful in educational curriculum, building and bridge construction and department of land records. These two new formulae are also useful to find the area of a triangular plots of lands, fields, farms, forests etc. by drawing their maps.

References

[1] Geometry concepts & pythagoras theorem.

Underground Water Prospecting In Rural Settings

E. C. Mabunda, Beng, Msc

Department of Electrical Engineering University of Zimbabwe, P. O. MP 167, Mt Pleasant, Harare ZIMBABWE

Abstract

This paper presents the design of a portable water table detector. The device can be used to identify where the water table is likely to be found. The heart of the design is on the microcontroller. The ground probes require high voltage and this is generated from a 12 volt battery using a 555 timer arranged as an a-stable multi-vibrator. The use of a battery is to make the device usable even at remote places where electrical power is not available. A suggested code in assemble language for the microcontroller is given as guide. However a high level language can also be implemented, to achieve the same results. The use of the microcontroller (μ processor) makes it feasible to produce a device that is cost effective for both urban and rural dwellers. The main activity of this design is centred on the development of the code (software program), design of a special power supply and the interfacing external hardware for the detector.

Key Words: Water table detector, electrode interface, PIC microcontroller, Geological strata, resistivity measurement, Analogue to Digital conversion.

1. Introduction

There are various types of water detectors available in the market, but most of these have been designed for countries that are very developed, hence they tend to be costly and more sophisticated for an ordinary user. This design results in a product that is cost effective in that it uses an inbuilt power supply based on the battery and virtually no moving parts that may require constant maintenance. The system constitutes a software program, control circuits and probe electrodes, as well as the power supply that is incorporated into the system. The device should be able to measure the depth from ground surface to the underground water, and should be easy to operate. The main focus of this paper is to generate motivation and interest in the design and production of devices that are simple to use and suitable for developing technologies.

2. System Overview

Figs 1 and fig 2 shows the setup of the water table detector. The system incorporates four electrodes, two of which are used to pass current through the ground and the other two are used to measure voltage across the specimen ground. Also there is need for signal conditioning to enable proper electrode interface to the microcontroller. Fig 1 illustrates the concept while fig 2 shows how the detector can be used.

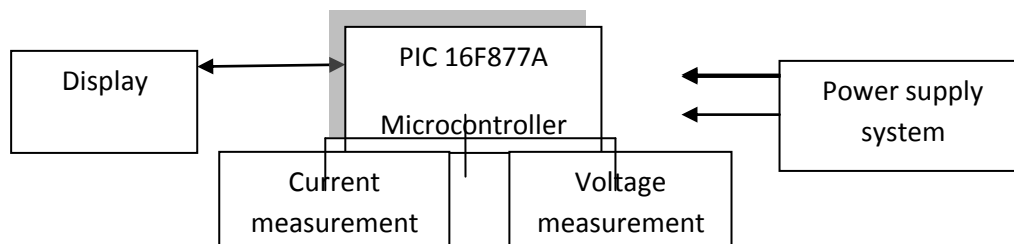


Fig.1. Underground water table detector block diagram

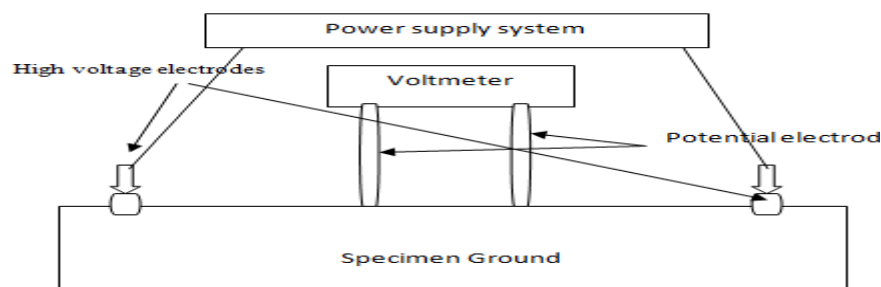


Fig.2. Deployment and usage of the Water table detector

To measure resistivity of subsurface formation, four electrodes are required. A current [I] is introduced between one pair of electrodes called current electrodes. The current electrodes can be identified as A and B or +I and -I to denote source and sink. The potential difference measured as a result of current flow is measured with another pair of electrodes called potential electrodes. These potential electrodes may be represented as M and N, and V will represent the resultant potential difference.

Resistivity = $K \left(\frac{V}{I}\right)$ where K is a geometrical constant

$$K = \frac{([\text{AB}]/2) - ([\text{MN}]/2)^2 \cdot \frac{\pi}{2}}{[\text{MN}]/2}$$

Where AB = distance between current electrodes
MN = distance between potential electrodes

The changes in the resistivity of geological strata may be measured by a method known as vertical electrical sounding. In the field, a series of resistivity measurements are made at various electrode spacing entered at a common point. Sampling depth is increased by increasing electrode spacing. The M and N electrode array is held fixed while the A and B current electrodes are moved outwardly by constant length. This movement is relative to the increase in depth of measurement as the current electrodes are moved further apart. The depth measured is AB/2. When the current electrodes are moved further apart, the potential recorded from the M and N electrodes will change as the current passes through different subsurface structures. The relationship $V = IR$ (Ohm's law) holds for simple circuits as well as earth materials. However, resistance is not a material constant; instead, resistivity is an intrinsic property of the medium describing the resistance of the flow of current in that medium. In general resistivity is defined as a unit change in resistance scaled by the ratio of a unit cross-sectional area and a unit length of the material through which the current is passing. Earth's resistivity can range over nine orders of magnitude from 1 to 10^8 ohm/m. Table 1 shows the common resistivity of different ground earth types.

Table.1

Material value	Resistivity range	Typical
Igneous and Metamorphic rocks	$10^2 - 10^8$	10^4
Sedimentary	$10 - 10^8$	10^3
Ground Water	1 - 10	5
Pure water		10^3

Common soil resistivity

3. Soil resistivity Processing Circuit

The computation of the resistivity and the subsequent water table results are performed in the microcontroller type PIC 16F877A. The choice of this particular type has been motivated by the fact that it is readily available and reasonably priced. This microcontroller is relatively simply to program; its instructions set has only 35 mnemonics yet performing very powerful operations.

3.1. Measuring resistivity at a depth of 20 meters.

The PIC 16F877A is used to perform the following computations under the control of the program code. The current electrode spacing in this case is 40 meters and the voltage electrode spacing is set at 4 meters, so that:

$$\text{AB} = 40 \text{ m}$$

$$\text{MN} = 4 \text{ m}$$

Plugging these figures into the previously mentioned formula we get:

$$\begin{aligned} \text{Resistivity} &= \left\{ \frac{(40/2)^2 - (4/2)^2 \cdot \frac{\pi}{2}}{(4/2)} \right\} V/I \\ &= \left\{ \frac{20^2 - 4 \cdot \frac{\pi}{2}}{2} \right\} V/I \\ &= \left\{ \frac{198\pi}{2} \right\} V/I \\ \text{Taking } \pi \text{ to be } 22/7 &\quad \text{we have } 310V/I. \end{aligned}$$

The condition for presence of the water table is that the value of the resistivity should lie in the range of 1 to 10 ohms per meter. Therefore the PIC is programmed to compute the following inequality and display a positive or negative result.

$$1\Omega/m < 310V/I < 10\Omega/m$$

$$= I < 310V < 10I$$

The denary number 310 when converted to binary is found to exceed 8 bits in size but the PIC microcontroller registers have got a maximum capacity of 8 bit numbers only. One way to alleviate this is to scale down by 2 so that the inequality becomes:

$$\frac{I}{2} < 155V < 5I$$

To obtain $\frac{I}{2}$ at the input of the system two resistors in parallel are used as shown in fig 3. This procedure will make the new inequality to be $I' < 155V < 10I'$ where I' is $\frac{I}{2}$

3.2. Measuring resistivity at a depth of 40meters

The procedure for measuring resistivity at the depth of 40 meters is the same as for 20 save for the current electrode spacing which is now 80m but the voltage electrode spacing remains at 4m. In this case AB = 80m. Resistivity becomes 1254V/I and the condition for presence of water remains the same i.e. between 1 and 10 Ω/m . The resulting inequality $1\Omega/m < 1254V/I < 10\Omega/m$ need to be scaled down to fit into the original range of $I' < 155V < 10I'$ by switching in resistances at the input. Fig. 3 show the implementation circuit diagram of the detector.

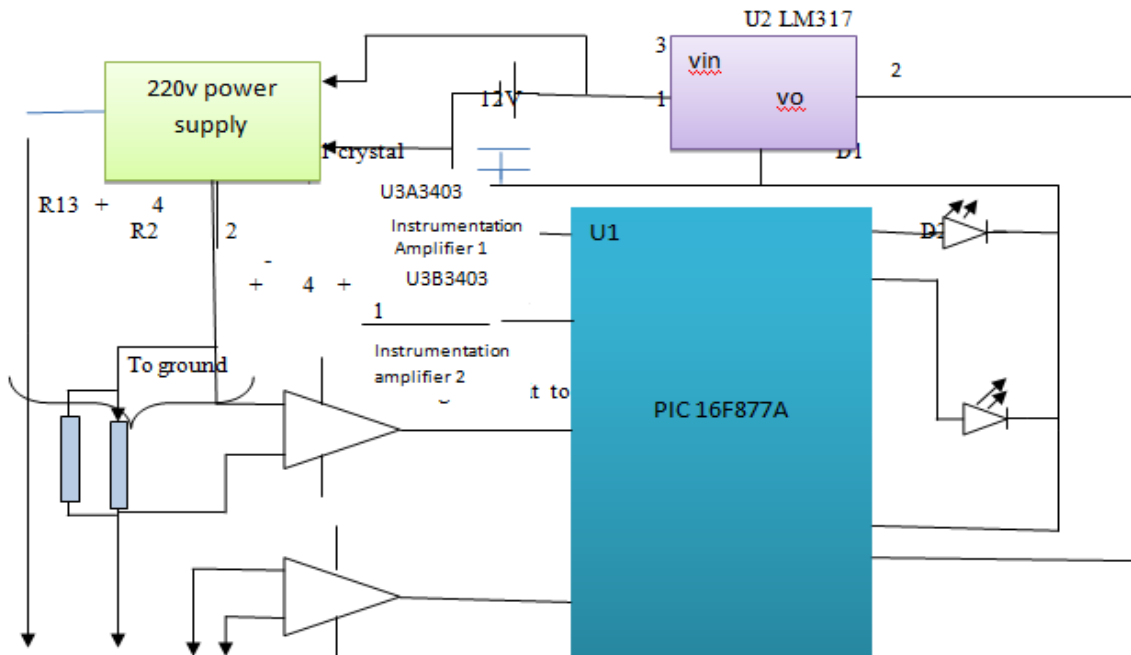


Fig.3.Circuit to measure resistivity

The instrumentation amplifier number 1 samples the value of voltage across the 1.2 k Ω resistors. This gives a value of voltage that is directly proportional to the current passing through the resistor which is also half the current passing through the circuit. The current $I/2$ is the one used for computing the resistivity by the microcontroller. Instrumentation amplifier 2 measures the underground voltage value. The two values, current passing through the circuit and the voltage across the underground are used to calculate resistivity of the underground structure. Since the groundwater resistivity as shown in table 1 is in the range of 1 to 10 ohms/m a positive result would be found out if the resistivity of the underground structure lies in this range. Microcontroller receives input voltage and current from which it calculates the resistivity and compares it with known range and gives an output signal to show the presence or absence of the water table. When the device is turned ON, one LED will light at any given moment. As long as the depth of measurement does not contain the water table it means that the red LED will be lighting. The lighting of these LEDs is done in software by the PIC microcontroller.

Fig 4 shows the detailed pin out diagram of the 16F877A microcontroller. The microcontroller makes use of an external clock which, for the purposes of this design uses a 4 MHz crystal oscillator connected to pins 9 and 10. Each instruction cycle takes 1µs to be executed.

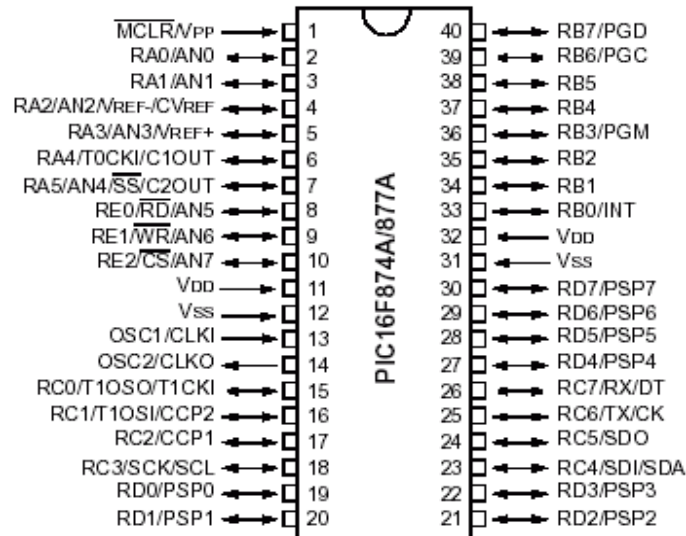


Fig.4. PIC 16F877A microcontroller pin out diagram

3.3 Analogue to Digital conversion

The PIC microcontroller is capable of converting an analogue signal to a digital one. It performs this for one signal at a time. Before the analogue to digital conversion is done there are registers that need to be initialized. These are ADCON0 and ADCON1 registers.

3.4 ADCON0 register

The pins for ADCON0 are configured as shown below. This register controls the operation of the analogue to digital module.

R/W-0	R/W-0	R/W-0	R/W-0	R/W-0	R/W-0	U/O	R/W-0
ADC1	ADCS0	CHS2	CHS1	CHS0	GO/DONE	-----	ADON

Bit 7-6

ADCS1:ADCS0: A/D conversions Clock select bits

00 = FOSC/2

01 = FOSC/8

10 = FOSC/32

11 = FRC (Clock derived from internal A/D module)

Bit 5-3

CHS2:CHS0: Analogue Select bits

000 = channel 0 (RA0/AN0)

001 = channel 1 (RA1/AN1)

010 = channel 2 (RA2/AN2)

011 = channel 3 (RA3/AN3)

100 = channel 4 (RA4/AN4)

101 = channel 5 (RA5/AN5)

110 = channel 6 (RA6/AN6)

111 = channel 7 (RA7/AN7)

Bit 2

GO/DONE: A/D Conversion status bit

If ADON = 1

1 = A/D Conversion in progress (setting the bit starts the A/D conversion)

0 = A/D Conversion not in progress (this bit is automatically cleared by hardware when A/D conversion is complete.

Bit 1

Unimplemented: read as 0

Bit 0

ADON: A/D on bit

1 = A/D converter module is operating

0 = A/D converter module is shut off and consume no operating current.

3.5 ADCON1 Register

This register initializes the control for analogue to digital conversion. The pins for ADCON1 register are configured as shown in the diagram below. The most significant bit selects the analogue to digital conversion format for reading the result. The next four bits are for Port configuration.

R/W-0	R/W-0	U/O	U/O	R/W-0	R/W-0	R/W-0	R/W-0
ADFM	ADCS2	-----	-----	PCFG3	PCGF2	PCGF1	PCFG0

Bit 7 **ADFM:** A/D Result Format Select bit 0 =
 1 = Right justified. Six (6) most significant bits of ADRESH are read as '0'
 Left justified six (6) least significant bits of ADRESL are read as '0'

Bit 6 **ADCS2:** A/D Conversion clock select bit

The steps followed when doing the analogue to digital conversion are as follows:

- Configure the A/D module
- Configure pins / voltage reference and digital input output (ADCON1)
- Select A/D input channel (ADCON0)
- Select A/D conversion clock (ADCON0)
- Turn on A/D module (ADCON0)
- Configure the A/D interrupt if desired
- Wait the required acquisition time
- Start the conversion by setting the GO/DONE bit
- Wait for the A/D conversion to complete by either polling the GO/DONE (low) bit or with interrupt enable you wait for the A/D interrupt.
- Read A/D result register pair (ADRESH: ADRESL).

The next page show shows the flow chart of the processes the microcontroller go through to achieve the measurement of the resistivity at 20m depth.

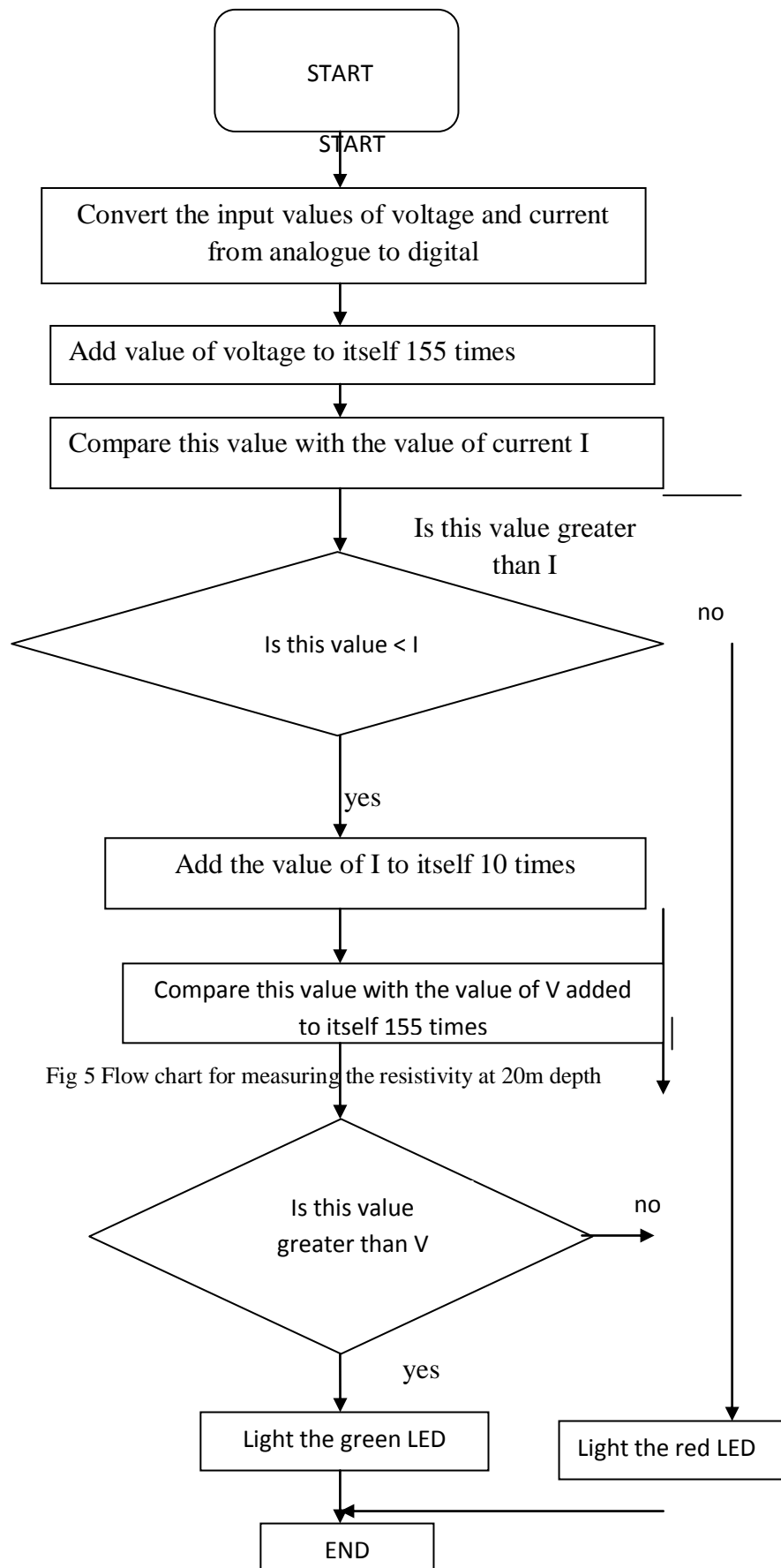


Fig 5 Flow chart for measuring the resistivity at 20m depth

4. Code for 20 M Depth Resistivity

The listing below (listing 1) is the suggested code that controls the operation of microcontroller in the calculation of the resistivity hence the depth of the underground water table.

Listing 1

```

Org 0x00
    RP0      equ    5
    RP1      equ    6

    Vic 1    equ    20h
    Vic 2    equ    21h
    Vic 3    equ    22h
    DEC      equ    23h
    DEC1     equ    24h
    ANS1     equ    25h
    ANS2     equ    26h
    Vic4     equ    27h
    Vic 5    equ    28h
    Vic6     equ    29h
    Init     equ    2Ah
    C        equ    2Bh
    RLED     equ    2Bh
    DEC2     equ    2Ch
    GLED     equ    2Dh
    Cham     equ    2Eh
    STATUS   equ    03h
    INTCON   equ    8Bh
    ADCON0   equ    1Fh
    ADCON1   equ    9Fh
    PORTA    equ    05h
    PORTB    equ    06h
    ADRESL   equ    9Eh
    PIR1     equ    0Ch

    Org      0x00
    Goto     Main
    BCF      STATUS,RPO
    MOVLW    0x80                ; all analogue input code
    MOVWF    ADCON1
    MOVLW    0x3F
    MOVWF    PORTA
    BCF      STATUS,RPO        ; reset to bank 0
    CLRF     PORTB

Volrcon CALL SelAN0
    CALL     AtoD
    CALL     Volt

    Return

Currcon CALL SelAN1
    CALL     AtoD
    CALL     Curr

    return

SelAN0 MOVLW    b'01000001'
    MOVWF    ADCON0

    Return
    
```



```

AtoD      BSF          ADCON0, 3
Z          BTFSS       PIR1, 6
          goto        Z
          return

Volt      MOVF        ADRESL, W
          MOVWF       vic1
          MOVWF       vic2

SelAN1    MOVLW      b'01001001'
          MOVWF       ADCON0
          return

Curr      MOVF        ASRESL, W
          MOVWF       vic4
          MOVWF       vic5
          MOVWF       vic6
          return

Cham      Banksel    ADCON1
          CLRF        ADCON1
          MOVLW      b'01000001'
          Banksel    ADCON0
          BCF        INTCON, 7
          return

main      CALL        Cham
          CALL        Voltcon
          CALL        Currcon

          MOVLW      0xFF
          MOVWF       DEC
          MOVFW      vic1

x         ADDWF      vic2, 0
          DECFSZ     DEC
          GOTO       x
          MOVWF     vic3
          MOVLW     b'00111000'
          MOVWF     DEC1
          MOVFW     vic3

y         ADDWF      vic2,0
          DECFSZ     DEC1
          GOTO       y
          MOVWF     ANS1
          MOVFW     vic4
          SUBWF     ANS1,1 ;ANS1-vic4
          BTFSC     STATUS,C
          GOT       RLED
          MOVLW     b'00001010'
          MOVWF     DEC2
          MOVFW     vic5

A         ADDWF      vic6,0
    
```

```

DECFSZ    DEC2
GOTO      A
MOVWF     ANS2
SUBWFANS1,0
BTFSC    STATUS,C
GOTO      GLED
GOTO      RLED
END

```

5. High Voltage Power Supply

In order to make the device truly portable the necessary 220 volt supply must be generated from the 12volt battery. The power supply schematic is shown in fig. 6. To keep the cost of the device low readily available components that are not highly specialized have been chosen. The NE555 timer has been used to generate a high frequency that drives Q1 and Q2 which in turn drives the transformer Tr1. The output voltage is then available across terminals 3and4 of Tr. 1.

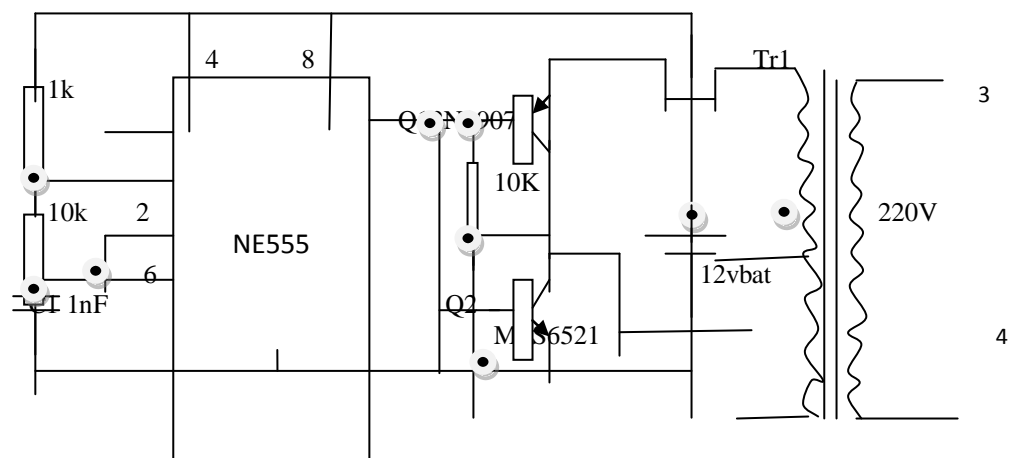


Fig.6 High voltage power supply

With the timing components given the NE 555 timer generates a square wave at a frequency, 68 kHz. The output pin 3 of the timer is fed onto the transistors. A high output which is 2/3 of the supply voltage causes transistor Q2 to conduct while transistor Q1 is not conducting. This is because Q2 is active high transistor. A low at the base of Q1 ensures conduction of this transistor. The 68 kHz value was chosen to minimize the size of the transformer as well as conserving power consumption from the battery making the device truly portable.

6. Conclusion

The design of a water table detector as shown here provides for an alternative way of constructing and production of a cheap and effective underground water table detector that is affordable, portable and can be useful in rural settings. This has been achieved by use of compact components such as the microcontroller, the NE555 timer and a high efficient transformer. The design is centred on three major components i.e. the PIC microcontroller, NE 555 and the program code. Further refinements in terms of packaging can make this device truly portable. The design objective is to provide for a simple and portable underground water detector that can be used by less sophisticated persons and this paper has successfully presented a possible solution to this end. Improvements to this device could be in making high voltage power supply that is more robust, by use of specialized components. However in so doing care must be exercised to avoid over pricing of the end device.

References

- [1] 2D and 3D Subsurface Resistivity Imaging using a constrained Least – Squares Algorithm April 14/17/1999, by UniversitatPolitecnica de Catalunya.
- [2] Corrosion-doctors.org <http://corrosion-doctors.org/Corrosion-Kinetics/Ohmic-drop-soil.htm> accessed 12/07/10
- [3] Ground Resistance Testers: http://www.aemc.com/technfo/appnotes/Ground_Resistance_Testers/App-Ground-SoilResistivity.pdf 12/07/10
- [4] Wileywater.com: http://www.wileywater.com/Controbutors/Sample_2.htm

- [5] Ground Water: Volume 14 issue 1 page 6 – 10 published online 6 July 2006
- [6] Groundwater NMR in conductive water: Geophysics Vol. 61 no. 4 July – August 1996.
- [7] Groundwater NMR: Geophysics Vol. 62 No 1 January – February 1997
- [8] Geophysical Research letters Vol. 18 No. 6 pages 1127 – 1130 June 1991
- [9] Ground Measuring Techniques: by Elvis R Sverko February 11, 1999, <http://www.electro-specialities.com/techhical/downloads/Grol> accessed 16/07/10
- [10] Soil resistance Measurement: <http://www.eijkelkamp.com/Portals/2/Eijkelkamp/Presentation/16/07/10> accessed 16/07/10
Accessed 10/07/10
- [11] Application of surface Geophysics to Ground-water investigations by A. A. R Zohdy, G. P. Eaton and D.R. Mobey Book 2 published by Science for a changing world.

Biosensors Based on Nano-Particles

Sidharth Singh Sisodia¹, Shalinee Dumoliya², Deepak Koli³

¹Lecturer-Computer Engineering, Pacific Institute of Technology, Udaipur, Rajasthan, India

²Lecturer-Electronic & Communication Engineering, Pacific Institute of Technology, Udaipur, Rajasthan, India

³Informatics Assistant, Department of Information Technology & Communication, Jaipur, Rajasthan, India

Abstract

Nano-particles have various unique features, which include biocompatibility, rapid and simple chemical synthesis, excellent electro-activity, and efficient coating by biomolecules. So if biosensors are built from nano-particles, it is proved to be a benefactor. Taking this in account, the paper discusses important features of nano-particle biosensors and R&D bibliometric analysis. Since R&D bibliometric analysis show that gold nano-particles are the best in class, this paper evaluates them in detail.

Keywords: Gold Nano-Particles, Bibliometric analysis.

1. Introduction

Bio-sensors are devices that are routinely applied in applications such as monitoring glucose content in blood, quality analysis of fresh and waste water. This is because bio-sensors react to the presence of bacteria, viruses or bio-molecules such as proteins, enzymes and DNA. Research on nano-particles based biosensors is rapidly gaining attention in the research community. More specifically, there is tremendous interest in applying nano-scale materials to biological material for sensors. Nano-materials are ideal candidates for building sensor devices. This is because even a few molecules of nano-materials can alter the properties very drastically. Such changes can be easily detected by optical, electrical and chemical means. Start-of-the art nano-material based biosensors have high sensitivity. This makes it possible to use them in applications where we need to detect one particular molecule against a background of many others. Use of metal and semiconductor based nano-particles is also gaining increased popularity in bio-sensors. Changes in color, fluorescence intensity, emission colour and electrical current can be used as sensing mechanisms.

2. Nano-Particle Biosensors

With the recent advancement in the field of nano-particle biosensors, there are various biosensors which have come into picture. These nano-particle biosensors and their special features are listed below

Bio-sensors	Unique features
Gold nano-particle based	Show potential to facilitate molecular bonding to detect glucose in the micromolar concentration range.
Amperometric biosensors	Are aided by silver nano-particles. Show increased biocompatibility, which aids in pesticide detection.
Palladium nano-particles	Fabricate a sensitivity-enhanced electrochemical DNA biosensor
Functional nano-particles	Bound to biological molecules. Developed for use in biosensors to detect and amplify signals.

Bibliometric Analysis Bibliometric analysis is employed to ascertain R&D trends and research networks for nano-particle-based biosensors. Bibliometric analysis is a tool for extracting information from large databases looking for patterns and explaining reasons for apparently unstructured behavior. Figure 1 shows trend line of article counts, based on the cumulative number of publications by each of the three datasets i.e. SCI, FACTIVA, INSP. Apparently the overall trend of the publication counts keeps increasing, which shows that nano-particles have played a more and more important role in the this research and this trend is likely to increase further.

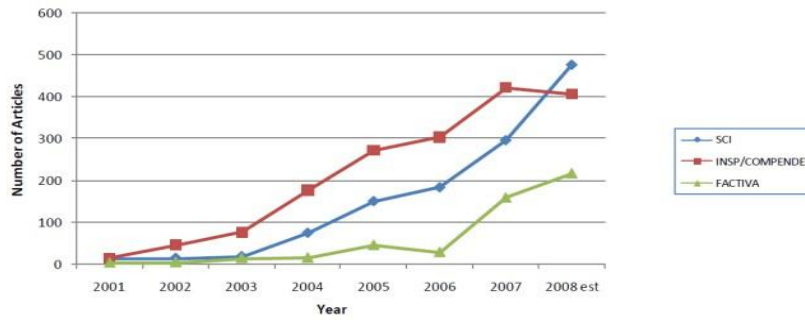


Figure 1: Trend of article counts for SCI, FACTIVE and ISP.

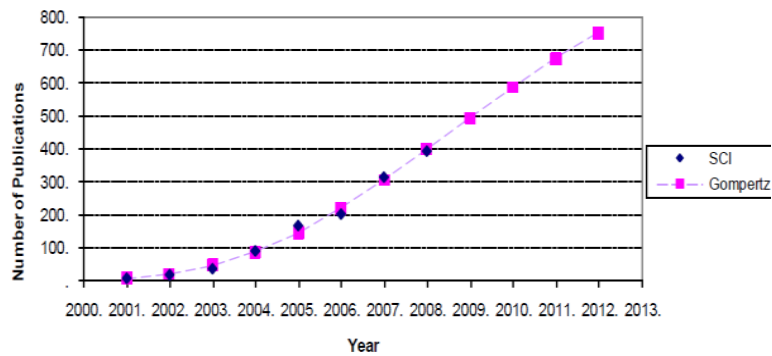


Figure 2: Trend of publication counts for SCI and Gompertz.

Figure 3 shows that the demand of metal nano- particle is increasing gradually. It further shows that the demand for gold nano-particles far exceeds the demand for platinum and silver nano-particles.

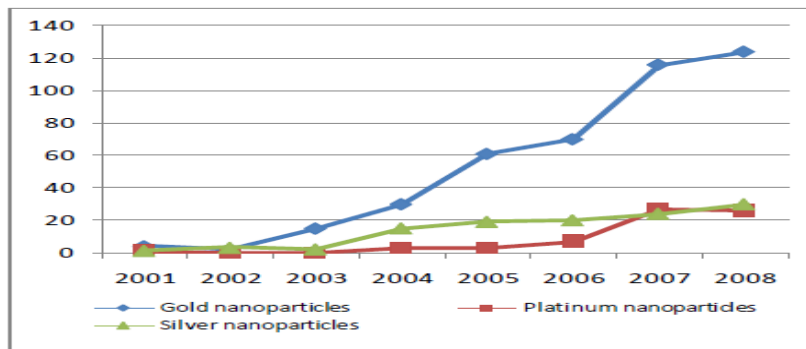


Figure 3(a): Increasing demand for gold nano-particles Figure 4 shows that metal nano-particles are on the top if we compare all types of nano-particle biosensors.

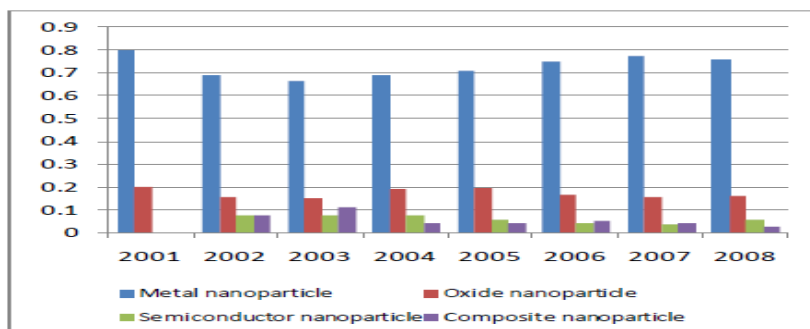


Figure 3(b): Increasing demand for metal based nano- particles

Gold Nano-particle Biosensors Gold nano-particles typically have dimensions ranging from 1-100nm. In addition, gold nano-particles display many interesting electrical and optical properties. Metals (like the gold in the nanoparticles) are good conductors, which is why they are used in electronics and wiring. Metals are good conductors for two reasons. First, electrons are not bound to individual atoms. Instead, they form a cloud around the atomic cores. This cloud of electrons is mobile allowing metal to transport charge (electrons) easily. Second, light is reflected off the surface of metals back to the eye. This is due to the electron cloud that surrounds the metal. Photons (individual units) of light cannot be absorbed by the atomic cores because they are blocked by the electron cloud. Consequently, photons are reflected back to the eye producing the sheen associated with metals. However, we also know from quantum mechanics that electrons can behave as either a wave or a particle. If we imagine electrons in the electron cloud as a wave with a certain energy value, we can envision a situation where it is possible for light of the same wavelength to be absorbed by the electron cloud, producing resonance. This is similar to what happens on stringed instruments, when a vibration occurs that matches the natural length of the string or one of its harmonics.

3. Principle

Metals are typically characterized by the presence of “free” electrons. In nanometer sized metal particles, there will be a strong absorption of light by the collective excitation of these unbound electrons. This absorption is referred to as a plasmon resonance and in the case of gold nano-particles they will have a spectral position and width that depends on its size, shape and to some extent the size distribution of the ensemble. When a metal absorbs light of a resonant wavelength, it causes the electron cloud to vibrate, dissipating energy. This process usually occurs at the surface of a material (as metals are not usually transparent to light) and is therefore called surface plasmon resonance. Figure 4 shows the plasmon resonance phenomena.

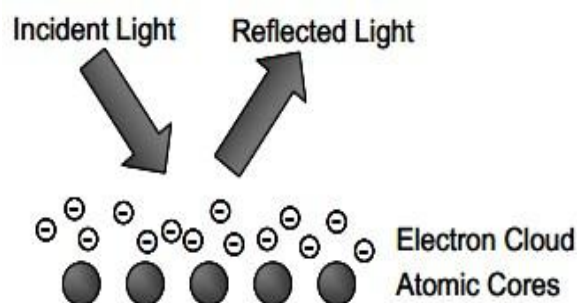


Figure 4: Plasmon resonance phenomenon

3.1 Equipments used

There are various equipments used to make measurements on nano-particles. This paper discusses three equipments listed below.

3.2 Scanning electron microscope (SEM) creates images of invisibly tiny things by bombarding them with a stream of electrons. This allows us to look at features on a scale as small as 10 nanometers (billionths of a meter). An SEM shoots a beam of electrons at the examination spot, transferring energy to the spot that it hits. The electrons in the beam (called *primary electrons*) break off electrons in the specimen. These dislodged electrons (called *secondary electrons*) are then pulled onto a positively charged grid, where they are translated into a signal. Moving the beam around the sample generates a whole bunch of signals, after which the SEM can build an image of the surface of the sample for display on a computer monitor [3].

3.3 Atomic force Microscope (AFM) scans the movement of a really tiny tip made of a ceramic or semiconductor material as it travels over the surface of a material. The tip positioned at the end of a *cantilever* (a solid beam) is either attracted to, or pushed away from the sample's surface. This deflects the cantilever beam and a laser measures the deflection. AFM then produces a visible profile of the little hills and valleys that make up the sample's surface.

3.4 Transmission electron microscope (TEM): Bouncing electrons off a sample is only one technique; you can also shoot electrons through the sample and watch what happens. That's the principle behind a transmission electron microscope (TEM). In effect, it's a kind of nano-scale slide projector. Instead of

shining a light through a photographic image (which allows certain parts of the light through), the TEM sends a beam of electrons through a sample. The electrons that get through then strike a phosphor screen, producing a projected image. Darker areas indicate that fewer electrons got through it, hence indicating that portion of the sample was denser. Lighter areas are where more electrons got through it, hence indicating that portion of the sample was less dense)[4].

4. Fabrication

There are various methods to fabricate gold nano- particle biosensors. This paper discusses two methods listed below.

4.1 Method: A glass slide is thoroughly cleaned in ethanol and deionized water for 15 min under ultrasonic agitation. Then, it is pretreated in a 30:70(v/v) mixture of H₂O₂ (30%) and H₂SO₄ (conc.) at 60-80°C for 45 min, washed with deionized water for 15 min and dried in an oven at 110°C for 45 min[7]. Surface of the substrate is modified by putting the glass slide in a solution of modifying agent, i.e. MPTMS, APTMS and PEI, in methanol for predetermined time (4, 12 and 20 hours). Then, the glass slide is washed with methanol and deionized water respectively, in an ultrasonic bath. Subsequently, the glass slide is immersed in gold colloidal solution prepared earlier. The deposition time for AuNPs is varied from 4, 12 and 20 hours, after which the glass slide is extensively rinsed with deionized water. Surface of the coated sample was characterized by X-ray photoelectron spectroscopy (XPS) and atomic force microscopy (AFM).

4.2 Method 2: 1.3 μm polystyrene latex (PSL) is used for template microsphere of colloidal crystal and 30 - 40 nm colloidal gold NPs is used to prepare assembled structure for SERS substrate. This process selected larger size gold NPs than 15 nm gold NPs which Kuncicky had used. This is because the apparent intensity of local plasmon resonance of 40 nm gold NPs is relatively larger than that of 15 nm and therefore more active substrate is expected as a result of experiments of colloidal aggregates. PSL and colloidal gold NPs were mixed and the volume fraction of PSL was adjusted from 2.5×10^{-3} to 5×10^{-3} . A glass plate is rinsed by the mixture solution of ethanol and water, and irradiated by ultraviolet light to make hydrophilic surface. Rinsed O-ring silicone rubber (5 mm diameter, 0.5 mm thickness) is put on the glass plate and the suspension of particle mixture is dropped into the ring for the fabrication of colloidal crystal with assembled structure of gold NPs. This O-ring is available to conserve the amount of gold NPs in the circumference of dried spots. After the drying process of the suspension, the PSL as template particles is removed by submersing the glass plate in methylene chloride for 15 min. A scanning electron microscope (S-4300, Hitachi, Tokyo, Japan) is used to observe the nanostructure of the substrates. SERS spectra is measured by a Raman spectroscope with a 785 nm incidental laser. A 10 μL of 30, 100 or 300 nM 4,4'-bipyridine (4bpy) aqueous solution is dropped on the SERS substrate and then the measurement is immediately performed. Raman spectrum of pure water is also measured as the background. The collection time of each SERS measurement is 10 seconds. Time course of SERS spectra were measured at the time of 1, 3, 5, 7 and 15 min after addition of 4bpy.

Figure 5 shows the schematic of the above prescribed method.

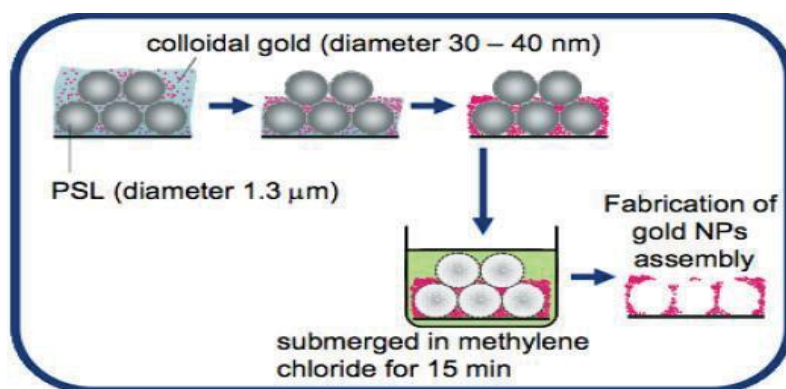


Figure 5: Schematic of Method 2

5. Characterization

Model gold nano-particles have diameter of 200 nm and length 2.5 – 4.0 μm . Surface modifications of gold nano-particles is done by the chemical compound 3-Mercapto-1-Hexanol (C₆H₁₄OS).

This paper focuses on surface characterization which includes size measurement (Inverted microscope Olympus IX70), electro-kinetic properties (ZetaPALS), and hydrophobicity (VCA Optima Goniometer). Electro-kinetic property is a particle's ability to move in the electromagnetic field. ZetaPALS measures the particles' mobility, and then calculates to give zeta potentials or the surface charge values. Figure 6 shows that the optimum concentration occurs at (OD546nm): **0.15 - 0.30**

Effect of concentration

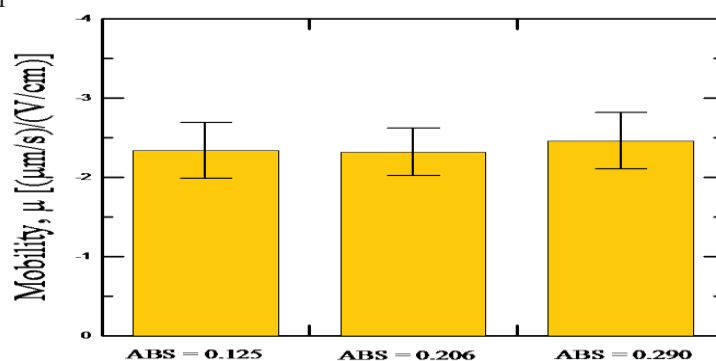


Figure 6: Mobility versus concentration

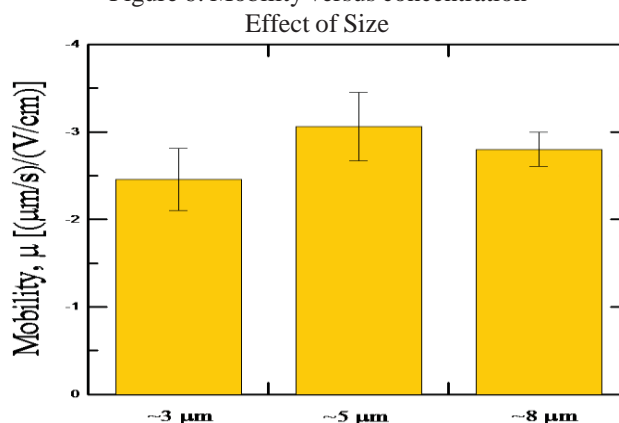


Figure 7: Mobility versus size, shows that mobility is not a function of size.

Figure 8 shows the effect of **valence** and **ionic strength**. As ionic strength increased in the presence of salt solutions, mobility became less negative (charge on particle approached neutral). Valence had an important role on mobility, in the presence of divalent cations, mobility was less negative than that in the presence of monovalent cations.

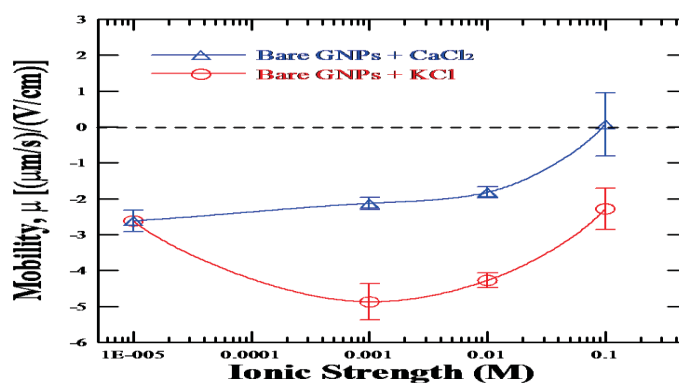


Figure 8: Mobility versus ionic strength

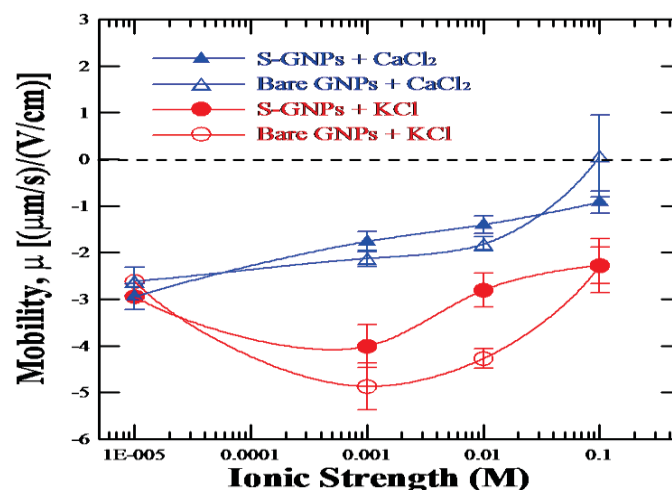


Figure 9: Mobility versus ionic strength for bare GNP versus S-GNP

Figure 9 shows the electro-kinetic properties of Bare GNPs vs. S-GNPs. The mobility of S-GNPs was less negative than that of bare GNPs in the presence of KCl. However, the difference was not significant in the presence of CaCl₂. Valence played an important role on GNPs' mobility regardless of the presence of 3-mercapto-1-hexanol groups. Moving on the other side, hydrophobicity refers to a surface's property of being water-repellent. Contact Angle method is used to know at what degree is GNPs hydrophobic. It is said to be hydrophobic if the contact angle is greater than 90° and hydrophilic otherwise. Solution concentration used is OD546nm : 1.684 (2.5x dilution). The optimum angle is observed at the concentration of 100μL. Contact angle of S- GNPs: $135.8 \pm 3.2^\circ$. This shows that the surface of S-GNPs is hydrophobic. Functional groups 3- mercapto-1-hexanol did not affect the hydrophobicity significantly.

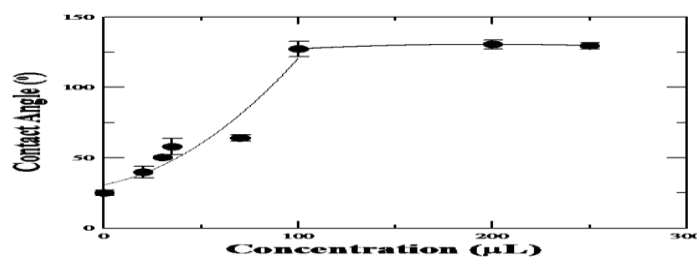


Figure 10: Contact angle as a function of concentration

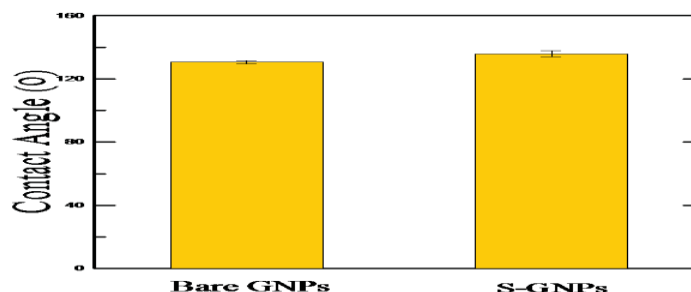


Figure 11: Comparison of contact angles for bare GNPs and S-GNPs

6. Applications

The most familiar application of nano-particles in sensing is the home pregnancy test. Nano-particles (< 50 nm) are bound to antibodies, complementary to a hormone produced by pregnant women. When the stick is submerged in urine flow, if the hormone is present it will bind to the microspheres (~ 500 μm) and nano-particles causing aggregates to form. The solution then passes through a paper filter. If the pregnancy hormone is present, the aggregates will be trapped by the filter producing a colored product. If the pregnancy hormone is not detected, the nano-particles will pass through the filter because of their

6. 1 small size.

Urine passes from the flow stick to a central reservoir containing gold nano-particles and latex micro- particles. If pregnancy hormone is present, particles aggregate and are prevented from passing through a downstream filter. This produces a red signal in the viewing window. Nano- and micro- particles are modified with antibodies (blue) that bind to pregnancy hormone (yellow) is present in urine, particles will aggregate and are unable to pass through the downstream filter[8].

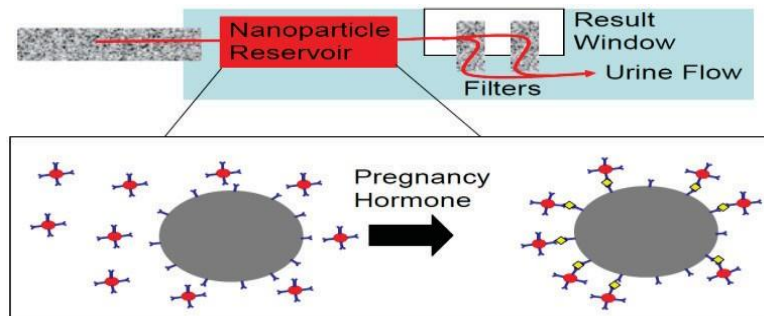


Figure 12: Application of nano-particles for home- pregnancy test

Functions	Biosensor	Sensor Advantage	Typical Examples
Bio-molecule Immobilization	Amperometric Biosensor	Improved Stability	For the determination of inulin in food
Catalysis of reactions	Glucose Biosensor	Improved sensitivity And	Glucose in gold nanoparticles
Labelling Bio-molecules	Optical Biosensor	Improved sensitivity and indirect detection	Self assembled nanoparticles probes for recognition and detection of biomolecules
Enhancement of electron transfer	Electrochemical Biosensor	Improved sensitivity and direct electrochemistry of proteins	Colloidal gold enhanced DNA immobilization for electrochemical detection of sequence specific DNA.

Other applications of gold nano-particles in different biosensor systems are listed in the table above.

7. Conclusion And Future Prospects:

Various aspects of gold nano-particles applications are presented in this paper. The properties of gold nano-particles can be modified by the adsorption of both polymers and biopolymers. The typical preparation strategies and applications of these gold nano-particle-polymer hybrids are summarized. The unique optical properties, special catalytic properties of gold nano-particles allow the use of these particles as labels for colorimetric detection of biomolecules, for developing sensitive biosensors. There is immense potential of gold nano-particles for cancer diagnosis and therapy. One of the most promising areas of gold nano-particles application is photothermal therapy, also antibacterial activity of drugs conjugated with gold nanoparticles.

References

- [1] <http://www.thevantagepoint.com/resources/articles/IDENTIFYING%20EMERGING%20NANOPARTICLE%20ROLES%20IN%20BIOSENSORS.pdf>
- [2] <http://onlinelibrary.wiley.com/doi/10.1002/wnan.84/pdf>
- [3] <http://www.sciencedirect.com/science/article/pii/S0921510710002370>
- [4] <http://ijaest.iserp.org/archieves/13-Jn-15-30-11/Vol-No.8-Issue-No.1/8.IJAEST-Vol-No-8-Issue-No-1-SYNTHESIS-OF-NANOPARTICLE-054-057.pdf>
- [5] <http://www.sciencedirect.com/science/article/pii/S0013468608003599>
- [6] http://www.nsec.ohio-state.edu/teacher_workshop/Gold_Nanoparticles.pdf
- [7] Zhuravlev, L.T., *Langmuir*, 3,316,1987.
- [8] http://www.nsec.ohiostate.edu/teacher_workshop/Gold_Nano_particles.pdf
- [9] <http://empl.snu.ac.kr/swchah/publications/ChemBiol12.pdf>
- [10] <http://www.electrochemsci.org/papers/vol5/5091213.pdf>

Comparative Study of Transcritical CO₂ Cycle with and Without Suction Line Heat Exchanger at High Ambienttemperature

¹A..D. Kadam, ² A.S. Padalkar, ³ V.U.Walekar

^{1,2,3}Pune University, Sinhgad college of Engineering, Vadgaon (Bk.), Pune, Maharashtra, India.

Abstract

Global warming and ozone depletion potential of chemical refrigerants have motivated to develop the refrigeration systems with natural refrigerants. Transcritical CO₂ refrigeration cycle losses its performance at higher ambient temperature due to lower critical temperature of CO₂. This paper discusses the comparative analysis of the transcritical cycle with and without suction line heat exchanger. At higher ambient conditions, the use of suction line heat exchanger improves the cycle performance by 2 to 4%. Due to more heat transfer rate the specific refrigeration capacity, mass flow rate and compressor power consumption. The performance of cycle does not improve significantly with increase in the effectiveness of the suction line heat exchanger.

Key Words: Transcritical cycle; CO₂; suction line heat exchanger; cycle simulation; gascooler; refrigerant

1. Introduction

Environmental issues have enforced all the researchers to find sustainable permanent alternative solutions to the current working fluids used in the refrigeration and air conditioning systems. Prof. Gustav Lorentzen through his research on natural refrigerant has given rebirth to CO₂, which was very popular in the late nineteen and early twenty century [7]. CO₂ is available in ample quantity in the nature and is not a toxic and inflammable refrigerant. It has very good thermo-physical and transport properties. CO₂ is being used in the heat pumps, display cabinets, and mobile air conditioners in the low ambient European countries. This paper discusses about the use of CO₂ in the air conditioning system working at high ambient conditions witnessed in the subtropical and tropical countries like India.

Few researchers have studied the effect of suction line heat exchanger (SLHX) on the energy performance of transcritical CO₂ cycle for low ambient temperatures and mobile air conditioning systems. Torrella et al. have evaluated the performance of transcritical CO₂ refrigeration system with internal heat exchanger for the evaporator saturation temperatures -5°C, -10°C, -15°C and gascooler outlet temperature 31°C and 34°C. They have concluded that use of internal heat exchanger increases the cooling capacity and COP by 12% [3]. The authors have not covered higher evaporator temperature range 0 to 5°C and ambient temperatures above 35°C. Aprea et al. have studied the transcritical CO₂ refrigeration system with internal heat exchanger for ambient temperature range 25 to 40°C and concluded 10% rise in the COP of the system at higher ambient temperatures [2]. Kim et al have studied the use of internal heat exchanger in transcritical CO₂ water heating system and concluded that optimum discharge pressure, which gives maximum capacity and COP decreases with increase of length of heat exchanger and noticed slight increase in the COP of the system with internal heat exchanger [8]. The Klein et al. have reported the influence of SLHX on the cycle performance for chemical refrigerants like R410a, R22, R134a, etc. excluding CO₂. and concluded there is 13% to 53% gain in the cooling capacity the subcritical refrigeration cycle [5]. Boewe et al. have found the gain in the capacity for the mobile CO₂ air conditioning system at higher ambient conditions [1].

2. Simulation Parameters

The cycle simulation for transcritical CO₂ system has carried out using numerical program Engineering Equation Solver (EES) [6]. Table 1 presents the input operating parameters considered for the cycle simulation.

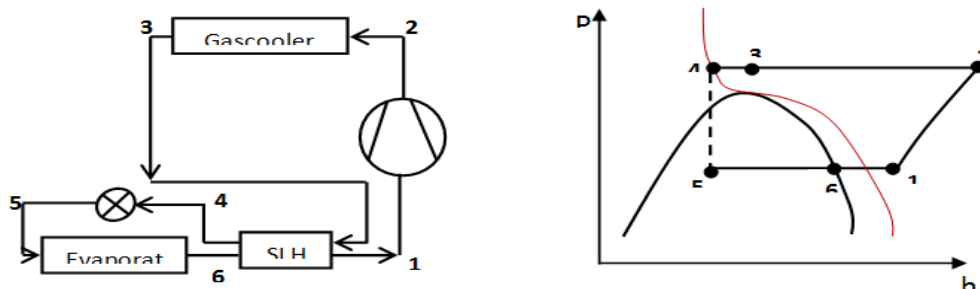


Figure 1. Schematic layout and P-h chart of transcritical CO₂ air conditioning system

The heat balance equations used in simulation are given in the Table 2. These are presented with their corresponding input and output parameters. The assumptions considered in the analysis are;

- steady state condition
- pressure drop losses in the heat exchangers and the connecting hoses lines are neglected
- convective and radiation heat losses from the components are neglected

Table 1. Input parameters for cycle simulation

Evaporator cooling load, kW	5.2
Compressor speed, rps	20
Isentropic efficiency of the compressor, [%]	70
Volumetric efficiency of the compressor, [%]	70
Evaporator saturation temperature, [°C]	5
Evaporator useful superheat, °C	5
Suction line heat ingress, %	10
Overall heat transfer coefficient for evaporator, U _o A _o , [W/k]	120
Overall heat transfer coefficient for gascooler, U _o A _o , [W/k]	310
Ambient temperature range, [°C]	30 - 45

As shown in Figure 1, due to ‘S’ shaped isothermal lines in the case of CO₂, the performance of transcritical cycle depends on optimization of gascooler pressure and temperature.

Table 2: Mathematical heat balance models for the components

Component	Equations	Input	Output
Compressor	$\dot{m}'_1(r) = V \rho_1 r N (\lambda v)$ $W_{1actual} = \dot{m}'_1(r) (h_1(2, is\epsilon) - h_2)$ $h_{2,act} = h_{2,sat} + C_{p,r} (T_{r,2} - T_{2,sat})$ $S_{1,is\epsilon} = S_{2,is\epsilon}$	V N ρ_r λv $(\lambda is\epsilon)$ h_2 N ρ_r	\dot{m}'_r W_{actual} $T_{r,2}$
Evaporator	$Q_a = \dot{m}_a \cdot C_{p,a} (T_{a_o} - T_{a_i})$ $Q_a = \dot{m}_r (h_6 - h_5)$ $Q_{max} = \dot{m}_r C_{p,r} (T_{r_i} - T_{a_i})$ $Q_{max} = \frac{Q_a}{\epsilon}$ $\epsilon \epsilon = 1 - \exp(-NTU)$ $U_o A_o = \left(\dot{m} C_p \right)_{min} NTU$	$U_o A_o$ \dot{m}_r T_{r_i} \dot{m}_a	Q_a Q_a h_6 T_6
Suction Line Heat exchanger	$\epsilon_{SX} (h_3 h_6) = (h_1 - h_6) = (h_3 - h_4)$	ϵ_{SX} h_3 h_6	h_1 h_4
Gascooler	$Q_a = \dot{m}_a \cdot C_{p,a} (T_{a_o} - T_{a_i})$ $Q_a Q_{max} = \frac{Q_a}{\epsilon}$ $\epsilon = 1 - \exp \left[\frac{NTU^{0.22}}{C_r} \{ \exp(-C_r \cdot NTU^{0.78}) - 1 \} \right]$	$U_o A_o$ $U_o A_o$ \dot{m}_r T_{r_i} \dot{m}_a T_{r_i} \dot{m}_a	Q_a Q_a h_3 T_3

	$C_r = \frac{\left(\dot{m} C_p \right)_{min}}{\left(\dot{m} C_p \right)_{max}}$ $U_o A_o = \left(\dot{m} C_p \right)_{min} NTU$		
Expansion valve	$h_4 = h_5$	h_4	h_5
Cycle	$COP = \frac{Q_a}{W_{actual}}$ $COP_{carnot} = \frac{T_{r, evap, sat}}{T_{r, gc, sat} - T_{r, eva, sat}}$	Q_a W_{actual}	COP COP_{carnot}

3. Results and Discussion

The results of the cycle simulation with and without suction line heat exchanger are presented in the form of figures.

3.1 Coefficient of Performance (COP)

Figure 3 shows variation of COP with gascooler exit pressure at various ambient temperatures. For ambient temperature more than 35°C, the use of SLHX improves the COP of the cycle by 2 to 4% as compared to cycle without SLHX. The improvement in COP is because of more specific heat rejection in the SLHX hence more refrigeration capacity. The use of SLHX effects in higher specific power consumption. However, the specific power consumption is less than specific heat rejection in the cycle using SLHX.

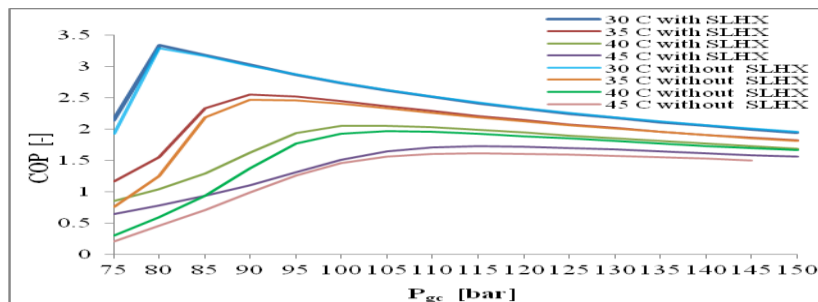


Fig. 3 Effect of gascooler pressure on the COP for different ambient conditions

Figure 4 depicts that use of SLHX improves the COP in the range 53.6% to 55.2% for rise in evaporator saturation temperature from -10°C to 5°C at ambient temperature 35°C. For ambient temperature 45°C, this change is from 40.40% to 41.38%. At 35°C ambient and 5°C evaporation temperature, COP with SLHX increases by 3.24% than that of without SLHX. For ambient 45°C, it increases by 56.30%.

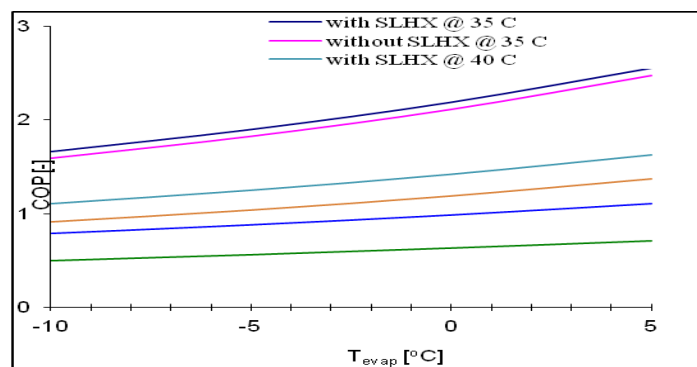


Fig. 4: Effect of evaporator temperature on COP for different ambient conditions

3.2 Gascooler Capacity

Figure 5 shows the variation of gascooler capacity for a range of evaporating temperatures. In case of CO₂transcritical system, the heat rejection capacity of the gascooler is very much sensitive to evaporation temperature and ambient temperature. For ambient temperatures 45°C and 35°C, the heat rejection capacity in the gascooler with SLHX is 29.28% and 1.56% lower than that of without SLHX respectively.

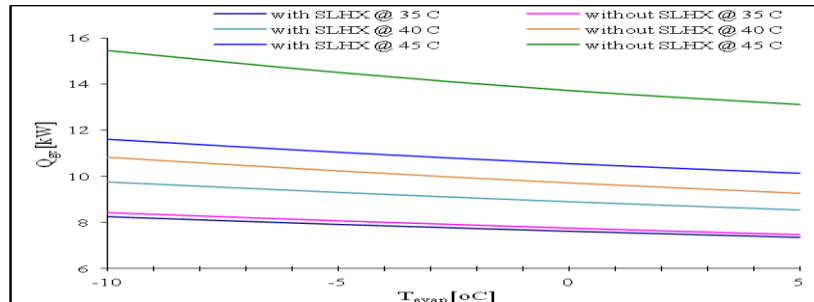


Fig. 5: Evaporator temperature versus actual heat rejection in the gascooler

3.3 Power Consumption

Figure 6 shows the power consumption for a range of evaporating temperature. The power consumption decreases with rise in evaporation temperature at all cases. For ambient 45°C, the power consumption decreases in the range 63.5% to 93% with SLHX than that of without SLHX for -10°C to 5°C change in evaporator saturation temperature. In the case of ambient 35°C, this change is in the range 11% to 22.7%. This indicates that use of SLHX has more advantage at higher ambient as compared to lower ambient.

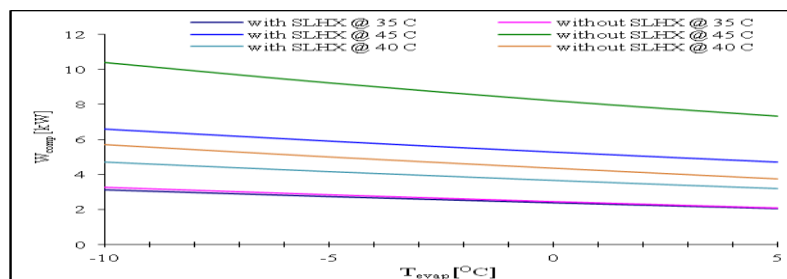


Fig. 6: Effect of evaporator temperature on actual compressor power consumption

3.4 Dryness fraction

Figure 7 shows the effect of SLHX on the inlet quality of refrigerant at evaporator. The dryness fraction of refrigerant decreases in the range of 30% to 27% with SLHX than that of without SLHX for -10°C to 5°C change in evaporator saturation temperature for ambient temperature 35°C.

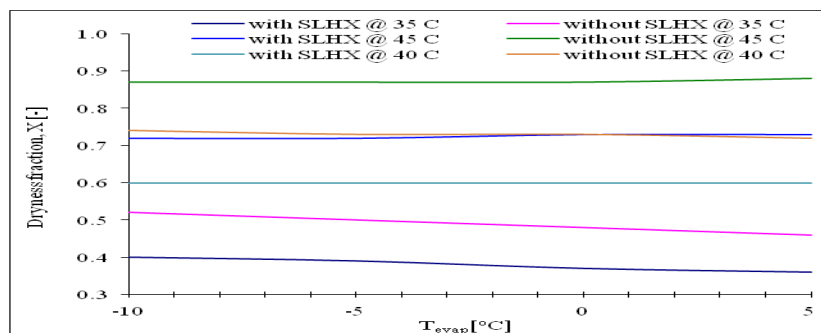


Fig. 7: Evaporator temperature versus dryness fraction for different ambient conditions

4. Conclusions

The performance of transcritical CO₂ refrigeration cycle depends on the ambient temperature and its corresponding optimized gascooler pressure. The use of suction line heat exchanger improves the COP in the range 2 to 4% for ambient temperature more than 35°C. For the evaporator temperature range -10°C to 5°C, the use of SLHX improves the COP in the range 50 to 55% for ambient temperature range 35°C to 45°C. The compressor power consumption decreases in the range of 60 to 95% at ambient temperature 45°C and 11 to 22%

at ambient temperature 35°C with SLHX. The share of liquid at evaporator inlet improves by 27 to 30% due to extra cooling of the gas at the gascooler outlet. The use of SLHX in the transcritical CO₂ system operating at high ambient conditions has major benefits in terms of the performance parameters of the system.

5. Nomenclature

Q	Actual heat flow [kW]	<i>Greek letter</i>	
A	Area [m ²]	å	Heat exchanger effectiveness [-]
COP	Coefficient of Performance [-]	<i>Subscripts</i>	
W	Compressor power [kW]	r	refrigerant
Cr	Heat capacity ratio [-]	v	volumetric
m	Mass flow of refrigerant [kg/s]	ise	Isentropic process
NTU	Number of transfer units	a	air
U _o	Overall heat transfer coefficient [W/m ² K]	max	maximum
h	Specific enthalpy [kJ/kg]	SX	Suction line heat exchanger
S	Specific entropy [kJ/kg]	sat	Saturation condition
C _p	Specific heat of refrigerant [kJ/kg K]	gc	gascooler
N	Speed of compressor [rps]	evap	evaporator
T	Temperature of refrigerant [°C]	i	Inlet
V	Volume flow capacity of compressor [m ³]	o	Outlet

References

- [1] Boewe, D., Yin J. M., Park Y. C., C. Bullard W., Hrnjak P. S. The role of the suction line heat exchanger in transcritical R744 mobile a/c systems, SAE paper 1999-01-0583, 1999
- [2] Ciro Aprea, Angelo Maiorino An experimental evaluation of the transcritical CO₂ refrigerator performances using an internal heat exchanger, *Int. Jr. of Refrigeration*, 31, 2008, 1006–1011
- [3] E. Torrella, D. Sa´nchez, R. Llopis, R. Cabello Energetic evaluation of an internal heat exchanger in a CO₂ transcritical refrigeration plant using experimental data, *Int. Jr. of Refrigeration*, 2010, Article in press
- [5] Klein S. A., Reindl D. T., Brownell K. Refrigeration system performance using liquid-suction heat exchangers, *International Jr. of Refrigeration*, 23 (98) 8, 2000, 588-596
- [6] Klein S. A. Engineering Equation Solver(EES), FChart Software, Inc., 2010
- [7] Lorentzen G. The use of natural refrigerants: a complete solution to CFCto CFC/HCFC predicament, *Int. Jr. of Refrigeration*, 18 (3), 1995, 190-197.
- [8] Sung Goo Kima, Yoon Jo Kimb, Gilbong Leeb, Min Soo Kimb The performance of a transcritical CO₂ cycle with an internal heat exchanger for hot water heating, *Int. Jr. of Refrigeration*, 28, and 2005, 1064–1072.

Novel Encoding and Decoding Algorithm for Block Turbo Codes over Rayleigh Fading Channel

¹M.Christhu Raju, ² Dr. Ch. D.V. Paradesi Rao

¹ECE DEPARTMENT, CVR COLLEGE OF ENGINEERING, AUTONOMOUS, Hyderabad

²ECE DEPARTMENT, AURORA ENGINEERING COLLEGE, Bhongir, Nalgonda dist.

Abstract

Proposed Error Correcting codes are widely used for error detecting and correcting which are present in during reception and they are also widely used in compact disc and wireless and digital communications. Proposed paper mainly discuss about the Block Encode and Decoder architectures with less complexity in terms of encoding and decoding. There are Six types of block codes are mainly discussed i.e Block (7, 3), Block (15,11), Block (31,15), Block (31,27), Block (255, 165) and Block(255,205). Simulation results over a AWGN and Rayleigh fading Chananel shows that Block Codes with higher block lengths are giving more gain compared to the lower block length and also error correcting capacity also higher for higher block lengths but complexity of encoding and decoding algorithms will increase and simulation results are shown for both voice and image and compared with existing algorithm. When I have used the single Block codes, error correction capacity is lower but it is doubled in case of block turbo codes and also performance is compared.

Keywords: Block codes, convolutional codes, forward error correctiong codes and decoding algorithms.

1. Review Of Work:

Block Codes(S,v) are mainly used in campact disks and mobile communications [1][2] and they are able to correct

$\frac{S-v}{2}$ of sequence of errors present in the received data. For example, if Block(31,15) is used then S =31 and

v=15 then this code can correct errors upto 4 symbols. And its correction capacity $Q_c = \frac{31-15}{2} = 4$ symbols.

This code able to correct upto 16 bits in sequence if at all 16 bits are corrupted. These block codes are mainly concentrated on symbols but not on bits. The Block codes are represented by the following characteristics.

Number of bits to represent one symbol	: λ
Code Length in symbols S	: $2^{\lambda} - 1$
Number of Information symbols v	: $2^{\lambda} - 1 - 2 Q_c$
Error correcting capability	: Q_c
Number of Check symbols	: $2 Q_c$
Minimum distance	: $d = 2 Q_c + 1$

1.1 Previous Work:

Proposed Encoder and decoder of block codes are used in any communication system and these block codes are classified as a forward error correcting codes in all aspects. Block codes (S, v) encoder architecture has been designed to produce the code word in terms of symbols rather than bits. One more type of error correcting code is called convolutional coding and which will produce the code word in terms of bits[3]. In order to transmit the data from source to the destinaiton, every communication system has to satisfy the condition of Shannon Capacity theorem[4][5].A lot of research is going on error correcting codes, which are linear Block codes, BCH codes, cyclic codes and convolutional codes. But each code having its own limitations. Out of all these codes, convolutional codes are very flexible in design and they will give better performance in terms of BER and SNR through the channel of AWGN compared to all other codes. But convolutional codes can not be used alone to correct sequence of errors are present in the received data. In order to avoid this problem, convolutional codes are connected in series[7] and parallel through interleaver is called product turbo codes[6]. Recently research is going on turbo codes, Soft out Veterbi Algorithm (SOVA) and which are very powerful error correcting codes because it has a iterative decoding algorithm. They have excellent Bit Error Rate performance against the Signal to Noise Ratio but still have some problems. First of all, their error

performance tails off, or exhibits an error “floor” at high signal-to-noise ratio (SNR)[8]. The complexity of the required soft-input, soft-output (SISO) decoder is such that a cost-efficient decoder was unavailable for most commercial applications. Block Codes are give better performance in terms of Bit Error Rate and in terms of sequence of Error Correction capability that’s why they are still used in Voice and Video applications This paper is organized as follows. In Section I, explained about *Block Encoder Descriptive Example*, while Section II summarizes with Block Decoder Descriptive example. Section III summarizes the simulation result of Block Codes for a random generated data with different modulation techniques over an AWGN Channel. Section IV briefly discuss about voice signal encoding and decoding using modulation techniques and section V gives a simulation result for image transmission through a AWGN channel. Section VI concludes my research work.

1.2 Proposed Work:

I have designed a new class of error correcting code called block code and denoted by Block (S,v). This Block code is tested for random generated data, voice signal and for image transmission. There are different types of Block codes are designed in my proposed work which are Block(7,3), Block(31,15), Block (255,205) and Block(255,225). All Block codes are simulated with different lengths of S and with different modulation techniques such as BPSK, QPSK AND QAM and transmitted from source to destination through the AWGN channel. From fig1. For proposed Block codes architecture, how the error rate has calculated as shown. I extended this work for block turbo codes. When i use the single Block codes, error correction capacity is lower but for error correction capacity becomes doubled in case of block turbo codes. For example (7,3) block code, error correction capacity is 2 while in case of block turbo codes it becomes 4.

2. Block Encoder Descriptive Example

Let $S = 2^\lambda - 1$ be the block length of a Block code of designed distance d in $GF(2^{m^\lambda})$. The number of λ -bit message symbols is $v = S - d + 1$.

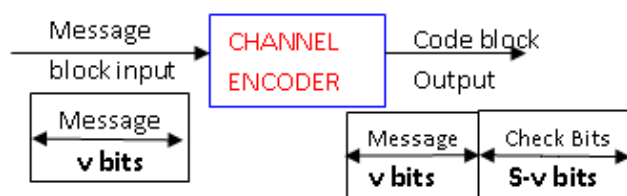


Fig:1 Block Encoder

First we define the generator polynomial to encode the v information symbols into length of $S = 2^\lambda - 1$ symbol Block code word is

$$\pi(y) = \prod_{i=1}^{2Q_c} (y - \beta^i) \text{ where } \pi(y) \text{ is the generator polynomial. Example Generator polynomial for Block (255,249) is } \pi(y) = (y - \beta^1)(y - \beta^2)(y - \beta^3)(y - \beta^4)(y - \beta^5)(y - \beta^6) \text{ or } \pi(y) = y^6 + \pi_5 y^5 + \pi_4 y^4 + \pi_3 y^3 + \pi_2 y^2 + \pi_1 y + \pi_0$$

Let $S = 15$ and consider a primitive, narrow sense, three-error correcting code over $GF(2^4)$, where the field is constructed modulo the primitive polynomial $y^4 + y + 1$. let β be a primitive element in the field and this generator has six roots of $\beta, \beta^1, \dots, \beta^{2Q_c}$. i. e $2Q_c = S - v$. roots are $\beta^1, \beta^2, \beta^3, \beta^4, \beta^5, \beta^6$

The generator of the (15, 9) code is

$$\Pi(y) = (y - \beta^1)(y - \beta^2)(y - \beta^3)(y - \beta^4)(y - \beta^5)(y - \beta^6) \text{ or } \Pi(y) = \beta^6 + \beta^9 y + \beta^6 y^2 + \beta^4 y^3 + \beta^{14} y^4 + \beta^{10} y^5 + \beta^6$$

Block codes may be encoded just as any other cyclic code. Given a input message vector polynomial $a(y) = a_0 + a_1 y + a_2 y^2 + \dots + a_{v-1} y^{v-1}$ where each $a_i \in GF(2^\lambda)$. And systematic encoding process is

$$H(y) = m(y) y^{S-v} + \text{rem}(y) = q(y) \cdot \Pi(y)$$

Let us assume that input message as 010 110 111 convert this into 3 bit data in decimal as $A = [2,6,7]$ for a Block code of [7,3] and corresponding message polynomial is written as $A(y) = \beta^1 + \beta^3 y + \beta^5 y^2$ and $y^4 (\beta^1 + \beta^3 y + \beta^5 y^2)$

is $A(y) = \beta^1 y^4 + \beta^3 y^5 + \beta^5 y^6$ Using vector to power conversion, we will divide the message polynomial by the generator polynomial as $\beta^3 + \beta^1 y + \beta^0 y^2 + \beta^3 y^3 + y^4$ And reminder the above division is gives by $p(y) = \beta^0 + \beta^2 y + \beta^4 y^2 + \beta^6 y^3$ and resulting codeword polynomial is written as $H(y) = p(y) + y^{S-v} m(y)$ is $\beta^0 + \beta^2 y + \beta^4 y^2 + \beta^6 y^3 + \beta^1 y^4 + \beta^3 y^5 + \beta^5 y^6$ In Encoder each symbol (β) is made with 3 bits of input data and which

is convenient for modems for processing. The input to the encoder is 7 symbol of information word. The conventional method to achieving this uses an arrangement containing multipliers and is expensive to implement in hardware. The implementation of block encoders based on an Linear shift register, which implements the polynomials division over the finite field [8]. The Block encoder architecture had slice blocks containing a constant multiplier, an adder, and a register . The number of slices to implement for an Block (S, v) code is s-v.. The additions and multiplications are performed on GF(2^k) and g_i are the coefficients of the generator polynomial π(y). Finally output codeword polynomial is written as

$$H(y) = \beta^0 + \beta^2 y + \beta^4 y^2 + \beta^6 y^3 + \beta^1 y^4 + \beta^3 y^5 + \beta^5 y^6$$

$$\text{Or } H(y) = (100) + (001)Y + (011) Y^2 + (101) Y^3 + (010) Y^4 + (110) Y^5 + (111) Y^6$$

3. Block Decoder

The algebraic decoding of block codes has the following general steps:

1. Computation of the syndrome
2. Determination of an error locator polynomial, whose roots provide an indication of where the errors are.
3. Finding the roots of the error locator polynomial. This is usually done using the novel search, which is an exhaustive search over all the elements in the field.
4. For block codes, the error values must also be determined. This is typically accomplished using proposed method search.

Suppose that received vector has v errors at locations of **i**₁, **i**₂, **i**₃,.....**i**_v with corresponding error values in these locations e_{ij} ≠ 0.

Error Locator polynomial is written as $W(Y) = \sum_{n=0}^6 W_n Y^n$

$W(Y) = (000) + (000)Y + (000) Y^2 + (001) Y^3 + (111) Y^4 + (000) Y^5 + (000) Y^6$. This Error polynomial is considered as one error at data location and other error is at parity symbol location.

Now received polynomial is written as $D(Y) = H(Y) + W(Y)$

$$D(Y) = (100) + (001)Y + (011) Y^2 + (101) Y^3 + (010) Y^4 + (110) Y^5 + (111) Y^6 + (000) + (000) Y + (000) Y^2 + (001) Y^3 + (111) Y^4 + (000) Y^5 + (000) Y^6$$

$D(Y) = (100) + (001)Y + (011) Y^2 + (100) Y^3 + (101) Y^4 + (110) Y^5 + (111) Y^6$ and above expression in polynomial form as

$D(Y) = \alpha^0 + \alpha^2 x + \alpha^4 x^2 + \alpha^0 x^3 + \alpha^6 x^4 + \alpha^3 x^5 + \alpha^5 x^6$ in order to detect the errors and correct the errors at the decoder, we need to calculate the syndrome and which is given by

$$O_i = D(Y) /_{Y=\beta^i} = D(\beta^i) \quad i = 1, \dots, S - v$$

Then we can find the syndromes in the following way.

O₁ = β³, **O**₂ = β⁵, **O**₃ = β⁶, **O**₄ = 0 Suppose in the received codeword, there are n number of errors are received then we have to find the Error locator polynomial in the form of Matrix as. Above Syndrome equations are written in the form Matrix form as

$$\begin{bmatrix} s_1 & s_2 \\ s_2 & s_3 \end{bmatrix} \begin{bmatrix} \sigma_2 \\ \sigma_1 \end{bmatrix} = \begin{bmatrix} s_3 \\ s_4 \end{bmatrix}$$

Substituting the syndrome values in matrix form as $\sigma_2 = \alpha^0$ and $\sigma_1 = \alpha^6$ Above

equation are used to find the locations of errors in the received polynomial is given by

$$\sigma(x) = \alpha^0 + \sigma_1 x + \sigma_2 x^2$$

$$\sigma(x) = \alpha^0 + \alpha^6 x + \alpha^0 x^2$$

$$\sigma(\alpha^0) = \alpha^6, \sigma(\alpha^1) = \alpha^2, \sigma(\alpha^2) = \alpha^6, \sigma(\alpha^3) = 0 \text{ (Error)},$$

$$\sigma(\alpha^4) = 0 \text{ (Error)}, \sigma(\alpha^5) = \alpha^2, \sigma(\alpha^6) = \alpha^0$$

$$S_1 = r(\alpha) = e_1 \beta_1 + e_2 \beta_2$$

$$S_2 = r(\alpha^2) = e_1 \beta_1^2 + e_2 \beta_2^2$$

$$\sigma(\alpha^3) = 0 \leftrightarrow 1/\beta_1 = \alpha^3 \leftrightarrow \beta_1 = \alpha^{-3} = \alpha^4 = \beta_1$$

$$\sigma(\alpha^4) = 0 \leftrightarrow 1/\beta_1 = \alpha^4 \leftrightarrow \beta_1 = \alpha^{-4} = \alpha^3 = \beta_1$$

In order to calculate the Errors present in the location are given by following matrix form as.

$$\begin{bmatrix} \alpha^3 & \alpha^4 \\ \alpha^6 & \alpha^8 \end{bmatrix} \begin{bmatrix} e_1 \\ e_2 \end{bmatrix} = \begin{bmatrix} \alpha^3 \\ \alpha^5 \end{bmatrix}$$

And two errors are given by e₁ = α², e₂ = α⁵. And Error Polynomial is given by.,

$$e(x) = e_1 x^{i1} + e_2 x^{i2} = \alpha^2 x^3 + \alpha^5 x^4$$

$$u(x) = r(x) + e(x)$$

$$u(x) = 4 + x + 3x^2 + 4x^3 + 5x^4 + 6x^5 + 7x^6 + 1x^3 + 7x^4$$

$$u(x) = 4 + x + 3x^2 + 5x^3 + 2x^4 + 6x^5 + 7x^6$$

From the above equation of U(x) has parity symbols and message symbols. Message polynomial is $2x^4 + 6x^5 + 7x^6$ and in binary form as 010 110 111 which is same as given input message.

4 .Rayleigh Slow Fading Channels:

The Rayleigh fading model is one of the most widely used fading channel model which assumes that there exist no direct line of sight path between the transmitter and the receiver and all the arriving signals at the receiver are due to reflected waves. This assumption is a typical characteristic of mobile communication scenario in urban areas. The normalized Rayleigh distribution, its mean and variance are as given below

$$p(r) = \begin{cases} \frac{r}{\sigma^2} e^{-\frac{r^2}{2\sigma^2}} & r \geq 0 \\ 0 & \text{otherwise} \end{cases}$$

With mean $m_r = 0.8862$ and variance is $\sigma^2 = 0.2146$

Channels dispersive in frequency are often referred to as time selective. More common term is frequency flat or simply flat fading channels. The term flat fading comes from the fact that ALL frequencies of transmitted signal are modulated by the same function. Frequency dispersion B often referred to as the Doppler spread or bandwidth. If the doppler spread is small compared to the reciprocal of the symbol rate T_s , the fading process is considered slow. For slow fading processes, the channel gain can be assumed constant over the symbol duration.

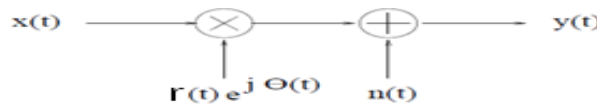


Fig2. Figure represents the Fading channel.

A sufficient and acceptable model is to consider the input-output relation of the digital channel of the form:

$$y_k = r_k \cdot x_k + n_k$$

where x_k and y_k are the transmitted and received data for the time slot k , respectively; the parameter r_k is a random value, fluctuations from symbol to symbol (fast fading) or from block to block (block fading). Its distribution determines the channel type: Rayleigh, Rice or Nakagami. The input sequence $\{x_k\}$ is binary, random, in NRZ bipolarformat,

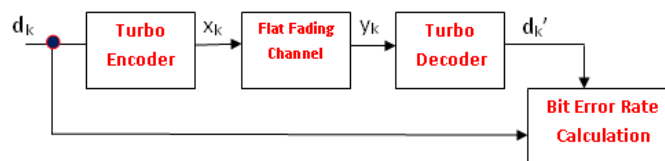


Fig 3. Turbo coded data transmission through different fading channels.

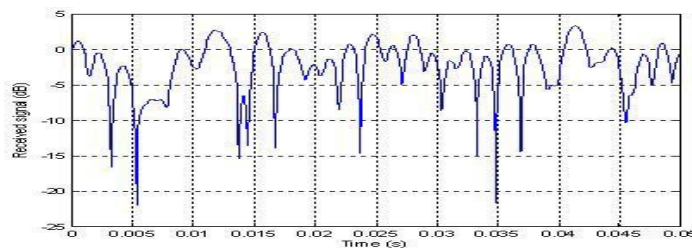


Fig4. Fading channel received signal amplitude characteristics.

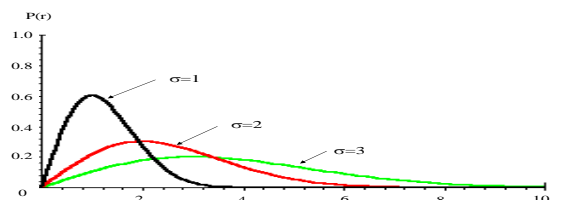


Fig.5 The pdf of the envelope variation

In order to generate the transmitted sequence $\{x_k\}$ another sequence denoted $\{u_k\}$ is generated by random numbers with uniform distribution in the interval $[0,1)$. The targeted required output is obtained after the following transformation:

$$\mathbf{X}_k = 2 \cdot [\mathbf{2} \mathbf{U}_k] - 1$$

In above equation, $[\]$ represents the truncated information of integer part, and $X_k^2 = 1$.

r_k represents rice distribution and $rk2 = 1$ and effective signal to noise ratio for transmission is defined as

$$\frac{E_b}{N_o} = \frac{1}{2} \cdot \frac{2E_b}{N_o} = \frac{1}{2} \frac{r_k^2 \cdot x_k^2}{w_k^2} = \frac{1}{2} \frac{1}{w_k^2}$$

Where E_b/n_o is SNR in dB and variance of additive noise can be expressed as

$$w_k^2 = \frac{1}{2.10^{10} \cdot SNR}$$

5. Block Turbo Codes:

Let us consider the two linear block codes B_1 and B_2 having parameters B_1 of (n_1, k_1, δ_1) and B_2 having parameters (n_2, k_2, δ_2) . The product code $P = B_1 \otimes B_2$

Block Turbo Code obtained by

1. Placing $(k_1 \times k_2)$ information symbols in an array of k_1 rows and k_2 columns.
2. Coding the k_1 rows using code B_2
3. Coding the n_2 columns using Code B_2 as shown in fig 1

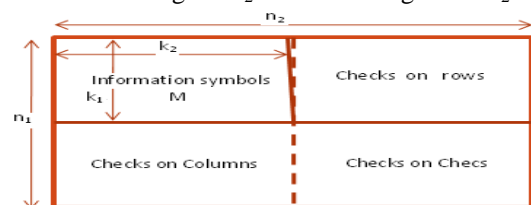


Fig6. Formation of data and check bits

$(n_1 - k_1)$ last rows of the matrix are code words of B_2 and $(n_2 - k_2)$ last columns of matrix are code words of B_1 by construction. Resulting Product Code P is

$$n = n_1 \times n_2 \quad k = k_1 \times k_2 \quad \delta = \delta_1 \times \delta_2$$

5.1 Decoding Algorithm for Block Turbo Codes

Scaling factors:

$$\alpha(k) = \{ 0, 0.2, 0.4, 0.43, 0.5, 0.56, 0.6, 0.7 \}$$

$$\beta(k) = \{ 0.64, 0.64, 0.64, 0.64, 0.7, 0.74, 0.8, 0.8 \}$$

R = received data matrix

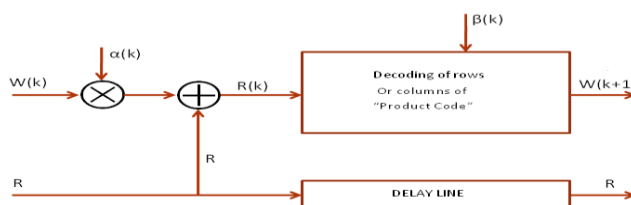


Fig7. Decoding of block Turbo codes block diagram

6. Simulation Results:

Observation#1. MATLAB is one of the high performance programming language in easy to use environment where problems and solutions are expressed in a frequent mathematical notation. A complete block diagram with Encoder and decoder and encoded data was modulated with Frequency shift keying as shown in fig1. Results with block codes with equal code rate of 0.7 approximately as shown in fig 4. The following Block codes with Block(15,11), Block(31,23), Block(63,47) and Block(127,95) for simulation in AWGN Channel. It is observed that Block codes are more efficient in large code size and it gives less noise effect compared to the lower codeword size of block codes and at the same time increases the complexity in the implementation of the transmission. For a Block Code (127,95) simulation, it is observed that for a BER of 10^{-2} respected SNR is 3dB and which is lowest noise effect compared to other block codes.

Block (S,v)	Code Rate CR = (v/S)
Block(15,11)	0.738
Block(31,23)	0.742
Block(63,47)	0.746
Block(127,95)	0.748

Table1. code rate for different Block lengths.

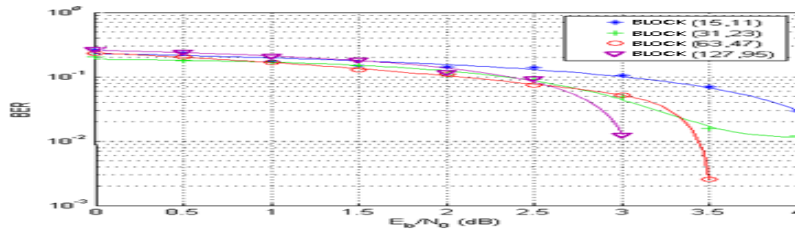


Fig 8. Block code performance in terms of Codeword Size at constant code rate

6.1 Observation. Now for next observation, I have performed the simulations for Block codes for different code rates as well as higher block lengths as shown in fig6. For a Block(255,245), Block(255,225), Block(255,205), Block(255,165) corresponding code rates are 0.96, 0.88, 0.80 and 0.647. As code rate decreasing from 0.96 to 0.647, noise effect also decreasing for a particular BER 10^{-2} . We can see that the absolute BER performance is approx. 2dB better for 0.647 code rate than 0.96. Another point i need to emphasize here that, for constant Block length with same error correcting capability, BER performance improved as shown in fig 6.

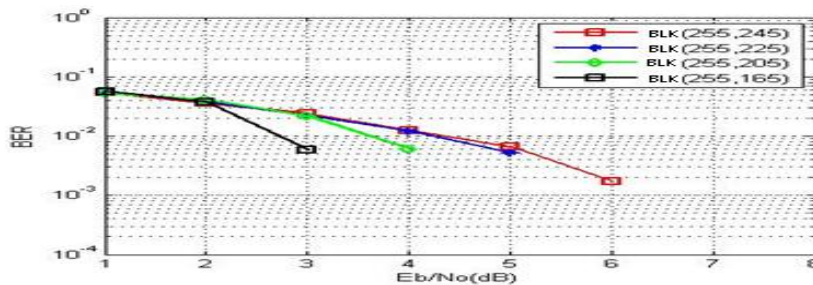


Fig 9. The BER performance comparison of Block codes for different code rates and fixed block length of 255

6.2 Observation. Previous simulation results are observed for Only FSK and now block codes are simulated with different lengths and different code rates are modulated with different modulation schemes. BPSK and QPSK with CR =0.5 has very less noise effect on signal compared to all other modulation schemes as shown in fig 8.

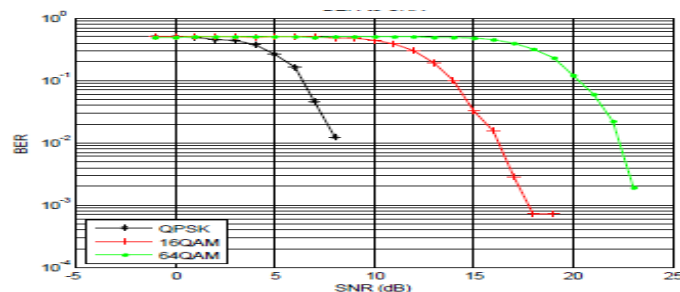


Fig 10. Performance of Block codes for code rate of 1/2(CR=0.5)

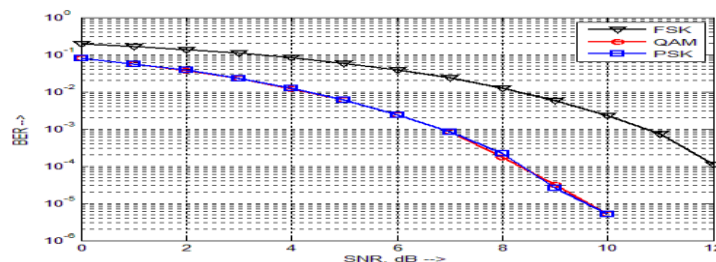


Fig 11. Performance of Block codes for code rate of 3/4(CR=0.7)

Block Codes Rate	QPSK at 10^{-2}	16QAM at 10^{-2}	64QAM at 10^{-2}
$1/2$	~ 8dB	~ 16.7dB	~ 23 dB
$3/4$	~ 13.5 dB	~ 18.7 dB	27.2 dB

Table 2. Block Codes with different code rates with QAM.

7. Result For Voice Signal.

Fig 9 is a original voice signal and which has recorded. This original voice signal is encoded and modulated with FSK, PSK and QAM and plotted its bit error rate with respect to signal to noise ratio. Block codes (127,123) has simulated with PSK and QAM has given lesser noise effect on signal compared to the FSK. Also observed that BER performance on signal is directly proportional to the Modulation order of M if it is modulated with M-ary Modulation schemes.

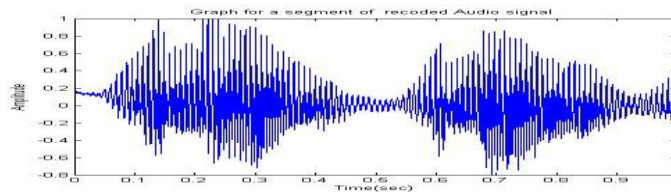


Fig 12. Original recorded audio signal

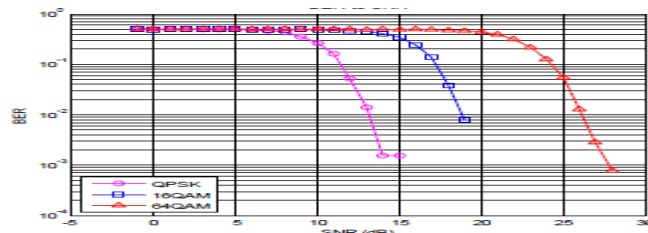


Fig 13. Block codes(127,123) for FSK,PSK and QAM

7.1 Result for Image Signal.

In order to use any forward error correcting code in digital communication it is required to transmit images through that FEC codes[7]. Simulation results shows the image quality degrades as the code rate increasing from lower to higher as shown in table 5. In order to transmit the image transmission using block codes, i suggest to use lower code rate compared to the higher order code rates where low Signal to Noise ratio is important.

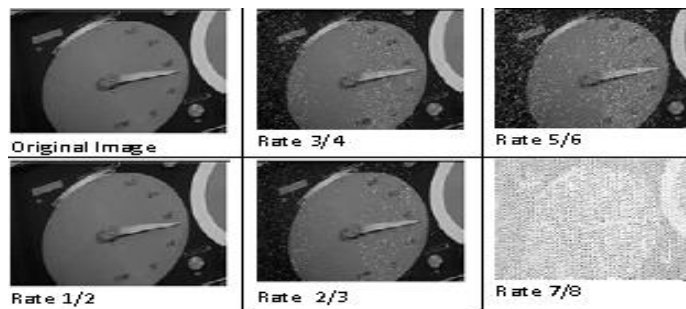


Fig 14. Recovered images with different rates with SNR=6dB

Modulation Scheme	BER at 10^{-2}
BPSK - $1/2$	3 dB
QPSK - $1/2$	7 dB
16 QAM - $1/2$	15 dB
64 QAM - $2/3$	17 dB
QPSK - $3/4$	9 dB
16 QAM - $3/4$	15 dB
64 QAM - $3/4$	20 dB

Table.4 Illustrates the modulation schemes are observed at BER 10^{-3}

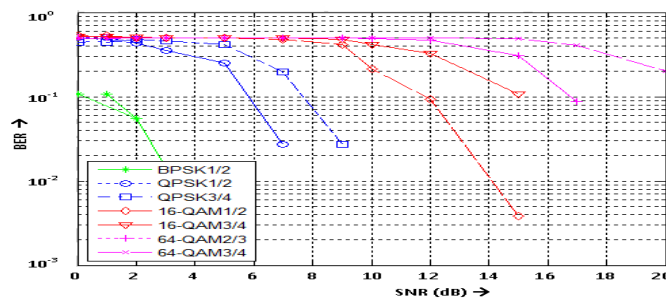


Fig 12. Image encoding for Block Codes for BPSK,QPSK AND QAM

E_b/N_0 (db)	0	9	20
16 QAM (Theoretical Symbol Error Rate)	0.9821	0.3919	0.0001721
16 QAM (Practical Symbol Error Rate)	0.7397	0.3540	0.0001652

Table.5. Block (15,11) codes are simulated over AWGN with 16 QAM Modulation.

E_b/N_0 (db)	0	9	20
16 QAM (Theoretical Symbol Error Rate)	0.9821	0.4751	0.013475
16 QAM (Practical Symbol Error Rate)	0.7428	0.4195	0.007829

Table 6. Block (15,11) codes are simulated over Rayleigh fading Channel with 16 QAM Modulation.

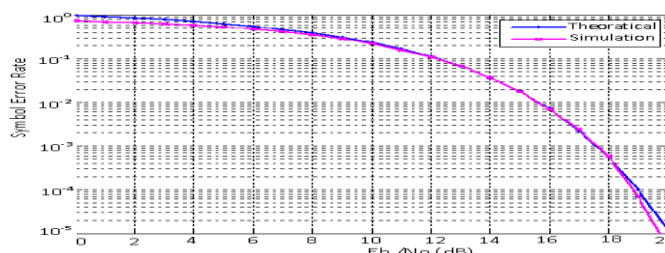


Fig. 13. Block (15,11) codes are simulated over Rayleigh Fading channel with 16 QAM Modulation.

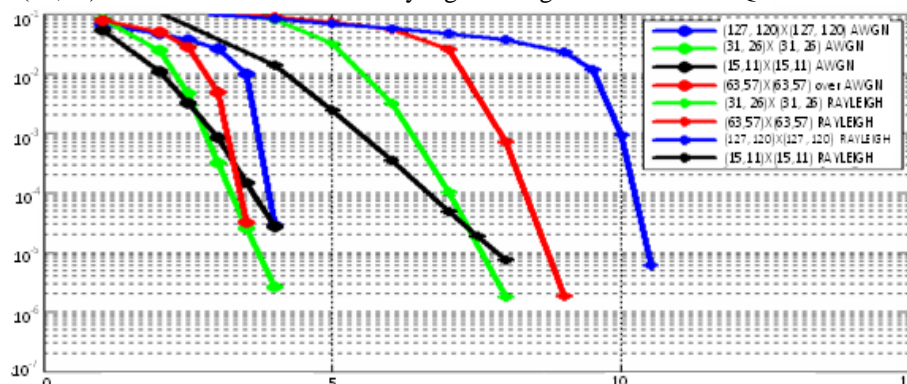


Fig. Performance of block turbo codes after 4 iterations through AWGN and Rayleigh fading channels using BPSK Modulation.

It has been shown that some of these high rate codes perform only at 1.2dB from the Shannon limit [15]. From above graph it was observed that decoding is easier with out errors over an AWGN Channel compared to rayleigh fading channel. If we compare the (31,26) and (63,57) will give the better performance compared survey of [15].

Block Turbo Code	SNR at 10^{-5} AWGN	SNR at 10^{-5} Rayleigh	Difference between channels(dB).
(15,11,4) ²	4.10	10.0	5.90
(31,26,4) ²	4.42	8.04	3.62
(63,57,6) ²	4.52	11.14	6.62
(127,120,4) ²	4.75	13.10	8.35

Table7. Performance of Block Turbo codes at fourth iteration over a Gaussian and a rayleigh Channels.

8. Conclusion:

In this paper, block codes are simulated with different lengths and different code rates for data, voice and image signals. From simulation results, it is revealed that, highest length of block codes has given the lowest noise effect than lower length of block codes, if input is a data is modulated with QPSK modulation. And if the input is voice signal then highest length of block codes has given lowest SNR for FSK and QAM. For voice signal, BPSK and QPSK has given lowest SNR for a particular BER as shown in fig 12 and proposed method had given better results compared with [5] and [6]. The block turbo codes simulations have shown very good results better than those obtained so far with other algorithms[9][10]. We have obtained BER curves for block turbo codes with identical slopes for Gaussian and Rayleigh channels. For a BER of 10^{-5} , the coding gain obtained is upto 5.5 dB and the difference with Shannon's limit is about 3.5 dB after four iteration on a Gaussian Channel. From table5 and 6 we can conclude that higher signal to noise ratio gives lower symbol Error rate.

References

- [1] C. Berrou, A. Glavieux, and P. Thitimajshima, Near Shannon Limit Error-correcting Coding and Decoding: Turbo-codes," *Proceedings of the 1993 International Conference on Communications*, pp. 1064-1069, May 1993.
- [2] Claude Berrou, Member, IEEE and Alain Glavieux, "Near Optimum Error Correcting Coding and Decoding: Turbo codes." *IEEE transactions on communications*, vol,44, No. 10, october 1996.
- [3] Nambirajan Seshadri, Carl-Erik W. Sundberg, "List Viterbi Decoding Algorithms with Applications", *IEEE transactions on communications*, vol.42, no2/3/4, February/March/April 1994.
- [4] A.J. Viterbi and J.K. Omura, principles of digital communications and coding, new york, MacGraw-hill, 1979.
- [5] Mahmut Ciftci and Douglas B.Williams, "Optimal Estimation for Chaotic sequences using the viterbi algorithm" *proceedings of IEEE*, 2001.
- [6] Vidhyacharan Bhaskar and Laurie L. Joiner, "Adaptive Rate Coding for Image Data Transmission" *proceedings of IEEE* 2002.
- [7] Shannon CE. "Communication in the presence of Noise". *Proceedings IRE*, Jan 1949, reprinted *Proceedings IEEE*, Vol 86, No 2 Feb 98.
- [8] B. Sklar, *Digital Communications Fundamentals and Applications*, 2nd Ed. Prentice Hall, New Jersey, 2001
- [9] Rong Zhou,, "Low complexity High Rate Reed solomon Block Turbo Codes, *IEEE Trans. On communications* , vol.55, no.9, september 2007.
- [10] S.M Reddy ,"On decoding iterated codes", *IEEE Trans. Inform. Theory*, vol IT-16, sept 1970, pp 624-627.
- [11] S.M Reddy and J.P. Robinson, "Random error and burst correction by iterated codes", *IEEE Trans. Inform. Theory*, vol IT-18, jan 1972, pp 182-185.
- [12] H. Schulze, and C. Luders, "Theory and Applications of OFDM and CDMA Wideband Wireless Communications", John Wiley & Sons, Ltd, 2005.
- [13] R. E. Blahut, "Theory and Practice of Error Control Codes. Reading", MA: Addison-Wesley, 1983.
- [14] S.B. Wicker, "Error Control Systems for Digital Communication and Storage". Prentice Hall, Upper Saddle River, NJ, 1995.
- [15] Hagenauer, J. Offer, E. Papke, L., Iterative decoding of binary block and convolutional codes, *Information Theory*, *IEEE Transactions on*, Volume 42, Issue 2, Mar 1996 Page(s): 429 – 445.

Secured Reversible Data Transmission by Using Gzip Deflector Algorithm for Encoded AVC Video

¹Gokiladeepa.G, ²Gayathri.S, ²Heeba.S.D, ²Pavithra.R

¹Assistant Professor, Department Of Information Technology, SNS College of Engineering, TamilNadu, India

²UG Scholar, Dept. of Information Technology, SNS College of Engineering, TamilNadu, India

Abstract

Reversible data transmission, visible watermarking and steganography schemes that can be employed along with multimedia applications. However, these methods are susceptible to quantization errors provided by standard image/video compression standards. In this work we present a secured data transmission using novel reversible visible watermarking scheme for H.264/AVC encoded video sequences. The proposed approach reversibly embeds the residual information that will then be used by the decoder to recover the original image or video frame. The residual information is losslessly compressed using the Gzip Deflector algorithm to minimize the information to be embedded and reduce the distortion provided by RCM. The compressed information is then encrypted using the 128-bit Advanced Encryption Standard (AES). Furthermore we add security in this work if the key does not match we provide irrelevant information or unwanted data's to the decoder. And finally we compared our proposed work with existing state of art.

Index Terms – Information embedding, data compression, lossless recovery, reversible watermarking scheme, DCT, AES, GZip Deflector algorithm.

1. INTRODUCTION

The recent growth of computer networks and multimedia systems has contributed to the proliferation of multimedia content. However, the availability of multimedia editing software has raised the issue of increased distortion level [1] unauthorized manipulation of proprietary material. Visible watermarking techniques have been extensively used to protect copyrighted material. However, traditional approaches, such as [2] are not able to recover the original image/video quality after watermarking extraction. The methods proposed for removable visible watermarking schemes where authenticated users are allowed to approximate the visible watermark. Nonetheless, these methods only manage to recover an approximate version of the original image after watermark extraction [12] and are therefore unsuitable for military, law and medical applications. There are several reversible visible watermarking schemes that can be employed for many applications [3]. However, these methods are susceptible to quantization errors provided by standard image/video compression standards. Therefore, these methods are not suitable for most Internet applications where multimedia content needs to be compressed prior transmission. In previous work, the same author has presented a reversible watermarking scheme for JPEG image compression. However, this method cannot be directly integrated within current video compression standards, mainly due to the spatio-temporal prediction mechanisms being employed by video standards.

This paper presents secured data transmission by an adaptation of the reversible visible watermarking scheme presented, for H.264/AVC video coding. The proposed method computes the residual error caused by the embedded watermark which is losslessly compressed using the GZip Deflector algorithm and then encrypted using the Advanced Encryption Standard (AES). The resulting information is embedded within the transform coefficients of every macroblock (MB) pair using the Reversible Contrast Mapping (RCM). The simulation results clearly show that the proposed mechanism outperforms the state of the art approach where Peak Signal-to-Noise Ratio (PSNR) gains of up to 7 dB were registered. The structure of this paper is as follows. Section II provides a detailed description of each component involved in the Reversible Visible Watermarking Embedding process while the Reversible Visible Watermark Extraction process is described in section III. Section IV presents the testing environment and presents the simulation results. The final comments and conclusion are delivered in section V.

2. Information Embedding

A High level description of the proposed Reversible Visible Watermark Embedding process for video content is illustrated in Fig.1. The original frame I is first fed to the information Embedding process which inserts a visible watermark within its Region of Interest (ROI) to generate the frame I_w . Given that the embedded watermark directly affects the image content, it makes this process irreversible. The resulting watermarked frame I_w is then compressed using the Video Encoder 1 process which employs motion estimation

and spatial prediction of the standard H.264/AVC encoder [4] to minimize the residual error E_{WC} to be entropy coded. The motion vectors and modes selected for each Macro block (MB) are registered in the Control Information module. This information is then used by the video encoder to compress the original image I which outputs the residual error E_C . This process computes neither motion estimation nor mode decision, but relies solely on the information contained within the Control Information module, thus significantly reduce the complexity of the system.

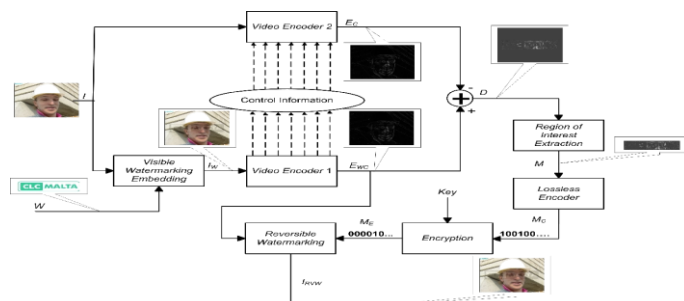


Fig.1 Schematic diagram of Information Embedding process.

The difference between the residual errors of the compressed watermarked image E_{WC} [5] and the compressed image E_C provides the discrepancy image D . This image contains 0 values outside the ROI, while having low magnitude values within the ROI. Therefore, in order to minimize the information to be embedded within the image, only the message M encompassing the Region of Interest within D is losslessly encoded and encrypted. The encrypted message M_E is then embedded within the watermarked image I_W using a re-visible watermarking approach. More information about each individual module is provided in the following sub-sections.

2.1 Data Embedding

The Visible Watermarking Embedding process is used to perceptibly insert a watermark W into a primary image I so that the watermark is visible by the human eye. The purpose of these watermarks is to be noticeable without significantly reducing the quality of the image. The method adopted in this work considers the human vision system (HVS model) and the image content to insert the watermark without significantly degrading the perceptual quality of the image/video content. This process dissects the host image I into non-overlapping 8×8 blocks. The watermark pattern W is then adaptively embedded into the host image using

$$I_n^W(i, j) = \begin{cases} [\alpha_n I_n(i, j)] & \text{if } W(i, j) = 1 \\ I_n(i, j) & \text{otherwise} \end{cases} \quad (1)$$

where $[\]$ represents the floor function, I_n^W and I_n denote the n^{th} 8×8 block of the watermarked image I_W and the host image I respectively, i and j are spatial coordinates within the block and n is the n^{th} adaptive scaling coefficient. The scaling coefficients α_n are dependent on both the human perception and image content and determine the visibility of the watermark pattern. More information about the derivation of these scaling coefficients can be found in [8] and [12].

2.2 Video Encoder and DCT

The Video Encoder process employs the standard H.264/AVC encoder [6] to compress the supplied video content. This process employs spatial prediction and motion estimation to minimize the residual error to be encoded. The encoder derives the residual information to be encoded by subtracting the predicted frame from the original frame. The resulting residual information is de-correlated using the discrete cosine transform (DCT) transformation [10][9] and quantized to keep the least amount of information while still achieving an acceptable level of image quality. The quantized transform coefficients are then inverse quantized and inverse transformed to recover the residual error E which also includes the quantization error introduced by the lossy nature of the standard video codec.

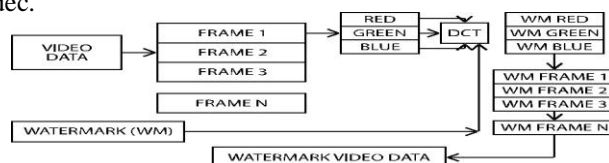


Fig. 2. DCT Based Watermark Technique.

The proposed method employs two Video Encoder processes. The Video Encoder 1 process receives the watermarked frame I_W and computes motion estimation and spatial prediction to compress the video. The resulting modes selected and motion vectors are then stored in the Control Information module while the resulting residual error E_{WC} is outputted. On the other hand, the Video Encoder 2 process receives the original video stream I and compresses it using the motion vectors and mode selected available in the Control Information module. This is done to ensure synchronization between the two processes and to minimize the computational complexity of the proposed system.

2.3 Data Compression and Encryption

The discrepancy message D is derived by subtracting the residual E_C from the residual E_{WC} . As it can be seen from Fig. 1, the non-zero coefficients reside only within the Region of Interest. Therefore, in order to minimize the data to be embedded, the Region of Interest is extracted from the discrepancy message D to generate the message M and this information is then passed through the Lossless Encoder process. The Lossless Encoder process adopts a simple encoding strategy, where each pixel in M is represented by a 10-bit codeword. The Most Significant Bit (MSB) is used to flag whether the pixel is a watermark (1) or not (0). The second MSB represents the polarity of the coefficient where negative coefficients are marked by a 1. The remaining 8-bits represent the magnitude of the coefficients of the residual error message M . Given that the decoder needs some extra information to be able to decode the encoded message (e.g. watermark dimensions and coordinates of the ROI), this information is concatenated to M prior to lossless encoding. The resulting 10-bit code words are then compressed using the public domain lossless Gzip Deflector algorithm [14].

2.4 AES (Advanced Encryption Standard)

To enhance the security, a 128-bit Advanced Encryption Standard (AES) [13] is used to encrypt the information to be embedded so that only authenticated users can recover the original image. The AES algorithm is a symmetric key algorithm which means the same key is used to both encrypt and decrypt a message. Also, the cipher text produced by the AES algorithm is the same size as the plain text message. Most of the operations in the AES algorithm take place on bytes of data or on words of data 4 bytes long, which are represented in the field $GF(2^8)$, called the Galois Field. AES is based on a design principle known as a Substitution permutation network. AES operates on a 4×4 matrix of bytes, termed the state. The AES cipher is specified as a number of repetitions of transformation rounds that convert the input plaintext into the final output of cipher text. Each round consists of several processing steps, including one that depends on the encryption key. A set of reverse rounds are applied to transform cipher text back into the original plaintext using the same encryption key. The AES algorithm loops through certain sections N_r times. It is fast in both software and hardware. AES Algorithm have following steps

- 1) Key Expansion—Round keys are derived from the cipher key using Rijndael's key schedule.
- 2) Initial Round
 - a) *Add Round Key*—each byte of the state is combined with the round key using bitwise XOR.
- 3) Rounds
 - a) *Sub Bytes*—a non-linear substitution step where each byte is replaced with another according to a lookup table.
 - b) *Shift Rows*—A transposition step where each row of the state is shifted cyclically a certain number of steps.
 - c) *Mix Columns*—a mixing operation which operates on the columns of the state, combining the four bytes in each column.
 - d) *Add Round Key*
- 4) Final Round (no Mix Columns)
 - a) Sub Bytes
 - b) Shift Rows
 - c) Add Round Key

Advantages of using AES algorithm:

- 1) Very Secure.
- 2) Reasonable Cost.
- 3) Main Characteristics
 - i) Flexibility, ii) Simplicity

2.5 Reversible Contrast Mapping (RCM)

The Reversible Watermarking process adopts the Reversible Contrast Mapping (RCM) mechanism presented in [15] to embed the encrypted information M_E within the watermarked image I_W . The RCM algorithm was used since it is reported to provide high-capacity data embedding without the requirement of the transmission of any additional side information. The RCM algorithm considers x and y to be a pair of coefficients whose values [11] reside in the range $[0; L]$. The forward RCM algorithm transforms the pixel pairs according to

$$x = 2x - y; \quad y = 2y - x \quad (2)$$

In order to prevent overflow and underflow, the transformed pixel pairs are restricted within the range

$$0 \leq x \leq L, 0 \leq y \leq L \quad (3)$$

The original coefficients can be recovered using the following inverse transformation

$$x = [(2/3)x + (1/3)y], Y = [(1/3)x + (2/3)y] \quad (4)$$

Where $[]$ is the ceil function.

The RCM method substitutes the Least Significant Bit (LSB) of x and y . The LSB of x is set to 1 to indicate a transformed pair while 0 otherwise. The information bit b is then embedded within the LSB of y . More information about this method can be found in [15]. The method proposed in [8], which is considered as the state of the art method, applies the RCM algorithm in the spatial domain. However, the RCM method cannot be applied in the spatial domain when considering compressed images since the embedded information will be distorted by the Quantization process of the image/video codec. It was further shown that the RCM method can modify the transformed coefficients prior entropy coding, thus making recovery of the original transform coefficients possible. However, the transform coefficients provide different levels of distortions, and therefore it is more desirable to embed the information within high frequency coefficients which provide the least distortion to the human vision system.

Therefore, considering a $P \times Q$ image, the Reversible Watermarking scans the blocks column-wise and grabs the first two neighbouring 4×4 transformed blocks. It embeds the first bit within the coordinate (3,3) which corresponds to the highest frequency coefficient. The remaining $\frac{P}{32} \times \frac{Q}{32} - 1$ bits are then stored within the coefficient with coordinates (3,3) of the remaining neighbour blocks. Once all the blocks have been used this process goes back to the first two neighbouring blocks and embeds the second $\frac{P}{32} \times \frac{Q}{32}$ bits within the coefficient coordinate (3,2). This process proceeds until either the whole bit stream is embedded or else when all the transform coefficients are used. It is important to notice that the RCM algorithm can be used to embed information more than once within the same coefficients. However, this will contribute to major distortions within the image. Therefore, the transform coefficients were only used once for embedding. The Reversible Watermarking process then outputs the image I_{RV_C} which is then entropy encoded and transmitted.

3. Information Extraction

The Information Extraction process inverts the computations performed by the Reversible Visible Watermark Embedding process. It receives the entropy coded information and decodes it to recover the image I_{RV_W} . The Reversible Data Extraction process then computes the inverse RCM function [13] to extract the encrypted message M_E and the visible watermarked residual E_W . The message M_E is then decrypted and decoded to derive the message M . The message M contains the residual watermark within a Region of Interest together with additional information suitable to reconstruct the discrepancy image D . The images D and E_{WC} are then summed to generate E_C . The Video Decoder then is able to recover the original compressed video sequence I_C .

4. Simulation Result

The proposed Reversible Visible Watermarking Scheme was implemented using the C++ programming language. The raw video sequences considered in these simulation results were encoded using a Common Intermediate Format (CIF) resolution at 30fps with a format IPPP using the Baseline Profile of H.264/AVC. The video was encoded using only the 4×4 transform size. The Quantization Parameter is set to a default of 20 unless otherwise specified. The logos employed in these experiments included some of the logos.

TABLE I

Performance Analysis of the Proposed Reversible Visible Watermarking Embedding Process

TABLE I

Performance Analysis of the Proposed Reversible Visible Watermarking Embedding Process

Logo	Width	Height	M _E Size (Bytes)	Comp. Ratio	I _w PSNR (dB)
ATLSS	163	216	14408	2.4436	26.2887
DARPA	130	263	16461	2.0770	26.9543
Censcir	82	225	8747	2.1093	30.1921
Robotics	130	108	5623	2.4969	31.4413
CIT	82	225	8472	2.1778	31.7764
HCII	65	65	2253	1.8753	37.4408

Table I illustrates the performance of the proposed Reversible Visible Watermarking Embedding mechanism. It can be clearly seen that the compression efficiency provided by the Lossless Encoder process is between 1.8 and 2.5. This compression efficiency is almost constant and thus not affected by the logo size. It can be further noticed that the larger the size of the logo to be embedded the lower is the quality of the Watermarked Video I_w. This is quite intuitive since larger logos need to modify more DCT coefficients thus inevitably reducing the perceptual quality of the Watermarked Video. The proposed system was compared to the Yang method which was adapted for compressed video. As it can be seen from Fig. 2, the quality of the proposed method is superior to the method adopted in [8]. In fact, it can be seen that no matter how much information is reversible embedded the proposed system manages to recover the original quality for authenticated users. This is mainly due to the fact that the information is being embedded on the compressed transform coefficients. On the other hand, the performance of the state of the art approach degrades with increasing embedding information since the information is hidden within the spatial domain which is corrupted by the Quantization process.

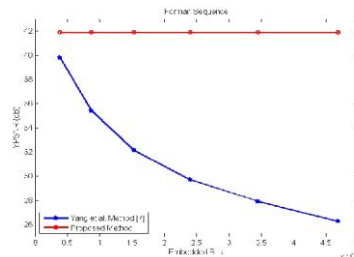


Fig. 3. Performance of the Yang method [8] and the proposed method at different number of embedded bits

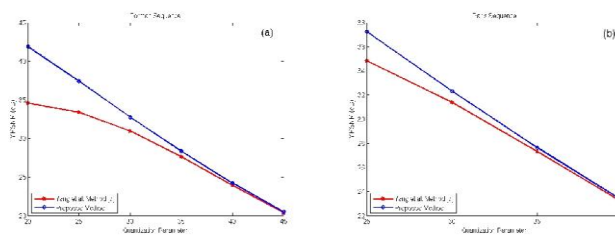


Fig. 4. Performance of the Yang [8] and the proposed method at different Quantization Parameters (a) Foreman (b) Paris Sequence



Fig. 5. Subjective results when using the (a) method proposed by Yang [8] and the (b) Proposed method. QP was set to 30.

The performance of the proposed scheme was further analysed using different Quantization Parameters. As

shown in Fig. 3, the proposed system clearly outperforms the method presented in [7] where PSNR gains of up to 7 dB were achieved. The superiority of the proposed method is more evident in Fig. 4 where it can be seen that the method proposed by Yang does not manage to extract the reversible information since it was corrupted by quantization errors induced by the lossy Video Encoder process. The quantization errors generally provide syntax and semantic violations in the De-Encryption and Lossless Decoding processes which are thus not able to recover the original embedded information. On the other hand the proposed method manages to recover the original compressed video when the user is authenticated.

5. Comments And Conclusion

This paper has presented a secured data Transmission with Advanced Encryption Standard (AES) using novel reversible visible water-marking scheme for H.264/AVC encoded video. The proposed method computes the information required by the decoder to recover the original compressed video when receiving the watermarked video sequence. The additional information is reversibly embedded within the transform coefficients of the watermarked video. The authenticated users are then enabled to extract the information hidden within the transform coefficients to recover the original compressed image. The experimental results have shown the superiority of the proposed system where PSNR gains of up to 7 dB was registered relative to the state of the art approach. It was further shown that the information to be hidden can be compressed with compression efficiency between 1.8 and 2.5. And the distortion provided by the RCM method is reduced. Furthermore, watermark estimation functions can be employed in order to reduce the energy within the message D to be decoded.

References

- [1] Reuben A. Farrugia "Reversible Visible Watermarking for H.264/AVC Encoded Video" IEEE Conference, May 2011
- [2] A. Watson, "Visually Optimal DCT Quantization Matrices for Individual Images", in Data Compression Conference, 1993. DCC '93., 1993, pp. 178-187.
- [3] S.-K. Yip, O. Au, C.-W. Ho, and H.-M. Wong, "Lossless Visible Water-Marking", in Multimedia and Expo, 2006 IEEE International Conference on, 9-12 2006, pp. 853-856
- [4] Xiao Zeng, Zhen-Yong Chen, Ming Chen and Zhang Xiong, "Reversible Video Watermarking Using Motion Estimation and Prediction Error Expansion," journal of information science and engineering 27, 465-479 (2011)
- [5] R. A. Farrugia, "A Reversible Visible Watermarking Scheme for Compressed Images", in MELECON 2010 - 2010 15th IEEE Mediterranean Electrotechnical Conference, 26-28 2010, pp. 212-217
- [6] T. Wiegand, G. Sullivan, G. Bjontegaard, and A. Luthra, "Overview of the H.264/AVC Video Coding Standard," IEEE Transactions on, Vol. 13, no. 7, pp. 560-576, July 2003
- [7] S.P. Mohanty, K.R. Ramakrishnan, and M.S. Kankanhalli, "A DCT Domain Visible Watermarking Technique for Images," in Multimedia and Expo, 2000, IEEE International Conference on, New York, USA, pp. 1029-1032
- [8] D. Coltuc and J.-M. Chassery, "Very Fast Watermarking by Reversible Contrast Mapping," Signal Processing Letters, IEEE, Vol. 14, no. 4, pp. 255-258, April 2007
- [9] A. Watson, "Visually Optimal DCT Quantization Matrices for Individual Images", in Data Compression Conference, 1993. DCC '93, 1993, pp. 178-187
- [10] Y. Yang, X. Sun, H. Yang, and C.-T. Li, "Removable Visible Image Watermarking Algorithm in the Discrete Cosine Transform Domain," Expo, 2000. ICME 2000. 2000 IEEE International Conference on, New York, NY, USA, pp. 1029-1032
- [11] A. Alattar, "Reversible of a Generalized Integer Transform," Image Processing, IEEE Transactions on, Vol. 13, no. 8, pp. 1147-1156, Aug. 2004
- [12] Y. Hu and B. Jeon, "Reversible Visible Watermarking and Lossless Recovery of Visible Watermarking and Original Images," Circuits and Systems for Video Technology IEEE Transactions on, Vol. 16, no. 11, pp. 1423-1429, Nov. 2006
- [13] Advanced Encryption Standard (AES), FIPS PUB Std. 197, 2001
- [14] (2010) Thezlib website. [Online]. Available <http://www.zlib.net/>
- [15] B.-B. Huang and S.-X. Tang, "A Contrast-Sensitive Visible Water-Marking Scheme," IEEE MultiMedia, vol. 13, no. 2, pp. 60-66, 2006.

“Isolation of Microorganism from Dairy Effluent for Activated Sludge Treatment”

¹Vishakha S. Shivsharan, ²Minal P. Wani, ³Suhas W. Kulkarani,

¹Dept. Of Plant And Animal Biotechnology And Environmental Sciences

²Dr. D.Y. Patil Biotechnology & Bioinformatics Institute, Tathawade, Pune.

³Dept. of Microbiology, Shriman Bhausaheb Zadbuke Mahavidyalaya, Barshi-413401.

Abstract

On current trends, it is estimated that, in the year 2030 most of our water resources would be exhausted or totally destroyed (UK Trade and Investment, 2002). Most water bodies have the ability to self-purify whereby they are pendent on environmental conditions, pollutant load and water retention times (Sanders and Yevjevich, 1996). But the natural contaminants are coupled with artificial pollutants, which are a result of human activities, the pollution load becomes too much for the water body to handle. The main pollutant derived from the industrial wastewaters are organic and inorganic substances, solved or in suspension, with different harmfulness degree (Banu, 1998). In the early 1960's U.S. senate committee noted that dairy industry was second most important single source of pollution in streams (Worner-1976). The dairy waste is basically organic and slightly alkaline in nature, when discharged in to streams without treatment, result in rapid depletion of dissolved oxygen (DO) and encourage the growth of algae i.e. eutrophication (Forsberg, 1998). Due to the overuse of surfactants in dairy, the waste can become unamenable to the biological treatment. The treatment of dairy wastewater, so that it is microbiologically and chemically acceptable for use in flush and irrigation applications, is of great importance (Ibekwe et al. 2003). Every Dairy is having particular characteristics of effluents and hence has the different effluent related problems. These problems can be revealed by effective treatment of the effluent a possible by the study of wastewater microbiota and to identify some new active strains adapted to the wastewater physical-chemical conditions, which metabolize organic compounds, similar to those which determine the pollution of wastewaters such as starch, casein, basic carbohydrates and lactic acid (Mihaela Palela et al.; 2007). There were identified strains able to produce a fast biodegradation of the organic compounds. Normally to isolate microbial culture of endogenous origin for the development of microbial biomass which can be used effectively under Activated sludge treatment to stabilize the effluent. For that purpose bacteria isolated from effluent and study morphological, cultural and biochemical characteristics and identified with the help of Bergey's Manuals of Systematic Bacteriology (1984)

Keyword: Dairy Effluent, Activated Sludge, Endogenous Culture, Isolation & Preliminary Identification, Microbiological And Biochemical Characterization.

1. Introduction:

Dairy wastewater disposal represents a major environmental problem. Numerous effective attempts have been made to resolve this problem by the activated sludge process is the mostly used biological treatment ever (Dashika Naidoo ;2005). This review discusses microorganisms associated with microbial digestion of dairy wastewater, biochemistry of the process, factors affecting microbial digestion, and efforts to develop defined cultures. To get an efficient biological wastewater treatment it is very important to know the wastewater microbiota composition and the biochemical properties correlated to the origin of pollutants, as well as the optimum metabolic activity and the physical -chemical conditions (Janczukowicz et al., 2007). Microbial digestion of dairy food wastewater offers many advantages over other treatments in that a high level of waste stabilization is achieved with much lower levels of sludge. As microbial digesters become increasingly used in dairy plants, more research should be directed toward selecting the best cultures that maximize environmental problem from dairy waste. The microbes responsible for the organic and inorganic luxury uptake occurring in the treatment plant (G.W. Fuhs & M.Chen ;1975) The isolation of bacteria and the study of their identification have been hampered by the unreliability of conventional microbiological techniques. This is largely due to their morphological variations and inconsistent characteristics and different biochemical Characteristics. To fully understand their role in promoting activated sludge process, bacteria need to be characterized. The aim of this study was, therefore, the bacteria in pure culture isolated. fifteen different cultures were used for this study. The cultures were identified using Bergey's Manuals of Systematic Bacteriology (1984).

2. Material And Methods:

The aim of this study is to evaluate the dairy wastewater microbiota and its biochemical activities, in order to obtain pure cultures adapted for wastewater treatment. To get an efficient biological wastewater treatment it is very important to know the wastewater microbiota composition and the biochemical properties correlated to the origin of pollutants, as well as the optimum metabolic activity and the physical-chemical conditions (Janczukowicz *et al.*, 2007).

1. Selection of source for isolation of micro organisms: The dairy effluent samples were collected from “Shivamrut Dudh Utpadak Sahkari Sangh Maryadit, Vijaynagar (Vizori) Akluj”. The sample was collected in a clean sterile plastic container and stored at 4°C until the analysis was carried out. (Trivedy and Goel ; 1984). Effluent samples were collected in duplicate from each station in pre sterilized bottles.

2. Primary screening: For primary screening the Dilutions of whey sample are prepared in distilled water. Selective dilutions are spread on nutrient agar, incubated and for 24hrs at room temperature. After incubation, isolated colonies are selected for further study. These selected colonies were restricted on nutrient agar for isolation by four quadrant method. These well isolated colonies were purified on nutrient agar and preserved on nutrient agar slant at 4°C for long time for further studies.

3. Characterization of the bacterial isolates : By following methods.

3.1 Cultural Characteristics: The various typical colony characteristics of the bacterial isolates were recorded after their appearance on nutrient agar after 24 hours of incubation at 28°C as described in sale (1974) Benson (1990) and Frobisher (1968).

3.2 Staining and Morphology: The Gram Characteristics and morphology of the isolates were studied by Gram staining method as described in Desai and Desai (1980).

4. Biochemical characterization: following two methods were used.

4.1 Enzymatic activities and 4.2 Carbohydrates utilization

4.1 Enzymatic activities: The extra-cellular production of various enzymes and their activities were studied using suitable method and materials described below.

4.1.1 Catalase: A loop full of growth of each bacterial isolate from nutrient agar slant was stirred in 30.0 v/v hydrogen peroxide and observed for evolution of gas as described in Blazevic (1975).

4.1.2. Gelatinase: Spot inoculation of the Bacterial isolates was done on sterile gelatin agar containing 0.4 % gelatin and incubated at 28°C for 24 hours. Gelatin hydrolyzing ability of micro-organisms was detected as the appearance of the clear zone after the addition of frazieres solution on the medium as described in Blazevic (1975).

4.1.3. Nitrate Reductase: Reduction of nitrate to nitrite was tested by inoculating bacterial isolates in tubes containing sterile peptone nitrate broth and detected by the sulphanilic acid - naphthyl-amine reaction as described in (Blazevic-1975).

4.1.4. Urease: Slants of sterile Christensen’s urea agar (1946) were inoculated with the bacterial isolates and incubated at 28°C for 24 hours Hydrolysis of urea was detected by the appearance of the pink colour in the medium as described in Blazevic (1975).

4.1.5. Oxidase: Colonies of the bacterial isolates are transferred by a glass rod on the filter paper strip moistened with freshly prepared 1% tetramethyl-1-p-phenylene diamine (TAPA) solution and observed for the appearance of a deep blue colour on the strip to indicate a positive result.

4.1.6. Starch hydrolysis: Spot inoculation of bacterial isolates was done on sterile starch agar containing 1% starch and incubated at 28°C for 24 hours and then Lugols iodine was poured on the plates to detect zones of starch hydrolysis around and beneath the colonies.

4.1.7. Hugh and Leifsons Test: The bacterial isolates were inoculated in to the two tubes of Hugh and Leifsons Medium (Aerobic and Anaerobic) in order to check oxidative and fermentative metabolism of sugar and incubated at 28°C for 24 hours. After incubation, tubes were observed for acid and gas production.

4.1.8. Hydrogen Sulphide Production Test: The bacterial isolates were inoculated in to sterile standard thiosulphate iron agar stab medium. Formation of black ferrous Sulphide precipitate in the medium indicated thiosulphate reduction.

4.2 Carbohydrates Utilization: Using peptone water as a basal medium in 5ml aliquots of each, the utilization of different carbohydrates by the bacterial isolates were studied. As described in Cruickshank (1973) The carbohydrates tested were :Disacclarides – Lactose, Maltose, Sucrose.;Hexoses- Glucose;Sugar alcohols – Mannitol, Sorbitol.;Sugar Vitamin – Inositol;Peptose – Xylose.

3. Result And Discussions:

Bacterial diversity has not been studied in detail in dairy effluent. However a few reports are available on the bacterial flora of certain effluents. Ravichandra et al. (2007) two strains of Thiobacillus sp were isolated from aerobic sludge of distillery and dairy effluent treatment plant . Dairy industry effluent in Chennai *Bacillus Subtilis* β -galactosidase has been used as a probiotic source organism by *Jayashree Natarajan et.al (2012)*

3.1 Isolation of Bacterial cultures from Whey :

3.2 Isolation of Bacteria:

Total fifteen bacterial isolates were isolated using sterile nutrient agar medium after incubation at room temperature for 24 hrs. from the “Shivamrut Dudh Utpadak Sakhari Sangh Maryadit, Vijaynagar (Vizori) Akluj” dairy plant effluent. Micro flora of the effluents from a dairy factory in Tehran (Pegah Dairy Processing Plant) were isolated and screened for their ability to reduce the organic matter content and COD of the effluents by Maghsoodi et.al(2007). R. Prakashveni and M. Jagadeesan(2008) study 19 bacterial genera isolated from the Thanjavur Co-operative Milk Products dairy effluent *Alcaligenes faecalis*, *Lueconostoc lactis* survive in all seasons .

3.3 Characterization of the bacterial isolates:

Morphological, cultured and biochemical characteristics of the isolates were studied. Micro flora of the effluents from a dairy factory in Tehran (Pegah Dairy Processing Plant) were isolated and screened for their ability to reduce the organic matter content and COD of the effluents by Maghsoodi et.al(2007)

3.4 Cultural characteristics :

The data on the cultural characteristics of the bacterial isolates on nutrient agar is presented in table:1. The colonies of the isolates on nutrient agar were circular to irregular ranging in size from <1mm to 2mm. The colour of colonies was dirty white and yellowish mostly. The colonies of all the isolates have regular to irregular margins with mostly flat to convex elevation, moist consistency and opaque to translucent in nature. Jain et. al (2001) isolated three different bacterial species such as *Bacillus megateriu*, *B. cereus* and *Xanthomonas fregariae* from distillery wastes effluent.

3.5 Staining and Morphology:

The bacterial isolates on nutrient agar were stained for their morphological characters and the results are presented in table 2. Out of the fifteen three were gram-negative short rod namely 3, 11, 13, Isolate 1,2,4,6 & 12 are gram positive rods and isolate number 8,9, & 10 are gram positive cocci . Isolate number 2,4,& 6 were seen to produce endospore . Isolate 1 to 10 all are motile and 11 to 15 are non-motile. Similar finding recorded that Sree kumar et.al (2010) have successfully isolated a new strain of spore forming Bacilli that it capable fermenting lactose from dairy effluents.

3.6

Enzymatic activities:

Out of total fifteen isolates tested for enzymatic activity, eight isolates with number 2,5,6,7,8,9,14,15 show amylase activity and 1,2,3,10,11,12,13 show Urease activity, 1,2,3,5,6,7,8,10,11 show Gelatinase activity. Nitrate reductase activity is shown by isolates 2, 4, 5,6,7,8,9,10,15. Catalase activity is shown by isolates viz 2,3,4,5,6,8,9,10,13,14 while isolates viz 1, 3,4,5,7,8,10,11,12,13 shows Oxidase activity. Caseinase activity shown by all the isolates except No. 2, 5, 8, 11, 12, 15. While none of the bacterial isolate shows the hydrogen Sulphide activity. Isolate number 10 show all test positive except H₂S & amylase and Isolate No. 15 show all test negative except nitrate reduction H.L. test & amylase activity. On the basis of biochemical characteristics of microbes it can be concluded that the abovementioned chemoorganotrophs utilize energy from dairy effluent and chemolithotrophs accelerates the corrosion process by converting ferrous ion to ferric and its oxides (Muthukumar et al., 2003, Dawood et al., 1998, Jayaraman et al., 1998, Rajasekar et al., 2005).

4.

Utilization Of Carbohydrates :

Glucose is the sugar which is most favored by bacteria as all isolates utilize it. Lactose and sucrose are also the sugar favored by the bacterial isolates as twelve isolates utilized it. Maltose, Mannitol and inositol were utilized by seven isolates. Isolate number 2 utilized all the sugars while isolate number 14 utilized all sugars. Isolate number 4 also utilized all the carbohydrates while isolate number 15 utilized only glucose and Mannitol as shown in table 5

Table 1 Colony Characters of bacterial isolates .

Bacterial isolate	Size (mm)	Shape	Colour	Margin	Elevation	Opacity	Consistency
1	1	Circular	Whitish	Regular	Flat	Opaque	Moist
2	<1	Round	Dirty white	Irregular	Slight Convex	Opaque	Moist
3	2	Circular	Pinkish	Regular	Flat	Opaque	Moist
4	2	Circular	Dirty white	Regular	Slight Convex	Opaque	Moist
5	<1	Irregular	White	Entire	Flat	Transparent	Moist
6	2	Circular	Faint red	Entire	Concave	Transparent	Moist
7	1	Irregular	Yellowish	Regular	Convex	Transparent	Moist
8	2	Regular	White	Irregular	Flat	Transparent	Moist
9	2	Irregular	Yellowish	Irregular	Flat	Transparent	Moist
10	<1	Circular	Yellowish	Regular	Convex	Transparent	Moist
11	<1	Circular	Colorless	Entire	Convex	Translucent	Moist
12	1	Circular	Yellowish	Entire	Convex	Opaque	Moist
13	2	Circular	Colorless	Entire	Convex	Opaque	Moist
14	1	Circular	Faint orange	Entire	Convex	Opaque	Moist
15	1	Circular	Whitish	Irregular	Raised	Opaque	Moist

Isolate No.	Gram Character	Sporulation	Shape of cell	Arrangement Of cell	Motility
1	Positive	-	Short rod	Pairs	Motile
2	Positive	+	Long rod	Long Chain	Motile
3	Negative	-	Short rod	Pairs	Motile
4	Positive	+	Long rod	Long Chain	Motile
5	Negative	-	Rods	Single	Motile
6	Positive	+	Rods	Single	Motile
7	Negative	-	Rods	Pairs	Motile
8	Positive	-	Cocci	Chains	Motile
9	Positive	-	Cocci	Bunches	Motile
10	Positive	-	Cocci	Bunches	Motile
11	Negative	-	Short rod	Chains	Non motile
12	Positive	-	Rods	Chains	Non motile
13	Negative	-	Short rod	Chains	Non motile
14	Negative	-	Rods	Chains	Non motile
15	Negative	-	Rods	Chains	Non motile

Table: 2 Staining and Morphology of the bacterial isolates.

Test No.	Catalase	Oxidase	H ₂ S	Nitrate Reduction	H.L. Test	Gelatinase	Urease	Amylase	Caseinase
1	-	+	-	-	-	+	+	-	+
2	+	-	-	+	+	+	+	+	-
3	+	+	-	-	+	+	+	-	+
4	+	+	-	+	-	-	-	-	+
5	+	+	-	+	+	+	-	+	-
6	+	-	-	+	+	+	-	+	+
7	-	+	-	+	-	+	-	+	+
8	+	+	-	+	-	+	-	+	-
9	+	-	-	+	+	-	-	+	+
10	+	+	-	+	+	+	+	-	+
11	-	+	-	-	-	+	+	-	-
12	-	+	-	-	+	-	+	-	-
13	+	+	-	-	+	-	+	-	+
14	+	-	-	-	+	-	-	+	+
15	-	-	-	+	+	-	-	+	-

Table 3 Biochemical Characteristics of the bacterial isolates.

Where “+” : Positive test
 “-” : Negative test

Table 4 Utilization of carbohydrates by the bacterial isolates

Isolate No.	Lactose	Sucrose	Glucose	Maltose	Mannitol	Inositol	Xylose
1	+	+	+	+	+	-	-
2	+	+	+	+	+	+	+
3	-	-	+	-	+	+	-
4	+	+	+	+	+	+	+
5	+	-	+	+	-	-	-
6	+	+	+	-	-	+	+
7	-	+	+	-	-	+	-
8	+	+	+	+	-	-	-
9	+	+	+	+	-	-	-
10	+	+	+	+	+	-	-
11	+	+	+	+	-	+	+
12	-	+	+	+	-	+	+
13	+	-	+	+	+	-	-
14	+	+	+	+	+	+	+
15	-	-	+	-	+	-	-

Where , “+” -positive test
 “-” -negative test

Table 5 Tentative identification of bacterial isolate from Bergey's Manuals of Systematic Bacteriology

Sr. No.	Isolate Number	Tentative identification
1	1	<i>Lactobacillus</i>
2	2	<i>Bacillus</i>
3	3	<i>Pseudomonas</i>
4	4	<i>Bacillus</i>
5	5	<i>Azotobacter</i>
6	6	<i>Arthrobacter</i>
7	7	<i>Zoogloea</i>
8	8	<i>Micro bacterium</i>
9	9	<i>Staphylococcus</i>
10	10	<i>Micrococcus</i>
11	11	<i>Cardiobacterium</i>
12	12	<i>Bifidobacterium</i>
13	13	<i>Pasterurella</i>
14	14	<i>Escherichia</i>
15	15	<i>Eikenella</i>

5. Conclusions :

According to the results, bacterial isolate are the most effective organisms for the activated sludge treatment to reduce the organic matter of high BOD- COD concentration of dairy effluent. It also decreased the carbohydrate ,nitrate to nitrite, fat, gelatin, urea, starch and protein content of the waste. We suggest that the addition of bacterium to the microbial mixture of the activated sludge will increase the overall efficiency of the treatment system. It can also reduce the bulking problems of the activated sludge by preventing the load of the organic matter from becoming too high. Thus industrial effluents from different industries may have been playing an important role in our social economy and creating serious problems solved by these isolates for the treatment of the effluents of Dairy.

References:

- [1] Ahring B.K., A.A Ibrahim, etui, (2001), "Effect of temperature increase from 55⁰C-65⁰C on performance & microbial population dynamics of an anaerobic reactor treating cattle" manure water research 35-41
- [2] APHA –AWWA-WPCP (1985) standard method for examination of water and waste water 16th ed. Washington
- [3] APHA-AWWA-WPCF (1980) standard methods for examination of water & waste water 15th ed American Public Health Association Washington.
- [4] Boczar B.A., Federte T.W. (2001), "Characterization and distribution of esterase activity in activated sludge." Water Research. Vol.35, pp 4208-4216.
- [5] Craggs R.J., Tanner C.C., Sukies JPS, Davies-Cotiey R.J. (2000), "Nitrification potential & attached biofilms in dairy form waste stabilization ponds" water science technology Vol. 42(10-11) 195-202.
- [6] Daigger G.T. & Littleton H.X. (2000) "Characterization of simultaneous nutrient removal in staged ,closed-loop bioreactors" Water Environment research Vol.72
- [7] Desai J.D. and A. J. Desai (1980), "Methods in microbiology microscopy and staining." Prashant Publishers Vallabh Vidyanagar.
- [8] Deshmukh A.M. (1997) "Hand book of media stain and reagent in microbiology" PAMA publication,Karad.
- [9] Eckles C.H., Combs U.b. macy H (2000), "Milk & milk products" 4th editors Tata Mcgeraw Hill publication company limited New Delhi.
- [10] Feroandez J.M., Omil F., Mendez R., Leena J.M., (2001), "Anaerobic treatment of fibreboard manufacturing wastewater in a pilot scale hybrid USBF reactor." Water Research Vol.35 (17) pp-475-508.
- [11] Gessesse A., Dueholm T., Petersen S.S., Nielsen P.H., (2003) "Lipase and protease extraction from activated sludge." Water Research Vol.37 Pp-213-365.

- [12] Hasur,C.Kinaci.A.Unlu (2004), “An alternative for pre-treatment of high-strength raw whey wastewater: submerged membrane bioreactors” Scientific and Technical Research Council of Turkey.
- [13] Hasur,C.Kinaci.A.Unlu (2004), “An alternative for pre-treatment of high-strength raw whey wastewater: submerged membrane bioreactors” Scientific and Technical Research Council of Turkey.
- [14] Sukumar De. (1994), “Outline of dairy technology”Oxford University Press. New Delhi.
Sneath PHA, Mair NS, Sharpe ME and Holt JG (1986)Endospore-forming gram-positive rods and cocci. In:Berger’s Manual of Systematic Bacteriology
- [15] Trivedy R.K. and P.K. Goel (1984), “Chemical and biological methods for water pollution studies.” Environmental Publication, Karad.
- [16] Watson S.D., Akhurst T., Whiteley C.G., Rose P.D., Pletschlce B.I.,(2004), “Primary dludge flow degradation is accelerated under biosulphide organic Conditions enzymological aspects.” Enzyme Microbe Technology. Vol 34 pp-595-602
- [17] [http:// www.elsevier.com/locate/watres](http://www.elsevier.com/locate/watres)
- [18] <http://www.dairy industry.com>
- [19] <http://www.anaerobic.htm>
- [20] <http://www.GWE.htm>
- [21] <http://www.scienceblog.com/community>
- [22] [http:// webmaster@pnl.gov](http://webmaster@pnl.gov)

Determining Pinpoint of Mobile Location in Global System for Mobile Communication Network (Gsm)

^{1,2}**Adnan Affandi, ²Mubashshir Husain**

^{1,2}Department of Elect. & Comp. Eng., King Abdul Aziz University, Jeddah, Saudi Arabia

Abstract:

The objective of this proposed paper is to present an extensive simple study about the mobile Location and the technologies that can enable them in conventional GSM networks, which do not require any significant changes to the network or the mobile device itself. A set of cell-based positioning techniques are proposed based on information available from the network and on accurate path loss models. We have also developed a program in matlab language for GSM vendors to use this feature without physical change in the network hardware.

Keywords: Global System For Mobile Communication, etc.

1. Introduction

In 1982, the Nordic PTT sent a proposal to Conférence Européenne des Postes et Télécommunications (CEPT) to specify a common European telecommunication service at 900 MHz. A Global System for Mobile Communications (GSM) standardization group was established to formulate the specifications for this pan-European mobile cellular radio system. During 1982 through 1985, discussions centered around whether to build an analog or a digital system. Then in 1985, GSM decided to develop a digital system. In 1986, companies participated in a field test in Paris to determine whether a narrowband or broadband solution should be employed. By May 1987, the narrowband Time Division Multiple Access (TDMA) solution was chosen. Concurrently, The terrain profile of a particular area needs to be taken into account for estimating the path loss. The terrain profile may vary from a simple curved earth profile to a highly mountainous profile. The presence of trees, buildings, and other obstacles also must be taken into account. A number of propagation models are available to predict path loss over irregular terrain.

While all these models aim to predict operators in 13 countries (two operators in the United Kingdom) signed the Memorandum of Understanding (MoU) which committed them to fulfilling GSM specifications and delivering a GSM system by July 1, 1991. This opened a large new market. In 1989 the ownership of the GSM standard was shifted to ETSI (European Telecommunications Standards Institute). ETSI has members from 54 countries inside and outside Europe, and represents administrations, network operators, manufacturers, service providers, research bodies and users. The next step in the GSM evolution was the specification of the Personal Communication Network (PCN) for the 1800 MHz frequency range. This was named the Digital Cellular System (DCS) 1800 (or GSM 1800). The Personal Communication Services (PCS) 1900 (or GSM 1900) for the 1900 MHz frequency range were also established for use in the Americas. Later GSM 800 and GSM 400 has been added. GSM 800 is using a frequency area currently being used by analog system in the Americas. GSM 400 is intended as a replacement of analog system around 450 MHz (NMT 450). This standard is not implemented by GPRS (General Packet Radio Services) is an extension of the GSM architecture. Packet data traffic runs on a new backbone IP network and is separate from the existing GSM core network that is used mainly for speech. GPRS was introduced in 2001. EDGE is a new modulation method enabling higher data bit rates introduced in R9.

2. Outdoor Propagation Models

Radio transmission in a mobile communications system often takes place over irregular terrain. signal strength at a particular receiving point or in a specific local area (called a sector), the methods vary widely in their approach, complexity, and accuracy. Most of these models are based on a systematic interpretation of measurement data obtained in the service area. Some of the commonly used outdoor propagation models are now discussed.

2.1 Longley-Rice Model

The Longley-Rice model [Ric67], [Lon68] is applicable to point-to-point communication systems in the frequency range from 40 MHz to 100 GHz, over different kinds of terrain. The median transmission loss is predicted using the path geometry of the terrain profile and the refractivity of the troposphere. Geometric optics techniques (primarily the 2-ray ground reflection model) are used to predict signal strengths within the radio horizon. Diffraction losses over isolated obstacles are estimated using the Fresnel-Kirchoff knife-edge models. Forward scatter theory is used to make troposcatter predictions over long distances, and far field diffraction losses

in double horizon paths are predicted using a modified Van der Pol-Bremmer method. The Longley-Rice propagation prediction model is also referred to as the ITS irregular terrain model. The Longley-Rice model is also available as a computer program [Lon78] to calculate large-scale median transmission loss relative to free space loss over irregular terrain for frequencies between 20 MHz and 10 GHz. For a given transmission path, the program takes as its input the transmission frequency, path length, polarization, antenna heights, surface refractivity, effective radius of earth, ground conductivity, ground dielectric constant, and climate. The program also operates on path-specific parameters such as horizon distance of the antennas, horizon elevation angle, angular trans-horizon distance, terrain irregularity and other specific inputs.

The Longley-Rice method operates in two modes. When a detailed terrain path profile is available, the path-specific parameters can be easily determined and the prediction is called a point-to-point mode prediction. On the other hand, if the terrain path profile is not available, the Longley-Rice method provides techniques to estimate the path-specific parameters, and such a prediction is called an area mode prediction. There have been many modifications and corrections to the Longley-Rice model since its original publication. One important modification [Lon78] deals with radio propagation in urban areas, and this is particularly relevant to mobile radio. This modification introduces an excess term as an allowance for the additional attenuation due to urban clutter near the receiving antenna. This extra term, called the urban factor (UF), has been derived by comparing the predictions by the original Longley-Rice model with those obtained by Okumura [Oku68]. One shortcoming of the Longley-Rice model is that it does not provide a way of determining corrections due to environmental factors in the immediate vicinity of the mobile receiver, or consider correction factors to account for the effects of buildings and foliage. Further, multipath is not considered.

2.2 Durkin's Model

The execution of the Durkin path loss simulator consists of two parts. The --first part accesses a topographic data base of a proposed service area and reconstructs the ground profile information along the radial joining the transmitter to the receiver. The assumption is that the receiving antenna receives all of its energy along that radial and, therefore, experiences no multipath propagation. In other words, the propagation phenomena that is modeled is simply LOS and diffraction from obstacles along the radial, and excludes reflections from other surrounding objects and local scatterers. The effect of this assumption is that the model is somewhat pessimistic in narrow valleys, although it identifies isolated weak reception areas rather well. The second part of the simulation algorithm calculates the expected path loss along that radial. After this is done, the simulated receiver location can be iteratively moved to different locations in the service area to deduce the signal strength contour.

2.3 Okumura Model

Okumura's model is one of the most widely used models for signal prediction in urban areas. This model is applicable for frequencies in the range 150 MHz to 1920 MHz (although it is typically extrapolated up to 3000 MHz) and distances of 1 km to 100 km. It can be used for base station antenna heights ranging from 30 m to 1000 m.

Okumura developed a set of curves giving the median attenuation relative to free space (A_{mu}), in an urban area over a quasi-smooth terrain with a base station effective antenna height (h_{te}) of 200m and a mobile antenna height (h_{re}) of 3 m. These curves were developed from extensive measurements using vertical Omni-directional antennas at both the base and mobile, and are plotted as a function of frequency in the range 100 MHz to 1920 MHz and as a function of distance from the base station in the range 1 km to 100 km. To determine path loss using Okumura's model, the free space path loss between the points of interest is first determined, and then the value of $A_{mu}(f, d)$ (as read from the curves) is added to it along with correction factors to account for the type of terrain. The model can be expressed as

$$L_{50} = L_F + A_{mu}(f, d) - G(h_{te}) - G(h_{re}) - G_{AREA} \quad (4.1)$$

where L_{50} is the 50th percentile (i.e., median) value of propagation path loss, L_F is the free space propagation loss, A_{mu} is the median attenuation relative to free space, $G(h_{te})$ is the base station antenna height gain factor, $G(h_{re})$ is the mobile antenna height gain factor, and G_{AREA} is the gain due to the type of environment. Note that the antenna height gains are strictly a function of height and have nothing to do with antenna patterns.

Plots of $A_{mu}(f, d)$ and G_{AREA} for a wide range of frequencies are shown in Figure 4.1 and Figure 4.2 . Furthermore, Okumura found that $G(h_{re})$ varies at a rate of 20 dB/decade and $G(h_{re})$ varies at a rate of 10 dB/decade for heights less than 3 m.

$$G(h_{re}) = 20 \log\left(\frac{h_{re}}{200}\right)$$

$$1000 \text{ m} \succ h_{re} \succ 10 \text{ m} \tag{4.2 a}$$

$$G(h_{re}) = 10 \log\left(\frac{h_{re}}{3}\right) \qquad h_{re} \leq 3 \text{ m} \tag{4.2 b}$$

$$G(h_{re}) = 20 \log\left(\frac{h_{re}}{3}\right)$$

$$10 \text{ m} \succ h_{re} \succ 3 \text{ m} \tag{4.2 c}$$

Other corrections may also be applied to Okumura’s model. Some of the important terrain related parameters are the terrain undulation height (Δh), isolated ridge height, average slope of the terrain and the mixed land-sea parameter. Once the terrain related parameters are calculated, the necessary correction factors can be added or subtracted as required. All these correction factors are also available as Okumura curves [Oku68]. Okumura’s model is wholly based on measured data and does not provide any analytical explanation. For many situations, extrapolations of the derived curves can be made to obtain values outside the measurement range, although the validity of such extrapolations depends on the circumstances and the smoothness of the curve in question.

Okumura’s model is considered to be among the simplest and best in terms of accuracy in path loss prediction for mature cellular and land mobile radio systems in cluttered environments. It is very practical and has become a standard for system planning in modern land mobile radio systems in Japan. The major disadvantage with the model is its slow response to rapid changes in terrain; therefore the model is fairly good in urban and suburban areas, but not as good in rural areas. Common standard deviations between predicted and measured path loss values are around 10 dB to 14 dB.

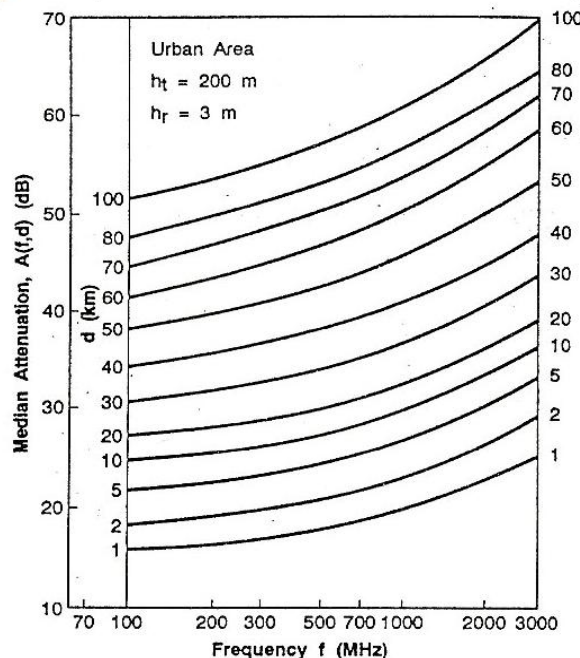


Figure 4.1 Median attenuation related to free space $A_{mu}(f, d)$, over a quasi-smooth terrain

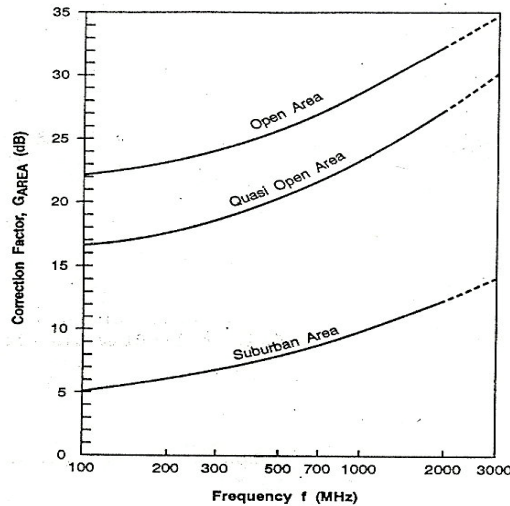


Figure 4.2 correction factor G_{AREA} , for different types of terrain

2.4 Hata Model

The Hata model [Hat90] is an empirical formulation of the graphical path loss data provided by Okumura, and is valid from 150 MHz to 1500 MHz. Hata presented the urban area propagation loss as a standard formula and supplied correction equations for application to other situations. The standard formula for median path loss in urban areas is given by

$$L_{50}(urban)(dB) = 69.55 + 26.16 \log f_c - 13.82 \log h_e - a(h_{re}) + (44.9 - 6.55 \log h_e) \log d \quad (4.3)$$

where f_c is the frequency (in MHz) from 150 MHz to 1500 MHz, h_e is the effective transmitter (base station) antenna height (in meters) ranging from 30 m to 200 m, h_{re} is the effective receiver (mobile) antenna height (in meters) ranging from 1 m to 10 m, d is the T-R separation distance (in km), and $a(h_{re})$ is the correction factor for effective mobile antenna height which is a function of the size of the coverage area. For a small to medium sized city, the mobile antenna correction factor is given by

$$a(h_{re}) = (1.1 \log f_c - 0.7) - (1.56 \log f_c - 0.8) \quad (4.4)$$

and for a large city, it is given by

$$f_c \leq 300MHz \text{ for } dB \quad a(h_{re}) = 8.29 * (\log 1.54 h_{re})^2 - 1.1 \quad (4.5 a)$$

$$a(h_{re}) = 3.2 * (\log 11.75 h_{re})^2 - 4.97 \text{ dB for } f_c \geq 300MHz \quad (4.5 b)$$

To obtain the path loss in a suburban area the standard Hata formula in equation (4.3) is modified as

$$L_{50}(dB) = L_{50}(urban) - 2[\log(f_c/28)]^2 - 5.4 \quad (4.6)$$

And for path loss in open rural areas, the formula is modified as

$$L_{50}(dB) = L_{50}(urban) - 4.78(\log f_c)^2 - 18.33 \log f_c - 40.98 \quad (4.7)$$

Although Hata's model does not have any of the path-specific corrections which are available in Okumura's model, the above expressions have significant practical value. The predictions of the Hata model compare very closely with the original Okumura model, as long as d exceeds 1 km. This model is well suited for large cell mobile systems, but not personal communications systems (PCS) which have cells on the order of 1km radius.

2.5 PCS Extension to Hata Model

The European Co-operative for Scientific and Technical research (EURO COST) formed the COST-231 working committee to develop an extended version of the Hata model. COST-231 proposed the following formula to extend Hata's model to 2 GHz. The proposed model for path loss is [EUR91]

$$L_{50}(\text{urban})(\text{dB}) = 46.3 + 33.9 \log f_c - 13.82 \log h_e - a(h_{re}) + (44.9 - 6.55 \log h_e) \log d + C_M \quad (4.8)$$

where $a(h_{re})$ is defined in equations (4.4), (4.5 a), and (4.5 b) and

$$C_M = 0 \text{ dB} \quad \text{for medium sized city and suburban areas} \quad (4.9)$$

$$C_M = 3 \text{ dB} \quad \text{for metropolitan centers}$$

The COST-231 extension of the Hata model is restricted to the following range of parameters:

$$\begin{aligned} f &: 1500\text{MHz to } 2000 \text{ MHz} \\ h_{te} &: 30 \text{ m to } 200\text{m} \\ h_{re} &: 1 \text{ m to } 10 \text{ m} \\ d &: 1 \text{ km to } 20 \text{ km} \end{aligned}$$

3. Locate A Mobile Position

By using Hata Model we can locate a Mobile position in the network by getting:

The Power value of Transmitting from the tower (from network data base)

The height of the tower (from network data base).

The receiving value in the mobile from the mobile (by using logical channels).

Carrier frequency (from network data base).

Mobile elevation which around 1.5 m.

Is the area urban , suburban or open rural (from network data base).

Calculate the Path loss by subtract the receiving value in the mobile (Rx) from Transmitting value from the tower (Tx).

$$L_{50} = Tx - Rx \quad (4.10)$$

Hata formula will be modifying for urban area to:

$$D = 10^{\frac{L_{50} - 69.55 - 26.16 \log f_c + 13.82 \log h_e + a(h_{re})}{44.9 - 6.55 \log h_e}} \quad (4.11)$$

Where

$$a(h_{re}) = (1.1 \log f_c - 0.7) - (1.56 \log f_c - 0.8) \text{ dB} \quad \text{(for small city)}$$

$$a(h_{re}) = 3.2 * (\log 11.75 h_{re})^2 - 4.97 \text{ dB} \quad \text{(for a large city)}$$

And for suburban area:

$$D = 10^{\frac{L_{50} - 69.55 - 26.16 \log f_c + 13.82 \log h_e + a(h_{re}) + 2[\log(f_c/28)]^2 + 5.4}{44.9 - 6.55 \log h_e}} \quad (4.12)$$

And for open rural areas:

$$D = 10^{\frac{L_{50} - 69.55 - 26.16 \log f_c + 13.82 \log h_e + a(h_{re}) + 4.78 (\log f_c)^2 + 18.33 \log f_c + 40.98}{44.9 - 6.55 \log h_e}} \quad (4.13)$$

From the above equations we can calculate the distance from the tower to the mobile for different areas (urban, suburban & open rural).after calculate the distance (D) we can create a circle as considering the position of the tower is origin of the circle and the distance D is the radius of the circle as shown below:

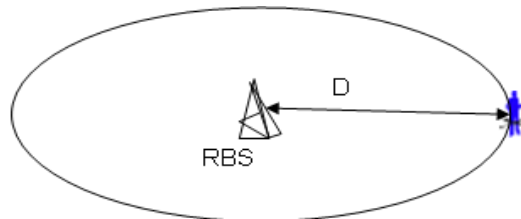


Figure 4-3 One Direction Estimation

And after repeat these process two times more for same mobile from different towers we will have three circles as shown below:

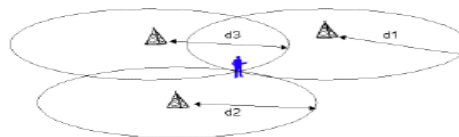


Figure 4-4 three directions estimation

The intersection between the three circles give us the location of the mobile .the intersection will be point or area depends on the receiving value (Rx) and we will locate Mobile position by placed our calculation and diagrams over good digitals Maps. These Maps programs can have them from good local vendor or use satellite Maps programs like Google earth.

4. Error and Correction

During our process maybe we will have some errors in the calculation and this is related to wrong reading values .this error in the reading values due to obstacles between the tower (transmitter) and mobile (receiver). some time no clear line of sight between RBS and MS which give us error in our estimation around 10 to 14 dB.

But we can overcome on these errors by using GSM techniques:

Handover to different towers (RBS's): we can our input by select different transmitters as we know the mobile receive from 6 different sites.

Frequency Hopping: this technique allows us to have varied frequencies to measure the mobile location because if we have a bad estimation from one frequency we will pick another one.

Take the measurement in different times or for some period to avoid the wrong estimation and take the good ones.

By these major techniques we will get a good estimation about customer location in any network. And there are a lot of techniques which are support our target.

As we know the GSM structure is very smart and always become smarter every day because it is a global system and whole the world deal with it.

We are hoping to lead the world in the development in the future.

5 .Development Of Software

Different Programs Have Been Developed In Matlab For The Simulation Of “ Determining Pinpoint Of Mobile Location In Global System For Mobile Communication network (GSM)”. In Fig.3 We Can See The Screenshot Of The Software.

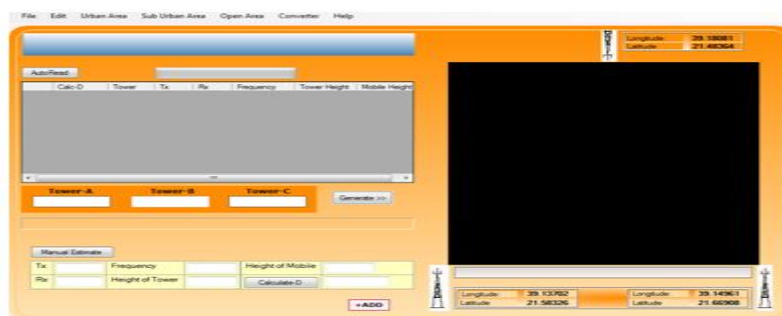


Fig 4.5

By using this simulator we can locate exact mobile location in Urban Area which is further divided into small and large city , in Sub urban area which is again divided into small and large city and finally in open area which is further divided into small and large city.

Determining pinpoint mobile location by using simulation software in Urban Area(Large City)

By using this software we demonstrated that how we can determine exact mobile location in Urban areas. Screenshot is shown in fig.4.6

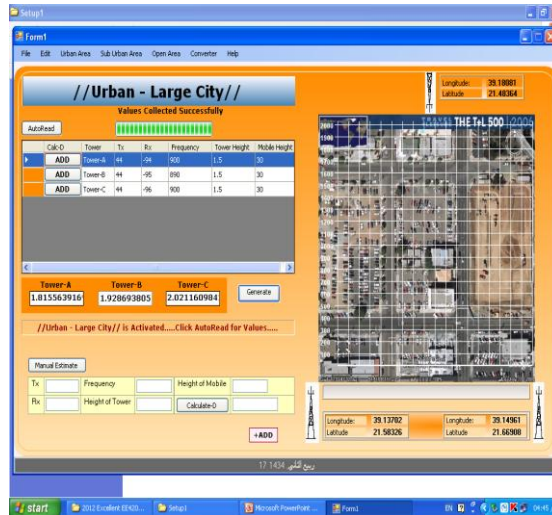


Fig 4.6

In this demonstration we have used the following values:

TValues					
Tower	Tx	Rx	Frq	Hte	Hre
Tower-A	44	-94	900	1.5	30
Tower-B	44	-95	890	1.5	30
Tower-C	44	-96	900	1.5	30

Where Tx=Transmitter
 Rx=Receiver
 Frq=Frequency
 Hte = Height of Transmitter
 Hre= Height of Receiver

Towerl		
Tower	Longitude	Latitude
Tower-A	39.13702	21.58326
Tower-B	39.14961	21.66908
Tower-C	39.18081	21.48364

Determining pinpoint mobile location by using simulation software in Sub-Urban Area (small city)

By using this software we demonstrated that how we can determine exact mobile location in Sub-Urban areas. Screenshot is shown in fig.4.7

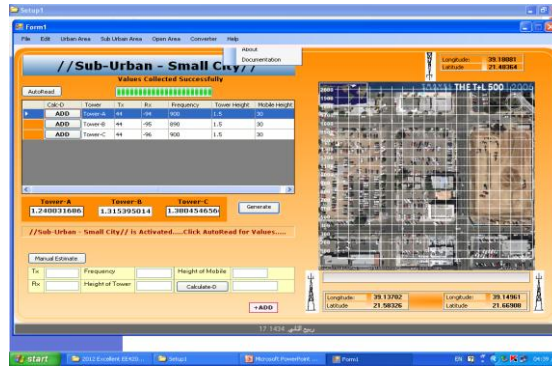


Fig 4.7

In this demonstration we have used the following values:

TValues					
Tower	Tx	Rx	Frq	Hte	Hre
Tower-A	44	-93	900	1.5	30
Tower-B	44	-95	890	1.5	30
Tower-C	44	-97	900	1.5	30

Where Tx=Transmitter
 Rx=Receiver
 Frq=Frequency
 Hte = Height of Transmitter
 Hre= Height of Receiver

Towerl		
Tower	Longitude	Latitude
Tower-A	39.10002	21.30003
Tower-B	39.14961	21.66908
Tower-C	39.18081	21.48364

Determining pinpoint location by using simulation software in Open Area (Large city)

By using this software we demonstrated that how we can determine exact mobile location in Open areas. Screenshot is shown in fig.

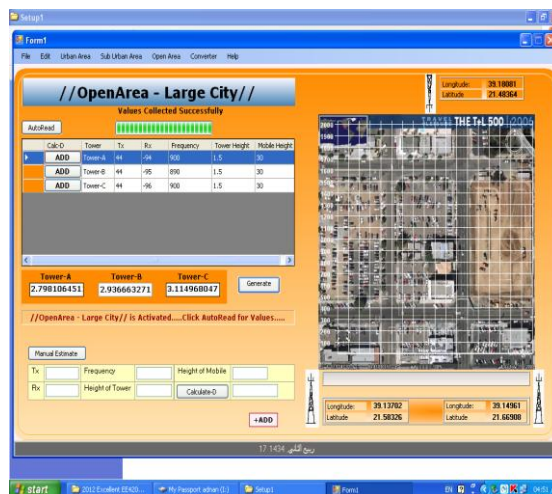


Fig 4.8

In this demonstration we have used the following values:

Tower1		
Tower	Longitude	Latitude
Tower-A	39.10002	21.30003
Tower-B	39.14961	21.66908
Tower-C	39.18081	21.48364

Where Tx=Transmitter
 Rx=Receiver
 Frq=Frequency
 Hte = Height of Transmitter
 Hre= Height of Receiver

Tower1		
Tower	Longitude	Latitude
Tower-A	39.20002	21.50234
Tower-B	39.14961	21.66908
Tower-C	39.18081	21.48364

4. Conclusion

- This research paper aims to present an extensive study about the mobile Location and the technologies that can enable them in conventional GSM networks.
- A set of cell-based positioning techniques are proposed based on information available from the network and on accurate path loss models.
- This paper creates a software methods program for GSM vendors to use this feature without physical change in the network hardware.

References

- [1] Theodore S. Rappaport, *Wireless Communication – Principles and Practice*, Prentice Hall, 1996.
- [2] Henry L. Bertoni , *Radio Propagation for Modern Wireless System* , Prentice Hall, 2000
- [3] Lucent Technologies course , *GSM 99/DCS 1800 System Introduction* , Lucent Company, 1996
- [4] Saudi Telecom Company course , *GSM RF Cellular Engineering*, Saudi Telecom Company ,2004.
- [5] Saudi Telecom Company course, *GSM Cell Planning Principles II*, Saudi Telecom Company ,2004.
- [6] Josef bajada. *Mobile Positioning for Location Dependent Services in GSM Networks* , 2000.M. Hellebrandt, R. Mathar, "Location tracking of mobiles in cellular radio networks", *IEEE Transactions on Vehicular Technology*, Sep. 1999,Vol. 48, No. 5, pp. 1558-1562.
- [7] Some training courses were giving to me by leadership companies like Saudi telecom company STC and Ericsson Company related to GSM and 3G.
- [8] Mouly & Pautet, *GSM system for mobile communication* , Jone Wily & Sons, 1989.
- [9] Rappaport , *wireless communication principles & practice* ,Marcel Dekker, 1994
- [10] http://www.mobilecomms-technology.com/contractors/gisservices/andrew_old/
- [11] <http://www.andrew.com/>
- [12] John Scurias, *A Brief Overview of GSM* ,
- [13] [http:// www. Barrow.uwaterloo.ca](http://www.Barrow.uwaterloo.ca) , 1994
- [14] Apostolis K. Salkintzis, " *A survey of Mobile Data Network* ",
- [15] [http:// www. columbia.uwaterloo.ca](http://www.columbia.uwaterloo.ca) , 1994

Fabrication And Implementation Of Turbo Charger In Two-Wheeler

¹,**AMALORPAVA DASS. J,** ², **Mr.SANKARLAL.P**

¹. M.E- (Thermal engineering) II-Year, J.J College of engineering and technology,Trichy.-620009.

².Asst.Proffessor, J.J College of engineering and technology,Trichy.-620009.

Abstract

The progress of automobiles for transportation has been intimately associated with the progress of civilization. The automobile of today is the result of the accumulation of many years of pioneering research and development. An attempt has been made in this project, the exhaust gas is used to rotate the turbine with blower arrangement. Exhaust gas is used to rotate the blower and this air is given to the ignition input supply. Our foremost aim in selecting this project is to use efficiency turbo charging. It is also good with regard to economical considerations and engine efficiency.

Key words: Turbocharger;Efficiency;IC engines.

1. Introduction

The output of the engine exhaust gas is given to the input of the turbine blades, so that the pressurized air produced. This power, the alternate power must be much more convenient in availability and usage. The next important reason for the search of effective, unadulterated power are to save the surrounding environments including men, machine and material of both the existing and the next forth generation from pollution, the cause for many harmful happenings and to reach the saturation point. The most talented power against the natural resource is supposed to be the electric and solar energies that best suit the automobiles. The unadulterated zero emission electrical and solar power, is the only easily attainable alternate source. Hence we decided to incorporate the solar power in the field of automobile, the concept of many Multi National Companies (MNC) and to get relieved from the incorrigible air pollution.

2. Turbocharger

BMW was the first to use turbo-charging in a production passenger car when they launched the 2002 in 1973. The car was brilliantly packaged too and paved the way for a simply magnificent 'Turbo Era' in the automotive world. Swedish giant Saab took its cue from this and its ensuing 900 series was one of the most characteristic turbo cars of its time. Intercoolers the latest turbo's they are used by most of today's turbo-diesel engines to make the compressed air denser. It works like this - on starting, exhaust gases spin the turbine and thus activate a compressor that pressurizes the air. This pressurised air from the turbo-charger is then sent through a duct to an air-cooled intercooler, which lowers the temperature of the intake charge and thus increases its density. The air-cooled intercoolers receive air through separate intakes and that explains the small scoops and louvers usually found on the hoods of turbo-charged cars. Modern turbo-diesel engines also make use of a temperature-sensitive, motor-driven fan which boosts airflow at low engine speeds or when the intake air temperature is high. Though there are diesel engines that 'earn' a turbo-charger mid-way through their life, the usual practice is to design and develop an engine with a turbo-charger in mind. Then, as and when a turbo-charged model is added to the stable, the engine can adapt to it without any additional strengthening and cooling of engine parts. A well-engineered, turbo-charged diesel engine offers better fuel efficiency (at times by 15 per cent), better overall performance (better torque and high-end power), reduced noise (compared to normally aspirated diesel engines) and minimum engine maintenance (owing to better combustion of diesel fuel). Turbo loses steam Multiple valves and double-overhead camshaft designs developed reasonable performance without the complication of turbo-charging, and these methods were politically correct too since they consumed less fuel. Consequently today there are only a few petrol-powered road cars that still use turbo-chargers for enhanced performance. Computers soon started playing an even bigger role in cars. Engine management systems linked to fuel-injection systems meant getting more out of the engine was even easier. For example, one can buy chips that can boost power by 100 bhp for some Japanese cars, such as the Nissan Skyline. Moreover, on-road speeds were being restricted all over the world. Though most of the sports cars today are capable of doing more, they are restricted electronically not to exceed 250 kmph even in autobahn-blessed Germany. Turbo-charging lost its edge towards the end of the '80s and today this technology is used only in select performance cars. Porsche, for example, is all set to build a turbo-charged version of its all-new 911(water-cooled) with added performance. Turbo engines were banned in Formula One too with the idea of restricting the performance of the cars (and thereby making them safer too). There are many who consider this a backward step in the world of Formula One, which is considered to represent the 'tomorrow' of automotive technology.

But if one analyses the performance of normally aspirated cars in F1 today, (3,500 cc non-turbo), they perform as well, if not better, than the turbo cars of the early '80s. So, there are no full stops in technology. While road cars and even sports and racing cars are going in for more efficient engines, better metallurgy and wilder-than-ever electronics to get their engines to perform at an optimum level without sacrificing the performance edge, turbo-chargers still continue to serve the same purpose they were invented for albeit more so with diesel engines.

3. Methodology

3.1 What is turbo-charging?

Turbo-charging, simply, is a method of increasing the output of the engine without increasing its size. The basic principle was simple and was already being used in big diesel engines. European car makers installed small turbines turned by the exhaust gases of the same engine. This turbine compressed the air that went on to the combustion chamber, thus ensuring a bigger explosion and an incremental boost in power. The fuel-injection system, on its part, made sure that only a definite quantity of fuel went into the combustion chamber.

3.2 What the turbo-charger does?

What the turbo-charger does is that it simply increases the volumetric efficiency of the engine. To give you an example: a 1,500 cc engine that produced, say, 60 bhp when it was normally aspirated, benefited at times with a 10- to 20-per cent power boost depending on the kind of turbo-charger used. Normally, the manufacturer would have had to resort to a bigger displacement in the engine, or design and develop an all-new engine to get more power from the same unit. In most piston engines, intake gases are "pulled" into the engine by the downward stroke of the piston (which creates a low-pressure area), similar to drawing liquid using a syringe. The amount of air which is actually inhaled, compared with the theoretical amount if the engine could maintain atmospheric pressure, is called volumetric efficiency. The objective of a turbocharger is to improve an engine's volumetric efficiency by increasing density of the intake gas (usually air). The turbocharger's compressor draws in ambient air and compresses it before it enters into the intake manifold at increased pressure. This results in a greater mass of air entering the cylinders on each intake stroke. The power needed to spin the centrifugal compressor is derived from the kinetic energy of the engine's exhaust gases. A turbocharger may also be used to increase fuel efficiency without increasing power. This is achieved by recovering waste energy in the exhaust and feeding it back into the engine intake. By using this otherwise wasted energy to increase the mass of air, it becomes easier to ensure that all fuel is burned before being vented at the start of the exhaust stage. The increased temperature from the higher pressure gives a higher Carnot efficiency. The control of turbochargers is very complex and has changed dramatically over the 100-plus years of its use. Modern turbochargers can use wastegates, blow-off valves and variable geometry, as discussed in later sections. The reduced density of intake air is often compounded by the loss of atmospheric density seen with elevated altitudes. Thus, a natural use of the turbocharger is with aircraft engines. As an aircraft climbs to higher altitudes, the pressure of the surrounding air quickly falls off. At 5,486 metres (17,999 ft), the air is at half the pressure of sea level, which means that the engine will produce less than half-power at this altitude.

4. Specification

4.1 Type Of Engine

Type of fuel used : Petrol
Cooling system : Air cooled
Number of cylinder : Single
Number of stroke : Two Stroke
Arrangement : Vertical
Cubic capacity : 100 cc

4.2 Spark Ignition Engine

A spark ignition (SI) engine runs on an Otto cycle—most gasoline engines run on a modified Otto cycle. This cycle uses a homogeneous air-fuel mixture which is combined prior to entering the combustion chamber. Once in the combustion chamber, the mixture is compressed, and then ignited using a spark plug (spark ignition). The SI engine is controlled by limiting the amount of air allowed into the engine. This is accomplished through the use of a throttling valve placed on the air intake (carburetor or throttle body). Mitsubishi is working on the development of a certain type of SI engine called the gasoline direct injection engine.

4.3 Advantages

- A century of development and refinement - For the last century the SI engine has been developed and used widely in automobiles. Continual development of this technology has produced an engine that easily meets emissions and fuel economy standards. With current computer controls and reformulated gasoline, today's engines are much more efficient and less polluting than those built 20 years ago.
- Low cost - The SI engine is the lowest cost engine because of the huge volume currently produced.

4.4 Disadvantages

The SI engine has a few weaknesses that have not been significant problems in the past, but may become problems in the future.

- Difficulty in meeting future emissions and fuel economy standards at a reasonable cost - Technology has progressed and will enable the SI engine to meet current standards, but as requirements become tougher to meet, the associated engine cost will continue to rise.
- Throttling loss lowers the efficiency - To control an SI engine, the air allowed into the engine is restricted using a throttling plate.
- The engine is constantly fighting to draw air past the throttle, which expends energy.
- Friction loss due to many moving parts - The SI engine is very complex and has many moving parts. The losses through bearing friction and sliding friction further reduce the efficiency of the engine.
- Limited compression ratio lowers efficiency - Because the fuel is already mixed with the air during compression, it will auto-ignite (undesirable in a gasoline engine) if the compression ratio is too high. The compression ratio of the engine is limited by the octane rating of the engine.

5. Emission Control System

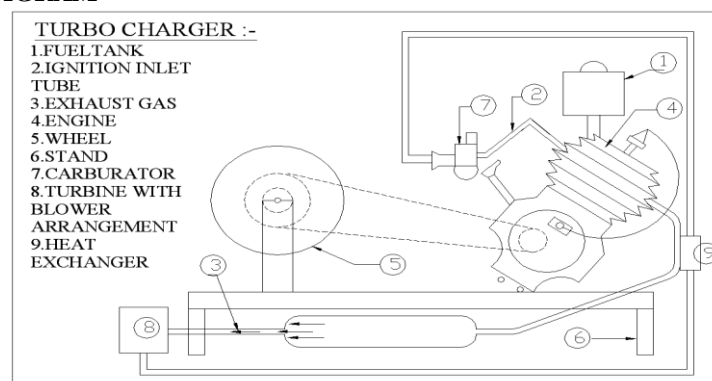
Automotive emissions contribute significantly to urban air quality problems. HEVs can reduce this contribution significantly through increased fuel economy, use of alternative fuels, and improved power unit and after treatment technology. A well-tuned spark ignition engine produces relatively low emissions. Significant emissions occur when the vehicle is started and warming up. During this time the engine must be choked to run properly. This creates excess unburned fuel in the exhaust, which leads to hydrocarbon and carbon monoxide emissions. During normal driving, emissions are relatively low because the air-to-fuel mixture is precisely controlled, allowing the catalytic converter to effectively reduce emissions. The diesel engine emissions are primarily nitrogen oxides (NO_x) and particulate matter (PM). NO_x is produced because the engine is operated with a lean air-to-fuel mixture. The high compression ratio of a diesel engine (required because of compression ignition) creates much higher pressure and temperature in the combustion cylinder. This lean mixture and high temperature cause the higher level of NO_x production. At high engine loads, where more fuel is injected, some of the fuel burns incompletely leading to the black smoke (PM) characteristic of a diesel engine.

6. Specification Of Four Stroke Petrol Engine:

Type	: Four stroke
Cooling System	: Air Cooled
Bore/Stroke	: 50 x 50mm
Piston Displacement	: 98.2 cc
Compression Ratio	: 6.6: 1
Maximum Torque	: 0.98 kg-m at 5500 rpm

7. Experimental Setup

BLOCK DIAGRAM



8. Advantages

1. Efficiency of the vehicle is improved.
2. Small modification is done in the vehicle.
3. Fuel consumption is less when compared to ordinary vehicle.
4. Less pollution.
5. Emissions are controlled in the Engine.

9. Applications

1. Automobile application.

10. Disadvantages

1. Additional cost is required.
2. Additional space is required to install this arrangement in vehicles.

11. Future Scope

1. The Efficiency of the engine can be increased .
2. The Emissions from the engine can be controlled.
3. Fuel consumption is less when compared to ordinary vehicle.
4. Experimental Analysis of the Engine with Turbo charger.
5. A prototype of the turbocharger could be fabricated by suitable processes and tested by properly installing it to a two-wheeler.

12. Conclusion

We have designed and fabricated a prototype of the Turbocharger was implemented in Two-wheeler, In which the efficiency of the Engine can be increased. Thus we have developed a method to increase the efficiency of the engine and at the same time to control the Emissions from the engine. The experimental setup of block diagram is shows the arrangement of turbocharger in two-wheeler. This type of engine will be more efficient than existing engines.

References

- [1] Achten, P. A. J. 1994. .A Review of Free Piston Engine Concepts,. SAE Paper 941776.
- [2] Alperstein, M., Swim, W. B. and Schweitzer, P. H. 1958. .Fumigation Kills Smoke . Improves Diesel Performance,. SAE Transactions, vol. 66, pp.574 . 588.
- [3] Baruah, P. C. 1988. .A Free Piston Engine Hydraulic Pump for an Automotive Propulsion System,. SAE Paper 880658.
- [4] Braun, A. T. and Schweitzer, P. H. 1973. .The Braun Linear Engine,. SAE Paper 730185.
- [5] Caris, D. F. and Nelson, E. E. 1959. .A New Look at High Compression Engines,. SAE Transactions, vol. 67, pp. 112-124.
- [6] Christensen, M., Johansson, B. and Einewall, P. 1997. .Homogeneous Charge Compression Ignition (HCCI) Using Isooctane, Ethanol, and Natural Gas . A Comparison With Spark Ignition Operation,. SAE Paper 972874.
- [7] Christensen, M., Johansson, B., Amneus, P. and Mauss, F. 1998. .Supercharged Homogeneous Charge Compression Ignition,. SAE Paper 980787.
- [8] Das, L. M. 1990. .Hydrogen Engines: A View of the Past and a Look Into the Future,. International Journal of Hydrogen Energy, vol. 15, no. 6, pp. 425 . 443.
- [9] Edson, M. H. 1964. .The Influence of Compression Ratio and Dissociation on Ideal Otto Cycle Engine Thermal Efficiency,. Digital Calculations of Engine Cycles, SAE Prog. in Technology, vol. 7, pp. 49-64.
- [10] Karim, G.A. and Watson, H.C. 1971. .Experimental and Computational Considerations of the Compression Ignition of Homogeneous Fuel-Oxidant Mixtures,. SAE Paper 710133.

Mining Association Rules From Time Series Data Using Hybrid Approaches

Hima Suresh¹, Dr. Kumudha Raimond²

¹ PG Scholar, Karunya University,

² Professor, Karunya University

Abstract:

Due to the frequent appearance of time series data in various fields, it has always been an essential and interesting research field. A time series analysis involves the methods for analyzing time series data, in order to mine meaningful and other relevant characteristics of the data. In most cases, time series data are quantitative values, so to come up with an intellectually appealing data mining algorithm to deal with quantitative type of data presents a biggest challenge to researchers in this field. In this paper, an extended Fuzzy Frequent Pattern (FP) growth approach is proposed and analyzed against the existing approach called Fuzzy Apriori (FA).

Keywords: Conditional Pattern Base, Fuzzy Apriori, Frequent Pattern, Fuzzy Logic, Genetic Algorithm, Neural Network and Frequent Pattern tree.

1. Introduction

Time series is defined as a series of well defined data values of a variable at successive time interval. The applications of time series includes FP analysis, predictions etc. FP analysis in time series data has become one of the most vital parts of data mining tasks and has attracted extreme interest among the researchers. Many approaches are available to examine time series data such as the Genetic Algorithm (GA), statistical methods etc. But the outputs of these approaches are difficult to understand/interpret the quantitative results. Apriori is the classic algorithm of association rules which determine the number of frequent items proposed by Agrawal et. al [6]. But uncertain time series are difficult to be dealt with this approach. So the fuzzy sets are used, in order to handle uncertain time series data. Fuzzy sets are the sets containing degrees of membership. Fuzzy set theory was introduced by L.A.Zadeh et. al [1] and this approach was followed by Hong et. al [2], [3], [4] and proposed several fuzzy algorithms to extract quantitative data and to mine meaningful association rules. The fuzzy mining algorithm integrates the concept of Apriori algorithm as well as fuzzy concepts.

However, in the Apriori algorithm, candidate generation suffers from significant costs such as: it may need to generate a huge number of candidate sets as well as it needs to scan the database repeatedly and to check a large set of candidates using pattern matching. This would be a tedious workload to go over each transaction in the database to determine the support value of candidate item sets. The approach to mine complete set of frequent item sets without candidate generation is one of the important motivations and also to generate efficient and scalable method for mining both long and short frequent patterns. An approach based on FP-Growth to find fuzzy association rules is proposed by Papadimitriou et. al [5]. In this approach each value in the transactions are transferred into two corresponding fuzzy regions. A support value is set and those fuzzy regions in the transaction which doesn't meet or exceed the predefined support would be removed. Here only the frequent fuzzy 1-itemsets obtained from each transaction are used for extracting. The expression of the fuzzy items with more fuzzy regions is successive. No fuzzy operation is used to combine the regions together. However, this made the rules mined to be difficult to interpret. The proposed extended Fuzzy FP growth approach overcomes this limitation to a certain extend. In this paper, an extended FP growth approach has been proposed and evaluated against the existing approach FA. It is an interesting method used for mining frequent item sets. The remainder of this paper is organized as follow: Section 2 describes the related works. Section 3 presents the hybrid approach using FA technique. Section 4 presents fuzzy FP-growth approach. Section 5 describes the experimental results. Finally, conclusion is discussed in Section 6.

2. Related Works

In this section some related concepts and algorithms are discussed such as: Apriori algorithm, FP-growth algorithm and Fuzzy set theory.

A. Apriori algorithm

The classic algorithm for mining frequent item sets and for learning association rule over the transactional database was proposed as Apriori algorithm by Agrawal et. al [6]. The algorithm involves two steps. Firstly, it find out the frequent item sets which exceeds or satisfies the minimum support. Secondly, the

rules are generated which satisfies the minimum confidence value. In this algorithmic method, the database is scanned repeatedly in order to generate all frequent item sets. It would be costly to go over each transaction and to count the support for each candidate item set. Also this approach generates huge number of candidate sets.

B. Frequent Pattern –Growth algorithm

One of the interesting methods to extract frequent item sets is FP-Growth algorithmic method and this is proposed by Han et. al [3]. The proposed algorithm does not require the candidate generations. The extraction of frequent patterns using Apriori is not efficient since it requires the repeated scanning of database and may need to generate large candidate item sets. In order to overcome this, an extended FP-Growth algorithm is used. The Approach involves several steps: First it scans the database to obtain all items with their corresponding support count. The items which exceed or satisfy the predefined minimum support are selected as the frequent 1-itemsets. Next step is to arrange the frequent 1-itemsets according to the decreasing order of their support count. Finally, the database is scanned again to construct the FP tree. All transactions are processed bottom up one by one and after processing all the transactions, a complete FP tree is constructed. Once the tree is constructed, FP-Growth procedure is executed to obtain all frequent item sets. FP growth generates the frequent patterns directly from the FP tree instead of candidate generation (C.W. Lin et.al [8]). For each frequent item, a conditional FP tree would be generated and the corresponding frequent item sets are derived from the same.

C. Fuzzy set theory

The word fuzzy means vagueness. Fuzzy sets have been introduced by Lotif A. Zadeh [1]. It is actually an extension of the classic set theory which defines the set membership as possibility distribution.

The rule for the fuzzy set theory can be expressed as:

$$f: [0, 1]^X = [0, 1] \quad (1)$$

Here “x” number of possibilities may occur.

A logic based on the truth values such as “true” and “false” would be sometimes inadequate while describing the human reasoning. Fuzzy logic uses the entire interval between 0 (false) and 1(true) for describing human reasoning.

3. Fuzzy Apriori Approach

The FA approach integrates the concept of Fuzzy as well as Apriori algorithm. The architecture for the FA approach implemented by C.H.Chen.et al [9] is shown in fig 1.

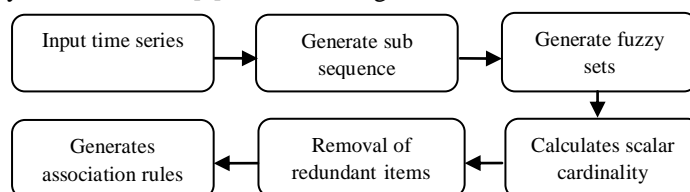


Fig 1: Architectural diagram of FA approach

The architecture describes the procedures for generating rules using FA algorithm. First, the time series data has been taken as input and from the given time series data, the subsequences of any length according to the sliding window size are generated. After the subsequence generation, each data point of the subsequences is transformed into fuzzy set. The total count or scalar cardinality of the corresponding fuzzy set based on the membership function is obtained. Frequent candidate sets are generated based on this support value which exceeds or satisfies the predefined support value. Pruning processes has been applied to filter away irrelevant large candidate sets. Finally the association rules are generated.

4. Fuzzy Frequent Pattern Growth Approach

The proposed approach uses the concept of fuzzy set and FP-growth approach to generate the frequent item sets without any candidate generation. The architecture for the proposed fuzzy FP-growth approach for time series data is shown in fig 2.

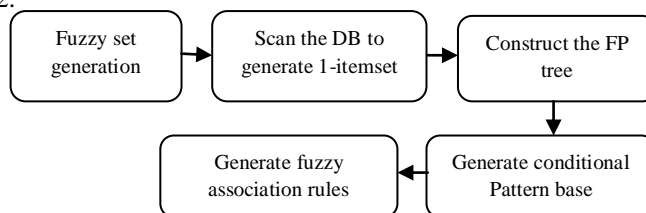


Fig 2: Architectural diagram of Fuzzy FP-growth approach

The approach uses the transformed fuzzy set for generating frequent patterns. It involves different phases. First step is to construct FP-tree from a database and from the resulting FP-tree, frequent patterns are generated. FP tree construction involves several steps such as: Scanning the databases to generate 1-itemset then rescanning to establish FP tree. Next generating conditional pattern base and corresponding conditional FP tree respectively. Finally fuzzy association rules are generated as proposed by C.W. Lin et. al [8].

5. Experimental Analysis

The Hybrid approach using both fuzzy concept and apriori algorithm is an efficient method for handling time series data to find linguistic association rules proposed by C.H. Chen et. al [9], A.M Palacios et. al [10]. Home price time series data over the years from 1999 to 2012 period has been used for analyzing the performance of the existing FA approach against the proposed Fuzzy FP growth approach [16]. The home price time series used for analyzing these two hybrid approaches are shown in table1.

Table 1: Home price time series data used as input

Years	Home price	Years	Home price
1999	127	2006	124
2000	129	2007	118
2001	132	2008	121
2002	130	2009	120
2003	126	2010	115
2004	132	2011	113
2005	129	2012	119

A. FA Method Analysis

The time series data is first transformed into subsequences according to the predefined window size, which could be of any length. Here in this example, window size is set as 5. So the total subsequence transactions will be 10 (T1, T2....T10) according to the formula (total length of time series – window size + 1). The transactions of subsequences generated are shown in table 2.

Table 2: Transaction of subsequences

TID	Transaction	TID	Transaction
T1	127,129,132,130,126	T6	132,129,124,118,121
T2	129,132,130,126,132	T7	129,124,118,121,120
T3	132,130,126,132,129	T8	124,118,121,120,115
T4	130,126,132,129,124	T9	118,121,120,115,113
T5	126,132,129,124,118	T10	121,120,115,113,119

After transforming the time series data into subsequences, the data points in each subsequence are converted to fuzzy values according to predefined membership function. The membership values used are Low, Middle and High and is used for the transformation of fuzzy sets from the given time series. The representation of membership function is given in fig 3.

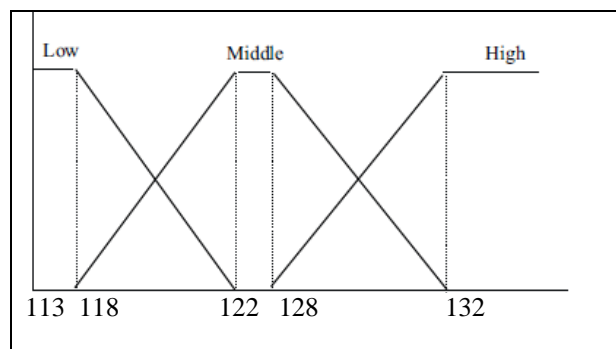


Fig 3: Membership function

The fuzzy values of each subsequence are shown in table 3. Each data point (A1, A2 ...An) in the transaction each subsequence will take the value of low (L), middle (M) and high (H).

Table 3: Fuzzy set transformed from time series

T	A1 L	A1 M	A1 H	A2 L	A2 M	A2 H	A3 L	A3 M	A3 H	A4 L	A4 M	A4 H	A5 L	A5 M	A5 H
T1	0	1	0	0	0.6 7	0.3 3	0	0	1	0	0	0	0	1	0
T2	0	0.6 7	0.3 3	0	0	1	0	0	0	0	1	0	0	0	1
T3	0	0	1	0	0	0	0	1	0	0	0	1	0	0.6 7	0.33
T4	0	0	0	0	1	0	0	0	1	0	0.6 7	0.3 3	0	1	0
T5	0	1	0	0	0	1	0	0.6 7	0.3 3	0	1	0	1	0	0
T6	0	0	1	0	0.6 7	0.3 3	0	1	0	1	0	0	0.6 7	0.3 3	0
T7	0	0.6 7	0.3 3	0	1	0	1	0	0	0.6 7	0.3 3	0	0.6 7	0.3 3	0
T8	0	1	0	1	0	0	0.6 7	0.3 3	0	0.6 7	0.3 3	0	1	0	0
T9	1	0	0	0.6 7	0.3 3	0	0.6 7	0.3 3	0	1	0	0	1	0	0
T10	0.6 7	0.3 3	0	0.6 7	0.3 3	0	1	0	0	1	0	0	0.6 7	0.3 3	0
Total	1.6 7	4.6 7	2.6 6	2.3 4	4	2.6 6	3.3 4	3.3 3	2.3 3	4.3 4	3.3 3	1.3 3	5.0 1	3.6 6	1.33

The total count or scalar cardinality has been calculated from the fuzzy set generated and is calculated as its count value. After the calculation, fuzzy items generated are collected as the 1-itemset [13], [14], [15]. The total count is then checked against the support value, which is predefined. Here in this example, support value is set as 30%. The item set whose values are greater than or equal to 30% has been taken and are the following: A1.Middle, A2.Middle, A3.Low, A3.Middle, A4.Low, A4.Middle, A5.Low, and A5.Middle. The 1-itemsets are represented in table 4:

Table 4: The 1-itemset generated with total count

1-Itemset	Total	1-Itemset	Total	1-Itemset	Total
A1.Middle	0.467	A2.Middle	0.4	A3.Low	0.334
A3.Middle	0.333	A4.Low	0.434	A4.Middle	0.333
A5.Low	0.501	A5.Middle	0.366	-	-

After the generation of 1-itemsets, corresponding 2-itemsets are obtained. The fuzzy items with the same attribute A_i are not put in to 2-itemset collection. The resulting 2-itemsets generated are shown in the table 5.

Table 5: The resulting 2-itemset satisfy the support

2-itemset	Total
A1.Middle \cap A5.Low	3
A3.Low \cap A4.Low	3.01
A4.Low \cap A5.Low	3.68

The association rules thus generated from the 2-itemsets with corresponding confidence values are shown in table 6:

Table 6: The Association rules with confidence values

Final Rule	Confidence
A1.Middle, A5.Low	0.64
A3.Low, A4.Low	0.9
A4.Low, A5.Low	0.84

The confidence value of the above association rules are calculated using the formula given below:

$$Confidence = \frac{Support(item.a \cup item.b)}{Support (item.a)} \quad (2)$$

The confidence value of rule is then compared with the predefined confidence threshold. The rule obtained here means that “if the value of a data point is low at the third time units then the value of a data point after fourth time units will also be low with a high probability”. Though the rule generated is useful to understand the corresponding time series data, the amount of effort required to generate the rules are more as candidate generation is more costly in time. In order to avoid the limitations of FA, the Fuzzy FP-Growth approach has been implemented and evaluated against FA approach.

B. FP-Growth Method Analysis

The Fuzzy FP-Growth approach is analyzed using the same home price time series data. The case study results of fuzzy FP growth approach are explained in table 7:

Table 7: Transactions and corresponding items

TID	Items
T1	(A1:127)(A2:129)(A3:132)(A4:130)(A5:126)
T2	(A1:129)(A2:132)(A3:130)(A4:126)(A5:132)
T3	(A1:132)(A2:130)(A3:126)(A4:132)(A5:129)
T4	(A1:130)(A2:126)(A3:132)(A4:129)(A5:124)
T5	(A1:126)(A2:132)(A3:129)(A4:124)(A5:118)
T6	(A1:132)(A2:129)(A3:124)(A4:118)(A5:121)
T7	(A1:129)(A2:124)(A3:118)(A4:121)(A5:120)
T8	(A1:124)(A2:118)(A3:121)(A4:120)(A5:115)
T9	(A1:118)(A2:121)(A3:120)(A4:115)(A5:113)
T10	(A1:121)(A2:120)(A3:115)(A4:113)(A5:119)

Each value of the transaction items are transformed in to fuzzy sets using this membership function. The fuzzy set transformed from the data is represented in table 8:

Table 8: Fuzzy sets generated from home price time series data

Tid	Items
T1	(1/A1Middle)(0.67/A2Middle+0.33/A2High)(1/A3High)(1/A5Middle)
T2	(0.67/A1Middle+0.33/A1High)(1/A2High) (1/A4Middle)(1/A5High)
T3	(1/A1High)(1/A3Middle)(1/A4High) (0.67/A5Middle+0.33/A5High)
T4	(1/A2Middle)(1/A3High)(0.67/A4Middle+0.33/A4High) (1/A5Middle)
T5	(1/A1Middle)(1/A2High)(0.67/A3Middle+0.33/A3High)(1/A4Middle)(1/A5Low)
T6	(1/A1High)(0.67/A2Middle+0.33/A2High) (1/A3Middle)(1/A4Low) (0.67/A5Low+0.33/A5Middle)
T7	(0.67/A1Middle+0.33/A1High)(1/A2Middle)(1/A3Low)(0.67/A4Low+0.33/A4Middle)(0.67/A5Low+ 0.33/A5Middle)
T8	(1/A1Middle)(1/A2Low)(0.67/A3Low+0.33/A3Middle)(0.67/A4Low+0.33/A4Middle)(1/A5Low)
T9	(1/A1Low)(0.67/A2Low+0.33/A2Middle)(0.67/A3Low+0.33/A3Middle)(1/A4Low)(1/A5Low)
T10	(0.67/A1Low+0.33/A1Middle)(0.67/A2Low+0.33/A2Middle)(1/A3Low)(1/A4Low)(0.67/A5Low+0.33/A5Middle)

The counts of all fuzzy regions are calculated. For example, in the case of A1.Low the total count will be 1+0.67=1.67. Likewise the steps are repeated for other regions. The corresponding results are shown in table 9.

Table 9: The scalar cardinality of each fuzzy region

Item	Count	Item	Count
A1.Low	1.67	A3.High	2.33
A1.Middle	4.67	A4.Low	4.34
A1.High	2.66	A4.Middle	3.33
A2.Low	2.34	A4.High	1.33
A2.Middle	2.66	A5.Low	5.01
A2.High	4	A5.Middle	3.66
A3.Low	3.34	A5.High	1.33
A3.Middle	3.33	-	-

The fuzzy region with the maximum count among the three possible regions for each item is selected. Take A1 as an example. Its count is 1.67 for low, 4.67 for middle and 2.66 for high. Since the count for middle is the maximum among three counts, the region middle is thus used to represent item A1 in the later mining process. This step would be repeated for the other items. The count of any region selected is checked against with the predefined minimum support value. Here support value assumed as 30%. That means $(10 \times 30\% = 3.0)$. The table 10 shows the set of frequent fuzzy region. Here every region satisfies the support 30%.

Table10: Frequent Fuzzy regions and count

Frequent fuzzy regions	Count
A1. Middle	4.67
A2.Middle	4
A3.Low	3.34
A4.Low	4.34
A5.Low	5.01

After finding the regions with higher counts, the header table is arranged based on the decreasing order of the support count. It is shown in table 11:

Table 11: The header table of the regions

Frequent fuzzy regions	Count
A5.Low	5.01
A1.Middle	4.67
A4.Low	4.34
A2.Middle	4
A3.Low	3.34

The fuzzy regions which are not in the header table are removed from each transaction [11]. The remaining fuzzy regions in each transaction are then sorted according to the membership values in a descending order. This is shown in table 12.

Table 12: The transactions transformed with the fuzzy regions

Tid	Frequent fuzzy region
T1	(1/A1Middle)(0.67/A2Middle)
T2	(0.67/A1Middle)
T3	0
T4	(1/A2Middle)
T5	(1/A1Middle)(1/A5Low)
T6	(0.67/A2Middle)(1/A4Low)(0.67/A5Low)
T7	(0.67/A1Middle)(1/A2Middle)(0.67/A4Low)(0.67/A5Low)
T8	(1/A1Middle)(0.67/A4Low)(1/A5Low)
T9	(0.33/A2Middle)(1/A4Low)(1/A5Low)
T10	(0.33/A1Middle)(0.33/A2Middle)(1/A4Low)(0.67/A5Low)

After this step, the transactions with only the sorted frequent fuzzy regions selected which are shown in table 13:

Table 13: The transactions with sorted the fuzzy regions

TID	Frequent fuzzy region
T1	(1/A1Middle)(0.67/A2Middle)
T2	(0.67/A1Middle)
T3	0
T4	(1/A2Middle)
T5	(1/A1Middle)(1/A5Low)
T6	(1/A4Low)(0.67/A2Middle)(0.67/A5Low)
T7	(1/A2Middle)(1/A3Low)(0.67/A1Middle)(0.67/A4Low)(0.67/A5Low)
T8	(1/A1Middle)(1/A5Low)(0.67/A3Low)(0.67/A4Low)
T9	(1/A4Low)(1/A5Low)(0.33/A2Middle)(0.67/A3Low)
T10	(1/A4Low)(1/A3Low)(0.67/A5Low)(0.33/A1Middle)(0.33/A2Middle)

All transactions up to 10 are inserted in the fuzzy FP tree [12]. In the FP tree representation, header table is shown in the left side and it contains the frequent Fuzzy Regions (FR) and their supporting count. The final fuzzy FP tree is shown in figure 4.

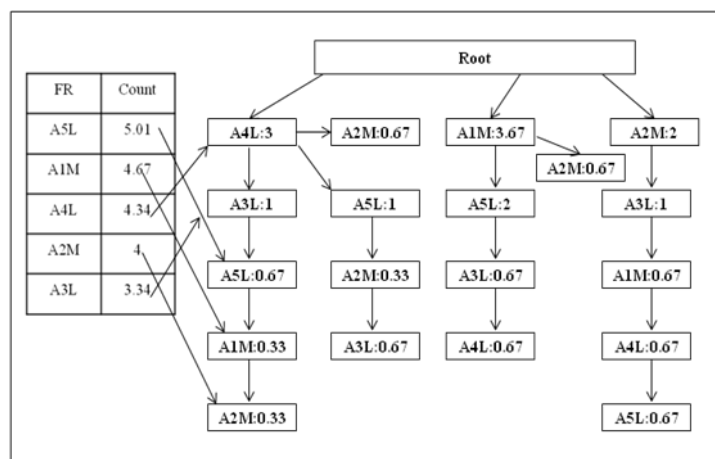


Fig 4: The Complete FP tree

While processing the items from bottom of the header table, first item would be **A3L**: the traversal from which **A3L** exist are:

- 1) (A4L:3)(A3L:1)
- 2) (A4L:3)(A5L:1)(A2M:0.33)(A3L:0.67)
- 3) (A1M:3.67)(A5L:2)(A3L:0.67)
- 4) (A2M:2)(A3L:1)

Table 14: The frequent item sets with A3L

1-Item	2-Item	3-Item
A5L:5.01	A4L, A3L:1.67	A1M, A5L, A3L:0.67
A1M:4.67	A5L, A3L:1.34	A4L, A5L, A3L:0.67
A4L:4.34	A2M, A3L:1.33	A5L, A2M, A3L:0.33
A2M:4	A1M, A3L:0.67	-
A3L:3.34	-	-

Here in this example taking the intersection (minimum) of items to obtain 2-itemset and 3-itemsets. For eg: A4L:3 and A3L:1 means1 (taking the smaller value or minimum operator) and then if the same transaction occurs again, it would be incremented with the corresponding value. Likewise all regions in the header table should be processed and frequent item sets are generated. On processing the items bottom up from the header table, corresponding item sets are obtained. Same item sets from all transactions are taken together and their count is evaluated using the intersection (minimum operator). From the corresponding item sets of all transactions, those exceed or meet the support count are chosen as the rules. The rules obtained are shown in table 15 and are similar to the rules generated by FA approach.

Table 15: The final rules generated

Final Rules	Count
A1.Middle,A5.Low	3
A3.Low, A4.Low	3
A4.Low, A5.Low	3.01

The two hybrid approaches are implemented in VB.NET at a personal computer with Intel Core i3, 2.10 GHZ and 4GB RAM. The data set used is the home price time series data over the period of 1999 to 2012. The sliding window size is predefined as 5. The experimental result shows the FA approach require more number of scans for each transaction compared to the proposed approach. In the case of FA approach, for 20 support value it requires 1001 total number of scans. Likewise for 25 support value, it requires a total scan of 539 and for 30, it requires 275 total scans. Whereas FP approach requires only 11 times total number of scans

for each transaction. This is one of the major advantages of the proposed approach over FA approach. The graphical representation of number of scans required for both the approaches shown in the fig 5.

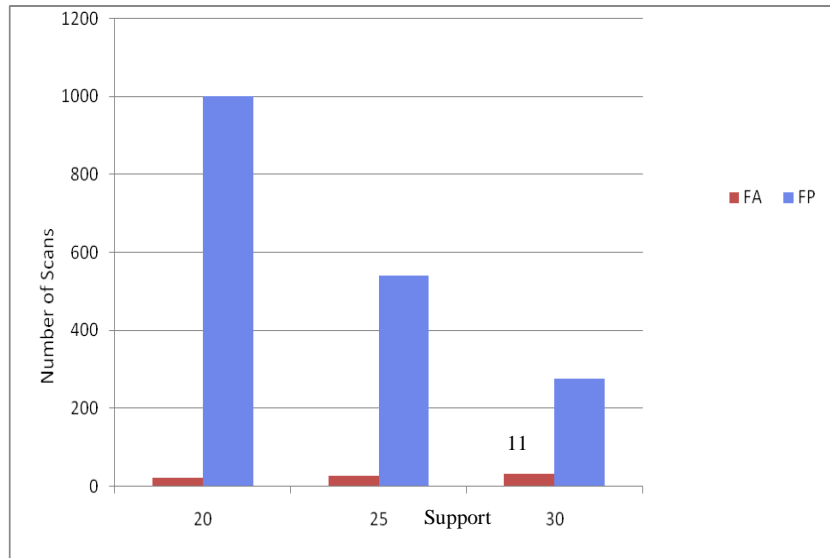


Fig 5: The graphical representation of number of scans

The execution time required for the proposed approach is less than FA approach. This is another benefit. The graph showing the execution time required for both the approaches are shown in fig 6.

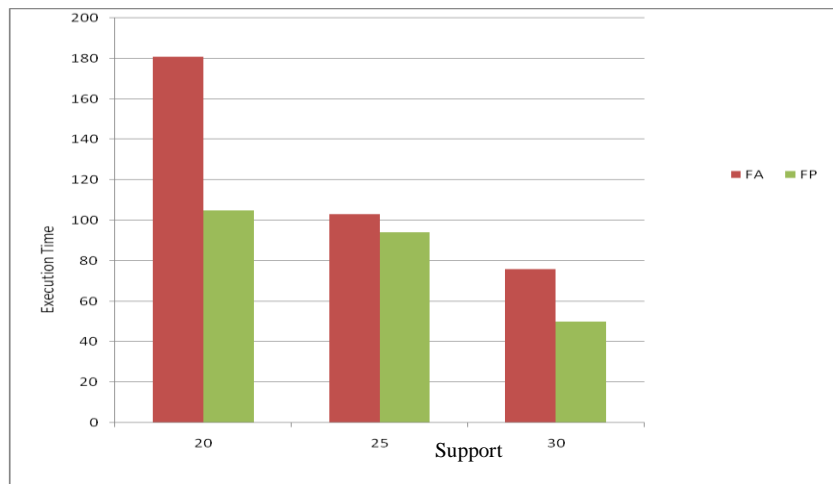


Fig 6: The graphical representation showing execution time

6. Conclusion

The paper discusses about two different hybrid approaches. The main aim of this analysis is to explore highly efficient method for generating non redundant and relevant rules. This technical report provides association rule mining on the existing hybrid approach and the proposed one. In this work, an efficient FP-Growth approach has been used to mine the complete set of frequent item sets without candidate generation. This approach helps to overcome the problems of FA, which requires a need to repeated scanning of the database and checking large set of candidates by pattern matching. The analytical study of this framework shows that it is efficient and scalable for extracting both small and long frequent patterns. The Fuzzy FP-Growth approach transforms the problem of finding long frequent patterns to search for shorter ones recursively and then concatenate the corresponding suffix. It uses the least frequent items as a suffix and there by offering good selectivity. The approach reduces the search costs to a great extend. FP growth approach provides less execution time compared to FA approach.

References

- [1] L.A. Zadeh, Fuzzy Sets. *Information and Control*, 8:338- 353, 1965.
- [2] T.P. Hong, C.S. Kuo, S.C. Chi, Mining association rules from quantitative data. *Intelligent Data Analysis*, no.3 (5), pages338- 353, 1965.
- [3] T.P. Hong, C.S. Kuo, S.C. Chi, Trade-off between Time Complexity and Number of Rules for Fuzzy Mining from Quantitative Data, *International Journal of Uncertainty: Fuzziness and Knowledge-based Systems*, 9 (5), pages338- 353, 2001.
- [4] Y.C. Lee, T.P. Hong, W.Y. Lin, Mining Fuzzy Association Rules with Multiple Minimum Supports using Maximum Constraints , Number of Rules. *Lecture Notes in Computer Science*. 3214: pages1283-1290, 2004.
- [5] S. Papadimitriou, S. Mavroudi, The Frequent Fuzzy Pattern Tree, Microsoft Corporation. Example Database Food Mart Of Microsoft Analysis Services: In the 19th WSEAS international conference on computers, 2005.
- [6] R. Agrawal, R. Srikant , Fast Algorithm for Mining Association Rules. *The International Conference on Very Large Data Bases*, pages487- 499, 1994.
- [7] S.M. Chen, J.R. Hwang, Temperature Prediction using Fuzzy Time Series. *IEEE Transactions on Systems, Man, and Cybernetics B: Cybernetics*, 30 (2), pages263- 275, 2000.
- [8] C.H. Lin, T.P. Hong, W.Y. Lu, Linguistic Data Mining with Fuzzy FP-trees, *Expert systems with applications*, 37, pages4560- 4567, 2010.
- [9] C.H. Chen, T.P. Hong, V.S. Tseng, Fuzzy data mining for time-series data, *Applied Soft Computing*, 12: pages536- 542, 2012.
- [10] A.M. Palacios , M.J. Gacto, J. Alcalá-Fdez, Mining Fuzzy Association Rules from Low Quality Data. *Soft Computing- A Fusion of Foundations, Methodologies and Applications*, Vol 16:pages883- 901, 2012.
- [11] J. Han, J. Pie, Y. Yin, Mining frequent patterns without candidate generation: In the ACM SIGMOD International Conference on Management of Data, pages1- 12, 2000.
- [12] K. Suriya Prabha, R Lawrance, Mining Fuzzy Frequent Item set using Compact Frequent Pattern Tree Algorithm. *International Conference On Computing and Control Engineering*, April 2012.
- [13] T.P. Hong, J.B. Chen, Finding Relevant Attributes and Membership Functions. *Fuzzy Sets and Systems- A Fusion of Foundations*, Vol 103, pages389- 404, 1999.
- [14] T.P. Hong, C.S. Kuo, S.L. Wang, A Fuzzy Apriori Tid Mining Algorithm with Reduced Computational Time, *Applied Soft Computing*, Vol 5, pages1-10, 2004.
- [15] T. Hua, S.Y. Sung, H.Xiong, Q. Fud, Discovery of Maximum Length Frequent Item sets, *Information Science: An International Journal*, Vol (178), Issue 1, 2008.
- [16] H. Suresh, K. Raimond, Analysis of Time Series Rule Extraction Techniques, *IOSR Journal of Computer Engineering (IOSR-JCE)*, Vol (8), Issue 5, pages22-27, 2013.

A Study of Influence of Electrochemical Process Parameters on the Material Removal Rate and Surface Roughness of SS AISI 304

¹S. S. Uttarwar, ²Dr. I. K. Chopde

¹Department of Mechanical Engineering, Priyadarshini College of Engineering, Nagpur, Maharashtra, India

²Department of Mechanical Engineering, Visvesvaraya National Institute of Technology, Nagpur
Maharashtra, India

Abstract

The machining of complex shaped designs was difficult earlier, but with the advent of the new machining processes incorporating in it chemical, electrical & mechanical processes, manufacturing has redefined itself. This paper presents results of the Electrochemical Machining (ECM) process, which was used to machine the SS AISI 304. Specifically, the Material Removal Rate (MRR) and Surface Roughness (SR) as a function of ECM were determined. The experimental work was based on the Taguchi approach of experimentation and table L₃₂ was used. Furthermore, a theoretical and computational model is presented to illustrate the influence parameter variations in results. The influence of independent parameters such as time of electrolysis, voltage, current, concentration of electrolyte, feed rate and pressure on output parameters material removal rate and SR is studied in this work. The results indicated that MRR was remarkably affected by variation in current and Surface Roughness decreased with increase in current. Hence, it was apparent that irregular MRR was more likely to occur at high currents. The results showed that MRR increased with increasing electrical voltage, molar concentration of electrolyte, time of electrolysis and feed rate. However, the time of electrolysis was the most influential parameter on the produced surface finish.

Keywords: Electrochemical machining; Material removal rate; Time; Feed rate; electrolyte concentration, Anova, Percentage error.

1. Introduction

Electrochemical machining (ECM), a nontraditional process for machining^[1,2] has been recognized now a days for performing numerous machining operations.^[4] Earlier the machining of complex shaped designs was difficult, however, with the advent of the new machining processes that incorporate in it chemical, electrical and mechanical processes, manufacturing process has redefined itself.^[3] New materials which have high strength to weight ratio, heat resistance, hardness and are also complex shapes needing greater accuracy demand development of newer type of machining process. The new and improved machining processes are often referred to as unconventional machining processes. For e.g. ECM removes material without heat. Almost all types of metals can be machined by this process. In today's high precision and time sensitive scenario, ECM has wide scope for applications.^[5] More specifically, ECM is a process based on the controlled anodic dissolution of the work piece anode,^[6] with the tool as the cathode, in an electrolytic solution.^[11] The electrolyte flows between the electrodes and carries away the dissolved metal.

Since the first introduction of ECM in 1929 by Gusseff, its industrial applications have been extended to electrochemical drilling, electrochemical deburring, electrochemical grinding and electrochemical polishing.^[13] More specifically, ECM was found more advantageous for high-strength alloys. Today, ECM has been increasingly recognized for its potential for machining,^[7] while the precision of the machined profile is a concern of its application.^[9,10] During the ECM process, electrical current passes through an electrolyte solution between a cathode tool and an anode work piece.

The work piece is eroded in accordance with Faraday's law of electrolysis.^[12] ECM processes find wide applicability in areas such as aerospace and electronic industries for shaping and finishing operations of a variety of parts that are a few microns in diameter.^[13] Furthermore, it has been reported that the accuracy of machining can be improved by the use of pulsed electrical current and controlling various process parameters. Amongst the often considered parameters are electrolyte concentration, voltage, current and inter electrode gap.^[14] Though there is a possibility of improving the precision of work, the dependency of accuracy on numerous parameters demand that a thorough investigation should be carried out to ascertain the causality to different parameters. In the backdrop of above information, this study was carried out to assess the best conditions (with respect to different process parameters) for improving the accuracy of ECM process. In this paper the authors propose an analytical model of electrochemical erosion to predict the finishing machined work

piece. The study envisaged an empirical data obtained from the experiments carried out to assess effect of operating parameter variations on material removal rate (MRR) and surface roughness (SR) for Stainless steel (AISI 202).

2. ECM Setup

Fig 1 and 2 shows the schematic set up of ECM in which two electrodes were placed at a distance of about 0.1 to 1mm and immersed in an electrolyte, which was a solution of sodium chloride.^[15] When an electrical potential (of about 20V) is applied between the electrodes, the ions existing in the electrolyte migrate toward the electrodes^[15].

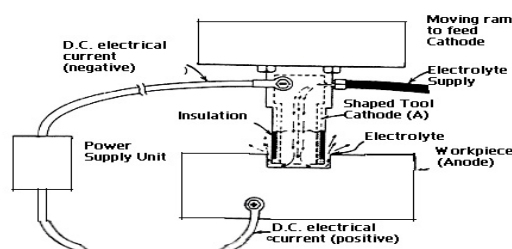


Fig 1. ECM Setup

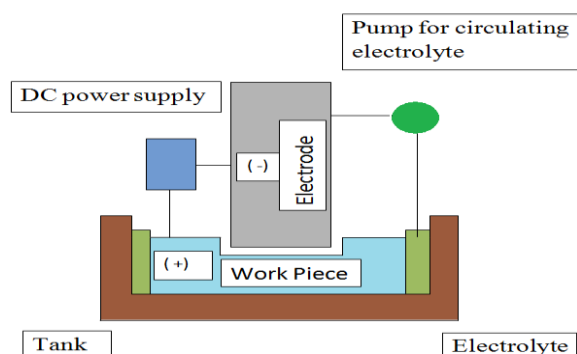


Fig 2. Block diagram of ECM setup

3. ECM Process Characteristics

3.1 Material removal rate:

The MRR primarily depends on the feed rates. The feed rate determines the amount of current that can pass through the work and the tool. As the tool approaches the work piece the length of the conductive current path decreases and the magnitude of current increases. This continues until the current is just sufficient to remove the metal at a rate corresponding to the rate of tool advance. Thereafter a stable cut is made available with a fixed spacing between the work and the tool, which is termed as the equilibrium-machining gap. If the tool feed rate is reduced, the tool advance will momentarily lag behind, increasing the gap and thus resulting in a reduction of current. This happens until a stable gap is once again established. Thus, the feed rate is an important parameter, which was given due consideration in the experiment.

3.2 Accuracy

Under ideal conditions and with properly designed tooling, ECM is capable of holding tolerance of the order of .02 mm & less. Repeatability of the ECM process is also very good. This is largely due to the fact that the tool wear is virtually non-existent on a good machine; tolerance can be maintained on a production basis in the region of .02-.04 mm. As a general rule, the more complex the shape of the work, the more difficult is to hold tight tolerances and the greater is the attention required for developing a proper tooling and electrode shape.

3.3 Surface Finish

ECM under certain conditions can produce surface finishes of the order of 0.4mm. This can be obtained by the frontal cut or the rotation of the tool or the work. Hence care was taken to control the important variables affecting the surface finish are feed rate, voltage, electrolyte composition, pressure, current & flow.

4. Operating Parameters In ECM

The operating parameters which are within the control of the operator and which influence ECM process capabilities are as follows: ^{[14],[15]}

4.1 Voltage

The nature of applied power supply is of two types, DC (full wave rectified) and pulse DC. A full wave rectified DC supplies continuous voltage and a pulse generator is used to supply pulses of voltage with specific on-time and off-time. The MRR is proportional to the applied voltage. But, the experimental values were found to be varying non-linearly with voltage. This is mainly because of less dissolution efficiency in the low voltage zone as compared to the high voltage zone. ^[12] However continuous voltage supply is used for this experimentation work.

4.2 Feed Rate

Feed rate governs the gap between the tool (cathode) and the work piece (anode) it is important for metal removal in ECM. ^[6] It plays a major role for accuracy in shape generation and hence was constantly monitored.

4.3 Electrolyte and its concentration

ECM electrolyte is generally classified into two categories, passivity electrolyte containing oxidizing anions e.g. sodium nitrate and sodium chlorate, etc. and non-passivity electrolyte containing relatively aggressive anions such as sodium chloride. Passivity electrolytes are known to give better machining precision. This is due to their ability to form oxide films and evolve oxygen in the stray current region. From review of past research, in most of the investigations researchers recommended NaClO₃, NaNO₃, and NaCl solution with different concentration for ECM and hence, NaCl was used as an electrolyte in this experimentation with concentration of 125gm/lit and 150gm/lit.

4.4 Current

Current plays a vital role in ECM. The MRR is directly proportions to the current (i.e. MRR increases with increase in current). However, this increase can be observed up to a certain limit and exceeding current beyond this level negatively affects accuracy and finishing of work piece. Hence, care was taken to apply current in the desired way.

5. Experimental Setup

Fig 3 shows actual photograph of the experimental set up of ECM on which the experimentation process was carried out.



Fig 3. Experimental set up of ECM process

5.1 Tool and Work piece Material

The tool used in this study was made up of copper while the work-piece used in this study was made up of Stainless Steel SS 304. This work piece was selected for this study as it has wide applications in various fields. The chemical composition of the used work piece i.e. SS 304 are as follows

Sample	C (%)	Si (%)	Mn (%)	P (%)	S (%)	Cr (%)	Ni (%)	Cu (%)	Fe (%)
SS 202	0.023	0.447	1.16	0.038	0.016	18.31	7.99	1.05	Remaining

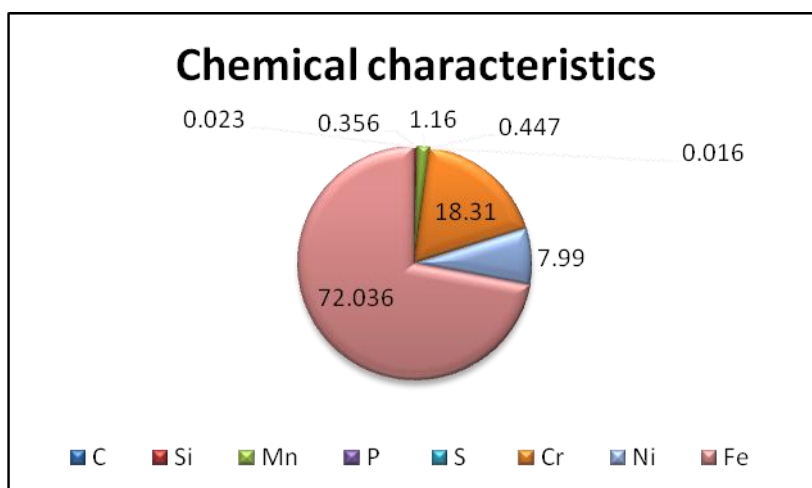


Fig 4. Chemical characteristics of work piece SS 304

5.2 Experimentation Work

An Orthogonal Array $L_{32}(2^1 \times 4^5)$ of Taguchi method was used for conducting the experimentation work. The results of dependent parameters (MRR and SR) with respect to all levels of independent parameters are shown in a following table.

Table 2 Values of Dependent and Independent Parameters (Orthogonal array L 32)

Run No.	Independent parameters						Dependent parameters	
	Electrolyte Conc. (gms/Ltr)	Voltage (V)	Current (Amp)	Feed (MM/min)	Electrolyte Flow (Ltrs/min)	Pressure (Kg/Cm ²)	MRR (mg/min)	SR (µm)
	E	B	A	0.1	C	F	G	H
1	125	10	100	0.2	4	3.4	5.277	4.074
2	125	10	125	0.3	5	3.6	5.224	3.788
3	125	10	150	0.4	6	3.7	5.259	3.775
4	125	10	175	0.1	7	3.8	6.380	5.591
5	125	14	100	0.2	5	3.6	4.430	3.626
6	125	14	125	0.3	4	3.4	5.586	3.306
7	125	14	150	0.4	7	3.8	5.161	3.491
8	125	14	175	0.2	6	3.7	4.136	3.304
9	125	18	100	0.1	6	3.8	4.705	3.677
10	125	18	125	0.4	7	3.7	5.859	3.603
11	125	18	150	0.3	4	3.6	6.056	5.099
12	125	18	175	0.2	5	3.4	4.811	4.474
13	125	22	100	0.1	7	3.7	4.497	4.013
14	125	22	125	0.4	6	3.8	5.365	3.573
15	125	22	150	0.3	5	3.4	5.086	3.760
16	125	22	175	0.4	4	3.6	4.789	3.458
17	150	10	100	0.3	4	3.8	5.612	4.299

18	150	10	125	0.2	5	3.7	4.922	3.362
19	150	10	150	0.1	6	3.6	5.373	3.510
20	150	10	175	0.4	7	3.4	5.343	3.259
21	150	14	100	0.3	5	3.7	6.703	6.402
22	150	14	125	0.2	4	3.8	4.514	3.268
23	150	14	150	0.1	7	3.4	6.705	5.971
24	150	14	175	0.3	6	3.6	5.468	3.713
25	150	18	100	0.4	6	3.4	5.144	3.149
26	150	18	125	0.1	7	3.6	4.657	3.602
27	150	18	150	0.2	4	3.7	5.439	4.612
28	150	18	175	0.3	5	3.8	6.754	4.474
29	150	22	100	0.4	7	3.6	4.772	3.947
30	150	22	125	0.1	6	3.4	4.540	3.530
31	150	22	150	0.2	5	3.8	5.362	3.589
32	150	22	175	0.3	4	3.7	3.607	3.270
Σ	4400	512	4400	0.4	176	112.2	165.044	124.566

5.3 Mathematical Model for MRR and SR

Using Regression Analysis Mathematical models were developed for MRR and SR with their indices. The six decision variables concerned for this model were Current, Voltage, feed rate, Pressure, Electrolyte concentration and flow of electrolyte.

6. Objectives

The various objectives under consideration for the formulation of model were

- a) Maximization of MRR and
- b) Improving SR (surface finish) and dimensional accuracy

6.1 Derived mathematical Models

Equation 1 and 2 are the mathematical models derived for calculation of MRR and SR.

$$\text{MRR} = \text{Constant} \times A^a \times B^b \times C^c \times D^d \times E^e \times F^f$$

Where a,b,c,d,e,f are the indices for current, voltage, electrolyte flow, feed rate, Electrolyte concentration and pressure . The formulated models are as follows

Mathematical Eqn for MRR is

$$\text{MRR} = 3.14695 A^{0.002050} B^{-0.01061875} C^{0.001225} D^{0.10975} E^{-0.00345} F^{-0.0104625}$$

--- Eqn 1

Mathematical Eqn for SR is

$$\text{SR} = 2.2425000 A^{0.0024500} B^{-0.0196875} C^{0.0212500} D^{0.0375000} E^{-0.0022500} F^{-0.0093750}$$

----- Eqn 2

From the Eqns. 1 and 2, it was evident that the MRR was positively influenced by the independent variables such as current, electrolyte flow and feed rate whereas negatively influenced by voltage, electrolyte concentration and pressure. Moreover, the SR was observed to be positively influenced by current, electrolyte flow, feed rate, and electrolyte concentration whereas it (SR) is negatively influenced by voltage and electrolyte concentration.

7. Comparison Of Practical V/S Theoretical Values Of MRR

A sample set of Comparison of Actual value of MRR calculated by formula and corresponding values derived by mathematical model is shown in Table 3 along with the calculated percentage error.

Table 3: Comparative assessment of the Practical v/s Theoretical values of MRR

Sr. No.	Values of Dependent Parameter (MRR)		Percentage Error
	By Mathematical Model	Actual Experimentation	
1	5.591386235	5.277	5.9577
2	4.994041391	5.224	-4.4020
3	4.671671187	5.259	-11.1681
4	4.458360504	6.380	-30.1197
5	5.636831741	4.430	27.2423
6	4.987908572	5.586	-10.7070

7.1 Comparison of Practical v/s Theoretical values of SR

A sample set of Comparison of Actual value of SR calculated by formula and corresponding values derived by mathematical model is shown in Table 4 with Percentage error.

Table 4: Comparative assessment of the Practical v/s Theoretical values of SR

Sr. No.	Values of Dependent Parameter (SR)		Percentage Error
	By Mathematical Model	Actual Experimentation	
1	3.367250843	4.074	-17.3478
2	3.374170425	3.788	8.8501
3	3.384412557	3.775	-10.3467
4	5.2312324	5.591	-6.4348
5	3.368413193	3.626	-7.1039
6	3.350383833	3.306	1.3425

8. Percentage Error

Percentage error graphs for difference in actual and theoretical values of MRR and SR are plotted with error on Y axis and readings on X axis. Fig 5 and 6 shows percentage error in actual and experimental values of MRR and SR. It was evident from the graphs that the different test runs showed noticeable variation in the percentage error of both the dependent parameters i.e. MRR and SR.

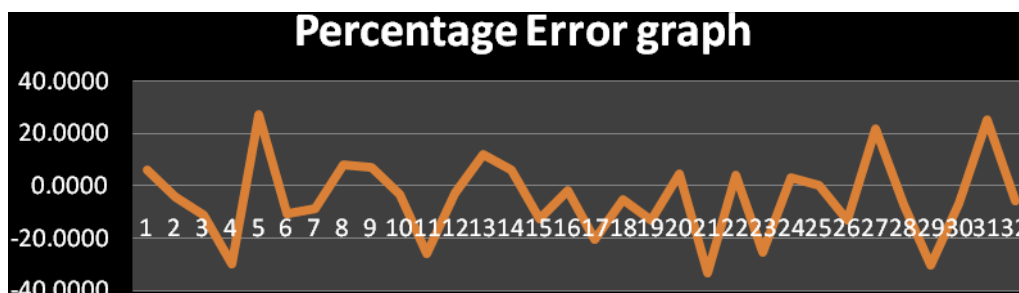


Fig 5. Percentage Error Graph for MRR



Fig 6. Percentage Error Graph for SR

9. Analysis of Variance or ANOVA

Analysis of Variance or ANOVA is a general technique that can be used to test the hypothesis that the means among two or more groups are equal, under the assumption that the sampled populations are normally distributed. The ANOVA procedure was used to test hypotheses that several means are same. In this study a total of 32 different conditions were selected to study the Material Removal Rate and Surface Roughness. The preliminary comparative assessment was carried out using the ANOVA procedure, followed by Post Hoc Test. The Post Hoc Test was employed to check, which means (obtained from the MRR and SR values as a function of 32 different runs. In addition to this, the Tukey’s HSD test was also performed to determine the HSD i.e. Honestly Significant Difference.

Anova and Post Hock Test

SS 304	N	Mean	Std. Deviation	Std. Error	95% Confidence Interval for Mean		Minimum	Maximum
					Lower Bound	Upper Bound		
1	3	3	5.2540	.09115	.05262	5.0276	5.4804	5.16
2	3	3	5.3193	.19453	.11231	4.8361	5.8026	5.12

ANOVA Results for MRR						
		Sum of Squares	df	Mean Square	F	Significance.
SS 304	Between Groups	50.491	31	1.629	29.513	.000
	Within Groups	3.532	64	.055		
	Total	54.023	95			

ANOVA Results for SR						
		Sum of Squares	df	Mean Square	F	Sig.
SS 304	Between Groups	74.024	31	2.388	18.957	.000
	Within Groups	8.062	64	.126		
	Total	82.086	95			

10. Results

It was observed that MRR was considerably affected by variation in current and SR decreased with increase in current. Hence, it was apparent that irregular removal of material was more likely to occur at high currents. The NaCl electrolyte was responsible for the lower SR and over-cut. Furthermore, MRR increased with flow rate because there was more mobility of the ions from the metal to the solution, thereby increasing the speed of the chemical reactions. Besides, there was a need to constantly remove the sludge formed during machining, which was necessary as the sludge accumulation could have negatively affected the machining efficiency of the ECM process. Results of entire experimentation work are as under:

A) Optimum value of MRR is as follows

	Actual	By Model
Optimum Value of MRR	6.754 mg/min	5.654 mg/min
Corresponding value of SR for this MRR	3.5574 μm	3.375 μm

Values of various parameters for above said maximum value of MRR is Current- 175A, Voltage 18 volts, Flow Rate 5Ltr/Min, Feed 0.3mm/min, Electrolyte concentration 150g/lit, Pressure 3.8 kg/cm²

B) Optimum value of SR is as follows

C)

	Actual	By Model
Optimum Value of SR	3.259 μm	3.46560 μm
Corresponding value of MRR for this SR	5.343mg/min	5.7883mg/min

Values of various parameters for above said optimum value of SR is Current- 125A, Voltage-10 volt, Flow Rate -7Ltr/Min, feed-0.4mm/min, Electrolyte concentration 150g/Lit, Pressure 3.4 kg/cm²

The mean MRR for SS304 varied between 3.6070 and 6.7540. Lowest MRR was observed for the run no. 32, while the highest value was recorded for the run no. 28. The analysis of data following ANOVA indicated significant difference in the mean values MRR and SR as a function of different conditions (set for different runs).

11. Conclusion

The experimentation work consists of study the influence of process parameters on MRR and SR. Process parameter such as machining voltage, feed, Current, Electrolyte concentration, electrolyte flow were successfully controlled and were allowed to vary according to need. The different combinations of the controlling factors were considered for the experimentation and to determine their (independent parameter's) influence on MRR and SR of SS304 work piece. The experimentation was carried out by varying all parameters in combination as per orthogonal array L₃₂. On the basis of the results obtained in this work, main conclusion can be stated as the selection of appropriate values for the different parameters of ECM process is crucial to achieve the efficiency and high quality of outcome from the process. Furthermore, similar experimental work can be continued to determine optimum process conditions for ECM process for other metals. In addition to this the difference between the theoretical and practical values of MRR and SR are also required (for other metals) to give some thought, so that % error can be reduced.

References

- [1] J.A. Mc Geough, *Principle of Electrochemical Machining*. Chapman and Hall, London, 1974.
- [2] P. Asokan, R Ravikumar, R Jeyapaul, M Santhi "Development of multi objective optimization models for Electrochemical Machining Process" Springer. Int J Adv. Munaf Technol(2008) 39:55-63 DOI 10.1007/s00170-007-1204-8
- [3] M. Hardopoulos · S. Turgeon · C. Sarra-Bournet · G. Laroche · D. Mantovani "Development of an optimized electrochemical process for subsequent coating of 316 stainless steel for stent applications" Received: 19 January 2004 / Accepted: 24 October 2005 Springer Science+Business Media, LLC 2006

- [4] K.L. Senthil Kumar, R. Sivasubramanian, K. Kalaiselvan, "Selection of Optimum Parameters in Non Conventional Machining of Metal Matrix Composite" *Portugalia Electrochemica Acta* 2009 27(4) 477-486.
- [5] R V Rao, P J Pawar, R Shankar "Multi objective optimization of electrochemical machining process parameters using a particle swarm optimization algorithm" DOI:10.1243/09544054JEM1158 *Proc. I mech E Vol 222 (2008) Part B*
- [6] J.A. McGeough and X. K. Chen, *Machining methods: electrochemical*, in "Kirk-Othmer J. I.
- [7] S K Mukherjee, s Kumar, P K shrivastava, Arbind Kumar " Effect of valency on material removal rate in electrochemical machining of aluminium" *Elsevier Journal of material processing Technology* 202(2008) 398-401
- [8] B Bhattacharyya S K Sorkhel " Investigation for controlled electrochemical machining through response surface methodology based approach" *Elsevier Journal of Processing Technology* 86(1999) 200-207.
- [9] Joˆao Cirilo da Silva Neto, Evaldo Malaquias da Silva, Marcio Bacci da Silva, 'Intervening variables in electrochemical machining' *Journal of Materials Processing Technology* 179 (2006) 92–96
- [10] J.A. McGeough, *Advanced Methods of Machining*, Chapman and Hall, London, 1988, pp. 55–88.
- [11] J. Tlusty, *Manufacturing Process and Equipment*, 1st ed., Prentice-Hall, USA, 2000.
- [12] M. Datta, Anodic dissolution of metals at high rates, *IBM J. Res. Develop.* 37 (2) (1993) 207–226.
- [13] M. Datta, R. V. Shenoy, L. T. Romankiw, "Recent advances in the study of electrochemical micromachining," *ASME J. Eng. Ind.* 118, 29–36, 1996.
- [14] P.C. Pandey, H.S. e Shan, *Modern Machining Processes*, Tata McGraw Hill, New Delhi, 1980.
- [15] G.F. Benedict, *Nontraditional Manufacturing Processes- Electrochemical Machining*, Marcel Dekker, New York and Basel, 1987, pp. 125–172.

Implementation of Data Mining Techniques for Weather Report Guidance for Ships Using Global Positioning System

P.Hemalatha

M.E Computer Science And Engineering IFET College Of Engineering Villupuram

Abstract

This paper deals with the implementation of data mining methods for guiding the path of the ships. The implementation uses a Global Positioning System(GPS) which helps in identifying the area in which the ship is currently navigating. The weather report on that area is compared with the existing database and the decision is made in accordance with the output obtained from the Data Mining technique. This decision about the weather condition of the navigating path is then instructed to the ship. This paper highlights some statistical themes and lessons that are directly relevant to data mining and attempts to identify opportunities where close cooperation between the statistical and computational communities might reasonably provide synergy for further progress in data analysis.

GLOBAL POSITIONING SYSTEM(GPS) provides specially coded satellite signals that can be processed in a GPS receiver enabling the receiver to compute position, velocity and time. Satellites were first used in position finding in a simple but reliable 2D Navy system called 'Transit' which laid the ground work for a system-"The Global Positioning System" that is funded and controlled by US Dept of Defense (DOD).

1. INTRODUCTION:

DATA MINING:

Data Mining means decision-making and data extraction. It also generates prediction mechanism from the available history. This implementation uses the Classification Models of Data Mining techniques. Data mining is a process of inferring knowledge from such huge data. Data Mining has three major components

1. Clustering or Classification,
2. Association Rules and
3. Sequence Analysis.

In classification/clustering we analyze a set of data and generate a set of grouping rules which can be used to classify future data. An association rule is a rule which implies certain association relationships among a set of objects in a database. In this process we discover a set of association rules at multiple levels of abstraction from the relevant set(s) of data in a database.

In sequential Analysis, we seek to discover patterns that occur in sequence. This deals with data that appear in separate transactions (as opposed to data that appear in the same transaction in the case of association).

2. CLASSIFICATION MODEL:

In Data classification one develops a description or model for each class in a database, based on the features present in a set of class-labeled training data. There have been many data classification methods studied, including decision-tree methods, such as C4.5, statistical methods, neural networks, rough sets, database-oriented methods etc. Using the training set, the Classification attempts to generate the description of the classes and these descriptions help to classify the unknown records. In addition to the training set, we can also have a test data set which is used to determine the effectiveness of a classification. The goal of the Classification is to build a concise model called Decision Tree that can be used to predict the class of the records whose class label is not known.

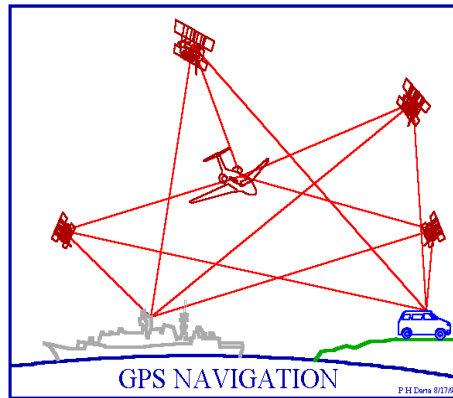
3. DECISION TREES:

A Decision tree is a Classification scheme, which generates a tree and a set of rules, representing the model of different classes, from a given data set. The set of records available for developing Classification methods is generally divided into two distinct subsets- a training set and a test set. The former is used for deriving the classifier, while the latter is used to measure the accuracy of the Classifier. The accuracy of the classifier is determined by the percentage of the test examples that are correctly classified. This implementation

uses the ID3 algorithm of the Classification Model to generate the Decision Tree.

4. The Global Positioning Systems

The US Global Positioning System (GPS) consists of a constellation of 24 satellites that emit radio signals for reception by specially designed devices. The GPS transmitter transmits the information regarding the latitude and longitude of the location where it is located to the satellite, which is then sent by the satellite to the receiver. If signals from one or more of these satellites are picked up by a GPS receiver, it can determine its location with high, reliable accuracy. The orbits are arranged such that there are, in fact, always at least 4 satellites visible from any point on the surface of the earth. Effectively, the satellite signal is continually marked with its own transmission time so that when received, the signal transit period can be measured with the synchronized receiver.



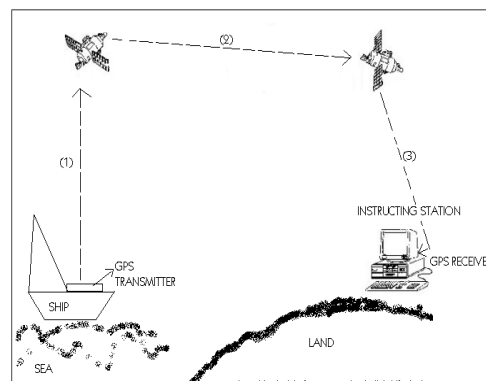
The satellites are so far out in space that the little distances we travel here on earth are insignificant. So if two receivers are fairly close to each other, say within a few hundred kilometers, the signals that reach both of them will have traveled through virtually the same slice of atmosphere, and so will have virtually the same.

5. Describing The Scenario

Steps involved:

- ❖ The GPS transmitter is placed in the ship and its receiver is placed in the instructing station.
- ❖ The analyzed weather report database is the training data.
- ❖ The Decision Tree is constructed for the Training Data.
- ❖ The GPS transmitter in the ship sends the information regarding the latitude and longitude of its current location to the nearby satellite.
- ❖ This satellite in turn sends this information to the satellite which is closer to the instructing station.
- ❖ The receiver present in the instructing station receives the GPS data from it.
- ❖ The weather information for that particular location is collected.
- ❖ The Decision Tree is traversed using this weather information and the required information is obtained.
- ❖ This predicted decision is then sent to the ship and the ship navigates accordingly.

THE REAL PICTURE:



6. Construction Of Decision Tree

ID3 and C4.5 are algorithms introduced by Quinlan for inducing Classification Models, also called Decision Trees, from data. We are given a set of records. Each record has the same structure, consisting of a number of attribute/value pairs. One of these attributes represents the goal of the record, i.e. the attribute whose values are most significant to us. The problem is to determine a decision tree on the basis of answers to questions about the non-goal attributes predicts correctly the value of the goal attribute. Usually the goal attributes take only the values {true, false} or {success, failure}, or something equivalent. In any case, one of its values will mean failure. Here, we are dealing with the records reporting the weather conditions for instructing the ship for its safe navigation. The goal attribute specifies whether or not to move forward.

ATTRIBUTE	POSSIBLE VALUES
Climate	Sunny, Cloudy, Rainy
Temperature	Continuous
Humidity	Continuous
Stormy	True, False

The non-goal attributes are:

and the training data is:

Climate	Temp (F)	Humidity(%)	Stormy?	Class
Sunny	75	70	true	Safe
Sunny	80	90	true	Unsafe
Sunny	85	85	false	Unsafe
Sunny	72	95	false	Unsafe
Sunny	69	70	false	Safe
Cloudy	72	90	true	Safe
Cloudy	83	78	false	Safe
Cloudy	64	65	true	Safe
Cloudy	81	75	false	Safe
Rainy	71	80	true	Unsafe
Rainy	65	70	true	Unsafe
Rainy	75	80	false	Safe
Rainy	68	80	false	Safe
Rainy	70	96	false	Safe

Notice that in this example two of the attributes have continuous ranges, temperature and humidity. ID3 does not directly deal with such cases, though below we examine how it can be extended to do so. A decision tree is important not because we hope it will classify correctly new cases. Thus when building classification models one should have both training data to build the model and test data to verify how well it actually works.

7. Basic Ideas Behind Id3:

- In the decision tree each node corresponds to a non-goal attribute and each arc to a possible value of that attribute. A leaf of the tree specifies the expected value of the goal attribute for the records described by the path from the root to that leaf. [This defines what is a decision tree].
- In the decision tree at each node should be associated the non-goal attribute which is most informative among the attributes not yet considered in the path from the root. [This establishes what a good decision tree is].
- Entropy is used to measure how informative is a node. [This defines what we mean by “good”].

7.1. Definitions:

If there are n equally probable possible messages, then the probability p of each is $1/n$ and the information conveyed by a message is $-\log(p) = \log(n)$. [All logarithms are in base 2]. That is, if there are 16 messages then $\log(16)=4$ and we need 4 bits to identify each message.

In general, if we are given a probability distribution $P = (p_1, p_2 \dots p_n)$ the information conveyed by this distribution, also called the Entropy of P , is: $I(P) = - (p_1 * \log(p_1) + p_2 * \log(p_2) + \dots + p_n * \log(p_n))$

For example, if P is $(0.5,0.5)$ then $I(P)$ is 1, if P is $(0.67,0.33)$ then $I(P)$ is 0.92, if P is $(1,0)$ then $I(P)$ is 0. The more uniform is the probability distribution, the greater is its information.

If a set T of records is partitioned into disjoint exhaustive classes C_1, C_2, \dots, C_k on the basis of the value of the goal attribute, then the information needed to identify the class of an element of T is $\text{info}(T) = I(P)$, where P is the probability distribution of the partition (C_1, C_2, \dots, C_k) :

$$P = (|C_1| / |T|, |C_2| / |T|, \dots, |C_k| / |T|)$$

In the training set T , $\text{Info}(T) = I(9/14, 5/14) = 0.94$.

If we first partition T on the basis of the value of a non-goal attribute X into sets T_1, T_2, \dots, T_n then the information needed to identify the class of an element of T becomes the weighted average of the information needed to identify the class of an element of T_i , i.e., the weighted average of $\text{Info}(T_i)$:

$$\text{Info}(X, T) = \sum \{ (|T_i| / |T|) * \text{Info}(T_i) \}$$

Here,

$$\text{Info}(\text{Climate}, T) = 5/14 * I(2/5, 3/5) + 4/14 * I(4/4, 0) + 5/14 * I(3/5, 2/5) = 0.694$$

Consider the quantity $\text{Gain}(X, T)$ defined as $\text{Gain}(X, T) = \text{Info}(T) - \text{Info}(X, T)$

This represents the difference between the information needed to identify an element of T and the information needed to identify an element of T after the value of attribute X has been obtained, that is, the gain in information due to attribute X .

In our example, for the Climate attribute the Gain is

$$\text{Gain}(\text{Climate}, T) = \text{Info}(T) - \text{Info}(\text{Climate}, T) = 0.94 - 0.694 = 0.246. \text{ Similarly,}$$

$$\text{Gain}(\text{Humidity}, T) = 0.151$$

$$\text{Gain}(\text{Stormy}, T) = 0.048$$

$$\text{Gain}(\text{Temperature}, T) = 0.029$$

We can use this notion of gain to rank attributes and to build decision trees where at each node is located the attribute with greatest gain among the attributes not yet considered in the path from the root.

The intent of this ordering is to create small decision trees so that the records can be identified after only a few questions.

7.2 The Id3 Algorithm:

The ID3 algorithm is used to build a decision tree, given a set of non-goal attributes C_1, C_2, \dots, C_n , the goal attribute C , and training set T of records. functionID3(R : a set of non-goal attributes,

C : the goal attribute,

S : a training set) returns a decision tree; Begin If S is empty, return a single node with value Failure;

If (S consists of records all with the same value for the goal attribute),

return a

single node with that value;

If R is empty, return a single node with as value the most frequent of the values of the goal attribute that are found in records of S ; [note that there will be errors, that is, records that will be improperly classified];

Let D be the attribute with largest $\text{Gain}(D, S)$ among attributes in R ;

Let $\{d_j \mid j=1, 2, \dots, m\}$ be the values of attribute D ;

Let $\{S_j \mid j=1, 2, \dots, m\}$ be the subsets of S consisting respectively of records with value d_j for attribute D ;

Return a tree with root labeled D and arcs labeled d_1, d_2, \dots, d_m going respectively to the trees

$\text{ID3}(R - \{D\}, C, S_1), \text{ID3}(R - \{D\}, C, S_2), \dots, \text{ID3}(R - \{D\}, C, S_m)$;

End ID3;

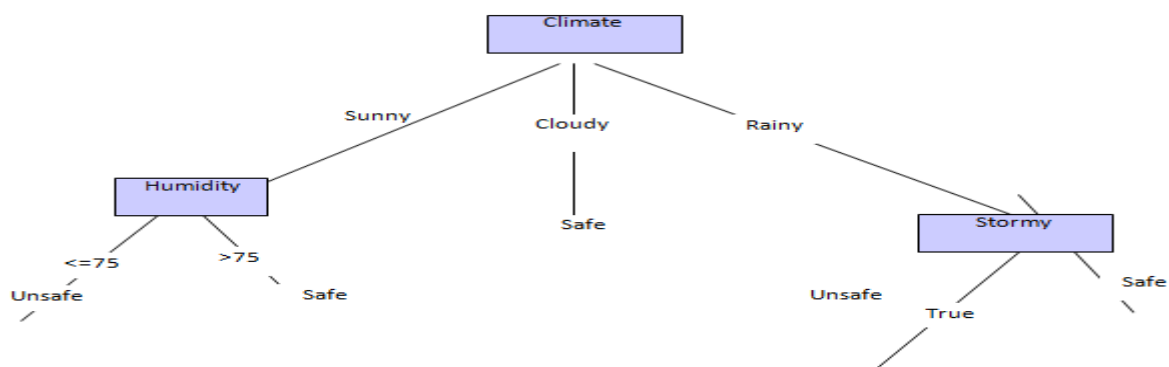
8. Conclusion:

The weather report of the ship’s location is made to traverse the Decision Tree and the corresponding decision is passed to the ship for its safe navigation. Thus this implementation, which uses many advanced concepts such as Data Mining and Global Positioning Systems, can also be extended for Aircrafts, Vehicle Tracking, Submarines, etc.

References:

- [1] UCLA Data Mining Laboratory
- [2] <http://nugget.cs.ucla.edu:8001/main.html>
- [3] IBM QUEST Data Mining Project <http://www.almaden.ibm.com/cs/quest/index.html>
- [4] Data Mining at Dun & Bradstreet
- [5] <http://www.santafe.edu/~kurt/text/wp9501/wp9501.shtml>
- [6] GPS Overview, by Peter.H.Dana. http://www.colorado.edu/geography/gcraft/notes/gps/gps_f.html

DECISION TREE FOR THE ABOVE ILLUSTRATION:



Equalization of Doppler Effect Using Constellation Diagram of 8-PSK Modulation

Vinay Negi¹, Sanjeev Kumar Shah², Sandeep Singh³, Arun Shekhar⁴ & Tanuja Sundriyal⁵

^{1,2,3} Uttarakhand Institute of Technology, Dehradun, Uttarakhand, India

^{4,5} H.N.B. Central University, Srinagar (Garhwal), Uttarakhand, India

Abstract: This paper describes the calculation and simulation results of the Doppler effect on a mobile user while walking with the help of constellation diagram for 8 PSK modulation when the walking user experienced the Rayleigh fading. And the equalizer is used to optimize the Doppler effect. Here LMS Linear equalizer is used to optimize the Doppler effect when the walking user having speed 1.5 m/sec. and the walking user is assumed on freeway. The results are taken at three position of mobile user i.e. at an angle of 5° , 60° and 85° . The calculation and simulation results of the Doppler effect on a mobile user with the help of constellation diagram for 8 PSK modulation is simulated in MATLAB.

Index Terms: 8 PSK modulation, LMS Linear equalizer, Rayleigh fading, Doppler effect, constellation diagram.

1. Constellation Diagram

A constellation diagram is a representation of a signal modulated by a digital modulation scheme such as quadrature amplitude modulation or phase-shift keying. It displays the signal as a two-dimensional scatter diagram in the complex plane at symbol sampling instants [1]. In a more abstract sense, it represents the possible symbols that may be selected by a given modulation scheme as points in the complex plane. Measured constellation diagrams can be used to recognize the type of interference and distortion in a signal. By representing a transmitted symbol as a complex number and modulating a cosine and sine carrier signal with the real and imaginary parts (respectively), the symbol can be sent with two carriers on the same frequency. They are often referred to as quadrature carriers. A coherent detector is able to independently demodulate these carriers. This principle of using two independently modulated carriers is the foundation of quadrature modulation. In pure phase modulation, the phase of the modulating symbol is the phase of the carrier itself [2].

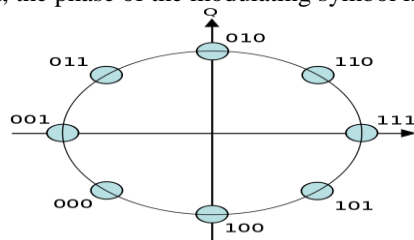


Fig.1 A constellation diagram for 8-PSK.

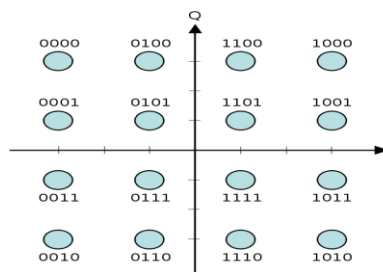


Fig.2 A constellation diagram for rect. 16-QAM.

As the symbols are represented as complex numbers, they can be visualized as points on the complex plane. The real and imaginary axes are often called the in phase, or I-axis and the quadrature, or Q-axis. Plotting several symbols in a scatter diagram produces the constellation diagram. The points on a constellation diagram are called constellation points. They are a set of modulation symbols which comprise the modulation alphabet. Also a diagram of the ideal positions, signal space diagram, in a modulation scheme can be called a constellation diagram. In this sense the constellation is not a scatter diagram but a representation of the scheme itself. The example shown here is for 8-PSK, which has also been given a Gray coded bit assignment [3].

2. Interpretation

Upon reception of the signal, the demodulator examines the received symbol, which may have been corrupted by the channel or the receiver (e.g. additive white Gaussian noise, distortion, phase noise or interference). It selects, as its estimate of what was actually transmitted, that point on the constellation diagram which is closest (in a Euclidean distance sense) to that of the received symbol. Thus it will demodulate incorrectly if the corruption has caused the received symbol to move closer to another constellation point than the one transmitted.

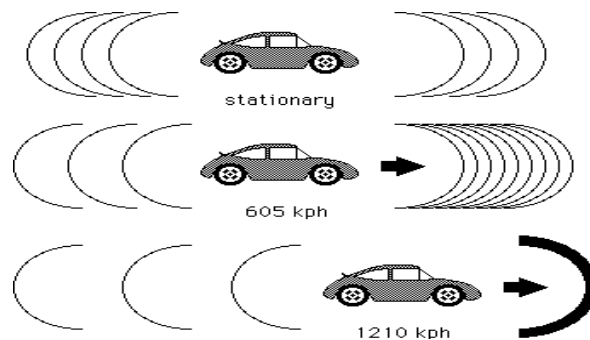
This is maximum likelihood detection. The constellation diagram allows a straightforward visualization of this process imagine the received symbol as an arbitrary point in the I-Q plane and then decide that the transmitted symbol is whichever constellation point is closest to it.

For the purpose of analyzing received signal quality, some types of corruption are very evident in the constellation diagram. For example:

1. Gaussian noise shows as fuzzy constellation points
2. Non-coherent single frequency interference shows as circular constellation points
3. Phase noise shows as rotationally spreading constellation points
4. Attenuation causes the corner points to move towards the center.

3. Doppler Effect

The Doppler Effect (or Doppler shift), is the change in frequency of a wave (or other periodic event) for an observer moving relative to its source. It is commonly heard when a vehicle sounding a siren or horn approaches, passes, and recedes from an observer [4]. The received frequency is higher (compared to the emitted frequency) during the approach, it is identical at the instant of passing by, and it is lower during the recession. The relative changes in frequency can be explained as follows. When the source of the waves is moving toward the observer, each successive wave crest is emitted from a position closer to the observer than the previous wave. Therefore each wave takes slightly less time to reach the observer than the previous wave. Therefore the time between the arrivals of successive wave crests at the observer is reduced, causing an increase in the frequency. While they are travelling, the distance between successive wave fronts is reduced; so the waves "bunch together". Conversely, if the source of waves is moving away from the observer, each wave is emitted from a position farther from the observer than the previous wave, so the arrival time between successive waves is increased, reducing the frequency. The distance between successive wave fronts is increased, so the waves "spread out".



The Doppler Effect for a Moving Sound Source

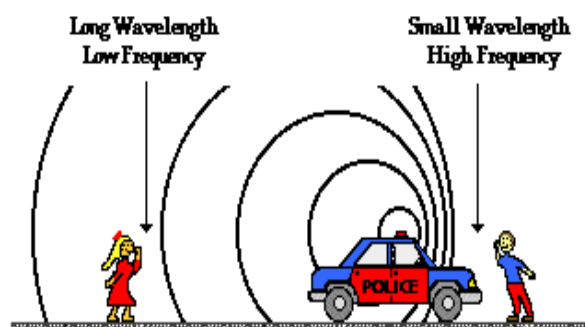


Fig.3 Doppler Effect

For waves that propagate in a medium, such as sound waves, the velocity of the observer and of the source is relative to the medium in which the waves are transmitted. The total Doppler Effect may therefore result from motion of the source, motion of the observer, or motion of the medium. Each of these effects is analyzed separately. For waves which do not require a medium, such as light or gravity in general relativity, only the relative difference in velocity between the observer and the source needs to be considered.

4. Mathematical Analysis For Simulation Results

1) Phase change in Rx signal $(\Delta\phi) = 2\pi\Delta l / \lambda = (2\pi v \Delta t / \lambda) * \cos\theta$

2) Doppler shift $(fd) = \Delta\phi / 2\pi\Delta t = (v / \lambda) * \cos\theta = v fc / c * \cos\theta$

Table 1.1 Mobile user having Walking speed of 1.5 m/sec on freeway (fd2)

Angle(θ) (Deg)	Gain(db)	fc(MHz)	fd2(Hz)
5	18	900	4.62
30	18	900	4
45	18	900	3.28
60	18	900	2.32
85	18	900	0.40
90	18	900	No doppler shift

Rayleigh fading is a reasonable model when there are many objects in the environment that scatter the radio signal before it arrives at the receiver. The central limit theorem holds that, if there is sufficiently much scatter, the channel impulse response will be well-modeled as a Gaussian process irrespective of the distribution of the individual components [5]. If there is no dominant component to the scatter, then such a process will have zero mean and phase evenly distributed between 0 and 2π radians. The envelope of the channel response will therefore be Rayleigh distributed.

5. Simulated Results

The constellation for the mobile user having speed 1.5 m/sec and the mobile car is assumed on freeway at an angle of 5° , 45° and 85° is simulated in MATLAB for 8-PSK are shown in fig.4 to fig. 10.

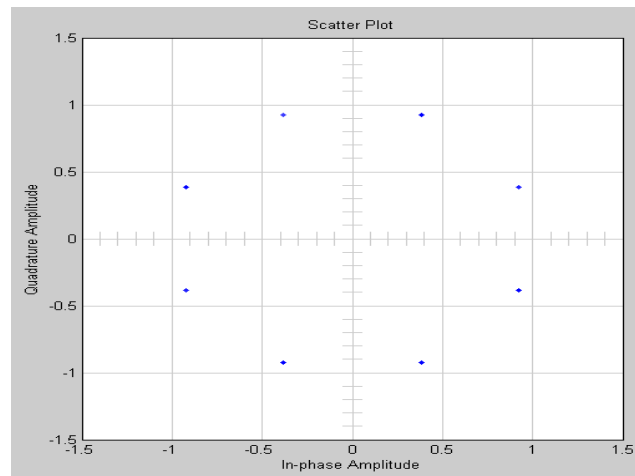


Fig.4 Constellation diagram of 8-PSK when mobile walking user is not experienced any fading & doppler effect

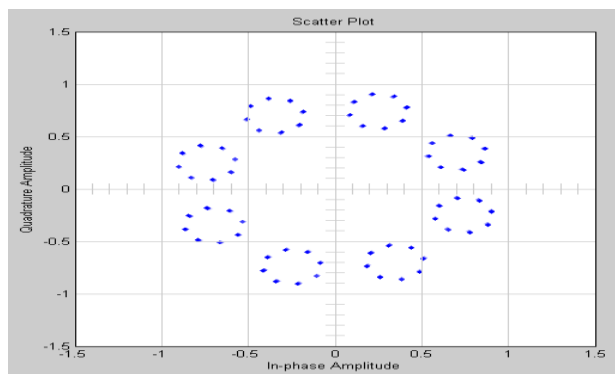


Fig.5 mobile walking user having speed 1.5 m/sec on freeway for angle 5° (MPSK, M=8) without equalizer

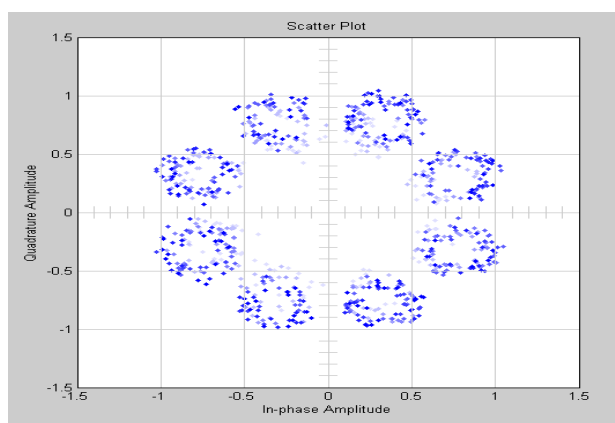


Fig.6 Mobile walking user having speed 1.5 m/sec on freeway for angle 5° (MPSK, M=8) with equalizer

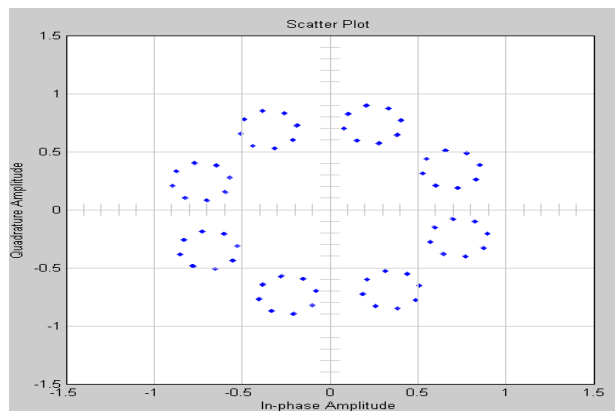


Fig.7 Mobile walking user having speed 1.5 m/sec on freeway for angle 60° (MPSK, M=8) without equalizer

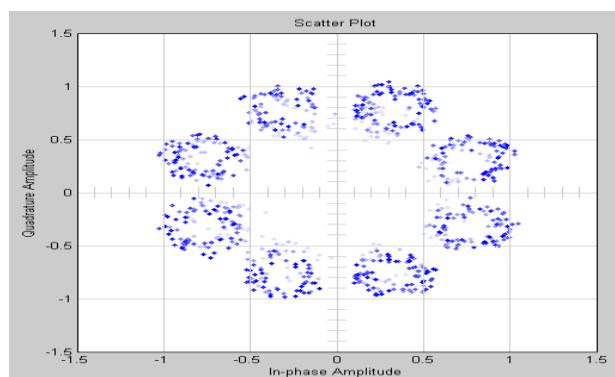


Fig.8 Mobile walking user having speed 1.5 m/sec on freeway for angle 60° (MPSK, M=8) with equalizer

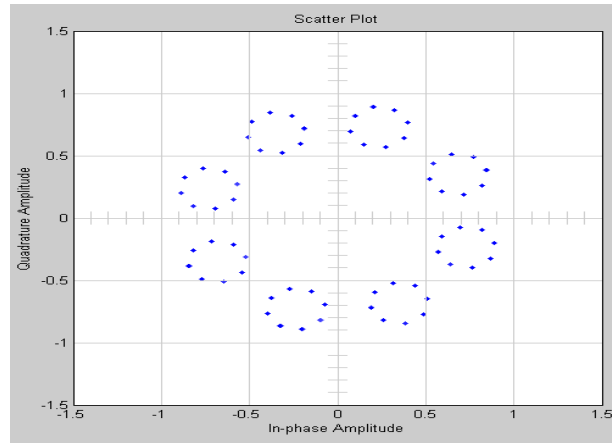


Fig.9 Mobile walking user having speed 1.5 m/sec on freeway for angle 85^0 (MPSK, M=8) without equalizer

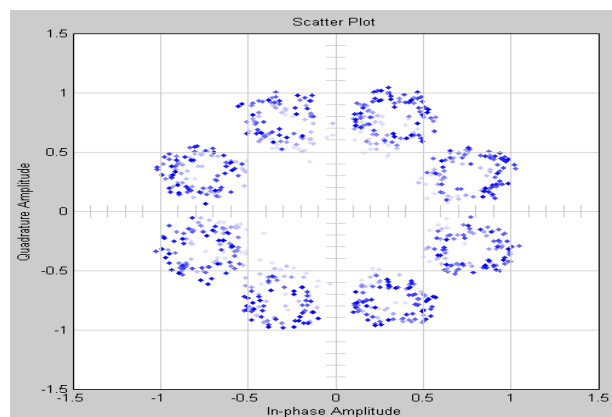


Fig.10 Mobile walking user having speed 1.5 m/sec on freeway for angle 85^0 (MPSK, M=8) with equalizer

6. CONCLUSION

This paper show the calculation and simulation results of the Doppler effect on a mobile walking user with the help of constellation diagram for 8 PSK modulation when the mobile walking user experienced the Rayleigh fading. And the LMS Linear equalizer is used to optimize the Doppler Effect when the mobile walking user having speed 1.5 m/sec and the mobile walking user is assumed on freeway. The results shows that the distorted constellation point because of Doppler effect when gain is taken 18 dB and carrier frequency is 900 MHz (i.e. U.S. digital cellular system) for each observation. And also the LMS Linear equalizer equalize those distorted constellation point for optimizing the Doppler Effect for every 5^0 , 60^0 and 85^0 .

REFERENCES

- [1] BER Performance of Reed-Solomon Code Using M-ary FSK Modulation in AWGN Channel, International Journal of Advances in Science and Technology, Vol. 3, No.1, 2011
- [2] Difference Threshold Test for M-FSK Signaling With Reed-Solomon Coding and Diversity Combining in Rayleigh Fading Channels, IEEE TRANSACTIONS ON VEHICULAR TECHNOLOGY, VOL. 54, NO. 3, MAY 2005
- [3] Performance Analysis of Combined Transmit Selection Diversity and Receive Generalized Selection Combining in Rayleigh Fading Channels Xiaodong Cai, Member, IEEE, and Georgios B. Giannakis, Fellow, IEEE, IEEE TRANSACTIONS ON WIRELESS COMMUNICATIONS, VOL. 3, NO. 6, NOVEMBER 2004
- [4] Bit-Error Probabilities of 2 and 4DPSK with Nonselective Rayleigh Fading, Diversity Reception, and Correlated Gaussian Interference, Pooi Yuen Kam, IEEE TRANSACTIONS ON COMMUNICATIONS, VOL. 45, NO. 4, APRIL 1997
- [5] T. S. Rappaport Wireless Communication. Prentice-hall, Upper Saddle River, N.J, 1996.



Vinay Negi was born in Uttarakhand, India, on June 30, 1990. He received B.Tech Degree in Electronics and Communication Engineering from Punjab College of Engineering and technology, Punjab in 2010 and M. Tech Degree in Communication System from Graphic era university, Uttarakhand in 2012. He joined the Faculty of Electronics in Uttaranchal Institute of Technology, Dehradun becoming an Assistant Professor. He has authored 1 scientific paper and co authored 3 scientific papers.
Department of Electronics and Communication
Uttaranchal Institute of Technology, Dehradun



Sanjeev Kumar Shah was born in U.P., India, on December 19, 1981. He received M.Tech Degree in Digital Communication from Dehradun Institute of Technology, Dehradun (Uttarakhand) in 2009. He joined the Faculty of Electronics in Uttaranchal Institute of Technology, Dehradun becoming an Assistant Professor. Currently, he is working toward Ph.D at Shri Venkateshwara University, Gajraula, Uttar Pradesh, India. He is also an Associate member of Institution of Electronics and Telecommunication Engineers. He has published 5 scientific papers.
Department of Electronics and Communication
Uttaranchal Institute of Technology, Dehradun



Sandeep Singh Negi was born in Uttarakhand, India, on July 11, 1980. He received B.Tech Degree in Electronics and communication engineering from Graphic era university, Uttarakhand and M.tech Degree in Communication System from Singhania University, Rajasthan. He joined the Faculty of Electronics in Uttaranchal Institute of Technology, Dehradun becoming an Assistant Professor. He has co authored 3 scientific papers.
Department of Electronics and Communication
Uttaranchal Institute of Technology, Dehradun



Arun Shekhar was born in Uttarakhand, India, on Feb 02, 1979. He received B.Tech Degree in Electronics and communication engineering from Dehradun Institute of Technology, Dehradun (Uttarakhand) and M.tech Degree in Communication System from GBPEC Pauri. He joined the Faculty of Electronics in HNB Garhwal Central University, Srinagar (Garhwal) becoming an Assistant Professor.
Department of Electronics and Communication
HNB Garhwal Central University, Srinagar (Garhwal)



Tanuja Sundriyal was born in Uttarakhand, India, on September 16, 1988. He received B.Tech Degree in instrumentation Engg. from USIC H.N.B.G. University (2006-2010), Uttarakhand in 2012 and M.tech Degree in control systems from graphic era university(2010-2012). He joined the Faculty of H.N.B.G. University (on contract) in Instrumentation Department.

Spectroscopic Constants & Potential Energy Function for Diatomic Molecules

¹Ratikant Thakur and ²Jagdish Mandal

^{1,2}University Department of Physics Tilka Manjhi Bhagalpur University, Bhagalpur – 812007, Bihar, India

Abstract

The interionic interaction potential energy functions consisting of an attractive term within the framework of 'effective charge model along with a short range repulsive interaction (SRRI) term incorporating the near values of molecular state polarizability, van der Waals dipole-dipole and dipole-quadrupole interaction and repulsive interaction of the Born-Mayer, Hellmann, Varshni-shukla and Ali-Hasan types have been used to compute the dipole moment, binding energy, rotation-vibration coupling constant and vibrational anharmonicity. The values of binding energies have been calculated with and without the inclusion of polarization. The inclusion of polarizable terms in the interaction-energy makes significant improvement in the result. This shows the interaction model must be dependent on this effect. The obtained values are in good agreement with the observed values available in the literature. The results are capable enough to establish the reliability and superiority of the interaction models.

Keywords: - Anharmonicity constant, Binding energy, Dipole moments, dipole-dipole and dipole-quadrupole interaction constants, vdWenergies

1. Introduction

Studies of interaction potential energy function in diatomic molecules play an important role in molecular physics as well as in the problems of astrophysical importance [1]. Recently there have been several investigations [2-5] on the potential energy function using the interaction originally due to Morse [6], Kratzer [7] and Rydberg [8]. Raghubanshi and Sharma [2] and Verma and Jha [5] have developed new potentials by combining Morse and Kratzer function and Rydberg and Kratzer functions respectively. The rotational vibrational constants α_e for diatomic molecules were calculated by using Morse-Kratzer (MK) and Rydberg-Kratzer (RK) potentials. But the results were far from satisfactory [1]. Rittner [9], for the first time proposed a polarizable ion model for alkali halide molecules by which interaction terms could be understood. Later on, Brumer and Karplus [10] modified Rittner model known as truncated Ritter model known as T-Rittner model expressed as.

$$U(r) = -\frac{z^2 e^2}{r} - \frac{(\alpha_1 + \alpha_2)}{2r^4} - \frac{C}{r^6} - \frac{D}{r^8} + U_R(r) \dots \dots \dots (1)$$

The first term is the electrostatic attraction between two point charges $z(+e)$ and $z(-e)$ separated by a distance r and known as Coulomb interaction. The second term is the polarization energy, the third and the fourth terms are the vander waals (vdw) dipole-dipole and dipole-quadrupole interaction energy and the last term is the short range repulsive interaction (SRRI). There are various repulsive interactions proposed by different theoretical workers from time to time to describe the structure and properties of ionic molecules [11]. The repulsive interactions in logarithmic functions [12-13] are also available in literature not free from error. In the present calculations, we introduce the modification in the previous work in order to improve the interaction potential model for calculating the spectroscopic constant of diatomic molecules. Four repulsive interactions namely, Born-Mayer [14] Hellmann [15], Varshni-Shukla [11] and Ali-Hasan [16] have been chosen as the short range repulsive interaction to investigate their validity for alkali halide molecules as the results obtained from other potential models are far from errors.

A generalized formula for short range repulsive interactions can be expressed as

$$U_R(r) = \frac{B}{r^m} \exp(-r/\rho) \dots \dots \dots (2)$$

which takes the form of Born-Mayer repulsive potential when $m=0$, Hellmann repulsive potential when $m=1$ and Varshni-Shukla potential when $m=2$. Ali-Hasan empirical repulsive potential is given by

$$U_R(r) = \frac{S}{r_m} \exp(-br^n) \dots \dots \dots (3)$$

In this potential $m=2$ and $n=3/2$. In eq^{ns} (2) and (3) B , S , ρ and b are repulsive potential parameters

2. Methods Of Calculation

The repulsive potential parameters are determined by applying the equilibrium criteria;

$$\left(\frac{dU(r)}{dr}\right)_{r=r_e} = 0 \dots \dots \dots (4)$$

and $\left(\frac{d^2U(r)}{dr^2}\right)_{r=r_e} = K_e = 4\pi^2 \omega_e^2 C^2 \mu_A \dots \dots \dots (5)$

K_e is the molecular force constant, ω_e is the equilibrium vibrational frequency, C is the speed of light in vacuum and μ_A is the reduced mass and r_e is the equilibrium interionic separation. The electronic polarizabilities of ions in the molecular state or bonded state differ from the free state polarizabilities. This is mainly due to the existence of the Coulomb interaction. Wilson and Curtis [17] have shown that the polarizability of cation remains unchanged whereas that of anion decreases significantly in the bonded state due to the effect of Coulomb interaction. The molecular state polarizability of anion (α_m) is calculated from the relation based on Ruffia energy analysis [18] given by

$$\alpha_2 = \alpha_m = \frac{e^2 h^2 n_0}{4\pi^2 m (E_f + e\varphi)^2} \dots \dots \dots (6)$$

Where $\varphi = e/r$

The values of E_f , known as energy parameter are calculated from free-ion polarizabilities α_f as reported by Cocker [19] given by.

$$E_f^2 = \frac{e^2 h^2 n_0}{4\pi^2 m \alpha_f} \dots \dots \dots (7)$$

where m is the electron mass, n_0 is the total no. of electrons in the ions and h is the Planck's constant. The molecular state polarizability of anions calculated from eq (6) and the free state polarizability of cations taken from Pauling [20] are used to estimate the dipole moment μ from the relation given by

$$\mu = er - \frac{e(\alpha_1 + \alpha_2)}{r^2} \dots \dots \dots (8)$$

and vdW dipole-dipole constant C and dipole – quadrupole constant D taken from Slater Kirkwood variational method [21] are expressed as

$$C = \frac{3 e h}{4\pi m^{3/2}} \frac{\alpha_1 \alpha_2}{\left(\frac{\alpha_1}{N_+}\right)^{1/2} + \left(\frac{\alpha_2}{N_-}\right)^{1/2}} \dots \dots \dots (9)$$

and $D = \frac{27 h^2 \alpha_1 \alpha_2 \left[\left(\frac{\alpha_1}{N_+}\right)^{1/2} + \left(\frac{\alpha_2}{N_-}\right)^{1/2} \right]^2}{32 \pi^2 m \left[\left(\frac{\alpha_1}{N_+}\right) - \frac{20}{3} \left(\frac{\alpha_1 \alpha_2}{N_+ N_-}\right)^{1/2} + \left(\frac{\alpha_2}{N_-}\right) \right]} \dots \dots \dots (10)$

Where N_+ and N_- are the effective no. of electrons in the ions and are defined by

$$N_+ = N + Z_+ \dots \dots \dots (11)$$

$$N_- = N - Z_- \dots \dots \dots (12)$$

Here N is the total no of electrons in the outer two shells.

The rotation vibration coupling constant (α_e) and vibrational anharmonicity constant ($\omega_e x_e$) are calculated from the relations [22]

$$\alpha_e = - \left(\frac{x_3 r_e^3}{3} + 1 \right) \frac{6 B_e^2}{\omega_e} \dots \dots \dots (13)$$

$$\omega_e x_e = \left(\frac{5}{3} x_3^2 - x_4 \right) \frac{h}{64 \pi^2 c \mu} \dots \dots \dots (14)$$

and $x_p = \left(\frac{d^p U(r)}{dr^p} \right)_{r=r_e} / \left(\frac{d^2 U(r)}{dr^2} \right)_{r=r_e} \dots \dots \dots (15)$

where p stands for order of derivative.

The binding energy D_i per mole of a diatomic molecule is given by

$$D_i = -NU(r_e) \dots \dots \dots (16)$$

Where N is the Avogadro's Number and r_e is the molecular equilibrium distance.

3. Results & Discussion

The molecular state polarizabilities for diatomic molecules have been calculated by using eq^{ns}. (6) and (7). They are calculated to obtain the improved values of polarization energies and vdW energies. Table – 1 shows their calculated values. The values of $N_+ N_-$ and r_e are taken from Mandal and Ghatak [23] and Huber and Hertzberg [1]. The different potential parameters have been computed with the help of molecular equilibrium

equations (4) and (5). Their values have been used to calculate spectroscopic constants. The constants C and D known as dipole-dipole, dipole quadrupole van der Waals interaction constants have been obtained with the help of eq^{ns} (9) and (10) given by Slater Kirkwood variational method. These values have been used in the evaluation of binding energy (D_e) and dissociation energy (D_e).

Table – 1 Calculated values of electronic polarizabilities $\alpha_1(A^{03})$ and $\alpha_2(A^{03})$, N+ and N- (total no. of electrons in the outer two shells) and values of $r_e(A^0)$,

Molecules	$\alpha_1(A^{03})$	$\alpha_2(A^{03})$	N+	N-	r_e
LiF	0.036 1.564	0.741	3	9	
LiCl	0.034 2.021	2.202	3	15	
LiBr	0.036 2.170	3.350	3	25	
Li I	0.033 2.392	5.224	3	25	
NaF	0.190 1.926	0.821	11	9	
NaCl	0.184 2.361	2.372	11	15	
NaBr	0.182 2.502	3.534	11	25	
Na I	0.180 2.711	5.455	11	25	
KF	1.143 2.172	0.865	17	9	
KCl	1.078 2.667	2.498	17	15	
KBr	1.063 3.680	2.821	17	25	
K I	1.045 3.048	5.659	17	25	
RbF	1.805 2.270	0.881	27	9	
RbCl	1.718 2.787	2.543	27	15	
RbBr	1.693 2.945	3.731	27	25	
Rb I	1.673 3.177	5.728	27	25	
CsF	3.154 2.345	0.893	27	9	
CsCl	2.989 2.906	2.534	27	15	
CsBr	2.952 3.072	3.779	27	25	
CsI	2.908 3.315	5.880	27	25	

Table- 2 shows the obtained values of the dipole moments of diatomic molecules. These calculation are based on the eq(8), Column (2) of this table shows the present calculation with possible errors Column(b) and (c) denote values of dipole moments for the mentioned molecules obtained by Rittner model [9] and point ion model the experimental values of μ . have been taken from Brumer and karplus [10]. The average percentage errors obtained by us and Ali-Hasan & Shankar et al are respectively 2.79, 13.58 and 31.29. The higher percentage errors in their values may be attributed to the omission of molecular polarizabilities. The values of μ obtained simply indicate the significance of molecular state polarizabilities.

Table2. calculated values of dipole moments μ in debye

Molecules	Expt. (1,22)' %error	present	%error	b calculation	%error	c
LiF	6.284 19.5	5.982	4.8	5.311	15.5	7.511
LiCl	7.085 36	7.07	0.2	5.241	26	9.706
LiBr	7.226 44.2	6.967	3.6	5.406	25.2	10.422

Li I	7.429 54.6	7.0703	4.8	5.375	27.5	11.488
NaF	8.123 7.77	8.387	3.25	7.492	13.8	9250
NaCl	8.972 26.4	9.132	1.78	7.773	13.4	11.339
NaBr	9.092 24.2	9.361	2.95	7.96	12.45	12.017
NaI	9.21 41.36	9.332	1.32	7.992	13.2	13.02
kF	8.558 21.8	8.383	2.04	8.074	5.6	10.432
KCl	10.238 25.1	10.389	1.47	9.181	10.3	12.809
kBr	10.603 27.78	10.68	0.73	9.575	9.69	13.549
KI	11.05 32.47	11.199	1.35	9.921	13.3	14.369
RbF	8.513 18.1	8.359	1.8	8.001	6	10.902
RbCl	10.483 32.3	10.745	2.49	9.469	9.8	13.885
RbBr	-	11.131	-	-	-	14.144
RbI	-	11.729	-	-	-	15.259
CsF	7.489 50.4	7.723	3.12	7.278	2.8	11.268
CsCl	10.858 28.5	10.782	0.69	9.364	13.7	13.957
CsBr	-	11.322	-	-	-	14.754
CsI	12.1 31.57	10.756	11.1	10.61	12.3	15.921
Average % deviation			2.793529		13.56118	
	30.70882					

Table- 3 (a) & 3 (b) Show the calculated values of binding energy (D_i) of molecules with and without the inclusion of molecular polarization energy. The calculation have been done for all the four short range repulsive interaction models. The average percentage errors in both cases for all the models are also very revealing. BM and VS interaction models give better results of binding energy in comparison to HM & AH models. The result indicates that the BM & VS interaction models are to be considered to be exact potential energy functions for the prediction of binding energy of these molecules. Results show that BM>VS>HM>AH. Thus the polarization energy has to be taken a reality for the evaluation of binding energy for halide molecules.

Table-3a Calculated Values of Binding Energy (D_i) in K. Calorie/mole (With Polarization)

Molecules	Expt (1,22) %Error	B.M With	%Error	Hell. With	%Error	V.S. With	%Error	A & H. With	
LiF	184.1	199.95	8.6	197.8	7.4	197.9	7.49	199.8	8.5
LiCl	153.3	159.6	4.1	157.1	2.4	160.3	4.5	161.45	5.2
LiBr	147.4	157.5	6.8	156.6	6.2	156.6	6.2	157.8	7.1
LiI	138.7	147.6	6.4	146.9	5.9	146.9	5.9	147.8	6.5
NaF	153.9	156.1	1.4	155.3	0.9	154.3	0.26	156.2	1.89
NaCl	132.6	133.8	0.9	134.8	1.6	132.8	0.15	134.1	1.13
NaBr	127.7	129.13	1.1	128.7	0.7	128.25	0.73	129.3	1.25
NaI	120.3	122.7	1.9	122.5	1.8	113.09	5.9	124.48	3.4
KF	139.2	152.4	9.5	151.9	8.6	151.5	8.8	167.4	20.2
KCl	118	128.4	8.8	123.2	4.4	134.4	13.8	133.4	13
KBr	113.6	121.8	7.2	110.5	2.7	110.4	2.8	111.24	2.07
KI	106.1	108.2	1.9	107.9	1.7	107.6	1.4	124.4	17.2
RbF	133.6	142.7	6.8	142.2	6.4	141.9	6.2	156.3	16.9

RbCl	113.4	114.2	0.7	114	0.4	113.6	0.17	124.7	9.96
RbBr	109	109.96	0.8	111	1.9	110.75	1.6	121.8	11.7
RbI	101.9	104.2	2.2	104.7	2.7	104.5	2.5	114.9	12.7
CsF	130.5	147.9	1.3	147.6	13.1	147.2	12.7	151.1	18.7
CsCl	112.3	114.45	1.9	114.1	1.6	113.95	1.46	111.9	.35
CsBr	130.5	109.4	16.1	109.1	9.65	109.1	9.6	107.6	17.6
CsI	101.1	104.06	2.9	103.9	2.8	102.2	1.1	100.6	.49
AVERAGE% DEVIATION			4.565			9.475		4.658	
			13.642						

Table-3b Calculated Values of Binding Energy (Di) in K. Calorie/mole (Without Polarization)

Molecules	Expt. (1,22) %Error	B.M Without	%Error	Hell. Without	%Error	V.S. Without	%Error	A & H. Without	
LiF	184.1 2.7	179.2	2.6	177.2	3.7	177.7	3.5	179.2	
LiCl	153.3 10.6	138.2	9.8	139	9.3	138.7	9.5	137	
LiBr	147.4 9.2	134.7	8.6	133.7	9.3	131.6	10.7	133.9	
LiI	138.7 12.1	146.9	2.9	121.2	12.6	121.1	12.6	121.9	
NaF	153.9	143.9	6.5	143.2	6.9	142.2	7.2	144.1	6
NaCl	132.6 9.12	128.8	2.9	121.24	8.5	122.8	7.4	120.5	
NaBr	127.7 10.94	113.48	11.1	113.1	11.4	112.59	11.9	113.72	
NaI	120.3 10.83	105.5	12.3	105.3	12.4	95.36	20.7	107.26	
KF	139.2 9.5	137.5	1.2	137.1	1.5	136.6	1.86	152.5	
KCl	118 3.2	111.7	5.3	111.5	5.5	122.8	4.06	121.8	
KBr	113.6 12.9	110.5	2.7	98.2	13.6	98.04	13.6	98.9	
KI	106.1 5.18	95.4	10.1	95.1	10.36	94.76	10.6	111.6	
RbF	133.6 4.4	126.1	5.6	126.1	5.6	125.2	6.3	139.5	
RbCl	113.4 0.32	102.6	9.5	101.3	10.6	101.9	10.1	113.03	
RbBr	109 5.32	98.2	1.1	99.2	8.9	98.9	9.26	103.6	
RbI	101.9 1.66	92.94	9.3	93.5	8.2	93.2	8.5	103.6	
CsF	130.5 4.99	125.9	3.5	125.6	3.7	125.13	4.11	137.02	
CsCl	112.3	101.6	9.5	101.3	9.7	101.2	9.8	112.3	0
CsBr	130.5	96.9	25.7	96.5	26.1	91.1	30.1	130.5	0
CsI	101.1	92.1	8.9	91.92	1.1	89.68	11.2	101.1	0
AVERAGE% DEVIATION			7.455			8.948		10.145	
			5.948						

Table 4 & 5 present the calculated values of α_e and $\omega_e x_e$ for halide molecules in the case of well-known four repulsive interaction models along with their experimental values. From the table it is evident that α_e for BM, HM, VS & AH are respectively 8.4, 10.21, 7.57, 6.28. The order of suitability of the models are

AH>VS>BM>HM. Similarly the percentage deviations of $\omega_e x_e$ for the above models are 5.57, 7.81, 6.27, 5.71 for BM, HM, VS & AH. Here VS and AH models give still more approximate values of anharmonicity. The small discrepancy between the observed and experimental values of the calculated quantities may be attributed due to overlap of electron clouding between anion & cations and hence the dependence of potential model on interionic separations.

Table-4 Calculated Values of Rotational constant α_e (in 10^{-4} cm)

Molecules	Expt.(1,22)	B.M	%Error	Hall.	%Error	V.S.	%Error	A&H	%Error
LiF	202.7	187.2	7.6	198.7	1.97	211.9	4.5	196.9	2.8
LiCl	80	87.6	9.5	91.5	14.3	97.7	2.1	74.6	6.7
LiBr	56.4	66.7	18.2	71.5	26.7	72.5	8.5	87.6	5.3
LiI	40.9	44.4	8.5	54.7	33.7	53.3	3.3	44.8	9.5
NaF	45.6	47.1	3.2	34.08	25.2	48.3	5.9	36	21
NaCl	16.3	15.5	4.9	16.4	0.6	17.2	5.5	15.4	5.5
NaBr	9.4	9.1	3.19	9.5	1.06	9.5	1	10.8	4.8
NaI	6.47	6.21	4	6.45	0.31	6.71	3.7	6.3	2.6
KF	28.3	23.28	17.7	22.5	10.9	24.6	13	23.7	16.2
KCl	7.89	9.8	24.2	10.2	9.8	7.38	6.4	4.3	5.5
KBr	4.05	4.03	0.5	5.1	5.9	3.75	7.4	3.5	3.5
KI	2.68	3.52	3	3.5	0.5	3.52	1.3	2.88	1.4
RbF	15.2	14.9	1.9	15.4	1.3	16.1	5.9	15.9	4.6
RbCl	4.53	4.42	2.48	4.18	7.6	4.76	5	3.54	1.8
RbBr	1.86	1.89	1.61	1.98	6.4	2.16	6.1	1.86	0
RbI	1.09	1.04	4.58	1.06	2.7	10.4	4.5	1.05	3.6
CsF	16.8	14.19	15.5	14.05	16.3	14.04	16.4	14.1	16
CsCl	3.39	3.64	7.3	3.75	10.6	4.2	23.8	3.6	0.61
CsBr	1.24	1	19.3	1.41	13.7	1.03	16.9	1	9.3
CsI	0.68	0.6	11.7	0.78	14.7	0.61	10.2	0.51	5
AVERAGE		% DEVIATION	8.443		10.212		7.57		6.2855

Table- 5 Calculated values of Vibrational anharmonicity constant $\omega_e x_e$ (in cm^{-1})

Molecules	Expt.	B.M	%Error	Hell. (1,22)	%Error	V.S.	%Error	A&H	% Error
LiF	8.1	8.3	0.24	8.17	0.86	7.4	8.6	8.46	4.4
LiCl	4.5	5.11	13.5	5.22	16	5.77	8.2	2.56	31
LiBr	3.53	4.54	8.6	2.12	9.9	4.89	8.5	8.68	5.8
LiI	3.39	3.9	15	3.7	9.6	3.7	9.1	3.8	12
NaF	3.83	4.24	10.7	3.05	20.3	4.4	4.8	3.51	8.3
NaCl	1.76	1.6	9	1.61	8.5	1.65	6.2	1.5	4.7
NaBr	1.16	1.13	2.5	1.15	8.5	1.1	5.1	1.57	5.3
NaI	0.96	0.94	2	1.1	4.5	1.95	1	1.93	3.1
KF	0.56	0.53	5.3	0.52	7.1	0.54	3.5	0.61	3.9
KCl	1.17	1.34	4.5	1.29	10.2	1.18	8.5	1.19	1.7
KBr	0.76	0.82	7.8	0.71	6.5	0.79	3.9	0.69	9.2
KI	2.43	2.46	1.2	1.35	4.4	2.45	8.2	2.26	6.9
RbF	1.8	1.79	5.5	1.89	5	1.64	8.8	1.95	8.3
RbCl	0.86	0.78	1.4	0.76	11.6	0.9	4.6	0.86	4.6
RbBr	0.46	0.44	4.3	0.42	3.6	0.49	6.5	0.47	2.8
RbI	0.34	0.34	0	0.36	3.8	0.36	5.8	0.33	2.9
CsF	1.62	1.6	1.2	1.3	9.7	1.75	8	1.69	4.3
CsCl	0.74	0.77	4	0.79	6.7	0.79	6.7	0.69	6.7
CsBr	0.36	0.37	2.7	0.38	0.38	5.5	0.33	0.33	8.3
CsI	0.25	0.22	12	0.24	4	0.24	4	0.27	8
AVERAGE		% DEVIATION	5.572		7.813		6.275		5.715

4. Acknowledgement.

We are extremely thankful to Prof. Md. Mazahir Hasan to suggest the problems and its relevance in the determination of interionic short range repulsive interaction.

References

- [1] Hertzberg G, Molecular Spectra and molecular structure; vol. I – spectra of diatomic molecules (Reinhold-Van Nostrand), New York, 1950.
- [2] Raghubanshi S.S. & Sharma L.K. Indian J. Pure & Applied phys 16, (1978) 1071
- [3] Ghodgankar AM & Ramani K, J. Chem. Soc Faraday Trans Part -2, 77 (1981) 209
- [4] Ghodgaonkar A.M. & Ramani K, Phys Status Solidib (Germany) 108 (1981) K 133
- [5] Verma M.P. & Jha B.L. Indian J. Phys part & 55 (1981) 170
- [6] Morse P.M. Phys Rev (USA) 34 (1929) 57
- [7] Kratzer A. Z. Phys (Germany) 3 (1920) 289
- [8] Rydberg B. Z. Phys (Germany) 73 (1931) 876
- [9] Rittner E.S. J. Chem. Phys 19 (1951) 1030
- [10] Brumer P.P. & Karplus M, J. Chem Phys 58 (1973) 3903
- [11] Varshni Y. P. & Shukla R.C. Rev Mod. Phys, 35 [1963] 130
- [12] Thakur K. P. Indian J. Pure appl. Phys 11 (1973) 549, Indian J. Chem. 12A (1974) 376
- [13] Thakur K.P. and Pandey J.P.J. Chem. Phys 71(1974) 850
- [14] Born M and Mayer J.E. Z. Phys. 75 (1932)
- [15] Hellmann, Acta physica, Chemica 2 (1934) 913, J. Chem. Phys. 3 (1935) 61
- [16] Ali MS and Hasan M. M. Indian J. phys 63 B (1989), 486
- [17] Wilson J.N & Curtis R.M. J.chem.phys 1970,187
- [18] Ruffia A.R.phys. Rev.130,1963,1412
- [19] Cocker.H, J.chen. phys80,1976,2078.
- [20] Pauling L,Proc.Royal soc .Londan A,114 ,1927,191.
- [21] Slater J.C&Kirkwood J.G.phys.Rev 37,1931,682.
- [22] Shankar J,kumar M& Kaur A.J.Indian J. phys 60B,1985,171.
- [23] Mandal & Ghatak J: Indian Chem. Soc Vol. 84, Feb 2007, 145-148

Lockme – Android Security Application

¹, Sumaiya Patel, ², Darshana Thakur, ³, Sujit Sherkar,
⁴, Priyanka Dhamane,

Information Technology Department

^{1,2,3,4}, Padmabhushan Vasantdada Patil Pratishthan's College of Engineering, Mumbai, India

Abstract: This paper presents an Android based App which is a security application. The idea behind this project is to develop an application which will help user of android to create Admin and Guest accounts like other computer based operating system. Security holes in Android operating system occur due to the permission based security model which is not properly enforced during system design. Permission based security model has central role hence it creates security holes in Android OS [1]. Google's android security model erased by its openness

Keywords: Android OS, Permission based security model, central role

I. Introduction

Android is a new, next-gen mobile operating system that runs on the Linux Kernel. Android Mobile Application Development is based on Java language codes, as it allows developers to write codes in the Java language. These codes can control mobile devices via Google-enabled Java libraries. It is an important platform to develop mobile applications using the software stack provided in the Google Android SDK. Android mobile OS provides a flexible environment for Android Mobile Application Development. With the increased pace of life and shrinking time people need everything in the palm of their hand, everything happening with a touch. Hence it all boils down to one point, which system provides the best applications? Android is winning the race globally, accounting for more than 50 percent of the market as of 2012. A tablet may be shared by many people in a organization or at home by family members. So there is a need for the owner to allow a guest account login, the way it is in Desktop PC. This feature is needed, in organizations where individuals are given company handsets. There are many situations where in a foreign (not the owner of handset but works within the same org as the owner) user may face the necessity of using the actual owner's phone (in case the owner is not present in the vicinity) in placing an internal call (call within the organization) or send emails or simply send a group sms. This functionality is precisely the one available on Desktop OS.

2. Existing System

By default the android phone allows only a single user sign on [2]. This person is the owner or the administrator for the phone. Owner has complete privileges. The current android Operating System [3] does not have a facility to create user account.

3. Proposed System

The device will facilitate user of device to create two user accounts viz.

- 1) Administrator
- 2) Guest

The Administrator has all the rights and permission to access all apps. The Guest has call and camera blocked. The guest has no permission to access the camera. She/he cannot make a call. In this application, we ensure that screen lock password of sufficient length is set up before displaying the secure content, as well as the screen lock timeout is also set. It also has an option to disable the camera. It stores all the policy that we set up, e.g. minimum password length, password complexity, screen timeout, etc. Once users enable the device admin application, they are subject to its policies. Complying with those policies typically confers benefits, such as access to sensitive systems and data. If users do not enable the device admin app, it remains on the device, but in an inactive state. Users will not be subject to its policies, and they will conversely not get any of the application's benefits—for example, they may not be able to sync data.

3. Technology Used

For developers:

OS : Windows XP or above
 IDE : Eclipse.
 SDK : android SDK.
 Emulator : any android emulator.
 System architecture : 32/64 bit.

For users:

OS : Android
 Hardware : any android phone
 Size on disk : minimum 1 MB.

4. Classes Used

BroadcastReceiver

android.content.BroadcastReceiver When a matching event is generated in the system, Android delivers the event to that broadcast receiver. Applications with Broadcast Receivers registered in the manifest don't have to be running when the Intent is broadcast for the receivers to execute. They will be started automatically when a matching. This is excellent for resource management as it lets you create event-driven applications that will still respond to broadcast events even after they've been closed or killed.

4.1 DevicePolicyManager

This service is provided through the **android.app.admin.DevicePolicyManager** class. The device administration API provides device administration [4] features at the system level. It allows development of security-aware applications that are useful in enterprise settings

Design

Android GUI is single-threaded, event-driven and built on a library of nest-able components. The Android UI framework is organized around the common Model-View-Controller pattern.

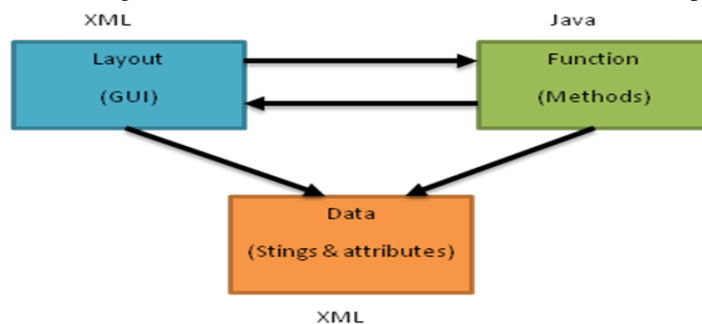


Fig Structure of the Application Design

Basically there are two ways to create a User Interface in Android, either through XML or by creating the UI Programmatically. The diagram shows the different tools used in developing the application for different purposes. The first step is GUI i.e. graphical user interface that is developed using the XML tags. Each form in Android is an Activity. To code for the function and for interconnection of the Activities we use Java. Java provides methods which will help to achieve all the task.

Block Diagram

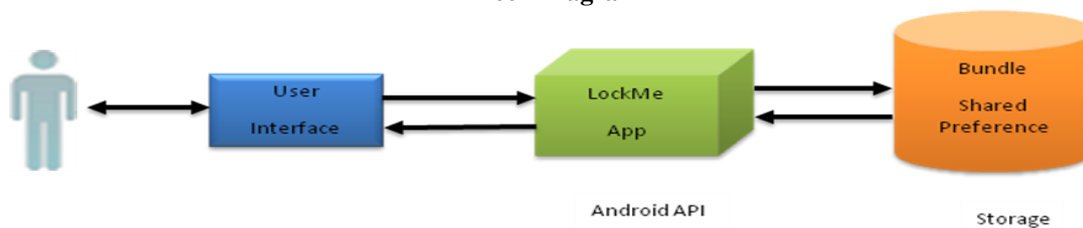


Fig: Architectural Block Diagram

The block diagram shows the architecture of the Application. The user will interact through User Interface which will consist of:

- Setting up Password policies
 - Logging on to device via Admin or guest account
- The LockMe app which is built on Android API will setup the policies for the password such as Numeric, Alphanumeric or Mixed as shown.

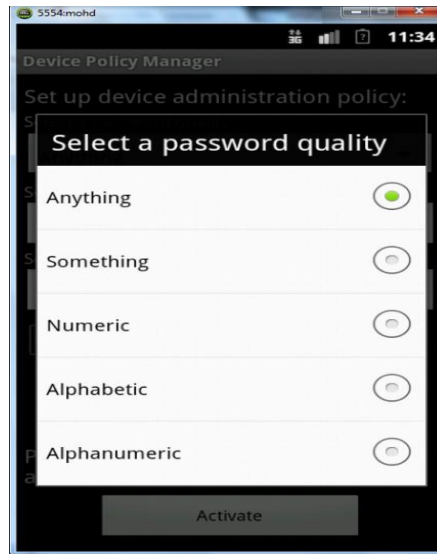


Fig: Selection of password quality

It will also block the calling facility and camera is user is logged on as Guest. For the storage of policies we use Shared Preferences where the policies are written to and read from while logging in. Finally, all the data that is used by the Java and XML is stored in form of values using XML.

4.2 Future Scope

The application has many options as its future scope. Development of mobile security application will be emphasized on following aspects:

- 1) Can be used to lock media folders for user's privacy.
- 2) Can be used to lock other apps.
- 3) Can be used to protect inbox so that no one can view messages.
- 4) Can be used enhance pattern changing.

5. Conclusion

Thus we have proposed an application targeted for android mobile and tablet users create a security-aware application that manages access to its content by enforcing device management policies. When device is protected using this application owner of device decides which content of device will be user see and access it. This application makes changes in OS through application this will help the easy to protect the device from unauthorized user. If other user gets access to device he/she will make change in the system or remove the security policies from device. This application protect user from doing system changes.

References

- [1] Android.com," Available: <http://www.android.com>
- [2] W. Enck, M. Ongtang, and P. McDaniel. Understanding Android security. IEEE Security & Privacy Magazine,7(1):10–17, 2009.
- [3] Technical Blog of Sai Geetha dedicated to Android, <http://saigeethamn.blogspot.com/>
- [4] Sayed Y Hashimi and Satya Komatineni, "Pro Android", Wiley India Pvt Ltd. (2009)
- [5] Android Developers official website, <http://developer.android.com/guide/topics/ui/index.html>
- [6] A visual interface editor for Android, <http://www.droiddraw.org/>
- [7] Static detection of malicious code in executable programs by J. Bergeron, M. Debbabi, J. Desharnais, M. M. Erhioui, Y. Lavoie, and N. Tawbi.
- [8] Android project. <http://source.android.com/>.

Computer Aided Engineering (CAE) Techniques Applied To Hip Implant

¹M. S. Abo_Elkhair, ²M. E. Abo-Elnor, ³A. E. Radi

¹Assoc. Prof, MTC, Cairo, Egypt

^{2,3}Professor of orthopedics, Faculty of medicine Ain-Shams Univ. Cairo, Egypt

Abstract: Methods to predict contact stresses in femoral prostheses can provide an improved understanding of load distribution. The objectives of this study is to apply advanced computer aided engineering techniques (CAE) for predicting stress transfer to femur after implantation of standard and short femoral stems (Proxima stem). A perspective three-dimensional geometry model for the femoral bone using subject-specific geometry from X-ray computed tomography image data (CTI) is used to create 3D CAD model. Forces acting on the femur in different gait regimes were reviewed and compared while loaded with standard and then with Proxima stem. And finally a developed finite element analysis model based on the created CAD model with forces acting on both femurs loaded with standard and Proxima stem is analyzed.

Keywords: Computer aided engineering, Biomechanics, Femur modeling, implant, Hip joint

I. Introduction:

Anatomic short femoral prostheses with a prominent lateral flare have the potential to reduce stress-shielding in the femur through a more physiological stress distribution to the proximal femur. Femur bone crack and fracture is one of the most common forms of injuries during accidents. Body weight is transferred through pelvis to femur by hip joint. Bone is a living tissue, which continuously rebuilds its structure according to the direction of loads exerted on it. After insertion of a metal prosthesis into the medullary canal, the load equilibrium and the remodel tissues in the bone are disturbed. Stress-shielding activity of the implant (Fig. 1), which is stiffer, makes the bone atrophies [1]. Reduction of stresses in bone with respect to the natural state causes its adaptation to the new conditions manifested by mass changing (external remodeling) or bone density changing (internal remodeling). The latter is especially dangerous because, as already indicated, it can cause aseptic loosening of the implant. Studying different factors affecting stress-shielding activity required appropriate modelling and simulation of the hip stem and femoral bone along with cemented media used in hip replacement surgery.

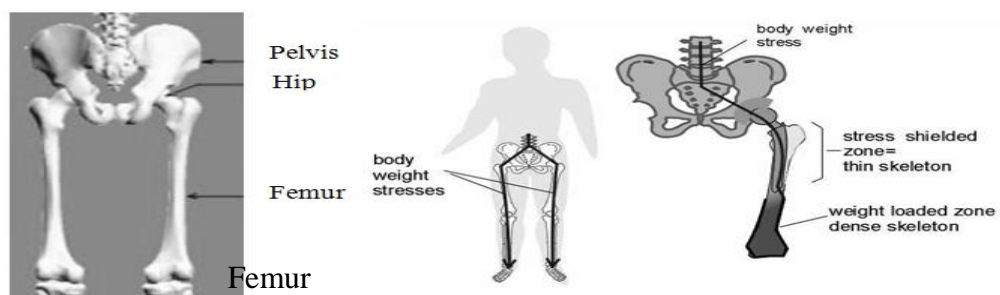


Fig. 1, Femur bone in human skeleton

The proper modeling of femur hip replacement can be achieved through the following processes:

- [1] Acquisition of computer tomography (CT) data of the femur.
- [2] Geometrical modeling of the femur and design of prosthesis stem in a computer-aided design (CAD) system.
- [3] Calculation of forces acting on hip during different gait regimes.
- [4] Finite element analysis of the selected implant prosthesis and bones.

2. Materials and Methods

2.1 Acquisition and processing of CT data:

Novel techniques have been developed to convert 3D image data, obtained from Computer Tomography, automatically into numerical meshes suitable for Finite Element (FE) analysis. CT measurements [2] of the diseased hip joint were performed in order to acquire coordinates of the points defining the femur

shape. The CT images obtained were then processed to filter the required data and detect the femur shape (Fig. 2).

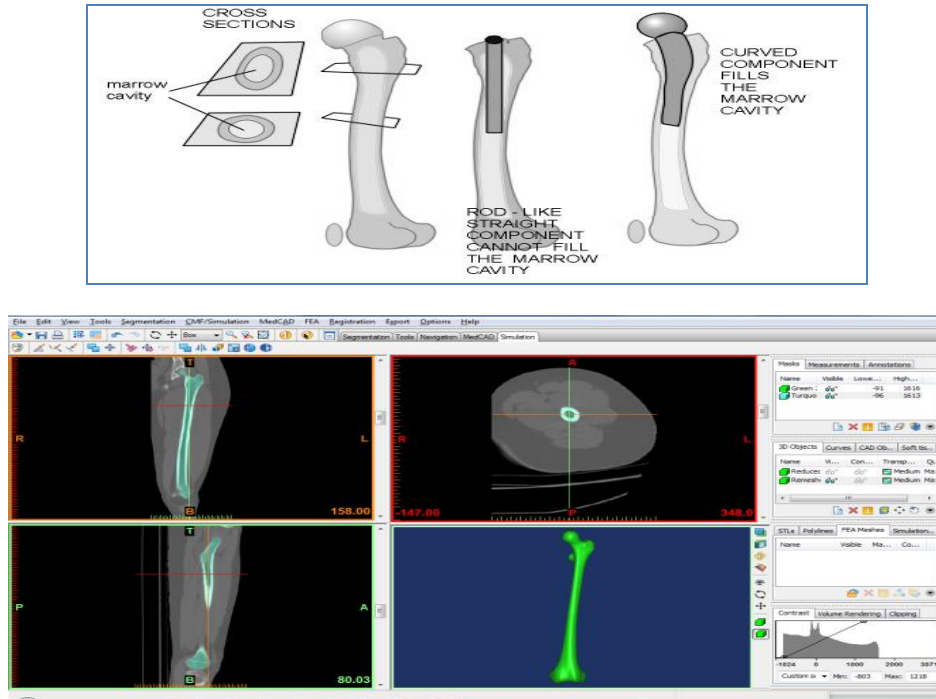
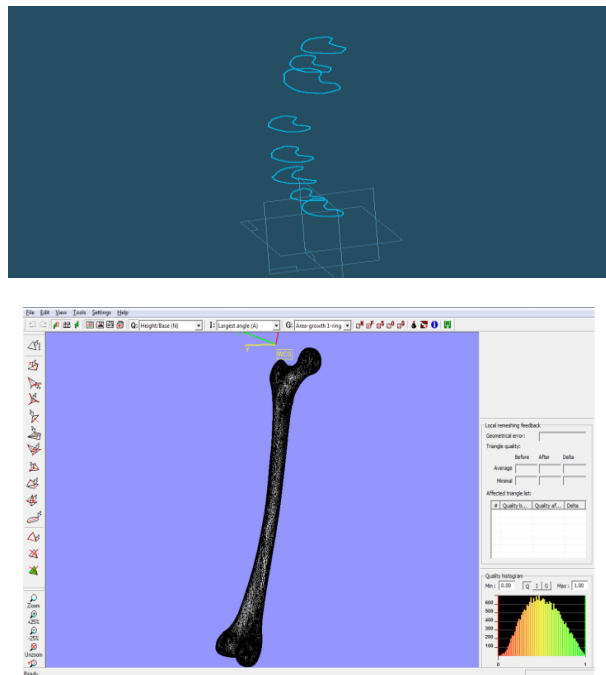


Fig. 2, CT images implementation to create 3D model of femur bone

MIMICS is a software suite that performs the segmentation of the anatomy through sophisticated three-dimensional selection and editing tools [3]. The Mimics software is an image-processing package with 3D visualization functions that interfaces with all common scanner formats.

2.2 Femur Geometrical modeling and prosthesis stem design

The processed CT data obtained by Mimics is then used either as a meshed model for rapid Finite Element Analysis of the femur or to create a 3D cad model, using AutoDesk Inventor CAD software, for prosthesis stem design as shown in figure (3).



Slices for further CAD uses

Mesh model for Finite Element Analysis
 Fig. 3, 2D slices and 3D mesh results of the processed CT data

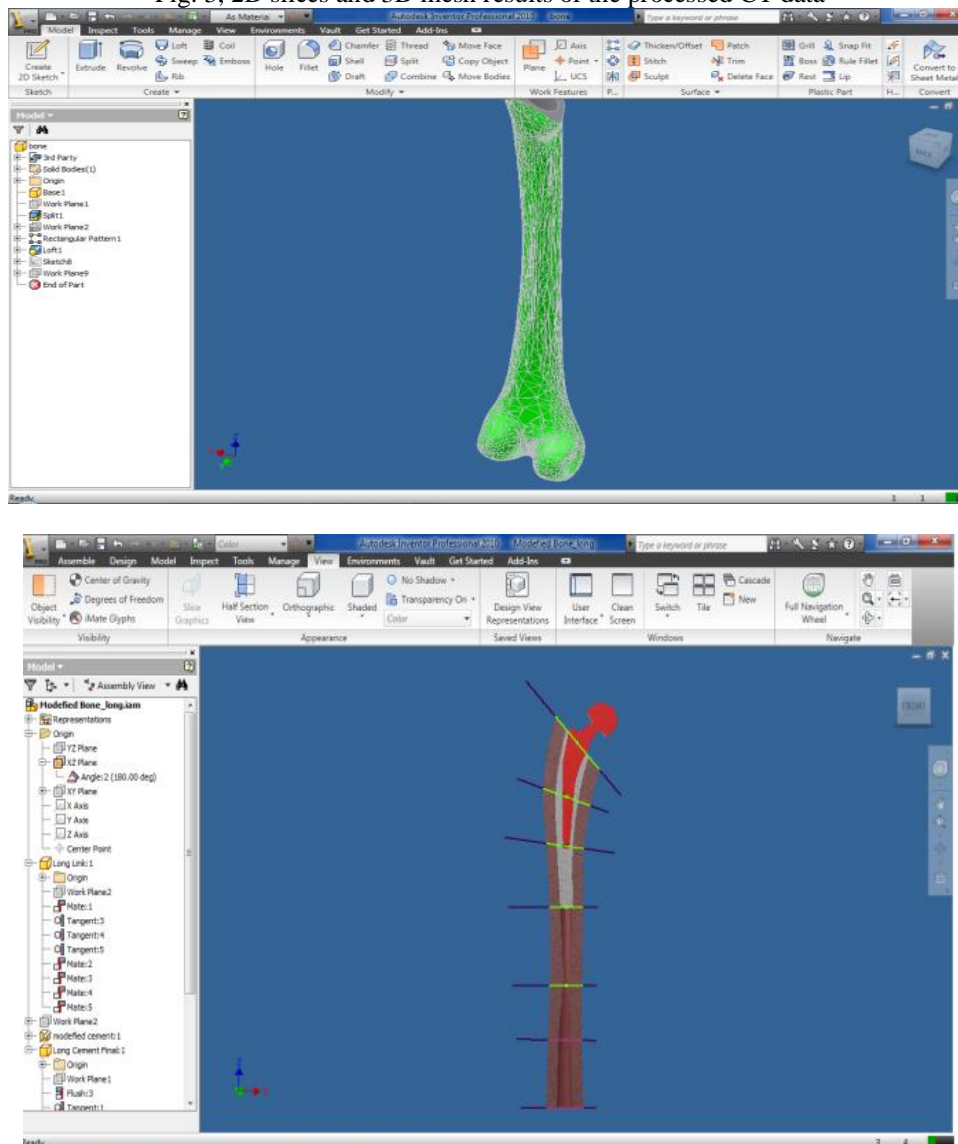


Fig. 4, Processing of the 3D model (cutting) in order to obtain the interested part of the femur

The proposed custom implant design was done using Autodesk Inventor CAD software (Fig. 4). A CAD model of the patient's distal femur was imported and used as the base for the design. The articulating surface was kept intact to avoid altering the gait and to preserve the correct patellar groove so as to prevent resurfacing and patellar dislocation. A set of spline curves were created along the interface surface in a radial pattern (Fig. 5), and a single spline was created to connect all curves in a central plane. A swept-blend command was used to create the smooth articulating surface. The bone-implant interface was created using a new set of curves in the same planes as the original curves. The inner curves were offset from the original curves and then manually edited to avoid any undercuts. The offset distance was kept uniform to create an implant with constant wall thickness. A new center plane curve was created as well to prevent the need for undercuts. A swept-blend-cut command was used to create the bone-implant interface. Additional cuts and fillets were added to provide an implant with smooth surfaces and edges.

2.3 Forces acting on hip during different gait regimes:

Muscle forces exerted during human movement provide insight in tissue load and muscle function and/or malfunction. The use of musculoskeletal models in the estimation of muscle force has been widely reported in the literature [4].

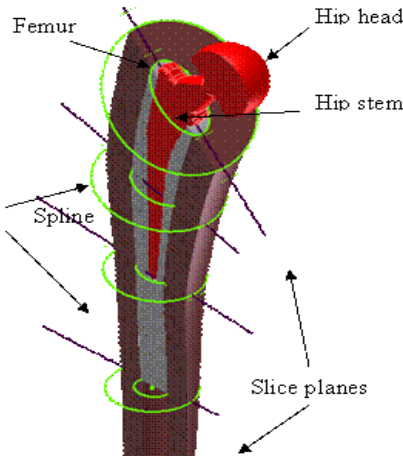


Fig. 5, Femur bone and prosthesis stem modeling

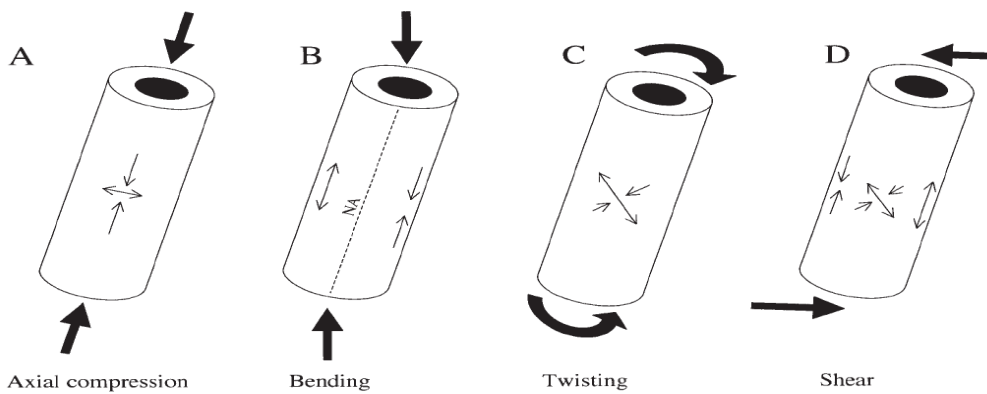


Fig. 6, Beam and cross-section views of applied forces and strain distributions in compression (A), bending (B), twisting (C), and shearing (D).

Bones are loaded in four possible ways [5], depicted in figure (6), they can be compressed axially, bent, sheared, and twisted. Often these loads occur in combination (most long bones are mostly bent, but also compressed and twisted to varying extents). Based on terminologies described in figure (7), a literature review of several analytical and experimental results [6] are plotted in figure (8) and figure (9). These results are used to simulate forces acting on femur hip for the finite element analysis.

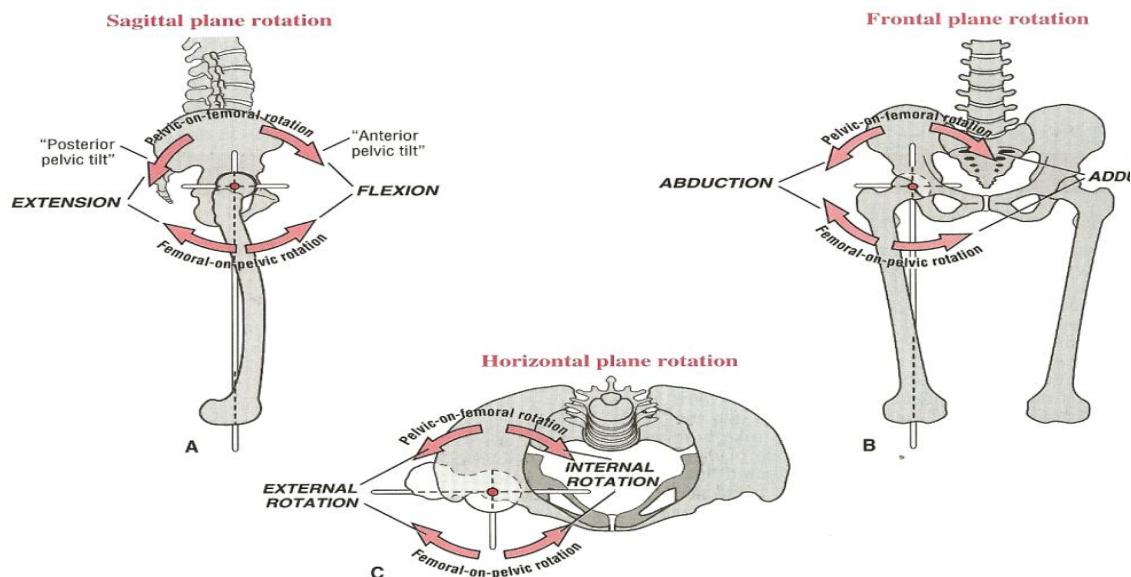


Fig. 7, femur degree of freedom terminology

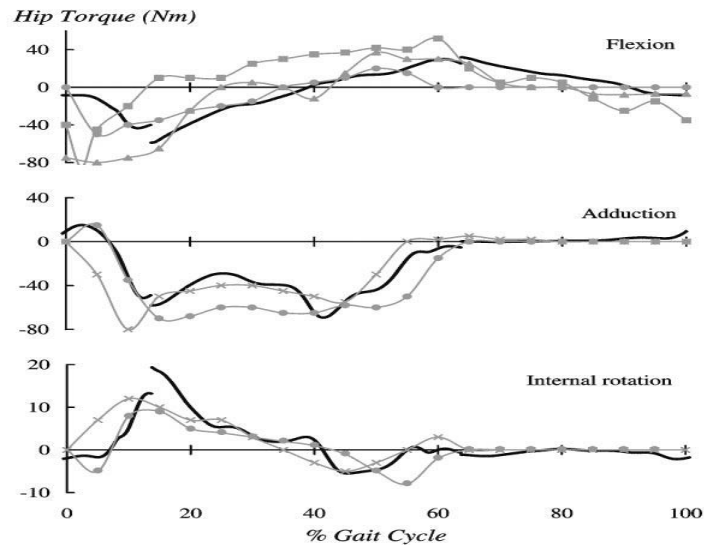


Fig. 8, The net muscle moments applied about the axes of the hip joint

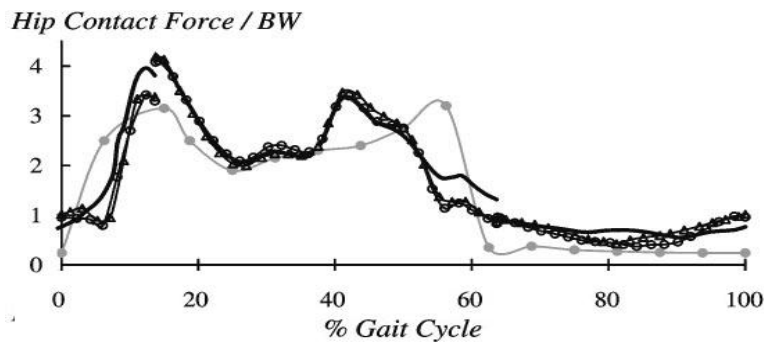
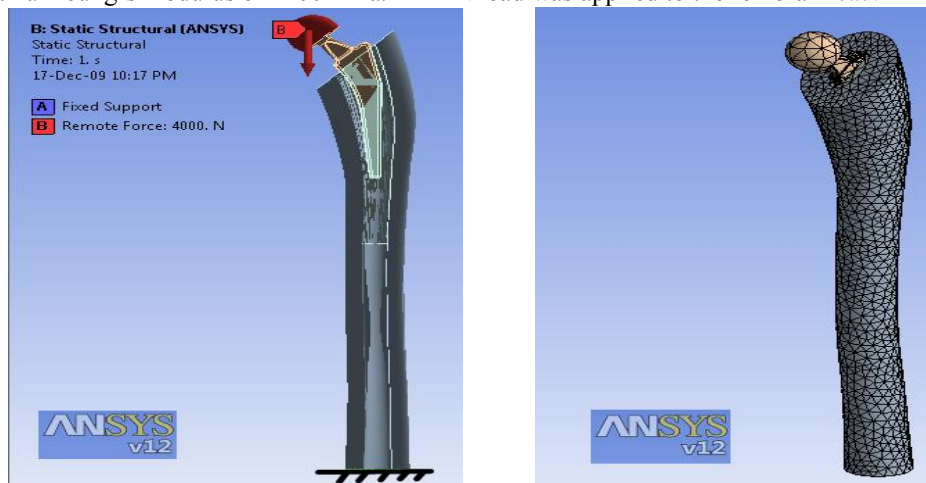


Fig. 9, Joint contact force in the hip

3. Finite Element Analysis

A finite element model of spacer and femur was developed to analyze stresses [7]. The analysis was performed using ANSYS, a FEA software (ANSYS Inc., Canonsburg, United States). CAD model was obtained as described before and transferred to ANSYS for FEA. Figure (10) shows both boundary condition and mesh distribution. Effect of knee-femur connection is modeled as fixed boundary for simplicity. The cancellous bone within the femur head has a Young's modulus of 1300 MPa and Poisson's ratio 0.28 while bone cement were analysed with a Young's modulus of 2200 MPa. A 4 kN load was applied to the femoral head.



femur force and boundary condition

mesh distribution

Fig. 10, Initial and boundary conditions for the FEA

4. Results and Discussion

Finite element results reveal the capability of the proposed computer aided design process to handle such an analysis requirements for orthopedic implants evaluation. As shown in figure (11) and figure (12), the homogenous distribution of the strain and stress fields across the contact layer between hip stem and cemented material and between cemented material and femur bone is an accepted proof of contact establishment of the cemented fill and both hip and femur. Extensive analysis of hip stem design, material and effect of using cement or cement-less installation of the hip stem along with studying the effect of cement material can be carried out using proposed model. Also the effect of different loads in gait regimes on stress-shielded zone will be analyzed latter on.

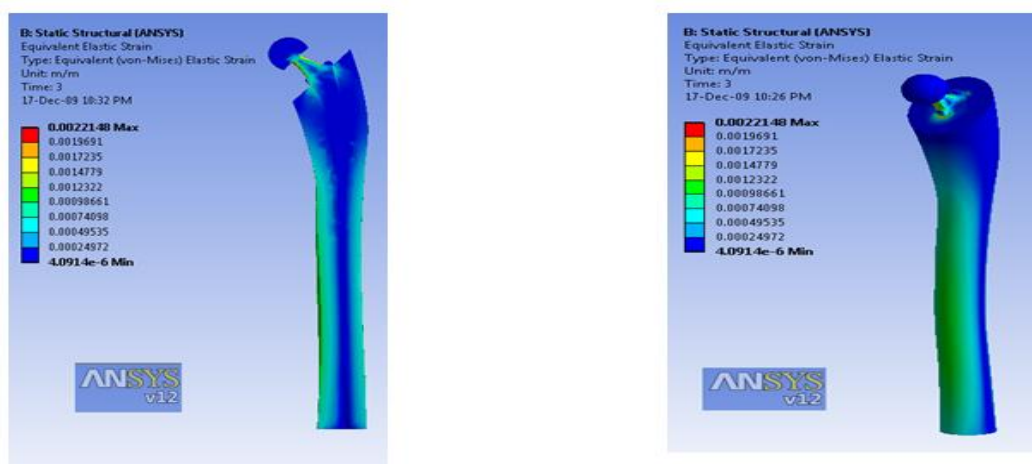


Fig. 11, Elastic strain distribution in section view (left) and 3D view (right)

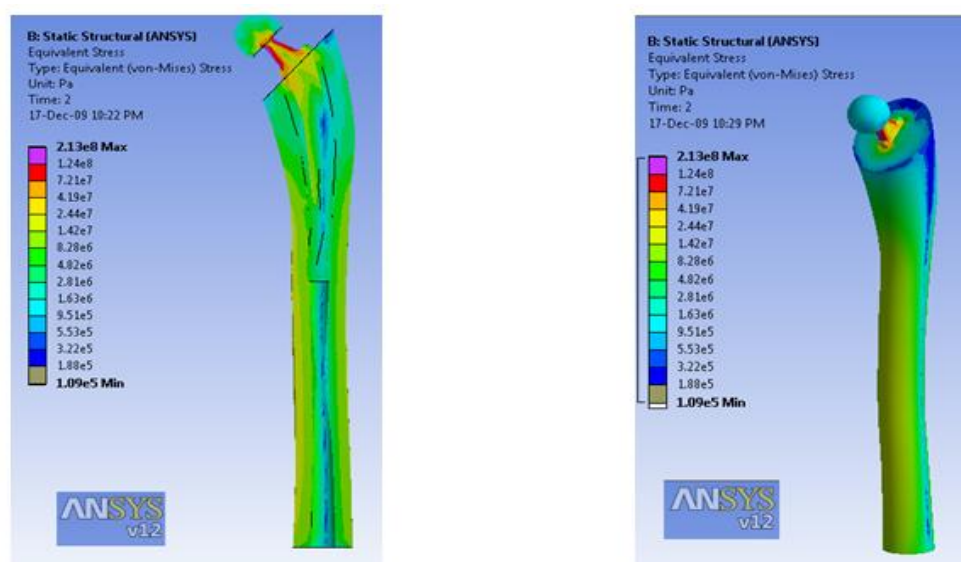


Fig. 12, (von-Mises) Stress distribution in section view (left) and 3D view (right)

5. Conclusions

Rapid custom modeling of human skeleton using advanced computed tomography (CT) techniques is believed to be the most effective way of selection of the right implant design for surgery. Advanced computer aided engineering (CAE) techniques such as CAD and FEA can provide better examination and analysis of the designed implant before surgery operation to insure high durability of the designed implant. In the research field, factors affecting stress distribution to human bones via the implant can be done using the CAE facilities for implant design optimization.

References

- [1] Mihai Ovidiu GHIBA, Lucian RUSU, "Geometrical design of custom-made femoral stem prostheses", Fascicle of Management and Technological Engineering, Vol. VII, No. XVII, 2008.
- [2] MIMICS (10.0) tutorial software package.
- [3] K. L. Chelule, Dr. T. Coole, D.G. Cheshire, "Fabrication of medical models from scan data via rapid prototyping techniques"
- [4] Erdemir, A., McLean, "Model-based estimation of muscle forces exerted during movements", Clinical Biomechanics Vol. 22, PP. 131-54, 2007.
- [5] Osbjorn M. Pearson, Daniel E. Lieberman, "The Aging of Wolff's "Law": Ontogeny and Responses to Mechanical Loading in Cortical Bone", YEARBOOK OF PHYSICAL ANTHROPOLOGY, Vol. 47, PP. 63-99, 2004.
- [6] Frank C. Anderson, Marcus G. Pandy, " Static and dynamic optimization solutions for gait are practically equivalent", Journal of Biomechanics, Vol. 34, PP. 153-161, 2001.
- [7] T. Thielen, S. Maas, A. Zuerbes, et al, "Mechanical behaviour of standardized endoskeleton-including hip spacers implanted into composite femurs", International Journal of Medical Sciences, Vol. 6, No.5, PP.280-286, 2009.

New Methods for Horizon Line Detection in Infrared and Visible Sea Images

Ilan Lifshitz¹, Evgeny Gershikov² and Benjamin Milgrom³

Department of Electrical Engineering,
Braude Academic College of Engineering,

Abstract:

In this work we propose methods for horizon line detection and target marking in marine images captured by either infra-red (IR) or visible light cameras. A common method for horizon line detection is based on edge detection and the Hough transform. This method suffers from serious drawbacks when the horizon is not a clear enough straight line or there are other straight lines present in the image. We improve the algorithm performance by proposing a pre-processing stage eliminating some of the false detections. We also propose a new method for horizon line detection. The new algorithm is based on the idea of segmenting the image into two regions (sky and sea) by comparing the regional probability distribution functions (PDFs) or histograms. The line maximizing a statistical distance between these PDFs is chosen. This method is highly complex and can be further improved. Thus, we proceed to introduce two new methods combining the basic edge detection and Hough transform (EDHT) method to detect several candidate lines in the image and a statistical criterion to find the optimal line among the candidates. The chosen criterion can be based on regional covariances or the distance between PDFs as described above. We show that choosing the first option provides the best performance among the methods tested, at least with respect to the angular error, and yields a low complexity fast algorithm. We compare all the examined methods not only quantitatively by their average accuracy and relative speed, but also visually for several test images. Our conclusion is that all the methods introduced in this work can be beneficial for automatic processing of marine images for the purpose of tracking, navigation, target recognition and other applications.

Keywords: horizon detection, marine images, edge detection, Hough transform, image analysis, covariance based method, histogram-based method

1. Introduction

The horizon line is used for different purposes, such as navigation in airborne and marine vehicles and military surveillance. A number of horizon line detection methods are known, for example, [3-5, 7, 9-15]. Some of these methods are based on edge detection [8], while others employ different techniques [9]. Due to the variety of techniques, a comparison of the detection performance that they can achieve can be very helpful. The goal of this research is to take construct a robust, efficient and high performance algorithm for horizon line detection in both infrared and visible light images by introducing new techniques and combining them with existing methods. For simplicity, we consider methods that use only the luminance information of the image. Considering that in the later stages of this research the proposed algorithm is to be implemented on a stand-alone hardware unit, algorithms complexity and their relative speed is also evaluated. First we examine some of the existing methods for sea-sky line detection that are of special interest in this work.

1.1. Edge detection and Hough transform based algorithm (H-EDHT)

The idea of using edge detection and the Hough transform [2] is not new. However, sometimes there are other strong edges present in the image that are confused for the horizon. We propose to use the pre-processing of Stages 1-3 to reduce the probability of this occurrence. The stages of this method can be summarized as follows.

- [1] Pre-process the image using morphological erosion [15] to reduce the probability of the detection of weak edges in the later stages. A small circular structuring element can be used here. Alternatively, the image can be smoothed using a low pass filter, but we found erosion to provide better performance.
- [2] In order to emphasize the horizon line and to decrease the non-relevant grayscale details we use standard deviation filtering [13] and mean filtering.
- [3] An optional stage for clearing non-dominant lines: apply Canny's [1] edge detector to the mean filtered image, then logically invert the image bits and use morphological erosion similar to Stage 1 to thicken the image edge lines.
- [4] Apply Canny's edge detector to the pre-processed image.
- [5] Apply the Hough transform [2] to the edges map.
- [6] Choose the horizon line to be the longest line found in the previous step.

1.2. Regional covariance based algorithm (H-COV)

An algorithm for horizon detection for remotely piloted micro air vehicles was introduced in [3]. The algorithm receives an image taken from the air as input and searches for an optimal partition of the image into two regions: sky and ground (or sky and sea) using a line, which is the detected horizon. The optimization criterion is based on the determinants and the traces of the covariance matrices of the two regions. More specifically, if we denote a sky pixel by $\mathbf{x}_{i,j}^s = [R_{i,j}^s \ G_{i,j}^s \ B_{i,j}^s]^T$, where $R_{i,j}^s, G_{i,j}^s, B_{i,j}^s$ are the primary red, green and blue values at the pixel (i,j) and, similarly, we denote a ground pixel by $\mathbf{x}_{i,j}^g = [R_{i,j}^g \ G_{i,j}^g \ B_{i,j}^g]^T$, then the covariance matrices of the regions are given by $\Lambda^s = E\left(\left(\mathbf{x}_{i,j}^s - \mu^s\right)\left(\mathbf{x}_{i,j}^s - \mu^s\right)^T\right)$, $\mu^s = E\left(\mathbf{x}_{i,j}^s\right)$ and $\Lambda^g = E\left(\left(\mathbf{x}_{i,j}^g - \mu^g\right)\left(\mathbf{x}_{i,j}^g - \mu^g\right)^T\right)$, $\mu^g = E\left(\mathbf{x}_{i,j}^g\right)$. $E()$ denotes here statistical mean. The optimization criterion, considered for all the possible horizon line orientations and positions and maximized is given by:

$$(1) \ J = \frac{1}{\det(\Lambda^s) + \det(\Lambda^g) + \text{trace}^2(\Lambda^s) + \text{trace}^2(\Lambda^g)},$$

where $\det()$ denotes the determinant and $\text{trace}()$ denotes the trace of the covariance matrices Λ^s and Λ^g . We consider a similar criterion to the one in [3] for the luminance image, thus the optimization term J becomes

$$(2) \ J = \frac{1}{\text{var}(Y^s) + \text{var}(Y^g) + \text{var}^2(Y^s) + \text{var}^2(Y^g)},$$

where $\text{var}()$ stands for variance and Y^s, Y^g are the luminance values of the sky and ground regions, respectively.

A simplified optimization criteria

$$(3) \ J = \frac{1}{\text{var}(Y^s) + \text{var}(Y^g)}$$

can be used instead of the one in [3] with similar results. Also, defining a region of interest (ROI) in the image and searching the horizon line only in this area speeds up the algorithm significantly. Alternatively, the input image can be down-sampled prior to the application of the algorithm to reduce its runtime, but this will decrease the accuracy as well. The structure of this paper is as follows. In the next section we present a new histogram based method for horizon line detection in marine images. Then in Section 3 we discuss algorithms combining the idea of edge detection and Hough transform with a statistical optimization criterion for determining the optimal line among a small set of candidates. In Section 4 we describe the methods and criteria used in the comparison of these algorithms and the horizon detection results: quantitative and visual. Section 5 presents a summary of this work and our conclusions.

2. A New Histogram Based Algorithm

The problem of finding the horizon line in sea images can be regarded as the problem of segmenting the image into two regions with different characteristics: the sky and the sea. We expect higher spatial correlations of the pixels inside each region than the inter-region correlations. This idea was exploited in Section 1.2 by calculating the covariance matrices in each region and maximizing a target function based on these matrices for all (or a set of) possible horizon line positions. Clearly, the target function is maximized when the covariance matrix of each region becomes closer to the matrix

$$(4) \ CM = \nu \begin{pmatrix} 1 & 1 & 1 \\ 1 & 1 & 1 \\ 1 & 1 & 1 \end{pmatrix},$$

where ν is a positive scalar, corresponding to the case of constant and equal red, blue and green values in each region. A distance metric between the sea and sky regions is not considered in Section 1.2, but can be added to the target function. For example, the terms $cov(R^{sky}, R^{sea})$, $cov(G^{sky}, G^{sea})$ and $cov(B^{sky}, B^{sea})$, standing for the covariances of the red, green and blue primary values, respectively, in the sky and sea regions, can be used. These covariances can be estimated using probability distributions or histograms of the image since usually the number of pixels in the two regions is not the same. Another idea is to measure the probability distribution functions (PDFs) in each of the regions and maximize the distance between those probability

functions. If the discrete PDF of the luminance in the sky region is denoted $p_Y^{Sky}(y)$ and the discrete PDF of the luminance in the sea region is denoted $p_Y^{Sea}(y)$ one can consider the Bhattacharyya distance between them, given by

$$(5) D_B(p_Y^{Sky}, p_Y^{Sea}) = -\ln(C_B(p_Y^{Sky}, p_Y^{Sea})),$$

where C_B is the Bhattacharyya coefficient, calculated as

$$(6) C_B(p_Y^{Sky}, p_Y^{Sea}) = \sum_y \sqrt{p_Y^{Sky}(y) p_Y^{Sea}(y)}.$$

We suggest maximizing the distance $D_B(p_Y^{Sky}, p_Y^{Sea})$ or equivalently minimizing the coefficient $C_B(p_Y^{Sky}, p_Y^{Sea})$ for a set of possible horizon line positions. One can also consider the Hellinger distance between the two PDFs, given by

$$(7) D_H(p_Y^{Sky}, p_Y^{Sea}) = \sqrt{\frac{\sum_y (\sqrt{p_Y^{Sky}(y)} - \sqrt{p_Y^{Sea}(y)})^2}{2}}$$

and related to the Bhattacharyya coefficient by

$$(8) D_H(p_Y^{Sky}, p_Y^{Sea}) = \sqrt{1 - C_B(p_Y^{Sky}, p_Y^{Sea})}.$$

Thus, maximizing the Hellinger distance or the Bhattacharyya distance is equivalent. Of course, other statistical distances for discrete PDFs can be considered as well. One could just replace the $D_B(p_Y^{Sky}, p_Y^{Sea})$ distance below with any other suitable statistical distance. Note that it does not have to be a metric. We denote the algorithm H-HIS (HIS stands for Histograms) and propose the following steps.

2.1. Stages of the algorithm

The horizon line spatial and angular position can be measured by its height above the center of the image and its angle relative to the horizontal line going from left to right.

For all possible heights and angles of the line, that are considered, the following stages are to be performed.

- [1] Segment the image using the line into two regions: sky and sea.
- [2] Calculate the PDFs of both regions p_Y^{Sky} and p_Y^{Sea} using the same number of gray levels, e.g., 64 for color depth of 8 bits per pixel (for the luminance component or each of the primary colors).
- [3] Calculate the Bhattacharyya distance D_B between the two histograms.

The line height and angle chosen are those corresponding to the maximum of $D_B(p_Y^{Sky}, p_Y^{Sea})$.

3. Improving The H-Edht Algorithm

The H-EDHT algorithm, described above, can be improved by combining it with the H-COV or H-HIS algorithms. The idea is that after the stages of pre-processing and edge detection, instead of just choosing the longest line in the edge map, several candidate lines are considered among the longest ones. Then the line yielding the best segmentation of the image into sky and sea regions among the candidates is taken. The criterion of optimality here can be the one proposed for H-COV or the one proposed for H-HIS. Thus, we consider three algorithms following the same first stages until the edge map is produced and a predefined number (e.g., 5 or 10) of the longest candidate lines is taken. Then we can do one of the following.

- a. Choose the candidate line having the maximal length. This is the basic H-EDHT algorithm.
- b. Choose the candidate line providing the best segmentation of the image into sky and sea regions. The best segmentation is determined based on the maximal value of the criterion function of (3). We denote this algorithm H-EDHT-COV.
- c. Once again we consider the best segmentation into two regions, but the criterion of optimality is that of (5). We denote this algorithm H-EDHT-HIS.

4. Comparison Methods And Results

Next, we describe the images and criteria used for the comparison of the algorithms described in this work.

4.1. Images used to compare the algorithms

The results of horizon detection for a group of 10 marine infra-red images and 10 marine visible light images are presented in this work. Image input format is true color (24 bit per pixel) non-compressed BMP. Resolutions used vary from around 300x200 to 1024x768 pixels. Most images contain a horizon line separating the sea and the sky clearly distinguished by the human eye. However, sometimes the horizon line is slightly distorted by camera optics and sea waves or concealed by marine vessels. To further challenge the selected algorithms, several images contained clouds or sun light effects near the surface of the sea water.

4.2. Comparison criteria

The algorithms were compared with respect to accuracy and speed. The accuracy was measured for the detected horizon angle (in degrees) relative to a horizontal line as well as the height of the line above the center of the image (in pixels). The errors provided in the next section for these two horizon line parameters are measured relative to the line height and angle as determined visually. The algorithms' speed was measured in terms of run time.

4.3. Quantitative results

The accuracy comparison for the algorithms described above (height and angle deviations) is given in Table 1 for infra-red images and in Table 2 for visible light images. In some of these images the horizon is not horizontally aligned (e.g., Figs. 1-3). As can be seen, the angular deviation is very small on average for the H-EDHT algorithms and especially H-EDHT-COV (0.06 degrees on average for IR images, 0.21 degrees for visible light images). The height deviation is smallest for the H-EDHT-COV method as well when considering IR images, but for visible light images, the best performers are H-COV and H-HIS. The run times of the methods are shown in Tables 3 and 4, as measured for a combined C++ and MATLAB implementation. When considering these results, the fastest technique is H-EDHT for both sizes of the images tested, but the H-EDHT-COV and H-EDHT-HIS methods are very close behind. The H-COV and H-HIS algorithms are significantly slower than H-EDHT due to the required intense computations of covariances or histograms in the process of the horizon detection.

4.4. Visual results

Visual results are provided in Figs. 1-2 for IR images and in Figs. 3-5 for visible light images. As can be seen, all the methods provide good results, however sometimes a small deviation can be observed from the horizon line as detected by the eye. Examples are H-COV result for IR_5 image (Fig. 1) or for IR_6 image (Fig. 2).

Table 1. Mean height deviation (pixels) and angle deviation (degrees) for the five algorithms when tested on IR images

Algorithm	Mean height deviation	Mean angle deviation
H-EDHT	1.49	0.14
H-COV	2.63	0.42
H-HIS	2.90	0.72
H-EDHT-COV	0.65	0.06
H-EDHT-HIS	1.41	0.15

Table 2. Mean height deviation (pixels) and angle deviation (degrees) for the five algorithms when tested on visible light images

Algorithm	Mean height deviation	Mean angle deviation
H-EDHT	3.69	0.28
H-COV	2.20	0.32
H-HIS	2.22	0.31
H-EDHT-COV	3.32	0.21
H-EDHT-HIS	3.25	0.24

Table 3. Mean run times (seconds) for the five horizon detection algorithms for images of size 640x480 [pixels]

Algorithm	Mean Time (sec.)
H-EDHT	0.2
H-COV	12.1
H-HIS	10.2
H-EDHT-COV	0.2
H-EDHT-HIS	0.2

Table 4. Mean run times (seconds) for the five horizon detection algorithms for images of size 1024x768 [pixels]

Algorithm	Mean Time (sec.)
H-EDHT	0.3
H-COV	61.1
H-HIS	48.9
H-EDHT-COV	0.4
H-EDHT-HIS	0.4

5. Conclusions

In this work we have compared five algorithms for automatic detection of the horizon line in marine images. These five algorithms include a method based on edge detection and Hough transform (H-EDHT), a covariance based method (H-COV), a new histogram based method (H-HIS) and two combinations of H-EDHT with the latter algorithms: H-EDHT-COV and H-EDHT-HIS. The H-EDHT method is commonly used for horizon line detection, but in this work we have added an improved pre-processing stage to it to enhance its performance, that includes the removal of noise and other obstructing details (like waves) from the image using morphological operations and other techniques. All five methods were implemented and tested on a group of infra-red images taken at night and on a group of visible light images taken during the day. We compared the algorithms with respect to angle and height deviations of the detected horizon line from the one determined manually and also with respect to run times. Our conclusion is that the H-EDHT-COV method is the most accurate algorithm with respect to the angle deviation, but it is sometimes less precise than H-COV or H-HIS with respect to the height deviation. If we consider the run times as well, the EDHT methods (H-EDHT, H-EDHT-COV and H-EDHT-HIS) are much faster than the covariance based H-COV or histogram based H-HIS algorithms. Thus, in applications where run-time is of primary importance, such as in real-time surveillance, we recommend using H-EDHT-COV, while for other applications H-COV can be a good candidate. All the methods, however, provide sufficiently good visual results. Note, that all the methods considered in this work use only the luminance information of the image for simplicity and low complexity of the algorithms. In the future, we intend to examine the use of the color information in visible light images [6] and determine whether it can improve the accuracy of horizon line detection.

6. Acknowledgement

We would like to thank the administration of Ort Braude Academic College of Engineering and the Department of Electrical Engineering for providing the opportunity and financial means to conduct this research.

References

- [1] J. Canny, "A computational approach to edge detection", IEEE Transactions on PAMI, 8(6), 1986, pp. 679-697.
- [2] R. O. Duda and P. E. Hart, "Use of the Hough Transformation to Detect Lines and Curves in Pictures", Comm. ACM, 15(1), 1972, pp. 11-15.
- [3] S. M. Ettinger, M. C. Nechyba, P. G. Ifju, and M. Waszak, "Vision-guided flight stability and control for micro air vehicles", Proc. IEEE Conf. on Intelligent Robots and Systems, Lausanne, Switzerland, 2002, pp. 2134 - 2140.

- [4] S. FefilatyeV, V. Smarodzinava, L.O. Hall, and D.B. Goldgof, "Horizon detection using machine learning techniques". Proc. Intern. Conf. on Machine Learning and App., 2006, pp. 17-21.
- [5] S. FefilatyeV, D.B. Goldgof, and L. Langebrake. "Towards detection of marine vehicles on horizon from buoy camera". Proc. SPIE, 2007, pp. 6736:67360O.
- [6] E. Gershikov and M. Porat, "On color transforms and bit allocation for optimal subband image compression", Signal Processing: Image Communication, 22(1), Jan. 2007, pp. 1-18.
- [7] C. Jiang, H. Jiang, C. Zhang and J. Wang; , "A New Method of Sea-Sky-Line Detection," Proc. of International Symposium on Intelligent Information Technology and Security Informatics (IITSI), April 2010, pp.740-743.
- [8] S. Kosolapov, "Robust Algorithms Sequence for Structured Light 3D Scanner Adapted for Human Foot 3D Imaging", Journal of Comm. and Computer, 8(7), 2011, pp. 595-598.
- [9] Tz. Libe, E. Gershikov and S. Kosolapov, "Comparison of methods for horizon line detection in sea images", Proc. CONTENT 2012, Nice, France, 2012, pp 79-85.
- [10] J.-W. Lu, Y.-Z. Dong, X.-H. Yuan and F.-L. Lu, "An algorithm for locating sky-sea line", Proc. of IEEE International Conference on Automation Science and Engineering, Oct. 2006, pp.615-619.
- [11] K. Nonami, F. Kendoul, S. Suzuki, W. Wang, and D. Nakazawa, Autonomous flying robots (Springer, Tokyo, Dordrecht, Heidelberg, London, New York, 2010).
- [12] Y. Wang, Z. Liao, H. Guo, T. Liu, and Y. Yang, "An approach for horizon extraction in ocean observation", Proc. IEEE Congress on Image and Signal Processing, 2009, Tianjin, China, pp. 1-5.
- [13] P. Wang, J. Tian and C. Gao, "Locating sea-sky line in infrared image based on complexed degree calculation", Proc. SPIE 7494, 74941P, 2009.
- [14] X. Wang, T. Zhang, L. Yan, X. Yang and G. Ao, "A method of sea-sky-line detection in complex sea background", Proc. SPIE 7495, 74950U, 2009.
- [15] D. Yan-zhi, S. Xiao-dong, W. Changjing, and X. Wei-gang, "Application of soft mathematical morphology in image segmentation of IR ship images", Proceedings ICSP 04, 2004, pp. 729-732.

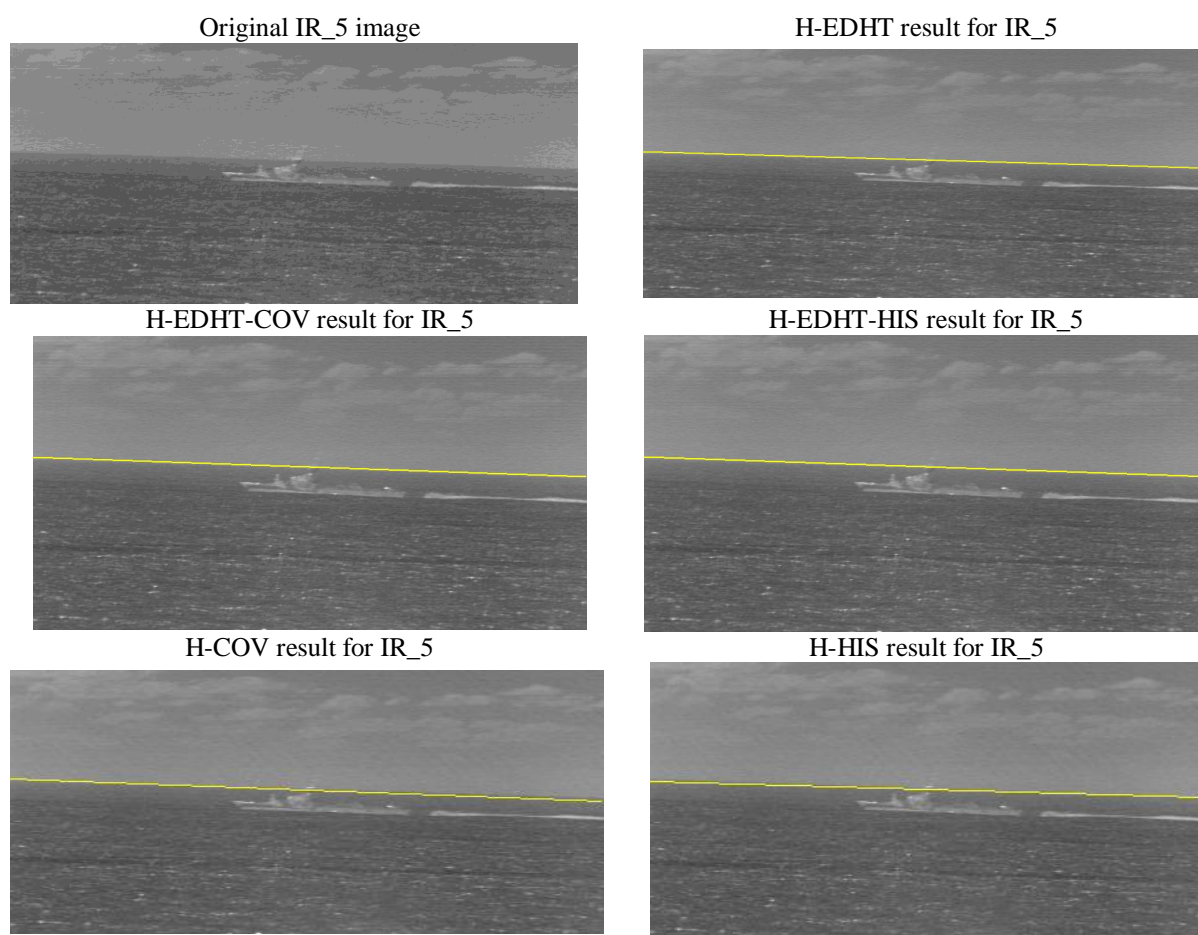


Figure 1. Horizon detection results for image IR_5. The (yellow) line marks the detected horizon.

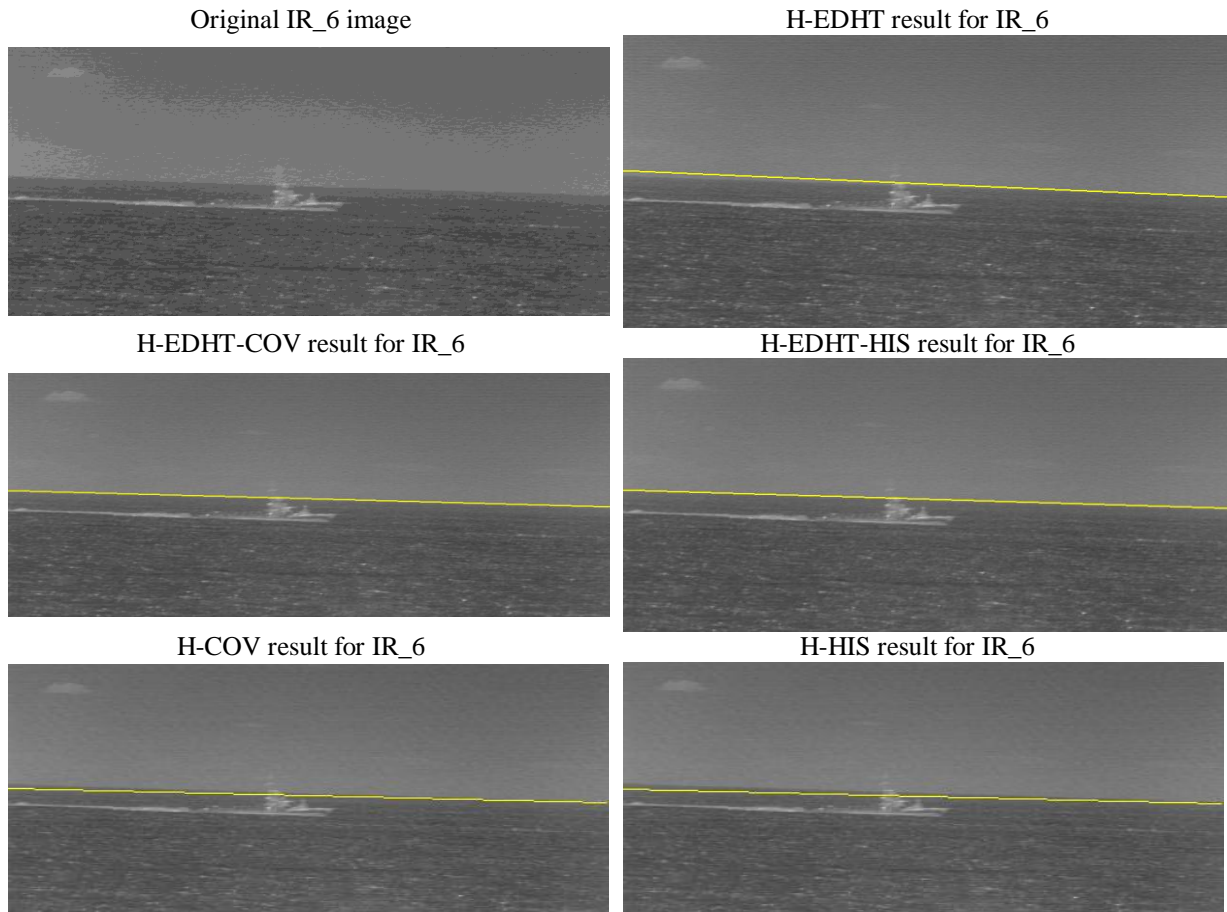


Figure 2. Horizon detection results for image IR_6. The (yellow) line marks the detected horizon.

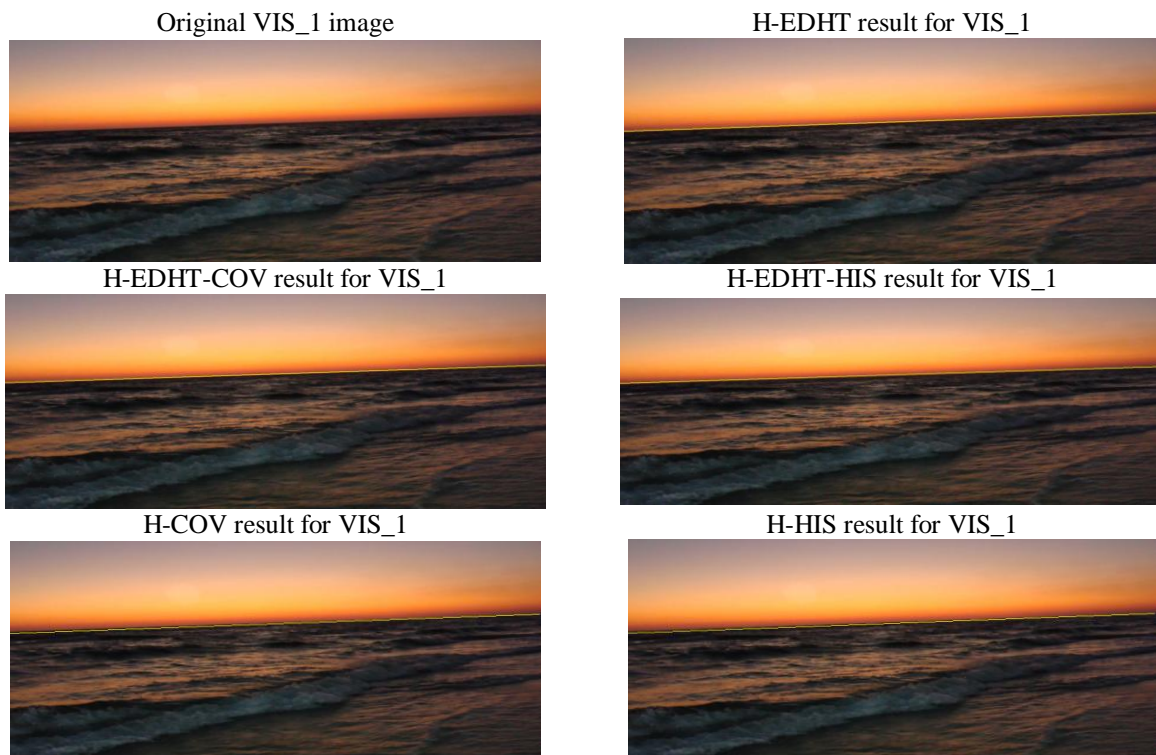


Figure 3. Horizon detection results for image VIS_1. The (yellow) line marks the detected horizon.

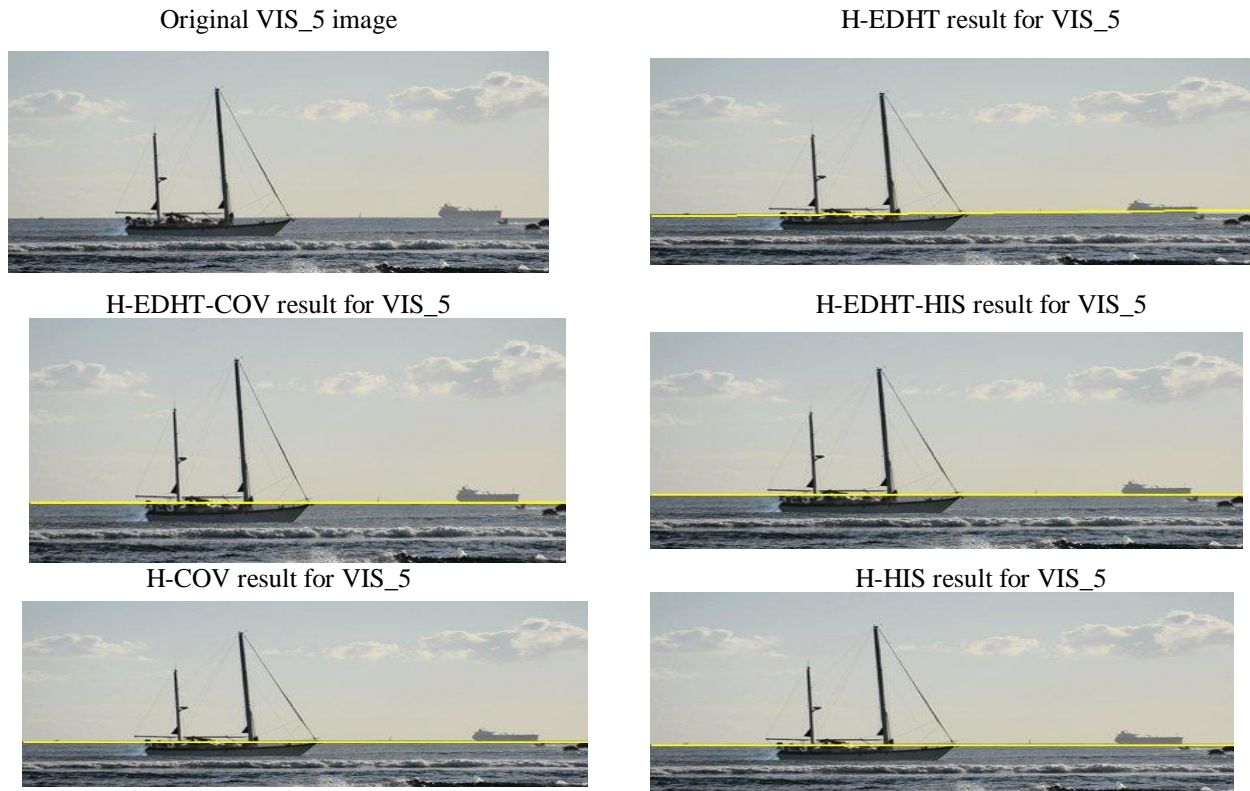


Figure 4. Horizon detection results for image VIS_5. The (yellow) line marks the detected horizon. Despite the waves and the ship present, all the algorithms detect the horizon correctly.

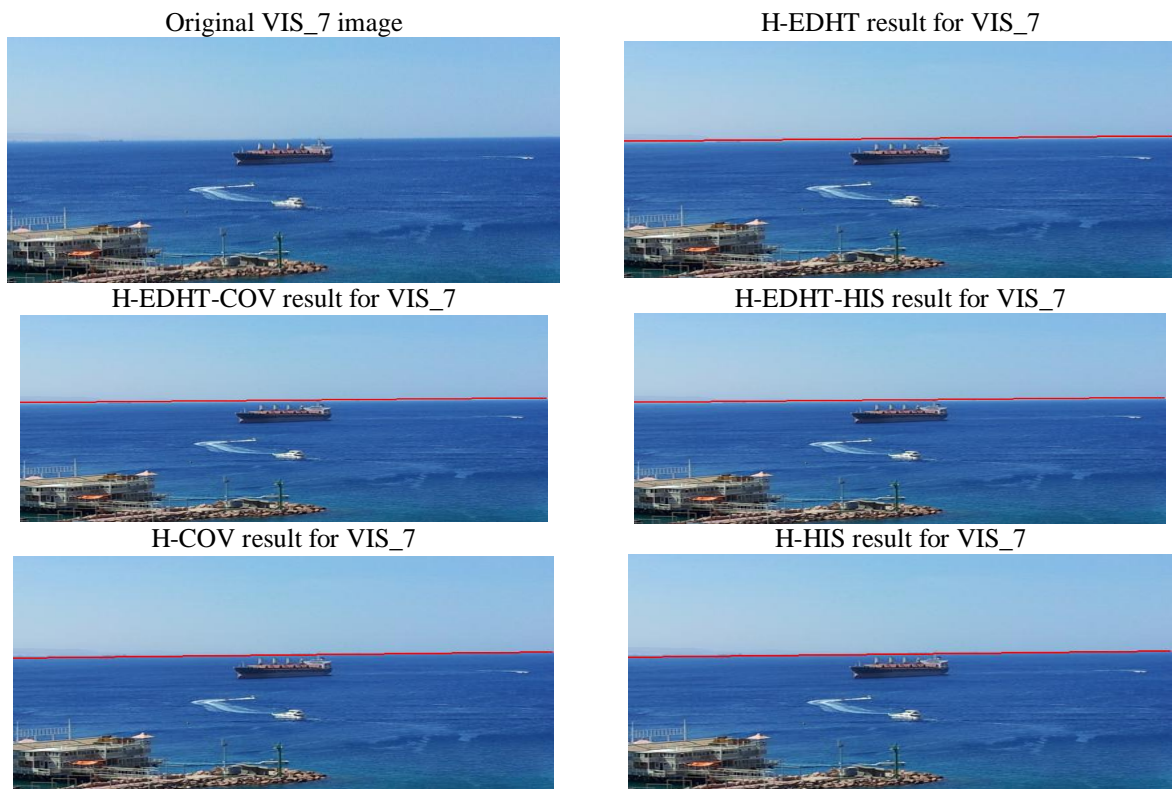


Figure 5. Horizon detection results for image VIS_7. The (red) line marks the detected horizon. Despite the waves, the ships and the land objects, all the algorithms detect the horizon correctly.

“A Study on Customer Preference of LG Lap-Top”

Dr. Srinivasa Rao Kasisomayajula

*Principal/Professor, Dept of Business Management, Vijaya P.G.College, Munaganoor, Hayathnagar, Ranga Reddy
Res: H.No.3-2-112/3, Meena Nagar, Bhongir-508116, Nalgonda District, Andhra Pradesh, India*

Abstract:

The consumers' tastes are changes rapidly. They want new models with the latest features. It is a very hard fight. The competition is on features differentiation, time to market and promotion, basically on every front. The dealer-push and brand pull, both plays a very crucial role. Hence the company concentrate on both fronts equally will have an upper hand over the others. Companies like *hp*, *Compaq*, *Lenovo*, *Sony* and *LG* have practices this very well and leading on the sales front. The dealers have to observe that the consumers add a lot of value after sales and service provided by the company while making a purchase decision. Today Management of Customers' relationship is assuming more and more importance and company cannot afford to ignore this. Based on the above response, *hp* and *Compaq*, provide better customer service as compared to others.

I. Introduction

By 2005, LG was in a Top 100 global brand, and in 2006, LG recorded a brand growth of 14%. Now the world's largest plasma panel manufacturer, its affiliate, L.G. Display is one of the largest manufacturers of liquid crystal displays. Also in 2006, the company's mobile Phone division, LG Mobile, marketed the L.G Chocolate phone, changing the company's image of the maker of thick 3G phones. It now focuses on the design and marketing of phones such as the L.G. shine, the LG Glimmer. As a result, the company was picked as "The Design Team of the Year" by the Red Dot Design Award in 2006~2007 and is often called the "New Apple" in the industry and online communities

1.1 Objectives of the Study

As part of this article, I undertook the study at the LG Electronics in the pertaining to consumer electronics. The following are the main objective of this article.

- To identify the consumer's taste and preference of laptops and desktops among consumers.
- To carry out detailed research on the preferences of LG desktops and laptops among the consumers
- To know the service and performance of the IT products between LG and its competitors.
- To know the product quality and pricing between LG and its competitors.

1.2 Scope of the Study

In order to achieve steady growth in this highly competitive market, the companies should be aware of its competitors. This study will provide an overall view of consumer perception about consumer electronics and market study of LG consumer products. This study can be viewed from qualitative nature as well as quantitative since it tries to know the opinions, view and suggestions of dealers and statistical tools have been used.

1.3 Limitation of the Study

The study is limited to Hyderabad only. Because of limited cost research is conducted with 50 samples of consumers only. The data is collected from the consumers are qualitative in nature i.e. Views options perceptions etc., these factors changes time to time. The data collected are primary in nature. Hence there is chance for a biased of misleading response from the consumers. On the other occasion consumers were reluctant to give information, because they were busy.

2. Methodology

Methodology states how research study should be undertaken. These include specification of research design, source of data, method of primary data collection, field work carried, analysis and interpretation done limited inherited in the conserved article. In the present research approached used in the survey method. All the consumers include in the survey were given a questionnaire and brief introduction about the company plan for strengthening their consumer support.

2.1 Research Design

A research design is generally a pure and simplified framework and certain plan for a study that will guide the collection and analysis of data where information needed. The function of the research design is to ensure that the required data is obtained and collected accurately and economically. Research design is basic

framework, which provides guideline for the best of research purpose. In short, research design is planned structure and strategy of investigation conceived so as to obtain specified answer or solution to research question and to control variance. Here the research design used for this research is descriptive.

Source of Data: Data sources consisted of both primary and secondary sources.

2.2 Primary Data

A questionnaire was used to conduct the whole survey. To control the response bias and to increase the reliability of the data, a structured pattern of question was also used in the questionnaire. The advantages of using this specified construction of the questionnaire are being administrative simplicity and easy in data processing analysis, and the interpretation. The questionnaire consists of dichotomous and the multi choice question to allow as possibilities to be covered. The question was asked directly to the consumers and in the direct disguised form so as to avoid confusion and to get the best and reliable answer.

2.3 Secondary Data

The information about the consumer’s number and their address were obtained which were formed as the secondary data sources.

2.4 Sampling Plan and Sampling Design

Sample selection of consumers throughout Hyderabad was taken for the survey to get the homogeneous and true representation of LG electronics.

2.5 Sample Size

50 Consumers are taken in Hyderabad.

2.6 Sampling Method

Judgment sampling was restored for the study of each respondent was assigned a number to identification, process the data analysis and the survey was conducted accordingly.

2.7 Tools Used for Analysis

- Chi square method
- Percentage Method

Results and Discussions

Table1- Observed Frequency

(No. of Respondents)

Parameter	Very good or very high	Per cent	Good or high	Per cent	Normal	Per cent	Sample size
Service	15	30%	25	50%	10	20%	50(B)
Performance	23	46%	15	30%	12	24%	50
Pricing	15	30%	18	36%	17	34%	50
Product quality	9	18%	26	52%	15	30%	50
Brand image	13	26%	23	46%	14	28%	50
Total Demand	(A) 75	30%	107	43%	68	27%	(N) 250

Table 2-Chi Square Value

Sl. No.	Parameter	Observed value O	Expected value E= {(A) * (B)}/ N	(O – E)	(O-E) ²	X ² = (O-E) ² /E
1	Service	15	15.0	0	0	0
		25	21.4	3.6	12.96	0.6056
		10	13.6	-3.6	12.96	0.9529
2	Performance	23	15.0	8.0	64.00	4.2667
		15	21.4	-6.4	40.96	1.9140
		12	13.6	-1.6	2.56	0.1882
3	Pricing	15	15.0	0	0	0
		18	21.4	-3.4	11.56	0.5402
		17	13.6	3.4	11.56	0.8500
4	Product quality	9	15.0	-6.0	36.00	2.4000
		26	21.4	4.6	21.16	0.9887
		15	13.6	1.4	1.96	0.1441
5	Brand image	13	15.0	-2	4.00	0.2667
		23	21.4	1.6	2.56	0.1196
		14	13.6	0.4	0.16	0.0117
<i>Chi Square value X² = Σ(O-E)²/E</i>						13.2484

Null Hypothesis $H_0(O) =$

There is no association between consumer opinions and various selection criteria of LG

Assumed, Level of Significance (α) = 5%

Degree of freedom (v) = $(r-1)(c-1)$ Where r = number of rows, c = number of columns

$v = 5 - 1 = 4, 3 - 1 = 2$, degree of freedom (V) $4 * 2 = 8$ Critical value = 15.5

The calculated value of X^2 (13.2484) is less than the Critical value (15.5) Hence the null hypothesis is rejected. i.e. There is an association between consumer opinions and selection criteria. In situations where there relative importance of all the items of the distribution is not the same name. If the same items in a distribution are more important than others, then this point must be born in mind, in order that average computed is the representative of the distribution. In such case, proper weight age is to be given to various items the weight attached to each item being proportional to the important of the item in the distribution. If 'N' is the sample size and 'W' are the weight, weighted average is calculated by:

2.8 INTERFACE:

Table value of X^2 at 5% level of significance is 15.5 since, calculated value is lesser than the tabulated value, null hypothesis is accepted i.e. consumers do not differ in their opinion on the various selection criteria of LG.

Table 2 Comparing Statement for various brands of similar products

Feature	HP	Per-cent	SONY	Per-cent	LG	Per-cent	ACER	Per-cent	Total Rsp.
Product quality	20	40%	15	30%	10	20%	5	10%	50
Pricing	15	30%	18	36%	9	18%	8	16%	50
Service	12	24%	20	40%	9	18%	9	18%	50
Performance	13	26%	16	32%	11	22%	10	20%	50
Brand Image	19	38%	16	32%	10	20%	5	10%	50
Overall rating	15	30%	17	34%	10	20%	8	16%	50
Ranking	Second Rank		First Rank		Third Rank		Fourth Rank		

3. Inference

Thus HP stands 1st among the product quality, Sony 2nd, LG 3rd and ACER stands 4th position. Consumers feel that price is higher for Sony, 2nd highest is HP, 3rd highest is LG and least is ACER. Consumers feel that Sony is the best amount various brands for service, HP is 2nd best and 3rd best are LG and ACER. Consumers feel that Sony is the best amount various brands for performance, 2nd best is HP, 3rd best are LG and least is ACER. Consumers feel that HP is the best amount various brands for brand image, 2nd best is Sony, 3rd best is LG and least is ACER. Consumers feel that SONY and HP provide more offerings with 30% but in case of LG and ACER it is quite less with 20%. It is seen that Consumers give first preference to SONY and it stands first with 34%, 2nd best is HP with 30%, 3rd best is LG with 20% and 4th is ACER with 16%.

3.1 FINDINGS

As far as product quality is concerned HP stands best with 40%, 2nd best is SONY with 30%, LG stands 3rd position with 20%, and ACER stands 4th position with 10%. As far as pricing is considered ACER is comparatively cheaper with 16%, 2nd stands LG with 18%, 3rd highest is HP with 30% and the most expensive is SONY with 36%. As far as service is concerned, SONY has scored 40% and stands best and 2nd best is HP with 24%, 3rd best are LG and ACER with 18%. As far as performance is concerned, SONY has scored 32% and stands best, 2nd HP with 26%, 3rd LG with 22%, and 4th ACER with 20%. As far as brand image is concerned HP has scored 38% and stands best, 2nd best is SONY with 32%, 3rd LG with 20% and 4th ACER with 10%. It is found that offers and promotions given by LG is not satisfied it stands around 20% whereas SONY and HP stands best with 30%. It is found that consumers give first preference to SONY and it stands first with 34%, 2nd best is HP with 30%, 3rd best is LG with 20% and 4th is ACER with 16%.

4. Conclusion

This article is done in order to find out the performance of LG IT products among its competitors as Hyderabad is a fast developing metropolitan city always buzzing with activities the rate of towards electronic product is high and they prefer customers, the best too. Any business and all the related activities revolve around the customers only. Customer satisfaction can be achieved only by offering better quality products backed up by performance and better services. This can be satisfied by designing the products in such a way that is suits the wants and preferences of the customer.

5. Suggestions

The company has to introduce more quality features to its existing laptops and desktops in order to increase their sales. As far as price is concerned it is normal but compared to Acer its price is little bit higher. Prompt service is available only for home appliances, if it is implemented for IT products it would satisfy the consumer and they would opt for our project. Battery backup and display clarity has to be improved in order to compete with the other brands. As far as offers are concerned, the company can give CD's like general knowledge, dictionary and encyclopedia, song CD's and also free accessories which is more useful to the consumers. In case of promotion, the company should promote their IT products by giving TV Ads, by distributing the pamphlets and by conducting more road shows. In order to improve the brand image the company has to start their own retail outlets in many places.

References

- [1] Philip Kotler, Marketing management . eleventh edition, Pearson Education
- [2] R.S.N. Pillai and Bagavathi, Modern marketing principles and Practices., Second Edition , S.chand and Company Ltd, New Delhi.
- [3] P.R. Vittal and V. Malini, Statistical and Numerical Methods, First Edition, Margam Publications, Chennai.
- [4] www.lglaptops.com

Flowshop Scheduling Using Multiagents with Adaptive Auction

¹, Amar Jukuntla, ², Dr. E. Grace Mary Kanaga,

¹, PG Scholar, ² Associate Professor,

^{1, 2}, Department of Computer Science and Engineering, Karunya University,
Coimbatore, India

Abstract:

In The Face Of Globalization And Rapidly Decreasing Of Product Lifecycle, Manufacturing Companies Trying To Improve The Machine Utilization And Product Life Cycle. Flowshop Scheduling Is Major Task For Manufacturing Companies In Terms Of Improving Machine Utilization And Scheduling Of Jobs. Here Agents Are Responsible To Solve Flowshop Scheduling Problem. The Differential Evolution Algorithms Are Employed To Obtain Solutions For Solving Flowshop Scheduling Problem. This Paper Describes Novel Approaches That Use The Price Utilization, Adaptive Auction Mechanism To Solve The Flowshop Scheduling Problem.

Keywords: Flowshop Scheduling, Auctions, Resource Allocation, Bidding, Adaptive Auction, Combinatorial Auction.

1. Introduction

Flow shop scheduling problems can be raised in scheduling Production Management System (PMS) in manufacturing industries systems. To take advantage of the production management system it is necessary to give full attention to the scheduling of such systems. This leads to problems in PMS resource allocation, planning and scheduling. Despite success of PMS in manufacturing industries a number of inefficiencies occur when PMS is used in allocating resources. The main problem is complementarities among resources, i.e when multiple independently allocated in order to complete the single task, an agent will complete with only part of the required resources, and efficiency. This issue is directly stated in a combinatorial auction mechanism. The scheduling problem and resource allocation in this paper originates from a PMS scheduling problem where between multiple agents of operations of a job on the same resource reallocating. Where agents seek to optimize goals by contending for resources from a common pool. When a job has finished processing on this machine it has to be processed in the second machine. For example consider the following problem scenario stated in [2]:

1. There are central pool of resources is available and that comprises multiple identical units of different machine types.
2. There are multiple automated software agents, each having a job list and is responsible to service jobs in its list by solving its respective scheduling problem. In this paper agent is used to solve generalized flow shop problem.

The above problem scenario occurs in variety of applications, like loading and unloading of containers operations and manufacturing. There different types of problems are raised for multiple decision makers contending for resources for a common pool and these agents are self interested. Bidding is done for utilize certain combination for machine resources from the pool over certain time periods. In multiple rounds combinatorial auction mechanism that is built on the general equilibrium solution [8] and prices of the machine resources over different periods will iterate over multiple rounds of the bidding process until price equilibrium is achieved.

2. Flowshop Scheduling

Scheduling can be termed as, "The allocation of resources over a period of time to perform a collection of tasks". Also, another form of scheduling is stated as, "It is a function to determine an actual (optimal or feasible) implementation plan as to the time schedule for all jobs to be executed; that is, when, with what machine, and who does what operation". For example flight scheduling, train scheduling are examples of the scheduling applications. According to the nature of scheduling can be divided into project scheduling and operations scheduling.

2.1 Project Scheduling:

In this scheduling all the activities of the scheduling are carried out in project. A project may be a construction of a building, manufacturing of a computer or maintenance and repair of a factory or a plant etc. Software based approaches are available to tackle this type of scheduling. They are like Graphical Evaluation and Review Technique (GERT), Critical Path Method (CPM) . . . etc.

2.2 Operations Scheduling:

Operations Scheduling can be stated as, “The processing of a set of jobs, in a given amount of time, on already allocated corresponding machines, in a workshop consisting of a several machines including operative workers”. Jain [1998] classified available operation scheduling as Job Sequencing, Flow shop scheduling, mixed flow shop scheduling, Job shop scheduling and Open shop scheduling. In Job Sequencing model defines that the sequence or order of the set of tasks to be processed on one machine. The sequence path is selected based on their maximization or minimization of objective functions. Flowshop Scheduling processing of sequence would be same for all jobs or tasks. Flowshop scheduling is used to find out job sequence in machines according to the multiple stages. Flowshop is a shop in which machines are arranged in a sequence Jobs begin processing on initial machine, process through several intermediary machines, and reaches the final machine to complete the scheduling. This flowshop scheduling is shown in Fig. 1. In Flowshop, every job must visit machine exactly once to complete the task and all jobs follow same route for visiting the machine.

In Job shop scheduling every job has its separate processing sequence. Scheduling of jobs complicated compared to flowshop scheduling.

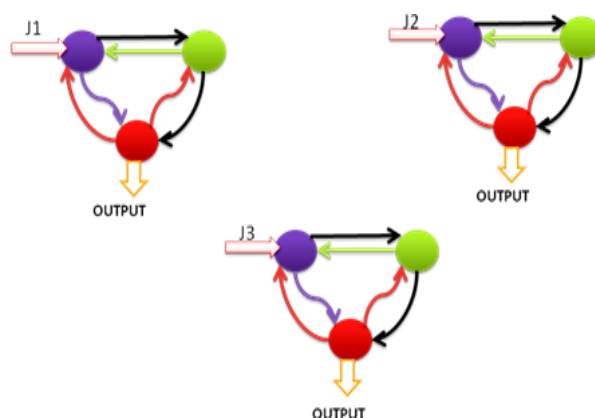


Fig 1. Flowshop Scheduling

A mixed shop scheduling is basically combination of both flowshop and job shop scheduling. In this case some jobs have fixed machine sequence like flowshop and other processed in an arbitrary like job shop [4]. A number of decision rules can be used for job sequence in the machines; they are FCFS, EDD, SPT, CR, and MP...etc.

3. Agent Based Scheduling

Multiagent System is stated as [1], “An agent is computer system which is situated in some environment, and that is capable to perform autonomous action in their environment in order to meet its design objectives”. Agents are responsible to solve flowshop scheduling problem in resource allocation and able to perform fast bidding for timeslots to schedule the jobs with specified time. Different types of agents are in this paper, Job Agents and Resource Agent. Job Agent seeks the resources for scheduling the jobs, solving the flowshop problem and able to generate bidding price quickly and participating the auction. Resource Agent is used to conduct auction between Job Agents based on the available resource on that time slot and able to solve conflicts between the Job Agents. In this paper agents are used to solve the flowshop problem and schedule all jobs with less makespan time with maximum utilization of machine resources. Different types of auction mechanisms are described in further sections.

4. Auction Mechanism

The bidding procedure is done in two ways. First, negotiation and auction, these methods are used to solve the conflicts between the bidders and auctioneers. Auction Mechanism is used to solve the conflicts between bidders and auctioneers. Negotiation [1] is the interaction between the multiple agents, used to resolve conflicts. It is useful for making possible proposals those agents to resolve conflicts. Agent negotiation is only applicable for only limited number of agents to solve the conflicts. But auction is used to solve this problem between the agents. An auction [6] is a mechanism to allocate resources to set of bidders on basics of bids. In a traditional auction, the auctioneer wants to allocate a resource to a single bidder from among a group of bidders. There are four different types of auctions are available: English auction, Dutch auction, First price sealed bid auction, and Vickrey auction. An English auction is an iterative auction where the bidders submit their bids

monotonically increasing order of bids. This process continues until a price is reached where a single bidder who is willing to buy. The item or resource is allocated to that bidder at the final bid price. The Dutch auction is exactly same as English Auction but it reverse of the price, i.e., bids price is monotonically decreased by auctioneer until there is a bidder who willing to buy that item at currently announced price. In both auctions one important note that can be observed as they are iterative in nature and price signals are continuously being fed back to the bidders. In this paper Adaptive Auction mechanism and Combinatorial Auction are used for allocating resources to the bidders. Adaptive Auction Mechanism [6] is an analytical process. This Adaptive Auction Mechanism is useful for online auction because auctioneer's doesn't know behavior of the bidders. This adaptive auction mechanism is used to maximize a given objective function based on observed outcomes. Over view of this approach is given in [6]. A parameterized mechanism shows that one or more auctions are conducted by a population of various bidders, potentially unknown bidding strategies. Result is input to the evaluator module; it revises the mechanism parameters and maximizes the seller's revenue. Any number of auction parameters is considered such as reserve prices, auctioneer fee...etc. The selection of mechanism is the key active element here. This mechanism doesn't depend on repeated interactions with the repeated bidders. It assumes that bidder's behavior remains constant. It helps to predict auction result as a function of the mechanism. This mechanism is commonly used in sequential auctions, auction design choice...etc. Combinatorial Auction Mechanism [7], is a kind of super market, where bidders can place all bids on combinations of items, rather than individual items. In this mechanism all the items should be traded at once, unlike the single-good auction. This mechanism helps to select the particular resources for the particular period and allocating the resources to particular Scheduling agent.

The price is calculated based on the resource utilization by using general equilibrium solution [8] and also calculating revenue for the auctioneer.

5. Bidirectional FLOWSHOP

This section gives a brief introduction about how multiple agents handle number of jobs. This Bidirectional Flowshop Scheduling under Critical Operation Sequence helps in handling the jobs with specific settings [2]. The objective of function is to minimize sum of the weighted tardiness and penalty and makespan cost. Based on the definition of Bidirectional FSP with multiple renewable machines and COS constraints [11], the resource allocation problem is to allocate the multiple renewable machines to contending job agents, while scheduling is to generate a schedule for each job agent with the allocated resources. Given the job release time, due time, and tardiness penalty, the objective is to minimize the weighted sum of makespan cost and tardiness penalty. The system overview is shown in Fig. 2.



Fig. 2. Resource allocation and scheduling for multiple agents

In BiFSP resource allocation and scheduling is preplanned, but allocating the resources to agents is difficult and does not consider the dynamics such as system failure, breakage. This method is concentrated only on centralized allocation and prescheduling. This problem can be explained in container terminal for loading and unloading the goods from yard to land. With the help of decision parameters calculating the resource utilization and cost estimation for that resource. These calculations are given below.

- Partitioning the total time into time horizon $\{1, 2, 3, \dots, \text{Tot}\}$ into F frames, $\{T_f: 1 < f < F\}$, all agents will be in same time partition.
- $P_{ij}^l, l \in \{1, 2, \dots, N\}, i \in \{1, 2, \dots, M\}, j \in \{1, 2, \dots, o_i\}$: processing time of operation j in job i in job l .
- D^l is due time for job l .
- W_d^l delay penalty of job l .
- W_m^l makespan price for job l .

Machine capacity and Constructive Heuristics Methods and Repair Heuristic Methods used for scheduling the jobs on machines. Continuous-Time-Domain use for resource allocation for different agents may have different timeslots.

Calculating machine capacity as follows

Machine Capacity

$$MC_{k(t)} = \sum_{m_{ij}=k} w_{ij} \tag{1}$$

$$W_{ij}(t) = \begin{cases} 0, & \text{ift} \leq \text{Time}_i^s \\ 1, & \text{ift} < \text{Time}_{ij}^s \leq \text{Tin} \\ 0, & \text{ift} > \text{Time}_i^e \end{cases} \tag{2}$$

Resource utilization is obtained and calculating the prices for those utilized resources by using Price Adjustment Methods [8, 9]. Notations are stated in Table 1.

TABLE I. LIST OF NOTATIONS

Symbol	Description
N	Total number of Agents
Tot	Total Number of periods
F	Total Time Frames
o_i^l	Total number of operations for job i in job list l
D^l	Due time of job list l
W_d^l	Delay penalty of job l
W_m^l	Makespan price for job l
Time_{ij}^s	Start Time of operation j in job i
Time_{ij}^e	End Time of operation j in job i

6. Resource Allocation And Scheduling

Although the adaptive auction mechanism can improve the speed of the bidding for obtaining feasible solutions through reallocation resources that has not been fully utilized after the auction process is completed. For each non-fully utilized resource, allocate the spare unites to the agent l . After each reallocation, agent will reconstruct its schedule and recalculate its objective value (Makespan Tardiness Cost for agent l), but allocation and scheduling, where information and decisions are decentralized [7]. Combinatorial Auction Mechanism that allows agents to participate in bid for the resources needed in a multi-period. This Mechanism is used to show how agents can decide optimal bidding strategies to respond to price adjustment strategies from the auctioneer. The price adjustment process was based on tatonnement process which was originally proposed by Walras [9] and enhanced by many other studies like Wellman [8]. This process resolves resource conflicts by updating the price based on excess demands iteratively. Several price adjustment process methods are available for calculating price for the particular period. Although the adaptive auction scheme can improve the speed of convergence and achieve feasibility, it often results as a local optimal solution. It is possible to obtain better

solutions through reallocation of resources that has not been completely utilized after the auction process is completed.

7. Conclusion

In this paper, an adaptive auction mechanism and combinatorial auction mechanisms are discussed, solving the conflicts between the agents for resource allocation. Although discussion is centered on the flowshop scheduling problem, these auction mechanism are used for generates the bid in each agent, based on the requirements of the resources on particular timeslot resources are allocated with minimum makespan time and these algorithms are readily replaces by another algorithms with modifications for increasing the system performance and reducing the total makespan time of jobs in future enhancement work.

References

- [1] Michael Wooldrige, "An Introduction to Multiagent Systems," John Wiley and Sons Ltd, 2009.
- [2] Z. J. Zhao, T. Y. Leong, S. S. Ge, and H. C. Lau, "Bidirectional flow shop scheduling with multi-machine capacity and critical operation sequencing," in Proc Int. Symp. Intell. Control (ISIC 2007), pp. 446–451.
- [3] Kenneth R Baker, "Introduction to Sequencing and Scheduling," John Wiley and Sons, NewYork, 1974.
- [4] J. Riezebos, G.J.C. Gaalman and J.N.D. Gupta, "flow shop scheduling with multiple operations and time lags," in the Journal of Intelligent Manufacturing, special issue on Production Planning and Scheduling, april 1995.
- [5] Aanen, E., (1988), Planning and scheduling in a flexible manufacturing system, PhD thesis, Faculty of Mechanical Engineering, University of Twente.
- [6] David Pardoe and Peter Stone, "Developing Adaptive Auction Mechanism," SIGecomExachanges, 2005, no.3, pp.1-10.
- [7] P.Cramton, Y.Shoham, and R.Steinberg, "Combinatorial Auctions," Cambridge, MA:MIT Press, 2006.
- [8] L. Walras, "Elements of Pure Economics," Homewood, IL: Richard Irwin, 1954.
- [9] H. C. Lau, Z. J. Zhao, Shuzhi Sam Ge, "Allocating Resources in Multiagent Flowshops With Adaptive Auctions," IEEE Transactions on Automation Science and Engineering, vol. 8, No. 4, October 2011.
- [10] S.S.Reddi and C.V. Ramamoorthy, On the flowshop sequencing problem with no wait in process, *OperationalResearch*, Q.23, pp323-331, 1972.
- [11] Z. J. Zhao, H. C. Lau, and S. S. Ge, "Integrated resource allocation and scheduling in a bidirectional flowshop with multimachine and cos constraints," IEEE Trans. Syst., Man, Cybern.—Part C: Appl. Rev., vol.39, no. 2, pp. 190–200, 2009.
- [12] J.Q.Cheng and M.P. Wellman, "The Walas algorithm: A convergent distributed implementation or general equilibrium outcomes," *Compt.Econ.*, p. 12, 1998.

Five Dimensional String Cosmological Model In General Relativity

¹ Kalpana Pawar (Mody), ² Vidhya Chauhan, ³ G. D. Rathod,

^{1,2} Department of Mathematics, Shivaji Science College, Nagpur,

³ VMIT, Nagpur.

Abstract:

In this paper we have investigated Five Dimensional String Cosmological Models with bulk viscosity and determined it's solution for three different cases. The various physical and kinematical properties are also studied.

Keywords: Bulk viscosity, Cosmic string, Five dimensional cosmological models.

1. Introduction

The study of cosmic strings attached considerable interest of cosmologists in the frame work of general relativity as it play an important role in the description of the universe in the early stages of its evolution (Kibble 1976) and give rise to density perturbations leading to the formation of galaxies (Zel'dovich 1980). The existence of a large scale network of strings in the early universe is not a contradiction with the present day observations of the universe. Various authors (Hogan and Ress 1984; Myung et al.1990; Banerjee et al. 1990; Gundlach and Ortiz 1990; Barros and Romero 1995; Yavuz and Yilmaz 1996; Sen et al.1997; Sen 2000; Bhattachajee and Baruah 2001; Barros et al.2001; Rahaman et al.2003; Reddy 2005) constructed string cosmological models in various theories of gravitation. Sez and Ballester (1986) formulated a scalar tensor theory of gravitation in which the metric is coupled with a dimensionless scalar field in a simple manner. Singh and Agrawal (1991), Shri Ram and Singh (1995) and Mohanty and Sahu (2003, 2004, 2005) studied various aspects of Sez and Ballester scalar tensor theory of gravitation. In particular Reddy (2003, 2006) studied some string cosmological models in Sez and Ballester scalar tensor theory of gravitation with the help of an excess ad hoc condition in five dimensional Kaluza-Klein space time, even though these solutions may not reveal the early universe.

2. The Field Equations

We consider the five dimensional line element in the form

$$(1) \quad ds^2 = -A^2(dX^2 + dY^2 + dZ^2) - B^2dM^2 + dt^2,$$

where A and B are functions of cosmic time t only.

The energy momentum tensor for a cloud of string dust with a bulk viscous fluid is given by Letelier (1979), Landau and Lifshitz (1963) as

$$(2) \quad T^j_i = \rho u_i u^j - \lambda x_i x^j - \xi u_{;k}^k (g^j_i + u_i u^j),$$

where ' ρ ' is the proper energy density for a cloud of strings with particles attached to them, ' λ ' is the string tension density, ' ξ ' is the bulk coefficient of viscosity, u^i is the five velocity of the cloud of particles and x^i is the direction of string i.e. direction of anisotropy satisfying the relation

$$(3) \quad u_i u^i = -1, \quad x^i x_i = 1 \quad \text{and} \quad u^i x_i = 0$$

The field equation in normal gauge for Lyra's manifold as obtained by Sen and Dunn are

$$(4) \quad R_{ij} - \frac{1}{2} g_{ij} R + \frac{3}{2} \phi_i \phi_j - \frac{3}{4} g_{ij} \phi_k \phi^k = -\chi T_{ij}$$

where ϕ_i is the displacement vector given by $\phi_i = (\beta(t), 0, 0, 0, 0)$.

The field equation (4) for the line element (1) leads to

$$(5) \quad \frac{-2A_4^2}{A^2} - \frac{2A_4 B_4}{AB} + \frac{3\beta^2}{4} = \chi \rho,$$

$$(6) \quad \frac{2A_{44}}{A} + \frac{A_4^2}{A^2} + \frac{2A_4 B_4}{AB} + \frac{B_{44}}{B} + \frac{3\beta^2}{4} = -\chi(\lambda + \xi\theta),$$

$$(7) \quad \frac{2A_{44}}{A} + \frac{A_4^2}{A^2} + \frac{2A_4 B_4}{AB} + \frac{B_{44}}{B} + \frac{3\beta^2}{4} = -\chi\xi\theta \quad \text{and}$$

$$(8) \quad \frac{3A_{44}}{A} + \frac{3A_4^2}{A^2} + \frac{3\beta^2}{4} = -\chi\xi\theta,$$

where the suffix '4' denotes ordinary differentiation with respect to 't'.

3. Solutions of Field Equations and Physical Properties

Here we have four independent field equations in six unknowns. Hence in order to get determinate solution, we consider the relation.

(9) $B=g(A(t))$.

From equations (7) & (8), we have

(10) $\frac{A_{44}}{A} - \frac{B_{44}}{B} + \frac{2A_4^2}{A^2} - \frac{2A_4B_4}{AB} = 0$.

Using (9), we have

(11) $A_{44} \left\{ \frac{1}{A} - \frac{g'}{g} \right\} + A_4^2 \left\{ -\frac{g''}{g} - \frac{2g'}{Ag} + \frac{2}{A^2} \right\} = 0$

Here prime indicates the differentiation with respect to the argument.

Equation (11) is satisfied for the following cases:

Case I: $A_4 = 0$

Case II: $A_{44} = 0$ and $\frac{g''}{g} + \frac{2g'}{Ag} - \frac{2}{A^2} = 0$

Case III: $\frac{g'}{g} - \frac{1}{A} = 0$ and $\frac{g''}{g} + \frac{2g'}{Ag} - \frac{2}{A^2} = 0$

Case I: $A_4 = 0$, leads to $A = K$ where $K \neq 0$ is a constant of integration.

With the help of (9), we have $B = g = K$

Hence five dimensional string models in this case, after using transformations, reduces to the form

(12) $dS^2 = dT^2 - (dX^2 + dY^2 + dZ^2) - dM^2$.

The energy density ρ , tensor density λ and the bulk viscosity ζ for the model (12) is given by

$\rho = \frac{3\beta^2}{4\chi}$,

$\lambda = 0$,

$\xi = -\frac{3\beta^2}{4\chi\theta}$.

Since $\theta = 0$, therefore we conclude that the Lyra geometry and cosmic strings do not survive in this case and space-time becomes Minkowskian.

Case II: $A_{44} = 0$ and $\frac{g''}{g} + \frac{2g'}{Ag} - \frac{2}{A^2} = 0$.

Here $A_{44} = 0$ leads to

(13) $A = L_1 t + L_2$,

where $L_1 \neq 0$ and L_2 is a constants of integration.

Where as solving

$\frac{g''}{g} + \frac{2g'}{Ag} - \frac{2}{A^2} = 0$,

After multiplying by A^2g and solving , we get

$g = C_1A + C_2A^{-2}$.

(14) $B = C_1A + C_2A^{-2}$.

After using some transformations the five dimensional string cosmological model in this case reduces to

(15) $dS^2 = -T^2(dX^2 + dY^2 + dZ^2) - \left[C_1T + \frac{C_2}{L_1^3 T^2} \right]^2 dM^2 + dT^2$.

The energy density ρ , tensor density λ and bulk viscosity ξ for this model are given by

$\rho = \frac{3\beta^2}{4\chi} - \frac{3}{\chi T^2} \left[\frac{2C_1L_1^3 T^3 - C_2}{C_1L_1^3 T^3 + C_2} \right], \lambda = 0$

Bulk viscosity is given by the relation

$\xi\theta + \rho = 0$

The scalar of expansion, spatial volume, deceleration parameter and shear for the model are given by

$\theta = -\left[\frac{3}{T} + \frac{C_1L_1^3 T^3 - 2C_2}{T(C_1L_1^3 T^3 + C_2)} \right]$,

$V = C_1L_1^4 T^4 + C_2L_1T$,

$q = \frac{3}{(4C_1L_1^3 T^3 + C_2)T} [3C_1^2 L_1^6 T^6 - 2C_1C_2L_1^3 T^3 + C_2^2 + C_1^3 L_1^9 T^6 - 2C_1^2 C_2 L_1^6 T^3] - 1$,

$\sigma = \frac{2}{3} \left[\frac{3}{T} + \frac{C_1L_1^3 T^2}{C_1L_1^3 T^3 + C_2} - \frac{2C_2}{C_1L_1^3 T^4 + C_2T} \right]$

In this model string tensor density vanishes but energy density is present and it is only due to bulk viscosity. Lyra geometry survives only due to the presence of bulk viscosity. In the absence of bulk the model reduces to five dimensional vacuum model in Einstein's theory. The model starts to expand with a big-bang and stops at $T = \infty$. Volume increases with time. As $T \rightarrow \infty$, the string energy density $\rho \rightarrow \frac{3\beta^2}{4\chi}$. Moreover string tension density $\lambda = 0$, therefore we can conclude that energy density is only due to the Lyra geometry. Shear decreases as time increases. Since, $\lim_{T \rightarrow \infty} \frac{\sigma}{\theta} \neq 0$, therefore the model is anisotropic for large values of T .

$$\Rightarrow \frac{g'}{g} = -\frac{1}{A}$$

$$\therefore \frac{g''}{g} + \frac{2}{A^2} - \frac{2}{A^2} = 0$$

$$g = zA + z_1,$$

$$(16) \therefore B = zA + z_1,$$

where $z \neq 0$, z_1 is a constant of integration.

In particular if we take $z_1 = 0$, then for this case, we arrive at the following mathematical models.

If $A = \sin(at + b)$, where $a \neq 0$, b are constants, then after suitable transformations we have the metric in the form

$$(17) dS^2 = -\sin^2(aT) \{dX^2 + dY^2 + dZ^2 - dM^2\} + dT^2,$$

For $T = \left(\frac{2n+1}{a}\right)\frac{\pi}{2}$, for $n = 0, 1, 2, \dots$ reduces to flat 5-dimension space-time.

If $A = e^{(at+b)}$, where $a \neq 0$, b are constants, then after some Transformations metric reduces to the form

$$(18) dS^2 = -e^{2aT} \{dX^2 + dY^2 + dZ^2 - dM^2\} + dT^2,$$

Here for $a < 0$, as T increases, model contracts in four directions. For $a > 0$, as T increases, model expands in four directions. The model becomes flat at initial epoch. The model follows exponential expansion.

If we take $A = (at + b)^m$, where $m \neq 0$, $a \neq 0$, $z_1 = 0$ are constants. Then model reduces to the form

$$(19) dS^2 = -T^{2m} \{dX^2 + dY^2 + dZ^2 - dM^2\} + dT^2.$$

Here model follows power law inflation.

References

- [1] D.K. Sen, K.A. Dunn, J. Math. Phys. 12,578,1971.
- [2] D.K. Sen, Z. Phys. 149, 311, 1957.
- [3] E.H. Brans and R.H. Dicke, Phys.Rev. 124, 925, 1961.
- [4] F. Rahaman, S. Das, N. Begum and M.Hossain, Pramana J. Phys. 61,153, 2003b.
- [5] F. Rahaman, G. Bag, B.C.Bhui, and S. Das, Fizika B12,193,2003b.
- [6] F. Rahaman, S. Chakraborty and J. Bera, Int.J. Mod. Phys. D11, 1501, 2002.
- [7] F.Rahaman, S.Chakraborty, S. Das, M.Hossian & J.Bera, Pramana J.Phys 60,453,2 2003a.
- [8] G. Lyra, Math. Z. 54,52, 1951.
- [9] G. Mohanty, K.L. Mahanta and R.R. Sahoo, Astrophys. Space Sci., 306, 269, 2006.
- [10] G. Mohanty, K.L. Mahanta and Bishi, B.K. Astrophys, Space Sci., 310, 273, 2007.
- [11] G.P. Singh, R.V. Despande and T. Singh ,Pramana J. Phys.63, 937, 2004.
- [12] J.S.Jeavons, C.B.J. Melntosh and D.K.Sen, J.Math.Phys.16,320, 1975.
- [13] R. Casana,C.A.M. DeMelo and B.M. Pimantal, Braz. J. Phys.35,1151,2005.
- [14] T. Singh and G. P. Singh, Fortschr. Phys. 41,737, 1993.
- [15] T. Singh and G. P. Singh, Math. Phys. 32, 24561991.
- [16] W.D. Halford, Aust. J. Phys. 23, 863, 1970.
- [17] W.D. Halford, J. Math. Phys. 13, 1699, 1972.
- [18] W.J. Marciano, Phys. Rev. Lett. 52,489, 1984.

Role of Software Agents in E-Commerce

Ramya S. Gowda, MS

Assistant Professor, Sikkim Manipal University, Bangalore-08, Karnataka, India

Abstract

This paper states how software agents will influence the present marketing prototype in interactive media. It focuses on the importance of these in E-Commerce. E-Commerce is a platform for the online activities of commerce, increase in the activities of trade in cyberspace increases the business opportunities over internet. Software agents are the useful tools to help individuals to undertake their activities on E-Commerce surroundings. Software agents create different paths for communication. Software agents increase the effectiveness and efficiency in several levels of market processes. The agent technology builds the bridge between the previously existing physical market and consequences of virtual markets. Software agents will have dramatic competition effects by quick transfer of information through new technology. As the name indicates software agents acts as mediators for the processes of choosing products and merchants. Overall software agents act as a vehicle between E-Commerce and business.

Keywords: agent, Agent-Based technology, collaborative agent, e-business, E-Commerce, ecommerce analysis, Mobile agent, reactive agent, Software Agents, technology

1. Introduction

Greater portion of daily activities such as shopping, socializing, and working are being transferred to the internet environment. Over the past few decades, human computer interaction, and electronic transactions are being used. Individual's online activities are getting more and more complex with growing opportunities of internet environment. The internet that has grown dramatically in the past few years would by now becomes unmanageable without E-Commerce for business [2]. It is claimed that within the next decade the internet could be populated with billions of agents exchanging information, goods and services with one another and with the people [3].

1.1 What is E-Commerce:

Modern methodology of news selling and merchandising tools that refers to the need of market by cost reduction in turns giving quality goods and services. E-commerce means doing business over interconnected networks. The term commerce is treated as transactions between business clients. So the meaning Electronic Commerce is narrow to some people thus there is a usage of term E-Business. But E-Commerce is not just buying and selling but also providing services to the clients and providing both inter and intra transactions of information in the organization irrespective of the type of company. This extended use of internet for trade and business led to the use of software agents in E-Commerce.

1.2 What are Software Agents:

Although the theory of agents stated that agent is given a very famous with the growth of internet. Software agents are a piece of software which works for the user. However software agent is not just a program. An agent is a system situated within and a part of an environment that senses that environment and acts on it. Over time in pursuit of its own agenda and so as to effect what it senses in the future [4]? Important use of agent concept is, as the tool for analysis not as dosage. As the system changes on can understand it.

1.3 Characteristics of Software agents:

Software agents are like guards and locomotives of most E-Commerce. The following are very few characteristics:

- Software agents can do their task without any outsource intervention.
- Social interaction with other software agents and human.
- Software agents are specific in their goals.
- Good software agent is the one which has the attitude to receive and adopt changes [9]. The agent must be programmed in a powerful language so as to express the rules.
- Safety of the information must be promised by the agent.
- Effective usage of the existing resources.
- Agent must be a good sailor
- Agents must be very careful in handling unauthorized users. The same information must be accessed by the user to which they have right.

1.4 Type of Software agents:

Agents are classified into different types based on the characteristics they possess. In order to possess the above properties agents must have distinct features such as locomotion, integration, co-operation, information, stimulation, etc. For the same sake software agents are classified into 8 agents.

1.5 Collaborative agents: A collaborative agent is a software program that helps users solve problem, especially in complex or unfamiliar domains by correcting errors, suggesting what to do next, and taking care of low level details. Collaborative agents are also referred as colligen. In spite of their behavior of autonomy, co-operation, and learning, colligen punctuate the first two behaviors. In order to perform these they have to agree on acceptable protocols.

1.6 Interface agents: Interface agents are computer programs that employ machine learning techniques in order to provide assistance to a user dealing with a particular application (Maes, 1994b). These agents take sufficient amount of time to understand and learn human behavior before they are onto work. In spite of their artificial learning thoughts they are limited co-operative with other agents [10].

1.7 Mobile agents: A mobile agent is an executing program that can migrate during execution from one machine to another in a heterogeneous network [11]. Mobile agents are used to solve many problem of network computing with minimum bandwidth and connectivity [12]. The theme behind these agents is, 'give program the ability to move'. The main advantage of mobile agent over stationery agent are:

(a) This is not bound to the system where it begins execution. (b) Can move from one system to another within the network. (c) Both the state and code is transported.

1.8 Information/Internet agents: The intelligent part of software which can automatically search for information on the website is termed as information agents. Information system can be considered as knowledge base system. These agents are defined by what they do unlike collaborative agents or interface agents which are defined by what they are. [10].

1.9 Reactive agents: These agents are responsible for stimulating the response to the present state of the environment in which they are embedded. These agents interact with other agents in a very simple and basic way. The important things which support reactive agents.(maes 1991 a ; p.1)

There is no prior specification of the behavior of these agents set since the dynamic interaction leads to the emergent complexity. (b) Reactive agents are responsible for collection of modules which operate autonomously. (c) Reactive agents tend to operate on representations which are close to raw sensor data [10]. (d) Intelligent behavior is the interaction of these agents with their environment.

(a) **Hybrid agents:** Combining two or more of the previous mentioned agent philosophies will yield a better functioning agent. E.g.: Synergy of reactive and collaborative model. The expectation is that this hypothesis will come true.

(b) **Heterogeneous agents:** These agent systems unlike hybrid, refers to an integrated set up of at least two or more agents which belong to two or more different agent classes. These may also contain two or more hybrid agents [10].

(c) **Smarts agents:** The smart agents are the new form of software agents that interface with other agents forming an artificial intelligence. SMART stands for System for Managing Agents for Real Time. The key concept lies here is not the entire individual agent need be intelligent. But by working together in a smart way the agents form a type of emergent intelligence that may appears to exhibit intelligence.

2. Literature Survey

There are several experimental agent projects at HP Labs in Palo Alto and Bristol, focusing on E-commerce and application management. Agents include standard libraries of measurement objects and methods to initiate, change, and dynamically update measurement. (See <http://beast.cs.utah.edu>). They have implemented a light-weight, dynamic agent infrastructure in Java (Chen, 1998, 1999), used for data mining and dynamic workflow integration and provisioning. Dynamic agents support "on demand". Several projects have focused on the agent mediated E-commerce, looking at negotiation in task allocation (Preist 1999), implementing a new facilitator architecture (Pearson, 1997), and playing a key role in the FIPA97 ACL specification. They are developing an experimental web-based economic simulation environment for a shopping mall, and integrating

that with personal agents and mobile appliances based on HP CoolTown (<http://www.cooltown.com>) (Griss, 2000), using Zeus (Nwana, 1999) as base.

3. Motivation:

It is a strong motivation for the use of software agents: agents with great powers should be carefully designed and analyzed. The role of software agents is very important in E-Commerce since it performs many functions like economic benefits, collaboration, integration, etc.. A full proof design is necessary to test the importance. Software agents mimic the way human individuals, organizations & societies succeed in very large complex tasks with the combination of E-Commerce. The fact is that a single human or any organization of humans is usually good in doing something, called Creating Value [1]. The fact that one earns money is because he/she creates value for their employer; the fact that some company makes money is because it creates value for its customers. So the general motivation for an architecture that tries to mimic human or human organization is to enable software to create value. It isn't that existing software today doesn't create value, the only reason software agents exists is because it creates value. But, unlike software agents, humans aren't (explicitly) programmed – they are given some initial knowledge (education/training), they are assigned some jobs, & they create value while collecting the knowledge & expertise in doing it. Something innovative is required to basically be able to claim that we can build such applications that create value without being programmed again and again, except for some basic business: when assigned with a job, performing it, improving in it & creating value without being specifically programmed as to how to solve each case. It can

- Solve unexpected situations,
- Create value in unexpected ways, employ both common sense & the ability to learn from situations,

improve its performance, i.e. by collaboration and by merely performing the job for sufficient amount of time.

The basic attribute of Intelligence can be assigned to three dimensions [5].i.e. Knowledge, Thinking, Learning.

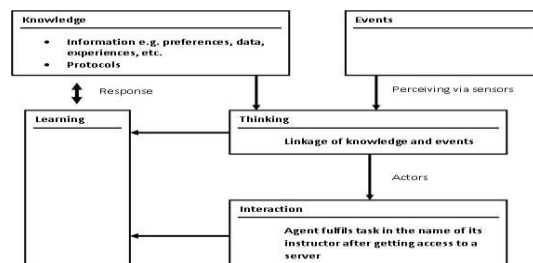
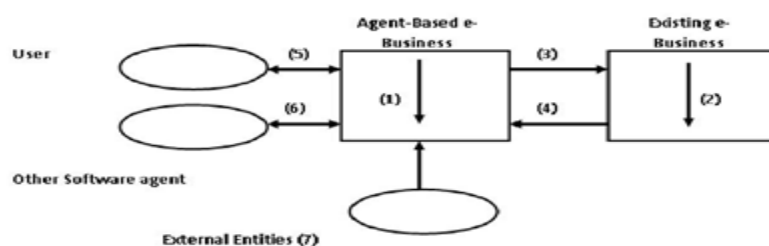


Figure 1. Mode of operation of software agents modified [main source [6]]

The knowledge of an agent consists of information and protocols. Information is to be understood data such as user preferences, or data. A protocol consists of simple if then relationships or represents also complex neural networks. For the use of knowledge the agent needs the ability to think, which is called agent machinery. The agent machinery requires two things. The agent must assume events in its environment over sensors and it must combine the assumed events with its knowledge in a thought process (6). From this linkage the agent can draw conclusions. And the agent can initiate autonomously, without intervention of the instructor, and act through the actors. The extension of the knowledge base results from learning processes. Learning is a behavior modification, which is the result of an experience. A software agent learns using its learning machinery [7]. The agents execute their task by replicating themselves within a network from one computer to another computer. Agent-based e-business in E-Commerce can be defined as a business enabled and operated by software agent technology. The primary roles in the agent-involved E-Commerce environment are played by users, agent-based e-business, existing e-business and other agents. The framework for agent-based E-Commerce analysis in



displayed in Figure 3 from the paper [13] .

Figure 2. Framework for Agent-Based E-Commerce Analysis

The classifications of researches by the framework for agent-based E-Commerce analysis are shown in the table.

Arrow 1-> Evolution of agent-based e-business [13].

Arrow 2-> Change of existing e-business [14]

Arrow 3-> Impact of agent-based e-business on existing e-business [15].

Arrow 4-> Effect of existing e-business sites on agent-based e-business [14]

Arrow 5-> Interaction with agent-based e-business and user [16]

Arrow 6-> Interaction between agents [17]

Arrow 7-> Influence of external entity (institutional, legal etc environments)[14],[5],[16].

The above discussed concepts, the Knowledge, Thinking, learning, and eventual change in e-business provokes to note the important role of software agents in the market.

4. Role of Software Agents In E-Commerce:

This part focus on the basic fundamentals including, the terms used in E-Commerce with respect to software agents and different examples which explains the role.

4.1. Software Agents enabling the formation of virtual organization:

Virtual systems are the decentralized business networks which work in flexible. To have efficient operation and productivity virtual organizations must be able to communicate, Co-operate and Co-ordinate (the 3Cs of business) with each other. Software agents are effective tool to virtual organizations since they provide mechanisms to automate several activities like, gathering data, refining information, negotiate business deals and also intelligent agents work like human beings in supplying and buying goods having the artificial machine knowledge. Software have variety of applications which includes, B2B E-Commerce, Internet based info systems, robotics, smart systems, DSS, data mining and Knowledge discovery. Agent technology helps in finding intranet or internet, Customer relation management, supply chain management and market pricing.

4.2. The reason behind the use of Software Agents:

The software agents are used due to the effect of following reasons:

- [1] Software Agents and Mobility: Mobile agents are a kind of software agent that represent a revolution in how programs are distributed, run and server resources shared and how computer users interact with online services.. They can act on behalf of their principals autonomously while performing their actions in some level of pro-activity and reactivity.
- [2] A software agent is a software entity that acts with autonomy to accomplish tasks on behalf of its users. They function continuously and autonomously in a particular environment, often inhabited by other agents of processes [20]. The idea here is the use of software agents for collaboration.
- [3] Coping with Emergencies: There are situations where people, organizations or computer systems will undergo stress. During this stage they fail to take quick actions which are common or daily tasks. For an individual, if there are some natural problems like death in the family, illness, or job problem etc. they fail to take care of simple thing like paying phone bill or electricity bill etc. For these kinds of problems it is not the solution to have a automated systems. Dynamic Distributed systems: Software agents provide a better figure for utilizing parallelism and dynamics of Computer networks which increases the usage of the available networks. Software agents give an ideal figure out for distributed computing.
- [4] Life agents: Life agents are software agents that are initiated and run in the background and act directly or indirectly on the client's side automatically, monitoring the progress over the period of time.

4.3. Technology behind Software Agents:

The idea here is enabling the intelligent agent as an instantly connected computing service on the network [18]. The use of WWW provides robustness and scalability of web servers; access of firewalls will also become easier. Since Intelligent Software Agents (ISAs) include problem domains that require *human-like intelligence* processing automated they need to have artificial human like intelligence. In order to process this they need the knowledge of the techniques like Artificial Intelligence, Pattern recognition, neural networks, embedded systems, and similarly such high end knowledge. Software agents offer great promise to build loosely-coupled, dynamically adaptive systems on increasingly pervasive message-based middleware, P2P and component technology, Java, XML, SOAP, HTML, HTTP and CGI etc. It can be seen that the knowledge of software engineering and enterprise modeling is also required for software agents.

4.4. Examples of Software Agents:

- **Buying agents:** Also known as shopping bots. These bots help the users to surf while finding the products and services they are searching for. For example, when a person surfs for an item on eBay, at the bottom of the page there is a list of similar products that other customers who did the same search looked at. This is because it is assumed the user tastes are relatively similar and they will be interested in the same products.
- **User agents:** Also known as personal agents. These agents carry out user tasks automatically. For example, some bots sort emails according to the user's order of preference, assemble customized news reports, or fill out webpage forms with the user's stored information.
- **Monitoring and Surveillance agents:** Also known as predictive agents. For example, the agents keep track of company inventory levels, observe competitor's prices and report them back to the company, watch stock manipulation by insider trading and rumors, etc.
- **Data-mining agents:** This agent uses information technology to find out the modern fashion in information from many different sources. For example, the agent that detects market conditions and changes and relays them back to a user/company so that the user/company can make decisions accordingly. The other examples are User agent, Mail Transfer agent, SNMP agent, DAML (Defense Agent Markup Language), 3APL (Artificial Autonomous Agent Programming Language), OWL (Web Ontology Language), Management agents, etc.

5. Applications And Benefits Of Software Agents:

- [1] Agents make less work for the end user and application developer.
- [2] The agent can adapt to its user preferences and habit over a course of time.
- [3] It will intelligently get shared among the community.
- [4] Mobile agents manage the user's E-mail, fax, phone and pager as well as linking the user to Telescript-enabled messaging and communication services such as America Online and AT&T PersonaLink Services [10].
- [5] The most favorite area with respect to reactive agents is games and entertainment industry [10].
- [6] Shopping agents are ideal applications of AgentBuilder agents. These agents can be used to locate
- [7] merchandise, compare prices, place orders, etc.

Intelligent Software agents will have numerous applications in the field of human like intelligence capabilities which is an area of research being done in Artificial Intelligence. Some of the applications are:

- [1] Logical Inference and Deduction
- [2] Contextual Domain Knowledge
- [3] Pattern Recognition
- [4] Learning and Adaptively.

Once the human-like intelligence capabilities are automated, autonomous operation permits software agents to process vast volumes of data which would be unmanageable by human agents.

6. Conclusion:

After studying the characteristics of software agents different conclusions were drawn that software agents are flexible enough to adopt and adjust themselves into changes. Software agents provide security to the information. Since E-commerce deal with business online, security plays the heart of business. Business needs lots of communication skills which is provided by software agents. Software agents are responsible for customer satisfaction in terms of B2B E-commerce. Software agents can be thus proved as an important entity with respect to E-Commerce. Without Software agents E-Commerce is like "a man having his leg cut".

References:

- [1] Dibau naum h under Multi-agent, agentier, agents, ai, architecture, emergence, emergence_engineering, knowledge_engineering, machines, memes, memetics, multiagent_systems, social_mechanism , December, 18, 2006.
- [2] Brown, J. and Duguid, P. (2000). Agents and Angels, Chapter 2 of the Social Life of Information, Harvard Business School Press.
- [3] Kephart, J. O. and Greenwald, A.R. (2000). When Bots Collide, Harvard Business Review, July-August.
- [4] Stan Franklin and Art Graesser. (1996), Workshop on Agent theories, Architectures and Languages, third international workshop conducted by the Institute for intelligent systems, Uni. Of Memphis.
- [5] Brenner, W.; Aarnekow, R.H.Wittig. (1998). Intelligente Softwareagenten-Grundlagen and Anwendungen. Berlin.
- [6] Caglayan, A.K. and C.G. Harrison, Intelligente software-Agenten. Munich 1998.

- [7] Rimmel, Gunnar and Clement, Michel and Runte, Matthias. (1999). Intelligent Software Agents: Implications for Marketing in E-Commerce, Göteborg, Department of Business Administration
- [8] Joseph. P.T, Published (2006), Book on E-Commerce: An Indian Perspective by Prentice Hall India.
- [9] Loannis Vlahavas, and Dimitris Vrakas, published (2005), Book on Intelligent Techniques for Planning.
- [10] Hyacinth S. Nwana, Divine T. Ndumu: An Introduction to Agent Technology, Re-Drawn by Mobile Computing, Dept. of IECS, Feng Chua University, R.O.C., (2003).
- [11] Brian Brewington, Robert Gray, Katsuhiko Moizumi, David Kotz, George Cybenko, and Daniela Rus, Copyright 1999 Springer Verlag. Chapter 15, pages 355-395, in "Intelligent Information Agents", edited by Matthias Klusch. Available at <http://agent.cs.dartmouth.edu/papers/brewington:ir.ps.Z>.
- [12] Holger Peine, an Introduction to Mobile Agent Programming and the Ara System, ZRI- Report 1/97.
- [13] Jin, D.S., Suh, Y.M. and Lee, K.J. (2003). Generation of hypotheses on the evolution of agent-based e-business using inductive learning, International Journal of Electronic Markets, Forthcoming.
- [14] Hhckjh Dongsu Jin, IACIS (2003). Evolution of Software Agent-Based E-Commerce: Based on Agent Competition Model.
- [15] Crowston, K. and MacInnes, I. (2000). The effects of market-enabling Internet agents on competition and prices, Journal of Electronic Commerce Research 1(4).
- [16] Smith, M. D. and Brynjolfsson, E. (2001) Consumer Decision-making at an Internet Shopbot: Brand Still Matters. Journal of Industrial Economics, 49(4), pp. 541-558.
- [17] Kephart, J. O. and Greenwald, A.R. (2000). When Bots Collide, Harvard Business Review, July-August.
- [18] J. Waldo, The JINI Architecture of network-centric computing, Communication of the ACM, July 1999, Vol 42, No. 7, pp.76-82.
- [19] Tomas Hruska, Masaki Hashimoto, Knowledge -based Software Engineering: Proceeding of the Fourth Joint Conference, September (2000).
- [20] Shoham, Y. (1997). An Overview of Agent-Oriented Programming, Software Agents Bradshaw, J. (ed.). AAAI Press/The MIT Press. P. 271-290.

Water Audit- A Tool for Assessment Of Water Losses

¹**R.A.Ganorkar**, ²**P.I.Rode**, ³**S.A Deshmukh**, ⁴**Dr.R.M.Dhoble**,

^{1,2}Asst.Prof. Civil Engg Dept, Priyadarshini Indira Gandhi College Of Engg Nagpur

³Asst.Prof. Civil Engg Dept, IBSS College Of Engg, Amravati

⁴Associate Professor In Civil Engineering Department, Priyadarshini Indira Gandhi College Of Engg, Nagpur (India)

Abstract:

The world's water resources are finite but exist on a planet with a constantly growing population. The development of water resources to man's benefit has been a fundamental factor in the evolution of civilizations throughout history. But, as our populations continue to grow and shift, the availability of quality water resources is in decline. Pollution, climate change and construction of cities in dry regions are some of the factors exacerbating evolving supply/demand imbalances. Many innovative technologies have been developed in recent times to assist the efficient delivery and utilization of drinking water. Water audits provide a rational, scientific framework that categorizes all water use in your system. It is a tool to overcome drought related problem, shortage, leakage and losses. International Water Association (IWA) / American Water Work Association (AWWA) initiated a large scale effort to asses reduced above related problem with the help of audit.

Key Words: IWA, AWWA, Water Audit

1. Introduction:

Water Audit comes into picture in late 80s to overcome a drought related problem, shortage, leakages and losses. The goal of an audit is to express an opinion on the person / organization / system etc., in question, under evaluation based on work done on a test basis. Water audits provide a rational, scientific framework that categorizes all water use in your system. It is a tool to overcome drought related problem, shortage, leakage and losses. International Water Association (IWA) / American Water Work Association (AWWA) initiated a large scale effort to asses reduced above related problem with the help of audit. Water audit is most effective tool for water management. With the help of water audit, we identify and quantify what steps can be taken to reduces water use and losses. Water audit and its analysis which can solve not only many water related problem but also saves precious resources and public money. Just as business routine, bank prepares statement of debits and credits for their customers and provides a statement of money, which is flowing into and out of accounts. The water audit display how quantity of water flows into and out of the distribution system and to the customer. Yet, as essential and commonplace as financial audit are to the world of commerce, water audit have been surprisingly uncommon in public water supply throughout most of the world.

1.1 Importance of Water Audit:

A portion of the total water use is leakage, some of it is due to inaccurate metering, some of it may be unauthorized use, and some of it is water delivered to customers. A water audit determines where the water ends up and how much of it got there. The level of detail in the water audit will vary based on the information on system has available. All water systems lose some amount of water for a variety of reasons. There are no accurate statistics for how much water is lost. Water loss costs money, paid by the system and customers. Utilities cannot reduce their water loss to zero. Some water loss is unavoidable, and it is not worth the expense to try to eliminate every drop escaping your system. However, most of the loss that occurs in water systems can be better managed by using a water audit. Managing a water utility is similar to managing any other business. In India, the land, water resources and population are 2.4 percent, 4 percent and 16 percent respectively of those of the globe. On an average the 50 percent of rain fall is within 15 days and in less than 100 hr, and this water is used for 365 days. The present water availability of India is 1820 m³ per capita per annum reduces from 6000 m³ per capita in 1947. In the context of prevailing scenario, the water audit becomes an inevitable activity in India and in World. Thus it is a tool to identify public money wastage due to the water loss, un-authorized connections as an advantage over the optimized use of water resources with environmental protection.

2. Objectives Of Water Audit:

Objectives of water audit is to find out physical losses due to pipe leakage and over flow, losses due to metering errors, un-authorized connections and free water supply given by Municipal authority for public stand post and park in the distribution system.

2.1 Advantage of Water Audit:

- [1] Water audits provide decision making tools to utility managers, directors, and operators. i.e., knowing where water is being used in your system allows you to make informed decisions about investing resources such as time, labor and money.
- [2] Water audits allow managers to efficiently reduce water losses in the system.
- [3] Reducing water used at the source may even result in delaying or avoiding capital investments such as a new well, more treatment technology or additional water rights.
- [4] Water audits also identify which water uses are earning revenue for the utility and which water uses are not. Thus, System personnel can increase revenue by ensuring all appropriate uses are being accurately measured and billed. This leads to more financial capacity in the water system, reduced cost per customer and better management of the water resource.
- [5] Creating awareness among water users i.e., customers can see and understand that the utility is taking proactive steps to manage wasted water and save for the future.
- [6] It is an effective educational and public relations tool for the water system.

3. Methodology Of Water Audit:

The standard water balance or methodology is the framework for categorizing and quantifying all water uses in the water audit. It is called a balance because when it is completed, all uses of water in the system equal the amount of water input by the sources. All water use is accounted for in the standard water balance (eliminating the need for the term unaccounted-for water). The standard water balance is really a series of simple equations. A graphical way to think about the standard water balance is presented in Figure 1. This is the most common way to view the standard water balance and developed by American Water Works Association (AWWA) and International Water Association (IWA) in 2000. It may also be presented in the form of separate equations, or in worksheet format. Begin by reading the graphical standard water balance from the left side, starting with the System Input category. It is important to understand that the vertical height of each category represents a proportional amount of water. Thus, the height of the System Input category represents all water pumped by the system in a given time period. This amount of water can be broken down into two additional categories, Authorized Use and Water Losses. Therefore, Authorized Use + Water Losses = System Input. This vertical height water measurement holds true across the entire standard water balance.

Following identify important relationships just by glancing at the standard water balance:-

- Water Losses = Apparent Losses + Real Losses.
- Nonrevenue Water = Water Losses + Unbilled Authorized Use.
- Apparent Losses = Metering Inaccuracies + Unauthorized Use.

System Input	Authorized Use	Billed Authorized Use	Revenue Water	Billed Metered Consumption
		Unbilled Authorized Use	Non Revenue Water	Billed Unmetered Consumption
	Water Losses	Apparent Losses		Unbilled Metered Use
		Real Losses		Unbilled Unmetered Use
				Unauthorized Use
				Leakage on Mains
				Overflows on Storages
				Leakage on Service Connections

Figure 1: AWWA/IWA Water Balance

Thus by following the five step process outlined below will able to complete these equations,

- Source Evaluation.
- Calculation of Authorized Consumption.
- Evaluation of Apparent Losses.
- Evaluation of Real Losses.
- Performance Measurement.

3.1 Source Evaluation:

The step first in completing the standard water balance is determining System Input. The System Input category may be comprised of various sources. A system may own multiple wells, springs or surface water intakes. This is a very important step, because even though it is only one category, the amount of water input should be balanced. Remember, in any type of balance, outputs must equal inputs. If this number is inaccurate, all of the remaining calculations you perform will be in error. The amount of water input to the balance is

determined by metering at the source. These meters are typically called master meters. Master meter readings are extremely important to all water systems. Accurate master meter readings are the only reliable way to determine how much total water the system is using; this may include dates of installation, warranties, maintenance records, or verbal communication with system personnel. These readings affect other critical aspects of the system, such as water rights compliance, mandatory taxes (i.e., the Water Conservation Fee), and payments for any water purchased from other systems. Master meters are larger and more expensive than customer meters. They will be subject to problems if they are not installed and maintained properly. Master meters should be tested regularly, and repaired or replaced as necessary. In order to properly maintain these meters, other appurtenances such as valves must be in good working order.

3.2 Calculation of Authorized Consumption:

This step should be fairly easy if system has been keeping good billing records. The first part involves calculating the category Revenue Water, which is made up of Billed Metered Consumption and Billed Unmetered Consumption. Since both of these categories are billed by the system, a review of the records should give you the information you need. Billed Metered Consumption includes residential, commercial and industrial customers. System may have different methods of billing these various customer classes. Other uses that should be placed in this category include any water that is metered and sold to other systems – this is known as exported water. Any other temporary or unconventional uses that are metered and billed during the month should be accounted for in this category. Billed Unmetered Consumption consists of any contracts the system has to provide unmetered water for a fee. An example is a contract to provide water to a construction site from a fire hydrant to water down roads. The utility should be estimating the amount of water used in this category as accurately as possible. For many systems, the water use in this category may vary over time, or it may be zero. After getting the information from the two categories above, simply add them together to determine Revenue Water. Also note that subtracting Revenue Water from System Input equals Nonrevenue Water. The final part of this step is to calculate Authorized Consumption. This includes Revenue Water plus any Unbilled Authorized Consumption. Since water use in this category is authorized by the system and might be expected that it will be simple to quantify.

Unbilled Authorized Consumption is most often made up of public uses in the community. This category is further broken down into Unbilled Metered Consumption and Unbilled Unmetered Consumption. Metered uses should be easier to quantify, as long as these meters are being read and recorded. Sometimes reading these meters is not a priority for system personnel since these uses are not being billed to anyone. Quantifying unmetered consumption will require estimation or installation of meters. Unbilled authorized consumption can be water uses like irrigation of public parks, fire flow for training or emergency use, and flushing of water lines by utility personnel. Water can also be consumed by treatment processes at the water or wastewater utility. Thus, at this stage it may be necessary to meet with other entities and educate them about the importance of estimating their water uses. After quantifying both components of Unbilled Authorized Consumption, add this category to Revenue Water, which is also Billed Authorized Consumption, to determine Authorized Consumption. Subtract this figure from System Input to calculate Water Losses.

3.3 Evaluate Apparent Losses:

Two categories i.e. Apparent Losses and Real Losses make up the components of Water Losses. The definition of these two terms is often confusing at first which are as follows. Apparent Losses of water occur as inaccuracies in water flow measurement, errors in water accounting, and unauthorized usage. Real Losses are the physical escape of water from the distribution system, and include leakage and overflows prior to the point of end use. Another way to think about Apparent Losses is that this category consists of water that is delivered to an end user – including unauthorized use – but is not properly measured or recorded. Sometimes apparent losses are called “paper losses” because they consist of water that is not properly recorded on paper. Apparent losses are more costly to the system than real losses. The cost of apparent losses occurs at the rate charged to the utility’s customers. The cost of real losses occurs at the cost of producing the water and pumping it through the distribution system. Thus the water audit allows understanding the true picture of water losses in water system. In the standard water balance, Apparent Losses is made up of Unauthorized Use and Customer Metering Inaccuracies. Unauthorized Use is theft or otherwise illegal consumption of water. There are different methods to detect and determine unauthorized use. Flow measurements on distribution lines can lead you in the right direction, particularly if the measurement can be limited to a few customers. Isolation of lines using valves may also work.

3.4 Evaluate Real Losses:

Real Losses are the physical escape of water from the distribution system, and include leakage and overflows prior to the point of end use. Real losses typically account for a greater volume of water lost by

utilities in comparison to apparent losses. The marginal cost of real water loss occurs at the cost of production – the expenses associated with extraction, treatment, delivery, operations & maintenance. Leakage on Mains is the first category of Real Losses. Leakage on mains refers to any physical loss of water in the distribution system other than storages or service connections. This category is often mistakenly confused with “water loss” or “unaccounted-for water” by people who are unfamiliar with the standard water balance. Leakage on mains will vary over time. It is important to keep good records of leak locations, repairs, and estimated losses. The amount of effort needed to perform a leak detection survey depends heavily on the information you have available, such as system maps, inventory of pipes and fittings, and history of repairs. Be sure that the information you are paying for will meet the needs of water audit. The new and most advanced real loss indicator (recommended by the IWA and AWWA Water Loss Committee) is the ILI, the infra structure leakage index. The development of the ILI started in 1997 when Allan Lambert the need for the real losses performance indicator which would allow international comparison between systems with very different characteristics, e.g. intermittent supply situation; low and high pressure system; differences in consumption level. The ILI, in the first few years known only to a few insiders, is now widely accepted and used by practitioners around the world, as it best describes the efficiency of the real losses management.

The ILI is a measure of how well a distribution network is managed (maintained, repaired and rehabilitated) for the control of real losses, at the current operation pressure. It is the ratio of Current Annual volume of Real Losses (CARL) to Unavoidable Annual Real Losses (UARL).

$$ILI = CARL/UARL$$

Being a ratio, the ILI has no units. But what are unavoidable losses and how are they calculated? Leakage management practitioners around the world are well aware that Real Losses will always exist – even in new and well managed systems. With the help of the following formula we can calculate the UARL.

$$UARL \text{ (liters/day)} = (18 \times L_m + 0.8 \times N_c + 25 \times L_p) \times P$$

Where;

L_m = Length of mains (km);

N_p = Number of service connections;

L_p = Total length of private pipe, curb-stop to customer meter (km);

P = average pressure (m).

Calculated components of Unavoidable Annual Real Losses are shown in table 1.

Sr. No.	Infrastructure Components	Background Losses	Reported Bursts	Unreported Bursts	UARL Total	Units
1	Mains	9.6	5.8	2.6	18	Liters/ km mains/Day /meter of pressure
2	Service Connection, meters at edge of street	0.6	0.04	0.16	0.8	Liters/Connection / day / meter of pressure
3	Underground pipes between edge of street and customer meters	16.0	1.9	7.1	25	Liters/km / Day / meter of pressure

Table No 1: Component of UARL

3.5 Performance Measurement:

One more step remains in the water audit process – interpreting the information that had been collected. A straight percentage performance measure does not account for variations in consumption or system input. Consider the following simple example:

	System Input	Total Gallons Consumed	Total Customers	Use per Capita	Total Real Losses	Percentage of Water Loss
System 1	1,000	800	10	80	200	20%
System 2	1,800	1,500	10	150	300	17%
System 3	1,300	1,000	10	100	300	23%

System 1 and System 2 serve an identical number of customers. System 2 has a higher amount of per capita use, a higher amount of total system input, and a higher amount of real losses. However, due to the ratio involved between real losses and system input, System 2 has a lower percentage of water loss. System 2 and System 3 also serve an identical number of customers, and they have an equal amount of real losses. System 2 has a higher use per capita, and a lower percentage of water loss. It should be clear from these hypothetical examples that a straight percentage of water loss should not be used to evaluate system water efficiency performance unless several other factors are taken into account. It is still a useful piece of information to consider, particularly when these other factors do not vary much. Other performance measures exist to help evaluate your utility's water use efficiency.

4. Conclusion:

Water audit study shall be covered the holistic approach towards total water resource, distribution and its efficient use to reduce the capital and operating cost as an added advantage over the optimized use of water resource with environment protection. With the help of Water Audit we can able to find the leakage and calculate the losses in the system and take the necessary measure for the future and fixed the performance target for improve the service level benchmark of the area.

References

- [1] Holmes Matthew (2007), "Water Use Auditing", New Mexico Rural Water Association, pp 1-20
- [2] Fanner V.P, Sturn R., J.Thornton (2007), "Evaluating Water Loss and Planning" Manual, Chapter -7, pp 75-93
- [3] Rathi Dinesh (2005), "Water audit in National scenario" National conference on water management conservation and sustainable development., Abstract Vol 1, pp 26-27
- [4] Liemberger R., Brothers K., Lambert A., McKenzie R., Rizzo A., Waldron T. (2006), "Water Loss Performance Indicator" pp 1-10
- [5] Lambert A.O, Brown Timothy G., Takizawa M., Weimer D (2000), "A Review of Performance Indicator for real Losses from Water Supply System" IWA/AQUA, pp 1-14
- [6] Kunkel George (2007), "Evaluating Water Loss and Planning" Manual, Chapter-4, pp 35-49
- [7] Halcrow Water Services Appendices Report (2003)
- [8] Nguyen Cong Thanh (2006), "Non-Revenue Water Assessment" pp 1-14
- [9] Kolbl J, Theuretzbacher-Fritz H., Neunteufel R., Perfler R., Gangl G., Kainz H., Haberl R. (2007), "Experiences with Water Loss PIs in the Austrian Benchmarking Project". Water Loss -2007, Conference Proceeding Vol 1, pp 176-186
- [10] Morrison J A E, Tooms S, Hall G (2007), "Sustainable District Metering". Water Loss -2007, Conference Proceeding Vol 1, pp 68-74
- [11] Halcrow Water Services and Bristol Water Services Report (2003), pp 12-58

An Efficient Semantic Web Through Semantic Mapping

Jenice Aroma R¹, Mathew Kurian²

¹ Post Graduation Student, ² Assistant Professor

Department of Computer Science and Engineering, Karunya University, Coimbatore

Abstract:

The outgrowth of web usage leads to the expectation of faster and easier access of web resources. Experts and even naïve users wish to have more advanced features on search schemes to acquire accurate results within a short time span. Semantic web can bring this expectation to real practice. To bring Semantic web in true, efficient Semantic Mapping is must. In this paper, a novel Two step Semantic Mapping algorithm and few related Semantic Mapping schemes are detailed with their functions and features. It helps one to acquire more knowledge on Semantic Mapping of concepts.

Keywords: Semantic web, WSDL, DAML-S, OWL-S.

1. Introduction

The Semantic web depends with machine interaction to acquire accuracy over information retrieval. The Conventional web resources includes syntactic discovery which could bring out related results not the relevant results. Thus it remains less efficient and needs an upgrade to the Semantic web. The Web 2.0 is termed for Conventional web today. To switch over web 3.0 (i.e) the Semantic web, a transition from WSDL (Web service description files) to OWL-S (Web Ontology Language for Services) files is must. This mode of transition is termed as Semantic Mapping of Concepts.

1.1 Mode of Semantic Mapping

The semantic mapping of concepts focuses towards the evolution of web 3.0 and the redefinition of conventional web resources in an efficient way. The ultimate goal of Semantic web is to bring an efficient Search scheme for retrieving related results. A novel Search discovery algorithm is must to be implemented for enabling the Semantic discovery of concepts.

To enhance the performance of this Search scheme, the conventional web services are mapped to Semantic web services. The Semantically mapped concepts are grouped into standard categories for enabling easier retrieval. On enabling rich semantics to the web resources through use of Web Ontology Language Services (OWL-S), the machine interoperability to understand the user's intention on information retrieval is enhanced. The Conventional Web services are prevalently XML based web services and it doesn't support efficient Automation of Web Services. The Automation of web services includes enhancing better mode of Discovery and Composition. The different modes of Discovery are Syntactic and Semantic Discovery. The Syntactic Discovery offers only Keyword based search Schemes.

The WSDL services that exist with the current web services provide only syntactic description of Data [1]. It analyses the supplied request from the user and finds a specific service based on the syntactical equivalence of input and output names. In Semantic Discovery, directory of Services be compiled which includes the ontological description for every service. It finds the suitable matching service from the compiled directory of services upon analyzing the user's requests.

2. Common Features Of Existing Semantic Mapping Tools

In semantic discovery, directory of Services be compiled which includes the ontological description for every service. The basic concepts on ontology modeling and various measures on extraction and matching of ontological concepts is shown. The different approaches on semantic mapping [2],[3],[4] applied are compared in the following Table 1.

Table 1. Common factors among the Semantic Mapping Approaches.

FEATURES	ASSAM	METEOR-S	WSDL TO DAML-S
Mapping Algorithm	Mapping the WSDL services using OWL-S are focused on Classification .	Mapping based on DAML-S ontologies.	Semantic mapping of concepts using DAML-S Annotations
Schemes on Classification	Using Iterative Relational Classifiers.	Use of Machine Learning Approach.	No Classification Schemes.
Support for Automation.	An Automated Tool for creating Semantic Data.	A Semi-Automated through use of schema matching.	An Automated Tool brings out Partial DAML-S file.
Standardized Concepts	Standardized concepts are absent.	Standardized concepts are absent.	Standardization of concepts is absent.
Performance Evaluation	Using Distance based Metrics.	Using Similarity Measures.	Using Edge base Metrics.

3. Semantic Mapping Algorithm

The Semantic Mapping of Concepts can be achieved through mapping the WSDL files into their corresponding OWL-S files. The DAML-S formats are earlier Semantic descriptions. The OWL-S supports more automation on complete generation of Information. Hence, it is more prevalent. The following Section details the sequences of Mapping in a two step Semantic Mapping algorithm over the WSDL and OWL-S files.

3.1 Two step Semantic Mapping Algorithm

The ‘Semantics’ is a sense of meaning which is added to the conventional web. It brings machine understanding and achieves more efficiency on information retrieval. This novel Semantic mapping algorithm includes a mapping process that maps the WSDL descriptions into upper ontologies called OWL-S. Normally the WSDL files are acquired from the Service Providers. Here, the WSDL descriptions are obtained from certain freely available web service sites. Those websites act like a repository for web services which can be applied for the Specified applications on research work.

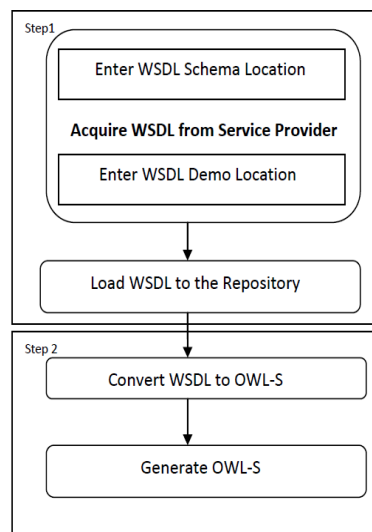


Fig.1: Mapping of WSDL to OWL-S

The Semantic Mapping Algorithm includes three main phases as (i) Loading WSDL file, (ii) Conversion using WSDL to OWL-S mapping and (iii) Generation of OWL-S files. The Mapping phase begins

at the stage of acquiring WSDL files as input from the service providers. As shown in Fig.1 the WSDL files are acquired from the freely available host websites through specifying the WSDL Demo and WSDL Schema locations of those WSDL files. On specifying the locations of the WSDL Schema, the WSDL descriptions are added to the repository and maintained as the input for mapping process. The WSDL files are converted to OWL-S through the conversion function using WSDL Translator.

3.2 WSDL to OWL-S Mapping

The Conversion function admits WSDL files into WSDL Translator for type conversion. This WSDL Translator is responsible for converting WSDL types into OWL format. In general, the WSDL components are of two types either Abstract definition or Concrete definition. The message and operation parts of WSDL Abstract definition are mapped into Service Information of OWL-S files. The Atomic process and Input-outputs of OWL-S comprises the Service Profile Information of OWL-S Files. The Service Profile Information helps to identify the type of Service, [6].

The Loading and mapping of abstract parts of WSDL components into OWL-S Components are clearly shown below with the following Fig.2. The mapping process shown in this algorithm is a simple process through use of WSDL Translator. The WSDL files are acquired from the Service Providers and the admitted to conversion function for mapping. Hence, this two phases leads to generation of OWL-S Files.

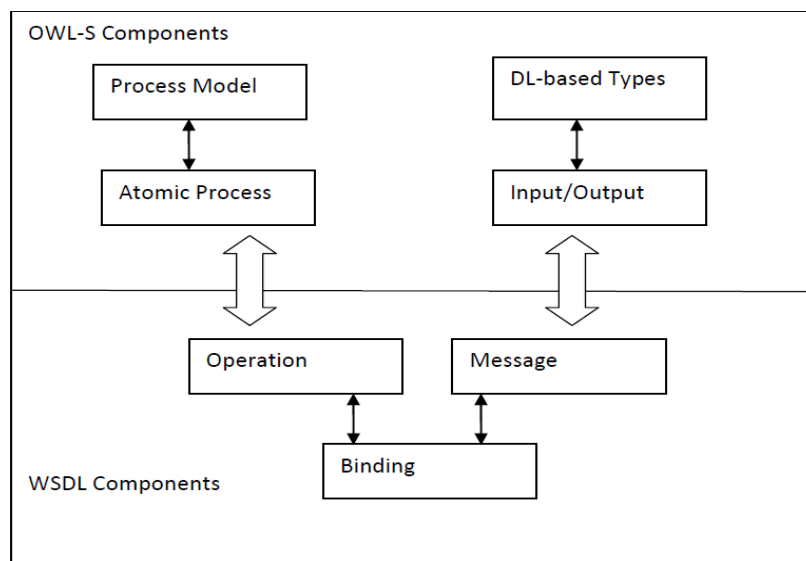


Fig.2: WSDL to OWL-S Mapping

The existing mapping schemes depend with schema matching and standardization before mapping. Though these schemes prove efficient, it leads to more time consumption due to lack of Standardization,[5]. However, the Standardization of mapping is more important and this proposed mapping algorithm extends further to add classification over the mapped web services in the enhancement work. A Simple Classification scheme can be applied to group the web services, which could achieve more efficiency on higher speed over information retrieval. This Simple Mapping Algorithm could achieve redefinition of Conventional web resources into Semantic Definitions with less time consumption and Efficiency on Information processing can be improved through adding a Classification scheme.

The Binding part of WSDL specifies the interface and style of SOAP binding. The Operation part specifies the type of Function being carried with the Web service. On mapping these concepts to Service Information, the OWL-S file is generated and added to the repository. Thus three phases of this Mapping algorithm could achieve redefinition of web 2.0.

4. Results

The following section shows the results for Semantic Mapping of Concepts. The admitted Web service description language files (WSDL) for semantic mapping undergoes two step of Semantic mapping phase. The Message parts of WSDL file be mapped into Grounding part of OWL-S file. The Operation parts of WSDL file be traced into Service Profile Information of OWL-S File.

```

</simpleType>
<complexType base="tns:ConversionRate">
  <sequence>
    <element minOccurs="1" maxOccurs="1" name="ConversionRateResult" type="tns:double" />
  </sequence>
</complexType>
<element name="double" type="tns:double" />
</schema>
</wsdl:types>
<wsdl:message name="ConversionRateSoapIn">
  <wsdl:part name="parameters" element="tns:ConversionRate" />
</wsdl:message>
<wsdl:message name="ConversionRateSoapOut">
  <wsdl:part name="parameters" element="tns:ConversionRateResponse" />
</wsdl:message>
<wsdl:message name="ConversionRateHttpGetIn">
  <wsdl:part name="FromCurrency" type="tns:string" />
  <wsdl:part name="ToCurrency" type="tns:string" />
</wsdl:message>
<wsdl:message name="ConversionRateHttpGetOut">
  <wsdl:part name="Body" element="tns:double" />
</wsdl:message>
<wsdl:message name="ConversionRateHttpPostIn">
  <wsdl:part name="FromCurrency" type="tns:string" />
  <wsdl:part name="ToCurrency" type="tns:string" />
</wsdl:message>
<wsdl:message name="ConversionRateHttpPostOut">
  <wsdl:part name="Body" element="tns:double" />
</wsdl:message>
<wsdl:portType name="CurrencyConverterSoap">
  <wsdl:operation name="ConversionRate">
    <wsdl:documentation xmlns:wsdl="http://schemas.xmlsoap.org/wsdl/">&lt;br&gt;&lt;b&gt;Get conversion rate from one currency to another currency &lt;b&gt;&lt;/wsdl:documentation>
    <wsdl:input message="tns:ConversionRateSoapIn" />
    <wsdl:output message="tns:ConversionRateSoapOut" />
  </wsdl:operation>
</wsdl:portType>
</wsdl:portType name="CurrencyConverterHttpGet">
  </wsdl:portType>
</wsdl:portType name="CurrencyConverterHttpPost">
  </wsdl:portType>

```

Fig 3.Message part in WSDL

```

<rdf:Property rdfs:label="ConversionRate" rdfs:domain="CurrencyConverterSoap" rdfs:range="double">
  <rdfs:Property rdfs:label="ConversionRateHttpGet" rdfs:domain="CurrencyConverterHttpGet" rdfs:range="double">
  <rdfs:Property rdfs:label="ConversionRateHttpPost" rdfs:domain="CurrencyConverterHttpPost" rdfs:range="double">
  </rdfs:Property>
</rdf:Property>

```

Fig 4. Grounding in OWL-S

```

<wsdl:portType name="CurrencyConverterSoap">
  <wsdl:operation name="ConversionRate">
    <wsdl:documentation xmlns:wsdl="http://schemas.xmlsoap.org/wsdl/">&lt;br&gt;&lt;b&gt;Get conversion rate from one currency to another currency &lt;b&gt;&lt;/wsdl:documentation>
    <wsdl:input message="tns:ConversionRateSoapIn" />
    <wsdl:output message="tns:ConversionRateSoapOut" />
  </wsdl:operation>
</wsdl:portType>
<wsdl:portType name="CurrencyConverterHttpGet">
  <wsdl:operation name="ConversionRate">
    <wsdl:documentation xmlns:wsdl="http://schemas.xmlsoap.org/wsdl/">&lt;br&gt;&lt;b&gt;Get conversion rate from one currency to another currency &lt;b&gt;&lt;/wsdl:documentation>
    <wsdl:input message="tns:ConversionRateHttpGetIn" />
    <wsdl:output message="tns:ConversionRateHttpGetOut" />
  </wsdl:operation>
</wsdl:portType>
<wsdl:portType name="CurrencyConverterHttpPost">
  <wsdl:operation name="ConversionRate">
    <wsdl:documentation xmlns:wsdl="http://schemas.xmlsoap.org/wsdl/">&lt;br&gt;&lt;b&gt;Get conversion rate from one currency to another currency &lt;b&gt;&lt;/wsdl:documentation>
    <wsdl:input message="tns:ConversionRateHttpPostIn" />
    <wsdl:output message="tns:ConversionRateHttpPostOut" />
  </wsdl:operation>
</wsdl:portType>
</wsdl:portTypes>
<wsdl:binding name="CurrencyConverterSoap" type="tns:CurrencyConverterSoap">
  <soap:binding transport="http://schemas.xmlsoap.org/soap/http" />
  <wsdl:operation name="ConversionRate">
    <soap:operation soapAction="http://www.webserviceX.NET/ConversionRate" style="document" />
    <wsdl:input />
    <soap:body use="literal" />
  </wsdl:operation>

```

Fig 5. Operations in WSDL

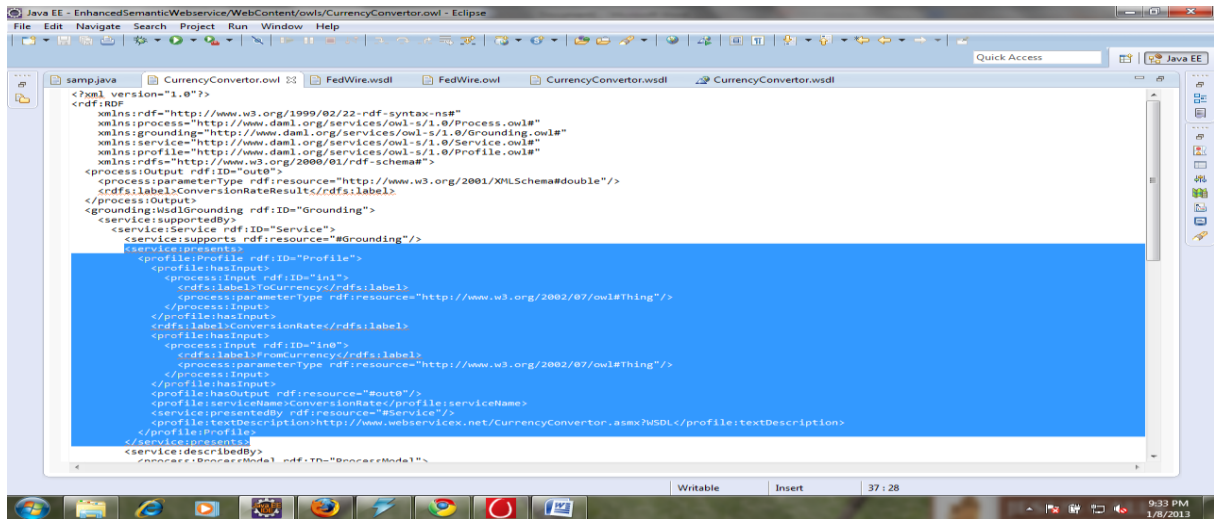


Fig 6. Service Profile in OWL-S

6. Conclusion

The semantic web is a dynamic field with enhanced approaches evolving everyday. It steps more higher on bringing a best model of Search. This paper proposes a novel scheme of mapping to generate semantic descriptions from the WSDL files. The special feature of this mapping algorithm is the simple automated mapping scheme with reduced time span. However, this mapping scheme can be made more efficient through addition of classification schemes for standardization.

References

- [1]. Web Services Description Lang., W3C, 2001, Online: <http://www.w3.org/TR/wsdl>
- [2]. Andreas Heß, Eddie Johnston and Nicholas Kushmerick, "ASSAM: A Tool for Semi-Automatically Annotating Semantic Web Services", 12th International Conference on Web Technologies, pages 470–475, 2008
- [3]. Abhijit A. Patil, Swapna A. Oundhakar, Amit P. Sheth and Kunal Verma, "METEOR-S Web Services annotation framework", proceedings of the 13th international conference on WWW. ACM Press, 2004.
- [4]. Massimo Paolucci, Naveen Srinivasan, Katia Sycara, Takuya Nishimura, "Towards a Semantic Choreography of Web Services: from WSDL to DAML-S", In Proceedings of the First International Conference on Web Services (ICWS'03), Las Vegas, Nevada, USA, pp 22-26, June 2003.
- [5]. Tamer A. Farrag, A. I. Saleh and H. A. Ali, "Towards SWSs discovery: mapping from WSDL to OWL-S based on ontology search and standardization engine", IEEE Transactions on Knowledge and Data Engineering, 2012.
- [6]. Web ontology language for services W3C Member Submission, 2004, Online: <http://www.w3.org/Submission/OWL-S/>

Lightweight Decentralized Algorithm for Localizing Reactive Jammers in Wireless Sensor Network

¹Vinothkumar.G, ²Ramya.G, ³Rengarajan.A

P.G.Scholar^(1,2), Associate Professor⁽³⁾

^{1,2,3}Veltech Multitech Dr.Rangarajan Dr.Sakunthala Engineering College, Chennai, India

Abstract:

In wireless sensor network one of the most security threats is the reactive jammer because of the mass destruction to the sensor communication and it is difficult to disclose. So we have to deactivate the reactive jammers by identifying all the trigger nodes, because the transmission invokes the jammer. Such a trigger identification procedure can work as an application-layer service and benefit many existing reactive jamming defending schemes. In this paper, on the one hand, we leverage several optimization problems to provide a complete trigger-identification service framework for unreliable wireless sensor networks. On the other hand, we provide an improved algorithm with regard to two sophisticated jamming models, in order to enhance its robustness for various network scenarios. Theoretical analysis and simulation results are included to validate the performance of this framework..

Keywords: Reactive jamming, jamming detection, trigger identification, error tolerant non adaptive group testing, optimization, NP-hardness.

1. Introduction

The security of wireless sensor networks has attracted numerous attentions, due to its wide applications in various monitoring systems and vulnerability toward sophisticated wireless attacks. Among these attacks, jamming attack in which a jammer node disrupts the message delivery of its neighboring sensor nodes with interference signals, has become a critical threat to WSNs. However a reactive variant of this attack, where jammer nodes stay quiet until an ongoing legitimate transmission (even has a single bit) is sensed over the channel, emerged recently and called for stronger defending system and more efficient detection schemes. Existing countermeasures for reactive jamming attacks consists of jamming detection and jamming mitigation. On the one hand detection of interference signals from jammer nodes is non-trivial discrimination between normal noises and adversarial signals over unstable wireless channels. A mapping service of jammed area has been presented in which detects the jammed areas and suggests that routing paths evade these areas. This works for proactive jamming, since all the jammed nodes are having low PDR and thus incapable for reliable message delay. However, in the case of reactive jamming, this is not always the case. By excluding the set of trigger nodes from the routing paths, the reactive jammers will have to stay idle since the transmissions cannot be sensed. Even though the jammers move around and detect new sensor signals, the list of trigger nodes will be quickly updated, so are the routing tables.

The basic idea of our solution is to first identify the set of victim nodes by investigating corresponding links PDR and RSS, then these victim nodes are grouped into multiple testing teams. Once the group testing schedule is made at the base station and routed to all the victim nodes, they then locally conduct the test to identify each of them as trigger or non-trigger.

2. Problem Models

2.1 NETWORK MODEL

Consider a wireless sensor network consisting of n sensor nodes and one stations can be split into small ones to satisfy the model. Each sensor node is equipped with a omnidirectional antennas, m radios for in total k channels throughout the network, where $k > m$.

2.2 Attacker Model

We consider both a basic attacker model and advanced attacker models in this paper.

2.3 Basic Attacker Model:

Three concepts are introduced to complete this model.

Jamming range(R): Similar to the sensors, the jammers are equipped with omnidirectional antennas with uniform power strength on each direction. The jammed area can be regarded as a circle centered at the jammer node.

Triggering range(r): On sensing an ongoing transmission, the decision whether or not to launch a jamming signal depends on the power of the sensor signal P_s .

Jammer distance: Any two jammer nodes are assumed not to be too close to each other, i.e., the distance between jammer J_1 and J_2 is $\delta(J_1; J_2) > R$.

2.4 Advanced Attacker Model:

To evade detections, the attackers may alter their behaviors to evade the detection, for which two advanced reactive jamming models: probabilistic attack and asymmetric response delay time.

Source_ID	Time_Stamp	Label	TTL	Main Message Body
V1	0950	victim	30	*****

Fig1: sensor periodical status report message

2.5 SENSOR MODEL

Besides monitoring the assigned network field and generating alarms in case of special events, each sensor periodically sends a status report message to the base station. The header is designated for anti-jamming purpose, which is 4-tuple: **Sensor_ID** as the ID of the sensor node, **Time_Stamp** as the sending out time indicating the sequence number, as well as a **Label** referring to the nodes current jamming status, and **TTL** as the time to live field.

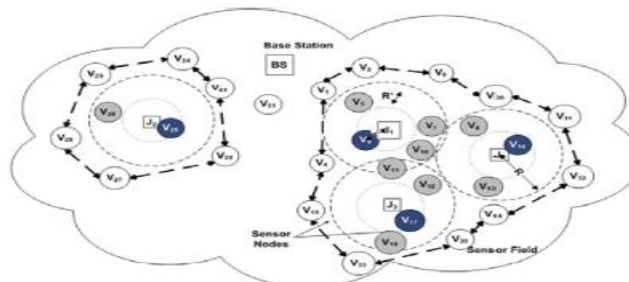


Fig 2: Nodes in Gray and Blue are victim nodes
And in blue is also a trigger node.

3. Kernal Techniques

3.1 Error Tolerant Randomized Non- Adaptive Group Testing:

Group testing was proposed since WWII to speed up the identification of affected blood samples from a large sample population. The traditional method of grouping items is based on a designated 0-1 matrix M_t , n where the matrix rows represent the testing group and each column refers to an item.

3.2 Minimum Disk Cover in a Polygon:

Given a simple polygon with a set of vertices inside, the problem of finding a minimum number of variable radii disks that not only cover all the given vertices, but also are all within the polygon, can be efficiently solved.

3.3 Cliques-Independent Set:

Clique-Independent set is the problem to find a set of maximum number of pair wise vertex disjoint maximal cliques, which is referred to as maximum clique-independent set.

4. Trigger Node Identification

The decentralized algorithm for trigger identification is a light weight procedure and the calculations are occur at the base station, the transmission overhead and complexity is low.

3 main steps of the procedure follow:

4.1 Anomaly Detection:

The base station detects potential reactive jamming attacks; each boundary node tries to report their identities to the base station. The base station waits for the status report from each node in each period of length P . If no reports have been received from node v with a maximum delay time, then v will be regarded as victim.

4.2 Jammer Property Estimation:

The base station calculates the estimated jammed area and jamming range R based on the locations of the boundary nodes.

4.3 Trigger Identification:

- a. Base station creates an encrypted message Z and broadcast to all boundary nodes.
- b. Boundary nodes keep broadcasting the Z to all victim nodes in the area.
- c. All victim nodes execute the procedure and identify themselves as trigger or non-trigger.

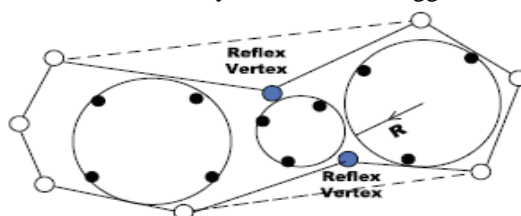


Fig 3: Estimated R and jammed area

4.4 Discovery of Interference Free Items:

It is possible to discover the set of victim nodes within the same jammed area, i.e., with a distance R from the same jammer node. Any two nodes within the same jammed area should be at most $2R$ far from each other.

4.5 Estimation of Trigger Upper Bound:

As mentioned in the attacker model, r depends not only on power of both sensors and jammers, but also the jamming threshold θ and path loss factor ζ .

$$r \geq ((P_n \cdot \theta) / (P_s \cdot Y))^{1/\zeta}$$

4.6 Analysis of Time and Message Complexity:

4.7 Time complexity:

By time complexity mean the identification delay counted since the attack happens till all nodes successfully identify themselves as trigger or non-trigger. Therefore, the complexity break downs into four parts:

- [1] Detection of interference signals at local links T_d .
- [2] Routing of sensor report to the base station from each sensor node, and the schedule to each victim node from the base station, aggregated as T_r .
- [3] Calculation of CIS and R at the base station T_c ;
- [4] Testing at each jammed area T_t .

4.8 Message Complexity:

On the one hand, the broadcasting schedule Z from the base station to all victim nodes costs $O(n)$ messages in the worst case. On the other hand, the overhead of routing reports toward the base station depends on the routing scheme used and the network topology as well as capacity.

5. Experimental Evaluation

5.1 Overview:

As a lightweight distributed trigger-identification service, our solution will be experimentally evaluated from four facets:

- [1] In order to show the benefit of this service, we compare it with JAM in terms of end-to-end delay and delivery ratio of our routes from the base station to all the sensor nodes.
- [2] In order to show the acceleration effect of CIS we compare the complexity solution with varying parameters.
- [3] In order to show the accuracy of estimating the jamming range we provide the range and error rate using disk cover algorithm.
- [4] In order to show its performance and robustness toward tricky attackers, we assess its false positive/negative rate and the estimation of R , for those two advanced jammer models.

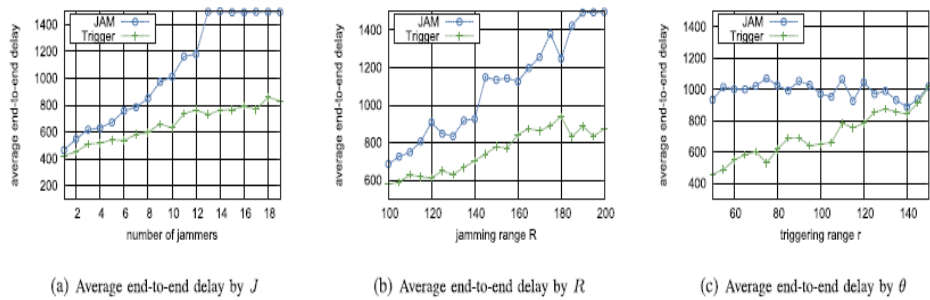


Fig 4: Benefits of Routing

5.2 Benefits for Jamming Routing:

This method is dedicated for proactive jamming attacks, which sacrifices significant packet delivery ratio due to unnecessarily long routes selected, though the effects of jamming signals are avoided. The length of routes based on JAM quickly climbs up to the upper bound, while that of our trigger method is much lower and more stable.

5.3 Improvements on Time Complexity:

The time complexity of our new clique based detection s proved to be asymptotically lower than the previous. Parameter values lower than these intervals would make the sensor network less connected and jamming attack less severe, while higher values would lead to impractical dense scenarios and unnecessary energy waste.

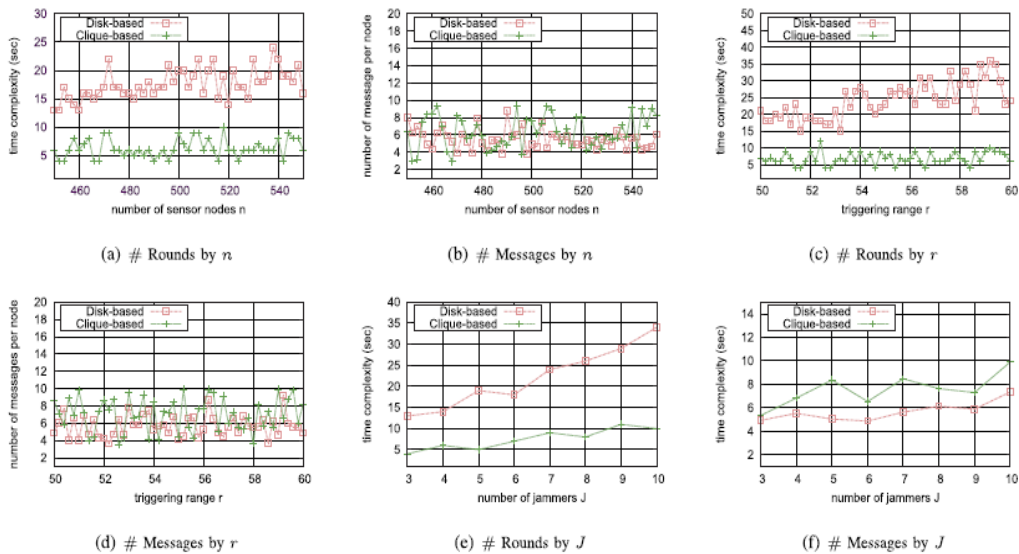


Fig 5: Time and Message Complexity

5.4 Accuracy in Estimating Jammer Properties:

Two observations are straightforward from these results:

- [1] All the estimated values are above the actual ones, however, less than 10 percent difference. This meets our
- [2] requirement for a tight upper bound of R .

The error rates in the case of fewer jammers are lower than those with more jammers. This is because the jammer areas can have larger overlaps, which introduces estimate inaccuracies.

5.5 Robustness to various Jammer Models:

Jammers in the simulation respond each sensed transmission with probability 0.5 as well. All the simulation results are derived by averaging 10 instances for each parameter team. We consider the extreme cases where jammers respond transmission signals with a probability as small as 0.1, or delay the signals upto 10 testing rounds later.

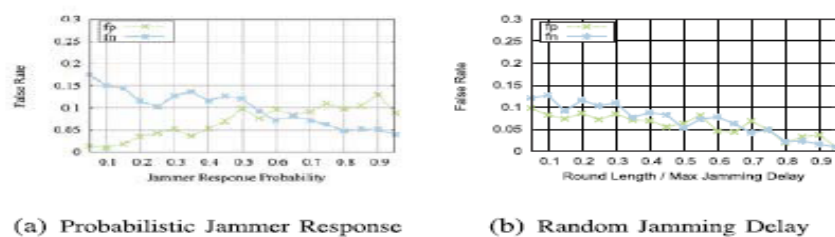


Fig 6: Solution Robustness

6. Further Enhancement

We further enhance our work to give more protection for trigger nodes. Trigger nodes will be given a **security code** to have protected communication once they had been identified. By doing this problem is controlled from spreading over the entire network. And we are **using Channel Surfing** to prevent from jamming. That means when we transmit a data successfully the channel was changed for next data.

7. Conclusion

Thus we are providing an efficient trigger identification service framework, we leverage several optimization problem models and provide corresponding algorithms to them, which includes the clique-independent problem, randomized error-tolerant group testing, and minimum disk cover for simple polygon. The efficiency of this framework is proved through both theoretically analysis toward various sophisticated attack models and simulations under different network settings.

References

- [1] W. Hang, W. Zanj, and W. Jingbo, "Performance of DSSS against Repeater Jamming", Proceeding IEEE13thInternational conference Electronics, Circuits and systems 2006.
- [2] I. Shin, Y. Shen, Y. Xuan, M.T. Thai, and T. Znati, "Reactive Jamming Attacks in Multi-Radio Wireless Sensor Networks: An Efficient Mitigating Measure by Identifying Trigger Nodes," Proc. Second ACM Int'l Workshop Foundations of Wireless Ad Hoc and Sensor Networking and Computing ,in conjunction with MobiHoc, 2009.
- [4] M. Strasser, B.Danev, and S. Capku, "Detection of Reactive jamming in Sensor Networks", ACM Trans. Sensor Networks, vol.7, pp. 1-29, 2010.
- [5] W. Xu, K. Ma, W. Trappe, and Y. Zhang, "Jamming Sensor Networks: Attack and Defense Strategies", IEEE Network, vol.20, no.3, pp. 41-47, May/June 2006.
- [6] W. Xu, T. Wood, W.Trappe, and Y. Zhang, "Channel Surfing and Spatial Retreats: Defenses against Denial of Service", Proc. ACM Workshop against Denial of Service

Secure Data Forwarding In Distributed Environment Using Cloud Storage System

S.Amritha¹, S.Saravana Kumar²

¹M.E.(Cse), Srinivasan Engg College,Perambalur,Tamilnadu,India.

²,Ap/Cse, Srinivasan Engg College,Perambalur,Tamilnadu,India.

Abstract:

A cloud storage system, used to store large number of data in storage server. Cloud system is used to provide large number storage servers, which provide long-term storage service over the Internet. Third party's cloud system does not provide data confidentiality. Constructing centralized storage system for the cloud system makes hackers stole data easily. General encryption schemes protect data confidentiality. In the proposed system a secure distributed storage system is formulated by integrating a threshold proxy re-encryption scheme with a decentralized erasure code. The distributed storage system not only supports secure and robust data storage and retrieval, but also lets a user forward data from one user to another without retrieving the data back. The main technical involvement is that the proxy re-encryption scheme supports encoding operations over encrypted messages as well as forwarding operations over encoded and encrypted messages. The method fully integrates encrypting, encoding, and forwarding. The proposed system is applied for military and hospital applications, then other secret data transmission.

Keywords: Decentralized erasure code, proxy re-encryption, threshold cryptography, secure storage system.

1. Introduction

Cloud computing is a model that treats the resources on the Internet as a unified entity, a cloud. Users use a service without being concerned about how computation is done and storage is managed. This method used to focus on designing a cloud storage system for robustness, privacy, and functionality. A cloud storage system is considered as a large scale distributed storage system that consists of many self-governing storage servers. Data robustness is a major obligation for storage systems. There are many proposals of storing data over storage servers. One way to present data robustness is to duplicate a message such that each storage server stores a copy of the message. It is robust because the message can be retrieved as long as one storage server survives. Another way is to encrypt a message of k symbols into a codeword of n symbols by erasure coding. To store a message, each of its encoded messages is stored in a various storage server. A storage server failure corresponds to an erasure error of the encode symbol. As long as the number of failure servers is under the acceptance threshold of the erasure code, the message can be recovered from the encode symbols stored in the available storage servers by the decoding process. This provides a trade off between the storage size and the acceptance threshold of failure servers. A decentralized erasure code is an erasure code that independently computes each codeword symbol for an encrypted message. Thus, the encoding process for a message used to split up message into n parallel tasks of generating codeword symbols. A distributed storage system is constructed a decentralized erasure code. After the messages are sent to storage servers, each storage server separately computes a codeword symbol for the received message and stores it. This finishes the encoding operation and storing process. The recovery process is also the same process like a encoding process. Storing data in a third party's cloud system will not provide a data confidentiality. In order to provide well-built confidentiality for messages in storage servers, a user encrypt messages by a threshold cryptography method before applying an erasure code method to encode and store messages. When user wants to use a message, user needs to recover the codeword symbols from storage servers, decode, and decrypt them by using cryptography keys. There are three problems in the above simple integration of encryption and encoding methods. First, the user has to do computation and the communication traffic between the user and storage servers is far above the ground. Second, the user has to manage his cryptography keys. If the user's tool of storing the keys is vanished or compromise, the security is broken. Finally, in addition data storing and retrieving, it is inflexible for storage servers to directly support other functions. For example, storage servers cannot frankly forward a user's messages to another user. The owner of messages has to retrieve message, decode, decrypt and then forward them to another user.

2. Related work

2.1. Ocean Store

Ocean Store is a utility infrastructure designed to span the globe and provide continuous access to persistent information. Since this infrastructure is comprised of untrusted servers, data is protected through

redundancy and cryptographic techniques. To improve performance, data is allowed to be cached anywhere, anytime. Additionally, monitoring of usage patterns allows adaptation to regional outages and denial of service attacks; monitoring also enhances performance through pro-active movement of data. A prototype implementation is currently under development. In the past decade it has seen astounding growth in the performance of computing devices. Even more significant has been the rapid pace of miniaturization and related reduction in power consumption of these devices. Before such a revolution can occur, however, computing devices must become so reliable and resilient that they are completely transparent to the user.

2.2. PAST

This technique sketches the design of PAST, a large-scale, Internet-based, global storage utility that provides scalability, high availability, persistence and security. PAST is a peer-to-peer Internet application and is entirely self organizing. PAST nodes serve as access points for clients, participate in the routing of client requests, and contribute storage to the system. Nodes are not trusted, they may join the system at any time and may silently leave the system Without warning. Yet, the system is able to provide strong assurances, efficient storage access, load balancing and scalability. Among the most interesting aspects of PAST's design are(1) the Pastry location and routing scheme, which reliably and efficiently routes client requests among the PAST nodes, has good network locality properties and automatically resolves node failures and node additions; (2) the use of randomization to ensure diversity in the set of nodes that store a file's replicas and to provide load balancing; and (3) the optional use of smartcards, which are held by each PAST user and issued by a third party called a broker. The smartcards support a quota system that balances supply and demand of storage in the system. There are currently many projects aimed at constructing peer-to-peer applications and understanding more of the issues and requirements of such applications and systems. Peer-to-peer systems can be characterized as distributed systems in which all nodes have identical capabilities and responsibilities and all communication is symmetric. We are developing PAST, an Internet-based, peer-to-peer global storage utility, which aims to provide strong persistence, high availability, scalability and security. The PAST system is composed of nodes connected to the Internet, where each node is capable of initiating and routing client requests to insert or retrieve files. Optionally, nodes may also contribute storage to the system. The PAST nodes form a self-organizing overlay network. Inserted files are replicated on multiple nodes to ensure persistence and availability.

3. System Model

3.1. Decentralized erasure code

In decentralized erasure code which is used to split up the messages or text data into n number of blocks. This is used for splitting purpose. Our result $n=ak^c$ allows that number of storage server be greater than the number of blocks of a text data's. Decentralized erasure code is a first phase of this project. This has been initiated. In the decentralized erasure code is an erasure code that independently computes each codeword symbol for a message. Thus, the encoding method for a message can be split into n parallel tasks of generating codeword symbols. A decentralized erasure code is used in a distributed storage system. The n blocked message is stored in for the integration process.

3.2. Integration

In an integration processes, the splinted message is joined into an m number of blocks, and stored into lager storage server. User A encrypts his message M is decomposed into k number of blocks m_1, m_2, \dots, m_k and which has an identifier ID. User A encrypts each block m_i into a cipher text C_i and sends it to v randomly chosen storage servers. Upon receiving cipher texts from a user, each storage server linearly combines them with randomly chosen coefficients into a codeword symbol and stores it. Note that a storage server may receive fewer than k message blocks and we assume that all storage servers know the value k in advance. Integration is used to combine messages into m number of block, which is encrypted and stored into a large number storage server. Then forward to user B. Data which is encrypted by using single key. This is produced by using hash key algorithm. In the data storage phase, user A encrypts his message M and dispatches it to storage servers. A message M is decomposed into k number of blocks m_1, m_2, \dots, m_k and which has an identifier ID. User A encrypts each block m_i into a cipher text C_i and sends it to v randomly chosen storage servers. Upon receiving cipher texts from a user, each storage server linearly combines them with randomly chosen coefficients into a codeword symbol and stores it. Note that a storage server may receive fewer than k message blocks and it assumes that all storage servers know the value k in advance.

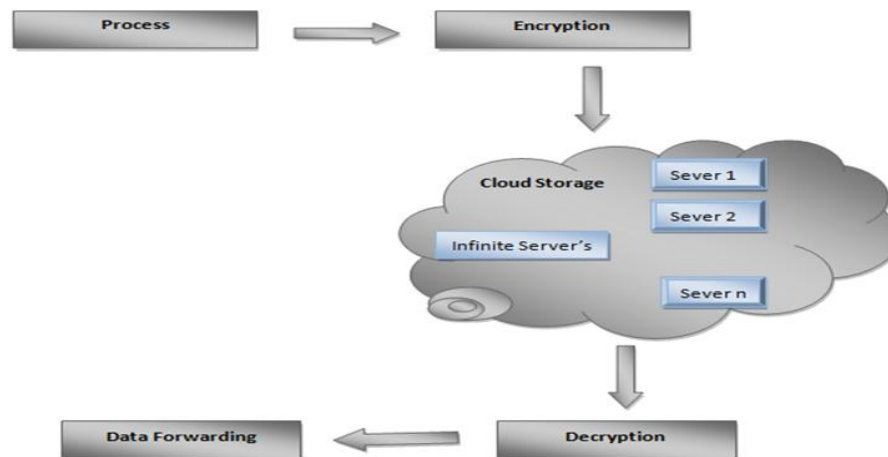


Fig 1: Overview architecture

3.3. Encryption

This is used to encrypt a plain text into a cipher text. Cipher text is produced along with a single key. This key is used to convert the cipher text again into a plain text. The integrated data is encrypted with a single key using random key generation method. Hash key algorithm using random key generation. This is used to generate, the random key. Whenever users encrypt the text, each session time a new key is generated. Storing data in a third party cloud does not provide Confidentiality in cloud storage. Data confidentiality is provided by threshold proxy re-encryption scheme. Using this technique the data is encrypted twice and key is generated by a random key generation methods using hash algorithm. This is used to generate the more than 10,000 key at the session time.

3.4. Data forwarding

In the data forwarding phase, user A forwards his encrypted message with an identifier ID stored in storage servers to user B such that B can decrypt the forwarded message by his secret key. To do so, A uses his secret key SK_A and B's public key PK_B to compute a re-encryption key $RK_{A \rightarrow B}^{ID}$ and then sends $RK_{A \rightarrow B}^{ID}$ to all storage servers. Every storage server uses the re encryption key to re-encrypt its codeword symbol for later retrieval needs by B. The re-encrypted codeword symbol is the grouping of cipher texts under B's public key. In order to differentiate re-encrypted codeword symbols from intact ones, we call them unique codeword symbols and re-encrypted codeword symbols, correspondingly.

3.5. Login

Log in page make user to access an account in a cloud server. When user has an account in the cloud server for accessing data and provides other services. User can sign up the page directly else users needed to create new account using create account option.

3.6. Uploading File

User after sing up his/her account. User forward data to another user using his/her account. Using id of an user and IP address. Upload encrypted files and forward to a user. User upload files along with a key which is used to encrypt the text.

3.7. Data Retrieval

Date retrieval is the final module of this project. User download data and using proxy re-encryption method text decoded and partial decrypted. A proxy server can transfer a cipher text under a public key PK_A to a new one under another public key PK_B by using the re-encryption key $RK_{A \rightarrow B}$. In the data retrieval phase, user A retrieves a message from storage servers. The message is either stored by user A or forwarded to user A. User A sends a recovery request to key servers. Upon receiving the recovery request and execute a proper verification process with user A, each key server KS_i needs u randomly chosen storage servers to get code symbols and does partial decryption on the received code symbols by using the key share $SK_{A,i}$. Finally, user A combine the partially decrypted codeword symbols to obtain the original message M . There are two suitcases for the data recovery phase. The first case is that a user A retrieves his own message from cloud. When user A needs to retrieve the message with an identifier ID, he informs all key servers with the individuality token A key server first retrieves original code symbols from u randomly chosen storage servers and then performs partial decryption Share Dec on every retrieved original codeword symbol. The result of partial decryption is called a partially decrypted code symbol. The key server sends the moderately decrypted codeword symbols and the

coefficients to user A. After user A collects replies from at smallest amount t key servers and at least k of them are originally from distinct storage servers, he executes Combine on the t partially decrypted codeword symbols to recover the blocks m_1, m_2, \dots, m_k . The second case is that a user B retrieves a message forwarded to user B. User B informs all key servers straight. The collection and combining parts are the same as the first case except that key servers retrieve re-encrypted codeword symbols and perform partial decryption Share-Decrypted on re-encrypted codeword symbols.

4. Experimental Result

This experiment shows that our approach is practical and could be used in secure data forwarding in distributed environment using cloud storage system. The empirical results show that cost reduction, time consuming, provide more security.

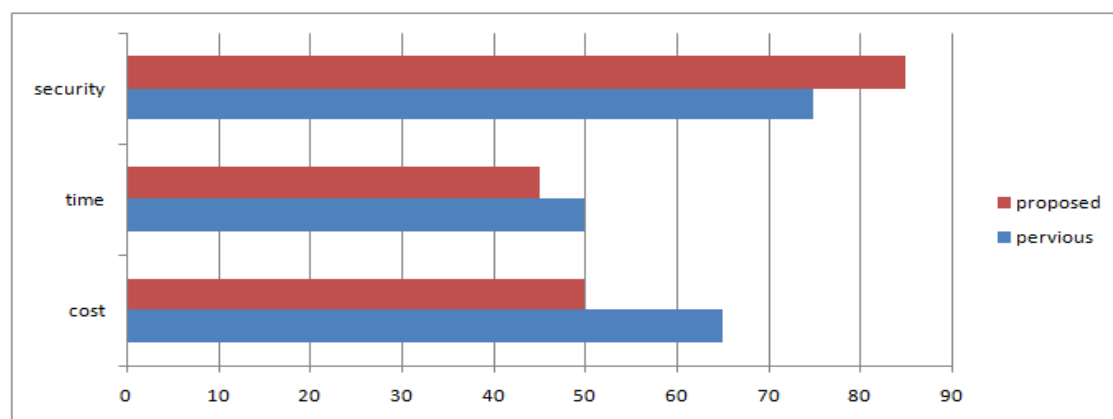


Fig 2: This result shows that compare to the previous system, the proposed system is provide more security, low cost, time consuming.

5. Conclusion

The study of existing system has revealed the use of centralized server, micro bench mark and Third Party Auditor (TPA). The implementations of the traditional systems have resulted in crashes, DOS attacks and unavailability due to regional network outages. In the proposed system a secure distributed storage system is formulated by integrating a threshold proxy re-encryption scheme with a decentralized erasure code. The proxy re-encryption scheme supports not only the expected encoding operations over encrypted messages but also the forwarding operations over encoded and encrypted messages.

6. Acknowledgements

This work was presented in part at the IEEE International Conference on Communications (ICC), 2012. This work was can be done in part of in our institution and support of all staff members.

References

- [1] Adya, W.J. Bolosky, M. Castro, G. Cermak, R. Chaiken, J.R.Douceur, J. Howell, J.R. Lorch, M. Theimer, and R. Wattenhofer, "Farsite: Federated, Available, and Reliable Storage for an Incompletely Trusted Environment," Proc. Fifth Symp. Operating System Design and Implementation (OSDI), pp. 1-14, 2002.
- [2] Ateniese.G, K. Fu, M. Green, and S. Hohenberger, "ImprovedProxy Re-Encryption Schemes with Applications to SecureDistributed Storage," ACM Trans. Information and System Security, vol. 9, no. 1, pp. 1-30, 2006.
- [3] Blaze.M, G. Bleumer, and M. Strauss, "Divertible Protocols and Atomic Proxy Cryptography," Proc. Int'l Conf. Theory and Application of Cryptographic Techniques (EUROCRYPT), pp. 127-144, 1998.
- [4] Brownbridge.D.R., L.F. Marshall, and B. Randell, "The Newcastle Connection or Unixes of the World Unite!," Software Practice and Experience, vol. 12, no. 12, pp. 1147-1162, 1982.
- [5] Dimakis. A.G, V. Prabhakaran, and K. Ramchandran, "Ubiquitous Access to Distributed Data in Large-Scale Sensor Networks through Decentralized Erasure Codes," Proc. Fourth Int'l Symp. Information Processing in Sensor Networks (IPSN), pp. 111- 117, 2005.
- [6] Dimakis.A.G., V. Prabhakaran, and K. Ramchandran, "Decentralized Erasure Codes for Distributed Networked Storage," IEEE Trans. Information Theory, vol. 52, no. 6 pp. 2809-2816, June 2006.

- [7] Druschel, P and A. Rowstron, "PAST: A Large-Scale, Persistent Peer-to-Peer Storage Utility," Proc. Eighth Workshop Hot Topics in Operating System (HotOS VIII), pp. 75-80, 2001.
- [8] Haerberlen, A, A. Mislove, and P. Druschel, "Glacier: Highly Durable, Decentralized Storage Despite Massive Correlated Failures," Proc. Second Symp. Networked Systems Design and Implementation (NSDI), pp. 143-158, 2005.
- [9] Hsiao-Ying Lin, Member, IEEE, and Wen-Guey Tzeng, Member "A Secure Erasure Code-Based Cloud Storage System with Secure Data Forwarding" vol. 23, no. 6, June 2012.
- [10] Kubiawicz, J, D. Bindel, Y. Chen, P. Eaton, D. Geels, R. Gummadi, S. Rhea, H. eatherspoon, W. Weimer, C. Wells, and B. Zhao, "Oceanstore: An Architecture for Global-Scale Persistent Storage," Proc. Ninth Int'l Conf. Architectural Support for Programming Languages and Operating Systems (ASPLOS), pp. 190- 201, 2000.
- [11] Mambo, M and E. Okamoto, "Proxy Cryptosystems: Delegation of the Power to Decrypt Ciphertexts," IEICE Trans. Fundamentals of Electronics, Comm. and Computer Sciences, vol. E80-A, no. 1, pp. 54-63, 1997.
- [12] Shao, J and Z. Cao, "CCA-Secure Proxy Re-Encryption without Pairings," Proc. 12th Int'l Conf. Practice and Theory in Public Key Cryptography (PKC), pp. 357-376, 2009.

AUTHORS PROFILE



S.Amritha received the B.E Degree computer science and engineering and now she is an M.E student in the Department of Computer Science & Engineering, Srinivasan Engineering College – Dhanalakshmi Srinivasan Group of Institutions, Perambalur, TN, India.

Her research interest includes Network Security and Mobile Computing.



S.Saravana kumar is working as Assistant Professor/CSE, Srinivasan Engineering College – Dhanalakshmi Srinivasan Group of Institutions, Perambalur, TN, India.

His research interest includes pervasive computing, Wireless Networks and Image Processing.

Seismic Analysis of High-Rise Building by Response Spectrum Method

¹Prof. S.S. Patil, ²Miss. S.A. Ghadge, ³Prof. C.G. Konapure, ⁴Prof. Mrs. C.A. Ghadge

^{1,3}Department of Civil Engineering, W.I.T. College of Engineering Solapur Maharashtra

²Student, W.I.T. College of Engineering, Solapur Maharashtra

⁴Department of Civil Engineering. S.T.B. College of Engineering, Tuljapur, Maharashtra

Abstract

This paper describes seismic analysis of high-rise building using program in STAADPro. with various conditions of lateral stiffness system. Some models are prepared that is bare frame, brace frame and shear wall frame. Analysis is done with response spectrum method. This analysis will produce the effect of higher modes of vibration & actual distribution of forces in elastic range in a better way. Test results including base shear, story drift and story deflections are presented and get effective lateral load resisting system.

Keywords: High-rise building, response spectrum method, seismic analysis, story deflection, time period, lateral load resisting system, storey drift

I. Introduction

A large portion of India is susceptible to damaging levels of seismic hazards. Hence, it is necessary to take in to account the seismic load for the design of high-rise structure. The different lateral load resisting systems used in high-rise building are: 1.Bare frame 2.Brace frame 3.Shear wall frame. In tall building the lateral loads due to earthquake are a matter of concern. These lateral forces can produce critical stresses in the structure, induce undesirable stresses in the structure, induce undesirable vibrations or cause excessive lateral sway of the structure.

Sway or drift is the magnitude of the lateral displacement at the top of the building relative to its base. Traditionally, seismic design approaches are stated, as the structure should be able to ensure the minor and frequent shaking intensity without sustaining any damage, thus leaving the structure serviceable after the event. The structure should withstand moderate level of earthquake ground motion without structural damage, but possibly with some structural as well as non-structural damage. This limit state may correspond to earthquake intensity equal to the strongest either experienced or forecast at the site. In present study the effect of bare frame, brace frame and shear wall frame is studied under the earthquake loading. The results are studied for response spectrum method. The main parameters considered in this study to compare the seismic performance of different models are storey drift, base shear, story deflection and time period.

2. Objective Of Studies

- [1] To analyze the building as per code IS 1893-2002 part I criteria for earthquake resistant structure.
- [2] Dynamic analysis of the building using response spectrum method
- [3] Building with different lateral stiffness systems
- [4] To get economical and efficient lateral stiffness system

2.1 Response Spectrum Method

The response spectrum represents an envelope of upper bound responses, based on several different ground motion records. For the purpose of seismic analysis, the design spectrum given in figure 1 of IS: 1893 (Part 1): 2002 is used. This spectrum is based on strong motion records of eight Indian earthquakes. This method is an elastic dynamic analysis approach that relies on the assumption that dynamic response of the structure may be found by considering the independent response of each natural mode of vibration and then combining the response of each in same way. This is advantageous in the fact that generally only few of the lowest modes of vibration have significance while calculating moments, shear and deflections at different levels of the building. Following procedure is generally used for the spectrum analysis:

- [1] Select the design spectrum.
- [2] Determine the mode shapes and periods of vibration to be included in the analysis.
- [3] Read the level of response from the spectrum for the period of each of the modes considered.

- [4] Calculate participation of each mode corresponding to the single-degree-of-freedom response read from the curve.
- [5] Add the effect of modes to obtain combined maximum response.
- [6] Convert the combined maximum response into shears and moments for use in design of the structure. Analyze the building for the resulting moments and shears in the same manner as the static loads. In this method, natural frequencies and mode shapes are to be obtained by a free vibration analysis. The design lateral force at each floor level in each mode of vibration is given by the equation. The peak shear force acting in storey i in mode k is given by the equation.

$$Q_i = A_k \theta_{ik} P_k W_i$$

$$P_k = \frac{\sum_{i=1}^n W_i \theta_{ik}}{\sum_{i=1}^n W_i (\theta_{ik})^2}$$

The peak storey shear force in storey i due to all modes considered is obtained by combining those due to each mode in accordance with using SRSS combination given by equation. So the lateral force at each storey due to all modes considered is calculated by the equation

$$F_{\text{roof}} = V_{\text{roof}}$$

$$F_i = V_i - V_{i+1}$$

In response spectrum method the peak response of the structure is calculated from model combination, where the following two methods can be used.

a) Square Root of Sum of Square (SRSS) Method

$$\lambda = \sqrt{\sum_{k=1}^r (\lambda_k)^2}$$

where, λ_k = Absolute value of quantity in mode k
 r = Number of modes being considered.

b) Complete Quadratic Combination Method:

$$\lambda = \sqrt{\sum_{i=1}^r \sum_{j=1}^r \lambda_i P_{ij} \lambda_j}$$

where, λ_i = Response quantity in mode i
 P_{ij} = Cross modal coefficient
 λ_j = Response quantity in mode j
 P_j = Cross-modal coefficient

$$P_{ij} = \frac{8}{(1 - \beta^2)^2 + 4}$$

where, ξ = Modal damping ratio in fraction
 β = Frequency ratio = ω_j / ω_i
 ω_i = Circular Frequency in i^{th} mode
 ω_j = Circular frequency in j^{th} mode

2.2 Response Spectrum Method by using StaadPro

This is accurate method of analysis. The design lateral force at each floor in each mode is computed by STAADPro in accordance with IS: 1893 (Part 1)-2002. The software provides result for design values, modal masses and storey wise base shear. Response Spectrum data specification is shown in figure 1.

Methodology: The design lateral shear force at each floor in each mode is computed by STAAD in accordance with the IS: 1893 (Part 1) -2002 following equation.

$$Q_{ik} = A_k * f_{ik} * P_k * W_k \text{ and } V_{ik} = Q_{ik}$$

STAAD utilizes the following procedure to generate the lateral seismic loads.

- [1] User provides the value for $\frac{Z}{2} \times \frac{I}{R}$ as factors for input spectrum.
- [2] Program calculates time periods for first six modes or as specified by the user.

- [3] Program calculates Sa/g for each mode utilizing time period and damping for each mode.
- [4] The program calculates design horizontal acceleration spectrum A_k for different modes.
- [5] The program then calculates mode participation factor for different modes.
- [6] The peak lateral seismic force at each floor in each mode is calculated.
- [7] All response quantities for each mode are calculated.
- [8] The peak response quantities are then combined as per method (CQC or SRSS or ABS or TEN or CSM) as defined by the user to get the final results.

3. Analysis of Building With Response Spectrum Method

Seismic Analysis of high-rise building having following data is analyzed for different models of lateral load resisting systems. Typical plan is shown in figure 2. Analysis is

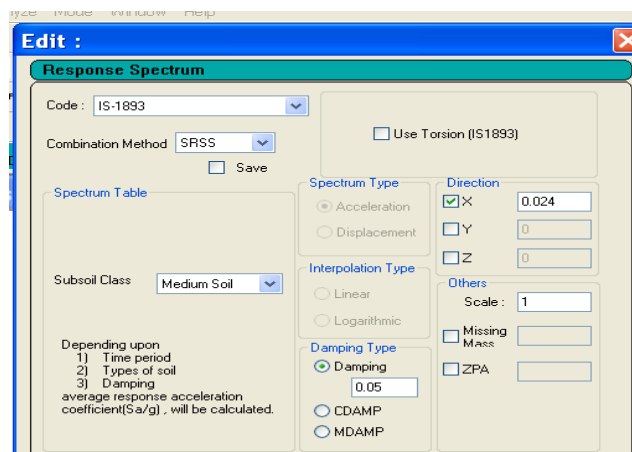


Figure:1 Response Spectrum data specification

done by taking into account the data from STAADpro. Space frame model is prepared. Member Properties are column size up to 6th storey 0.45 X 0.60m, column size above 6th storey 0.30 X 0.45m, beam size 0.23 X 0.30m, shear wall 0.2m, concrete bracing 0.23 X 0.23m, thickness of slab 0.1m. Loads considered are floor load, wall load, live load and earthquake load. The grade of concrete is M₂₀ & steel used is Fe₄₁₅. The parametric study for following mentioned models is carried.

- [1] Bare frame
- [2] Brace frame

- Case 1 Bracing at location A in plan- Bracing is centrally located at exterior frame of Z direction through out height.
- Case 2 Bracing at location B in plan- Bracing is centrally located at exterior frame of X direction through out height.
- Case 3 Bracing at location A and B in plan- Bracing is centrally located at exterior frame of both X and Z direction through out height.
- Case 4 Bracing at location C in plan- Bracing is located at exterior frame end corners of both X and Z direction through out height.

3.1 Shear wall frame

- Case 1 Shear wall at location A in plan- Shear wall is centrally located at exterior frame of Z direction through out height.
- Case 2 Shear wall at location B in plan- Shear wall is centrally located at exterior frame of X direction through out height.
- Case 3 Shear wall at location A and B in plan- Shear wall is centrally located at exterior frame of both X and Z direction through out height.
- Case 4 Shear wall at location C in plan- Shear wall is located at exterior frame end corners of both X and Z direction through out height.

For present work response spectrum method as per IS:1893-2002 is carried out for reinforced concrete moment resisting frame having (G+14) storey situated in zone IV. The floor to floor height of the building is 3m. The total height of building is 45m.

Load combinations considered in this analysis are

- 1) 1.5(DL+LL)
- 2) 1.2(DL+LL+EQX)
- 3) 1.2(DL+LL-EQX)
- 4) 1.2(DL+LL+EQZ)
- 5) 1.2(DL+LL-EQZ)
- 6) DL+1.5EQX
- 7) DL-1.5EQX
- 8) DL+1.5EQZ
- 9) DL-1.5EQZ

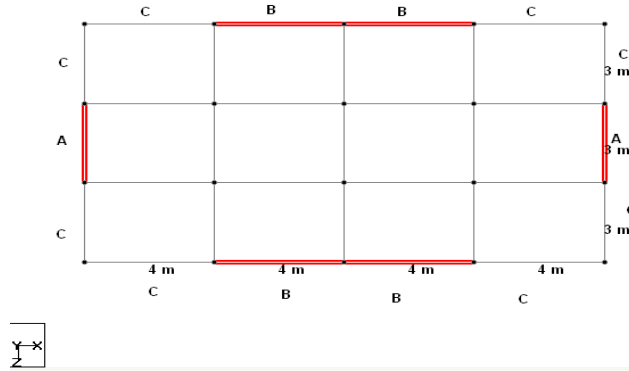


Figure 2 Plan of building showing location of braced frame & shear wall frame

Design Parameters: The design spectrum used is of medium soil as per IS 1893 Part I (2002). A response spectrum is shown in figure 3.

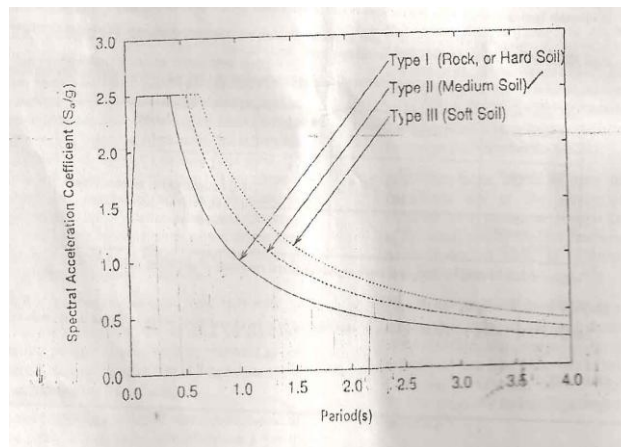


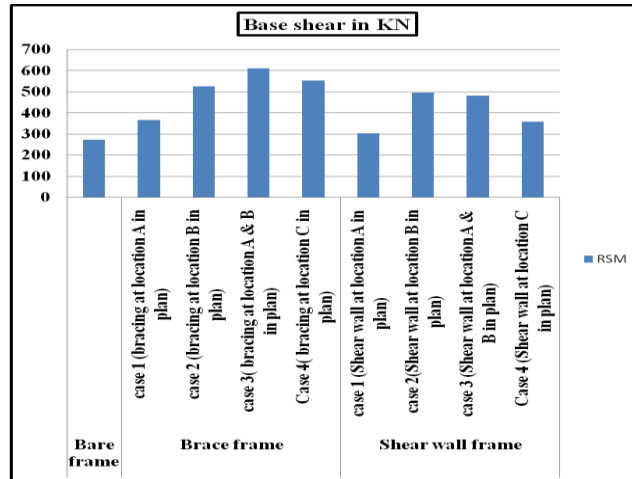
Figure 3 Response spectrum for soil as per IS 1893 Part I (2002)

4. Result and Discussion

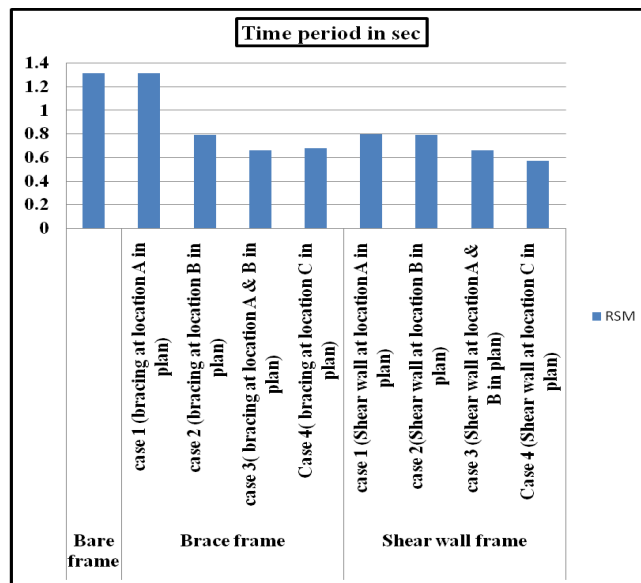
The variation of storey drift, base shear, story deflection and time period is evaluated for all these models and compared with response spectrum method.

4.1 Variation of base shear, story deflection, storey drift and time period

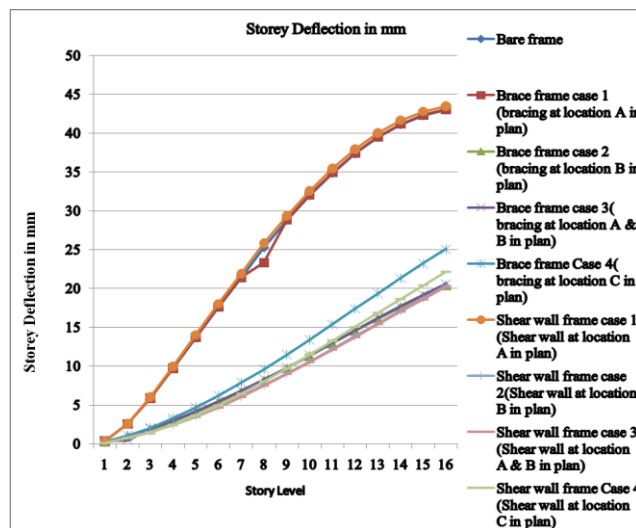
The parametric study to know base shear, story deflection, storey drift & time period in case of all models is performed here. The results are shown in table I to IV & in graph 1 to 4 which are listed below. From Table I and graph 1, it is observed that base shear minimum for case 2 and 3 in both brace frame and shear wall frame. From Table II and graph 2, time period is also less for case 2 and 3 in both brace frame and shear wall frame. As base shear increases time period of models decreases and vice versa. Building with short time period tends to suffer higher accelerations but smaller displacement. Therefore, from table III & IV, graph 3 & 4 story deflections is also minimum for case 2 and 3 in both brace frame and shear wall frame. Story drift i.e. top story displacement is also reduced for case 2 and 3 in both brace frame and shear wall frame.



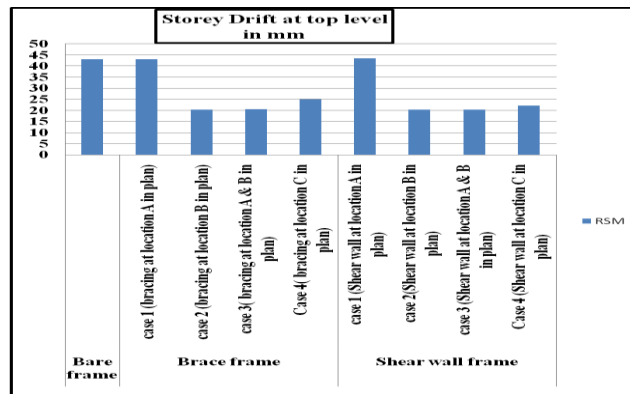
Graph 1 Design Base Shear in KN



Graph 2 Time period in sec



Graph 3 Storey deflection in mm



Graph 4 Storey drift in mm

Method	Bare frame	Brace frame				Shear wall frame			
		case 1 (bracing at location A in plan)	case 2 (bracing at location B in plan)	case 3 (bracing at location A & B in plan)	Case 4 (bracing at location C in plan)	case 1 (Shear wall at location A in plan)	case 2 (Shear wall at location B in plan)	case 3 (Shear wall at location A & B in plan)	Case 4 (Shear wall at location C in plan)
RSM	272.5	366.92	527.2	612.9	553.9	304.05	495.4	482.9	358

Table I Design Base Shear in KN

Method	Bare frame	Brace frame				Shear wall frame			
		case 1 (bracing at location A in plan)	case 2 (bracing at location B in plan)	case 3 (bracing at location A & B in plan)	Case 4 (bracing at location C in plan)	case 1 (Shear wall at location A in plan)	case 2 (Shear wall at location B in plan)	case 3 (Shear wall at location A & B in plan)	Case 4 (Shear wall at location C in plan)
RSM	1.315	1.319	0.794	0.66	0.68	0.8	0.79	0.66	0.57

Table II Time Period in sec

Story Level	Bare frame	Brace frame				Shear wall frame			
		case 1 (bracing at location A in plan)	case 2 (bracing at location B in plan)	case 3 (bracing at location A & B in plan)	Case 4 (bracing at location C in plan)	case 1 (Shear wall at location A in plan)	case 2 (Shear wall at location B in plan)	case 3 (Shear wall at location A & B in plan)	Case 4 (Shear wall at location C in plan)
1	0.34	0.34	0.23	0.39	0.3	0.35	0.14	0.14	0.09
2	2.55	2.56	1	0.48	1.06	2.63	0.87	0.87	0.7
3	5.88	5.9	1.85	1.98	2.05	6.06	1.58	1.57	1.44
4	9.69	9.73	2.87	3.03	3.32	9.99	2.48	2.45	2.42
5	13.65	13.71	4.04	4.21	4.71	14.05	3.55	3.51	3.6
6	17.58	17.64	5.32	5.49	6.24	18.05	4.77	4.72	4.95
7	21.38	21.46	6.68	6.85	7.86	21.92	6.11	6.05	6.44

8	25.26	23.35	8.16	8.3	9.61	25.85	7.55	7.48	8.05
9	28.79	28.89	9.71	9.82	11.47	29.4	9.07	8.99	9.74
10	31.98	32.09	11.31	11.4	13.4	32.61	10.64	10.55	11.49
11	34.84	34.96	12.92	13	15.39	35.48	12.25	12.15	13.28
12	37.34	37.47	14.52	14.6	17.38	37.98	13.88	13.76	15.08
13	39.45	39.58	16.09	16.18	19.37	40.06	15.51	15.39	16.88
14	41.09	41.23	17.58	17.71	21.33	41.69	17.15	17.02	18.68
15	42.25	42.39	19.04	19.2	23.23	42.82	18.78	18.64	20.46
16	42.99	43.12	20.38	20.6	25.09	43.51	20.38	20.23	22.19

Table III Storey deflection in mm

Method	Bare frame	Brace frame				Shear wall frame			
		case 1 (bracing at location A in plan)	case 2 (bracing at location B in plan)	case 3 (bracing at location A & B in plan)	Case 4 (bracing at location C in plan)	case 1 (Shear wall at location A in plan)	case 2 (Shear wall at location B in plan)	case 3 (Shear wall at location A & B in plan)	Case 4 (Shear wall at location C in plan)
RSM	42.99	43.12	20.38	20.6	25.09	43.51	20.38	20.23	22.19

Table IV Storey drift (Top storey displacement) in mm

5. Conclusions

- A significant amount of decrease in story drift has been observed in case 2 and 3 i.e. lateral stiffness system is centrally located at exterior frame of X direction through out height and lateral stiffness system is centrally located at exterior frame of X & Z direction through out height in both brace frame and shear wall frame compared to other models. Also shear wall models in case 3 gives less storey deflection and storey drift than bare frame and brace frame.
- A significant amount of decrease in time period of model in case 2 and 3 i.e. lateral stiffness system is centrally located at exterior frame of X direction through out height and lateral stiffness system is centrally located at exterior frame of X & Z direction through out height in both brace frame and shear wall frame compared to other models, therefore displacements in the structure are minimized.
- Building with short time period tends to suffer higher accelerations but smaller displacement.
- Comparing the top storey drift in the longitudinal direction, it can be seen that it decrease by 52.59%, 52.08% & 41.63% in case 2, 3 and 4 of brace frame as compared to bare frame and it decreases by 52.59%, 52.94 & 48.38% in case 2, 3 and 4 of shear wall frame as compared to bare frame. The models with shear wall located at exterior frame of X & Z direction through out height is found most effective in resisting lateral loads because it shows least deflection as compare with other models.
- A significant amount of increase in the lateral stiffness has been observed in all models of brace frame and shear wall frame as compared to bare frame.
- More accurate values of response may be obtained for buildings by the modal analysis method, using modified design response spectra for inelastic analysis.

References

- [1] IS 1893-2002, 'Indian Standard Criteria of practice for Earthquake Resistant Design of Structures', Bureau of Indian Standards, New Delhi, India
- [2] Pankaj Agrawal, Manish Shrikhande, 'Earthquake Resistant Design of Structures', Prentice Hall India Publication

- [3] Liu Haufeng, Zhao Ning, '*Study on Tall buildings structure Analysis*', Joint international Conference on Computing and decision making in Civil and Building Engineering, Montreal, Canada, June 14-16, 2006, pp 4018-4024
- [4] Bangle S. Taranath, Textbook of McGraw Hill International Editions, '*Structural Analysis and Design of Tall Buildings*' 1988, pp 563-569
- [5] D.-G. Lee & H.S. Kim, '*Efficient seismic analysis of high-rise buildings considering the basements*', NZSEE Conference, 2001, pp 1-9
- [6] Yongqi Chen, Tiezhu Cao, Liangzhe Ma, and ChaoYing lu, '*Seismic protection system and its economic analysis on the beijing high-rise building pangu plaza*', The 14 World Conference on Earthquake Engineering, October 12-17, 2008, Beijing, China
- [7] Andreas J. Kappos, Alireza Manafpour, '*Seismic design of R/C buildings with the aid of advanced analytical techniques*', Engineering Structures 23 (2001), pp 319–332

Sensing of Faults and Condition Monitoring in Gearbox of the Wind Turbine

¹Mr.B.Babu, ²Mr.R.Vinod Kumar Reddy ³Mr. R.Devananda Reddy

¹Head of The Department, ^{2,3}student
^{1,2,3}EEE Dept., M.R.R.I.T.S/ J.N.T.U.A/ A.P/INDIA

Abstract

Data mining algorithms and statistical methods are applied to analyze the jerk data obtained from monitoring the gearbox of a wind turbine. Two types of analyses are performed— failure component identification and monitoring vibration excitement. In failure component identification, the failed stages of the gearbox are identified in time-domain analysis and frequency-domain analysis. In the time domain, correlation coefficient and clustering analysis are applied. The fast Fourier transformation with time windows is utilized to analyze the frequency data. To monitor the vibration excitement of the gearbox in its high-speed stage, data mining algorithms and statistical quality control theory are combined to develop a monitoring model. The capability of the monitoring model to detect changes in the gearbox vibration excitement is validated by the collected data.

Index Terms—Data mining, failure component identification, fast Fourier, jerk, transformation with time windows, vibration excitement monitoring, wind turbine gearbox.

I. Introduction

WIND energy has experienced a remarkable expansion in recent years. As wind farms are aging, their operations and maintenance issues are gaining significance. The wind industry has been affected by failures of wind turbine components, such as main bearings, gearboxes, and generators. High cost in replacing failed components impacts the energy cost. Therefore, research in fault identification and condition monitoring is warranted. Fault identification is concerned with a fault that has occurred and its labeling. In condition monitoring, parameters reflecting the component conditions are identified and their changes are analyzed to detect an emerging failure. Fault detection and condition monitoring of wind turbine blade and generator has been widely discussed. Tsai *et al.* [1] presented a wavelet transform-based approach to the damage detection of wind turbine blades [1]. Kusiak and Verma [2] applied a data-driven approach for monitoring wind turbine blade faults [2]. Watson *et al.* [3] utilized wavelet techniques to extract bearing failure faults of doubly fed induction generator based on power output data [3]. The literature on gearbox faults is focused on the frequency-domain analysis. Wavelet and the Fourier transformation are the two widely applied techniques. Mohanty and Kar [4] discussed fault detection of a multistage gearbox by applying discrete wavelet transformation to demodulate the current signal [4]. Wang and McFadden [5] applied a wavelet transform to the vibration signal to detect faults in a helicopter gearbox [5]. Yuan and Cai [6], [7] developed a modified Fourier transform method, the variable amplitude Fourier series, to study gearbox diagnosis based on vibration signals [6], [7]. Wang *et al.* [8] applied complex Morlet continuous wavelet transform to fault diagnosis of a gearbox with fluctuating loads [8].

Although the frequency analysis may lead to detection of faults of a gearbox, it has some drawbacks. One disadvantage is that frequency-domain analysis is more effective in fault identification but less effective in condition monitoring. Another drawback is that the commonly used techniques in frequency domain analysis, such as the Fourier transformation, assume that the underlying process is linear and stationary. Moreover, the time factor is omitted in the frequency-domain analysis and the change of a process is not considered. In this paper, the fault identification analysis is studied in both the time domain and frequency domain based on the vibration data of an impaired gearbox tested by the National Renewable Energy Laboratory (NREL). The identified faults are validated by the gearbox inspection report provided by the NREL. Besides fault identification, the vibration excitement monitoring model is also discussed in this paper. The monitoring model is developed by combining data mining with statistical control theory. Data mining algorithms are utilized to establish models for predicting vibration excitement. As an emerging science, data mining has been successfully applied in various domains [9]–[11]. Its capability in building high-quality predictions models has also been proven in our previous research [12]–[15]. Statistical control charts are then applied to detect the increase in the vibration excitement by monitoring the prediction residuals. The capability of the proposed monitoring model in detecting the increase of vibration excitement is validated by the data.

2. Gearbox Test Environment

The data used in this research came from a damaged gear-box of a test wind turbine. The gearbox was retested at the Dynamometer Test Facility (DTF) at NREL. To retest the gear-box, the complete nacelle and the drivetrain of the test wind turbine were installed at the DTF. The nacelle was hard-fixed to the floor without hub, rotor, and yaw bearing. The gearbox included three stages—low-speed stage (LSST), intermediate-speed stage (ISST), and high-speed stage (HSST). It was instrumented with over 125 sensors. Fig. 1 shows the side view of the gearbox. As shown in Fig. 1, the LSST is connected to the rotor, and the HSST is connected to the generator.

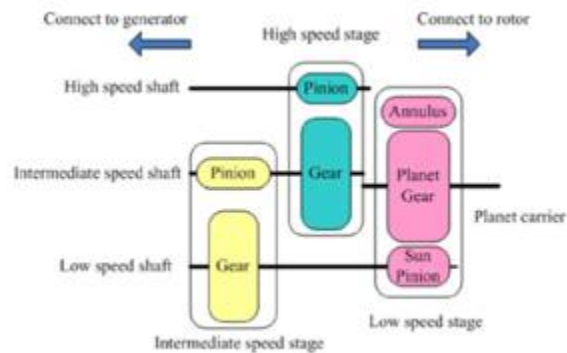


Fig. 1. Structure of gearbox.

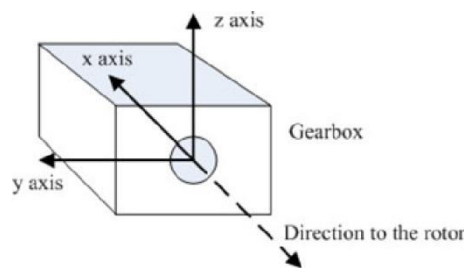


Fig. 2. Coordinate system of vibration acceleration.

To investigate the root cause of the gearbox damage and develop the condition monitoring strategies, vibration data were collected. Thus, 12 accelerometers were mounted on the out-side of the gearbox, generator, and main bearing to measure the vibration acceleration. Vibration data of all 12 accelerometers were collected at 40 kHz using a high-speed data acquisition system. Besides the vibration data, the corresponding torque of the low-speed shaft and the generator speed were recorded. The direction of the drivetrain vibration acceleration is described as a 3-D coordinate system and sensed by accelerometers. The origin of the coordinate system is the intersection of the planet-carrier rotation axis and the plane cutting the torque arm cylinder in half along their length. The x -axis describes the system acceleration along the main shaft axis and the downwind side, and the y -axis represents the vibration acceleration direction, which is horizontally perpendicular to the x -axis. The z -axis is orthogonal to the x - and y -axes. Fig. 2 illustrates the coordinate system of the vibration acceleration. Although the vibration acceleration of the system is depicted by a 3-D coordinate system, the mounted accelerometers can only sense one or two directions of acceleration. Table I presents the locations of the accelerometers, the measured directions of vibration acceleration, and the units of the recorded data. In the research presented in this paper, three test cases, Case 1, Case 2, and Case 3, are analyzed. In Case 1, the nominal speed of the high-speed shaft is set to 1800 r/min and the electricity power is set to 25% of the rated power. In Case 2, the nominal speed of the high-speed shaft is the same as in Case 1, but the electricity power is set to 50% of the rated power. This indicates that the

TABLE I
LOCATIONS AND DESCRIPTIONS OF THE SENSORS

Sensor	Symbol	Location	Plus acceleration direction	Units
Accelerometer No. 1	AN1	Main bearing radial	+Z and -Y	m/s ²
Accelerometer No. 2	AN2	Main bearing axial	-X	m/s ²
Accelerometer No. 3	AN3	Ring gear radial 6 o'clock	-Z	m/s ²
Accelerometer No. 4	AN4	Ring gear radial 12 o'clock	+Z	m/s ²
Accelerometer No. 5	AN5	Low-speed shaft radial	+Y and -Z	m/s ²
Accelerometer No. 6	AN6	Intermediate-speed shaft radial	+Y and -Z	m/s ²
Accelerometer No. 7	AN7	High-speed shaft radial	+Y and +Z	m/s ²
Accelerometer No. 8	AN8	High-speed shaft upwind bearing radial	+Z	m/s ²
Accelerometer No. 9	AN9	High-speed shaft downwind bearing radial	-Z	m/s ²
Accelerometer No. 10	AN10	Camier downwind radial	+Y	m/s ²
Accelerometer No. 11	AN11	Generator upwind radial	+Z and -Y	m/s ²
Accelerometer No. 12	AN12	Generator downwind axial	+Z and -Y	m/s ²
Generator speed	ω	Encoder on high-speed shaft	Null	rpm
Low-speed shaft torque	τ	Strain gauges on low-speed shaft	Null	kNm

torque in Case 2 is twice the amount of torque in Case 1.

In this section, a blind study is discussed. The study considers identification of component failures in the gearbox using the vibration acceleration data while the failed components are unknown. Time- and frequency-domain analysis of the vibration acceleration data is performed to investigate the failed components and the root causes of the failure.

2.1 Data Processing and Description

To analyze the gearbox vibration in the time domain, jerk is utilized. Jerk describes the rate of acceleration change, and it is often used to indicate the excitement of vibration. For the high-frequency vibration acceleration data in Section II, the jerk is approximated in

$$\vec{J} \approx \frac{\vec{a}_t - \vec{a}_{t-T}}{T} \quad (1)$$

Expression (1) is derived in the following:

$$\vec{J} = \frac{d\vec{a}}{dt} = \lim_{\Delta t \rightarrow 0} \frac{\Delta \vec{a}}{\Delta t} \approx \frac{\vec{a}_t - \vec{a}_{t-T}}{t - (t-T)} = \frac{\vec{a}_t - \vec{a}_{t-T}}{T} \quad (1)$$

$$\Delta \vec{a} = \vec{a}_t - \vec{a}_{t-T} \quad \text{and} \quad \Delta t = t - (t-T) \quad (2)$$

where \vec{J} is jerk, \vec{a} is acceleration, t is the time index, and T represents the sampling interval, 1/40 000 s.

Since the sampling frequency is high (i.e., 40 kHz), the number of data points within 10 min length is large. Therefore, vibration, the high-frequency jerk data (40 kHz), is then converted into much lower frequency data (1/15 Hz) by computing the mean of jerk at 15-s intervals. The standard deviation and the maximum value of the jerk data in each 15-s interval are also computed. The sampling frequency, 1/15 Hz, reduces the data size for ease of time-domain analysis.

2.2 Time-Domain Analysis

In Section III-B, the correlation coefficient [16] and clustering analysis [17] are utilized to investigate the failed components in the gearbox. The component failure can be identified by examining the pattern similarity of the jerk data measured by accelerometers mounted at different locations of the drivetrain.

- 1) Correlation Coefficient Analysis: Correlation coefficient [16] is a fundamental but useful tool to analyze the linear

TABLE II
CORRELATION COEFFICIENT OF THE DATA IN CASE 1

	J_{AN1}	J_{AN2}	J_{AN3}	J_{AN4}	J_{AN5}	J_{AN6}	J_{AN7}	J_{AN8}	J_{AN9}	J_{AN10}	J_{AN11}	J_{AN12}
J_{AN1}	1.00	0.98	0.53	0.20	0.02	0.14	0.00	-0.11	0.16	0.16	0.16	0.03
J_{AN2}	0.98	1.00	0.59	0.06	0.18	0.30	0.17	0.05	0.32	0.25	0.33	0.19
J_{AN3}	0.53	0.59	1.00	0.09	0.31	0.53	0.41	0.19	0.62	0.77	0.48	0.32
J_{AN4}	0.20	0.06	0.09	1.00	-0.88	-0.78	-0.85	-0.94	-0.70	-0.11	-0.76	-0.89
J_{AN5}	0.02	0.18	0.31	-0.88	1.00	0.94	0.97	0.97	0.90	0.50	0.92	0.97
J_{AN6}	0.14	0.30	0.53	-0.78	0.94	1.00	0.98	0.93	0.99	0.60	0.95	0.96
J_{AN7}	0.00	0.17	0.41	-0.85	0.97	0.98	1.00	0.97	0.96	0.56	0.94	0.97
J_{AN8}	-0.11	0.05	0.19	-0.94	0.97	0.93	0.97	1.00	0.88	0.39	0.90	0.98
J_{AN9}	0.16	0.32	0.62	-0.70	0.90	0.99	0.96	0.88	1.00	0.67	0.92	0.93
J_{AN10}	0.16	0.25	0.77	-0.11	0.50	0.60	0.56	0.39	0.67	1.00	0.59	0.42
J_{AN11}	0.16	0.33	0.48	-0.76	0.92	0.95	0.94	0.90	0.92	0.59	1.00	0.92
J_{AN12}	0.03	0.19	0.32	-0.89	0.97	0.96	0.97	0.98	0.93	0.42	0.92	1.00

TABLE III
CORRELATION COEFFICIENT OF THE DATA IN CASE 2

	J_{AN1}	J_{AN2}	J_{AN3}	J_{AN4}	J_{AN5}	J_{AN6}	J_{AN7}	J_{AN8}	J_{AN9}	J_{AN10}	J_{AN11}	J_{AN12}
J_{AN1}	1.00	0.83	0.32	-0.73	0.50	0.56	0.49	0.67	0.49	0.48	0.64	0.56
J_{AN2}	0.83	1.00	0.76	-0.91	0.88	0.90	0.87	0.92	0.87	0.86	0.91	0.91
J_{AN3}	0.32	0.76	1.00	-0.67	0.94	0.92	0.95	0.78	0.96	0.95	0.80	0.90
J_{AN4}	-0.73	-0.91	-0.67	1.00	-0.85	-0.90	-0.84	-0.97	-0.83	-0.80	-0.94	-0.91
J_{AN5}	0.50	0.88	0.94	-0.85	1.00	0.99	0.99	0.92	0.99	0.98	0.92	0.98
J_{AN6}	0.56	0.90	0.92	-0.90	0.99	1.00	0.99	0.95	0.98	0.97	0.95	0.99
J_{AN7}	0.49	0.87	0.95	-0.84	0.99	0.99	1.00	0.91	0.99	0.98	0.92	0.98
J_{AN8}	0.67	0.92	0.78	-0.97	0.92	0.95	0.91	1.00	0.91	0.88	0.96	0.96
J_{AN9}	0.49	0.87	0.96	-0.83	0.99	0.98	0.99	0.91	1.00	0.98	0.90	0.98
J_{AN10}	0.48	0.86	0.95	-0.80	0.98	0.97	0.98	0.88	0.98	1.00	0.88	0.96
J_{AN11}	0.64	0.91	0.80	-0.94	0.92	0.95	0.92	0.96	0.90	0.88	1.00	0.96
J_{AN12}	0.56	0.91	0.90	-0.91	0.98	0.99	0.98	0.96	0.98	0.96	0.96	1.00

dependence between parameters and it is widely used in research. In this study, a correlation coefficient analysis is performed based on the processed jerk data discussed in Section III-A to examine the linear relationship between sensors for Cases 1 and 2. Tables II and III present the results of correlation coefficient analysis for the two cases. The data in Tables II and III show that the jerks of sensors AN5, AN6, AN7, AN8, and AN9 are positively correlated. However, the correlation with the other sensors is relatively low. Besides Cases 1 and 2, the gearbox was tested in another Case 3 with generator speed of 1200 r/min and the torque set at 25%. In Case 3, the linear correlation between the jerks of all sensors is above 90%. This is due to the fact that the drivetrain system is highly coupled and the abnormal vibration patterns of some damaged components do not appear for low generator speed and torque. When the generator speed increases to 1800 r/min in Case 1 and the torque increases to 50% in Case 2, the correlation among these sensors changes as shown in Tables II and III. Since the main bearing sensed by AN1 and AN2 is healthy, the low correlation between the main bearing accelerometer signal and accelerometers in ISST and HSST point to some issues in the health condition of components in ISST and HSST.

2.3 Clustering Analysis: To further analyze jerk patterns of the 12 sensors in Table I, clustering analysis is applied. Clustering analysis is an unsupervised method of data analysis. Clustering algorithms group observations into clusters by evaluating similarities among the observed data. The clustering analysis in Section III-B2 aims at grouping data from 12 sensors using the jerk data. The time series of the jerk of Section III-A is utilized in the clustering analysis. The k -means algorithm [17] is modified in this study to establish clusters. In the original version of k -means algorithm, the number of clusters k should be arbitrarily set by the analyst. In this study, a clustering cost function is introduced to evaluate the cluster quality with k . The clustering cost function is formulated as (3) and used in a tenfold cross-validation scheme [18], [19]

$$d(k, \mathbf{x}, \mathbf{c}) = \frac{1}{\sum_{i=1}^k m_i} \sum_{i=1}^k \left(\sum_{\mathbf{x}_j \in C_i} \|\mathbf{x}_j - \mathbf{c}_i\|^2 \right) \quad (3)$$

where d is the clustering cost, k is the number of clusters, m is the number of observations (sensors) contained in each cluster, \mathbf{x} is a vector of parameters used in this research, \mathbf{c} presents the centroid of each cluster, j is the index of each data point, and C_i represents cluster i .

The modified k -means algorithm involves the following steps: Step 1. Set the initial value of k to 2.

Step 2. Divide the dataset into 10 subsets of equal size. Step 3. Repeat ten times.

Step 3.1. Randomly select nine subsets for training and use the tenth subset for testing.

Step 3.2. Initialize k centroids.

Step 3.3. Repeat the following two steps until the centroids do not change.

Step 3.3.1. Assign data point to the closest cluster by

$$C_i^t = \{\mathbf{x}_j : \|\mathbf{x}_j - \mathbf{c}_i^t\| \leq \|\mathbf{x}_j - \mathbf{c}_{i^*}^t\|, i^* = 1, 2, \dots, k\}.$$

Step 3.3.2. Update the values of the centroids by $\mathbf{c}_i = \sum_{\mathbf{x}_j \in C_i} \mathbf{x}_j / n$, where n is the total number of observations.

Step 3.4. Compute the clustering cost d .

Step 4. Estimate the average of clustering cost d in tenfold cross-validation.

Step 5. Stop the algorithm if $d(k, \mathbf{x}, \mathbf{c}) - d(k-1, \mathbf{x}, \mathbf{c}) \leq \zeta$ or $k = 12$; otherwise, go back to Step 1.

To implement the modified k -means algorithm, the parameter ζ is set to 0.05. The results of clustering analysis for Cases 1 and 2 are presented in Table IV, respectively.

Three clusters are generated by the modified k -means algorithm (see Table IV). In Cluster 1, most of the sensors sense the vibration acceleration of the gearbox low-speed stage. Cluster 2 contains data from two sensors that monitor the acceleration of the main bearing. Sensors that measure the vibration acceleration in the intermediate and high-speed stage make Cluster 3. To further analyze the data in the three clusters, the Euclidean distance between the centroids of clusters is calculated. The shorter the distance, the more similar the two clusters are. Since the gearbox test experiment was conducted to examine the failure components of the gearbox, the vibration of the main

TABLE IV
CLUSTERING RESULTS FOR CASES 1 AND 2

Case 1		Case 2	
Sensor	Cluster No.	Sensor	Cluster No.
AN1	2	AN1	2
AN2	2	AN2	2
AN3	1	AN3	1
AN4	1	AN4	1
AN5	1	AN5	1
AN6	3	AN6	3
AN7	1	AN7	1
AN8	3	AN8	3
AN9	3	AN9	3
AN10	1	AN10	1
AN11	1	AN11	1
AN12	3	AN12	3

TABLE V
CLUSTER DISTANCES FOR CASES 1 AND 2

Case 1	Cluster 1	Cluster 2	Cluster 3
Cluster 1	0.00	2.31	3.41
Cluster 2	2.31	0.00	5.72
Cluster 3	3.41	5.72	0.00
Case 2	Cluster 1	Cluster 2	Cluster 3
Cluster 1	0.00	2.26	3.26
Cluster 2	2.26	0.00	5.52
Cluster 3	3.26	5.52	0.00

Fig. 3. Jerk data measured by AN9.

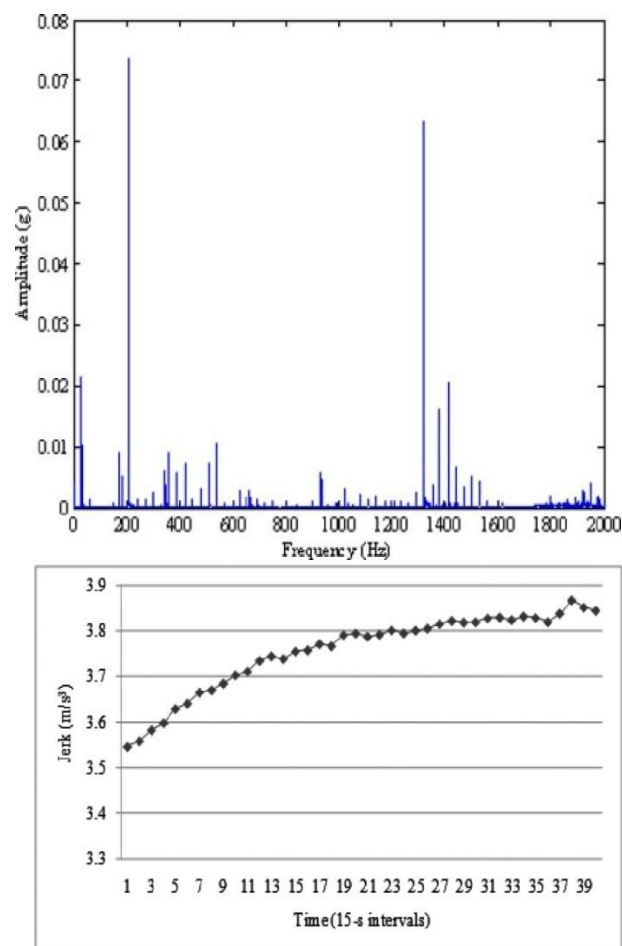


Fig. 4. Power spectrum of second-minute acceleration data of Case 1.

bearing was normal in this research. In Table V, the distance between the centroids of Clusters 1 and 2 is 2.31 while the distance between the centroids of Clusters 3 and 2 is 5.72. Based on the results in Table V, the components sensed by the accelerometers in Cluster 3 are considered to be primarily failed because the distance between Clusters 1 and 2 is small. Some components sensed by the sensors in Cluster 1 are also considered as failed since the data from the two sensors belong to two different clusters. The clustering algorithm is also applied to Case 3. The distance between Clusters 1 and 2 is 2, the distance between Clusters 1 and 3 is 3, and the distance between Clusters 2 and 3 is 5. The distance between two clusters should be less than the distance in Case 3 because the abnormal vibration in ISST and HSST is not fully excited in Case 3.

3. Root Cause Analysis:

The correlation coefficient and clustering analysis in Sections III-B1 and III-B2 both point to the failure of components in the gearbox at the intermediate- and high-speed stage. The main reason is that the jerk data measured by the sensors mounted at intermediate- and high-speed stage have an extremely similar pattern which should be different in normal condition. Fig. 3 illustrates the trend of the jerk data sensed by AN9 during the 10-min test in Case 2. In Fig. 3, it is observable that the change of vibration acceleration is gradually increased from the beginning to the end of the test experiment. This trend of jerk data indicates that the excitement of vibration in the high-speed stage gradually becomes stronger during the test. This is highly possible due to the gradually increased friction between gears in the high-speed stage. The possible root cause of the increasing friction is lubrication starvation and damaged gears. The analysis of the failure component and possible root cause is then proved according to the inspection report of the disassembled gearbox provided by the NREL.

3.1 Frequency-Domain Analysis

In Section III-C, fast Fourier Transformation with time windows [20] is applied to develop power spectrums based on the original vibration acceleration data of both Cases 1 and 2 measured by accelerometers described in Section II. The pattern of vibration excitement gradually increasing in the high-speed stage of a gearbox, shown in Fig. 3, can also be observed from the power spectrums with time windows. In time-domain analysis, the failure of the high-speed stage of the gearbox has been identified. To monitor the vibration acceleration in the high-speed stage, three accelerometers—AN7, AN8, and AN9—are utilized. Since the frequency-domain analysis results of all three sensors are similar, the result of AN7 is selected as the representative in the following discussion. Figs. 4 and 5 depict the power spectrum developed based on the second- and tenth-minute acceleration data of AN7 in Case 1. Figs. 6 and 7 show the same content of AN7 in Case 2. In Figs. 4 and 5, it is obvious that the magnitude of power is

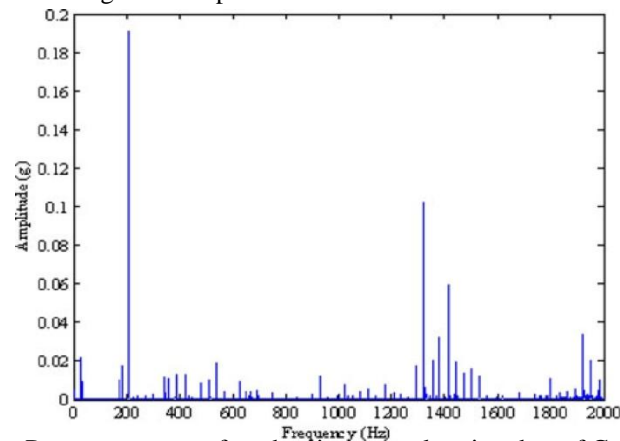


Fig. 5. Power spectrum of tenth-minute acceleration data of Case 1.

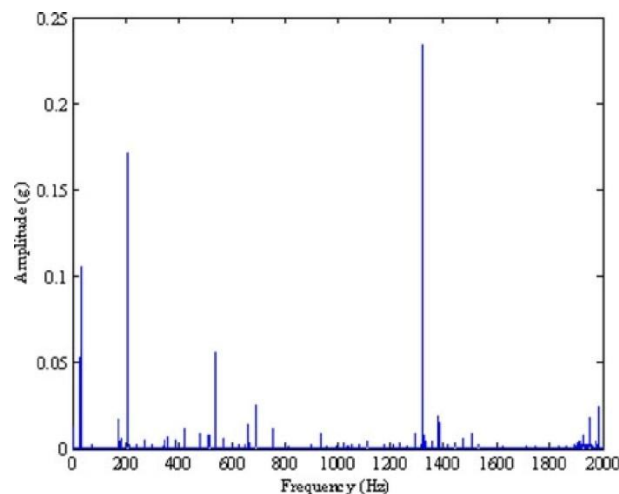


Fig. 6. Power spectrum of second-minute acceleration data of Case 2.

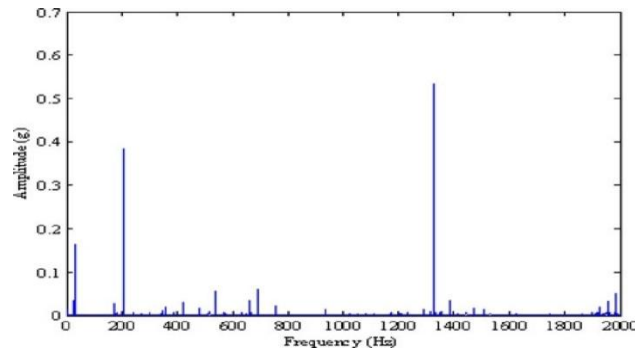


Fig. 7. Power spectrum of tenth-minute acceleration data of Case 2.

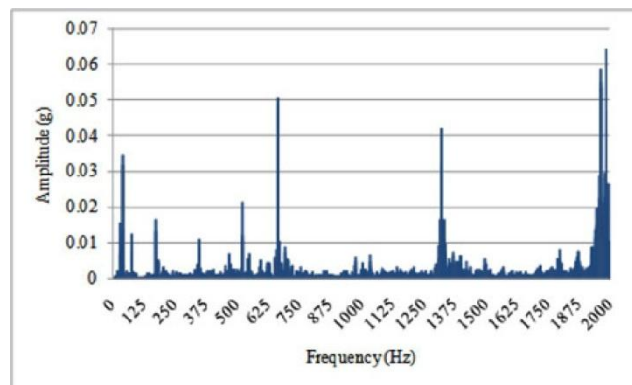


Fig. 8. Power spectrum of the gearbox in healthy condition.

increased from the second minute to the tenth minute in Case 1. Figs. 6 and 7 present the same pattern as in Case 2. Moreover, by comparing the power spectrums of Case 1 to those of Case 2, it is observable that the magnitude of power becomes much larger when the rated power is increased from 25 to 50%. This indicates that the vibration in the high-speed stage of the gearbox in Case 2 becomes more significant due to the increase of rated power. To identify that the gearbox is in abnormal status, the power spectrums based on the vibration acceleration data in the tenth minute of a damaged gearbox can be compared to the power spectrum based on the acceleration data of a healthy gearbox. Fig. 8 presents the power spectrum of a gearbox in healthy condition. In Figs. 5 and 7, the spike at around 200 and 1375 Hz (HST modulations) is much higher than the same spike displayed in Fig. 8. In this frequency-domain analysis, the damage in the high-speed stage of the gearbox is identified. However, it is difficult to identify the details of the damage in the high-speed stage, such as fretting corrosion, scuffing, and dents of the high-speed gear set. To identify the details of the damage, the gearbox needs to be disassembled.

4. Monitoring Vibration of Gearbox

4.1 HIGH-SPEED STAGE

In this section, a framework of monitoring vibration acceleration at the high-speed stage of the gearbox is developed. Data-driven prediction models are integrated with the control chart theory to build the vibration monitoring model. The vibration monitoring model is capable of detecting the level of vibration excitement at the high-speed stage of the gearbox.

4.2 Data Description

In this section, data used to develop the vibration monitoring model are discussed. Jerk of vibration acceleration data of AN7 discussed in Section II is applied for training data-driven models. As mentioned in Section II, the sampling frequency of jerk data sensed by AN7 in this study is 40 kHz, which is unrealistic in industrial applications. Thus, the high-frequency (40 kHz) jerk data is averaged to a lower frequency, 10 Hz, with the corresponding sampling interval of 0.1 s. The standard deviation and maximum value of the 40 kHz jerk data is calculated at each 0.1-s interval. Since faults may occur in a short time, e.g., as 10 s, the 0.1-s data are monitored to detect the emerging faults.

Dataset	Data points	No. of data points
Training dataset	From 1 st data point to 3000 th data point	3000
Test dataset	From 3001 st data point to 4000 th data point	1000
Analysis dataset	From 5001 st data point to 6000 th data point	1000

The processed dataset contains 6000 data points. The dataset is then split into three subsets—the training dataset, test dataset, and analysis dataset—for developing data-driven models. The first 3000 data points are selected to form the training dataset utilized for the development of data-driven models. To validate the data-driven models, a test dataset is needed. The test dataset contains 1000 data points, immediately following the 3000 data points in the training dataset. The analysis dataset is composed of the last 1000 data points in the original processed dataset. The 1000 data points between the test dataset and the analysis dataset are not utilized in this study. The three datasets are characterized in Table VI.

4.3 Data-Driven Models

To monitor the vibration excitement of the high-speed stage of the gearbox, data-driven models need to be developed that are able to predict the jerk derived from the acceleration data measured by AN7. In this section, three types of models—single-signal model I, single-signal model II, multisignal model—are discussed to predict the jerk at the gearbox high-speed stage. These three types of models are developed by considering three different sensor conditions of the gearbox. Single-signal model I reflects a scenario wherein only one sensor is mounted on the high-speed stage of the gearbox; while in single-signal model II, the mounted sensor on the high-speed stage records data at a higher frequency than needed. Multisignal model reflects a scenario wherein the multisensors are mounted on the gearbox and the sensor on the high-speed stage fails. Seven data-mining algorithms—neural network (NN) [21]–[23], neural network ensemble (NNE) [24], boosting tree regression (BT) [25], [26], random forest regression (RF) [27], classification and regression tree (CART) [28], support vector machine (SVM) [29], [30], and k nearest neighbor (kNN) [31]—are selected to construct the data-driven models.

Parameter	Importance	Parameter	Importance
$J_{AN7,t-T}$	100	$J_{AN7,t-2T}$	92
$J_{AN7,t-2T}$	96	$J_{AN7,t-4T}$	90
$J_{AN7,t-3T}$	93	$J_{AN7,t-5T}$	90
$J_{AN7,t-4T}$	93	$J_{AN7,t-7T}$	89
$J_{AN7,t-5T}$	92	$J_{AN7,t-8T}$	82

4.4 Single-Signal Model I: In this section, the single signal model I, a data-driven time series model, is introduced to predict the jerk of AN7 at time t . To predict the jerk of AN7 at time t , the past ten states of jerk of AN7 at time t are derived from the dataset of Section IV-A. A parameter selection strategy, the importance analysis by the boosting tree algorithm, is utilized to select the five most important past states of jerk of AN7 at time t as the input to the single-signal model I. Table VII presents the ten past states of jerk of AN7 and the associated importance evaluated by the importance analysis. In Table VII, symbol J means quantity jerk, AN7 presents the sensor name, t is the current time, and T describes the data sampling interval. Based on the parameter importance provided in Table VII, five past states— $J_{AN7,t-T}$, $J_{AN7,t-2T}$, $J_{AN7,t-3T}$, $J_{AN7,t-4T}$, and $J_{AN7,t-5T}$ —are considered as the inputs of the single-signal model I. Then, the single-signal model I is formulated

as

$$J_{AN7,t} = f(J_{AN7,t-T}, J_{AN7,t-2T}, J_{AN7,t-3T}, J_{AN7,t-4T}, J_{AN7,t-5T}) \quad (4)$$

$$J_{AN7,t} = f(J_{AN7,t-T}, J_{AN7,t-2T}, J_{AN7,t-3T}, J_{AN7,t-4T}, J_{AN7,t-5T}) \quad (4)$$

where $f(\cdot)$ is the model developed by data-mining algorithms. Seven data-mining algorithms—NN, NNE, BT, RF, CART, SVM, and kNN—are all applied to train the data-driven models (single-signal model I) based on the training dataset. The test dataset then is used to validate and compare the trained models. Four metrics—used in model evaluation of the mean absolute error (MAE), standard deviation of absolute error (SDofAE), mean absolute percentage error (MAPE), and standard deviation of absolute percentage error (SDofAPE)—for validation of data-driven models are formulated in (5)–(8), respectively,

$$MAE = \frac{1}{n} \sum_{i=1}^n |\hat{y}_i - y_i| \tag{5}$$

$$SDofAE = \sqrt{\frac{1}{n} \sum_{i=1}^n \left(|\hat{y}_i - y_i| - \frac{1}{n} \sum_{i=1}^n |\hat{y}_i - y_i| \right)^2} \tag{6}$$

$$MAPE = \frac{1}{n} \sum_{i=1}^n \left(\left| \frac{\hat{y}_i - y_i}{y_i} \right| \right) \times 100\% \tag{7}$$

$$SDofAPE = \sqrt{\frac{1}{n} \sum_{i=1}^n \left(\left| \frac{\hat{y}_i - y_i}{y_i} \right| - \frac{1}{n} \sum_{i=1}^n \left| \frac{\hat{y}_i - y_i}{y_i} \right| \right)^2} \times 100\% \tag{8}$$

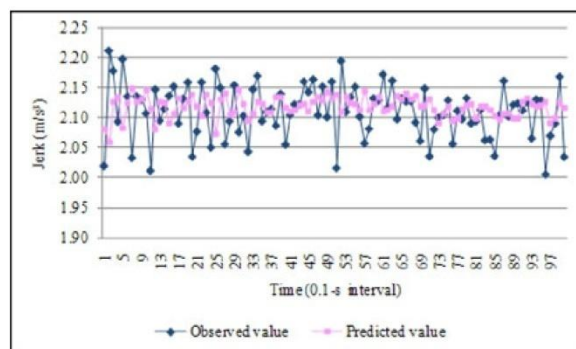
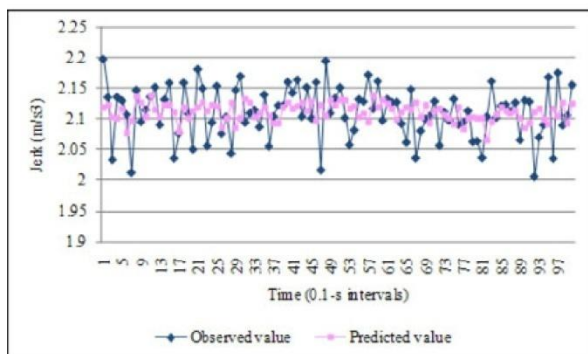
where \hat{y} is the predicted value by a model, y is the observed value, and n means the total number of data points in training or the test dataset Table VIII presents the test results of data-driven models with seven data-mining algorithms. As shown in Table VIII, all seven data-mining algorithms can develop good quality data-driven models to predict the jerk of AN7. The accuracy of data-driven models is about 98% (MAPE is about 2%). However, since SVM provides relatively higher prediction accuracy, it is selected to develop the single-signal model I. Fig. 9 illustrates the first 100 test results of the model developed by the SVM algorithm.

4.5 Single-Signal Model II:

In Section IV-A, the standard deviation and the maximum of the jerk of AN7 were derived. The past states of the derived data, such as its standard deviation and maximum, could benefit the prediction model. In Section IV-B2, the five past states of the jerk of AN7, its derived standard deviation and its maximum are all considered to construct the

Algorithm	MAE	SDofAE	MAPE	SDofAPE
NN	0.0445	0.0329	0.0207	0.0150
NNE	0.0446	0.0331	0.0208	0.0151
BT	0.0427	0.0315	0.0200	0.0144
RF	0.0505	0.0361	0.0235	0.0163
CART	0.0573	0.0391	0.0266	0.0176
SVM	0.0408	0.0296	0.0192	0.0138
KNN	0.0505	0.0388	0.0235	0.0178

Algorithm	MAE	SDofAE	MAPE	SDofAPE
NN	0.0461	0.0339	0.0215	0.0154
NNE	0.0465	0.0341	0.0216	0.0155
BT	0.0430	0.0324	0.0201	0.0149
RF	0.0492	0.0357	0.0229	0.0161
CART	0.0574	0.0390	0.0267	0.0176
SVM	0.0403	0.0299	0.0190	0.0141
KNN	0.0517	0.0383	0.0241	0.0175



Parameter	Importance	Parameter	Importance	Parameter	Importance
$J_{AN7,t-T}$	100	$J_{AN7,t-3T}$	93	$M_{AN7,t-2T}$	42
$J_{AN7,t-2T}$	100	$S_{AN7,t-5T}$	91	$M_{AN7,t-4T}$	38
$J_{AN7,t-T}$	99	$S_{AN7,t-2T}$	91	$M_{AN7,t-T}$	31
$J_{AN7,t-4T}$	97	$S_{AN7,t-T}$	83	$M_{AN7,t-3T}$	29
$S_{AN7,t-4T}$	94	$S_{AN7,t-3T}$	80	$M_{AN7,t-5T}$	28

Parameters	Importance	Parameters	Importance	Parameters	Importance
$J_{AN6,t}$	100	$J_{AN3,t}$	59	$J_{AN1,t}$	27
$J_{AN5,t}$	88	$J_{AN12,t}$	56	$R_{a,t}$	21
$J_{AN9,t}$	85	$J_{AN11,t}$	36	$R_{z,t}$	19
$J_{AN8,t}$	84	$J_{AN2,t}$	32		
$J_{AN10,t}$	64	$J_{AN4,t}$	32		

single-signal model II to predict jerk of AN7 at time t . The same parameter selection strategy in Section IV-B1 is utilized to select the five most important parameters as the inputs of the single-signal model II.

Table IX presents the results of importance analysis. Sym-bol S represents the standard deviation and M represents the maximum. The remaining notation is defined in Section IV-B1. The most important five important parameters are $J_{AN7,t-T}$, $J_{AN7,t-5T}$, $J_{AN7,t-2T}$, $J_{AN7,t-4T}$, and $S_{AN7,t-4T}$ (see

Table IX). These five parameters are selected as the inputs of the single-signal model II. The single-signal model II is expressed in the following:

$$J_{AN7,t} = f(J_{AN7,t-T} \cdot J_{AN7,t-5T} \cdot J_{AN7,t-2T} \cdot J_{AN7,t-4T} \cdot S_{AN7,t-4T}) \quad (9)$$

where $f(\cdot)$ is the data-driven model.

The seven data-mining algorithms of Section IV-B1 are applied to develop the single-signal model II. The test results of the data-driven models are illustrated in Table X. In Table X, the

best-performed algorithm is SVM with the prediction accuracy higher than that in Table VIII.

Fig. 10 presents the first 100 test points of the single-signal model II trained by the SVM algorithm.

4.6 Multisignal Model: Besides the information of jerk of AN7 itself, the jerk derived based on acceleration data mea-sured by other sensors can be used to predict the jerk of AN7. Table XI describes the pool of parameters used in the parameter selection and the result of parameter selection based on the same procedure discussed in Section IV-B1. In the fifth column, the presents the rate of generator speed ω or torque τ at time t . Based on the importance illustrated in Table XI, $J_{AN6,t}$,

$J_{AN5,t}$, $J_{AN9,t}$, $J_{AN8,t}$ and $J_{AN10,t}$, are considered as the inputs of multisignal model, and the multisignal model is formulated as

$$J_{AN7,t} = f(J_{AN6,t} \cdot J_{AN5,t} \cdot J_{AN9,t} \cdot J_{AN8,t} \cdot J_{AN10,t}) \quad (10)$$

Table XII interprets the test results of data-driven models (mul-tisignal model) developed by data-mining algorithms discussed

TABLE XII
TEST RESULTS OF MULTISIGNAL MODEL DEVELOPED BY SEVEN ALGORITHMS

Algorithm	MAE	SDofAE	MAPE	SDofAPE
NN	0.0411	0.0311	0.0192	0.0142
NNE	0.0405	0.0307	0.0189	0.0140
BT	0.0400	0.0306	0.0187	0.0141
RF	0.0522	0.0367	0.0242	0.0166
CART	0.0483	0.0357	0.0224	0.0162
SVM	0.0412	0.0311	0.0192	0.0143
KNN	0.0453	0.0350	0.0212	0.0160

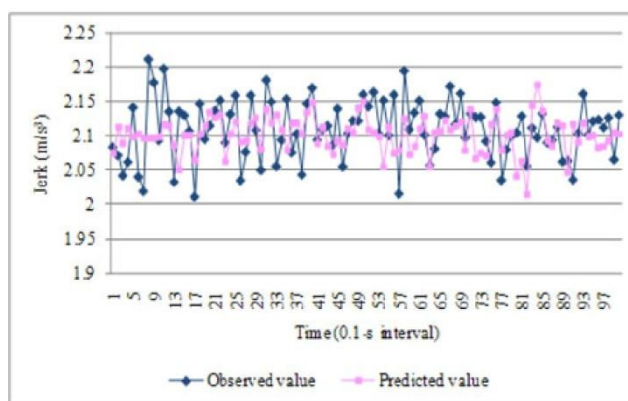


Fig. 11. First 100 test points of the multisignal model developed by BT.

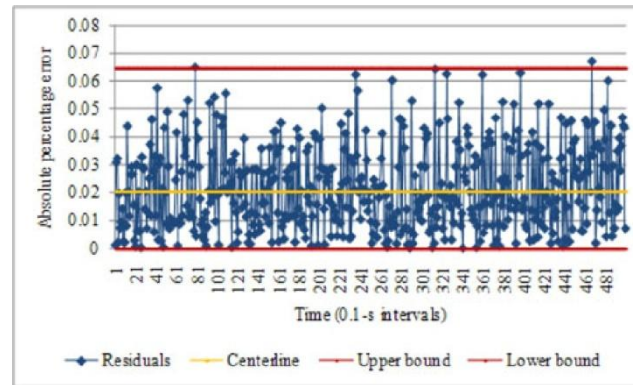


Fig. 12. Modified \bar{x} -bar chart for the test dataset.

the mean and the standard deviation of the test dataset need to be computed according to (11) and (12), respectively,

$$\mu_t = \frac{[\sum_{i=1}^m (\hat{y}_i - y_i)]}{m} \quad (11)$$

$$s_t = \sqrt{\left[\sum_{i=1}^m \frac{((\hat{y}_i - y_i) - \mu_t)^2}{(m - 1)} \right]} \quad (12)$$

in Section IV-B1. In Table XII, the BT algorithm provides the most accurate and stable prediction results of jerk of AN7 based on the five most important parameters in Table XI. In addition, by comparing Table XII with Tables VIII and X, it is observable that the information of other sensors is beneficial to developing the prediction model of jerk of AN7. Fig. 11 shows the first 100 test results of the multisignal model trained by the BT algorithm in predicting the jerk of AN7.

4.7 Monitoring Models

Two monitoring models are discussed in this section to detect the increase in vibration excitement at the high-speed stage of the gearbox. To detect the increase in vibration excitement, two statistical control methods are applied to monitor the prediction residuals of the single-signal model I.

5. Modified X-Bar Chart:

The single-signal model I, developed by the SVM algorithm in Section IV-B1, offers 98% accurate predictions based on the test dataset. Unlike multisignal models, the single-signal model I uses only one signal to predict $J_{AN7,t}$. If the modeled system changes in the future and the changes do are reflected in the training dataset, then the single-signal model I will not be able to provide accurate predictions. The degradation of prediction performance is manifested in the increase of the prediction residuals. Therefore, the shift in the vibration excitement at the high-speed stage of the gearbox can be detected by analysis of the prediction residuals of the single-signal model I. To analyze the prediction residuals, in this section, a modified \bar{x} -bar chart where μ_t represents the mean of the test dataset, s_t describes the standard deviation of the test dataset, and m is the total number of data points in the test dataset.

Based on the computed μ_t and s_t , the modified \bar{x} -bar chart is formulated as

$$UCL_x = \mu_t + c \left(\frac{s_t}{\sqrt{q}} \right) \quad (13)$$

$$CL_x = \mu_t \quad (14)$$

$$LCL_x = \max \left\{ 0, \mu_t - c \left(\frac{s_t}{\sqrt{q}} \right) \right\}. \quad (15)$$

The UCL_x , CL_x , and LCL_x in (13)–(15) represent the upper control limit, centerline, and lower control limit of the modified \bar{x} -bar chart, respectively. The parameter c controls the width between the upper and lower control limit. The parameter q denotes the number of sampling data points.

To monitor the prediction residuals of the single-signal model I by the modified x-bar chart, two datasets—a test dataset and an analysis dataset—are utilized. The test dataset is applied to de-velop the modified x-bar chart and then the trained modified x-bar chart is employed to examine whether the vibration ex-citement at the high-speed stage has shifted for the analysis dataset. *Definition 1:* If the number of prediction residuals greater than the upper control limit or lower than the lower control limit in the analysis dataset is larger than that in the test dataset, then the vibration excitement is considered as shifted. Otherwise, the vibration excitement is considered normal. Fig. 12 presents the residual analysis results based on the test dataset using the modified x-bar chart. To

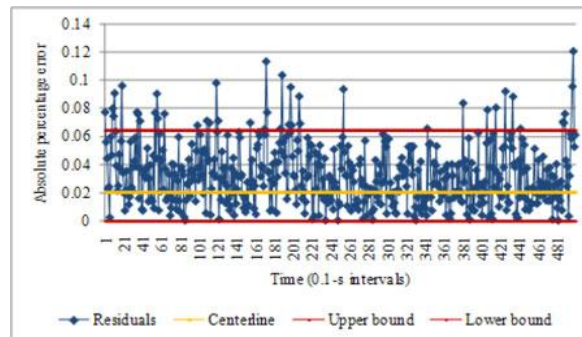


Fig. 13. Modified x-bar chart for the analysis dataset
display the concept clearly, only the data points in the second half of the test dataset

are included in Fig. 12. Fig. 13 shows the prediction residuals based on the analysis dataset monitored by the modified x-bar chart. The first 500 prediction residuals of the analysis dataset are included. As shown in Figs. 12 and 13, it is quite obvious that the shift of the vibration excitement is detected because there are more residuals that exceed the upper control limit in Fig. 13 than in Fig. 12

5.6 Exponentially Weighted Moving Average Chart: In statistical quality control, the exponentially weighted moving average (EWMA) chart [32] is commonly applied to detect a small shift in a process. As shown in Fig. 3, the vibration excitement at the high-speed stage shows a gradually increasing pattern that is similar to a small shift in a process. The pattern of signal sensed by AN7 is similar to that of AN9 (see Fig. 3). Therefore, the EWMA chart is able to detect the increase of vibration excitement at the high-speed stage of the gearbox. Compared to the modified x-bar chart in Section IV-C1, the detection result of the EWMA chart is clearer and easier to understand. In the EWMA chart, the value of a quantity, EWMA, is monitored and estimated by

$$z_i = \lambda x_i + (1 - \lambda)z_{i-1} \tag{16}$$

where z presents the EWMA, x is the prediction residual and i is the index of a data point

$$UCL_{EWMA} = \mu_t + Ls_t \sqrt{\frac{\lambda}{2-\lambda} [1 - (1-\lambda)^{2i}]} \tag{17}$$

$$CL_{EWMA} = \mu_t \tag{18}$$

$$LCL_{EWMA} = \max \left\{ 0, \mu_t - Ls_t \sqrt{\frac{\lambda}{2-\lambda} [1 - (1-\lambda)^{2i}]} \right\} \tag{19}$$

where L and λ are two parameters that need to be arbitrarily set to develop the EWMA chart and the remaining notation is presented in Section IV-C1.

Fig. 14 shows the EWMA chart of the analysis dataset. The test dataset is utilized to calculate the μ_t and s_t in (16)–(18). The parameter L is set to 3 and λ is set to 0.1, according to the recommendation in [32]. In the EWMA chart, $L = 3$ indicates

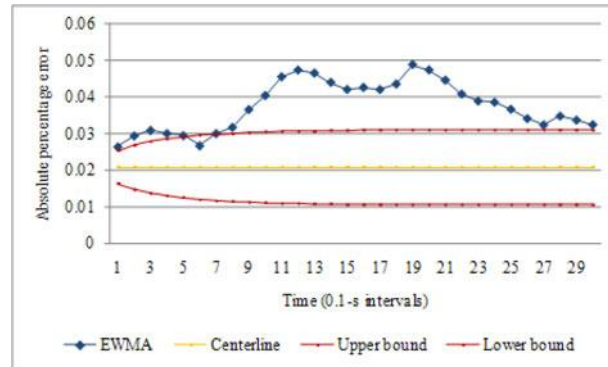


Fig. 14. Result of EWMA chart

that a three-sigma limit is considered and a small λ indicates a small weight of new data in the estimation of EWMA which ensure the effectiveness of EWMA in detection of small shifts. As shown in Fig. 14, the vibration excitement described in the analysis dataset is clearly different from that of the test dataset. This is because EWMA is above the upper control limit most of the time in Fig. 14.

6. Conclusion

Analysis of jerk data derived from vibration acceleration data of the wind turbine gearbox was discussed in this paper. The vibration acceleration data were collected in the test facility of the NREL. To test the gearbox, the drivetrain system (without blades or hub) were removed from a wind turbine and fixed on the floor of the NREL test facility. Twelve vibration accelerometers were mounted on different locations of the drivetrain system to sense the vibration acceleration. Based on the jerk data, two types of analysis—component failure identification and monitoring gearbox high-speed stage vibration—were addressed. In the analysis of the component failure identification, the correlation coefficient analysis and clustering analysis were applied to identify the failure stage of the gearbox in the time domain. In the frequency-domain analysis, fast Fourier transformation with time windows was applied. The failure of the intermediate- and high-speed stages of the gearbox was correctly identified by the approaches discussed in this paper. Some root causes could be inferred based on the data patterns of some specific sensors. However, to confirm the root cause of the gearbox fault, the actual inspection of the disassembled gearbox was undertaken. Besides the component failure identification analysis, models for monitoring the vibration excitement of the gearbox highspeed stage were introduced. Data-driven models and statistical control theory were integrated to develop a monitoring model. Four types of data-driven models were introduced to predict the jerk indicated by the vibration excitement of the gearbox highspeed stage. Each data-driven model represented a condition of sensors in the test. Two statistical control charts were established based on the developed data-driven model. The shift of vibration excitement at the high-speed stage was effectively detected. Although, in this paper, only the monitoring model for the high speed stage vibration was discussed, this framework could be applied to monitor the vibration excitement of other parts of the gearbox. The main shortcoming of this study was the gearbox test condition. Since the drivetrain was fixed to the floor, other factors (e.g., force from the wind and tower) that could impact the vibration excitement were not resented. To develop a more applicable monitoring model, gearbox vibration acceleration data collected from field-operated wind turbines is needed.

7. Acknowledgment

The authors would like to thank the NREL for providing the data used in this research

References

- [1] C. Tsai, C. Hsieh, and S. Huang, "Enhancement of damage-detection of wind turbine blades via CWT-based approaches," *IEEE Trans. Energy Convers.*, vol. 21, no. 3, pp. 776–781, Sep. 2006.
- [2] A. Kusiak and A. Verma, "A data-driven approach for monitoring blade pitch faults in wind turbines," *IEEE Trans. Sustainable Energy*, vol. 2, no. 1, pp. 87–96, Jan. 2011.
- [3] S. J. Watson, B. J. Xiang, W. Yang, P. J. Tavner, and C. J. Crabtree, "Condition monitoring of the power output of wind turbine generators using wavelets," *IEEE Trans. Energy Convers.*, vol. 25, no. 3, pp. 715–721, Sep. 2010.
- [4] A. R. Mohanty and C. Kar, "Fault detection in a multistage gearbox by demodulation of motor current waveform," *IEEE Trans. Ind. Electron.*, vol. 53, no. 4, pp. 1285–1297, Jun. 2006.

- [5] W. J. Wang and P. D. McFadden, "Application of wavelets to gearbox vibration signals for fault detection," *J. Sound Vibration*, vol. 192, no. 5, pp. 927–939, 1996.
- [6] X. Yuan and L. Cai, "Variable amplitude Fourier series with its application in gearbox diagnosis-Part I: Principle and simulation," *Mech. Syst. Signal Process.*, vol. 19, no. 5, pp. 1055–1066, 2005.
- [7] X. Yuan and L. Cai, "Variable amplitude Fourier series with its application in gearbox diagnosis-Part II: Experiment and application," *Mech. Syst. Signal Process.*, vol. 19, no. 5, pp. 1067–1081, 2005.
- [8] X. Wang, V. Makis, and M. Yang, "A wavelet approach to fault diagnosis of a gearbox under varying load conditions," *J. Sound Vibration*, vol. 329, no. 9, pp. 1570–1585, 2010.
- [9] J. A. Harding, M. Shahbaz, S. Srinivas, and A. Kusiak, "Data mining in manufacturing: A review," *J. Manuf. Sci. Eng.*, vol. 128, no. 4, pp. 969–976, 2006.
- [10] M. J. A. Berry and G. S. Linoff, *Data Mining Techniques: For Marketing, Sales, and Customer Relationship Management*, 2nd ed. New York: Wiley, 2004.
- [11] S. Shah, A. Kusiak, and M. O'Donnell, "Patient-recognition data-mining model for BCG-plus interferon immunotherapy bladder cancer treatment," *Comput. Biol. Med.*, vol. 36, no. 6, pp. 634–655, 2006.
- [12] A. Kusiak and Z. Zhang, "Analysis of wind turbine vibrations based on SCADA data," *ASME J. Sol. Eng.*, vol. 132, no. 3, pp. 031008-1–031008-12, 2010.
- [13] A. Kusiak and Z. Zhang, "Short-horizon prediction of wind power: A data-driven approach," *IEEE Trans. Energy Convers.*, vol. 25, no. 4, pp. 1112–1122, Dec. 2010.
- [14] A. Kusiak, M. Y. Li, and Z. Zhang, "A data-driven approach for steamload prediction in buildings," *Appl. Energy*, vol. 87, no. 3, pp. 925–933, 2010.
- [15] A. Kusiak, M. Y. Li, and H.-Y. Zheng, "Virtual models of indoor-airquality sensors," *Appl. Energy*, vol. 87, no. 6, pp. 2087–2094, 2010.
- [16] R. A. Fisher, "Frequency distribution of the values of the correlation coefficient in samples from an indefinitely large population," *Biometrika*, vol. 10, no. 4, pp. 507–521, 1915.
- [17] P. N. Tan, M. Steinbach, and V. Kumar, *Introduction to Data Mining*. Boston, MA: Addison Wesley, 2006.
- [18] P. A. Devijver and J. Kittler, *Pattern Recognition: A Statistical Approach*. London, UK: Prentice-Hall, 1982.
- [19] F. Mosteller, "A k-sample slippage test for an extreme population," *Ann. Math. Statistics*, vol. 19, no. 1, pp. 58–65, 1948.
- [20] R. N. Bracewell, *The Fourier Transform and Its Applications*. Boston: McGraw-Hill, 2000.
- [21] H. Siegelmann and E. Sontag, "Analog computation via neural networks," *Theor. Comput. Sci.*, vol. 131, no. 2, pp. 331–360, 1994.
- [22] G. P. Liu, *Nonlinear Identification and Control: A Neural Network Approach*. London, UK: Springer, 2001.
- [23] M. Smith, *Neural Networks for Statistical Modeling*. New York: Van Nostrand Reinhold, 1993.
- [24] L. K. Hansen and P. Salamon, "Neural network ensembles," *IEEE Trans. Pattern Anal. Mach. Intell.*, vol. 12, no. 10, pp. 993–1001, 1990.
- [25] J. H. Friedman, "Stochastic gradient boosting," *Comput. Statist. Data Anal.*, vol. 38, no. 4, pp. 367–378, 2002.
- [26] J. H. Friedman, "Greedy function approximation: A gradient boosting machine," *Ann. Statist.*, vol. 29, no. 5, pp. 1189–1232, 2001.
- [27] L. Breiman, "Random Forests," *Mach. Learning*, vol. 45, no. 1, pp. 5–32, 2001.
- [28] L. Breiman, J. H. Friedman, R. A. Olshen, and C. J. Stone, *Classification and Regression Trees*. Monterey, CA: Wadsworth, 1984.
- [29] B. Schölkopf, C. J. C. Burges, and A. J. Smola, "Cambridge," in *Advances in Kernel Methods: Support Vector Learning*, MA: The MIT Press, 1999.
- [30] I. Steinwart and A. Christmann, *Support Vector Machines*. New York: Springer-Verlag, 2008.
- [31] G. Shakhnarovich, T. Darrell, and P. Indyk, *Nearest-Neighbor Methods in Learning and Vision*. Cambridge, MA: The MIT Press, 2005.
- [32] D. C. Montgomery, *Introduction to Statistical Quality Control*. New York: John Wiley, 2005.



B.BABU was born in A.P, INDIA., in **1983 and** received the B.Tech.,(hons) degree in electrical and electronic engineering and the M.Tech degree from S.V.UNIVERSITY, TIRUPATI, INDIA., in 2005 and 2010, respectively. His research interests include direct ac–ac power conversion, variable-speed ac motor drives using different circuit topologies, and more- electric/electric automobiles. From 2006 to 2008, Lecturer at the CRIT, involved in teaching and research in power electronic systems. Since 2010, he has been with the Power Electronics, Machines and Control Group, School of Electrical and Electronic Engineering, MRRITS , udayagiri ,INDIA., where he is currently a Senior Lecturer in Power Electronics. His research interests are power electronic converters and modulation strategies, variable-speed drive systems, and electromagnetic compatibility..



R.VINOD KUMAR REDDY is doing his graduation in electrical and electronics engineering in MRRITS, udayagiri, A.P, INDIA. He also completed his project in the field of GENERATION OF POWER FROM WIND in SUZLON ENERGY LIMITED-TIRUMALA .He presented seminars on the “new design of 3MW wind turbine”.



R.DEVANANDA REDDY is pursuing his graduation in the department of electrical and electronics engineering in did his project on wind energy generation in SUZLON ENERGY LIMITED, TIRUMALA. He presented seminars on various topics which include DIRECT DRIVE WIND TURBINE-the third generation in the harnessing of power from wind. his research interests are applications of fuzzy logics in the controlling and monitoring of wind turbines.

Estimation of Wind Power Generation Based On Performance Curves

¹Mr.B.Babu, ²Mr.J.Vikram Kumar Reddy, ³A.Keerthi
^{1,2,3}(EEE Dept., M.R.R.I.T.S/ J.N.T.U.A/ A.P/INDIA)

Abstract

Three different operational curves—the power curve, rotor curve, and blade pitch curve—are presented for monitoring a wind farm’s performance. A five-year historical data set has been assembled for constructing the reference curves of wind power, rotor speed, and blade pitch angle, with wind speed as an input variable. A multivariate outlier detection approach based on -means clustering and Mahalanobis distance is applied to this data to produce a data set for modeling turbines. Performance monitoring of wind turbines is accomplished with the Hotelling control chart.

Index Terms—Control chart, -means clustering, Mahalanobis distance, performance monitoring, turbine performance curves.

I. Introduction

Recent years have witnessed a rapid expansion of wind energy. The growing number of wind turbine installations presents the asset operators with turbine operations and maintenance issues [1]. Variable wind conditions contribute to varying loads, which in turn lead to wind turbine faults, e.g., spalled bearings and fractured gears. Failures of wind turbines require repairs and negatively impact their performance [2]–[4]. Monitoring the performance of wind turbines is the key to reduction of operations and maintenance costs. Wind turbine performance is affected by: 1) external factors such as wind turbulence, storms, and icing; and 2) internal factors such as components’ temperature and lubrication. While the external factors cannot be controlled, events associated with the internal factors can be predicted. An efficient way to measure the impact of internal factors is through turbine operations. The operational characteristics of turbines depend on parameters such as rotor power, torque, and pitch angle. Continuous monitoring of these parameters can be useful in assessing wind turbine performance. State-of-the-art turbine monitoring applications are discussed in [3]–[5]. Condition monitoring approaches, namely vibration analysis [6], oil analysis [7], and strain measurement [8], are widely used in the literature. Data-mining-based approaches have gained their popularity in wind turbine research. Related applications of data mining include: 1) power curve monitoring [9], 2) monitoring and prediction of wind turbine states [10],

TABLE I
DATA DESCRIPTION

Task	Data Period
Extracting reference curves	August 2005-08
Validating reference curves	August 2009
Monitoring wind turbines	August 2011

[11], 3) modeling turbine abnormal behavior [12], [13], and 4) prognosis of turbine faults [14].

In this paper, turbine performance is assessed with three performance curves—power curve, rotor curve, and blade pitch curve. To perform such an assessment, operational wind turbine data is needed. Supervisory control and data acquisition (SCADA) systems record wind turbine parameters at different time intervals. SCADA data may be effectively used to tune a wind farm and provide early warnings of possible failures. In the research reported in this paper, historical wind turbine data is used to extract reference curves. The paper is organized as follows. Section II presents the data set used in the research, along with a description of turbine performance curves. In Section III, the solution methodology is presented, which consists of: 1) reference curve construction, 2) outlier detection, and 3) moment calculation. In Section IV, a statistical control chart is employed for performance monitoring of wind turbines. Section V concludes the paper with topics for future research.

2. Data for Turbine Performance Curves

The data used in this paper has been collected from a wind farm of over 100 wind turbines. Three wind turbine performance curves—power curve (power versus wind speed), rotor curve (rotor speed versus wind speed), and blade pitch curve (blade pitch angle versus wind speed)—are constructed for wind turbine

performance. The data set analyzed in this paper is di-vided into three parts. First, a four-year historical data (August 2005–August 2008) from 22 turbines is available to extract the reference curves for the month of August. The data is aver-aged over 10-min intervals (10-min data). The reference curves are validated with data from the following year (August 2009). To conduct performance monitoring, one month of data from 22 wind turbines was collected in August 2011. Table I presents the data used in the research. Descriptions of the three turbine performance curves are pro-vided in Section II-A.

2.1 Wind Turbine Performance Curves

A power curve indicates power generated by a wind turbine at various wind speeds. Malfunctions of a wind turbine will impact its power- generation capability. A typical wind power curve re-sembles a sigmoid function; however, due to various malfunc-tions (e.g., sensors and components), the power curve acquires a shape of its own

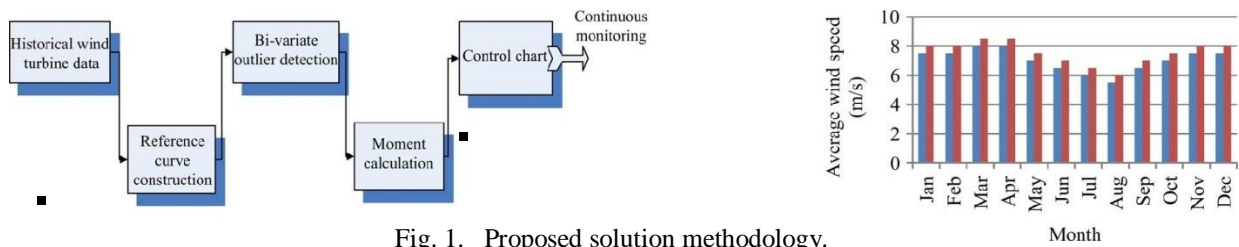


Fig. 1. Proposed solution methodology.

A rotor curve represents a mapping between rotor speed and wind speed. Failures of turbine components impact its shape. A typical rotor curve is a monotonically increasing function of the wind speed. A blade pitch curve shows the relationship between the tur-bine pitch angle and wind speed. The turbine’s control system adjusts the blade angle for maximum power capture. A malfunc-tion of the control system and high wind speed causes a turbine to stall, i.e., blade pitch angle becomes 90 . During the normal operations of a wind turbine, the pitch angle is set to, e.g., 0 , 66 , and 83 . In general, during the startup of a wind turbine, the blade pitch is set to a high value. A negative value of the pitch angle reflects the presence of a strong wind. In the cut-in to cut-out region of the wind speed, the blade pitch settings are adjusted by the control system for the max-imum power output. At the rated wind speed, the blade pitch angle is continuously adjusted to maintain the power required. In Section III, the proposed solution methodology is discussed.

3. Solution Methodology

The proposed solution methodology includes four phases (see Fig. 1). The historical wind farm data from several wind turbines is scanned initially to select wind turbine data (Phase 1). Due to the stochastic nature of the wind and inherent variability in the individual turbines, the noisy raw data is processed using a multivariate outlier detection approach (Phase 2). The resulting reference curves are used as a benchmark to evaluate the perfor-mance of individual turbines (Phase 3). Skewness and kurtosis of performance curves are calculated for each wind turbine and compared against the corresponding reference curves. In Phase 4, a quality control chart is used for performance monitoring of wind turbines.

All solution phases are discussed in the subsequent sections.

3.1 Construction of Reference Curves

Wind turbine performance depends on wind speed. The data used in this research is obtained from a large wind farm lo-cated in Blairsburg, Iowa. The monthly average distribution of wind speed at this location is investigated. Fig. 2 provides the monthly distribution of wind speed. The average wind speed varies across different months. Constructing reference curves using the yearly performance data may not be ideal as many de-tails may be missed. Based on the distribution of the wind speed, the reference curves for individual months are constructed. Based on the completeness of data across different years, per-formance curves for the month of August are extracted from the turbine data collected on 22 turbines over a four -year pe-riod (i.e., August 2005–August 2008). Based on the analysis,

Fig. 2. Average monthly wind speed distribution near the wind farm location (source: Iowa Energy Center).

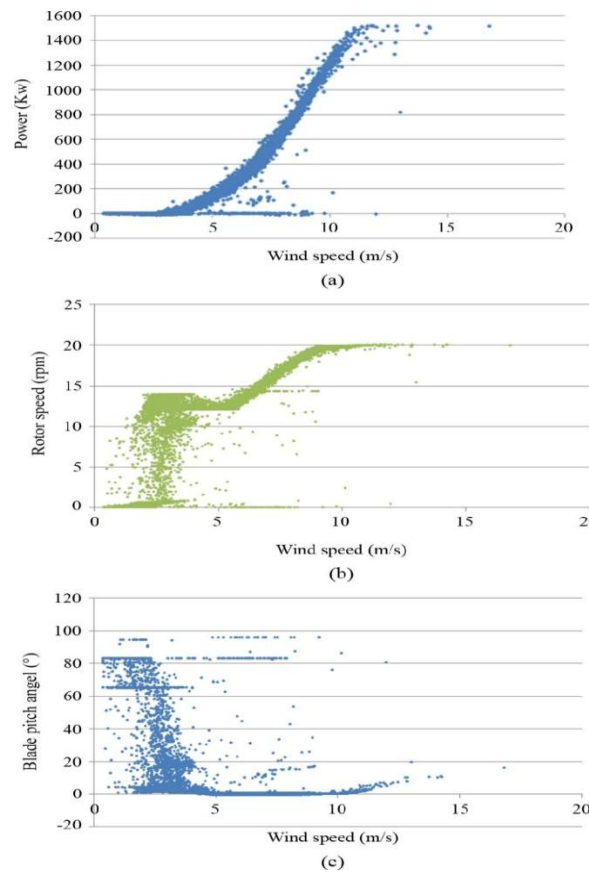


Fig. 3. Performance curves for the month of August (August 2005–August 2008). (a) Power curve. (b) Rotor curve. (c) Blade pitch curve.

data from 22 wind turbines is averaged to obtain three reference curves. Fig. 3(a)–(c) provides the reference power curve, rotor curve, and blade pitch curve of the historical monthly data for the month of August.

In Section III-B, a bivariate outlier selection approach is discussed.

3.1 Bivariate Outlier Detection

The reference curves constructed from the historical data contain outliers which need to be removed for clear depiction of normal turbine behavior. These outliers are largely due to the sensor errors and fluctuations in the turbine performance. In this paper, a multivariate outlier detection approach based on Mahalanobis distance is used. The Mahalanobis metric expresses the distance of an instance to the centroid in the multidimensional space [15], and it is calculated based on the correlation-covariance matrix. Therefore, Mahalanobis distance indicates whether an instance is an outlier with respect to the independent variable values

$$D_{st}^2 = (x_s - x_t) \text{Cov}^{-1} (x_s - x_t)^{-1}, \quad s \neq t. \quad (1)$$

In (1), D_{st}^2 the Mahalanobis distance between instance 's' and 't', and COV^{-1} is the inverse of covariance matrix. Due to distinct shape of performance curves, calculating Mahalanobis distance for an overall curve can be misleading as the centroid (usually for wind speeds between 4.5 and 7m/s) will consider the extreme data points (points close to cut-in wind speed, or/and near in order to improve outlier detection, the performance curve data is grouped into smaller clusters. The -means clustering algorithm determines the number of clusters for each curve by minimizing the cost function in the following [16]:

$$\Delta(k, x, c) = \frac{\sum_{i=1}^k \left(\sum_{x \in C_i} \|x - C_i\|^2 \right)}{\sum_{i=1}^k \text{Obs}_i} \quad (2)$$

where is the clustering cost, is the number of clusters, is the number of data points in cluster i , represents the data points, and represents cluster . The proposed procedure for identifying outliers in the bivariate performance curves is presented next.

3.2 Procedure: Extracting Smooth Performance Curves

Parameters:perf-C={PC,RC,BPC} , optimal number of clusters (kopt), maximum number of data subsets (Max_fold), Mahalanobis distance threshold

Begin

For each x €;perf-C

Set initial number of clusters

Divide the data set intoMax_fold

For f = 1 : Max-fold

Randomly select 90% subset for training and 10% for testing.

Initialize K centroids

Repeat, until the centroid does not change.

Evaluate the training error using the cost function in

End for

Output: (Optimal number of clusters)

For j=1 : kopt

Evaluate the Mahalanobis distance(D_{pq}) (1) for each data pair from the cluster mean

Sort the data pairs(p,q) based on the distance (D_{pq})

Retain data pairs(p,q) with (D_{pq}) <= δ

End for

Output: Mahalanobis distance between all data points for clusters

Repeat

Do until x = |perf-C|

End

3.3 Output: Smooth performance curves:

In the above procedure, the Mahalanobis distances between the data points and the cluster centers (centroids) are computed. The K-means clustering algorithm applied to the monthly reference curves provides 14, 11, and 9 clusters for the power curve, the rotor curve, and the blade pitch curve, respectively. Fig. 4(a)–(c) illustrates the clustered reference curves with training errors 0.039, 0.062, and 0.075 for these same curves, respectively. Fig. 5 depicts the Mahalanobis distance of power curve for individual clusters. The outlier data points can be easily identified in Fig. 5. Similarly, rotor curve and blade pitch curve are analyzed. The aim here is to extract smooth reference curves; therefore, a conservative approach based on the Mahalanobis distance metric is used to remove the outlier data points. The threshold distance is chosen in such a way that the data points corresponding to the high-density clouds in the clusters are selected. Table II presents the threshold distance for each cluster. Using the threshold distance indicated in Table II, 10%–15% of the data points were considered as outliers and thus are discarded. The refined performance curves are illustrated in Fig. 6(a)–(c). In Section III-C, the moment of the performance curves is discussed. Scalar performance matrices, namely, skewness and kurtosis of bivariate data, are evaluated.

3.4 Moment Calculation:

The third- and fourth-order moments, namely kurtosis and skewness, are often used to describe the shape of the data distribution. The multivariate kurtosis and skewness can also be used as a data compression technique providing a single value describing the shape of the distribution. Due to the high frequency data that is used in the proposed research, the performance curves are described using kurtosis and skewness. The refined reference curves obtained in Section III-B are used as a

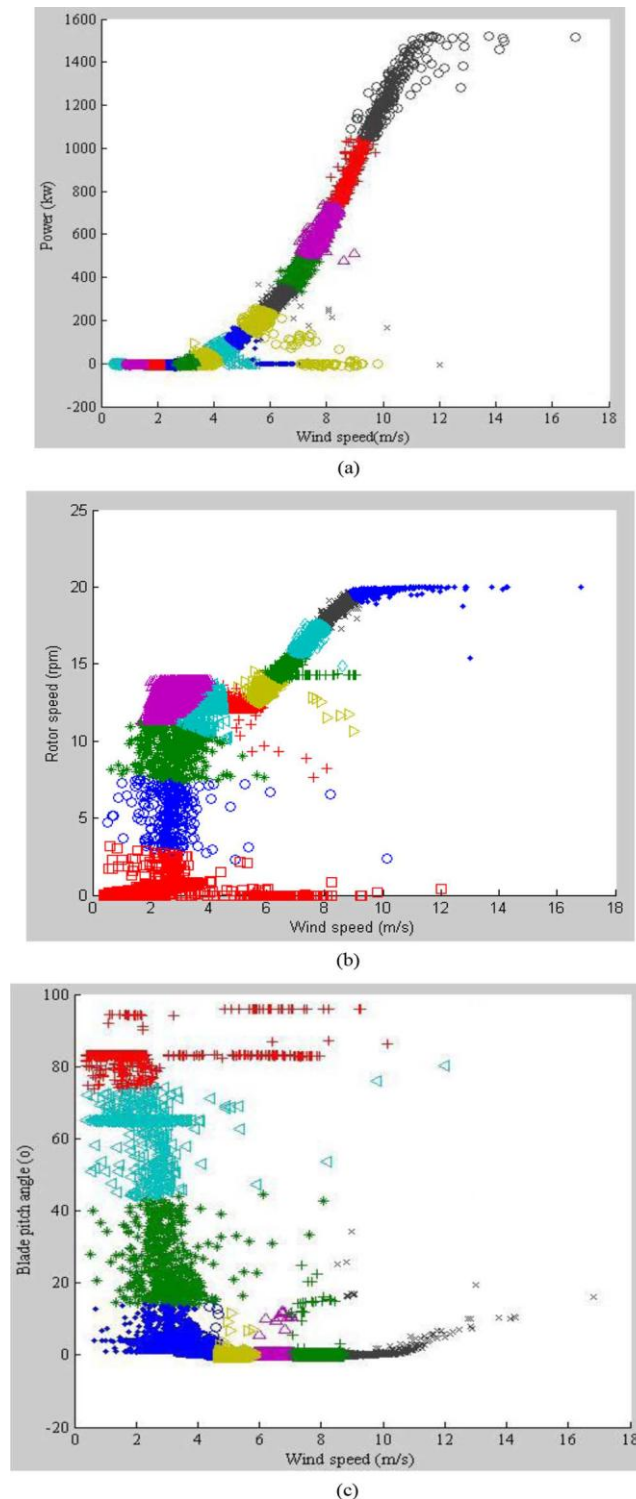


Fig. 4. Performance curves with clusters. (a) Power curve. (b) Rotor curve.

3.5 Blade pitch curve.

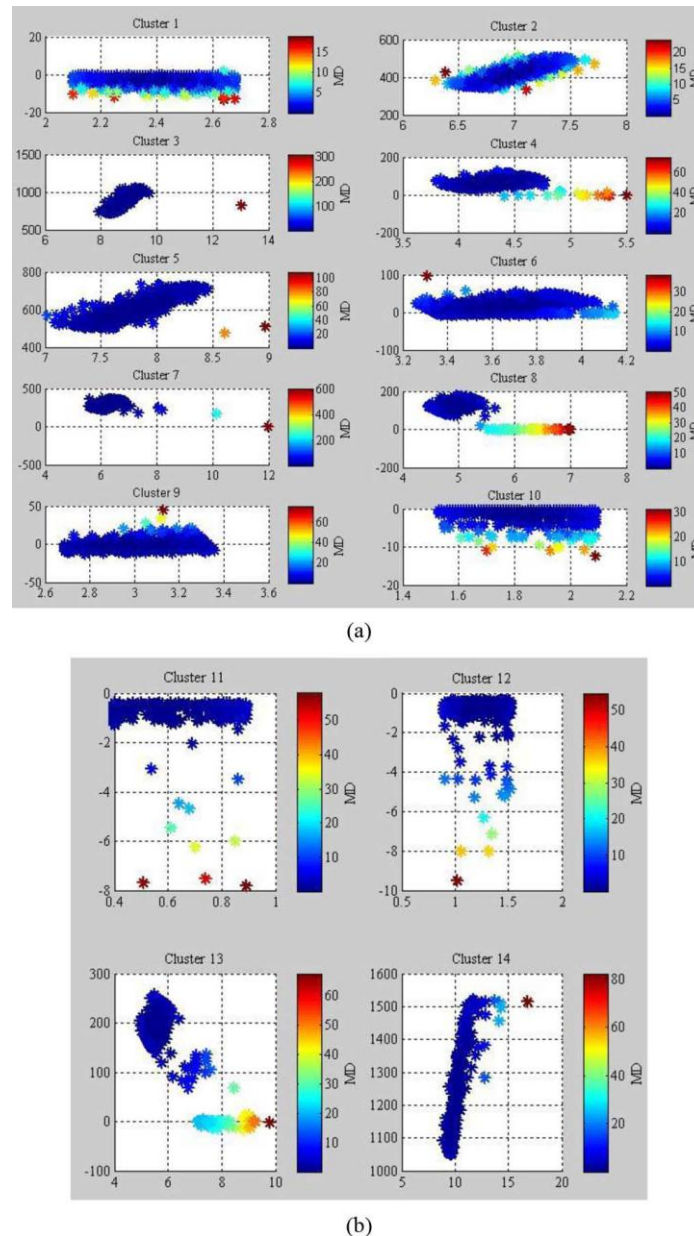


Fig. 5. Mahalanobis distance (MD) of power-curve-based clusters. (a) Clusters 1–10. (b) Clusters 11–14.

benchmark for performance monitoring of the wind farm. Multivariate skewness is a univariate measure of skewness for mul- tivariate data, where a value close to zero indicate elliptical symmetry. The multivariate skewness is defined [17], [18]

$$Skew_{multi} = \frac{1}{n^2} \sum_i \sum_j \left((x_i - \bar{x})^T \cdot Cov^{-1} \cdot (x_j - \bar{x}) \right)^3 \quad (3)$$

where \bar{x} is the matrix mean, and cov^{-1} is the estimated population covariance matrix. Similarly, multivariate kurtosis is a univariate measure of kurtosis for multivariate data. For column matrix, a value of kurtosis coefficient close to $p(p+2)$ indicates approximate multi-normality. Multivariate kurtosis is mathematically described in the following [18], [19]:

$$Kurt_{multi} = \frac{1}{n^2} \sum_i \left((x_i - \bar{x})^T \cdot Cov^{-1} \cdot (x_i - \bar{x}) \right)^2 \quad (4)$$

In general, under-performing wind turbines will deviate from the reference curves, resulting in different values of kurtosis and skewness that can be tracked in a 2D-graph. depending on the requirements, performance monitoring can take place on a daily, weekly, or monthly basis.

TABLE II
MAHALANOBIS DISTANCE THRESHOLD FOR PERFORMANCE CURVE CLUSTERS

Cluster No.	Power Curve	Rotor Curve	Blade Pitch Curve
1	2.5	10	25
2	2.5	2.5	5.0
3	50	50	5.0
4	10	5	25
5	10	1	25
6	5.0	25	50
7	100	2.5	10
8	5.0	25	2.5
9	10	10	25
10	5.0	10	NA
11	5.0	25	NA
12	5.0	NA	NA
13	10	NA	NA
14	10	NA	NA

TABLE III
MULTIVARIATE KURTOSIS AND SKEWNESS OF REFERENCE CURVES

Data Type	Criteria	PC	RC	BPC
Yearly	Skewness	2.25	2.11	4.17
	Kurtosis	9.34	8.41	9.12
Monthly	Skewness	8.24	1.75	2.38
	Kurtosis	15.13	7.89	8.35
Test	Skewness	10.25	1.98	3.18
	Kurtosis	17.33	8.87	8.67

table III compares the kurtosis and skewness of yearly and monthly reference curves with respect to the test data (August 2009). The kurtosis and skewness of reference curves constructed based on the yearly data (January 2008–December 2008) is obtained in a similar way. The values presented in Table III indicate that the skewness and kurtosis of monthly reference curves are much closer than of the yearly reference curves. Thus, monthly reference curves are used for monitoring the wind farm.

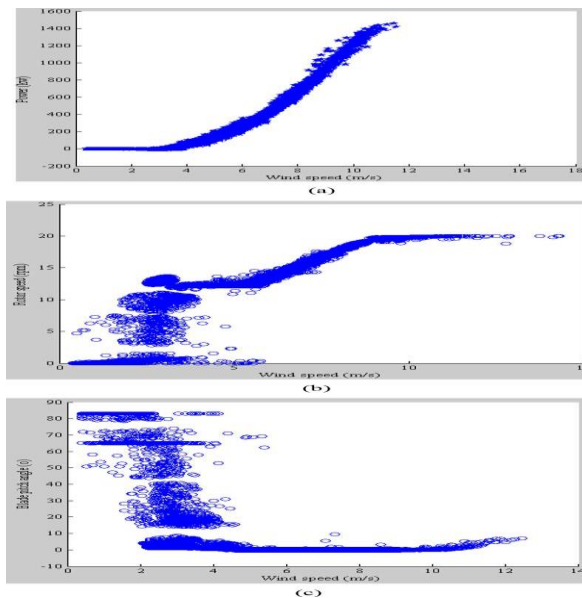


Fig. 6. Refined performance curves. (a) Power curve. (b) Rotor curve. (c) Blade pitch curve.

3.6 Monitoring a Wind Farm:

In this section, data from 22 wind turbines over a period of a month (August 2011) are analyzed using kurtosis and skewness for three performance curves. The analysis is based on the 10-min average data. Turbines located farthest from the reference points (see Table III) are considered to be abnormal. Euclidean distance is used to evaluate the distance of individual wind turbines from the reference points. Figs. 7–9 provide a 2-D scatter plot of the performance curves, where each point (diamond) represents an individual wind turbine. In addition, kurtosis and skewness of the reference curves are included in Figs. 7–9. Depending on the distribution of data points across the performance curves, the kurtosis and skewness distribution varies. Due to the distinct shape of the power curves, the kurtosis and skewness values are higher and more spread out than those of the rotor and blade pitch curves. In the 2-D skewness-kurtosis graph, wind turbine performance can be assessed by: 1) relative location of individual turbines with respect to the reference curves, and 2) location of individual turbines with respect to the turbine clusters. In general, turbine showing the same behavior will form a distinct cluster. Any abnormal turbine behavior can be easily visualized in a 2-D scatter graph. The possible reasons for the distinct location of individual turbines in the skewness-kurtosis plot could be:

- [1] under-performance due to system abnormalities,
- [2] under-performance due to different wind speeds, and
- [3] over-performance due to errors in wind speed measurement.

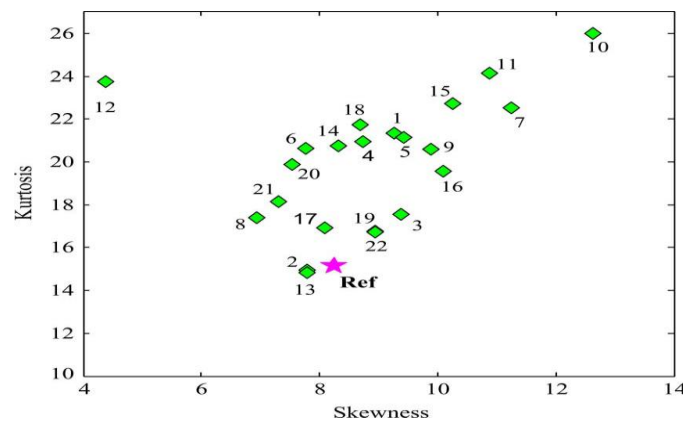


Fig. 7. Status of a wind farm reflected by the power curve.

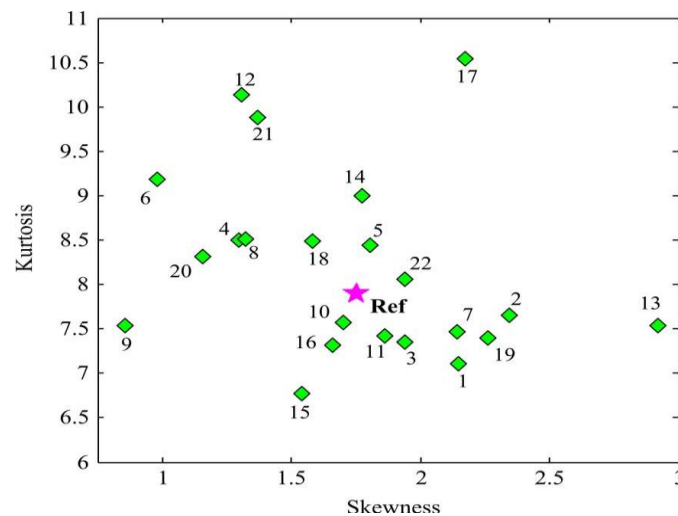


Fig. 8. Status of a wind farm reflected by the rotor curve

Using the guidelines mentioned earlier in this section, the power-curve-based skewness-kurtosis graph identifies turbines 10 and 12 as abnormal, whereas turbines 6, 9, 13, and 17 behave differently in the rotor and blade pitch curves.

Fig. 10 illustrates the power curve of turbine 10. The abnormal behavior of turbine 10 is clearly visible as the fault logs confirm the faults associated with generator windings. More information about turbine fault logs is provided in [3] and [20]. Performance of wind turbines can be assessed with the 2-D kurtosis-skewness graph; however, time is not depicted in the scatter plot. Therefore, to keep track of time, control charts are utilized.

4. Performance Monitoring Of Wind Turbines

In this section, performance monitoring of wind turbines is performed using a quality control chart. The overall monitoring of the wind farm can be done on a weekly or monthly basis; however, for performance monitoring of a wind farm over time, quality control charts are required. In this paper, two output metrics are used—skewness and kurtosis.

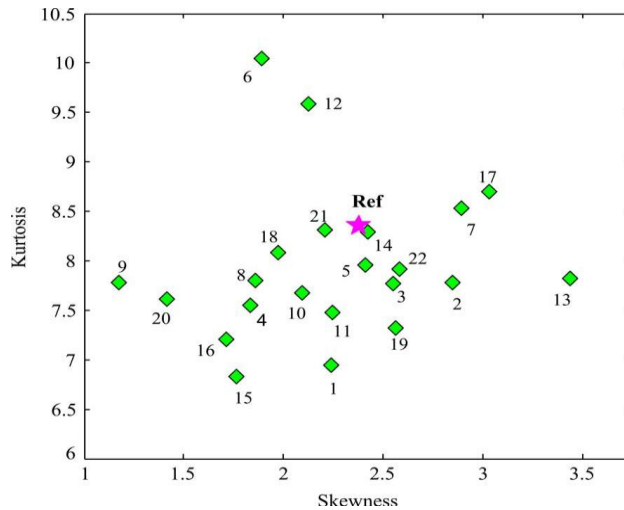


Fig. 9. Status of a wind farm reflected by the blade pitch curve.

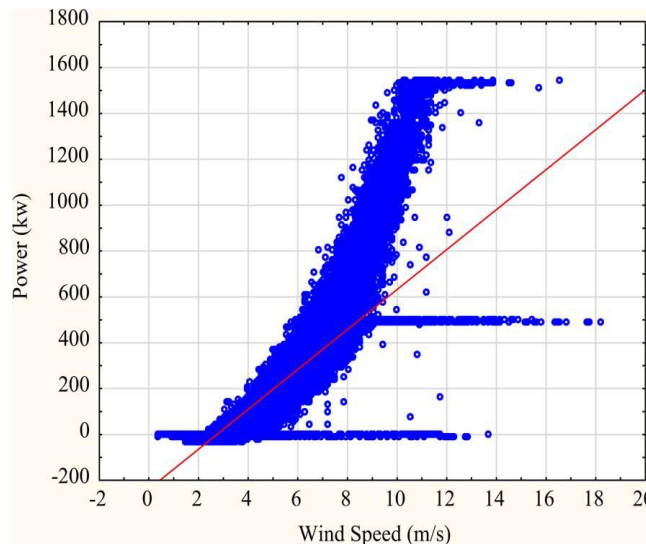


Fig. 10. Power curve of turbine showing abnormal behavior (turbine 10).

Monitoring the matrices independently can be misleading. Therefore, bivariate process monitoring using Hotelling’s control chart is employed. In the literature, Hotelling’s chart has been widely used to simultaneously monitor two or more output variables [21]. Equations (5)–(7) define the statistic as follows:

$$T^2 = (x_{ij} - \bar{X}_j) S^{-1} (x_{ij} - \bar{X}_j)' \tag{5}$$

In (5), is the individual observation, is the mean, is the covariance matrix inverse, and is the index of input variables. Since the subgroup size is 1, the covariance matrix is evaluated by pooling all observations [22], [23]

$$S = \frac{1}{m-1} \sum_{i=1}^m (x_{ij} - \bar{X}_j)(x_{ij} - \bar{X}_j)'. \quad (6)$$

For two output variables, the covariance matrix will take the form

$$S = \begin{bmatrix} s_1^2 & s_{12} \\ s_{21} & s_2^2 \end{bmatrix}. \quad (7)$$

The lower control limit (LCL) is always 0, whereas the upper control limit (UCL) is calculated from (7)

$$UCL = \frac{p(m+1)(m-1)}{m^2 - mp} F_{\alpha, p, m-p}. \quad (8)$$

In (8), is the number of output variables, is obtained from distribution. The value of is set to 0.001. The kurtosis and the skewness can be monitored simultaneously; however, the Hotelling test requires the data to be normal. Therefore, the initial data is normalized using the Box-Cox approach. A value varies from 5.0 to 5.0. Fig. 11 provides a comparison of initial and transformed skewness data of turbine 1 obtained using the Box-Cox approach. For equal to 0.552, the transformed data resembles a normal distribution. This process is repeated for all turbines. The transformed bivariate data of turbines is divided into two parts, e.g., training and testing.

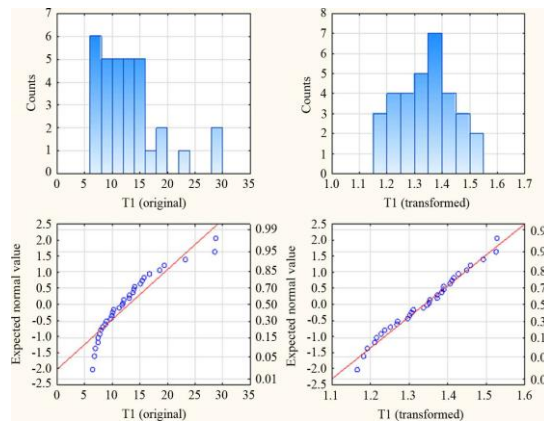


Fig. 11. The Box-Cox transformation of turbine 1 data ($\lambda = -0.552$)

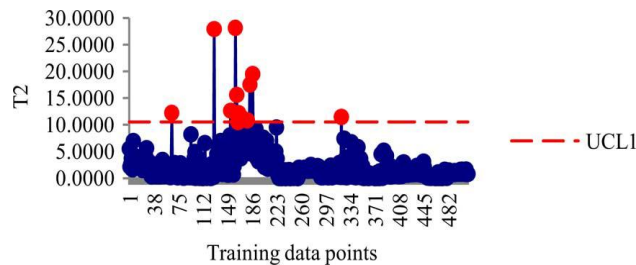


Fig. 12. Control limits for training data points (iteration 1).

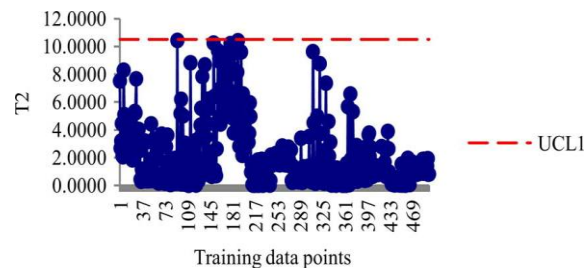


Fig. 13. Control limits for training data points (iteration 3)

Using the information presented in the power-curve-based kurtosis skewness data (see Fig. 7), turbines 7, 10, 11, 12, and 15 are used for testing, whereas the control limits are obtained by using data from the remaining turbines. Fig. 12 provides the UCL of 10.507, resulting in 12 data points out of control. The out-of control data points are removed, and the training process is iterated until all data-points meet the control limits. After three training process iterations, all data points were found in control, with the resulting UCL of 10.505 (Fig. 13). Fig. 14(a)–(e) illustrates the test data corresponding to turbines 7, 10, 11, 12, and 15. Based on the obtained UCL values, turbines 7, and 11 were found to be affected by an abnormal day in a month, whereas, two abnormal days were found for turbine 10. The remaining turbines, e.g., turbines 12 and 15 were found to operate normally. In general, various faults (cable twisting left, faulty pitch controller) contributed to the abnormal days of turbines 7, 10, and 11. However, the main reason for abnormal days is the power curtailment. Due to the limited number of observations, no significant pattern in the value was observed.

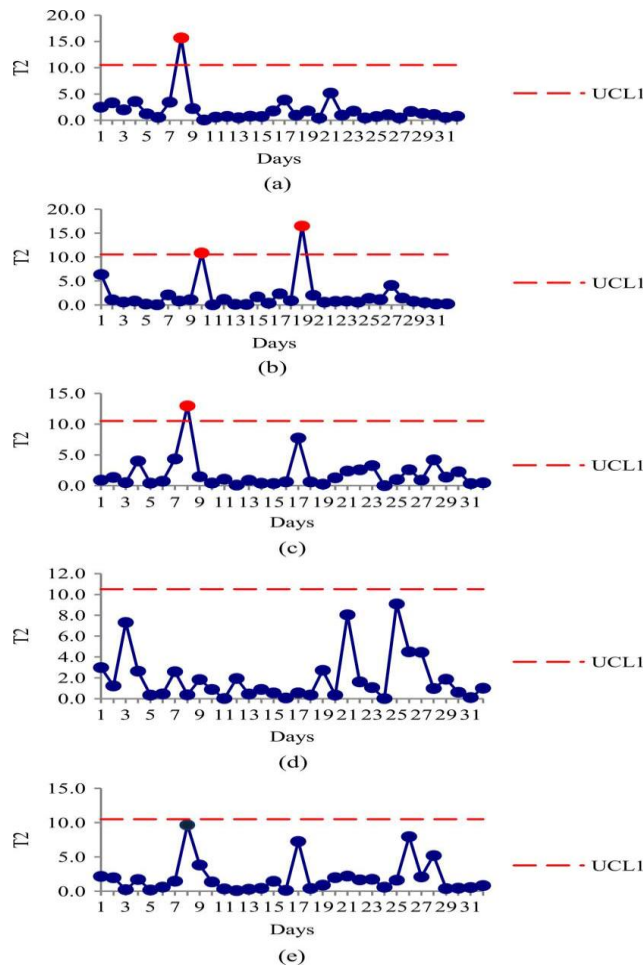


Fig. 14. Hotelling's T^2 chart for the test data (a) turbine 7, (b) turbine 10, (c) turbine 11, (d) turbine 12, and (e) turbine 15.

5. Conclusion:

A systematic approach for monitoring the performance of a wind farm was presented. Three performance curves—the power curve, rotor curve, and blade pitch curves—were used. The Mahalanobis distance was computed to identify outliers in the performance curves. The bivariate performance curve data was grouped into several clusters for better identification of outliers. Using the skewness and kurtosis of bivariate data, the initial high-frequency data was compressed to a single value. Hotelling's control chart was used for performance monitoring of the data points in time. The transformed kurtosis-skewness graphs were determined to be better suited for turbine monitoring than the high-frequency performance curves. The Hotelling control chart was applied to the daily average data. Future research will focus on hourly data. The impact of the output variables on Hotelling's control chart deserves further study.

References

- [1] A. Zaher, S. D. McArthur, and D. G. Infield, "Online wind turbine fault detection through automated SCADA data analysis," *Wind Energy*, vol. 12, no. 6, pp. 574–593, 2009
- [2] Z. Hameed, Y. S. Hong, Y. M. Cho, S. H. Ahn, and C.K. Song, "Condition monitoring and fault detection of wind turbines and related algorithms: A review," *Renew. Sustain. Energy Rev.*, vol. 13, no. 1, pp. 1–39, 2009.
- [3] R. Hyers, J. McGowan, K. Sullivan, J. Manwell, and B. Syrett, "Condition monitoring and prognosis of utility scale wind turbines," *Energy Mater.*, vol. 1, no. 3, pp. 187–203, 2006.
- [4] Y. Amirat, M. E. H. Benbouzid, E. Al-Ahmar, B. Bensaker, and R. Wamkeue, "A brief status on condition monitoring and fault diagnosis in wind energy conversion systems," *Renew. Sustain. Energy Rev.*, vol. 13, no. 9, pp. 2629–2636, 2009.
- [5] P. Tavner, G. W. Bussel, and F. Spinato, "Machine and converter reliabilities in wind turbines," in *Proc. 3rd IET Int. Conf. Power Electronics Machines and Drives*, Ireland, 2006, pp. 127–130.
- [6] P. Caselitz and J. Giebhardt, "Rotor condition monitoring for improved operational safety of offshore wind energy converters," *J. Solar Energy Eng.*, vol. 127, no. 2, pp. 253–261, 2005.
- [7] E. Becker and P. Posta, "Keeping the blades turning: Condition monitoring of wind turbine gears," *Refocus*, vol. 7, no. 2, pp. 26–32, 2006.
- [8] T.W. Verbruggen, *Wind Turbine Operation and Maintenance Based on Condition Monitoring*, WT- , Final Report Energy Research Center, The Netherlands, ECN-C-03-047, 2003, pp. 1–39.
- [9] A. Kusiak, H.-Y. Zheng, and Z. Song, "On-line monitoring of power curves," *Renew. Energy*, vol. 34, no. 6, pp. 1487–1493, 2009.
- [10] A. Kusiak and A. Verma, "Prediction of status patterns of wind turbines: A data-mining approach," *ASME J. Solar Eng.*, vol. 133, no. 1, pp. 011008–1–011008–10, 2011.
- [11] A. Kusiak and A. Verma, "A data-mining approach to monitoring wind turbines," *IEEE Trans. Sustain. Energy*, vol. 3, no. 1, pp. 150–157, Jan. 2012.
- [12] A. Zaher and S. McArthur, "A multi-agent fault detection system for wind turbine defect recognition and diagnosis," in *Proc. IEEE*, Lausanne, Switzerland, Jul. 2007, pp. 22–27, POWERTECH.
- [13] M. A. Sanz-Bobi, M. C. Garcia, and J. D. Pico, "SIMAP: Intelligent system for predictive maintenance: Application to the health condition monitoring of a wind turbine gearbox," *Comput. Industry*, vol. 57, no. 6, pp. 552–68, 2006.
- [14] A. Kusiak and W. Y. Li, "The prediction and diagnosis of wind turbine faults," *Renew. Energy*, vol. 36, no. 1, pp. 16–23, 2011.
- [15] P. Mahalanobis, "On the generalized distance in statistics," *Proc. National Institute of Sciences of India*, vol. 2, no. 1, pp. 49–55, 1936.
- [16] M. Inaba, N. Katoh, and H. H. Imai, "Applications of weighted voronoi diagrams and randomization to variance-based K-clustering," in *Proc. 10th ACM Symp. Computational Geometry*, 1994, pp. 332–339.
- [17] K. V. Mardia, "Measures of multivariate skewness and kurtosis with applications," *Biometrika*, vol. 57, no. 3, pp. 519–530, 1970.
- [18] K. V. Mardia, "Applications of some measures of multivariate skewness and kurtosis in testing normality and robustness studies," *Sankhya*, ser. B, vol. 36, no. 2, pp. 115–128, 1974.
- [19] K. V. Mardia, "Tests of Univariate and Multivariate Normality," in *Handbook of Statistics*, P. Krishnaiah, Ed. Amsterdam, The Netherlands: North Holland, 1980, vol. 1, pp. 279–320.
- [20] A. Kusiak and A. Verma, "Enhanced turbine performance monitoring," *Wind Syst. Mag.*, vol. 3, no. 24, pp. 36–41, 2011.

- [21] R. A. Johnson and D. W. Wichern, *Applied Multivariate Statistical Analysis*. Upper Saddle River, NJ: Prentice-Hall, 2002.
- [22] J. D. Williams, W. H. Woodall, J. B. Birch, and J. H. Sullivan, "Distribution of Hotelling's T₂ statistic based on successive difference estimator," *J. Quality Technol.*, vol. 38, no. 3, pp. 217–229, 2006.
- [23] J. H. Sullivan and W. H. Woodall, "A comparison of multivariate quality control charts for individual observations," *J. Quality Technol.*, vol. 28, no. 4, pp. 398–408, 1995.



J. BABU was born in A.P, INDIA., in **1983 and** received the B.Tech.,(hons) degree in electrical and electronics engineering and the M.Tech degree from S.V.UNIVERSITY, TIRUPATI, INDIA., in 2005 and 2011, respectively. His research interests include direct ac–ac power conversion, variable-speed ac motor drives using different circuit topologies, and more-electric/electric automobiles. From 2006 to 2008, Lecturer at the CREC, involved in teaching and research in power electronic systems. Since 2010, he has been with the Power Electronics, Machines and Control Group, School of Electrical and Electronic Engineering, MRRITS , udayagiri ,INDIA., where he is currently a Senior Lecturer in Power Electronics. His research interests are power electronic converters and modulation strategies, variable-speed drive systems, and electromagnetic compatibility..



J. VIKRAM KUMAR REDDY is pursuing his graduation in the department of electrical and electronics engineering in MRRITS, udayagiri, A.P, INDIA. He did his project on wind energy generation in SUZLON ENERGY LIMITED, TIRUMALA. He presented seminars on various topics which include WIND AMPLIFIED ROTOR PLATFORMS (WARP SYSTEM)-the fourth generation in the harnessing of power from wind. his research interests are applications of fuzzy logics in the controlling and monitoring of wind turbines.



A. KEERTHI is doing her graduation in electrical and electronics engineering in MRRITS, udayagiri, A.P, INDIA. she also completed her project in the field of GENERATION OF POWER FROM WIND in SUZLON ENERGY LIMITED-TIRUMALA. she reviewed seminars on different strategies which include "hybrid generation of power from wind and solar". she is very much enthusiastic to do her research in the development of computational intelligence in the areas of power generation from wind and solar and even their automation.

Automatic Cash Deposite Machine With Currency Detection Using Fluorescent And UV Light

¹Dhiraj Vasant Kapare , ² Sadashiv Lokhande, ³Sayaji Kale

^{1,2,3} Department of E&TC Engineering Imperial College of engineering, Pune, India

Abstract:

Cash Deposit Machines (CDM) has altered the relationship between banks and their depositors, as well as the competitive relationships among banks. In this paper, I survey the literature to describe the ways have influenced these aspects of banking markets. The project is designed to provide fully automatic cash deposit machine. It is combination of Embedded, DIP & Automation. In Mat lab every data image of note is compared with ideal stored image of every appropriate type of note. Every note is passed through UV light to detect the originality of note which consequently results in acceptance and rejection of faulty notes.

.Keywords: Currency, Fake Detection, Spindle, Storage, UV light.

1. Introduction

Automated cash deposit machines can offer significant benefits to both banks and their depositors. The machines can enable depositors to deposit cash at more convenient times and places than during banking hours at branches. At the same time, by automating services that were previously completed manually, CDMs can reduce the costs of servicing some depositor demands. These potential benefits are multiplied when banks share their CDMs, allowing depositors of other banks to access their accounts through a bank's CDM. In this paper, I will review the literature on CDM pricing and focused both on the motives for sharing CDM facilities.

2. System Overview

The project is designed to provide fully automatic cash deposit machine. The hardware consists of LCD screen for displaying option to select the bank and enter Acc. No in which cash is to be deposited and also guides the customer to next steps .The carriage is provided to carry the currency notes one by one from customer where camera captures image of every note and send the data image to PC with Matlab. Every data image of note is compared with ideal stored image of every appropriate type of note. Every note is passed through UV light to detect the originality of note which consequently results in acceptance and rejection of faulty notes.



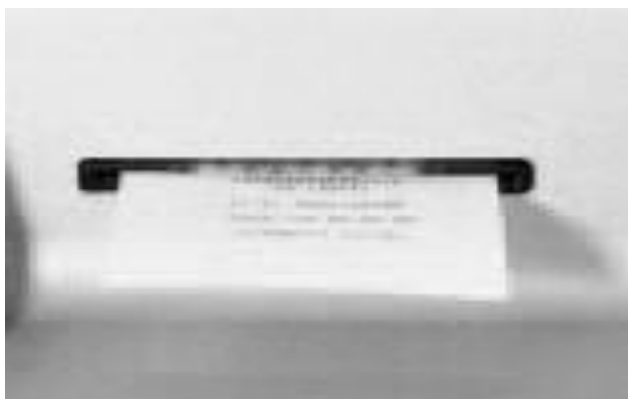
“Figure1. Database contexts”

Spindle is used to push notes from carriage to storage container of notes. Counter is provided to count the cash and counted data will be sending to MC.



“Figure2. System overview”

Finally LCD screen will show the new balance of customers account and will also give printed receipt



“Figure3. Unique receipt”

If there is any fault in machine then buzzer will make sound. Likewise there is one note is duplicate then buzzer will be make a sound. There is LED which indicate that machine is ready to use.

2.1. CDM Provide Busy Customer Service

- [1] Improved levels of convenience and security
- [2] Improved speed of deposit and ease of use
- [3] Reduced queuing time, increased customer satisfaction
- [4] Unique receipt slip issued after each deposit made
- [5] Revenue generating opportunities, created by re-deploying staff to more profitable activities
- [6] Flexibility to process cash at a convenient time or to outsource task
- [7] Speed of transaction minimizes customer exposure to risk of attack
- [8] Enhanced management information

2.2. Customer Requirement

Banks customers' taste and desire have begun to raise the stakes of expectation of exceptional services. Customers want to transact their banking transactions at any time and location convenient for their life-style. They want to pay their regular household bills. The four forces - customers, technology, convergence and globalisation have the most important effect. The success of electronic banking, as argued by many researchers, depends probably on bank service quality, customer preferences and satisfaction. Recent studies found that consumer behaviour is changing partly because of more spare time. The way of use of financial services is characterised by individuality, mobility, independence of place and time, and flexibility. Historically, banks have taken the attitude that they will provide customers with the services and, the banks, wish to provide. In order to survive both from domestic and the increasing level of global cross-border competition, banks need to change their process of servicing their customers

2.3. Benefit of automatic Banking

The perceived benefits of electronic banking have been documented in recent studies, especially several electronic distribution channels available for banks in United States and concluded that customer orientations towards convenience, service, technology, change, knowledge about computing and the Internet affected the usage of different channels. Convenience of conducting banking outside the branch official opening hours has been found significant in cases of adoption. Banks provide customers convenient, inexpensive access to the bank 24 hours a day and seven days a week. Literatures indicate the movement away from cash transactions and in words of the use of non-cash payment has continued to rise with increasing value. Tellers are today equipped to issue receipts (deposit slips) for cash deposits the service of ordering bank draft of certified cheques made payable to third parties has also been increasingly automated. A reduction in the percentage of customers visiting banks with an increase in alternative channels of distribution will also minimize the queues in the branches. Increased availability and accessibility of more self-service distribution channels helps bank administration in reducing the expensive branch network and its associate staff overheads. Bank employees and office space that are released in this way may be used for some other profitable ventures

2.4. Customer always require fast technology

New technology has raised your customers' expectations, and whilst they may come from many different backgrounds, lifestyles and professions, your customers have one thing in common: Choice of leisure time, work patterns, shopping, and the choice of how, when and with whom they carry out their banking requirements. In this competitive environment the winners are responding to their customer's needs, and improving the banking experience with

- [1] A convenient customer service
- [2] A modern retail environment
- [3] Faster transactions and improved security
- [4] Extended hours access to services

Communications – complete with a monitoring system to constantly verify operation and status of the CDM, whether remotely or centrally located. A file transfer utility is also available for retrieving audit and event history files. Automated Cash Deposits help you deliver more efficient Self-Service solutions. Our range of Cash Deposit Machines has been designed either for free standing or in the wall installation

2.5. Risks Associated with Electronic Banking

Although, electronic banking provides many opportunities for the banks, it is also the case that the current banking services provided through Internet are limited due to security concerns, complexity and technological problems Hewer and Howcroft used the term trust to describe a measure of risk. Viewed risk in the context of security concerns and risk in the context of trust in one's bank .Finally, a number of studies found trust and perceived risks have a significant positive influence on commitment and ultimately leads towards overall satisfaction Reputation of a service provider is another important factor affecting trust

3. Application

- [1] Banks and other financial institutions: Personal and business customers making cash/cheque deposit.
- [2] Local Government Offices: Payment of rents, taxes, court fines, parking fines.
- [3] Utility company Offices:
Payment of water, gas, electricity, telephone bills.
- [4] Transport: Airline cabin crew, bus or train drivers and conductors who need to deposit fares or payments received.
- [5] Retail Outlets :Convenient cash deposit system for daily takings and offers customers a paying in point for store cards

4. Conclusion

With incorporation of cash deposit machine we will be able to solve the problems like fake note detection. Main purpose of cash deposit machine is to provide flexibility depositing money 24x7 in particular bank account so that we could get lead from queuing in front of bank window and inconvenience in time availability. Reduction in queuing time increases customer satisfaction. It also improves speed of deposit and level of convenience with security.

References

- [1] Bhandari v.b. "Design of machine element"
- [2] www.posb.com.sg/posb/others/cam/default
- [3] www.bankmuscat.com/en-us/ConsumerBanking/ExpatServices/Pages/CDM.aspx
- [4] www.atmmarketplace.com
- [5] www.glory-global.com
- [6] www.banking-automation.com
- [7] Balto, D. and J. Mc Andrews (1998) "Joint Venture Payment Networks and Public Policy," Electronic Banking Report,
- [8] www.atmia.com/ClassLibrary/Page/Information/DataInstances/1690/Files/657/Future_of_Cash_Article_-2.pdf
- [9] www.leaninnovations.ca/seven
- [10] Mc Andrews, James (1998) "ATM Surcharges," Federal Reserve Bank of New York

Simulink Design Of Pipelined CORDIC For Generation of Sine and Cosine Values

Richa Upadhyay¹, Dr. Nisha Sarwade², Shrugal Varde³

^{1,2,3}Electrical Department, V.J.T.I. Mumbai

Abstract

In recent researches, there are countless applications where sine and cosine wave are used, like in Physics, Digital Signal Processing for various transforms, several modulation and demodulation techniques etc. There are numerous ways to generate digital sine and cosine waves, the use of previously calculated tables is one of the choices, but it requires excessive memory usage when good quantization level is needed. CORDIC algorithm, on the other hand, offers an excellent alternative, and its best characteristic is flexibility. Its quantization accuracy is a function of word length. In this paper a simple Pipelined CORDIC structure for generation of sine and cosine values has been implemented and verified using Simulink tool by MATLAB.

Keywords: CORDIC, Simulink, Pipeline Architecture, Shift And Add, Trigonometric, Unscaled, HDL, Hardwired.

I. Introduction

The CORDIC is hardware-efficient algorithms for computation of trigonometric and other elementary functions by only shift and adds operations. The CORDIC set of algorithms for the computation of trigonometric functions was designed by Jack E. Volder in 1959 to help building a real-time navigational system for the B-58 bomber [1]. Later, J. Walther in 1971 extended the CORDIC scheme to other functions [2]. The CORDIC method of functional computation is used by most calculators (such as the ones by Texas Instruments and HP) to approximate the normal transcendental functions.

The popularity of CORDIC was very much enhanced there-after primarily due to its potential for efficient and low-cost implementation of a large class of applications which include: the generation of trigonometric, logarithmic and transcendental elementary functions; complex number multiplication, Eigen-value computation, matrix inversion, solution of linear systems and singular value decomposition (SVD)[4] for signal processing, Fourier and related Transforms[3], image processing, and general scientific computation. Some other popular and upcoming applications are:

- [1] Direct frequency synthesis, digital modulation and coding for speech/music synthesis and communication;
- [2] Direct and inverse kinematics computation for robot manipulation;
- [3] Planar and three-dimensional vector rotation for graphics and animation

Although CORDIC may not be the fastest technique to perform these operations, it is attractive due to the simplicity of its hardware implementation, since the same iterative algorithm could be used for all these applications using the basic shift-add operations. In this paper, our purpose is to demonstrate the utility of the simulation tool Simulink by MATLAB to implement the basic CORDIC algorithm for calculating the trigonometric values. Simulink, developed by MathWorks, is a data flow graphical programming language tool for modeling, simulating and analyzing multidomain dynamic systems. Its primary interface is a graphical block diagramming tool and a customizable set of block libraries. It offers tight integration with the rest of the MATLAB and XILINX environment and can either drive them or be scripted from them. Simulink is widely used in control theory and digital signal processing for multidomain simulation and Model-Based Design. The remainder of this paper is organized as follows. In Section II, describes the principles of CORDIC operation, covering the elementary ideas from coordinate transformation to rotation mode and vectoring model operations. In section III, the implementation of CORDIC for calculation of sine and cosine values is discussed. The CORDIC architecture applied for this paper has been described in Section IV along with its implementation in Simulink. The conclusion along with future research directions are discussed in Section V.

2. Basic Cordic Algorithm

The CORDIC algorithm performs a planar rotation as shown in Fig 1. Graphically, planar rotation means transforming a vector (X_i, Y_i) into a new vector (X_j, Y_j) . Using a matrix form, a planar rotation for a vector of (X_i, Y_i) is defined as-

$$\begin{bmatrix} X_j \\ Y_j \end{bmatrix} = \begin{bmatrix} \cos \theta & -\sin \theta \\ \sin \theta & \cos \theta \end{bmatrix} \begin{bmatrix} X_i \\ Y_i \end{bmatrix} \quad (1)$$

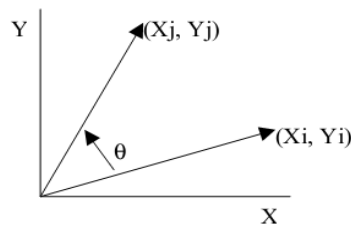


Fig-1: Planar rotation of a vector

The θ angle rotation can be executed in several steps, using an iterative process. Each step completes a small part of the rotation. Many steps will compose one planar rotation. A single step is defined by the following equation:

$$\begin{bmatrix} X_{n+1} \\ Y_{n+1} \end{bmatrix} = \begin{bmatrix} \cos \theta_n & -\sin \theta_n \\ \sin \theta_n & \cos \theta_n \end{bmatrix} \begin{bmatrix} X_n \\ Y_n \end{bmatrix} \quad (2)$$

Here n = no. of iterations. Equation 2 can be modified by eliminating the $\cos \theta_n$ factor.

$$\begin{bmatrix} X_{n+1} \\ Y_{n+1} \end{bmatrix} = \cos \theta_n \begin{bmatrix} 1 & -\tan \theta_n \\ \tan \theta_n & 1 \end{bmatrix} \begin{bmatrix} X_n \\ Y_n \end{bmatrix} \quad (3)$$

Equation 3 requires three multiplies, compared to the four needed in equation 2. Additional multipliers can be eliminated by selecting the angle steps such that the tangent of a step is a power of 2. Multiplying or dividing by a power of 2 can be implemented using a simple shift operation. The angle for each step is given by eq (4) and All iteration angles summed must equal the rotation angle θ as in eq (5).

$$\theta_n = \arctan \left(\frac{1}{2^n} \right) \quad (4)$$

$$\sum_{n=0}^{\infty} S_n \theta_n = \theta \quad (5)$$

Where $S = \{+1, -1\}$

This results in the following equation for $\tan \theta_n$

$$\tan \theta_n = S_n 2^{-n} \quad (7)$$

Combining equation 3 and 7 results in-

$$\begin{bmatrix} X_{n+1} \\ Y_{n+1} \end{bmatrix} = \cos \theta_n \begin{bmatrix} 1 & -S_n 2^{-n} \\ S_n 2^{-n} & 1 \end{bmatrix} \begin{bmatrix} X_n \\ Y_n \end{bmatrix} \quad (8)$$

Besides for the $\cos \theta_n$ coefficient, the algorithm has been reduced to a few simple shifts and additions. The coefficient can be eliminated by pre-computing the final result. The first step is to rewrite the coefficient.

$$\cos \theta_n = \cos \left(\arctan \left(\frac{1}{2^n} \right) \right) \quad (9)$$

The second step is to compute equation 9 for all values of 'n' and multiplying the results, which we will refer to as K.

$$K = \frac{1}{P} = \prod_{n=0}^{\infty} \cos \left(\arctan \left(\frac{1}{2^n} \right) \right) \approx 0.60725 \quad (10)$$

K is constant for all initial vectors and for all values of the rotation angle; it is normally referred to as the congrate constant.

Because the coefficient K is pre-computed and taken into account at a later stage, equation 8 may be written as

$$\begin{bmatrix} X_{n+1} \\ Y_{n+1} \end{bmatrix} = \begin{bmatrix} 1 & -S_n 2^{-n} \\ S_n 2^{-n} & 1 \end{bmatrix} \begin{bmatrix} X_n \\ Y_n \end{bmatrix} \quad (11)$$

or as

$$X_{n+1} = X_n - S_n 2^{-n} Y_n, \quad Y_{n+1} = Y_n + S_n 2^{-n} X_n \quad (12)$$

At this point a new variable called 'Z' is introduced. Z represents the part of the angle θ which has not been rotated yet.

$$Z_{n+1} = \theta - \sum_{i=0}^n \theta_i \quad (13)$$

Combining equations 5 and 13 results in a system which reduces the not rotated part of angle θ to zero.

$$Z_{n+1} = Z_n - S_n \arctan \left(\frac{1}{2^n} \right) \quad (14)$$

Thus the basic CORDIC equations are –

$$X_{n+1} = X_n - S_n 2^{-n} Y_n$$

$$Y_{n+1} = Y_n + S_n 2^{-n} X_n$$

$$Z_{n+1} = Z_n - S_n \arctan \left(\frac{1}{2^n} \right)$$

So, the CORDIC method evaluates elementary functions merely by table-look-up, shift and add operations. A small number (of the order of n, where n bits of precision is required in the evaluation of the functions) of pre-calculated fixed constants is all that is required to be stored in the look-up table. The CORDIC algorithm has nice geometrical interpretations: trigonometric, exponential, multiply functions are evaluated via rotations in the circular, hyperbolic and linear coordinate systems, respectively. Their inverses (i.e., inverse trigonometric functions, logarithm and division) can be implemented in a “vectoring” mode in the appropriate coordinate system. Thus, there exist two modalities of CORDIC algorithm, **VECTORING** and **ROTATION** mode. In vectoring mode, coordinates (X_n, Y_n) are rotated until Y_n converges to zero. In rotation mode, initial vector (X_n, Y_n) starts aligned with the x axis and is rotated by an angle of θ_i every cycle, so after n iterations, θ_n is the obtained angle. Also,

$$S_n = \begin{bmatrix} \text{sign}(Z_n) & \text{for rotation mode} \\ -\text{sign}(Y_n) & \text{for vectoring mode} \end{bmatrix}$$

Hence, in ROTATION MODE

$$S_n = \begin{bmatrix} 1 & ; & Z_n > 0 \\ -1 & ; & Z_n \leq 0 \end{bmatrix}$$

And in VECTORING MODE

$$S_n = \begin{bmatrix} -1 & ; & Y_n > 0 \\ 1 & ; & Y_n \leq 0 \end{bmatrix}$$

3. CORDIC Theory for Trigonometric Functions

3.1 SINE AND COSINE

The rotation mode CORDIC operation can simultaneously compute the sine and cosine of the input angle. Setting the y component of the input vector to zero reduces the rotation mode result to:

$$x_n = \frac{1}{K} \cdot x_0 \cos z_0, \quad y_n = \frac{1}{K} \cdot x_0 \sin z_0$$

By setting x_0 to K the rotation produces unscaled sine and cosine of angle argument, z_0 . Very often sine cosine values modulate a magnitude value. Using other techniques (for example: look up table) requires a pair of multipliers to obtain the modulation. The CORDIC technique performs the multiply as a part of rotation operation, and therefore eliminates the need for a pair of explicit multipliers. The output of CORDIC rotator is scaled by the rotator gain. If the gain is not acceptable, a single multiply by the reciprocal of gain constant placed before CORDIC rotator will yield unscaled results. It is worth noting that the hardware complexity of CORDIC rotator is approximately similar to that of a single multiplier with the same word size.

Summary:

Mode: Rotation mode

Initial values: $[x, y, z] = [K, 0, \theta]$ (θ = input angle)

Direction: Reduce z to Zero

Output: $[x, y, z] = [\cos \theta, \sin \theta, 0]$

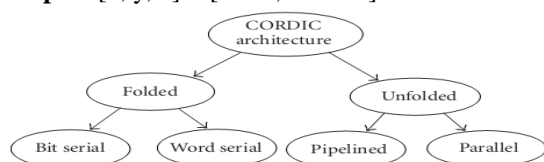


Fig-2: Taxonomy of CORDIC architectures

4. Proposed Cordic Architecture

As in fig-2, there are number of ways to implement CORDIC processor. The ideal architecture depends on the speed versus area tradeoff in the intended application. The CORDIC algorithm has traditionally been implemented using bit serial architecture with all iterations executed in the same hardware [6]. This slows down the computational device and hence, is not suitable for high speed implementation. For this paper we use a **Pipelined Architecture** [6, 10]. Instead of buffering the output of one iteration and using the same resources again, one could simply cascade the iterative CORDIC, which means rebuilding the basic CORDIC structure for each iteration. Consequently, the output of one stage is the input of the next one, as shown in Fig. 6, and in the face of separate stages two simplifications become possible. First, the shift operations for each step can be performed by wiring the connections between stages appropriately. Second, there is no need for changing constant values and those can therefore be hardwired as well. The purely unrolled design only consists of combinatorial components. Input values find their path through the architecture on their own and do not need to be controlled. While implementation a single iteration of the basic CORDIC structure like in fig-4, the Generic resource report which is obtained from the HDL code generator of Simulink is as follows:

Multipliers	0
Adders/Subtractors	6
Registers	0
RAMs	0
Multiplexers	6

Fig-3: Resource report of a Single CORDIC iteration

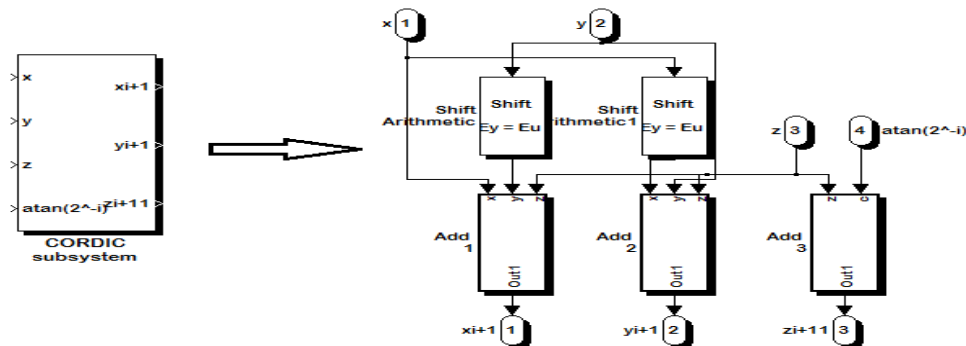


Fig-4: Hardware implementation of single CORDIC iteration

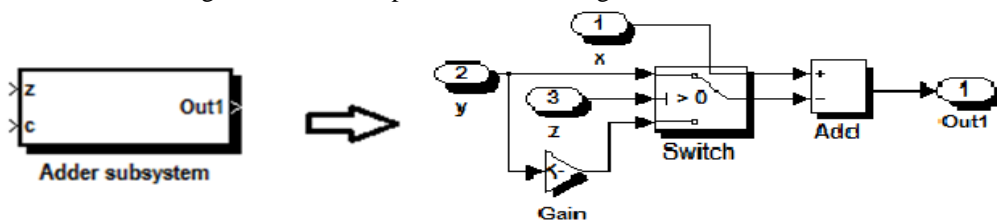


Fig-5: The Addition/Subtraction Logic Subsystem

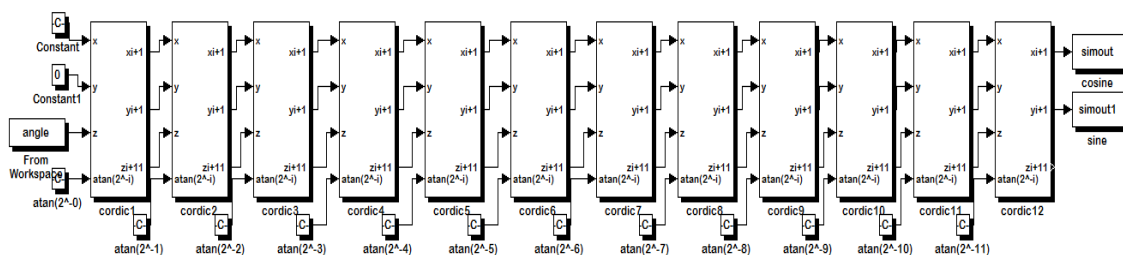
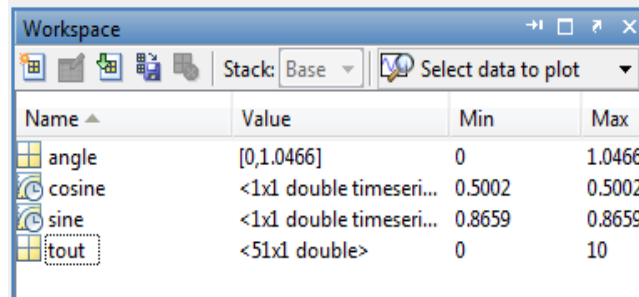


Fig-6: Pipeline architecture of CORDIC for sine and cosine.



Name	Value	Min	Max
angle	[0,1.0466]	0	1.0466
cosine	<1x1 double timeseri...	0.5002	0.5002
sine	<1x1 double timeseri...	0.8659	0.8659
tout	<51x1 double>	0	10

Fig-7: Output obtained on the workspace window

Here the input angle is 60° i.e. 1.0466 radians and

as shown in the figure above the output values attained are: $\sin 60^{\circ} = 0.8659$ and $\cos 60^{\circ} = 0.5002$.

5. Conclusion

In this paper simple calculation of sine and cosine of the input angles is done, CORDIC algorithm is implemented by using simple hardware through repeated shift-add operations and this is the feature which makes it attractive for a wide variety of applications. The code above implements a pipeline algorithm of a 12-stage CORDIC operating within the rotation mode. Here since the number of shifts to be performed by the shifters at different stages is fixed (shift-operation through i bit positions is performed at the i^{th} stage), the shift operations could be hardwired with adders.

The same is the case with the constant arctan (2^{-i}). This is to help reduce the no. of resources and also the latency of computation. In all of these ways, the CORDIC algorithm proves its merit as a simple but powerful algorithm that all FPGA designers should be aware of. Using CORDIC algorithm to generate these waveforms can, if correctly done, result in a high spurious-free dynamic range. Good SFDR performance is required for most signal-processing applications. Also, Simulink being a graphical language makes it easy to implement and understand the physical meaning of CORDIC. As future work the HDL code (can be VHDL or VERILOG) can be generated from the Simulink graphical program and can further be used on FPGA. Also the implementation of the CORDIC algorithm can be done on FPAA (Field Programmable Analog Array), the analog cousin of FPGA by using SIM2SPICE tool that automatically converts analog systems from Simulink design to Spice netlist and further the placing and routing can be done on FPAA with the help of other tools.

References

- [1] J. E. Volder, "The CORDIC Trigonometric Computing Technique," IRE Trans. on Electronic Computers, vol. EC-8, pp. 330-334, Sep. 1959.
- [2] J. S. Walther, "A unified Algorithm for Elementary Functions," in Proceedings of the 38th Spring Joint Computer Conference, pp. 379-385, 1971
- [3] A. M. Despain, "Fourier Transform Computers Using CORDIC Iterations," IEEE Transactions on Computers, vol. C-30, pp. 993-1001, Oct. 1974
- [4] J. R. Cavallaro and F. T. Luk, "CORDIC Arithmetic for a SVD processor," Journal of Parallel and Distributed Computing, vol. 5, pp. 271-290, 1988.
- [5] J. Duprat and J. Muller, "The CORDIC Algorithm: New Results for Fast VLSI Implementation," IEEE Transactions on Computers, vol. 42, no. 2, pp. 168-178, 1993.
- [6] J. P. Meher, J. Valls, T. Juang, K. Sridharan and K. Maharatna, "50 Years of CORDIC: Algorithms, Architectures, and Applications," IEEE Transactions on Circuits and Systems, vol. 56, no. 9, pp. 1893-1907, 2009.
- [7] E. O. Garcia, R. Cumplido, M. Arias, "Pipelined CORDIC Design on FPGA for a Digital Sine and Cosine Waves Generator," 3rd IEEE Transactions on Computers, vol. 59, no. 4, pp. 522-531, 2010.
- [8] R. Bhakthavathalu, M. Sinith, P. Nair and K. Jismi, "A Comparison of Pipelined Parallel and Iterative CORDIC Design on FPGA," International Conference on Industrial and Information Systems, pp. 239-243, 2010
- [9] Vladimirova, T. and Tiggler, "FPGA Implementation of Sine and Cosine Generators Using the CORDIC Algorithm", Proc. of Military and Aerospace Application of Programmable Devices and Technologies Conference (MAPLD 99), Sep. 1999, Laurel, MA, A-2, pp. 28-30.
- [10] Naveen Kumar and Amandeep Singh Sappal "Coordinate Rotation Digital Computer Algorithm: Design and Architectures", International Journal of Advanced Computer Science and Applications, Vol. 2, No. 4, 2011, pp 68-71.
- [11] "System Generator for DSP user guide", UG640 (v 12.1) April 19, 2010.

Discrimination of Fault from Non-Fault Event in Transformer Using Concept of Symmetrical Component

¹Mr. R.V.KATRE, ²Prof. Mr. D. S. Chavan, ³Prof.S.S.Sardey

Abstract

In this paper a overcurrent protection using concept of symmetrical component for power transformer is presented .first we review the concept of symmetrical component. Secondly we investigate how the concept of symmetrical component can be used to improve the transformer protection scheme and how it helps to discriminate the fault and non fault events. For this an algorithm and discrimination criteria is analysed for various fault condition and switching event.

Keywords : Fault, overcurrent relay, symmetrical Components, type of Faults, Transformer energizing, PSCAD, Switching event

1. Introduction

The Concept of symmetrical components provides a practical technology for understanding and analyzing power system operation during unbalanced conditions such as those caused by faults between phases and/or ground, open phases, unbalance impedances, and so on. Also, many protective relays operate from the symmetrical component quantities. Thus a good understanding of this subject is of great value and a very important tool in protection.

1.1 Methodology For Improved Protection Schemes:

For any unbalanced or nonsymmetrical network, such as unsymmetrical fault occurs or having unbalanced load, symmetrical component conversion can decouple three-phase system into three independent sequence equivalent networks, namely positive, negative and zero sequence network. Therefore these three sequence networks can be analyzed separately. Then we can convert the sequence value back into phase variables. This analysis procedure is commonly used in analyzing the unbalanced system network, including fault. Symmetrical components can be viewed as a mathematical tool on which we can entirely based to analysis system without converting back to phase variable. For example, the amplitude of zero sequence signifies the degree of unbalance, and therefore can be used to detect the unbalanced fault.

1.2 Theoretical background

The symmetrical component transformation for an arbitrary three-phase set of variables (balanced or unbalanced), for example the three-phase current, and inverse transformation is given in (1) and (2).

$$\begin{bmatrix} I_0 \\ I_1 \\ I_2 \end{bmatrix} = \frac{1}{3} \times \begin{bmatrix} 1 & 1 & 1 \\ 1 & \alpha & \alpha^2 \\ 1 & \alpha^2 & \alpha \end{bmatrix} \times \begin{bmatrix} I_a \\ I_b \\ I_c \end{bmatrix} \text{----- (1)}$$

Here I_1 , I_2 and I_0 denote the positive, negative and zero sequences respectively. And $\alpha = 1 \angle 120^\circ = -0.5 + j0.866$

In general application in power system analysis, we typically begin with information in “phase variables” denoted by subscripts a, b, and c. Note that phase variables corresponds to actual physical quantities. The value of converting physical quantities to symmetrical components is in visualizing and quantization the degree of unbalanced system network. For a balanced three-phase system, it won't be difficult to calculate that the zero and negative sequences are zero, and the positive sequence is equal to phase a, no matter current or voltage.

2. Operation And Principle Of Overcurrent Relays

There are two characteristics for overcurrent relays:

- 1) definite- time characteristic and 2) inverse-time characteristic. In the definite-time characteristic relays, if the current amplitude exceeds a pre-defined value, the relay trips after a definite time. In the protection of motors, these relays are used to prevent the unbalanced operation of the motors. According to IEC standard [19], the characteristic of inverse time overcurrent relays (excluding induction type) is depicted by the following expression:

$$T = \frac{C}{\left(\frac{I}{I_s}\right)^{\alpha} - 1} \text{----- (2)}$$

T- the relay operation time;
C- constant for relay characteristic;
I_s-current setting threshold;
I- current detected by relay (normally the effective value) ; *I* > *I_s*
α- constant representing inverse-time type *α* > 0
 By assigning different values to *α* and *C*, different types of inverse characteristics are obtained.

2.1 Proposed Algorithm

Any three-phase voltage and current consist of three components in sequence space which are related to each other as follows:

$$\begin{bmatrix} I_0 \\ I_1 \\ I_2 \end{bmatrix} = \frac{1}{3} \times \begin{bmatrix} 1 & 1 & 1 \\ 1 & \alpha & \alpha^2 \\ 1 & \alpha^2 & \alpha \end{bmatrix} \times \begin{bmatrix} I_a \\ I_b \\ I_c \end{bmatrix}$$

Here *I₁*, *I₂* and *I₀* denote the positive, negative and zero sequences respectively. And $\alpha = 1 \angle 120^\circ = -0.5 + j0.866$

Also $1 + \alpha + \alpha^2 = 0$ if currents *I_a*, *I_b* and *I_c* are balanced (i.e., *I_a* = *I* ∠ 0, *I_b* = *I* ∠ -120° and *I_c* = *I* ∠ +120°). So existence of the negative components means that the system is unbalanced. except over a transient period that may be as a result of different switching method or non identical saturated case of three-phase transformers, three phases are almost affected simultaneously during switching event. Consequently, the negative component is not considerably changed in this case. On the other hand, faults are classified into symmetrical and asymmetrical parts. The major feature of these faults is the large value of the negative component, such that there are the theoretical following cases-

For phase-ground fault

$$I_2 = I_1 = \frac{V_f}{Z_0 + Z_1 + Z_2 + (3Z_f)} \text{..... (4)}$$

Where *Z_f* is the fault impedance between the line and ground *Z₀*, is the zero component impedance *Z₁*, is the positive component impedance, and *Z₂* is the negative component impedance.

For phase-phase fault:

$$I_2 = -I_1 = \frac{V_f}{Z_1 + Z_2 + Z_f} \text{..... (5)}$$

For phase-phase- ground fault:

$$I_2 = (-I_1) \times \frac{Z_0 + 3Z_f}{Z_0 + 3Z_f + Z_2} \text{..... (6)}$$

Therefore, the negative component in the asymmetrical faults is considerable. For symmetrical faults the negative component tends to zero. Not often, the three-phase fault occurs and the negative component of the current is negligible and almost equal to zero similar with the switching case. The criterion function for discriminating fault from nonfault switching is defined as follows

. The criterion function for discriminating fault from non fault switching is defined as follows:

$$R = \frac{|I_1| - |I_2|}{|I_1| + |I_2|} \text{----- (7)}$$

Since there is a considerable negative component in the asymmetrical fault case, according to criterion function the value of *R* is close to zero. In the switching case, the negative component is very small and *R* is close to 1. In the switching case, the negative component is very small and *R* is close to 1. Except over a transient period that may be as a result of different switching methods or a non identical saturated case of three-phase transformers, three phases are almost affected simultaneously and the three-phase network has not a major

unbalance, during the switching event. In the calculation of I_2 and I_1 in equation (1), I_a , I_b , and I_c are phasor value (amplitude of the fundamental harmonic). Therefore, dc values and its harmonics are largely eliminated. So the difference in dc value in the current is not important. According to the above, $R < 0.35$ indicates the fault; otherwise, over current is the result of switching. The suggested criterion is based on the different behavior of the current components during fault and non fault conditions and is independent of the amplitude of the current which is advantageous. The reason is that it operates based on the relative difference between the negative and positive component of the current. Another advantage of the suggested criterion function is that its proper operation is independent of the power system balancing. Actually, the suggested criterion function in the asymmetrical distribution networks also operates properly. The reason is that during the asymmetrical fault, the negative component of current increases and the value of R is much smaller than that before fault event. Thus, it is enough that the threshold value be lower than at the value of R in the normal state of the network.

3. Simulation

To show the advantage of the proposed algorithm, a part of a distribution system shown in Fig.1 is modeled; using the EMTDC/ PSCAD package. The network parameter of the 2-bus distribution system is illustrated in this figure. Several nonfault events are applied to this system along with some short circuit events at different times. The simulation results show that how the proposed algorithm could help the overcurrent relay to discriminate fault from nonfault events. The following cases are presented here:

- Transformer energizing;
- Induction motor starting;

4. Transformer Energizing

When the primary winding of an unloaded transformer is switched on to normal voltage supply, it acts as a nonlinear inductor. In this situation there is a transient inrush current that is required to establish the magnetic field of the transformer. The magnitude of this current depends on the applied voltage magnitude at the instant of switching, supply impedance, transformer size and design. Residual flux in the core can aggravate the condition. The initial inrush current could reach values several times full load current and will decay with time until a normal exciting current value is reached. The decay of the inrush current may vary from as short as 20 cycles to as long as minutes for highly inductive circuits. The inrush current contains both odd and even order harmonics. In order to study a transformer energizing, various inrush current conditions were simulated at different parts of the power system. Various parameters which have considerable effect on the characteristic of the current signal (e.g., core residual magnetization, nonlinearity of transformer core and switching instant) were changed and the current signal was analyzed by the proposed method. In all cases, correctness of the proposed algorithm has been proved.

Malfunctioning of transformers is mainly because of following reasons:

Due to magnetizing inrush current, Harmonics generated due to occurrence of internal faults, Short Circuit in core winding, Symmetrical or Asymmetrical Faults Symmetrical components consist of three quantities: positive-sequence (exists during all system conditions, but are prevalent for balanced conditions on a power system including three-phase faults); negative-sequence (exist during unbalanced conditions); zero-sequence (exist when ground is involved in an unbalanced condition). Negative and zero-sequence components have relatively large values during unbalanced fault conditions on a power system and can be used to determine when these fault conditions occur. Negative-sequence components indicate phase-to-phase, phase-to-ground, and phase-to-phase-to-ground faults. Zero sequence components indicate phase-to-ground and phase -to-phase-to-ground faults

4.1 Inrush due to switching-in

Initial magnetizing due to switching a transformer in is considered the most severe case of an inrush. When a transformer is de-energized (switched-off), the magnetizing voltage is taken away, the magnetizing current goes to zero while the flux follows the hysteresis loop of the core. This results in certain remanent flux left in the core. When, afterwards, the transformer is re-energized by an alternating sinusoidal voltage, the flux becomes also sinusoidal but biased by the remanence. The residual flux may be as high as 80-90% of the rated flux, and therefore, it may shift the flux-current trajectories far above the knee-point of the characteristic resulting in both large peak values and heavy distortions of the magnetizing current. A detailed study of a typical case is presented below. In this case transformer at busbar 1-2 is switched on at instant $t = 0.25s$ and three-phase currents are measured at busbar 7. Fig. 2 shows these three-phase currents. As shown in Fig. 3, except over a transient period, R is close to 1 and is larger than setting $R = 0.35s$ that shows nonfault case. In this case tripping signal is prevented.

4.2 Fault

In this case a phase-ground fault (A-G) occurs at busbar 1 at instant $t = 0.25s$ and three-phase currents are measured at busbar 7. Fig. 4 shows these three-phase currents. As shown in Fig. 5, R is close to zero that shows a fault case in which the tripping signal is issued.

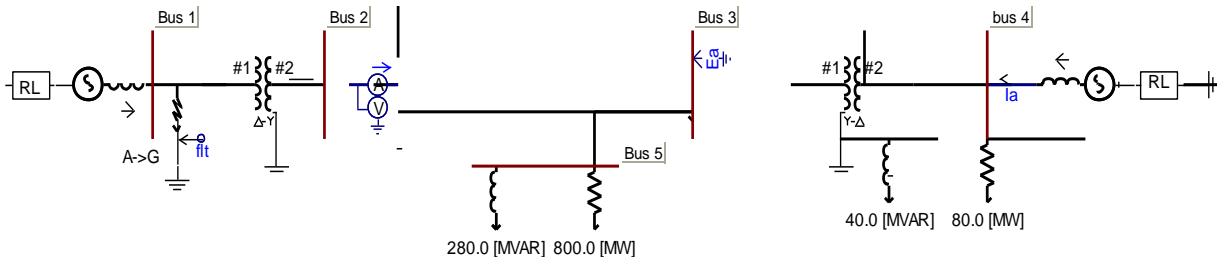


Fig 1. 5-bus system model

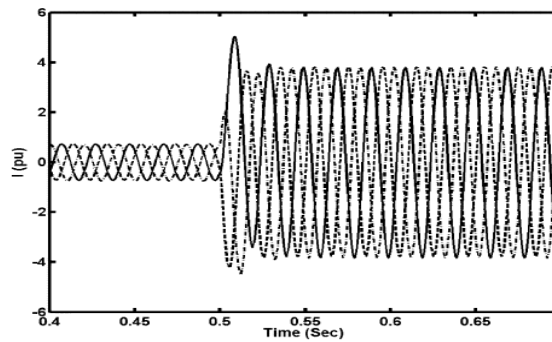


Fig.2. 3- phase current due to transformer energizing

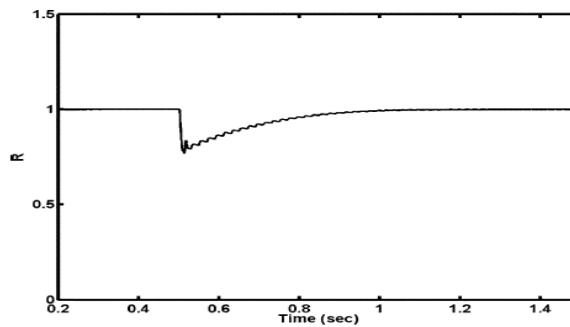


Fig 3. Value of R versus time due to transformer Energizing

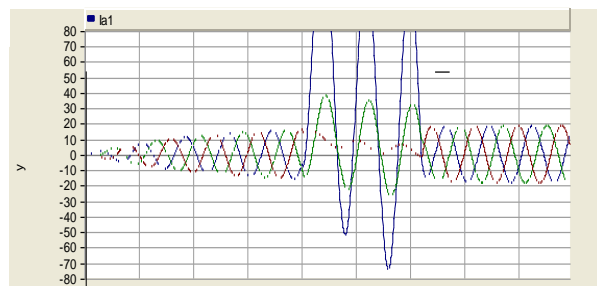


Fig 4 Three phase current due to fault (A-G)

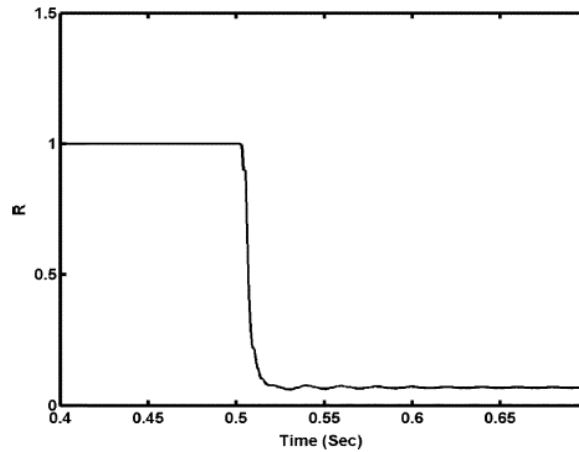


Fig. 5 Value of R versus time due to fault (A-G)

Three-phase currents are measured at the busbar 1 Fig. 4 shows these currents is close to zero which indicates that there is a fault and the relay trips. In fact, one more advantage of the suggested algorithm is that, in addition to the diagnosis of the fault in the individual occurrence from the nonfault case, it enables to discriminate a fault from simultaneous switching properly. This is necessary because, if in the case of fault, the operation of the relay is prevented and it is assumed switching case, it may lead to a serious damage.

5. Theoretical Analysis

Sr No.	Calculated Parameter	Value	Value
Positive and negative Sequence Network parameters			
	Transmission line voltage base	3.2Kv	12
	Motor line Voltage base	8 Kv	13.
	% Reactance of transformer	43%	7.8
	% Reactance of motor	6%	24.
	% Reactance of line	7%	16.
Zero Sequence Network parameters			
	% Neutral Reactance	5%	94.
	% Reactance of transformer	43%	7.8
	% Reactance of line	6%	41.
	% Reactance of line	7%	16.

6. Conclusion

In this paper, from simulations results it indicates that enhanced sensitivity can be achieved with a symmetrical component based overcurrent protection. Also the paper presents a new algorithm- overcurrent protection based on symmetrical component and shows vastly improved performance over conventional techniques, to discriminate fault and non fault events like switching and magnetizing inrushes in transformer. Undesirable operation of relay due to the switching is prevented. The capability of the new method has been demonstrated by simulating various cases on a suitable power system for various types of asymmetrical faults.

7. Future Scope

Here only the fault cases related to Transformer is studied but in future it can be studied for Alternator, Turbo-generators etc.

Reference

[1] F. Wang and M. H. J. Bollen, "Quantification of transient current signals in the viewpoint of overcurrent relays," in Proc. Power Eng. Soc. General Meeting, Jul. 13–17, 2003, vol. 4, pp. 2122–2127.

[2] "Classification of component switching transients in the viewpoint of protection relays," *Elect. Power Syst. Res.*, vol. 64, pp. 197–207, 2003.

[3] J. H. Brunke and H. J. Frohlich, "Elimination of transformer inrush currents by controlled switching-Part II: Application and performance considerations," *IEEE Trans. Power Del.*, vol. 16, no. 2, pp. 281–285, Apr. 2001.

[4] M. A. Rahman and B. Jeyasurya, "A state-of-the-art review of transformer protection algorithms," *IEEE Trans. Power Del.*, vol. 3, no. 2, pp. 534–544, Apr. 1988.

[5] P. Liu, O. P. Malik, C. Chen, G. S. Hope, and Y. Guo, "Improved operation of differential protection of power transformers for internal faults," *IEEE Trans. Power Del.*, vol. 7, no. 4, pp. 1912–1919, Oct. 1992.

[6] T. A. Sidhu, M. S. Sachdev, H. C. Wood, and M. Nagpal, "Design, implementation and testing of a micro-processor-based high-speed relay for detecting transformer winding faults," *IEEE Trans. Power Del.*, vol. 7, no. 1, pp. 108–117, sJan. 1992, .

[7] K. Yabe, "Power differential method for discrimination between fault and magnetizing inrush current in transformers," *IEEE Trans. Power Del.*, vol. 3, no. 3, pp. 1109–1117, Jul. 1997.

[8] P. Bastard, M. Meunier, and H. Regal, "Neural network-based algorithm for power transformer differential relays," *Proc. Inst. Elect. Eng. C*, vol. 142, no. 4, pp. 386–392, 1995.

[9] M. C. Shin, C. W. Park, and J. H. Kim, "Fuzzy logic-based for large power transformer protection," *IEEE Trans. Power Del.*, vol. 18, no. 3, pp. 718–724, Jul. 2003.

[10] A. T. Johns and S. K. Salman, *Digital Protection for Power Systems*. Stevenage, U.K.: Peregrinus, 1995.

[11] S. Emmanouil, M. H. J. Bollen, and I. Y. H. Gu, "Expert system for classification and analysis of power system events," *IEEE Trans. Power Del.*, vol. 17, no. 2, pp. 423–428, Apr. 2002.

[12] W. A. Elmore, C. A. Kramer, and S. E. Zocholl, "Effects of waveform distortion on protective relays," *IEEE Trans. Ind. Appl.*, vol. 29, no. 2, pp. 404–411, Mar./Apr. 1993.

[13] J. F. Witte, F. P. Decesaro, and S. R. Mendis, "Damaging long-term over voltages on industrial capacitor banks due to transformer energization inrush currents," *IEEE Trans. Ind. Appl.*, vol. 30, no. 4, pp. 1107–1115, Jul./Aug. 1994.

[14] R. Rudenberg, *Transient Performance of Electric Power System*. Cambridge, MA: MIT Press, 1965.

[15] Improved Overcurrent Protection Using Symmetrical Components Saeed Lotfi-fard, Student Member, IEEE, Jawad Faiz, Senior ion of Member, IEEE, and Reza Irvani, Fellow, IEEE

[16] Overcurrent Protection Solution based on symmetrical component Method; Mr. K. K. Rajput, Mrs. K. D. Thakur Mrs. C. H. Chavan, *Journal of Information ,knowledge and research in electronics and communication engineering*, ISSN 0975-6779,Nov 10 to Oct 11 ,Vol-01,issue-02.



Rohit Katre: M.Tech Student in Electrical Power Systems, Bharati Vidyapeeth Deemed University College of Engineering, Pune, Maharashtra, India



Prof.D.S.Chavan: Ph D (Registered), ME (Electrical), BE (Electrical), DEE Associate Professor, Co-Ordinator (R&D Cell), Co-Ordinator (PH.D.Programme Management) Bharati Vidyapeeth Deemed University College Of Engineering Pune 411043. He Is Pursuing Ph D. He Received ME (Electrical)(Power Systems) Achieved Rank Certificate In Pune University For ME

Prof. S.S.sardey.: ME (Electrical Power system), BE (Electrical), Assistant Professor, Bharati Vidyapeeth Deemed University College Of Engineering Pune 411043.

Image Segmentation and Classification of Mri Brain Tumors Based On Cellular Automata and Neural Network

R.Fany Jesintha Darathi¹, K.S.Archana²

¹ student in Vels University, M.E Computer Science, Chennai

² Assist. Professor in Vels University, M.E. Computer Science, Chennai

Abstract:

Cellular automata (CA) based seeded tumor segmentation method on magnetic resonance (MR) images, which uses Region of interest and seed selection. The region of tumor is selected from the image for getting seed point from abnormal region. This seed is selected by finding Co occurrence feature and run length features. Seed based segmentation is performed in the image for detecting the tumor region by highlighting the region with the help of level set method. The brain images are classified into three stages Normal, Benign and Malignant. For this non knowledge based automatic image classification, image texture features and Artificial Neural Network are employed. The conventional method for medical resonance brain images classification and tumors detection is by human inspection. Decision making is performed in two stages: Feature extraction using Gray level Co occurrence matrix and the Classification using Radial basis function which is the type of ANN. The performance of the ANN classifier is evaluated in terms of training performance and classification accuracies. Artificial Neural Network gives fast and accurate classification than other neural networks and it is a promising tool for classification of the tumors.

Segmentation of brain tissues in gray matter, white matter and tumor on medical images is not only of high interest in serial treatment monitoring of “disease burden” in oncologic imaging, but also gaining popularity with the advance of image guided surgical approaches. Outlining the brain tumor contour is a major step in planning spatially localized radiotherapy (e.g., Cyber knife, iMRT) which is usually done manually on contrast enhanced T1-weighted magnetic resonance images (MRI) in current clinical practice. On T1 MR Images acquired after administration of a contrast agent (gadolinium), blood vessels and parts of the tumor, where the contrast can pass the blood–brain barrier are observed as hyper intense areas. There are various attempts for brain tumor segmentation in the literature which use a single modality, combine multi modalities and use priors obtained from population atlases. Using gray scale, spatial information and thresholding method, region growing was applied to segment the region. The region of tumor is selected from the image for getting seed point from abnormal region. This seed is selected by finding Co occurrence feature and run length features. Seed based segmentation is performed in the image for detecting the tumor region by highlighting the region with the help of level set method.

I. Introduction

Ultrasound image segmentation is a critical issue in medical image analysis and visualization because these images contain strong speckle noises and attenuation artifacts. It is difficult to properly segment the interested objects with correct position and shape. In addition, poor image contrast and missing boundaries is a challenging task. Large numbers of different methods was proposed on ultrasound medical image segmentation. Some of them use a semi automated approach and need some operator interaction. Others are fully automatic and the operator has only a verification role. These methods can be represented by threshold based technique, boundary based methods, region based methods, mixture techniques that combined boundary and region criteria and active contour based approaches. Threshold technique uses only gray level information and do not consider the spatial information of the pixels and do not manage well with noise or poor boundaries which generally encountered in ultrasound images. Boundary based methods use the gradient of pixel values at the boundary between adjacent regions. In these methods an algorithm searches for pixels with high gradient values that are usually edge pixels and then tries to connect them to produce a curve which represents a boundary of the object. But to convert the edge pixels into close boundary is difficult for the ultrasound image segmentation. Region based segmentation is based on the principle that neighboring pixels within the one region have similar value. FCM algorithm is best known region based category for the segmentation. These methods affect the results due to speckle noises in ultrasound images. Another method is active contour method which is suitable for finding edges of a region whose gray scale intensities are significantly different from the surrounding region in the image. To segment homogenous regions, the semi automatic region growing methods first requires users to identify a seed point. In this paper, A full automatic region-growing segmentation technique is proposed. First we found the seed automatically using textural features from Co-occurrence matrix (COM) and run length features. Then using gray scale, spatial information and thresholding method, region growing was applied to

segment the region. With the advances in imaging technology, diagnostic imaging has become an indispensable tool in medicine today. X-ray angiography (XRA), magnetic resonance angiography (MRA), magnetic resonance imaging (MRI), computed tomography (CT), and other imaging modalities are heavily used in clinical practice. Such images provide complementary information about the patient. While increased size and volume in medical images required the automation of the diagnosis process, the latest advances in computer technology and reduced costs have made it possible to develop such systems. Blood vessel delineation on medical images forms an essential step in solving several practical applications such as diagnosis of the vessels (e.g. stenosis or malformations) and registration of patient images obtained at different times. Segmentation algorithms form the essence of medical image applications such as radiological diagnostic systems, multimodal image registration, creating anatomical atlases, visualization, and computer-aided surgery.

2. Automatic Selection Seed Point

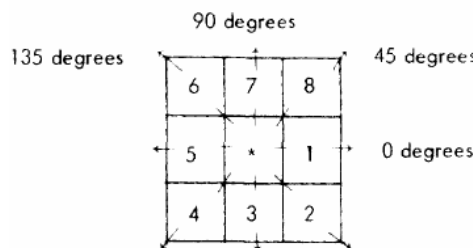
In this section we describe the method for automatic selection of abnormal region from ultrasound image using Co occurrence matrix probability feature and run length method

3. Co-Occurrence Matrix Probability Feature

A Co-Occurrence Matrix (COM) is square matrices of relative frequencies $P(i, j, d, \theta)$ with which two neighboring pixels separated by distance d at orientation θ occur in the image, one with gray level i and the other with gray level j “Fig. 1” [6]. A COM is therefore a square matrix that has the size of the largest pixel value in the image and presents the relative frequency distributions of gray levels and describe how often one gray level will appear in a specified spatial relationship to another gray level within each image region. Fig 3.1. Co occurrence matrix with its orientations There are 14 features that may be extracted from COM matrix, but usually 4 or 5 features are more interested ones. In this paper 2 textural features were calculated from the COM for direction θ values of 0° and a distance d of 1. The matrix was normalized by the following function:

$$p(i, j, d, \theta) = \frac{P(i, j, d, \theta)}{R} \tag{1}$$

R is the normalized function, which is usually set as the sum of the matrix.



For example; with an 8 grey-level image representation and a vector t that considers only one neighbor, we would find [1]:

1	2	1	3	4
2	3	1	2	4
3	3	2	1	1

Fig 3.2 Image example

	0	1	2	3	4	5	6	7
0	0	0	0	0	0	0	0	0
1	0	1	2	0	0	0	0	0
2	0	1	0	2	0	0	0	0
3	0	0	1	1	0	0	0	0
4	0	1	0	0	1	0	0	0
5	0	0	0	0	0	0	0	0
6	0	0	0	0	0	0	0	0
7	0	0	0	0	0	0	0	0

Fig 3.3 Classical Co-occurrence matrix

In this work the co-occurrence features energy and entropy which can easily differentiate non-homogeneous region from homogeneous region are considered. Energy is called Angular Second Moment. It is a measure the homogeneity of the image and can be calculated from the normalized COM. It is a suitable measure for detection of disorder in texture image. Higher values for this feature mean that less changes in the image amplitude or intensity result in a much sparser COM. The energy is formulated by the following equation:

$$J = \sum_{i=1} \sum_{j=1} (p(i, j))^2$$

Entropy gives a measure of complexity of the image. Complex textures tend to have higher entropy. Entropy is represented by the following equation

$$S = -\sum_{i=1} \sum_{j=1} p(i, j) \log(p(i, j))$$

The value of energy and entropy are high for homogeneous regions and low for non-homogeneous regions. The abnormal region in the ultrasound images appears to be homogeneous. So these parameters can identify a seed pixel from the abnormal regions. Some cases the seed pixel is selected from the normal region which appears to be homogeneous. This drawback can be avoided by the calculating run length features that will describe in next section.

4. Gray Level Runlength Features

Run length features are based on computation of continuous probability of the length and gray level of the primitive in the texture. After the selection of seed pixel from co-occurrence features, we can check whether the selected seed pixel belongs to abnormal region or not. This can be checked by calculating the Run length features. These features are calculated from the Run length matrix $P(i, j)$ which describes the number of times that the image contains a run of length j in a given direction consisting of points having gray level i .

The following two features that give the good difference between homogeneous and non-homogeneous regions are considered.

Long run emphasis

$$\frac{\sum_{i=1}^G \sum_{j=1}^R j^2 p(i, j)}{\sum_{i=1}^G \sum_{j=1}^R p(i, j)}$$

Run length Non Uniformity

$$\frac{\sum_{i=1}^G \sum_{j=1}^R j p(i, j)^2}{\sum_{i=1}^G \sum_{j=1}^R p(i, j)}$$

That $P(i, j)$ is run length matrix, G denotes number of gray levels and R is longest run. The long run length emphasis is high for homogeneous region and low for non homogeneous region and the run length non uniformity is low for ,homogeneous and high for non homogeneous. The run length features have been calculated around the points selected by co occurrence features. If all the run length features of selected point and its neighborhood points are equal then the point is considered as a seed point.

5. CA ALGORITHM BASED ON SEED BASED SELECTION

A cellular automata is basically a computer algorithm that is discrete in space and time and operates on a lattice of cells. Since it was first proposed by Von Neumann and Ulam, Cellular Automata has attracted researchers from various fields in both physical and social sciences because of its simplicity, and potential in modeling complex systems. Each individual cell is in a specific state and changes synchronously depending on the states of some neighbors as determined by a local update rule. They are parallel, local and homogeneous, since the state of any cell depends only on the states of the local neighbors at the previous time step and the update rules are same for every cell.

Formally, a cellular automaton (CA) is a triple $A=(S, N, \delta)$, where S is a nonempty set, called the state set, N is the neighborhood, and $\delta: S^N \rightarrow S$ is the neighborhood; S^N , which is the argument of, indicates the states of the neighborhood cells at a given time, while, which is its value, is the state of the central cell at the next time step. Although the usual definition for “Cellular Automata” is in favor of a finite state set (discrete and bounded), continuous state sets in which the states are real numbers are also used in CA literature under the name “Continuous CA” or “Coupled Map Lattices”. A detailed discussion and some of the issues that can arise while using a continuous state set on a finite machine. There are various attempts of using CA in image processing problems including: image enhancement (sharpening and smoothing), image filtering, edge detection and image segmentation (Grow-cut). Grow-cut method uses a continuous state cellular automaton to interactively label images using user supplied seeds. The cells are corresponding to image pixels, and the feature vector is RGB or gray scale intensities. The state set for each image pixel consists of a “strength” value in a continuous interval $[0,1]$, a label and an image feature vector. The automata are initialized by assigning corresponding labels at seeds with a strength value between 0 and 1 where a higher value reflects a higher confidence in choosing the seed. Strengths for unlabeled cells are set to 0.

Where g is a pixel similarity function bounded to $[0, 1]$ depending on the image features i.e.,

$$g(x) = 1 - \frac{x}{\max \|\vec{C}\|_2}$$

Where the argument x is for instance, the absolute difference between the intensities of two neighboring pixels. The surprising success of this simple algorithm, especially on medical images, motivated us to further analyze the algorithm. We showed that the result of the iterations of this algorithm converges to that of the shortest paths algorithm by modifying the similarity function used: $g(x) =$. We note that, the original similarity function used in Grow-cut is a first order approximation to the one we utilized. In connecting shortest paths to cellular automata framework, maximizing the product of the edge weight ω_{ij} was shown to be equivalent to minimizing the sum of the $-\log \omega_{ij}$'s, i.e., $\|_{ij}\|$'s resulting in the shortest path between a seed node to any non seed node in the graph over the negative logarithm edge weights.

These weights can be interpreted similarly to the reciprocal weight ω_{ij} defined in Sinop and Grady, which was shown to infer a connection between the shortest path algorithm and the general seeded segmentation optimization with L_∞ norm minimization. Simultaneously and independently from our work, it has also been shown that the Grow-cut algorithm is equivalent to the Belman–Ford algorithm, which calculates the shortest paths on a weighted graph. However, there, the motivation and emphasis was on fast hardware implementation of the CA algorithms, due both increasing availability of low-cost graphical hardware (GPUs), and CA algorithm's suitability to run on parallel processors. Shortest path idea was utilized in other works such as, where the Eikonal equation was solved with two different boundary conditions constructed from foreground and background seeds. Image-dependent speed functions were inserted into the right hand side of the Eikonal equation, whose solutions led to two distance functions: shortest paths of each pixel from the foreground seeds and the background seeds. For each pixel, the smaller distance to the foreground seeds produced the resulting segmentation.

The grow cut method, first find the maximum intensity variation which means that from this intensity to 0 we are sure that this is not the ROI. Second we cut the histogram from MAX to 0. Then, find the threshold from MAX to the highest intensity which separates the uncertainty area from the ROI. This is simply done using the well-known Otsu thresholding method. This is a parameter free thresholding technique which maximizes the inter-class variance. It is interesting to observe that the Otsu method is more accurate in cutting into two classes than a k-means for example, because the k-means just measures distances between data and classes' centroids but Otsu also take care to get compact clusters using the inter-class variance.

6. Morphological Process

A shape (in blue) and its morphological dilation (in green) and erosion (in yellow) by a diamond-shape structuring element Mathematical morphology (MM) is a theory and technique for the analysis and processing of geometrical structures, based on set theory, lattice theory, topology, and random functions. MM is most commonly applied to digital images, but it can be employed as well on graphs, surface meshes, solids, and many other spatial structures. Topological and geometrical continuous-space concepts such as size, shape, convexity, connectivity, and geodesic distance, can be characterized by MM on both continuous and discrete spaces. MM is also the foundation of morphological image processing, which consists of a set of operators that transform images according to the above characterizations.

7. Binary Morphology

In binary morphology, an image is viewed as a subset of an Euclidean space \mathbb{R}^d or the integer grid \mathbb{Z}^d , for some dimension d . Example application: Assume we have received a fax of a dark photocopy. Everything looks like it was written with a pen that is bleeding. Erosion process will allow thicker lines to get skinny and detect the hole inside the letter "o".

8. Grayscale Morphology

In grayscale morphology, images are functions mapping an Euclidean space or grid E into $\mathbb{R} \cup \{\infty, -\infty\}$, where \mathbb{R} is the set of real's, ∞ is an element larger than any real number, and $-\infty$ is an element smaller than any real number. Grayscale structuring elements are also functions of the same format, called "structuring functions".

9. Conclusion

A Segmentation algorithm for the problem of tumor delineation which exhibit varying tissue characteristics, as the change in enhancing part of the tumor after radiation therapy becomes important. The segmentation to partition the tumor tissues further into enhancing parts. Seed based segmentation is performed in the image for detecting the tumor region and then highlighting the region with help of level set method pre-processing. More importantly, the supervised segmentation method requires considerable amount of training and testing data which comparatively complicates the process. Whereas, this study can be applied to the minimal amount of data with reliable results. As future work, we will be trying to improve classification of Tumor using Radial basis function which is the type of ANN. The performance of the ANN classifier was evaluated in terms of training performance and classification accuracies. Artificial Neural Network gives fast and accurate classification than other neural networks and it is a promising tool for classification of the tumors.

References

- [1] S. Warfield, K. Zou, and W. Wells, "Simultaneous truth and performance level estimation (STAPLE): An algorithm for the validation of image segmentation," *IEEE Trans. Med Imag.*, vol. 23, no. 7, pp. 903–921, Jul. 2004.
- [2] K. H. Zou, S. K. Warfield, A. Bharatha, C. M. C. Tempany, M. R. Kaus, S. J. Haker, W. M. Wells, F. A. Jolesz, and R. Kikinis, "Statistical validation of image segmentation quality based on a spatial overlap index," *Acad. Radiol.*, vol. 11, no. 2, pp. 178–189, 2004.
- [3] M. Prastawa, E. Bullitt, S. Ho, and G. Gerig, "A brain tumor segmentation framework based on outlier detection," *Med. Image Anal.*, vol. 8, no. 3, pp. 275–283, 2004.
- [4] Georgiadis. Et all , "Improving brain tumor characterization on MRI by probabilistic neural networks and non-linear transformation of textural features", *Computer Methods and program in biomedicine*, vol 89, pp24-32, 2008
- [5] M. T. Hagan, H. B. Demut, and M. H. Beale, *Neural Network Design*, 2002.
- [6] Chowdhury, M.H.; Little, W.D.; "Image thresholding techniques" *IEEE Pacific Rim Conference on Communications, Computers, and Signal Processing*, 1995. Proceedings. 17-19 May 1995 Page(s): 585 – 589
- [7] Zhou, J.; Chan, K.L.; Chong, V.F.H.; Krishnan, S.M "Extraction of Brain Tumor from MRI Images Using One-Class Support Vector Machine" *27th Annual International Conference of the Engineering in Medicine and Biology Society*, 2005. *IEEE-EMBS 2005*, Page(s): 6411 – 6414
- [8] Pan, Zhigeng; Lu, Jianfeng; "A Bayes-Based Region-Growing Algorithm for Medical Image Segmentation" *Computing in Science & Engineering*, Volume 9, Issue 4, July-Aug. 2007 Page(s): 32 – 38
- [9] J. C. Bezdek, L. O. Hall, L. P. Clarke "Review of MR image segmentation techniques using pattern recognition." *Medical Physics* vol. 20, no. 4, pp. 1033 (1993).
- [10] Velthuizen RP, Clarke LP, Phuphanich S, Hall LO, Bensaid AM, Arrington JA, Greenberg HM and Silbiger ML. "Unsupervised Tumor Volume Measurement Using Magnetic Resonance Brain Images," *Journal of Magnetic Resonance Imaging*, Vol. 5, No. 5, pp.

The Industrial Maintenance Management and Implementing Maintenance Policies for Improvement in Productivity

Ajay S. Bonde¹, Ashwadeep C. Fulzele²

1,2,Department Of Mechanical Engineering, Yashvantrao Chavan College Of Engineering, Nagpur,

Abstract:

As a consequence, of the implementation of advanced manufacturing technologies and just-in-time production systems, the nature of the production environment has changed during the last two decades. This has allowed companies to massively produce products in a customized way. But the increase in automation and the reduction in buffers of inventory in the plants clearly put more pressure on the maintenance system. The present maintenance management policy has been proposed in order to diminish this pressure. Whatever the policy an organization adopts, it has to be evolving to continue being useful against the fast changes that occur in business, communications and industry. Most companies lack a formal method to address maintainability during the project delivery process, yet maintenance can seriously affect productivity. This paper outlines the proposed model process and describes the potential roles and benefits of maintenance policy [1].

Keywords: Maintainability, Maintenance, Organization, Production Environment, Productivity, Maintenance Policy,

1. Introduction

Maintenance is defined as the combination of all technical, administrative and managerial actions during the life cycle of an item intended to retain it in, or restore it to, a state in which it can perform the required function. In the same standards, maintenance management is defined as all the activities of the management that determine the maintenance objectives or priorities, strategies, and responsibilities and implement them by means such as maintenance planning, maintenance control and supervision, and several improving the methods including economical aspects in the organization. The maintenance management policy can be viewed as one of the basic and integral parts of the maintenance management function. The maintenance management function consists of planning, organizing, implementing and controlling maintenance activities. The management organizes, provides resources (personnel, capital, assets, material and hardware, *etc.*) and leads to performing tasks and accomplishing targets. Once the plans are created, the management's task is to ensure that they are carried out in an effective and efficient manner. Having a clear mission, strategy, and objectives facilitated by a corporate culture, organizing starts the process of implementation by clarifying job and working relations (chain of command, span of control, delegation of authority, *etc.*) [2].

2. Maintenance Management Policy

2.1 The Maintenance Schedule

It is generally accepted that, in any maintenance department where there are more than 10 crafts persons and more than two or three crafts, some planning, other than day-to-day allocation of work by supervisor or leadsperson, can result in improved efficiency. As the size of the maintenance organization, for example, scheduling, increases, the extent to which work planning can be formalized and the amount of time that should be spent on this activity are increased. There should be only as much planning as necessary for maximum overall efficiency so long as the system costs less than the cost of operating without it.

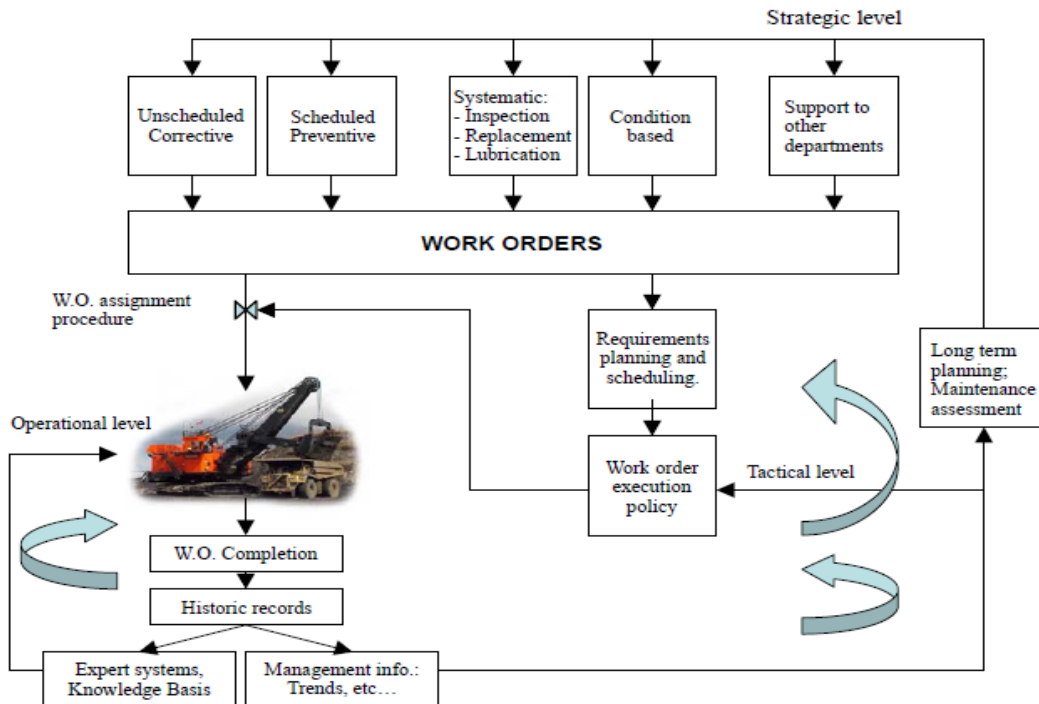


Fig: 1. The Maintenance policy [3].

2.2 The Procedure for Scheduling

There are practical limitations to any scheduling system. A very detailed schedule that because of emergencies becomes obsolete after the first hour or two of use is of little value. If, however, actual performance indicates from 60 to 80 percent adherence during normal operation, the value of the schedule is real. Justification of any scheduling system requires proof of its effectiveness in dollars saved. Where some form of incentive system or work measurement exists, such proof is readily available. But in most maintenance departments no such definitive method is available and the only criteria of measurement are overall trends in maintenance costs and quality of service. Some aspects to be considered in arriving at a sound work-scheduling procedure are work unit, size of jobs scheduled, percent of total work load scheduled, and lead time for scheduling.

Work Unit. Most detailed schedules are laid out in terms of labour-hours or, if standard times are used, fractions of hours. Other scheduling systems use a half craft-day as a minimum work unit. Others may use a craft-day or even a craft-week as a basis.

Size of Jobs Scheduled. Some work-scheduling systems handle small jobs as well as large ones. Others schedule only handle major work where the number of crafts persons and the length of time involved are appreciable.

Percent of Total Work Load Scheduled. Although in some cases all work may be scheduled, the most effective systems recognize the inability of any maintenance engineering department to anticipate all jobs, especially those of an emergency nature, and do not attempt scheduling for the entire work force. A portion of the available work force is left free for quick assignment to emergency jobs or other priority work not anticipated at the time of scheduling.

Lead Time for Scheduling. Lead time for scheduling, or the length of time covered by the schedule, is another variable to be considered. Some scheduling systems do not attempt to cover breakdown repairs and are limited to the routine preventive maintenance and to major work that can be anticipated and scheduled well in advance. In these cases a monthly or biweekly allocation of manpower suffices. In most instances, however, a weekly schedule with a 2- or 3-day lead time results in good performance, yet is sufficiently flexible to handle most unexpected work. In extreme situations a daily schedule with a 16- to 18-hr lead time may be necessary to provide the necessary control. A more workable solution for this situation, however, involves use of a master schedule for a minimum of 2 weeks with provision for modifying it daily.

3. Selection And Implementation Of A Scheduling System

3.1 Flow-of-Work Requests.

Before any formalized scheduling program can be initiated, the method of requesting work from the maintenance department should be formalized. This request may take the form of a work description or job ticket, listing labour hours or equipment requirement, or it can be in the form of a work sheet on which the same type of information is accumulated by either verbal or written communication. Regardless of the form this information takes, it must be routed to one central point if a scheduling system is to be used. In a small plant this can be the supervisor, self direct team leader, the maintenance superintendent, or the maintenance engineer. In a larger maintenance department it should be through a staff individual or group. The amount of information on the work request depends upon the type of talent used in the scheduling group. If the individual charged with planning is completely familiar with the job requirements and can determine the craft skills and labour-hours involved, the necessary equipment, and any other information required for scheduling, a summary of the jobs will suffice. On the other hand, where complexity of work is such that it is practically impossible for any individual to have this information, or if the person charged with scheduling does not have the training necessary to analyze the work, then the information on the work request must be presented in more detail. The number of labour-hours required, by craft, the timing, the relation between crafts, the location and availability of parts and equipment, and any special requirements concerning coordination with production schedules or personnel should be included. In addition to job information required for planning, it is equally important to have a feedback on actual performance in terms of notification of completion and actual time consumed, by craft. This may be incorporated in the work-request system, but provision must be made for channelling this information back to the scheduling centre. The scheduling system should also provide for work scheduled but not completed becoming a part of the work backlog. As such, it is considered, along with new work, for new scheduling.

3.2 Determination of Priority.

In any maintenance organization which is efficiently manned, the work load, in terms of quantity or timing, exceeds the availability of men and/or equipment. For this reason the problem of defining the order in which the work is to be carried out, or establishing priority, exists and is an important factor in scheduling. In a small plant with one operating department and a small maintenance organization, establishment of priorities may amount to casual discussion between maintenance and production. However, as the plant grows and the maintenance department is called upon to provide service to more than one production department, the problem of equitable and efficient priority assignment becomes more involved. One of the most serious problems in maintaining good relations between maintenance and production departments is in this sphere. Too frequently personalities, working conditions, accessibility, or geographic location with respect to central shops influence the order of work assignment. This may decrease the overall efficiency of the plant. The means for determining work priority figures most importantly in the establishment of a work-scheduling system. On the surface a solution to this problem would reserve decisions concerning priorities to an individual who is in position to judge the effect on overall plant performance.

In a plant of any size, it is usually most effective to handle such decisions at a lower level of management, with the plant manager having the final say when no decision as to priority of work can be reached. A method which has proved satisfactory in many instances has been to assign a rough allocation of craft manpower to each production department, then to establish the priority of work within each department by consultation with its supervision. When it is necessary to vary the allocation of men, this should be done by negotiation between production departments to arrange a mutually agreeable exchange. If such a reallocation cannot be concluded, as a last resort the plant manager must make the decision.

3.3 Coordinating and Dispatching.

In the execution of an effective scheduling system it is necessary to compromise with the practical considerations of getting the work done, and done economically. If a supervisor or team leader guided his or her crafts persons on the assumption that the job must be completed at the exact time he had estimated and then continued to assign work on the basis of his estimate of the time necessary, it is obvious that confusion, incomplete work, and idle craft time would result. A formal schedule, issued weekly and followed blindly, would have the same effects. Instead, the schedule should be used as a guide, and modifications can be made as needed. Rapid communication of such modifications to the men responsible for carrying them out is essential to the success of a work schedule. It is also essential that any changes or unexpected work for which provision has not been made in the schedule be funnelled through the dispatch centre. Usually the dispatch centre can incorporate this type of work more efficiently than is possible by random selection of the nearest craftsmen or injection of higher authority into the picture [4].

4. Preventive versus Breakdown Maintenance

Preventive maintenance has long been recognized as extremely important in the reduction of maintenance costs and improvement of asset reliability. In practice it takes many forms. Two major factors that should control the extent of a preventive program are first, the cost of the program compared with the carefully measured reduction in total repair costs and improved asset performance; second, the percent utilization of the asset being maintained. If the cost of preparation for a preventive-maintenance inspection is essentially the same as the cost of repair after a failure accompanied by preventive inspections, the justification is small. If, on the other hand, breakdown could result in severe damage to the asset and a far more costly repair, the scheduled inspection time should be considered. Furthermore, in the average plant preventive maintenance should be tailored to fit the function of different items of equipment rather than applied in the same manner to all equipment. Key pieces of equipment in many other integrated manufacturing lines are in the same category. Conversely, periodic inspections of small electric motors and power transmissions can easily exceed the cost of unit replacement at the time of failure. Indeed, a program of asset or component replacements can result in considerably lower maintenance costs where complete preventive maintenance is impractical. In a plant using many pumps, for instance, a program of standardization, coupled with an inventory of complete units of pumps most widely used, may provide a satisfactory program for this equipment. This spare-tire philosophy can be extended to many other components or subassemblies with gratifying results. Sometimes, instead of using a centrally administered formal preventive program, qualified mechanics are assigned to individual pieces of equipment, or equipment groups, as mechanical custodians. Operating without clerical assistance and with a minimum of paperwork, these men, because of familiarity with equipment and ability to sense mechanical difficulties in advance, can effectively reduce maintenance costs and breakdowns. These compromise devices can frequently be used to greater advantage, even in plants where equipment is not in continuous operation and a more comprehensive preventive program might be set up.

Periodic shutdown for complete overhaul of a whole production unit, similar to the turnaround period in oil refineries, is another method of minimizing breakdowns and performing maintenance most efficiently. Unfortunately, this is a difficult approach to sell to management of a 7-day, around the-clock manufacturing plant not accustomed to this method. One of the most effective methods of tempering ideal preventive maintenance with practical considerations of a continuous operation is that of taking advantage of a breakdown in some component of the line to perform vital inspections and replacements which can be accomplished in about the same time as the primary repair. This requires recording of deficiencies observed during operating inspections and moving in quickly with craftsmen and supervision prepared to work until the job is done. Production supervision usually can be sold the need for a few more hours' time for additional work with repair of a breakdown much more easily than they can be convinced of its necessity when things are apparently running smoothly [5].

References

- [1] A. Crespo Ma´rquez, P. Moreu de Leo´n, J.F. Go´mez Ferna´ndez, C. Parra Ma´rquez and M. Lo´pez Campos Department of Industrial Management, School of Engineering, University of Seville, Seville, Spain.
- [2] Bradley PS (2002) Designing the Best Maintenance. <http://www.samicorp.com>:1–5
- [3] Morel G, Suhner M, Iung B, L´eger JB. (2001, October). Maintenance holistic framework for optimizing the cost/availability compromise of manufacturing systems. In: Proceedings of the sixth IFAC symposium on cost oriented automation. Survey Paper, Berlin, Germany, October, 2001. ISBN:0-08-043907-1.
- [4] Chelson VJ, Payne CA, Reavill RP (2005) Management for Engineers Scientists and Technologists, 2nd edn. Wiley, Chichester England
- [5] Lindley R, Higgins Darrin J, Wikoff, Maintenance Engineering Handbook. Duffuaa, S.O. (2000), “Mathematical models in maintenance planning and scheduling”, in Ben-Daya, M., Duffuaa, S.O. and Raouf, A. (Eds), Maintenance, Modelling and Optimization, Kluwer Academic Publishers, Boston, MA.

Azotobacter Chroococcum Mass Culture for Production of Bio-Fertilizer, Its Sustained Efficacy on Nitrogen Fixation and Crop Productivity in Mulberry Garden

¹S.Rajaram , ²Klisdamon Nongrang , ³S.K.Mandal, ⁴M.K.Ghosh and
B.B.Bindroo.

^{1,2,3,4}Central Sericultural Research and Training Institute, Central Silk Board, Berhampore - 742 101, Murshidabad, West Bengal, India.

Abstract :

Mulberry is cultivated by farmers for its leaves, the sole food for silkworm (*Bombyx mori* L.) for commercial production of raw silk in Sericulture Industry. As mulberry is a perennial crop can be maintained for several years in the field, selection of suitable land and follow-up of recommended package of practices are inevitable for maintenance of potential productivity of the variety selected for cultivation. As the quality of mulberry leaves alone contributes about 38.2% for the success of silkworm cocoon crop, quality linked leaf productivity of mulberry leaves can be achieved through adequate supply of all required input into soil. Nitrogen is one of the important macronutrient required for mulberry in larger quantity. In order to reduce the high cost involved towards nitrogenous chemical fertilizers and to maintain the soil health in an eco-friendly way Integrated Nutrient Management (INM) approach in agriculture sector became popular and the same has been followed in mulberry cultivation as well in recent years. Use of different kinds of microbial inoculants as bio-fertilizer to fix atmospheric nitrogen in mulberry garden brought improvements in soil health maintenance and helps to reduce nitrogenous chemical fertilizer requirements and expenditure to farmers considerably without affecting the quality linked productivity.

Keeping in view of the above an experiment study was conducted to ascertain the consistent efficacy of *Azotobacter chroococcum* inoculants @ $10^{8.9}$ cells per g charcoal carrier material used as nitrofert bio-fertilizer application in mulberry garden during July to September 2012 crop. S1635 mulberry variety in Paired Row System [PRS] of plantation with (150+90) x 60 cm spacing under irrigated condition with two treatments i.e., T1 as control with basal dose of application of 20 MT FYM $\text{ha}^{-1} \text{year}^{-1}$ in two split doses and recommended 336:180:112 NPK $\text{ha}^{-1} \text{year}^{-1}$ in 5 split doses and in T2, except 50% of N replaced by 20 kg nitrofert bio-fertilizer $\text{ha}^{-1} \text{year}^{-1}$ in 5 split doses all other nutrients and package of practices as followed in T1 with 13 replications in CRD. Average leaf yield of 7.35 & 7.34 and total biomass of 12.95 & 13.0 tons ha^{-1} obtained in T1 and T2 respectively and quality of leaves on economic characters found without significant difference between the treatments revealed the consistent efficiency of *Azotobacter chroococcum* in fixing atmospheric nitrogen in the soil of mulberry garden to reduce nitrogenous chemical fertilizer and expenditure without affecting the quality linked leaf productivity and mass culture of the bacteria for preparation of Nitrofert bio-fertilizer, its application techniques are discussed in the paper.

Key Words : Mulberry leaf, bio-fertilizer, biological nitrogen fixation, eco-friendly soil health, potential productivity.

1. Introduction :

Mulberry is cultivated by farmers for its leaves, the sole food for silkworm (*Bombyx mori* L.) for commercial production of raw silk in Sericulture Industry. As mulberry is a perennial crop can be maintained for many years, selection of land and follow-up of recommended package of practices are inevitable for quality linked potential productivity throughout. Further the quality of mulberry leaves as single factor contributes about 38.2% for the success of silkworm crop (Miyashita, 1986), adequate supply of all required input into soil is very much essential. In India, during the Green Revolution period more emphasis was given for increase unit area productivity of crops which facilitated in indiscriminate application of inorganic chemical fertilizers, chemicals to control various pests and diseases without considering the soil health maintenance for long-term use for agriculture purposes resulted in considerable damage to the soils of agriculture land. It was reported that out of 235 mha of cultivable area, soils of 166 mha have been damaged (Swaminathan, 1994) in the country, necessitated alternate methods to improve the soil health. Excessive uses of nitrate and phosphatic fertilizers have led to extensive contamination of surface and ground waters (Dahama, 2003). To complete life cycle normally, living organism requires a large numbers of substances from outside are called nutrition. Green plants being autotrophic, requires only inorganic substances from outside (Pandey and Sinha, 1972). An essential element is defined as one whose absence prevents plants from completing its life cycle or one that has clear

physiological role (Arnon and Stout, 1939). Though the atmosphere contains more than 70% of nitrogen, only about 0.1% of fixed nitrogen is present in the soil and small traces of nitrogen from the atmosphere reach the soil in a dissolved state in rain water (Rangaswami and Bagyaraj, 2004). The fate of nitrogen fertilizers in the soil is controlled by several physical, chemical and biological factors. The percentage of recovery of nutrients varies between the different types of fertilizers reported as 50-60; 5-15 and 75% of N P K respectively and nitrogen deficiency is observed in plants grown on soils with low organic matter (< 0.4 % organic carbon) and also reported that nearly 62 % soils are deficient in Nitrogen (Anonymous, 2011).

Nitrogen fixation is the reduction of N₂ (atmospheric nitrogen) to NH₃ (ammonia). Free living prokaryotes with the ability to fix atmospheric dinitrogen (diazotrophs) are ubiquitous in soil. But our knowledge of their ecological importance and their diversity remains incomplete. In natural ecosystems, biological N₂ fixation is most important source of N. The capacity for nitrogen fixation is widespread among bacteria and archaea. The estimated contribution of free-living N-fixing prokaryotes to the N input of soil ranges from 0-60 kg. ha⁻¹ year⁻¹ (Bürgmann *et al.*, 2003). Bio-fertilizers can make significant contribution towards the development of strategies for productivity improvement which do not lead to an exponential rise in the consumption of non-renewable forms of energy (Subba Rao, 1982) and the use of bio-fertilizers is currently gaining interest as a cheap, safe alternative to chemical fertilizers (Sharma, 2002).

After isolation of two aerobic free living nitrogen fixing bacteria in 1901 by Martinus Beijerinck, and named them as *Azotobacter chroococcum* and *A. agile* study on practical applicability of these *Azotobacter* spp. attracted several workers. Yamagata and Itano (1923) reported that *Azoto-bacter* is ubiquitous in neutral and weakly basic soils, but not in acidic soils and the growth of bacteria favored at a temperature of 20-30°C and Moreno *et al.*, (1986) observed that in dry soils, *Azotobacter* can survive upto 24 years in the form of cysts. Use of variety of carbohydrates, alcohols and salts of organic acids as sources of carbon and pH 4.8 to 8.5 found optimum for growth of the bacteria George (2005).

Wong and Maier (1985) reported that hydrogen dependent mixotrophic growth of *Azotobacter* in a nitrogen-free medium containing mannose and availability of hydrogen in the soil facilitates the growth of *Azotobacter* in nature. Culture media inoculated with *A. chroococcum* with high NaCl concentration, incubated on rotary shaker for 60 hours at 200 rpm facilitated full growth of colony and shown brown colour pigment. *A. chroococcum* being a non-symbiotic bacteria have a great potential for use in production of bio-fertilizer due to its ability to fix N₂ (Nakade *et al.*, (2012). Besides, nitrogen fixation, it also produces, Thiamin, Riboflavin, IAA and gibberellins, when applied to seeds, seed germination is improved to a considerable extent and also controls plant diseases due to the above substances (Kader *et al.*, 2002).

Presence of ferredoxin, hydrogenase and an important enzyme nitrogenase required for nitrogen fixation was reported by Shank *et al.*, (2005) and of the different type of nitrogenase, the basic one is Molybdenum- iron nitrogenase was reported by Howard and Rees (2006). Chen *et al.*, (1995) observed that *Azotobacter* spp. facilitate the mobility of heavy metals in the soil and thus enhance bioremediation of soil from heavy metals, such as cadmium, mercury and lead. Emtiazia *et al.*, (2004) reported that *Azotobacter* biodegrade chlorine-containing aromatic compounds, such as 2,4,6-trichlorophenol which was used as an insecticide, fungicide and herbicide till its mutagenic and carcinogenic effect was found (Li *et al.*, 1991).

Like other agricultural crops, mulberry requires all sixteen nutrients and nitrogen in large quantity. Based on the high cost involved in application of nitrogenous chemical fertilizers and to maintain the soil health in an eco-friendly manner, Integrated Nutrient Management (INM) approach in agriculture sector became popular in recent years, the same has been followed in mulberry cultivation as well.

A. chroococcum cells blended with peat soil/charcoal/FYM in powdered form as carrier material containing 10⁸⁻⁹ cells g⁻¹ observed as optimum for application in mulberry garden. CSR&TI., Berhampore, India has standardized the mass culture technique for production of a bio-fertilizer under the name "Nitrofert" to reduce nitrogenous fertilizer requirement and expenditure in mulberry cultivation without affecting the quality linked leaf productivity and for eco-friendly way of soil health improvement (Sudhakar *et al.*, 2000). Mass culture of *A. chroococcum* for production of nitrofert bio-fertilizer, findings of the experiment conducted on its application and crop productivity in S1635 mulberry garden are discussed in detail in this paper.

2. Materials And Methods

2.1 Mass multiplication of *Azotobacter chroococcum* for Nitrofert bio-fertilizer production in laboratory :

Preparation of Walkman's bacterial culture medium and inoculation of *A. chroococcum* mother culture for mass culturing and production of bio-fertilizer in charcoal powder as carrier material maintaining 10^{8-9} cells g^{-1} as described by Sudhakar *et al.*, 2000 rotary shaker for shaking at 200 rpm for 60 hours for mass (**Plates : 1-10**).

2.2 Efficacy of Nitrofert on nitrogenous fertilizer saving and crop productivity in mulberry garden :

The experiment was carried out in **Plot No. A-9** Agronomy Section of CSR&TI, Berhampore West Bengal, India, well established irrigated mulberry garden raised in alluvial soil with S1635 high yielding variety under Paired Row System with plant spacing of (150+90) x 60 cms the mulberry garden during July to September 2012. After pruning of plants, 26 number of plots demarcated each with two paired rows and 10 plants and thus a total 40 number of plants per plot (Chaturvedi and Sarkar, 2000) in Completely Randomized Design [CRD] as described by Sukhatme and Amble (1985) was drawn as experiment plan to accommodate 2 treatments with 13 replications each. In T1, recommended quantity of FYM @ 20 ton ha^{-1} year $^{-1}$ in two equal split doses and chemical fertilizers NPK @ 336 : 180 : 112 kg. ha^{-1} year $^{-1}$ in 5 equal split doses (Ray *et al.*, 1973) as control and in T2 FYM @ 20 ton ha^{-1} year $^{-1}$ in two equal split doses and chemical fertilizers NPK @ 168 : 180 : 112 kg. and Nitrofert 20 kgs ha^{-1} year $^{-1}$ in 5 equal split doses (**Plates : 11-16**). Irrigation water applied as and when required and all other package of practices recommended for mulberry garden maintenance were followed uniformly in all plots. On 70th day 5 randomly selected plants from each plot were pruned and observations made on the following parameters individually and yield was estimated as suggested by Sreenivasa Shetty *et al.*, (1990).

2.3 Growth Parameters

like Number of branches / plant, Branch height (cm), Total shoot length / plant (m), Number of leaves / branch, Number of leaves / plant, Total leaf weight / plant (kg), Total shoot weight /plant (kg), Green biomass weight / plant (kg), Leaf weight ha^{-1} crop $^{-1}$ (ton), Shoot weight ha^{-1} crop $^{-1}$ (ton), Biomass green weight ha^{-1} crop $^{-1}$ (ton), Biomass dry weight ha^{-1} crop $^{-1}$ (ton) and **Leaf quality Parameters** like Moisture Content of leaf (MC) and Moisture Retention Capacity (MRC) (Vijayan *et al.*, 1997). All data of the experiment were subjected to statistical analysis using AGRES Software and the results were tabulated and discussed separately.

3. Results And Discussion

3.1 Mass multiplication of *Azotobacter chroococcum* for Nitrofert bio-fertilizer production in laboratory :

From 10 litres of *Azotobacter chroococcum* bacteria media charcoal powder mixed 23 kgs of Nitrofert bio-fertilizer with 10^{8-9} cells g^{-1} carrier material prepared.

3.2 Efficacy of Nitrofert on nitrogenous fertilizer saving and crop productivity in mulberry garden :

Microbial inoculants in carrier based preparations containing beneficial microorganisms in a viable state intended for seed or soil application and designed to improve soil fertility and help plant growth by increasing the population and biological activity of desired microorganism in the root environment (Subba Rao, 1982). Inoculation of *Azotobacter* and AM fungus in mulberry has proved beneficial in terms of economizing N and P fertilizer application by 50% without adverse effect on leaf yield and quality (Das *et al.*, 1994). Application of n-triacontanol (Vipul) as foliar spray and use of *Azotobacter* bio-fertilizer could increase the leaf yield by 15-20% besides, 50% reduction in nitrogenous fertilizer (Rajanna *et al.*, 2005). *Azotobacter* bio-fertilizer application @ 20 kg ha^{-1} year $^{-1}$ was able to curtail 50% nitrogenous fertilizer requirement of mulberry without affecting yield and quality of leaves (Sudhakar *et al.*, 2000). Similar results (Table 1 & Fig. 1-2) obtained in the experiment conducted are discussed as below:

3.3 Number of branches / plant : An average of 15.92 and 13.92 number of branches recorded per plant in T2, T1 respectively and the difference between the two treatments was statistically significant @ CD 5% level.

3.4 Branch height (cm) and total shoot length plant $^{-1}$ (m) The difference in the average height of branches in T1 and T2 recorded was statistically non significant @ CD 5% level the same was reflected in as well.

3.5 Number of leaves branch $^{-1}$ and plant $^{-1}$: Though the difference in average number of leaves per branch observed was statistically significant @ CD 5% level and the same per plant was non significant in T1 and T2.

- 3.6 Total leaf weight and shoot weight plant⁻¹ (kg) :** An average of 0.5285 kg of leaves produced per plant during the crop period in T1 and T2. Similarly, there was no difference in weight of shoots among the treatments.
- 3.7 Green biomass weight plant⁻¹ (kg) :** As there was no difference in the weight of leaves and shoots produced per plant during the crop period in T1 and T2 the same was reflected in the total biomass green weight as well.
- 3.8 Leaf weight ha⁻¹ crop⁻¹ (ton) :** Average estimated yield of 7.35 and 7.34 tons of mulberry leaves ha⁻¹ crop⁻¹ in T1 and T2 respectively are on par statistically @ CD 5% level.
- 3.9 Shoot weight ha⁻¹ crop⁻¹ (ton) :** Average estimated shoot weight of 5.55 and 5.67 tons harvested during the crop in T1 and T2 respectively are on par statistically @ CD 5% level.
- 3.10 Biomass green weight ha⁻¹ crop⁻¹ (ton) :** Average estimated biomass green weight of 12.90 and 13.00 tons ha⁻¹ produced during the crop in T1 and T2 respectively and its dry weight recorded are on par statistically @ CD 5% level.

b) Leaf quality Parameters :

- 3.11 Moisture Content of leaf (%) :** Average Moisture Content of leaf of 81.79 and 81.71% recorded during this crop in T1 and T2 respectively are on par statistically @ CD 5% level
- 3.12 Moisture Retention Capacity of leaf (%) :** Average Moisture Retention Capacity of leaf of 94.00 and 94.94% recorded during this crop in T1 and T2 respectively are on par statistically @ CD 5% level.

4. Conclusion :

It may be concluded that the maintenance of *A. chroococcum* bacteria culture and mass multiplication in Walkman's culture medium under laboratory conditions for production of "Nitrofert" bio-fertilizer is viable. "Nitrofert" bio-fertilizer application @ 20 kgs. ha⁻¹ year⁻¹ in 5 split doses in mulberry garden helps to reduce upto 50% nitrogenous chemical fertilizer requirement and saves expenditure without affecting the quality linked productivity, in addition it improves the soil health in an eco-friendly way.

References :

- [1] Anonymous (2002) Crops and drops making the best use of water for agriculture. Published by the Director, Information Division, FAO. UN., Viale delle Terme di Caracalla, 00100 Rome, Italy : 17-19.
- [2] Anonymous (2011). Scientific and Technological Annual Report. ICAR. New Delhi.
- [3] Arnon, D. L. and Stout, P. R (1939). The essentiality of certain elements in minute quantity for plants with special reference to copper. *Plant Physiology*. 14: 371-375.
- [4] Bürgmann, H.; Manuel Pesaro.; Franco Widmer. and Josef Zeyer. (2003). Strategy for optimizing quality and quantity of DNA extracted from soil. *Bacteriological Reviews*. 36(2) : .295 - 341
- [5] Chaturvedi, H.K. and Sarkar, A. (2000) Optimum size and shape of the plot for mulberry experiment. *Indian J. Seric*. 39 (1) : 66 - 69.
- [6] Chen, J. H.; Czajka, D. R.; Lion, L. W.; Shuler, M. L. and Ghiorse, W. C. (1995). Trace metal mobilization in soil by bacterial polymers. *Environmental Health Perspectives* 103(1): 53 - 58.
- [7] Church, M J.; Cindy M. Short.; Bethany D. Jenkins.; David M. Karl. and Jonathan P. Zehr. (2005). Temporal Patterns of Nitrogenase Gene (NifH) Expression in the Oligotrophic North Pacific Ocean, *Environmental Microbiology*. 134(1) : 155 - 193.
- [8] Dahama, A.K. (2003). Organic farming for sustainable agriculture. Updesh Purohit for Agrobios (India), Jodhpur. ISBN 81-7754-058-0.
- [9] Das, P.K.; Choudhury, P.C.; Ghosh, A; Katiyar,R.S; Madhav Rao, A.R.; Mathur, V.B. and Mazhumder, M.K. (1994). Studies on the effect of bacterial bio-fertilizers in irrigated mulberry (*Morus alba* L.) *Indian J. Seric*. 33:170 -173.
- [10] Emtiazia, G.; Ethemadifara, Z. and Habibib M. H. (2004). Production of extra-cellular polymer in Azotobacter and biosorption of metal by exopolymer. *African J of Biotechnol*. 3(6) : 330 - 333.
- [11] George M. Garrity. (2005). Bergey's Manual of Systematic Bacteriology Springer 2nd edition NewYork ISBN-13 : 978-0387241432.
- [12] Howard, J. B. and Rees, D.C. (2006). How many metals does it take to fix N₂? A mechanistic overview of biological nitrogen fixation. *Proceedings of the National Academy of Sciences of the United States of America* 103 : 46.
- [13] Kader. M.A.; Mian. M.H. and Hoque. M.S.(2002) Effect or Azotobacter inoculants on the yield and nitrogen uptake by wheat. *J. Biol Sci.*, 2 (4) : 259-261.

- [14] Li, D.Y.; Eberspächer, J.; Wagner, B.; Kuntzer, J. and Lingens, F. (1991). Degradation of 2,4,6-trichlorophenol by *Azotobacter* spp. strain GP1. *Applied and Environmental Microbiology*. 57 (7): 1920 - 1928
- [15] Miyashita, V. (1986) A report on mulberry cultivation and trainings methods suitable to bivoltine rearing in Karnataka, Central Silk Board, Bangalore, India.
- [16] Moreno J.; Gonzalez-Lopez J. and Vela, G. R. (1986). Survival of *Azotobacter* spp. in Dry Soils. *Applied and Environmental Microbiology* 51 (1): 123 - 125.
- [17] Nakade Dhanraj, B.; Chonde Sonal G. and Bhosale Pallavi (2012). Hallophilic nitrogen fixing *Azotobacter chroococcum* N-21 and its use as a bio-fertilizer for saline soils. *J. Microbiol. Biotech. Res.*, 2 (2) : 319 - 326
- [18] Pandey, S.H., Sinha B.K., (1972) Plant Physiology. Vikas Publishing House Pvt. Ltd. ISBN 0-7069-1327-4 : 111.
- [19] Rajanna, L.; Das, P.K.; Ravindran, S.; Bhogsha, K.; Mishra R.K.; Singhvi, N.R.; Katiyar, R.S. and Jayaram, H. (2005). Mulberry cultivation and physiology. Published by Central silk board Bangalore : 82.
- [20] Ray, D.; Mandal,L.N.; Pain, A.K. and Mondal,S.K. (1973). Effect of NPK and FYM on the yield and nutritive value of mulberry leaf. *Indian J. of Seric.* 12(1)7 - 12.
- [21] Rangaswami, G. and Bagyaraj, D.J. (2004). Agricultural Microbiology. Prentice Hall of India private limited, New Delhi. ISBN 81-203-0668-6: 131 - 138.
- [22] Shank Yu.; Demin O. and Bogachev AV. (2005). Respiratory Protection nitrogenase complex in *Azotobacter vinelandii*. *Success. Biological Chemistry* 45: 205 - 234
- [23] Sharma Arun, K. (2002). A handbook of Organic farming. Updesh Purohit for Agrobios (India), Jodhpur. ISBN 81-7754-099-8 : 219 - 229.
- [24] Sreenivasa Shetty, N.K.; Devaiah, M.C. and Shankar, M.A. (1990). Effect of ammonium chloride on growth and yield of mulberry in comparison with other nitrogenous fertilizers. *Indian J. Seric.* 29 (1) : 101 -1 09
- [25] Subba Rao, N.S. (1982). Biofertilizers in Agriculture. Oxford and IBH Publishing Co.,New Delhi.ISBN 81-204-0125-5:8.
- [26] Sudhakar, P.; Chattopadhyay, G.N., Gangwar, S.K. and Ghosh, J. K. (2000). Effect of *Azotobacter* biofertilizer with inorganic nitrogen on leaf yield and quality of mulberry (*Morus alba* L) *Trop. Sci.* 40 (2) : 75 - 82.
- [27] Sukhatme, P.V. and Amble, V.N. (1985) Statistical methods for agriculture workers. Published by Publications and Information Division, Indian Council of Agricultural Research, New Delhi.
- [28] Swaminathan, S. (1994) Population and food - A crisis on the horizon. The Hindu survey of the environment : 7 - 9.
- [29] Vijayan, K.; Reghunath, M.K.; Das, K.K.; Tikader, A.; Chakraborty, S.P.; Roy, B.N. and Quadri, S.M.H. (1997) Studies on leaf moisture of mulberry germplasm varieties. *Indian J. Seric.* 36 (2):155 - 157.
- [30] Wong, T.Y. and Maier R.J. (1985). H₂-Dependent Mixotrophic Growth of N₂-Fixing *Azotobacter vinelandii*. *Journal of Bacteriology* 163(2): 528 - 533
- [31] Yamagata U. and Itano A. (1923). *Physiological Study of Azotobacter chroococcum*, *beijerinckii* and *vinelandii* types. *Journal of Bacteriology* 8 (6): 521 - 531.

Fig.1 Showing Leaf, shoot & biomass weight

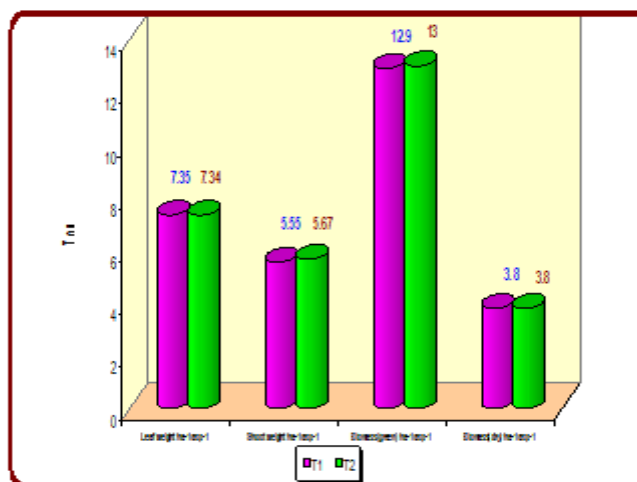


Fig. 1 Showing Moisture Content & Moisture Retention Capacity of leaf

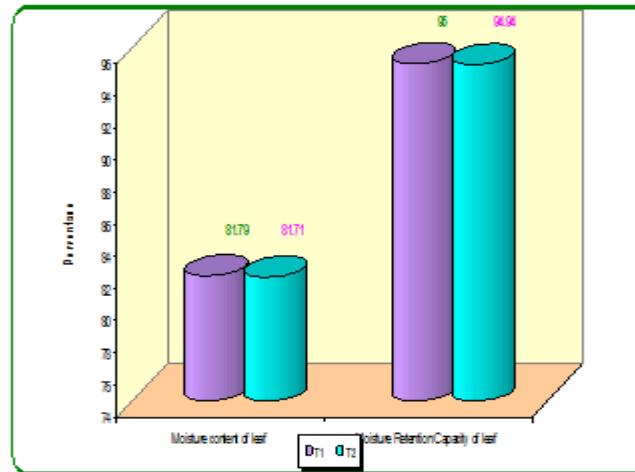


Table : Showing the effect of *A. chroococcum* bio-fertilizer (liberty) on quality and productivity of 6 year mulberry. Va. recommended dose of chemical fertilizer

Treatment	Growth parameters						Quality parameters							
	No. of branches / plant	Height of branch (cm)	Total shoot length / plant(m)	No. of leaves / branch	No. of leaves / plant	Leaf weight / plant(g)	Leaf weight / plant(g)	Total shoot weight / plant(g)	Leaf weight / plant(g)	Total shoot weight / plant(g)	Total biomass weight ha ⁻¹ crop ⁻¹ (ton)	Total biomass weight ha ⁻¹ crop ⁻¹ (ton)	Moisture content of leaf (%)	Moisture Retention Capacity of leaf (%)
1	2	3	4	6	6	7	8	8	10	11	12	13	14	15
T1	13.92	120.62	16.70	20.75	283.57	0.53	0.40	0.93	7.35	5.55	12.90	3.80	81.79	95.00
T2	15.92	113.54	17.94	18.63	291.45	0.53	0.41	0.94	7.34	5.67	13.00	3.82	81.71	94.94
Grand Mean	14.9235	117.076	17.3215	19.6862	287.5073	0.5285	0.405	0.9331	7.3412	5.6469	12.9504	3.8092	81.7527	94.9742
SEd	0.919	3.7835	1.0557	0.6383	12.9319	0.0395	0.0397	0.0771	0.5466	0.5394	1.069	0.3145	0.2125	0.1323
CD @ 5% level	1.8669 ^{ns}	7.6013 ^{ns}	2.1112 ^{ns}	1.2702 ^{ns}	24.4932 ^{ns}	0.0813 ^{ns}	0.0822 ^{ns}	0.1591 ^{ns}	1.1323 ^{ns}	1.1323 ^{ns}	2.2063 ^{ns}	0.649 ^{ns}	0.4282 ^{ns}	0.2731 ^{ns}

ns : Standard Error (within); CD : Critical Difference; * Significant at CD 5% level; NS: Non significant

**Plates showing different stages in mass multiplication of
Azotobacter chroococcum and Nitrofert biofertilizer production**



Plates : 1 & 2 Culture media preparation



Plate: 3 Sterilization of culture media



Plate : 4 Inoculation of *A. chroococcum*



Plate : 5 *A. chroococcum* culture



Plate : 6 Shaking for growth of culture



Plate : 7 Microscopic observation



Plate : 8 Mixing of culture in carrier material

Plates showing Nitrofert biofertilizer production & experiment in the field



Plate : 9 Nitrofert weighing & packing



Plate : 10 Nitrofert Bio-fertilizer



Plate : 11 Experiment Plot layout



Plate : 12 Mixing of NPK fertilizer



Plate : 13 Nitrofert mixing with FYM



Plate : 14 Treatment in progress



Plate : 15 Experimental plot



Plate : 16 Data collection

Realization Of Gateway Relocation Using AC And LB Algorithms In Mobile Wimax Networks

K.Sujatha¹, C.Nandagopal²

¹, Second M.E (Communication Systems),

²,Lecturer,ECE department

Abstract:

The WiMAX Forum has defined a two-tiered mobility management to minimize handover delay and packet loss. However, it leads to another problem: When to perform ASN GW relocation? The standards only define the ASN GW relocation procedures without specifying when the ASN GW relocation should be performed. It is left for vendors and operators to develop their own proprietary solutions. In this paper, we propose an algorithm, which incorporates traditional Admission Control (AC) and Wiener Process (WP)-based prediction algorithms to determine when to carry out ASN GW relocation. We further develop an analytical model to analyze the proposed algorithm. Simulations are also conducted to evaluate the performance of the proposed algorithm. The results show that the proposed algorithm can improve the performance significantly in terms of blocking probability, dropping probability, average serving rate, and average signaling overhead. The performance is checked with hard handoff and compared with the existing system.

Keywords: Admission control Wi-MAX networks, Mobility management, resource management, statistics and stochastic process and wireless networks

1. Introduction:

The IEEE 802.16-series standards [1], [2] are expected to provide broadband wireless access for a variety of multimedia services. The working group standardizes physical (PHY) layer and Medium Access Control (MAC) layer only. To build a complete system, higher layers are still necessary. One of the major objectives of WiMAX Forum thus, is to develop and standardize the WiMAX Forum Network Architecture [4],[5],[6],[7] which is evolving into Internet Protocol (IP)-based Service Network (ASN) which provides wireless radio access for WiMAX subscribers. It consists of one ASN Gateway (ASN GW) and many base stations (BSs). Each ASN is connected to Connectivity Service Network (CSN), which provides IP connectivity services. To support IP mobility, Mobile IP (MIP) 1 is adopted. The Home Agent (HA) of a Mobile Station (MS) is located in the CSN of the MS's Home Network Service Provider (H-NSP). In the shown fig :1 there takes place two mobility's:

They are as follows

- i) ASN Anchored mobility
- ii) CSN Anchored mobility

ASN Anchored Mobility refers to MS's movement between BSs that belong to the same or different ASN GWs. In ASN Anchored Mobility, the context of the designated MS is transferred from the previous BS to the new BS. Without performing CSN Anchored Mobility, ASN Anchored Mobility can minimize handover delay and packet loss. An MS may perform intra-ASN handover (e.g., changing from Flow (1) to Flow (2) in Fig. 1) while still attaching to the same ASN GW. In addition, an MS may perform inter-ASN handover (e.g., changing from Flow (2) to Flow (3) in Fig. 1) where the ASN GW A is the traffic anchor point and responsible for ASN CSN tunneling. That is, traffic is still sent to ASN GW A, which then further tunnels traffic to ASN GW B. In Flow (1) and Flow (2), the MS is called Serving MS of ASN GW A. In Flow (3), the MS is called Anchored MS of ASN GW A and handover MS of ASN GW B. In such case, the ASN GW A and ASN GW B are called anchored ASN GW and Serving ASN GW, respectively. CSN Anchored Mobility refers to the process of changing the traffic anchor point and is independent of the MS's link layer handover [4]. It is also called ASN GW relocation. For example, if CSN Anchored Mobility is not performed, when the MS roams from ASN GW B to ASN GW C in Fig. 1, ASN GW A will tunnel traffic to ASN GW C. The MS is still served by two ASN GWs (ASN GW A and ASN GW C). As aforementioned discussion, the MS is called Anchored MS of ASN GW A.

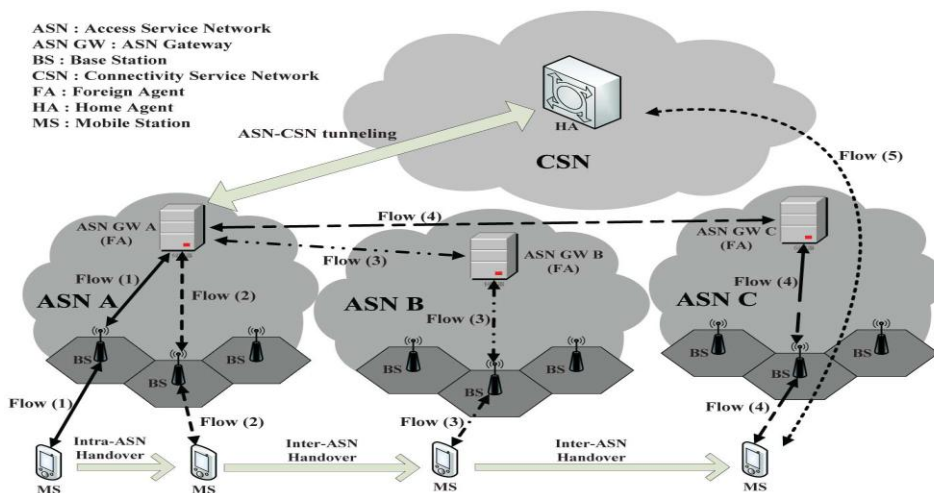


Fig: 1 ASN Anchored Mobility and CSN Anchored mobility in WiMAX Networks

The ASN GW A may request the MS to carry out CSN Anchored Mobility, i.e., ASN GW relocation. This may happen due to the heavy load of the ASN GW A, to reduce end-to-end latency, or for resource optimization purposes [4], [5]. After performing ASN GW relocation, the traffic anchor point is changed to ASN GW C. The MS then is not served by ASN GW A. This is shown in Fig. 1 after changing from Flow (4) to Flow (5).

2. Algorithms

2.1 Gateway Relocation Admission Control Algorithm (Grac)

The ASN GW relocation may be initiated at different times with different reasons. For example, as aforementioned discussion, an MS may perform ASN Anchored Mobility without performing CSN Anchored Mobility to reduce handover latency. After the handover is completed (i.e., the handover delay has been reduced), the MS may perform ASN GW relocation immediately so the number of Anchored MSs can be kept small. However, it may not be a good strategy always to relocate an Anchored MS so quick. For example, an MS may move fast and keep changing its Serving ASN GW. In this example, it might be better to keep the Anchored ASN GW unchanged. In some other examples, if the system load is light, there is no emergent need to perform ASN GW relocation. However, when more and more MSs are served by two ASN GWs, the system load will become heavy. New users may be blocked. Handover users may be dropped as well. The network performance may be reduced significantly. Therefore, performing ASN GW relocation is essential. In WiMAX standards [4], [5] it is specified that ASN GW can decide when to perform ASN GW relocation. In this paper, we consider that the system load is heavy so Anchored MSs are forced to perform ASN GW relocation. The proposed GRAC determines when to request Anchored MSs to perform ASN GW relocation and how many Anchored MSs should be relocated. After ASN GW relocation, resources are released and system performance is improved.

The proposed algorithm does not need to exchange information between neighboring ASN GWs. It also does not require centralized coordination and any assistance from extra servers. In addition, the proposed algorithm does not need to predict the movement of the mobile stations. It combines AC algorithm with a prediction technique to determine when is necessary to perform ASN GW relocation. Thus, it is called Gateway Relocation AC (GRAC).

2.2 New call bounding algorithm

The GRAC can work with any AC algorithm. In this section, we simply pick up the new call bounding algorithm. For simplicity, here we assume that the resource assigned to each MS in one ASN GW is equal. The main point is not on a specific AC algorithm. The focus is on how to modify an AC algorithm for the two-tier mobility management in WiMAX. The proposed GRAC with the new call bounding Algorithm will limit the number of Serving MSs and Anchored MSs in one ASN GW. The maximum number of MSs in the network and Tncb is the limit for the number of new MSs, which have been admitted into the network. when a new call enter the network it will either accepted or dropped based on the network resource availability.

2.3 WP-based prediction algorithm

In the above algorithm, we can set C_0 as C because a new coming MS can be queued until the resource is available after ASN GW relocation is completed. However, this approach cannot be applied to handover MSs because handover MSs are sensitive to handover latency. The acceptable handover delay is much less than the queuing delays of a new MS. Assuming that a handover MS arrives and C is reached. If the handover MS needs to wait for the ASN GW relocation of one Anchored MS, the handover latency will be too high. Actually, if ASN GW relocation is performed just when a handover MS arrives, it is equivalent to performing both ASN Anchored Mobility and CSN Anchored Mobility. The handover latency cannot be reduced. On the other hand, one may perform ASN GW relocation much earlier than C is reached. However, this may force many Anchored MSs to perform ASN GW relocation, which may not be preferable as already discussed earlier. Thus, for handover MSs, it is critical to perform ASN GW relocation at an appropriate time. Therefore, we propose a prediction algorithm based on Wiener Process (WP) which provides a systematic way to determine when to request Anchored MSs to perform ASN GW relocation. In addition, the algorithm can also estimate how many Anchored MSs should be relocated. The proposed algorithm is simple and accurate.

Wiener Process has been proven effective in modeling Stochastic processes where the values of the random variables are affected by a large number of independent or weakly dependent factors, each with a relatively small impact [18]. The $W(t)$ we want to model is impacted by a large number of factors. These factors are either independent or weakly dependent of each other. For example, $W(t)$ is impacted by the arrival rate of new MSs, arrival rate of handover MSs, average connection holding time, average network residence time, and so on.

2.4 Load balancing algorithm(LB)

The load balancing algorithm will reduce the overload of packets and reduce the blocking and dropping of the packets. After the handover is completed (i.e., the handover delay has been reduced), the MS may perform ASN GW relocation immediately so the number of Anchored MSs can be kept small. Here the load balancing is done with the hard handoff. Here once the gateway is overloaded then the entire gateway is relocated immediately, therefore the mobile users can communicate with the new gateways. Because of the gateway relocation the dropping and blocking of packets will be reduced. Hence the average serving rate of the packets within the network will be increased. Hence the performance of the network will also be increased.

3. Performance analysis

We propose an analytical model to investigate the performance of the proposed algorithm. In the analysis, the connection holding time is defined as the time from an MS connects to the network until it is disconnected. The network residence time is the time an MS is served by an ASN GW. We assume each ASN GW has two arrival processes which are Poisson distributed with rate λ_n and λ_h for new MSs and handover MSs, respectively. If a new MS is admitted into the network, we assume the connection holding time and network residence time follow exponential distribution with mean $1/\mu_c$ and $1/\mu_n$, respectively. For a handover MS, only network residence time is required. It is also assumed to be exponentially distributed with mean $1/\mu_n$. To analyze the proposed GRAC, there are three major factors are —the number of Serving MSs, the number of handover MSs, and the number of Anchored MSs. Intuitively, a 3-D Markov chain may be used to investigate the performance. Unfortunately, the computational complexity of a 3-D Markov chain will be increased dramatically when the number of MSs in the system becomes large.

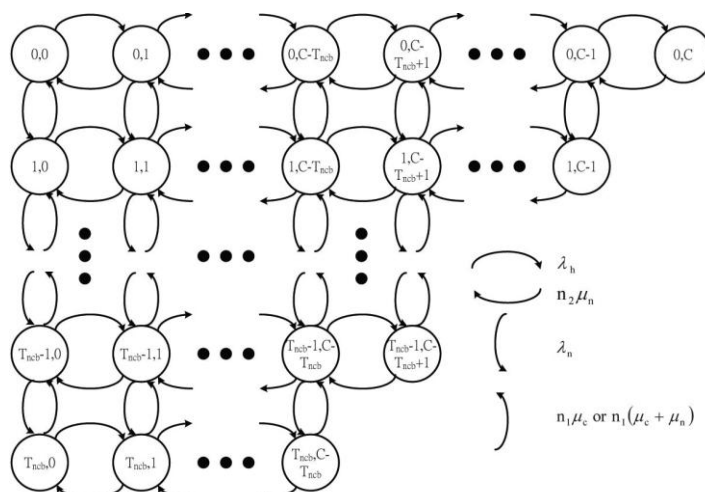


Fig: 2-State transition diagram

Upper bound: If we assume each MS never performs ASN GW relocation, it will always be served by two ASN GWs. For each ASN GW, the average service time of new MSs is $1/\mu_c$. That is, the MSs will stay in the ASN GW for the duration of whole connection holding time. It will result in the highest blocking probability for new MSs and dropping probability for handover MSs.

Lower bound: If each MS always performs ASN GW relocation immediately after each inter-ASN handover, the average service time of new MSs becomes $1/(\mu_c + \mu_n)$ for each ASN GW

4.Numerical Results

The analysis is validated by extensive simulations by using Network Simulator-version 2 (ns-2). The analytical results of both upper-bound and lower-bound cases are close to the simulation results. In addition to the upper-bound analysis and lower-bound analysis, we also provide simulation results for the proposed GRAC with WP-based prediction. The parameters and values used in simulations are listed in Table:1. The following sections present the results with various performance metrics. The results are based on exponential distribution for connection holding time and network residence time. We have also conducted simulations by using gamma distribution to model connection holding time and network residence time with mean $1/\mu_c$ and $1/\mu_n$

TABLE: 1 Parameters for simulation

Parameter	Value
C	50
T_{ncb}	25
$1/\mu_c$	1000 (s)
T_{wnr}	45
τ	5 (s)
k	25
α	$N(0, 1)$

- C: Maximum number of MSs in one ASN GW
- Tncb: Threshold for blocking a new MS
- $1/\mu_c$: Average connection holding time for new MSs
- Twnr: Threshold for carrying out WP-based prediction
- T: Sampling time interval
- K: Number of latest samples
- α : Standard normal random variable

4.1 Blocking probability of New MSs

The blocking probability of new MSs when λn is varied from 0.01 (1/s) to 0.1 (1/s). We set $\lambda h = 0.04$ (1/s) and $1/\mu n = 400$ (s). As expected, for both upper-bound and lower-bound cases, the blocking probability increases significantly when λn increases. Nevertheless, Fig. 4 shows that the blocking probability of the proposed GRAC is close to that of the lower-bound case regardless of the value of Δt . This is because our algorithm can appropriately request Anchored MSs to perform ASN GW relocation when a new MS arrives. We also investigate the blocking probability with Different mean network residence time, $l = \mu n$. In this case, we choose $\lambda n = 0.04$ (1/s) and $\lambda h = 0.04$ (1/s). When $1/\mu n$ increases, the MSs will be served by the ASN GW longer. Thus, they perform inter-ASN handover less. Therefore, the blocking probability in the lower-bound case and the proposed GRAC is increased even if λn and λh are fixed. On the other hand, because the new MSs never perform ASN GW relocation, the blocking probability of the upper-bound case is irrelevant to $1/\mu n$. Therefore, it remains constant. Comparing the upper-bound case with the lower-bound case, when $1/\mu n$ is much lower than $1/\mu c$, many new MSs become Anchored MSs. The incoming new MSs can be accepted easily by requesting the Anchored MSs to perform ASN GW relocation in the lower-bound case. Here HH referred to as Hardhandoff.

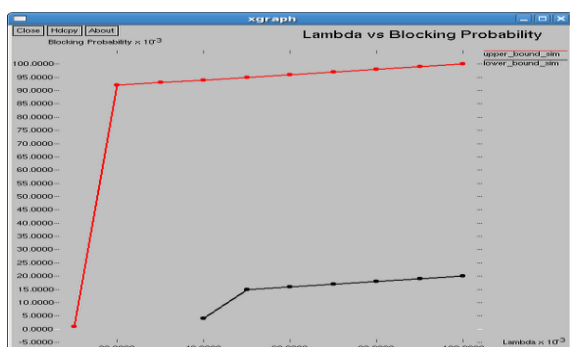


Fig: 3 Arrival rate vs. Blocking probability with AC with LB (HH)

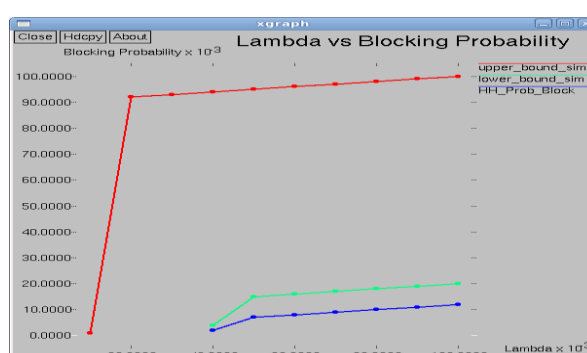


Fig :4 Arrival rate vs blocking probability

4.2 Dropping Probability of Handover MS

The dropping probability of handover MSs when λn is varied from 0.01 (1/s) to 0.1 (1/s) we set $\lambda h = 0.04$ (1/s) and $1/\mu n = 400$ (s). When λn increases, i.e., there are more MSs in the system, the dropping probability increases too. The handover MS is dropped when C in the AC algorithm is reached. In the proposed GRAC, however, the WP-based prediction is sensitive to the variation of the samples. The Anchored MSs are requested to perform ASN GW relocation when the system is expected to be overloaded. Thus, the dropping probability of handover MSs is reduced significantly. Thus, they perform inter-ASN handover less. Therefore, the dropping probability is increased even if λn and λh are fixed. The dropping probability of the upper-bound case is also increased. This is because the handover MSs are also served by one ASN GW longer. In addition, in the proposed GRAC, the dropping probability of $\Delta t = 10$ (s) is lower than that of $\Delta t = 5$ (s).

4.3 Average Serving Rate

The average serving rate is defined as the average number of MSs served by an ASN GW per minute. It includes both new MSs and handover MSs. The average serving rate versus λn , where λn is varied from 0.01 (1/s) to 0.1 (1/s). We choose $\lambda h = 0.04$ (1/s) and $1/\mu n = 400$ (s). The upper-bound case and lowerbound case are almost equal when $\lambda n \leq 0.02$ (1/s). This is because the blocking and dropping probabilities are small in both cases. However, when λn increases, the average serving rate of lower-bound case increases faster than that of upper-bound case. This is because the blocking and dropping probabilities in the upper-bound case are higher than those in the lower-bound case. Thus, less MSs are served in the upper-bound case. Please also note that the average serving rate of the proposed GRAC is very close to that of the lower-bound case.

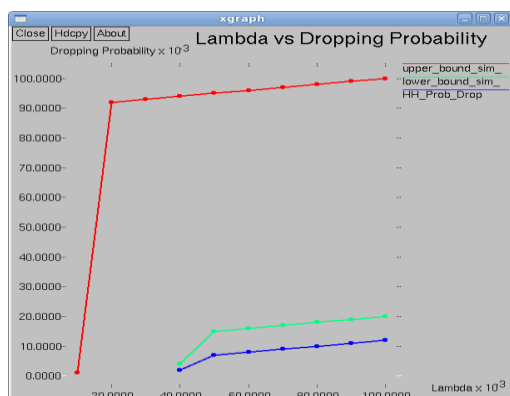


Fig: 5 Arrival rate vs dropping probability with AC with LB(HH).

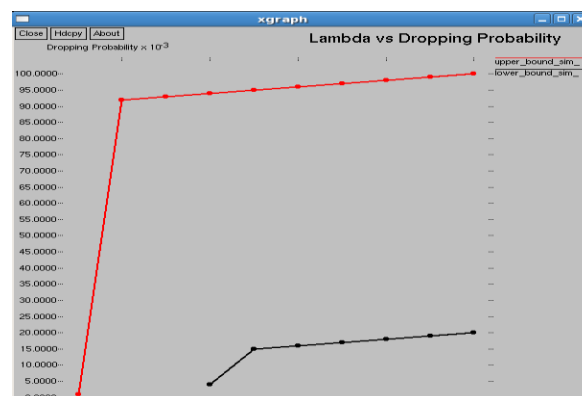


Fig:6 Arrival rate vs dropping probability

4.4 Average Signaling Overhead

The average signaling overhead per minute versus λn , where λn is varied from 0.01 (1/s) to 0.1 (1/s). We set $\lambda h = 0.04$ (1/s) and $1/\mu n = 400$ (s). The amount of signaling traffic generated by executing CSN Anchored Mobility can be measured by the number of ASN GW relocation performed in the system. As, the signaling overhead of the upper-bound case is 0, because new MSs never perform ASN GW relocation in the upper-bound case. In the lower-bound case, the signaling overhead is increased when λn increases. However, the signaling overhead of the proposed GRAC is always lower than that of the lower-bound case. This is because with WP based prediction, the proposed GRAC can request ASN GW relocation only when the system is expected to be overloaded. Furthermore, we also investigate the average signaling overhead with different mean network residence time, $1/\mu n$. We still set $\lambda n = 0.04$ (1/s) and $\lambda h = 0.04$ (1/s). Again, the signaling overhead of the upper bound case is 0

5.conclusion

In WiMAX standards, an ASN GW can decide when to perform ASN GW relocation. In this paper, we consider that the system load is heavy hence more number of packets will be either blocked or dropped. In order to reduce that we can increase the threshold value and the capacity of the network using load balancing algorithm. It is done with the Hard handoff. Hence here the capacity and threshold has been increased than in the existing system using hard handoff. The numerical results show that the proposed algorithm can effectively reduce the blocking probability, dropping probability, and average signaling overhead. It also increases the average serving rate. Hence we compare the proposed system with the existing system.

References

- [1] IEEE 802.16-2004 Std., Air Interface for Fixed Broadband Wireless Access Systems, IEEE, Oct. 2004.
- [2] IEEE 802.16e-2005 Std., Part 16: Air Interface for Fixed and Mobile Broadband Wireless Access Systems-Amendment 2: Physical and Medium Access Control Layers for Combined Fixed and Mobile Operation in Licensed Bands, IEEE, Feb. 2006.
- [3] WiMAX Forum Std. 1.0, Rev. 4, WiMAX Forum Network Architecture (Stage 2: Architecture Tenets, Reference Model and Reference Points), WiMAX, Feb. 2009.
- [4] WiMAX forum Std. 1.0, Rev. 4, WiMAX Forum Network Architecture (Stage 3: Detailed Protocols and Procedures), WiMAX, Feb. 2009.
- [5] L. Nuaymi, WiMAX: Technology for Broadband Wireless Access. John Wiley, 2007.
- [6] K. Etemad, "Overview of Mobile WiMAX Technology and Evolution," IEEE Comm. Mag., vol. 46, no. 10, pp. 31-40, Oct. 2008..
- [7] Y. Fang and Y. Zhang, "Call Admission Control Schemes and Performance Analysis in Wireless Mobile Networks," IEEE Trans. Vehicular Technology, vol. 51, no. 2, pp. 371-382, Mar. 2002.
- [8] D. Hong and S.S. Rappaport, "Traffic Model and Performance Analysis for Cellular Mobile Radio Telephone Systems with

- Prioritized and Nonprioritized Handoff Procedures,” IEEE Trans. Vehicular Technology, vol. 35, no. 3, pp. 77-92, Aug. 1986.
- [9] Y.-B. Lin, S. Mohan, and A. Noerpel, “Queuing Priority Channel Assignment Strategies for PCS Hand-Off and Initial Access,” IEEE Trans. Vehicular Technology, vol. 43, no. 3, pp. 704-712, Mar. 1994.
- [10] B. Li, S.T. Chanson, and C. Lin, “Analysis of a Hybrid Cutoff Priority Scheme for Multiple Classes of Traffic in Multimedia Wireless Networks,” Wireless Networks, vol. 4, no. 4, pp. 279-290, 1998.
- [11] R. Ramjee, D. Towsley, and R. Nagarajan, “On Optimal Call Admission Control in Cellular Networks,” Wireless Networks, vol. 3, no. 1, pp. 29-41, 1997.

Convective Heat Transfer in Maxwell-Cattaneo Dielectric Fluids

S. Maruthamanikandan¹ and Smita S. Nagouda²

^{1,2}Department of Mathematics, Christ University, Bangalore-560 029, INDIA

Abstract:

The effect of second sound on the onset of Rayleigh-Bénard instability in a dielectric fluid subject to the simultaneous action of a vertical ac electric field and a vertical temperature gradient is investigated theoretically by means of the method of small perturbation. The horizontal layer of the fluid is cooled from the upper boundary, while an isothermal boundary condition is imposed at the lower boundary. The eigenvalues are obtained for free-free, isothermal boundary combinations and the influence of various parameters on the onset of electrothermal convection has been analyzed. Some of the known cases are derived as special cases. The Rayleigh-Bénard problem for a Maxwell-Cattaneo dielectric fluid is always less stable than that with classical heat conduction. It is shown that the destabilizing influence of the Cattaneo number is not attenuated by that of the dielectrophoretic force and vice versa, and that both second sound and electric forces change the aspect ratio of convection cells appreciably.

Keywords: AC electric field, Dielectric fluid, Electroconvection, Hyperbolic energy equation, Maxwell-Cattaneo heat flux, Roberts number, Stationary instability.

1. Introduction

The problems of natural convection in dielectric fluids have received widespread attention because they are representative of a variety of non-isothermal situations. The dielectric liquids are characterized by very slight electrical conductivity. Transformer oil (and most other organic substances) and distilled water are examples of such fluids. Compared to magnetic liquids, these liquids are easier to prepare. Under the influence of an external electric field such a fluid exhibits a large polarization and as soon as the field is removed, the fluid attains zero polarization state at once. Dielectric liquids can be controlled by electric forces and the relevant details were addressed by Melcher [1]. The general topic of electrically enhanced heat transfer in fluids and possible practical applications has been reviewed by Jones [2] and Chen *et al.* [3]. Electrically induced convection in dielectric liquids has been the subject of investigation for many decades right from the experimental work of Gross and Porter [4]. They observed that the convection pattern established by the electric field is quite similar to the familiar Bénard cells in normal convection. Turnbull [5] examined the effect of dielectrophoretic forces on the Bénard instability. The principle of exchange of stabilities is shown to hold for a certain set of boundary conditions. Approximate solutions for the critical temperature gradient as a function of the wavelength and the electric field are found using the variational principles and the Galerkin method.

The effect of uniform rotation on the onset of convective instability in a dielectric fluid under the simultaneous action of a vertical ac electric field and a vertical temperature gradient was considered by Takashima [6]. It is shown that the principle of exchange of stabilities is valid for most dielectric fluids. It is shown that, even when the electrical effects are taken into account, the coriolis force has an inhibiting effect on the onset of instability and as the speed of rotation increases the coupling between the two agencies causing instability (electrical and buoyancy force) becomes tighter. Stiles [7] investigated the problem of an electrically insulating liquid layer confined between horizontal conducting electrodes, the upper of which is warmer. It is found that the system becomes unstable with respect to the onset of steady convection when the electric field strength reaches a critical value, which in a rapidly varying ac field is due to the polarization body force. Maekawa *et al.* [8] considered the convective instability problem in ac and dc electric fields. Linearized perturbation equations are solved analytically.

Stiles *et al.* [9] studied the problem of convective heat transfer through polarized dielectric liquids. It is shown that for a critical voltage, as the gravitational Rayleigh number becomes increasingly negative, the critical wavenumber at the onset of convection becomes very large. As the temperature drop between the plates increases the fraction of the heat transfer associated with convection is found to pass through a maximum value when the critical horizontal wavenumber is close to four times its value when gravity is absent. Smorodin [10] analyzed the effect of an alternating arbitrary-frequency electric field on the stability of convective flow of a dielectric liquid occupying a vertical layer in the *EHD* approximation. The stability thresholds are determined in the linear approximation using Floquet theory. Maruthamanikandan [11] investigated the problem of gravitational instability in a dielectric liquid in the presence of internal heat generation, surface tension,

radiation and viscoelasticity. Mikheev *et al.* [12] experimentally verified that dielectric liquids can be purified by means of turbulent electroconvection under the action of ponderomotive forces arising in an inhomogeneous alternating electric field. Radhakrishna and Siddheshwar [13] investigated linear and a weakly nonlinear stability analysis of thermal convection in a dielectric liquid permeated by a vertical, uniform ac electric field using the normal mode method and truncated representation of Fourier series respectively. It is found that the effect of increasing the electric number is to enhance the amplitudes and thereby the heat transport.

The propagation of thermal waves is sometimes referred to as second sound effect. The classical energy equation allows for an infinite speed for the propagation of heat, which is physically unacceptable. The energy equation to be considered in the present work is effectively a damped wave equation and is therefore hyperbolic rather than parabolic. The knowledge of second sound has provided a rich source of information for the study and understanding of the superfluid state. Second sound is not in any sense a sound wave, but a temperature or entropy wave. In ordinary or first sound, pressure and density variations propagate with very small accompanying variations in temperature; in second sound, temperature variations propagate with no appreciable variations in density or pressure. Recently, it has been realized that this is not just a low temperature phenomenon, but has important applications in such fields as skin burns, phase changes, biological materials, and in nanofluids (Straughan [14]).

Straughan and Franchi [15] investigated the effect of thermal waves (second sound) upon the onset of convective instability of a Newtonian fluid confined between a horizontal layer of finite thickness. They obtained critical Rayleigh number for the onset of convection when the Maxwell-Cattaneo heat flux law is employed, which allows for thermal waves of finite speed. Stress-free boundaries have been considered. It is found that convection is possible in both heated above and below cases and that the Bénard problem for a Maxwell-Cattaneo fluid is always less stable than the classical one and overstability only occurs in the heated below case. Lebon and Cloot [16] examined the effects resulting from the substitution of the classical Fourier law of heat conduction by the Maxwell-Cattaneo law in Bénard's and Marangoni's problems. Considering only infinitesimally small perturbations, it is shown that when buoyancy is the single factor of instability, no stationary convection can develop in a fluid layer heated from above, but oscillatory convection is possible. It is found that, in Maxwell-Cattaneo fluid, oscillatory convection does not play an important practical role.

Straughan [14] investigated the problem of thermal convection for a layer of fluid when the heat flux law of Cattaneo is adopted. The boundary conditions are taken to be rigid-rigid and isothermal. It is shown that for small Cattaneo number, the critical Rayleigh number initially increases from its classical value until a critical value of the Cattaneo number is reached. For Cattaneo numbers greater than this critical value a notable Hopf-bifurcation is observed with convection occurring at lower Rayleigh numbers and by oscillatory rather than stationary convection. It is also found that the aspect ratio of the convection cells likewise changes. Smita and Pranesh [17] studied the problem of the onset of Rayleigh-Bénard convection in a second order Colemann-Noll fluid by replacing the classical Fourier heat flux law with non-classical Maxwell-Cattaneo law. The eigenvalue problem is solved using the general boundary conditions on velocity and third type of boundary conditions on temperature. It is found that the classical Fourier heat flux law overestimates the critical Rayleigh number compared to that predicted by the non-classical law and that the results are noteworthy at short times.

While the effect of a variety of non-uniform basic temperature gradients on the onset of electroconvection has been studied intensely, this paper is devoted to studying qualitatively the effect of propagation of thermal waves upon the onset of electroconvection in a horizontal layer of dielectric fluid. The linear stability analysis is based on the normal mode technique and we allow for a thermal wave of finite speed by adopting the heat flux model of Cattaneo.

2. Mathematical Formulation

We consider a Boussinesq dielectric fluid layer of thickness ' d ' with a uniform vertical ac electric field applied across the layer. The lower and upper boundaries of the fluid layer are maintained at uniform, but different temperatures T_0 and T_1 (with $T_0 > T_1$) respectively. A Cartesian coordinate system (x, y, z) is chosen with the origin at the bottom of the fluid layer and the z -axis normal to the fluid layer.

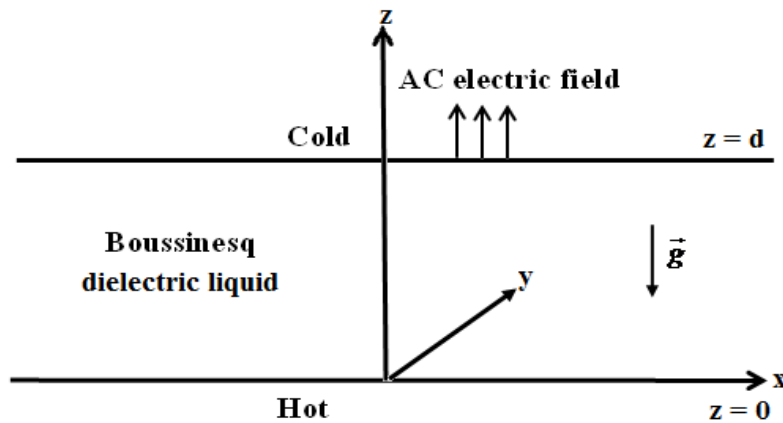


Fig. 1 Configuration of the problem.

The relevant governing equations for an incompressible dielectric fluid under the Boussinesq approximation are

$$\nabla \cdot \vec{q} = 0 \quad (1)$$

$$\rho_0 \left[\frac{\partial \vec{q}}{\partial t} + (\vec{q} \cdot \nabla) \vec{q} \right] = -\nabla p + \rho \vec{g} + \mu \nabla^2 \vec{q} + (\vec{P} \cdot \nabla) \vec{E} \quad (2)$$

$$\frac{\partial T}{\partial t} + (\nabla \cdot \vec{q}) T = -\nabla \cdot \vec{Q} \quad (3)$$

$$\tau \left[\frac{\partial \vec{Q}}{\partial t} + (\nabla \cdot \vec{q}) \vec{Q} + \vec{\omega} \times \vec{Q} \right] = -\vec{Q} - \kappa \nabla T \quad (4)$$

$$\rho = \rho_0 [1 - \alpha(T - T_0)] \quad (5)$$

where \vec{q} is the velocity vector, \vec{P} the dielectric polarization, \vec{E} the electric field, T the temperature, p the pressure, ρ the fluid density, κ the thermal diffusivity, μ the fluid viscosity, \vec{g} the acceleration due to gravity, α the coefficient of thermal expansion, ρ_0 the density at a reference temperature $T = T_0$, \vec{Q} the heat flux vector, τ the constant relaxation time and $\vec{\omega} = \frac{1}{2}(\nabla \times \vec{q})$. The electric properties involved in the Kelvin body force are the polarization \vec{P} and the electric field gradient $\nabla \vec{E}$. In a dielectric liquid the polarization vector \vec{P} measures the electric dipole moment per unit volume of fluid due to partial alignment of intrinsic molecular dipoles induced by the applied electric field \vec{E} . It should be noted that if the frequency of the electric field becomes too high there can be appreciable heating associated with dielectric loss. Fortunately, this form of dielectric heating is negligible for the frequencies discussed in this paper.

The relevant Maxwell equations are

$$\vec{P} = \epsilon_0 [\epsilon_r - 1] \vec{E} \quad (6)$$

$$\nabla \cdot (\epsilon_0 \epsilon_r \vec{E}) = 0 \quad (7)$$

$$\nabla \times \vec{E} = 0 \text{ or } \vec{E} = \nabla \phi \quad (8)$$

where ϵ_0 is the electric permittivity, ϵ_r the relative permittivity or dielectric constant and ϕ the electric potential. The dielectric constant is assumed to be a linear function of temperature according to

$$\epsilon_r = \epsilon_r^0 - e(T - T_0) \quad (9)$$

where $e > 0$ is the dielectric permittivity and $\epsilon_r^0 = 1 + \chi_e$ with χ_e being the electric susceptibility.

2.1 Basic state

The basic state is quiescent and is described by

$$\begin{aligned} \vec{q} = \vec{q}_b = (0, 0, 0), \quad p = p_b(z), \quad \rho = \rho_b(z), \quad T = T_b(z), \quad \vec{E} = \vec{E}_b = (0, 0, E_b(z)), \\ \vec{P} = \vec{P}_b = (0, 0, P_b(z)), \quad \varepsilon_r = \varepsilon_{rb}(z), \quad \phi = \phi_b(z), \quad \vec{Q} = \vec{Q}_b = (0, 0, \kappa\beta), \quad \beta = \frac{T_0 - T_1}{d} \end{aligned} \tag{10}$$

where the subscript *b* denotes the basic state. The quiescent basic state has a solution given by

$$T_b = T_0 - \beta z \tag{11}$$

$$\rho_b = \rho_0 [1 + \alpha\beta z] \tag{12}$$

$$\varepsilon_{rb} = (1 + \chi_e) \left[1 + \frac{e\beta z}{1 + \chi_e} \right] \tag{13}$$

$$E_b = \frac{E_0 (1 + \chi_e)}{1 + \chi_e + e\beta z} \tag{14}$$

$$\vec{P}_b = \varepsilon_0 E_0 \left[(1 + \chi_e) - \frac{1}{\left(1 + \frac{e\beta z}{1 + \chi_e} \right)} \right] \hat{k} \tag{15}$$

$$\phi_b = \frac{(1 + \chi_e) E_0}{e\beta} \log \left[1 + \frac{e\beta z}{1 + \chi_e} \right] \tag{16}$$

where E_0 is the value of the electric field at $z=0$.

2.2. Perturbed State

Since we are interested in the stability of the basic state, we superimpose infinitesimally small perturbations on the basic state according to

$$\begin{aligned} \vec{q} = \vec{q}_b + \vec{q}' = (u', v', w'), \quad p = p_b + p', \quad \rho = \rho_b + \rho', \quad T = T_b + T', \\ \vec{E} = \vec{E}_b + \vec{E}', \quad \vec{P} = \vec{P}_b + \vec{P}', \quad \varepsilon_r = \varepsilon_{rb} + \varepsilon'_r, \quad \phi = \phi_b + \phi', \quad \vec{Q} = \vec{Q}_b + \vec{Q}' \end{aligned} \tag{17}$$

where primes denote perturbed quantities. Following the classical procedure of linear stability analysis, the linearized equations governing small perturbations turn out to be

$$\rho_0 \frac{\partial}{\partial t} (\nabla^2 w') = \mu (\nabla^4 w') + \alpha \rho_0 g \nabla_1^2 T' + \frac{\varepsilon_0 e^2 E_0^2 \beta}{1 + \chi_e} \nabla_1^2 T' - \varepsilon_0 e E_0 \beta \frac{\partial}{\partial z} (\nabla_1^2 \phi') \tag{18}$$

$$\left(1 + \tau \frac{\partial}{\partial t} \right) \left(\frac{\partial T'}{\partial t} - \beta w' \right) = -\kappa \nabla^2 T' - \frac{\tau \kappa \beta}{2} \nabla^2 w' \tag{19}$$

$$(1 + \chi_e) \nabla^2 \phi' - e E_0 \frac{\partial T'}{\partial z} = 0 \tag{20}$$

where $\nabla_1^2 = \frac{\partial^2}{\partial x^2} + \frac{\partial^2}{\partial y^2}$. Non-dimensionalizing (18), (19) and (20) using the length, time, velocity, temperature

and electric potential scales $d, \frac{d^2}{\kappa}, \frac{\kappa}{d}, \beta d$ and $\frac{e E_0 \beta d^2}{1 + \chi_e}$, we obtain (after neglecting the primes for simplicity)

$$\frac{1}{Pr} \frac{\partial}{\partial t} (\nabla^2 w) = \nabla^4 w + (R + L) \nabla_1^2 T - L \frac{\partial}{\partial z} (\nabla_1^2 \phi) \tag{21}$$

$$\left(1 + 2C \frac{\partial}{\partial t} \right) \left(\frac{\partial T}{\partial t} - w \right) = \nabla^2 T - C \nabla^2 w \tag{22}$$

$$\nabla^2 \phi - \frac{\partial T}{\partial z} = 0 \tag{23}$$

where $Pr = \frac{\mu}{\rho_o \kappa}$ is the Prandtl number, $R = \frac{\alpha \rho_o g \beta d^4}{\mu \kappa}$ is the thermal Rayleigh number, $L = \frac{\epsilon_o (e E_o \beta d^2)^2}{\mu \kappa (1 + \chi_e)}$ is the Roberts number and $C = \frac{\tau \kappa}{2d^2}$ is the Cattaneo number. The boundary conditions are taken to be free-free, isothermal and their importance will be made clear in Section 5. So the boundary conditions are

$$w = D^2 w = T = D\phi = 0 \text{ at } z = 0, 1. \tag{24}$$

It should be mentioned that Takashima and Ghosh [18] used the boundary condition $D\phi = 0$ in order to obtain exact solution to the problem of electrohydrodynamic instability in a viscoelastic fluid with free-free, isothermal boundaries. The derivation of the general boundary conditions for the electric potential ϕ is given in the work of Maruthamanikandan [11].

3. Linear Stability Analysis

We use the normal mode solution for the dependent variables according to

$$[w, T, \phi] = [W(z), \Theta(z), \Phi(z)] \exp\{i(lx + my) + \sigma t\} \tag{25}$$

where l and m are the dimensionless wavenumbers in the x and y directions respectively and σ is the growth rate. Because the linear eigenvalue system (21) – (23) has constant coefficients, it has a general solution with an exponential dependence on z . Substituting (25) into (21), (22) and (23), noting that the principle of exchange of stabilities is valid [6, 16], we arrive at the following stability equations

$$(D^2 - a^2)^2 W - (R + L)a^2 \Theta + La^2 D\Phi = 0 \tag{26}$$

$$(D^2 - a^2)\Theta = [C(D^2 - a^2) - 1]W \tag{27}$$

$$(D^2 - a^2)\Phi - D\Theta = 0 \tag{28}$$

where $D = \frac{d}{dz}$ and $a = \sqrt{l^2 + m^2}$ is the non-dimensional wavenumber of the convective disturbance. In view of (25), the boundary conditions (24) take the form

$$W = D^2 W = \Theta = D\Phi = 0 \text{ at } z = 0, 1. \tag{29}$$

4. Exact Solution

Equations (26), (27) and (28) together with boundary conditions (29) constitute an eigenvalue problem with R being the eigenvalue. Let us assume the solution in the following form so that they satisfy the boundary conditions (29). The solution is therefore given by

$$W = A_1 \sin \pi z, \quad \Theta = A_2 \sin \pi z, \quad D\Phi = A_3 \sin \pi z, \tag{30}$$

where A_1, A_2 and A_3 are constants. The condition for the existence of a non-trivial eigenvalue leads to the following expression for R

$$R = \frac{(\pi^2 + a^2)^3}{a^2 [1 + C(\pi^2 + a^2)]} - \frac{La^2}{\pi^2 + a^2}. \tag{31}$$

Before developing the consequences of (31), we mention a couple of limiting cases that can be derived from (31). In the limiting case of $L = 0$, one recovers the result of Lebon and Cloot [16] and the associated Rayleigh number R is given by

$$R = \frac{(\pi^2 + a^2)^3}{a^2 [1 + C(\pi^2 + a^2)]}. \tag{32}$$

In this case R assumes its minimum value at the critical wavenumber $a_c^2 = \frac{\sqrt{1+C\pi^2(1+C\pi^2)}-1}{C}$. In the limiting case of $C = 0$, one recovers the classical result established for Fourier dielectric liquid (Turnbull [5]) and the corresponding Rayleigh number R is given by

$$R = \frac{(\pi^2 + a^2)^3}{a^2} - \frac{La^2}{\pi^2 + a^2}. \quad (33)$$

Moreover, in the limiting case when $L=C=0$, we obtain

$$R = \frac{(\pi^2 + a^2)^3}{a^2} \quad (34)$$

which is the well-known expression concerning the problem of Rayleigh-Bénard convection in a Newtonian Fourier fluid [19]. We find that R assumes its minimum value $R_c = 27\pi^4/4$ at $a_c = \pi/\sqrt{2}$.

5. Results and Discussion

The problem of convective instability induced by a coupling of thermal and dielectrophoretic effects in an initially quiescent polarised dielectric liquid is investigated analytically by the method of small perturbation. The non-classical Maxwell-Cattaneo heat flux law involves a wave type heat transport and does not suffer from the physically unacceptable drawback of infinite heat propagation speed. The eigenvalues are obtained for free-free, isothermal boundary conditions. It was corroborated, in Maxwell-Cattaneo fluid convection and dielectric liquid convection, that oscillatory convection does not play an important practical role [8, 16]. Indeed, it is known from thermodynamics that the relaxation time and consequently the Cattaneo number C are positive quantities. It has been established that oscillatory convection occurs only for C above a threshold value and since the C values encountered with laboratory fluids appear well below this threshold, it is advantageous to concentrate on stationary convection.

It should be remarked that the use of realistic flow boundary conditions does not qualitatively, but quantitatively change the critical values (Chandrasekhar [19]). Similarly the use of realistic boundary conditions on the electric potential is of only very limited impact on the stability of the system [5]. It is well known that rigid-rigid boundaries offer most stabilizing effect against the fluid motion and the least suppression is offered by free-free boundaries [19]. For non-dissipative flows there is an alternative variational approach to stability which relies on determining whether or not the energy of the flow is a minimum at equilibrium (Straughan [20]). Neutral stability curves in the (R, a) plane are plotted for different values of the governing parameters. The coordinates of the lowest point on these curves designate the critical values of R and a .

Before we embark upon a discussion of the results obtained, it should be noted that the heat is transferred purely by conduction in the quiescent state and by both conduction and convection in the steady convective state. The thermal Rayleigh number R , characterising the stability of the system, is calculated as a function of the Roberts number L and the Cattaneo number C . The variation of thermal Rayleigh number R with the wavenumber a for different values of the Roberts number L and for the Cattaneo number $C = 0$ is shown in Fig. 2. The Roberts number L is the measure of the ratio of electric to dissipative forces. Dissipative forces can be neglected when L is extremely large. It is observed that as L increases, R_c decreases monotonically. From Figs. 3 and 4, it is seen that this trend continues to be the same even for $C = 0.01$ and $C = 0.1$. This means that the dielectrophoretic force has a destabilizing influence on the system. So higher the electric field strength, the less stable the system due to an increase in the destabilizing electrostatic energy to the system. In other words, the presence of electric field facilitates heat transfer more effectively and hence hastens the onset of electroconvection at a lower value of the thermal Rayleigh number.

Moreover, as can be seen from Figs. 2 through 4, R_c decreases monotonically with an increase in the Cattaneo number C . The reason for the destabilizing effect of second sound is that the energy equation considered is effectively a damped wave equation and is, therefore, hyperbolic rather than parabolic. Noticeably, the band width of the neutral stability curves increases with an increase in C indicating that large values of C augment the destabilizing influence of the electric forces and vice versa. It is also obvious that maximum

destabilization is achieved when both L and C are large. Consequently, the onset of electroconvective instability in a dielectric fluid layer is hastened by increasing the magnitudes of second sound and electric forces.

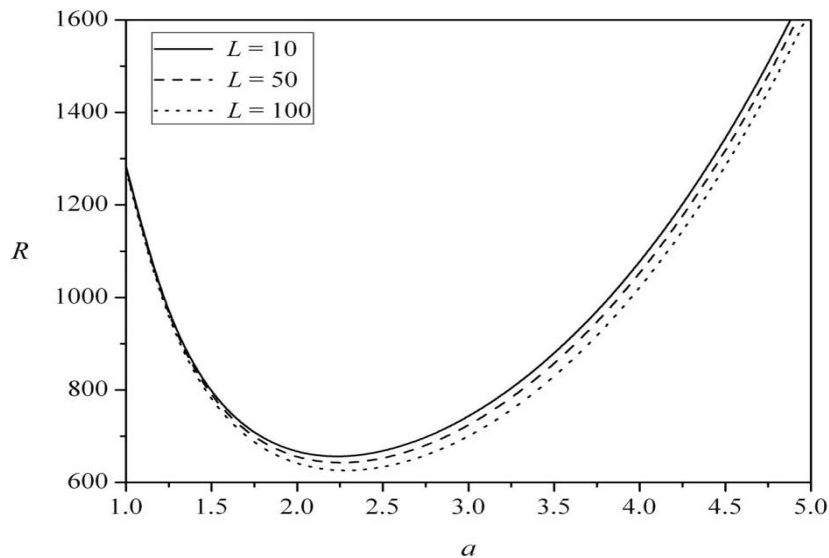


Fig. 2 Variation of thermal Rayleigh number R with a for different values of Roberts number L when $C = 0$.

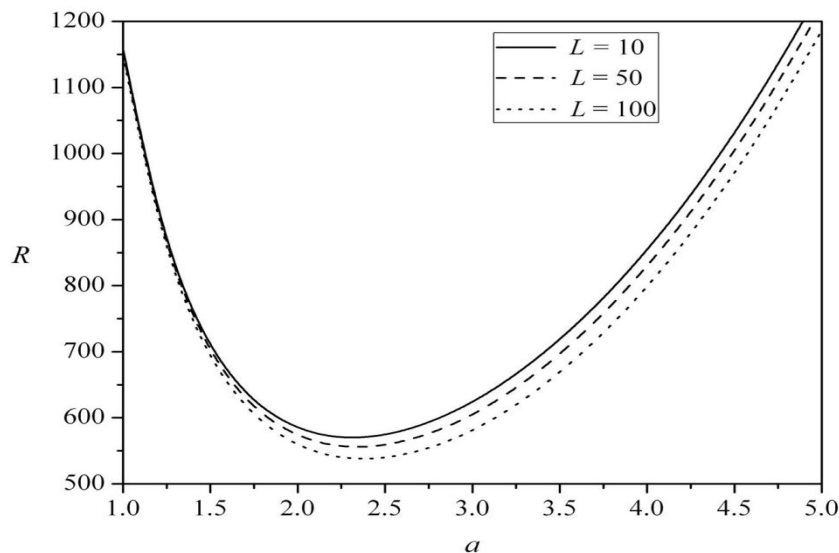


Fig. 3 Variation of thermal Rayleigh number R with a for different values of Roberts number L when $C = 0.01$.

On the other hand, the dimensionless number a is the characteristic of the convection cell shape and size. It is evident from Figs. 2 through 4 that the effect of increasing the values of both L and C is to increase a_c monotonically. This means that the convection cell size is contracted when both L and C are increased. It follows that the transition from equilibrium state to destabilization is accompanied by the shorter wavelength electroconvection on account of the presence of second sound and the dielectrophoretic force. We believe that the present study offers some insights into the heat transfer mechanism that can take place in devices wherein dielectric fluids play a vital role. Undoubtedly, the problem would be more challenging if the magnetic and couple-stress effects are taken into account (Saravanan [21, 22]).

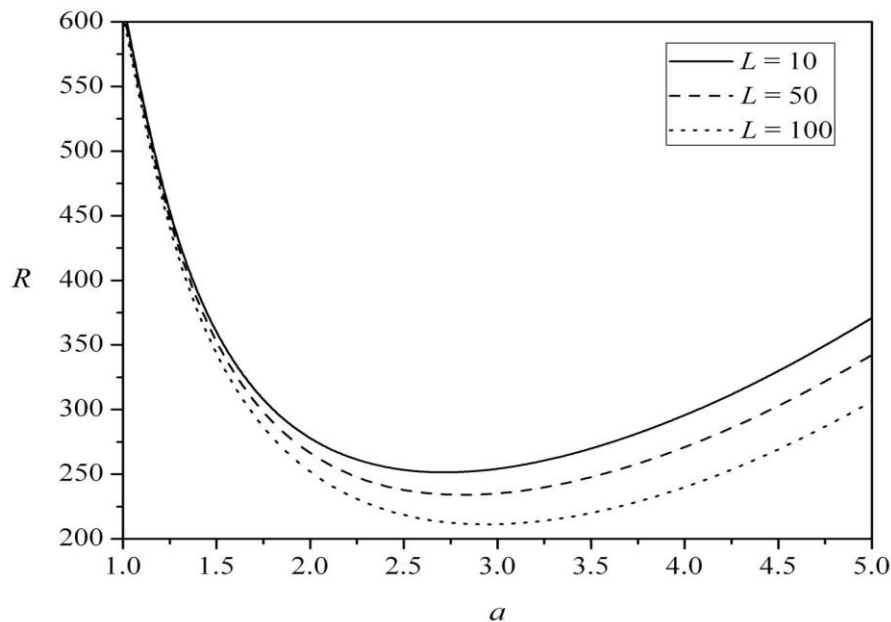


Fig. 4 Variation of thermal Rayleigh number R with a for different values of Roberts number L when $C = 0.1$.

6. Conclusions

The effect of non-classical heat conduction on the onset of Rayleigh-Bénard instability in a horizontal layer of a Cattaneo-dielectric fluid subject to the simultaneous action of a vertical ac electric field and a vertical temperature gradient is investigated analytically by the method of small perturbation. The instability criteria are determined in terms of the thermal Rayleigh number, wavenumber, the Cattaneo number and Roberts number. The following conclusions are drawn:

- (i) The Rayleigh-Bénard problem for a Cattaneo-dielectric fluid layer is always less stable than that with the Fourier-dielectric fluid.
- (ii) The system is considerably influenced by the effect of second sound in the presence of dielectrophoretic forces.
- (iii) The effect of second sound reinforces the destabilising influence of dielectrophoretic forces and vice versa, and maximum destabilization is achieved for large values of the Roberts number and the Cattaneo number.
- (iv) The threshold for the stationary instability decreases with increase in the electric forces and the Cattaneo number.
- (v) Increase in the magnitude of electric forces and second sound causes the convective motion to occur at shorter wavelengths.

7. Acknowledgements

The authors would like to thank the management of Christ University, Bangalore, India for their support and encouragement. The authors are appreciative of the comments of the anonymous reviewers.

References

- [1] J.R. Melcher. Continuum electromechanics. MIT Press, 1981.
- [2] T.B. Jones. Electrodynamically enhanced heat transfer in liquids: A review. *Adv. Heat Transfer*, 14: 107-148, 1978.
- [3] X. Chen, J. Cheng and X. Yin. Advances and applications of electrohydrodynamics. *Chinese Science Bulletin*, 48: 1055-1063, 2003.
- [4] M.J. Gross and J.E. Porter. Electrically induced convection in dielectric liquids. *Nature*, 212: 1343-1345, 1966.
- [5] R.J. Turnbull. Effect of dielectrophoretic forces on the Bénard instability. *Phys. Fluids*, 12: 1809-1815, 1969.
- [6] M. Takashima. The effect of rotation on the electrohydrodynamic instability. *Can. J. Phys.*, 54: 342-347, 1976.
- [7] P.J. Stiles. Electrothermal convection in dielectric liquids. *Chem. Phys. Lett.*, 179: 311-315, 1991.
- [8] T. Maekawa, K. Abe and I. Tanasawa. Onset of natural convection under an electric field. *Int. J. Heat Mass Trans.*, 35: 613-621, 1992.

- [9] P.J. Stiles, F. Lin and P.J. Blennerhassett. Convective heat transfer through polarized dielectric liquids. *Phys. Fluids*, 5: 3273-3279, 1993.
- [10] B.L. Smorodin. Stability of plane flow of a liquid dielectric in a transverse alternating electric field. *Fluid Dynamics*, 36: 548–555, 2001.
- [11] S. Maruthamanikandan. Convective instabilities in ferromagnetic, dielectric and other complex liquids. Ph.D. Thesis, Bangalore University, India, 2005.
- [12] G.M. Mikheev, Gr.M. Mikheev, V.A. Tarasov. and T.G. Mikheeva. Electroconvective purification of dielectric liquids. *Tech. Phys. Lett.*, 34: 391-393, 2008.
- [13] D. Radhakrishna. and P.G. Siddeshwar. Linear and nonlinear electroconvection under ac electric field. *Commun. Nonlinear. Sci. Numer. Simul.*, 17: 2883-2895, 2012.
- [14] B. Straughan. Oscillatory convection and the Cattaneo law of heat conduction. *Ricerche. Mat.*, 58: 157-162, 2009.
- [15] B. Straughan and F. Franchi. Bénard convection and the Cattaneo law of heat conduction. *Proc. Roy. Soc. Edinburgh*, 96: 175-178, 1984.
- [16] G. Lebon and A. Cloot. Bénard-Marangoni instability in Maxwell-Cattaneo fluid. *Phys. Lett.*, 105A: 361-364, 1984.
- [17] S.N. Smita and S. Pranesh. Rayleigh-Bénard convection in a second-order fluid with Maxwell-Cattaneo Law. *Bull. Soc. Math. Services and Standards*, 1: 33-48, 2012.
- [18] M. Takashima and A.K. Ghosh. Electrohydrodynamic instability in a viscoelastic liquid layer. *J. Phys. Soc. Japan*, 47: 1717-1722, 1979.
- [19] S. Chandrasekhar. *Hydrodynamic and hydromagnetic stability*. Oxford University Press, 1961.
- [20] B. Straughan. *The energy method, stability and nonlinear convection*. Springer, 2004.
- [21] S. Saravanan. Centrifugal acceleration induced convection in a magnetic fluid saturated anisotropic rotating porous medium. *Trans. Porous Media*, 77: 79-86, 2009.
- [22] S. Saravanan and D. Premalatha. Effect of couple stress on the onset of thermovibrational convection in a porous medium. *Int. J. Thermal Sci.*, 57: 71-77, 2012.

Enhancing Degraded Color Images Using Fuzzy Logic and Artificial Bee Colony

Adlin Sharo T¹, Dr. Kumudha Raimond²

¹P.G Student, Computer Science & Engineering, Karunya University, India.

²Professor, Computer Science & Engineering, Karunya University, India.

Abstract:

The principal objective of image enhancement is to modify attributes of an image to make it more suitable for a given task and a specific observer. Many research works have been carried out to enhance the degraded images using many techniques including hybrid approaches such as fuzzy logic and Ant Colony Optimization (ACO). Besides, many works have adopted optimization techniques to improve the quality of the degraded images where convergence of optimizing parameters plays an important role. An approach has been proposed in this paper using fuzzy logic and Artificial Bee Colony (ABC) optimization technique to improve the convergence time as well as quality of the degraded images. This approach has yielded better results than ACO with respect to convergence time.

Keywords: ABC, ACO, Fuzzification, Gaussian membership function, Hue Saturation Value (HSV), Overexposed, Underexposed.

1. Introduction

Enhancing the visual clarity of an image is termed as image enhancement which helps to maximize the clarity of the captured image. Because of the limited capabilities of the hardware device which is used for image acquisition, the atmospheric effects such as mist, fog and cloud adds unwanted information which results the image to blur and so it is an essential factor in the imaging domain. In addition to this reason, image enhancement technique is needed in many areas such as remote sensing, robot navigation, textiles, military, film industry, document processing, graphic arts, printing industry, biomedical image analysis and forensic image analysis. Several techniques have been developed to serve this purpose. This research work contributes further to enrich the visual clarity of the degraded images.

2. Image Enhancement

Histogram equalization is a technique for adjusting image intensities to enhance contrast. In histogram equalization, the pixel will be uniformly distributed instead of original pixel distribution and hence the image gains more clarity. For color images, histogram equalization is more tedious due to the vectorial nature of color. Individual pixel value is represented by a vector in a proper color space i.e., (Red, Green and Blue) RGB in the RGB space with as many components as the color. Nikoletta Bassiou and Constantine Kotropoulos use probability smoothing and a multilevel smoothing to derive the transformations of the original intensity and saturation color components to uniformly distributed ones. This method produces more visually appealing images [1]. Duan has introduced a novel histogram processing algorithm which considers the original distribution of pixel in the equalization process [2]. Low-complexity algorithm for contrast enhancement was introduced by T. Arich in which histogram modification techniques such as adjustable histogram equalization, histogram smoothing, weighted histogram approximation, black and white stretching are done by computing histogram and by adjusting the level of enhancement [3]. But it cannot be applied to other types of degraded color images. Color image enhancement technique applied to RGB color space is not suitable for human visual system.

When boundary values are not clear for any image, it will lead to vagueness which means that there is a need for fuzzification and so operations of fuzzy sets like AND, OR, NEGATION are performed for fuzzification. Fuzzy classification is mainly done by conditions and rule based smoothing. For getting the crisp output values, defuzzification is done. For classification of image values fuzzy logic method is used [4]. In Khandelwal's algorithm, the fuzzy logic rules are generated which will differentiate between ambiguous colors [5]. The fuzzy sets are classified based on the HSV color components in Lior Shamir's approach. For example, the rule "Dark Orange, Medium, Medium Dark gives Dark Brown" is defined manually by classifying the HSV color component. Fuzzy logic-based method provides a more accurate color classification [6]. Sarode M.K.V have introduced a new algorithm to retrieve the features related to a specific tumor disease in which only hue is

preserved, whereas saturation and value are changed. Author was able to detect the serious tumor regions and remove the noisy pixels by applying the fuzzy logic rules [7].

H.D. Cheng proposed a novel adaptive direct fuzzy contrast enhancement where the sigmoidal membership function is used to map an image from spatial to fuzzy domain. While transforming the image from one color space (RGB) to another color space (HSV, HIS, YIQ), only the intensity and saturation components were altered without modifying the hue component but it resulted in gamut problem [8]. S.K. Naik tried to keep the transformed values within the range of the RGB space so as to avoid the gamut problem [9]. B. Tang et.al in his approach has changed the color data into chromaticity and brightness and carried the processing further [10].

A HVS Controlled Color Image Enhancement and Evaluation (HCCIEE) algorithm was proposed by K.-Q. Huang which mostly concentrated on the visual effect and the image is enhanced without ringing or halo artifacts [11]. D. Yu have introduced hue preserving correction algorithm named normalized SI correction appropriate for different kinds of enhancement [12]. Fuzzy intensification method was proposed by M. Hanmandlu in which the hue value is preserved, and changes made only on saturation and value and by minimizing the fuzzy entropy. This has resulted in more visual quality image in the contrast enhancement perception [13].

In order to enhance the image, many optimization techniques are used such as greedy, genetic, fuzzy, bacterial foraging and ACO. It is used for optimizing the parameters in color image enhancement techniques [14]. Knowledge about various color image enhancement techniques are gained through a survey on color image enhancement technique [15]. ABC optimization [16-19] is used to optimize the objective function in the proposed approach. The rest of this paper is organized as follows: Section 3 covers the proposed system and the working of the optimization algorithm with its results and analysis of this work. Conclusions are given in Section 4.

3. Proposed Methodology

In this proposed methodology, a degraded image which is either underexposed or overexposed is enhanced by using fuzzy logic and ABC technique. The RGB color value of the image is converted into HSV color value. Only the value and the saturation components of the image changed whereas the hue component remains unaltered. The diagrammatic representation of the proposed approach is shown in Figure 1.

3.1 Fuzzy Approach

The word ‘Fuzzy’ means vagueness. Fuzziness occurs when the boundary of a piece of information is not clear. In [14], the degraded images are enhanced by combining fuzzy logic and ACO optimization technique. In this approach, a degraded image is taken as input. The image is categorized into underexposed, mixed-exposed and overexposed regions. In [14], only the luminance component is fuzzified by preserving the hue component. Gaussian membership function has been used to fuzzify the underexposed and overexposed regions. The parameters in the membership function are optimized using ACO optimization techniques. The fuzzy approach followed in this research work is mainly based on the work adopted in [14].

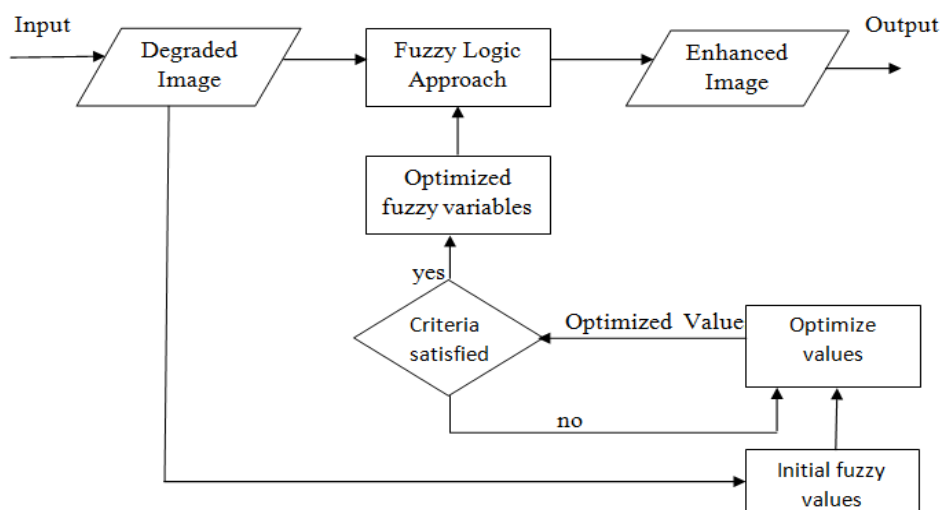


Figure 1: Block diagram of Proposed Methodology

3.2 Optimization using ABC

The revolution of Bee's algorithm is started during 2005 for optimizing parameters [16-19]. This technique is based on intelligent foraging behavior of honey bee swarms. The purpose of bees is to find the places of food sources where high amount of nectar is present. It consists of three phases: employee bees, onlooker bees and scout bees. The overall flowchart of the ABC algorithm is shown in Figure 2 [20].

3.2.1 The employed bees

It flies around the multidimensional search space and find food sources depending on their experiences and their neighbor bees. The colony size consists of sum of same number of employee bees and onlooker bees. Initially the food source positions are randomly generated by using the equation (1). Then by using the fitness function the fitness value is calculated [17]. If the current fitness value is higher than that of the previous fitness value then the current value is replaced by the previous one. Otherwise the value is not replaced and remains the same. By using greedy mechanism the process of comparing and replacing the value is done.

$$v_{ij} = x_{ij} + \phi_{ij} (x_{ij} - x_{kj}) \quad (1)$$

Where V_{ij} is the new food position, k and j are the randomly chosen parameters of different values, where $k \in [1, 2, \dots, SN]$ and $j \in [1, 2, \dots, D]$. $(X_{ij} - X_{kj})$ is the difference between two old food source positions. D is the number of optimization parameters and SN is the number of employed bees. Φ_{ij} is a random number between $[-1, 1]$.

3.2.2 The onlooker bees

It gets the information of food sources from the employed bees and selects one of the best food position which is having high nectar amount. Then by using equation (2) the probability value is calculated. Now based on the probability information the current and previous value are compared by using greedy approach. If the present value is higher than the previous then the current value is replaced by the best value. During this process a limit value is assigned. Each time when the values are compared and if best result is obtained then the counter is set to zero otherwise the limit value will be incremented. Similarly the process is repeated for other bees.

$$P_i = \frac{fit_i}{\sum_{j=1}^{SN} fit_j} \quad (2)$$

Where, P_i is the probability value associated with i^{th} food source. fit_i represents i^{th} food source's nectar amounts. SN is the number of food source which is equal to the number of employed bees.

3.2.3 Best food source

The best value that is obtained from the above process is stored in the memory.

3.2.4 The scout bees

It finds the new food positions randomly without any experience for the exhausted food sources and the iteration are repeated. The scout bee finds a new random food source position using the equation (3).

$$x_i^j = x_{\min}^j + rand(0,1)(x_{\max}^j - x_{\min}^j) \quad (3)$$

where x_{\min} and x_{\max} are lower and upper bounds of parameter j , respectively.

3.2.5 Stopping criteria

1) If the previous value is equal to the current value while comparing the value by using greedy mechanism then the algorithm is stopped. 2) A particular limit value is assigned while comparing the value by using greedy if until the limit, the value obtained is not best then the algorithm is stopped. 3) If the maximum numbers of iterations are executed then the algorithm is terminated.

3.3 Defuzzification:

By using the optimized values of the parameters, the fuzzy membership values are enhanced in the under and overexposed regions. After enhancing membership values defuzzification is done in the underexposed and overexposed regions of the image using inverse functions. By combining the under and overexposed region and applying the original histogram in the middle region gives an image which is then converted from HSV to RGB to get the final enhanced image.

3.4 Results and analysis

The degraded image such as underexposed and overexposed images and the histogram of the original image is shown in Figure 3(a), Figure 4(a), Figure 5(a) and Figure 6(a). The over and underexposed region in the original image is classified by two threshold values and then it is fuzzified. After that the intensification and exposure parameters are optimized using ABC, and then defuzzification is done on the image to get the enhanced image. The enhanced image and their histogram are shown in Figure 3(b), Figure 4(b), Figure 5(b), and Figure 6(b). The time taken by proposed approach is compared with ACO based approach and is found to be better ie, faster than ACO and is shown in Table 1.

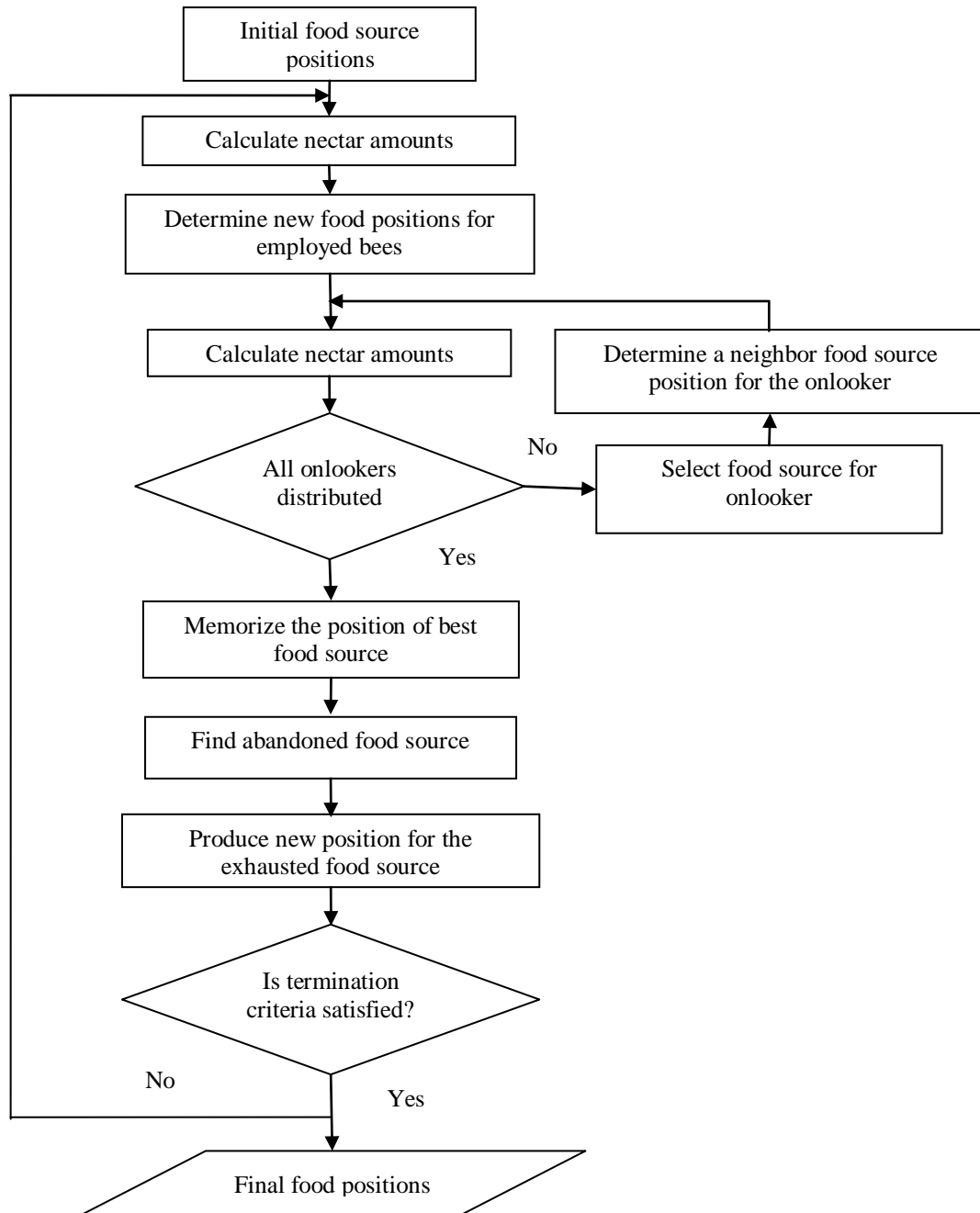


Figure 2: Flowchart of ABC algorithm [20]

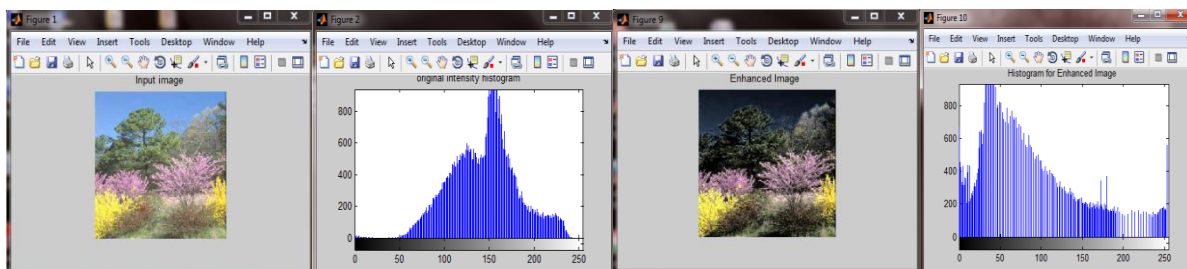


Figure 3(a): Tree image (over exposed image) and its histogram, (b): Enhanced image and its histogram with the proposed approach.

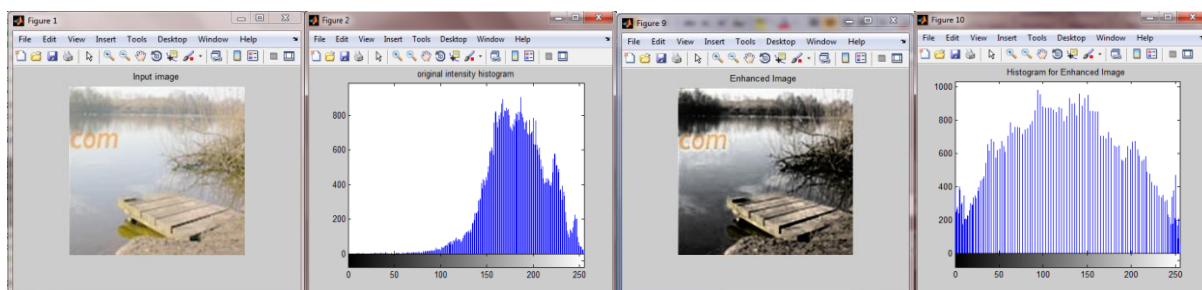


Figure 4(a): Scenery image (over exposed image) and its histogram, (b): Enhanced image and its histogram with the proposed approach.

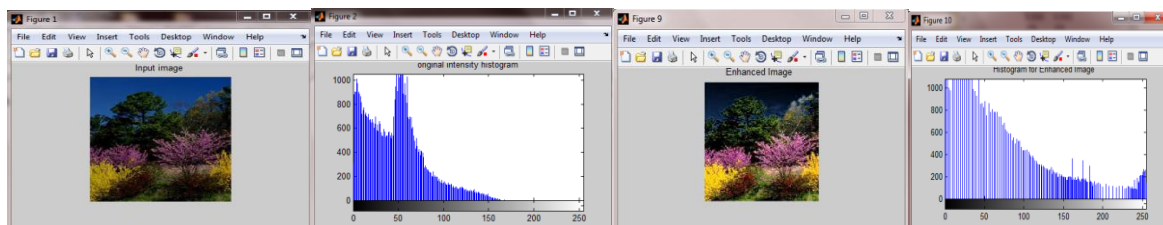


Figure 5(a): Tree image (underexposed image) and its histogram, (b): Enhanced image and its histogram with the proposed approach.

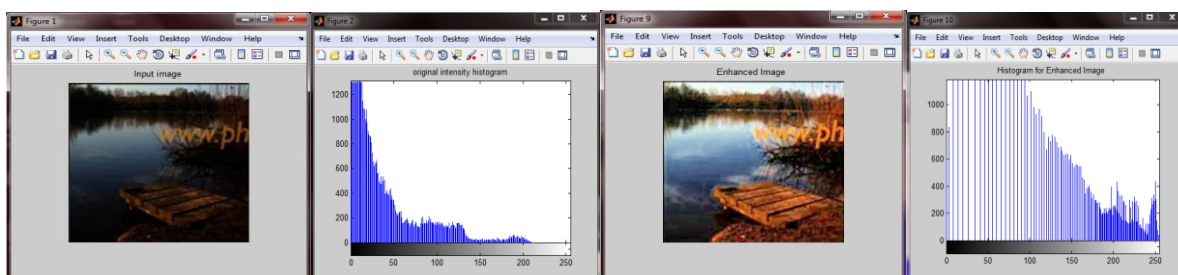


Figure 6(a): Scenery image (underexposed image) and its histogram, (b): Enhanced image and its histogram with the proposed approach.

Table 1. Comparison of time taken by ABC (proposed approach) with ACO.

Test Image	Time taken by ACO (sec)	Time taken by ABC (sec) proposed approach
Figure 3(a)	195.73	19.73
Figure 4(a)	194.40	11.49
Figure 5(a)	197.79	13.82
Figure 6(a)	173.95	12.42

4. Conclusion

In this paper a degraded image is taken as input and divided into underexposed, mixed-exposed and overexposed regions. Gaussian membership function has been used to fuzzify the underexposed and overexposed regions. The parameters in the membership function are optimized using ACO and ABC optimization techniques. Based on the simulation results, it has been found that ABC has given better results than ACO approach.

References

- [1] Nikoletta Bassiou, Constantine Kotropoulos, "Color image histogram equalization by absolute discounting back-off", *Computer Vision and Image Understanding* vol 107, pp.108–122, Jan 2007.
- [2] J. Duan, G. Qiu, "Novel histogram processing for colour image enhancement", *Third International Conference on Image and Graphics*, vol 4, pp. 55–58, Dec 2004.
- [3] T. Arich, S. Dikbas, "A histogram modification framework and its application for image contrast enhancement", *IEEE Trans. Image Process.*, vol 18, 2009.
- [4] Manglesh Khandelwal, Shweta Saxena, Priya Bharti, "An efficient algorithm for Image Enhancement", *Indian Journal of Computer Science and Engineering (IJCSSE)*, Vol. 2, pp. 118-123, 2005. M.Hellmann, "Fuzzy logic Introduction", *Info. & Ctl.*, pp. 94-102., vol 12, 1968.
- [6] Lior Shamir, "Human Perception-based Color Segmentation Using Fuzzy Logic", *IPCV*, pp.496-502, vol 2, 2006.
- [7] Sarode M.K.V., S.A. Ladhake, P.R. Deshmukh, "Fuzzy system for color image enhancement", *World Academy of Science, Engineering and Technology*, vol 48, pp.311-316, 2008.
- [8] H.D. Cheng, Huijuan Xu, "A novel fuzzy logic approach to contrast enhancement", *Pattern Recognition*, vol-33. pp.809-819, 2000.
- [9] S.K. Naik, C.A. Murthy, "Hue-preserving color image enhancement without gamut problem", *IEEE Trans. Image Process.*, vol 12, pp.1591–1598., Dec 2003.
- [10] B. Tang, G. Sapiro, V. Caselles, "Color image enhancement via chromaticity diffusion", *IEEE Trans. Image Process.*, vol 10, pp. 701–707, May 2001.
- [11] K.-Q. Huang, Q. Wang, Z.-Y. Wu, "Natural color image enhancement and evaluation algorithm based on human visual system", *Comput. Vis. Image Underst.*, vol 103, pp. 52–63, 2006.
- [12] D. Yu, L.-H. Ma, H.-Q. Lu, "Normalized SI correction for hue-preserving color image enhancement", *International Conference on Machine Learning and Cybernetics*, pp. 1498–1503, 2007.
- [13] M. Hanmandlu, D. Jha, R. Sharma, "Color image enhancement by fuzzy intensification", *Pattern Recognit. Lett.*, vol 24, pp. 81–87, 2003.
- [14] Om Prakash Vermaa, Puneet Kumarb, Madasu Hanmandluc, Sidharth Chhabrad, "High dynamic range optimal fuzzy color image enhancement using Artificial Ant Colony System", *Applied Soft Computing* 12, pp.394-404, Aug 2011.
- [15] T. Adlin Sharo, Kumudha Raimond, "A Survey on Color Image Enhancement Techniques", *IOSRJEN*, vol 3, pp. 20-24, Feb 2013
- [16] D. Karaboga, B. Basturk "On the performance of artificial bee colony (ABC) algorithm", *Applied Soft Computing*, Vol. 8, pp. 687–697, June.2008.
- [17] D. Karaboga, C. Ozturk "A novel clustering approach: Artificial Bee Colony (ABC) Algorithm", *Applied Soft Computing*, Vol. 11, pp. 652–657, Dec.2011.
- [18] P.Tsai, J.S. Pan.et.al "Enhanced Artificial Bee Colony Optimization", *Innovative Computing*, Vol.5, pp. 1349- 4198, Aug.2009.
- [19] W. Zou, Y. Zhu, H. Chen and X. Sui "A Clustering Approach Using Cooperative Artificial Bee Colony Algorithm", *Discrete Dynamics in Nature and Society*, Vol.10, pp. 1-16, Oct.2010.
- [20] R. Venkata Rao, P.J. Pawar, "Parameter optimization of a multi-pass milling process using non-traditional optimization algorithms", *Applied Soft Computing*, vol 10, pp. 445–456, 2010.